2018

Supramolecular Luminescent Sensors

Teresa L. Mako
University of Rhode Island

Joan M. Racicot
University of Rhode Island

Mindy Levine
University of Rhode Island, m_levine@uri.edu

Citation/Publisher Attribution

Mako, T. L., Racicot, J. M., & Levine, M. (2018). Supramolecular Luminescent Sensors. *Chem. Rev.* In press. doi: 10.1021/acs.chemrev.8b00260
Available at: http://dx.doi.org/10.1021/acs.chemrev.8b00260

TITLE Supramolecular Luminescent Sensors

AUTHORS Teresa L. Mako, Joan M. Racicot, Mindy Levine

AUTHOR AFFILIATION Department of Chemistry, University of Rhode Island, 140 Flagg Road, Kingston, RI 02881; tel: 401-874-4243; fax: 401-874-5072; email: mindy.levine@gmail.com; m_levine@uri.edu

ABSTRACT There is great need for stand-alone luminescence-based chemosensors that exemplify selectivity, sensitivity, and applicability, and that overcome the challenges that arise from complex, real-world media. Discussed herein are recent developments toward that goal in the field of supramolecular luminescent chemosensors, including macrocycles, polymers, and nanomaterials. Specific focus is placed on the development of new macrocycle hosts since 2010, coupled with considerations of the underlying principles of supramolecular chemistry as well as analytes of interest and common luminophores. State-of-the-art developments in the fields of polymer and nanomaterial sensors are also examined, and some remaining unsolved challenges in the area of chemosensors are discussed.

Contents

1. Introduction

The ability to detect a broad variety of analytes under a wide variety of real-world conditions is critical for a number of applications and in a wide range of scientific, medical, political, and security realms. Broadly speaking, chemists have been highly successful at developing detection methods for small organic molecules,[1,2] anions[3,4] and cations;[5,6] biological macromolecules including peptides,[7,8] and oligonucleotides;[9] and whole cells[10,11] and organisms, including bacteria[12,13] and fungi.[14,15] Notable successes include the use of these systems for the detection of 2,4,6-trinitrotoluene (TNT)[16,17] in the air above land mines,[18] for demarcation of tumor boundaries to enable highly effective tumor resection surgeries,[19] and for the detection of bacteria in food,[20] liquid,[21] and the human body. [22]

In all cases, the rational design of chemical sensors, or chemosensors, for detection applications requires thorough consideration of all system components: (1) the analyte, defined as the target for detection; (2) the recognition element, defined as the part of the sensor that recognizes the analyte; (3) the transducer, defined as the sensor component that responds to the presence of the analyte with a change in signal; (4) the environment (solvent[23] and/or solvent additives;[24] gas-phase environment;[25] solid-state backing),[26-28] and (5) all other experimental parameters, including the system temperature[29] and the concentrations of all components.[30]

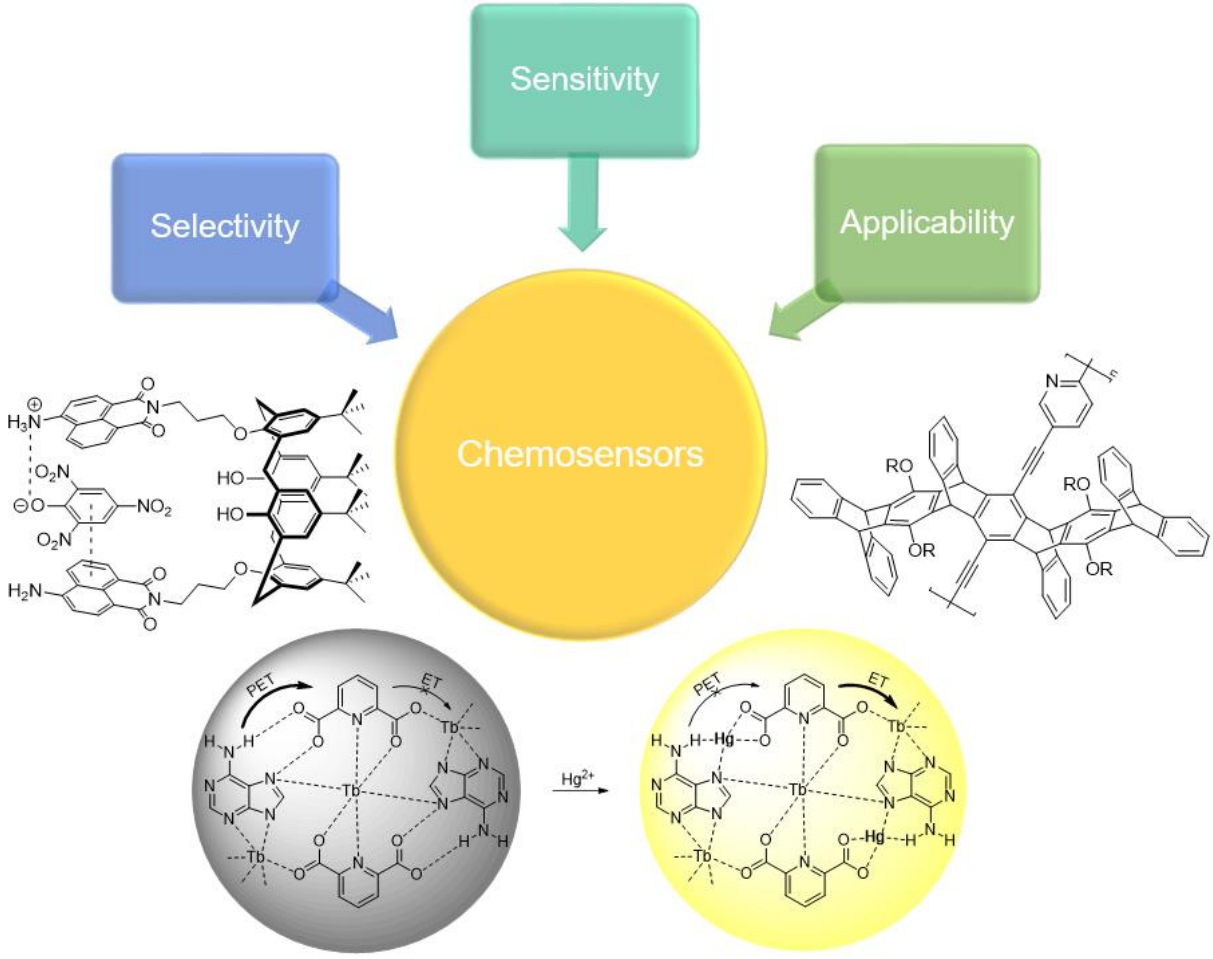

Figure 1. Examples of recently developed chemosensors that have all three aspects of an ideal chemosensor: selectivity, sensitivity, and applicability.[31-33]

One classification system for understanding sensor platforms is to divide such platforms into two categories: those that are sensitive and those that are selective. Selective sensor platforms, in this

classification, refer to those that detect only one analyte, whereas sensitive platforms refer to those that use multidimensional analyses for the (often simultaneous) detection of multiple analytes.[34] Selective detection schemes require sensor molecules, such as antibodies,[35,36] enzymes,[37,38] or aptamers,[39,40] that are specific for binding and detecting one analyte. Such systems have strong commercial successes in pregnancy tests,[41,42] HIV diagnostic systems,[43,44] and glucose monitoring equipment.[45,46] all of which require specificity for one analyte. However, since most analytes share similar structural features with a large range of other molecules, identifying a sensor that binds only a single target analyte is often impractical, and sensitive detection can be the most feasible option. To accomplish such sensitive detection, array-based statistical analytical methods are used to create unique fingerprints for the desired analytes, which are then used for accurate unknown identification.[47]

Overarching goals of sensor chemistry is to develop sensors that have general applicability in multiple environments, high levels of sensitivity for low concentrations of the target analyte, and good selectivity in distinguishing that analyte from other, often structurally related or commonly co-existing compounds (Figure 1). Often, in controlled lab settings, sensitive detection platforms will fare well, only to fall short in circumstances where multiple analytes are present or in relatively complex environments. Selective sensors are generally more successful in complex environments because of the extremely strong analyte-sensor binding displayed by the sensor elements, but there is a relatively small range of molecules that can be detected by selective methods. As discussed in a recent review by Rotello and coworkers,[34] a key challenge in sensor development is the design, optimization, and implementation of systems that are highly selective, highly sensitive, and work well in real-world environments.

Supramolecules are molecular assemblies that are held together by intermolecular forces rather than by covalent bonds. Several features inherent to such systems make them ideal candidates for use as chemosensors, including:[48] (1) Ease of formation: Supramolecules are able to form highly ordered and complex systems without the need for covalent bond formation, which avoids lengthy synthetic processes, and facilitates rapid sensor development;[49] and (2) Adaptive nature: The relatively weak nature of the intermolecular interactions that underlie supramolecular assemblies means that the assemblies are adaptive, and can change their configurations in response to a variety of external stimuli, including the introduction of the target analyte. Such configurational changes, in turn, often lead to a measurable change in an optical signal, including fluorescence and absorption changes. High levels of reversibility, another feature of supramolecular assemblies that is a consequence of the labile intermolecular interactions, means that once the external stimulus is removed, the supramolecular host can reorder to its original state.[50] Supramolecular luminescent sensors often rely on non-covalent supramolecular interactions in all areas of the sensor system, including in sensor-analyte, sensor-fluorophore, and fluorophore-analyte interactions.[51,52] System reversibility provides significant practical advantages, especially compared with sensors that rely on covalent bond formation, which is often irreversible and leads to single-use sensors.[53] This review will discuss luminescent supramolecular hosts, focused in particular on macrocycles, polymers, and nanomaterials, and their use in chemosensor design. Although metal organic frameworks are also prominent luminescent supramolecular hosts, they will not be discussed in this review, and the authors direct interested readers to several other reviews on the topic.[54-58] We would also like to apologize to any researcher whose work has been inadvertently overlooked.

Changes in a detectable signal that occur in the presence of the analyte can refer to a broad variety of signaling elements and various types of read-outs, including changes in color (for colorimetric or absorption-based detection);[59-61] changes in the Raman spectral signal (for Raman-based detection);[62,63] changes in the mass of the sensor after a target analyte binds (for quartz crystal microbalance detection);[64-66] or changes in any other spectroscopic,[67] quantitative,[68] or analytical property.[69] Luminescence-based chemosensors refer to those sensors that respond to the presence of the target analyte with a detectable change in the luminescence signal, with the main types of luminescence being fluorescence, characterized as an allowed, singlet-to-singlet relaxation with photon emission, and phosphorescence, characterized as a forbidden, triplet-to-singlet relaxation with photon emission. More details about the mechanism of

fluorescence and phosphorescence are discussed in Section 2.2, below. Luminescent chemosensors require a component that is photophysically active, in order for the target analyte to induce a measurable change in that photophysical activity.[70] The change of photophysical activity may occur through a change in the magnitude of emission intensity, the wavelength of the emission maximum, the quantum yield, or the relative ratios of various fluorescence/phosphorescence-emitting components.[71] Multiple types of emission changes can also occur simultaneously,[72,73] especially in complex detection environments.[74]

This review focuses on luminescent chemosensors, including their rational design, and broad-ranging applications of such sensors in a variety of realms, including in materials science, biomedical imaging, and national security. It starts with a review of some of the underlying principles of chemosensors, including the non-covalent forces that govern such systems, and the mechanisms of recognition between an analyte and chemosensor via non-covalent interactions. From there, we will review particular classes of luminescent chemosensors, including luminescent macrocycles, luminescent polymers (both with conjugated luminescent backbones and with luminescent pendant side chains), and luminescent nanomaterials. Fluorescent chemosensors are much more common than those based on other types of luminescence, and thus the majority of discussions herein are focused on fluorescence. The concluding section of the review article includes a discussion of unsolved issues in the field of chemosensors, and how future directions of luminescent chemosensors might address those issues.

Of note, the field of chemosensors in general, and fluorescent chemosensors in particular, is highly active with significant numbers of chemists publishing in this field. Readers are directed to other reviews on this important topic to supplement this one, including reviews by Anslyn,[75,76] Rotello,[77,78] Gibb,[79,80] Rebek,[81,82] Liu,[83,84] and Swager.[85-87]

2. Underlying Principles of Chemosensors

2.1. Non-Covalent Interactions

In order for a chemosensor to detect an analyte of interest, the presence of the analyte must induce a measurable change in a read-out signal that can be detected by a user, or operator, of the sensing device. This requires association between the analyte and the chemosensor, which can occur either via covalent[88] or non-covalent interactions.**Error! Bookmark not defined.** Association via non-covalent interactions in sensor design is significantly more common in the scientific literature compared with covalent association,[89,90] because covalent association is often irreversible (with the exception of dynamic covalent chemistry), leading to single-use sensors. Common non-covalent interactions between the analyte and the chemosensor include: hydrophobic association,[91] electrostatic interactions,[92,93] intermolecular hydrogen bonding,[94] cation-π[95] and anion-π[96] interactions, and other aromatic interactions, including π-π stacking[97] and edge-face interactions.[98] When designing a sensor, it is important to note that very rarely do supramolecular complexes rely on just one non-covalent interaction.[99] Combinations of several interactions are often present, and efforts toward designing a system to achieve a myriad of non-covalent interactions are complex and varied. Examples of such cooperativity include: a combination of π-π interactions and weak hydrogen bonding allowing for the formation of oligophenyleneethynylene-based amphiphilic platinum(II) complexes;[100] and a combination of cation-π, anion-π, and intermolecular hydrogen bonding facilitating the assembly of ternary complexes of 1,3,5-triamino-2,4,6-trinitrobenzene, an anion, and a cation.[101]

2.1.1. Hydrophobic Association. Hydrophobic association refers to favorable interactions that exist between two non-polar molecules when they are found in an aqueous environment,[102] with the two molecules associating in a geometry that allows the exclusion of water.[103] Fewer interactions between the aqueous solvent and the non-polar molecules result in a more energetically favorable system[104] because water molecules at the interface with the non-polar molecules are highly ordered, and hydrophobic association reduces the size of that interface. The history of the hydrophobic effect began in earnest in the biochemistry community in the 1960s, with very few examples reporting hydrophobic association before that decade.[105-107] In 1967, a biochemist named Bernard Randall Baker first reported the existence of hydrophobic association as key factor in facilitating enzyme-substrate binding and enzymatic catalysis.[108]

Other biochemists soon reported similar effects,[109-111] highlighting the ubiquity of this interaction in biological systems. Soon after that, in 1970, Ronald Breslow and coworkers reported the first synthetic use of the hydrophobic effect to drive the design and performance of a cyclodextrin-based artificial enzyme.[112,113]

Examples of hydrophobic association between a supramolecular host and a target analyte include cyclodextrin binding a hydrophobic guest in its hydrophobic interior cavity,[114,115] which results in displacing high energy water from the cavity[116] (so named because of its inability to form the full complement of hydrogen bonds, Figure 2)[117,118] and an overall energetically favorable binding. Such binding has been used in chemical sensors, in cases where the binding of an analyte induces changes in the fluorescence emission signal of a fluorophore bound (covalently[119,120] or non-covalently)[121,122] in close proximity, in cases where analyte binding induces displacement of a photophysically active guest from the cavity; and in cases where the analyte itself is photophysically active and displays photophysical changes as a result of encapsulation in the cyclodextrin cavity.

Cucurbiturils (CBs) are another class of macrocyclic chemosensors that rely on hydrophobic association to bind a small-molecule analyte in the interior of the cavity. As with cyclodextrins, these interactions are favored due to the displacement of high-energy water from the macrocycle cavity. Many isomers of these compounds exist, with the most common ones being CB[6], CB[7],[123] and CB[8].[124] Isaacs,[125,126] Masson,[127,128] Nau,[129] Kaifer,[53] and others[130] have demonstrated unprecedentedly high levels of affinity between the CB hosts and small molecule guests. Although these supramolecular hosts are often not photophysically active (with few exceptions),[131,132] the attachment of a photophysically active moiety to the CB core results in a read-out signal that changes in the presence of the target analyte. Synthetic cavitands, including those developed by Gibb,[133,134] Rebek,[135,136] and Anslyn,[75,76] demonstrate markedly improved hydrophobic association and binding affinities compared to naturally-occurring and synthetically-modified cyclodextrins and cucurbiturils. Many of these synthetic cavitands have significant conformational rigidity,[137] which eliminates undesired flexibility in the cavity and facilitates extremely strong binding.[138]

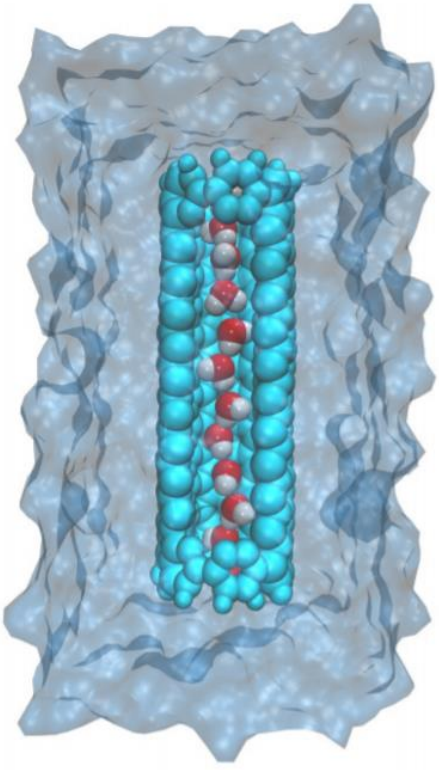

Figure 2. "High energy" water, i.e. water without a full complement of intermolecular hydrogen bonds, in a single-file arrangement inside of a single-walled carbon nanotube. Reproduced from Ref. 139. Copyright 2017 American Chemical Society.

Hydrophobic association also occurs for polymeric chemosensors.[140,141] In one example, researchers reported the use of highly hydrophobic nanostructures derived from block copolymers for the detection of small-molecule nitroaromatics.[142] These nanostructures were rendered water dispersible as a result of the inclusion of non-conjugated segments, and were highly fluorescent due to their poly(*p*-phenylenevinylene) block components. Analyte-induced quenching of the nanostructure's fluorescence was used to detect nitroaromatics at 0.5 ppm in fully aqueous environments. A variety of other examples have also been reported.[143,144]

Of note, the strength of hydrophobic association between two non-polar molecules is intimately dependent on the solvent composition,[145] which must be highly polar (usually aqueous) in order to favor solvent exclusion between the non-polar molecules.[146,147] Moreover, a variety of solvent additives can be used to tune the strength of the effective hydrophobic interactions, with additives such as chaotropic agents decreasing the effective hydrophobicity,[148] and additives such as kosmotropic agents increasing it.[149]

Hydrophobic interactions are highly prevalent in well-solubilized solutions, but they can also occur in the solid-state, at interfaces, or in a variety of other situations. For example, at the air-water interface, hydrophobic interactions occur between non-polar molecules.[150] These interactions drive the self-assembly of ionic liquids,[151] determine how amino acids interact with lipid monolayers,[152] and are instrumental in determining the three-dimensional conformation of enzymes.[153] Computational investigations of molecules at the air-water interface point to factors such as significant aqueous surface tension,[154] relatively high polarity of the air,[155] and the decreases in entropy associated with organized assemblies of molecules[156] as factors that determine molecular and supramolecular behavior at these interfaces.[157] In highly polar solid matrices, two non-polar analytes associate with energetics and geometries that closely mimic solution-state hydrophobic binding.[158] By contrast, hydrophobic interactions in the gas state are almost unheard of,[159] due to the lack of an energetic driving force to compel two non-polar molecules into close proximity.[160]

Classical hydrophobic interactions are entropy-driven and occur due to the increase in the disorder of water molecules when they are removed from the well-ordered interface with the non-polar analyte and become part of the bulk aqueous solvent. Of note, small enthalpic contributions are generally also present.[161,162] Rigorous studies of certain systems, such as the inclusion complexes formed between bile salts and β-cyclodextrin,[163] have described non-classical hydrophobic effects that are driven by enthalpy.[164] Because the energetic driving force of hydrophobic association can have both entropic and enthalpic contributions, the primary thermodynamic driving force for a given host-guest system cannot be fully assumed unless proper studies are conducted, including isothermal titration calorimetry (ITC)[163] and computational studies.[165]

Hydrophobic interactions are usually measured by determining the strength of binding between two non-polar molecules and conducting rigorous experiments to rule out other possible interactions, thus determining by exclusion that hydrophobic interactions must be occurring. Various types of computational modeling have also been used to support the existence of a hydrophobic interaction, although questions about the simplifying assumptions inherent in such computational methods remain, as do questions about the accuracy of some of the results.[166,167] These questions arise because although computational work can be highly accurate for extremely small systems, the significant computing resources required to achieve similar accuracy for larger systems is often prohibitive, resulting in the use of multiple simplifying assumptions. To address this issue, Chia-en Chang[168-170] and others[171,172] have developed new computational models that are particularly effective at predicting hydrophobic association, especially in large, flexible supramolecular structures such as cyclodextrins.

2.1.2. Electrostatic Interactions. Electrostatic interactions are significantly stronger than interactions involved in intermolecular hydrophobic association, with gas-phase binding strengths that approach

covalent bond interactions, although they are often weakened in water due to ion solvation.[173,174] Examples of using electrostatic interactions in luminescent chemosensors include the use of fluorescent cationic polyelectrolytes, developed by Bazan,[9,175,176] Heeger,[177,178] LeClerc,[179] and Liu,[180,181] to bind polyanionic DNA and transduce that binding into noticeable photophysical changes.

One weakness that is traditionally associated with electrostatically-driven chemosensors is that of low selectivity, because electrostatic interactions are highly promiscuous.[182,183] Oftentimes, selectivity in chemosensors needs to be balanced against sensitivity in the same systems, as factors that benefit one of these elements can work against the other.[34] Selectivity is particularly challenging for high strength, promiscuous interactions such as electrostatic interactions, especially in complex environments.[184] In the use of cationic polyelectrolytes to bind polyanionic DNA, the authors achieve reasonable selectivity through the use of multiple favorable electrostatic interactions,[185,186] which act cooperatively to enable high selectivity to occur.[187,188]

Non-classical electrostatic interactions have been reported by Flood and coworkers in which two or more anions were found to stabilize each other through the formation of anti-electrostatic hydrogen bonds.[189] For example, dimers or multimers of bisulfate[4] or phosphate,[190] chaotropic anions, were stabilized by encapsulation in a macrocyclic cavity, leading to the formation of stable 2:2 and higher order, host-guest complexes. A crystal structure that shows an example of this binding is shown in Figure 3. Other anions, including I^-, ClO_4^-, and NO_3^-, formed 1:1 host-guest complexes with cyanostars, with anion dimers not forming due to their lack of hydrogen atoms.[191]

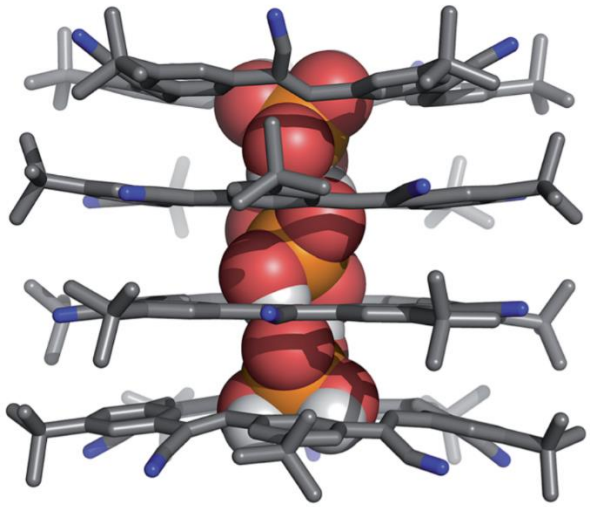

Figure 3. A crystal structure of three phosphate anions stacked inside four cyanostar hosts as reported by Flood and coworkers. Reproduced with permission from Ref. 190. Copyright 2018 Royal Society of Chemistry.

The strength of electrostatic interactions, much like that of hydrophobic interactions, are intimately dependent on the solvent environment.[192,193] Highly polar solvents interact directly with the charged components, and as a result partially mitigate the charge that is felt by the other system component, resulting in a lower "effective" charge.[194] Aqueous solvents, for example, orient water around both cations[195] and anions[196] in a way that facilitates solvation of the anions but decreases the effective charges and the strength of the electrostatic interactions.[197] Electrostatic interactions in non-polar solvents, by contrast, are generally magnified, due the inability of the solvent to solvate charged species effectively.[198,199]

Electrostatic interactions exist in non-solution-state systems and are often stronger in these systems due to lack of solvent interference. In particular, solid-state fluorescent chemosensors use electrostatic interactions to bind polyanionic dengue viral DNA[200] and polycationic serine-containing proteases.[201]

Electrostatic interactions also exist in the gas phase,[202] and have been studied using gas-phase IR multiple photon dissociation (IRMPD) spectroscopy, ion mobility-mass spectrometry (IM-MS),[203] and various UV and other IR techniques.[202]

2.1.3. Intermolecular Hydrogen Bonding. The traditional definition of an intermolecular hydrogen bond is a favorable interaction between a hydrogen atom attached to an electronegative atom on one molecule, termed the hydrogen bond donor, and an atom with a lone pair of electrons on a different molecule, termed the hydrogen bond acceptor (Figure 4).[204] These interactions are generally weaker than electrostatic interactions, but stronger than hydrophobic and other non-polar interactions. Of note, recent work has expanded the traditional definition of a hydrogen bond to include a greater variety of hydrogen bond donors, as long as the atom directly attached to the participating hydrogen has significant electronegative character.[205] Hydrogen bonding under this expanded definition has been reported between a C-H bond and an iodide anion,[206] between a molybdenum and phenol proton,[207] between an sp^3-hybridized C-H proton and aromatic ring,[208] and between carboranes and aromatic rings.[209]

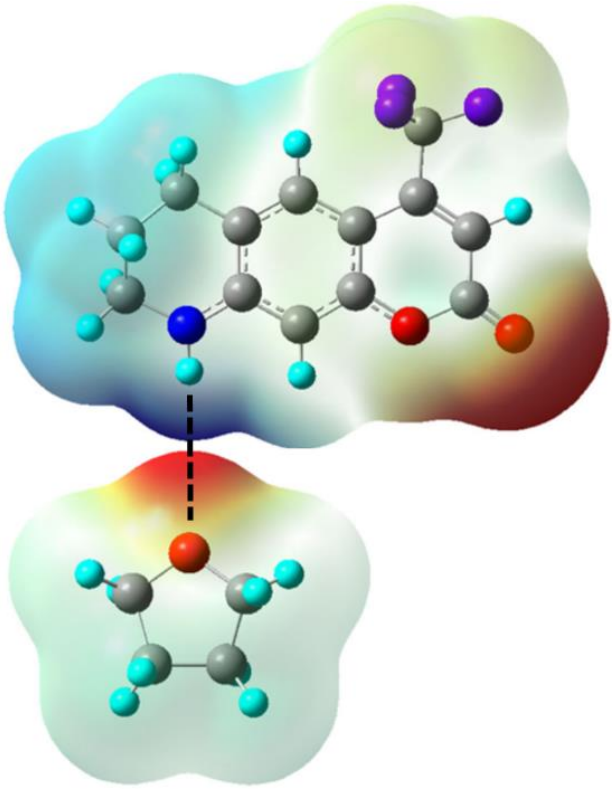

Figure 4. Electrostatic potential map of the intermolecular hydrogen bonding between Coumarin 30 and tetrahydrofuran (THF). Adapted with permission from Ref. 210. Copyright 2018 Springer.

Some structural motifs typically used in hydrogen bonding include squaramides,[211] ureas,[212] and thioureas.[213] Often, these motifs are used to drive self-assembly,[214] including the self-assembly of supramolecular hosts.[215,216] In one example, Bruce Gibb reported the design, synthesis, and applications of a series of self-assembled supramolecular cavitands,[217-219] where the driving force for self-assembly is through intermolecular hydrogen bonding.[220,221] In another example, hydrogen bond-driven chemosensors in chloroform were reported by Zimmerman and coworkers.[222,223] Such self-assembled architectures bound a variety of small molecule guests, including nitroaromatics,[224] guanosine,[225,226] and other nucleotide bases[227] with extremely high affinities, due to favorable binding of host and guest molecules with alternating donor and acceptor groups.

Unlike intermolecular hydrophobic association, hydrogen bonding is primarily driven by enthalpy, although highly solvent dependent[228] enthalpy/entropy compensation balances have also been reported.[229] A report by Ross and Subramanian studied the thermodynamics of protein association, discovering a temperature-dependent system in which the processes are driven by entropy and hydrophobic associations at low temperatures, and by enthalpy and hydrogen bonding at high temperatures.[230] The researchers asserted that the presence of hydrogen bonding can be revealed by negative values of entropy and enthalpy, indicating that hydrogen bonds produce favorable enthalpic contributions. David van der Spoel and coworkers employed classical molecular dynamic simulations of alcohol/water mixtures to derive thermodynamic parameters of the hydrogen bonds present in the solvent mixtures.[231] In these situations, the formation of hydrogen bonds was almost always enthalpically favorable and for higher concentrations of alcohol in water, entropic barriers were present. Leung, Peng, Chou and coworkers developed a series of oligo-α-aminopyridines with a high propensity for hydrogen bond-promoted dimerization, finding that increasing the number of hydrogen bonding sites present led to significant enthalpic stabilization of the dimers.[229]

The existence of hydrogen bonding can be inferred through solid-state X-ray crystallography,[232,233] although not visualized directly, because hydrogen atoms are generally too small to be seen.[234] Moreover, the existence of hydrogen bonding in the solid state does not provide direct information about solution-state hydrogen bonding, even when comparing the same molecule, as ample literature precedent supports the fact that intermolecular interactions in the two states can differ widely.[235,236] Direct solution-state measurements of intermolecular hydrogen bonding generally rely on spectroscopic measurements including ^{1}H NMR[237] and near-[238] and far-infrared spectroscopy.[239]

2.1.4. Cation-π Interactions. The history of the cation-π interaction began in 1981, when chemists found that the gas-phase interaction between a potassium cation and benzene was stronger than the gas-phase interaction between the potassium cation and water.[240] Similar results were measured for the interactions of other cations, including sodium and lithium cations, with benzene, demonstrating the generality of this phenomenon and pointing to the existence of favorable cation-π interactions. Following this initial discovery, Dougherty and coworkers used such interactions to bind a positively charged quaternary amine guest, adamantyltrimethylammonium iodide, inside an aromatic catenane.[241,242] An example of a cation-π interaction between benzene and NH_4^+ is shown in Figure 5.

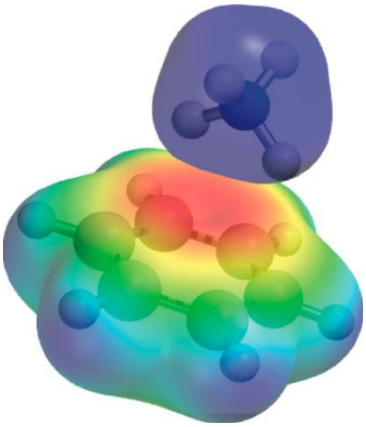

Figure 5. Electrostatic potential map of the cation-π interaction between benzene and NH_4^+. Reproduced from Ref. 242. Copyright 2013 American Chemical Society.

Scientific consensus about the nature of the cation-π interaction is that it is primarily an electrostatic interaction between a positively charged cation and the negative charge density that exists above an aromatic ring.[243] Like most electrostatic interactions, larger ions produce weaker interactions because of lower charge densities.[244] Therefore, in the gas phase, the strength of cation-π interactions follows the following order, with the smallest cation (lithium) participating in the strongest cation-π interactions:[245]

$Li^+ > Na^+ > K^+ > Rb^+$

The use of the cation-π interactions in fluorescent chemosensor design focuses on the detection of cations including potassium,[246] mercury,[247] and cesium.[248] Such chemosensors have been designed to take advantage of cation-π interactions, including in the development of a supramolecular hydrogel containing an aromatic pillar[5]arene with pendant naphthalimide arms that bind, detect, and remove mercury cations;[247] and with the use of a naphthylamine-derived host for the selective detection of copper.[249]

The existence of cation-π interactions has been measured with a variety of methods, including the imaging of charge transfer in a cation-π system in the gas phase.[250] Initial gas-phase measurements of cation-π interactions were much higher in magnitude that subsequent solution-phase measurements due to the solvation of cations that occurs, to varying degrees, in virtually all solvents investigated. Nonetheless, solution-phase cation-π interactions are particularly favored in non-polar and aprotic solvents that have limited interactions with the cation.[251-253] Particular examples of such interactions in biological systems have been reported,[254,255] including as essential components in the formation of tertiary protein structures.[256]

Moreover, solid-state cation-π interactions have also been measured, and include examples such as interactions between aromatic triphenylene and potassium cations,[257] between a cationic surfactant and aromatic PAHs in a clay matrix,[258] and between alkali metal cations and an aromatic macrocyclic host.[259] The limited mobility of the cations and the aromatic moieties within the matrix limits the ability to voluntarily adopt the most favorable intermolecular distances, but systems that position each component in the appropriate location can use these interactions to achieve highly stable multicomponent architectures.[260]

2.1.5. Anion-π Interactions. The anion-π interaction[96] is a relatively newly investigated intermolecular phenomenon, especially compared to many of the aforementioned non-covalent interactions,[261,262] and there was initially some controversy around the legitimacy of such interactions, due to their counterintuitive nature,[263] when they were first introduced.[264,265] A crystal structure demonstrating a close-range interaction between an anion and aromatic ring, reported in 2004, unambiguously proved that anion-π interactions exist in the solid state.[266] Following that report, evidence of solution-state anion-π interactions was discovered via spectroscopic methods,[267] and computational methods were used to obtain significantly improved understanding of such forces.[268,269] In contrast to the negative electron density that exists over an unsubstituted benzene ring, a significant region of positive electron density exists over aromatic rings with highly electronegative substituents, such as hexafluorobenzene.[270,271] This positive region of electron density can, in turn, bind to a broad variety of anions in a phenomenon termed an "anion-π interaction" (Figure 6).

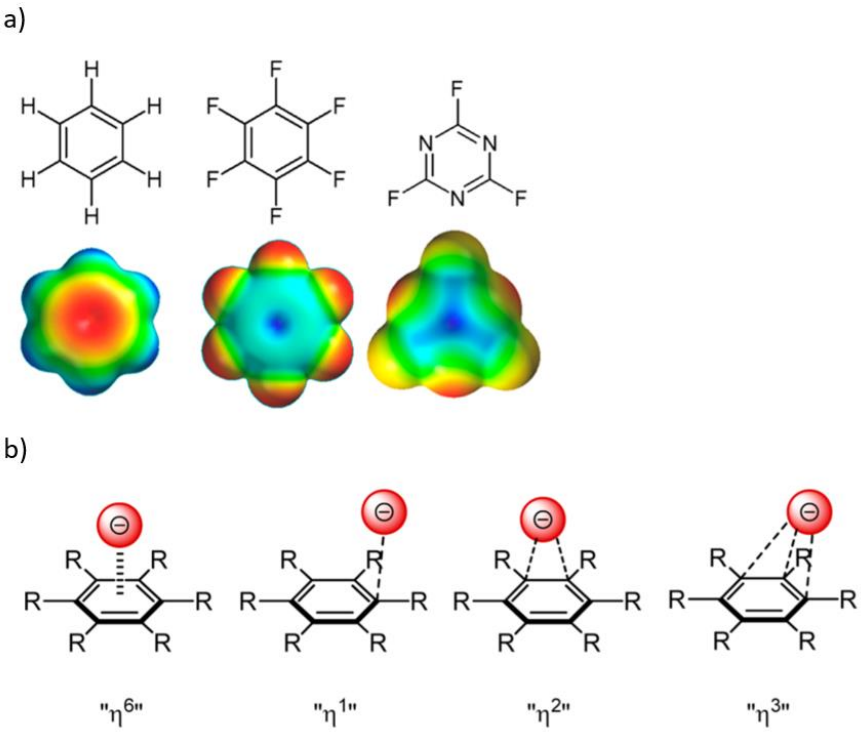

Figure 6. (a) Electrostatic potential maps of benzene, hexafluorobenzene, and trifluorotriazene and (b) modes of anion-π interactions as reported by Hay[272] and Albrecht.[273] Reproduced from Ref. 262. Copyright 2013 American Chemical Society.

Anion-π interactions are particularly useful in designing sensors that can detect anions, including those with significant public health, agricultural, and security interests such as fluoride,[274] nitrate,[275] and perchlorate.[276] Of note, because anions are generally strongly solvated in aqueous solutions, anion binding motifs generally need to be designed to either bind solvated anions or to strip (or partially strip) the aqueous solvation shell prior to binding.[277] The extent to which anions are solvated/desolvated and how such solvation impacts binding affinities and selectivities is a highly active research area.[278,279]

2.1.6. π-π Interactions. π-π Interactions refer to the interaction between the negative electron density of one aromatic ring and a second aromatic ring to form one of three possible structures:[280] a sandwich structure,[281] a T-shaped structure,[282,283] or a parallel displaced structure[284] (Figure 7). The actual structure of the dimer that forms depends on a number of experimental and structural parameters, with two benzene molecules in the gas phase interacting in a T-shaped geometry,[285] where the negative electron cloud on one molecule interacts with a proton (with partial positive charge) on the second aromatic molecule. In contrast, differently substituted aromatic rings, especially those with widely disparate charge densities, will interact to form a sandwich structure. For example, benzene and hexafluorobenzene, with significantly different charge densities, crystallize in infinite stacks with alternating benzene and hexafluorobenzene moieties.[286] This phenomenon was first reported in 1960, where the mixture of C_6H_6 and C_6F_6 was characterized as a "molecular complex."[287] The third possible geometry, parallel displaced structures, is extremely rare for single-ring aromatic moieties, and is markedly more prevalent in intermolecular interactions involving medium and large-sized polycyclic aromatic compounds.[288,289]

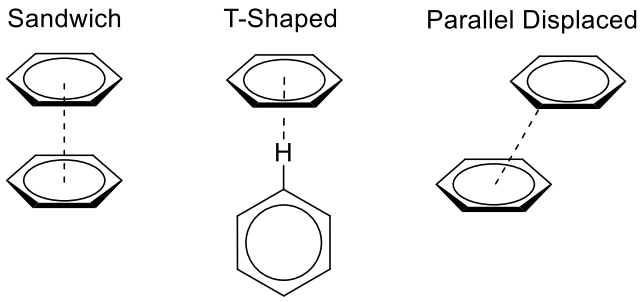

Figure 7. Depictions of sandwich, T-shaped, and parallel displaced modes of π-π stacking.[285,290]

π-π interactions are extremely useful in sensing applications, especially for the sensing of aromatic analytes.[291] For example, Stoddart and coworkers have synthesized a variety of aromatic hosts that are capable of binding aromatic guests with high affinities via π-π stacking.[292] There are large varieties of aromatic guests that are important targets for detection due to their environmental prevalence and high toxicities to humans, including polycyclic aromatic hydrocarbons,[293] polychlorinated biphenyls,[294] bisphenol A and other bisphenol analogues,[295] and aromatic pesticides such as DDT.[296] Work in the Levine group has included the design and synthesis of aromatic ring-containing macrocycles, which have demonstrated enhanced binding affinities for aromatic guests compared to non-aromatic cyclodextrin hosts,[297] and more efficient energy transfer between an aromatic analyte and high quantum yield aromatic fluorophore when both are bound in the macrocycle's interior.[298] Much of this enhanced performance is attributed to favorable π-π stacking interactions, and computational modeling of the complexes supports favorable and close-range interactions between the aromatic rings in the various system components.[299]

2.1.7 Halogen Bonding. Halogen bonding, which is defined as the non-covalent interaction between a Lewis acidic halogen and a Lewis base, has gained significant attention in recent years due to its utility in supramolecular sensing (specifically anion recognition), templated self-assembly, and catalysis.[300,301] Halogen atoms, due to their high electronegativity, can participate as electron donors in interactions with electron acceptors including hydrogen atoms, alkali metals, or alkaline earth metals.[301] In cases where the halogen atom is bound covalently to another atom, the electron density about the halogen atom becomes anisotropically distributed, as shown in Figure 8. A band of increased electronegativity about the center of the halogen atom, orthogonal to the covalent bond, is formed, while the end of the atom becomes electropositive. This electropositive region is then able to form non-covalent interactions with electron-rich sites, such as other halogen atoms. This model of explaining halogen bonding is referred to as a sigma-hole model.[302] Other models, including a lump-hole model,[303] have been proposed, and significant theoretical efforts to fully explain the halogen bonding interaction have also been reported.[304]

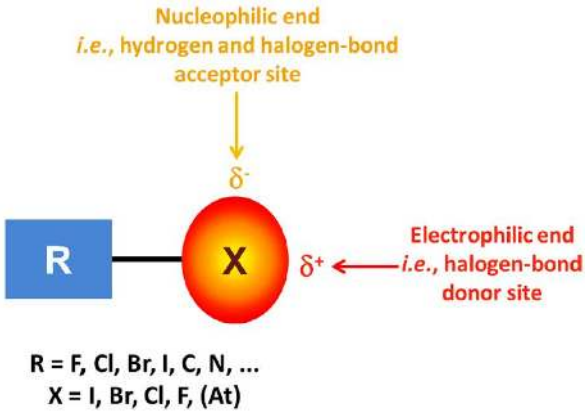

Figure 8. Depiction of anisotropic distribution in a halogen atom covalently bound to another atom. Reproduced from Ref. 301. Copyright 2016 American Chemical Society.

Efforts to use non-covalent halogen bonding in supramolecular chemical sensing have taken a variety of forms. Diedrich and co-workers reported the use of halogen bonding for directing the self-assembly of complex resorcinarene cavitands,[305] with interactions gained from a single halogen bond competitive enthalpically with that of an intermolecular hydrogen bond.[306] Halogen bonding has also found utility in luminescent chemical sensing in cases where halogen bonding can trigger assembly and/or disassembly of a sensing element;[307] in the detection of anions in which halogen bonding between the anion and sensor is used to achieve high selectivity;[308] and in the development of sensors for biological processes, through use of halogen bonding to modulate molecular conformations and achieve target selectivity.[309]

2.2. Mechanisms of Fluorescence

The process of luminescence is characterized by the radiative release of a photon from a molecule as it transitions from an excited state back to its ground state configuration.[174,310,311] Fluorescence and phosphorescence, the two main categories of luminescence, are differentiated based on the excited state from which the photon is released. The Jablonski diagram, shown in Figure 9, illustrates the difference in these two phenomena. When a molecule is irradiated, it transitions from the ground S_0 state to the excited S_1 state. In many cases, the molecule transitions back to the ground state via a non-radiative pathway, known as internal conversion, in which no photon is emitted and luminescence is not observed.[310] Alternatively, radiative decay can occur as the molecule relaxes from S_1 to S_0. During this process, termed fluorescence, a photon is released. This radiative decay is promoted by conjugation of the molecule or the presence of inherently luminescent atoms such as terbium or europium.[311] In a final instance, the molecule can undergo the spin-forbidden transition from an excited singlet state, S_1, to an excited triplet state, T_1, through non-radiative intersystem crossing. Because this is technically a forbidden transition, the likelihood of this transition occurring is generally low, although it can be increased in cases of similarity between the molecular geometry and vibrational levels of the molecule's excited singlet and triplet states, as well as in cases where strong spin-orbit coupling, often due to the heavy atom effect, is possible and can promote the necessary spin flip.[174] Spin-orbit coupling is the mixing of the spin and orbital quantum numbers of a molecule, and heavier atoms have a higher mixing of these two states than do lighter atoms. After undergoing the forbidden transition, the molecule then relaxes from T_1 to S_0 in a radiative pathway referred to as phosphorescence. Due to the spin-forbidden nature of phosphorescence, the lifetimes of fluorescent and phosphorescent emissions are vastly dissimilar, with the former occurring on micro- or nano-second timescales and the latter on millisecond-to-second timescales. It is very common to observe a change in the fluorescence or phosphorescence emission spectra upon the formation of a host-guest association complex; however, host-guest complexation can also lead to measurable changes is phosphorescence lifetimes, allowing for time-gated detection[312-316] in which the presence of an analyte can be detected based on the longevity of a phosphorescence signal.[174]

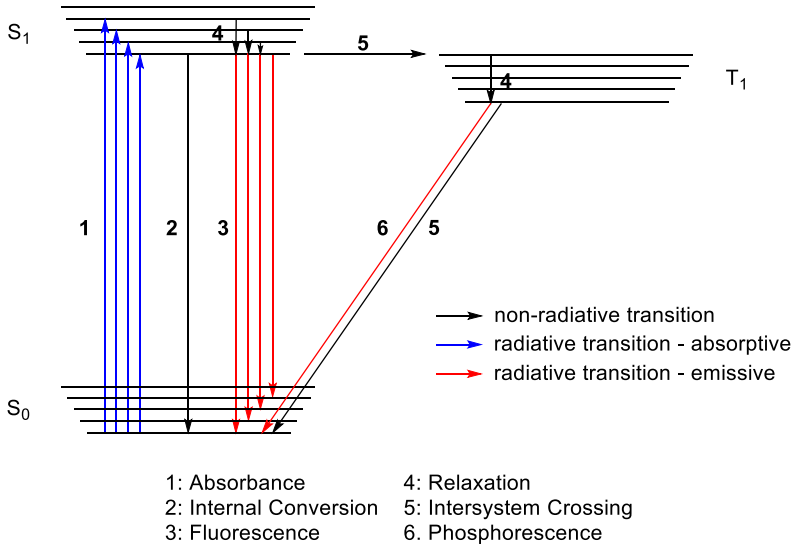

Figure 9. Jablonski Diagram illustrating the electronic transitions that lead to absorbance, fluorescence, and phosphorescence[174,310,311]

Luminescent supramolecular detection schemes often rely on the ability of an analyte to change the fluorescent or phosphorescent emission of a sensor molecule through the transfer of energy.[311] There are several different mechanisms by which this energy transfer can occur: Förster resonance energy transfer (FRET), photo-induced electron transfer (PET), and electron exchange (EE). Of note, in any given system, multiple energy transfer mechanisms can occur simultaneously, and the possibility of multiple coexisting mechanisms should be explicitly considered in any mechanistic investigation. The transfers are characterized based on differences in the electron movements between the lowest unoccupied molecular orbital (LUMO) and highest occupied molecular orbital (HOMO) of the participating molecules as illustratedin Figure 10, as well as by the observed changes in the emission profile.[174] The fluorescent or phosphorescent molecule in a host-guest complex can be either the energy donor, energy acceptor, or both, depending on the electronics of the system, and thus the aforementioned transitions can lead to either emission quenching or emission enhancement. Emission quenching occurs via the transfer of energy to the excited state of a molecule that undergoes non-radiative decay as it transitions back to the ground state. Conversely, emission enhancement occurs when energy is transferred to a molecule that undergoes a radiative transition from an excited state to the ground state. Ratiometric changes in emission can also occur, in which one peak in the emission spectrum decreases while a new peak at a significantly different wavelength increases.[311] Often, this type of emission change is a result of the formation of aggregates of excited state molecules. One such type of aggregate, termed an exciplex, is a complex formed from the excited states of the donor and acceptor molecules. Excimers, in contrast, refer to aggregates of the excited states of two of the same molecule. Other aggregates, including H-aggregates and J-aggregates, can also form.[317] H-aggregates are characterized by co-facial stacking between the monomeric units that results in hypsochromic shifts (or H-shifts) in the absorption spectra relative to the monomeric species.[318] J-aggregates, in contrast, are slipped-stack arrangements of monomeric units that have bathochromic shifts in their absorption spectra and increased extinction coefficients in those bathochromically-shifted bands.[319]

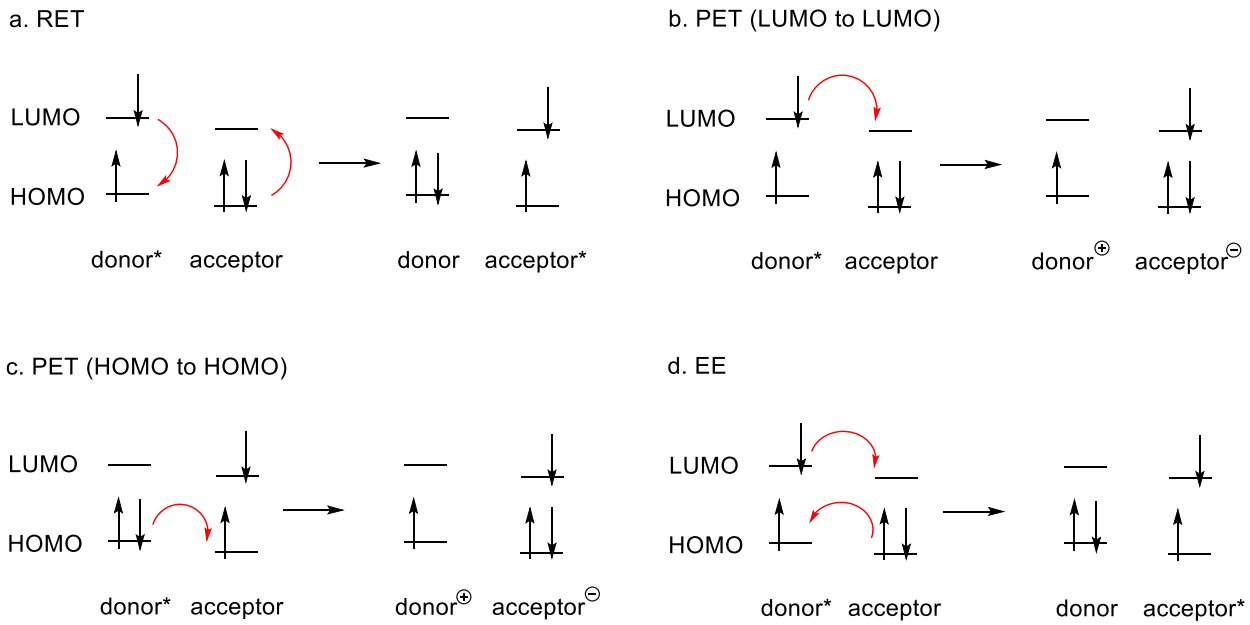

Figure 10. Molecular orbital diagram representations of the mechanisms of a) resonance energy transfer (RET); b) photo-induced electron transfer (PET) between LUMOs; c) photo-induced electron transfer (PET) between HOMOs; and d) electron exchange (EE)

The molecular orientation between the donor and acceptor can have profound effects on the efficiency of energy transfer processes, with the effects intimately dependent on the particular energy transfer mechanism. Specifically, Förster resonance energy transfer theory considers the relative orientation of the donor and acceptor explicitly in the Förster equation as the orientational factor, κ^2.[320,321] Most commonly this orientational factor is approximated to have a value of 2/3, which is accurate in cases where there is unrestricted movement of both the donor and acceptor dipoles and where the movement is markedly faster than the fluorescence lifetime of the donor.[322] Additional mathematical relationships between the energy transfer efficiency and the orientation of the donor and acceptor dipoles have been derived in cases where these experimental conditions cannot be guaranteed,[323] and the ability of the orientational factor to reveal important information about the system geometry and other system-wide structural features has also been demonstrated.[324]

For energy transfer that proceeds via a photoinduced electron transfer mechanism, energy transfer efficiencies are maximal for a co-facial, pi-stacked relationship between the electron donor and electron acceptor.[325] This orientation allows for direct orbital overlap between the two system components, and directly enables effective electron transfer to occur.[326] Such co-facial relationships have been found in a broad variety of biologically-relevant[327,328] and materials science-related systems.[329,330] Similarly, energy transfer that results from direct electron exchange between the donor and acceptor is most efficient for co-facially arranged donor and acceptor moieties.[331,332]

2.2.1. FRET. Förster resonance energy transfer, or FRET, is governed by the Förster energy transfer mechanism[174] which treats the energy donor and acceptor as two interacting dipoles.[333] Although commonly known as fluorescence resonance energy transfer, this mechanism is also applicable to phosphorescence and other types of luminescence. FRET occurs when there is an energy match and spectral overlap between the fluorescent emission of the donor molecule and the absorption of the acceptor molecule.[311] When this resonance condition is met, photons emitted by the donor are absorbed by the acceptor (Figure 10a), raising the acceptor to an excited state. The acceptor then fluoresces or phosphoresces at its characteristic wavelength, even without direct excitation. In cases where the acceptor is not emissive, however, fluorescence quenching due to energy transfer is observed. The extent of this energy transfer is determined

by the degree of spectral overlap between the emission and absorption profiles of the donor and acceptor, respectively, referred to as the spectral overlap integral, or J.[334] As a result, the energy transfer mechanism can be assessed by using the same energy donor in combination with a broad variety of fluorophores, calculating the spectral overlap integral for each donor-acceptor combination, and comparing that to the efficiency of the energy transfer.[335] If Förster resonance energy transfer is the predominant mechanism, the ratio of energy transfer efficiency to spectral overlap integral should be constant.[336] Additionally, FRET is operative over relatively long-range distances,[337] and is inversely proportional to R^6, where R is the average distance between the energy donor and energy acceptor.[338] An example of a FRET-based sensing mechanism is shown in Figure 11.

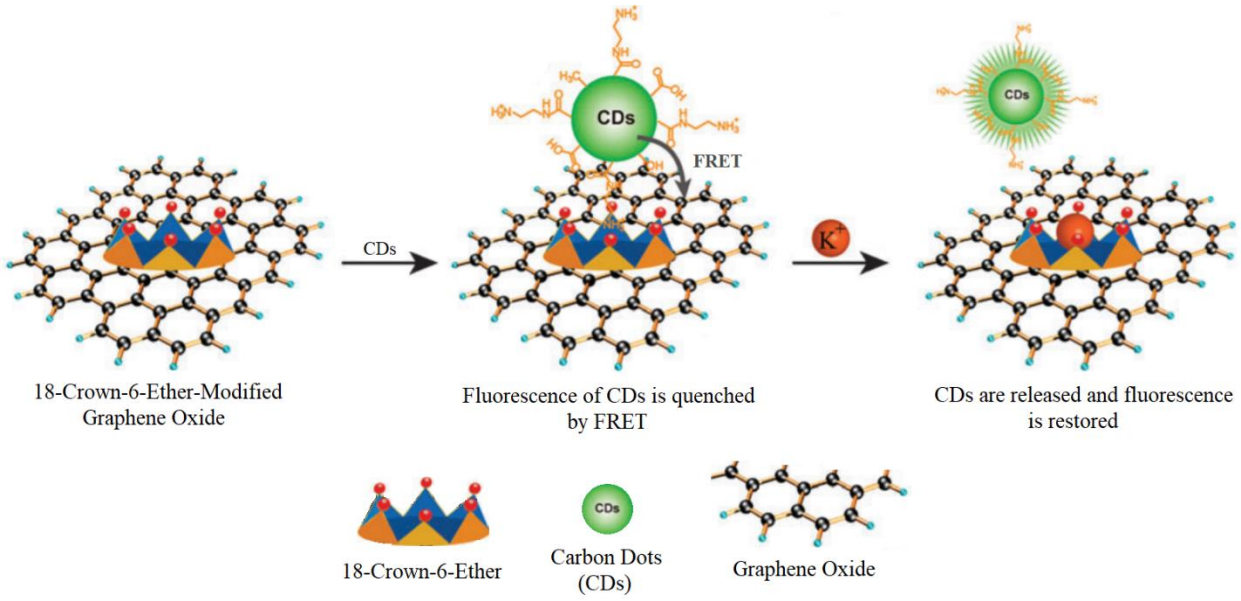

Figure 11. Example of a FRET-based sensing mechanism. Cationic ethylene diamine appendages of a carbon dot were encapsulated in a crown ether affixed to a graphene oxide surface, leading to quenching by FRET from the carbon dot to graphene oxide. Addition of potassium cation displaced the carbon dot, prohibiting FRET and increasing fluorescence. Adapted with permission from Ref. 339. Copyright 2012 Royal Society of Chemistry.

Practical ramifications of Förster energy transfer in detection systems relates to the spectral overlap requirement of Förster theory, which often has, as an unintended consequence, spectral overlap between the emission spectrum of the donor and the emission spectrum of the acceptor.[340] This emission spectra overlap means that for sensing systems that respond to the presence of an analyte with an increase in the acceptor emission signal, residual emission from the donor is often observed even in the absence of the target analyte. System sensitivity in such cases is compromised, often times severely, by the inability to achieve a completely dark background. As a result, energy transfer that operates with reduced spectral overlap between the donor and acceptor can potentially lead to higher system performance,[341] and efforts towards the development of such systems have been reported.

The inner filter effect (IFE) also describes a phenomenon wherein spectral overlap between two species leads to the emission of an energy donor being absorbed by an energy acceptor. In this case, however, the energy acceptor is not the luminophore, and absorption of excited state energy by the energy acceptor prevents the excitation energy from reaching the luminophore, resulting in a filtering of the excited state energy and a lower overall amount reaching the target compound.[342,343] Although IFEs have been seen in many cases as an undesirable mechanism, it is quickly emerging as an important non-irradiative energy conversion model. IFE is commonly observed with nanomaterial detection platforms,[344,345] as the nanomaterials have high absorbing capacity and extinction coefficients.[342]

2.2.2. PET. Photo-induced electron transfer, or PET, occurs when a donor-acceptor complex is formed in which an electron can shuttle from the donor directly to the acceptor, unlike FRET in which no electron is transferred.[346] In PET, an electron is relocated directly from the LUMO of the excited state donor to the LUMO of the ground state acceptor, in the case where the LUMO of the donor is higher in energy than that of the acceptor (Figure 10b); or when an electron moves from the ground state HOMO of the donor to the excited state HOMO of the acceptor, when the former is higher in energy than the latter (Figure 10c). Both instances of PET result in the donor having a singly occupied HOMO and the acceptor having a full HOMO and singly occupied LUMO.[174] Close proximity of the acceptor and donor is required, and the use of covalently linked donor-acceptor pairs increases the likelihood of PET occurring. The distance dependence of the donor and acceptor in energy transfer schemes depends largely on the operative energy transfer mechanism. Photoinduced electron transfer in particular requires close proximity between the donor and acceptor in order for effective orbital overlap to occur.[347] Of note, the exploitation of such strong distance dependence to determine key structural information about a variety of experimental systems has also been reported.[348,349] In some cases, the charge transfer complex undergoes a non-radiative transition back to the ground state and no emission profile is seen. A common mode of supramolecular sensing involves a host that has internal PET between covalently linked donor and acceptor moieties that quenches the emission of the species. Upon complexation with an analyte, the PET is disrupted, leading to an increase in fluorescence.[311] In other cases, the charge transfer complex can undergo a radiative transition to the ground state. An example of a PET-based chemosensor is shown in Figure 12.

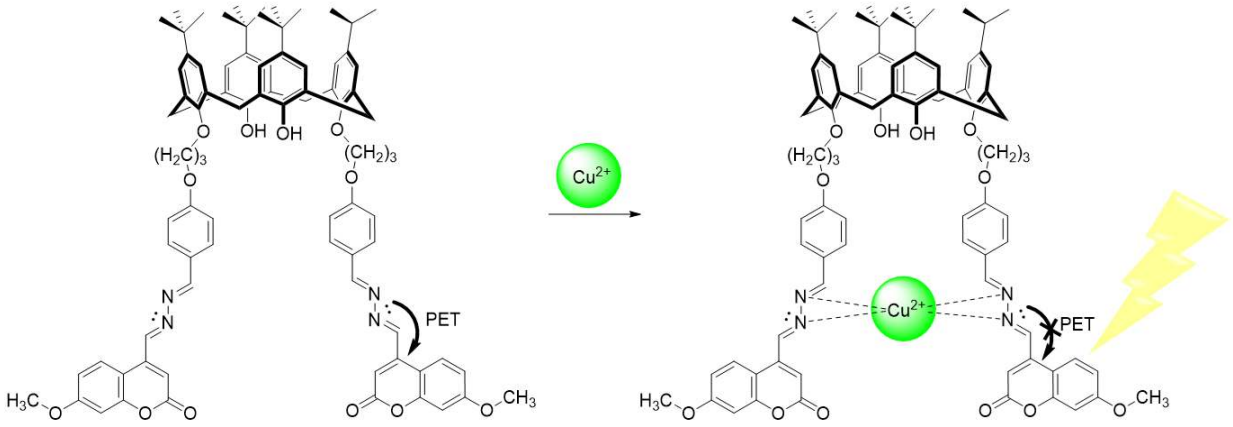

Figure 12. A calixarene host in which PET existing between the imine nitrogen lone pair and the coumarin fluorophore is interrupted by the presence of Cu^{2+}, leading to an increase in fluorescence.[350]

Other electron transfer mechanisms that can be considered classes of PET are internal (or intramolecular) charge transfer (ICT) and metal-ligand charge transfer (MLCT), and twisted internal (or intramolecular) charge transfer (TICT) in which the fluorescence of a compound, such as thioflavin T,[351,352] is related to the rotary motion of certain bonds on the molecule.[353] The former case typically involves conjugated π-systems in which an electron donor and an electron acceptor are bridged by conjugation, which allows for the migration of an excited state electron.[354] In the excited state, many conjugated systems, including those with heteroatoms, have larger dipoles than in their ground state, allowing for enhanced charge transfer.[355] Due to these strong dipoles, these species generally aggregate in solution. MLCT describes the charge transfer that occurs from a ligand to the metal. The efficiency of MLCT is strongly dependent on a number of experimental parameters, including the solvent environment[356] and the identity of the metal center, which is often a transition metal.[357,358]

2.2.3. EE. Electron exchange (EE), or Dexter-type interactions, rely on the quantum mechanical interactions of donor and acceptor molecules when they are in close proximity.[174] In such interactions, an electron is transferred from the LUMO of the excited donor to the LUMO of the acceptor. Simultaneously, an electron is transferred from the HOMO of the acceptor to that of the donor, (Figure 10d). This exchange

of electrons, rather than the transfer of one single electron, is what differentiates this mechanism from PET. In contrast to FRET, Dexter energy transfer requires close-range interactions between the donor and acceptor to enable direct orbital overlap between the interacting moieties,[359] and the efficiency of such energy transfer decreases dramatically as the distance between the donor and acceptor increases.[347,360,361,] Collisions of the donor and acceptor molecules induce direct interactions of the wavefunctions of the molecules, which is necessary for the electron exchange to occur, and which requires close intermolecular distances.[310] In order to ensure close proximity between the molecules and induce Dexter interactions, donor and acceptor molecules can be held in fixed media such as frozen solvents or polymeric scaffolds.[174] A particularly useful application of EE involves electron transfer between the triplet states of the donor and acceptor molecules in a process called "sensitization."[174] Sensitization is useful in instances where an acceptor molecule cannot undergo intersystem crossing, but instead EE from a donor molecule allows for the phosphorescence of the acceptor molecule.

2.2.4. Other Mechanisms. Other phenomena commonly cited in the publications reviewed herein as inducing changes in fluorescent or phosphorescent emission are: chelation enhanced fluorescence (CHEF), chelation enhanced fluorescence quenching (CHEQ), and aggregation-induced emission (AIE). CHEF and CHEQ describe the occurrence of fluorescence enhancement[362-364] or quenching[365-367] upon the chelation of a metal center to the sensor molecule, and thus are mentioned primarily in cation detection schemes. The chelation of a metal center changes the electronic structure of the molecule, allowing one or more of the aforementioned processes to take place. AIE refers to the aggregation of molecules, often induced by complexation with a guest for the most effective detection schemes, to produce an emission response, again most likely through one of the aforementioned mechanisms.[368-370]

2.2.5. Fluorescence Enhancement of Encapsulated Dyes. In the majority of cases, binding of a small molecule fluorophore inside the hydrophobic cavity of a macrocycle host results in enhancement of the fluorophore's emission, with concomitant attenuation of the fluorescence signal upon displacement from the cavity. The mechanisms that underlie such fluorescence changes strongly depend on the chemical structures, and can occur via sterically-induced blocking of single bond rotation,[371] and/or blocking the formation of a non-radiative charge transfer excited state.[372] For hydrophobically-driven inclusion complexes in particular, the non-polar environment around a complexed fluorophore can also contribute to increases in the fluorophore's emission intensity through inducing changes in the fluorophore's observed dipole moment[373] and through blocking interactions between the fluorophore and the bulk solvent.[374] The ability of macrocycle complexation to lead to decreased aggregation of the fluorophore and concomitant fluorescence enhancements has also been reported.[375] These effects combine with the increased steric hindrance that occurs when the fluorophore is complexed inside the macrocycle's cavity to lead to the overall observed fluorescence enhancement.

2.3. Quantifying Supramolecular Complexation

2.3.1. Benesi-Hildebrand Binding Constants. In 1948, Benesi and Hildebrand realized that association complexes were forming between iodine and aromatic hydrocarbons, based on the formation of a new absorption peak when both species were combined.[376] In a subsequent publication, the same authors reported an equation to quantify the equilibrium constant, defined as the binding strength between iodine and an aromatic hydrocarbon, with the numerical representation of such a binding strength now recognized as an association constant.[377] Many variations of the Benesi-Hildebrand equation have developed since the initially reported equation (Equation 1, below), in which [G] is the initial concentration of guest, [H] is the initial concentration of host, I is the signal intensity in the presence of guest (reported as absorbance, luminescence, fluorescence, or phosphorescence values), I_0 is the signal intensity in the absence of quest, ε_0 is the molar extinction coefficient, and K is the association constant.

(1) $$\frac{[G]\cdot l}{log\left({}^{I_0}/_{I}\right)} = \left(\frac{1}{K\varepsilon_0}\right)\frac{1}{[H]} + \frac{1}{\varepsilon_0}$$

Practically, the numerical data represented in this equation is often derived by plotting 1/[Host] on the *x*-axis and 1/ΔI on the *y*-axis. If a linear relationship is obtained, the slope of this line is taken to represent the association constant.[378,379,380] While useful, this method is only valid in cases where the concentration of host is much higher than the concentration of the complex, and is typically only used for 1:1 host-guest complexes,[377] although other binding stoichiometries have also been reported.[381]

2.3.2. Stern-Volmer Quenching Constants. The Stern-Volmer equation, first reported in 1920,[382] describes the quenching of a fluorophore through a dynamic, or collisional, quenching process as a result of diffusive interactions between the fluorophore and quencher.[383] The Stern-Volmer relationship is expressed by Equation 2, below, where F_0 is the fluorescence intensity in the absence of quencher, F is the fluorescence intensity in the presence of quencher, [Q] is the quencher concentration, and K_{SV} is the Stern-Volmer constant.[85]

(2) $$\frac{F_0}{F} = (1 + K_{SV}[Q])$$

This relationship can also be expressed in terms of luminescence lifetimes, as shown by Equation 3, below, where τ_0 is the luminescence lifetime in the absence of quencher, τ is the luminescence lifetime in the presence of quencher, and k_q is the diffusional quenching constant.[85]

(3) $$\frac{\tau_0}{\tau} = (1 + k_q \tau_0 [Q])$$

A linear relationship is obtained in instances where dynamic quenching is the only process occurring, and thus K_{SV} and k_q can be calculated by plotting F_0/F vs. [Q] or τ_0/τ vs. τ_0[Q], respectively. However, in some cases, static quenching, in which the fluorophore forms a stable non-fluorescent ground state complex with a quencher, is occurring simultaneously.[384] This results in a nonlinear relationship between F_0/F and [Q], which can be described by Equation 4, below, where K_S represents the static quenching constant and K_D represents the dynamic quenching constant.

(4) $$\frac{F_0}{F} = (1 + K_S[Q])(1 + K_D[Q])$$

Despite its widespread usage throughout the fluorescence sensor literature, the Stern-Volmer relationship is based on a number of assumptions, including that of a pseudo-first order quenching mechanism and an assumption of a 1:1 relationship between fluorophore and quencher molecules.[385] Thus, a number of fluorescence systems in which analyte-induced quenching occurs cannot be described via the Stern-Volmer relationship.

2.3.3. Association/Binding Constants. While Benesi-Hildebrand and Stern-Volmer constants are widely recognized as sufficient estimations of binding constants, it has been realized that much more complicated intermolecular interactions are commonly present, and thus more detailed equations that account for this complexity are required for the calculation of more accurate binding constants. Furthermore, with the advent of more advanced computer technologies that can process more complex equations, researchers are moving towards the use of these equations that can provide more accurate information.[386] Because these calculations can be difficult or time consuming, a number of computer programs have been devised for the purpose of analyzing data and determining accurate association constants, including Hyperquad[362,387,388] and Specfit.[389,390] Readers who are interested in determining association constants manually are directed to an excellent tutorial review by Thordarson.[386]

2.3.4. Job's Plots. The aforementioned Benesi-Hildebrand and Stern-Volmer relationships generally rely on the assumption of a 1:1 host-guest binding stoichiometry, yet in many instances of supramolecular binding events formation, other stoichiometries are favored, including 1:2 complexes, 2:1 complexes, and complicated combinations of simultaneous, co-occurring multiple stoichiometries. In 1928, Paul Job described a method to determine the stoichiometry of a binding event,[391] and this method is now known as Job's plot, Job's method, or the method of continuous variation. To use this method, the total concentration of a solution of A and B is held constant, while the relative proportions of A and B are varied.[392] The mole

fraction of A (χ_a) is then plotted versus the normalized physical parameter (P), which is obtained using a variety of spectroscopic techniques (fluorescence, absorbance, NMR, etc.). In cases where a 1:1 AB stoichiometry is in effect, P_{max} occurs when $\chi_a = 0.5$. Likewise, P_{max} occurs at $\chi_a = 0.67$ with an A_2B binding mode and at $\chi_a = 0.33$ with an AB_2 binding mode. However, care must be taken when utilizing this method, as more complicated stoichiometric combinations, or instances where multiple stoichiometries are present, cannot be determined using this method. These plots are also useful in gaining a rough estimation of host-guest association constants, in that sharper peaks generally correspond to higher constants and broader peaks correspond to lower constants.[392]

2.3.5. Limits of Detection and Quantification. Determining a detection limit, the smallest amount of analyte that will give an unmistakable signal, and a quantification limit, the smallest amount of analyte that can be accurately quantified, of a given system is invaluable for the analysis of any sensor that could potentially have any commercial or industrial application.[393] The most common approach is to obtain a calibration line of the system in question and to use the equation of that line to calculate the concentration of analyte at the point where the signal is three times the standard deviation of the blank, for detection limit, or ten times the standard deviation of the blank, for quantitation limit. However, there are numerous methods for the determination of these limits, many of which are described in a review by Belter et al.[393]

3. Common Fluorophores.

The rational selection of fluorophores for a particular sensor application can be guided by a range of theoretical and/or practical considerations, including: (a) the need for fluorophores that absorb and/or emit in a target spectral region, in order to act as effective energy acceptors; (b) concerns about solubility of the fluorophores in a broad range of environments, in order to maintain high performance for biological, aqueous-phase applications; (c) stability of the fluorophore to a range of temperatures, solvents, pH values, and other experimental parameters, as dictated by the target application; and (d) the ability to access the fluorophores readily via synthetic means and/or via commercial sources. Table 1 briefly reviews some key parameters of various fluorophore classes associated with these considerations, and the reader is encouraged to consult this table as a helpful guide for their rational fluorophore selection procedures.

Fluorophore	Solubility	Absorbance (nm)	Emission (nm)	Quantum yield	Stokes shifts (nm)	Molar extinction coefficients ($M\ cm^{-1}$)	References
BODIPY	Poor aqueous solubility	500-620	505-750	0.60-0.90	5-130	40000-110000	394,395,396
Squaraines	Poor aqueous solubility	630-670	650-680	0.9 in organic solvents	10-60	300000	397,398,399
Cyanines	organic solvents, aqueous	645-800	660-920	0.0025-0.32	15-200	130000-688000	400,401,402,403
Fluorescein	Aqueous	499	510	0.97 in ethanol	11	92300	404,405,406,407
Eosin Y	Polar organic, and aqueous	526	539	0.67 in ethanol	13	112000	408,409,407
Pyronine Y	Polar organic and aqueous	547	5669	0.48 in ethanol	26	69200	410,411
Rhodamine	Polar organic solvents, Weak fluorescence in water	500-570	520-580	0.7-0.98 in ethanol	10-80	85700-116000	412,406,413,407

Acridine Orange	Polar organic, aqueous	435	530	0.2 in ethanol	95	27000	404, 407 414,415,416
N-Methylacridinium	Polar organic, aqueous	360	490	a	130	19953	417, 418
Lucigenin	Polar organic	368, 455	506	0.67	138	342000/7400	419
Methylene Blue	Polar organic, aqueous	666	686	0.04 in ethanol	20	92000 in ethanol 84000 in water	420, 421, 422
Thionine	Polar organic, aqueous	460	610-625	0.020 in ethanol	150-165	28000	423, 424
Neutral Red	Polar organic and aqueous	460	625	0.044 in ethanol	165	15500	425, 407
Nile Blue	Aqueous	625	674	0.27 in ethanol	49	67000	426
Isoquinolines	Acetonitrile	260	368	0.24	108	a	427
Berberine	Aqueous, Poor solubility in THF	257, 340, 421	555	0.028 in ethanol	134	a	428, 429
Palmatine	Aqueous	349, 420	525	0.001 in DMSO	125	a	430 431
Coptisine	Polar organic, aqueous	402	559	a	157	a	432,433, 434
Rylene Luminophores	Insoluble in polar solvents	350-650	380-670	0.08-0.99	20	38000-85000	435,436,407
Perylene Diimide	Insoluble in polar solvents, soluble in chloroform and toluene	552	536	0.97 in toluene	11	50000	420, 407
Coumarins	Nonpolar solvents	308-454	395-550	0.0032-0.82 in ethanol	< 30	5700-54000	437, 407, 438, 439
Thiazole Orange	Moderate aqueous solubility, soluble in methanol	500	533	0.08 in PBS	33	63000	440, 441, 442,443,444
Luminol	Poor aqueous solubility	365	415	0.50 in ethanol	50	7636	445, 446
Diketopyrrolopyrrole	Poor solubility in most solvents	499-655	560-695	0.009-0.96	34-107	34000-556000	447,448,449,450

Table 1. Comparison table of the physical properties of common fluorophores. a) No relevant information found.

The full list of fluorophore classes discussed in this review are shown schematically in Figures 13-19, and include the following important classes:

3.1. Zwitterionic. (Figure 13)

3.1.1. BODIPY: Boron dipyrromethene, abbreviated as BODIPY, represents a class of fluorophores with extremely high quantum yields,[451] with absorption and emission maxima usually in the green spectral region.[396,452] The position of these maxima, as well as other photophysical properties of these compounds, can be tuned via substitution, at the central (i.e. meso) carbon,[453] on the pyrrole rings,[454] or at the boron center directly.[455] BODIPY dyes with emission maxima in the near-infrared spectral region have been reported,[456] with extended aromatic conjugation, increasing the absorption and emission maxima.[457] Many BODIPY fluorophores are commercially available, and others are readily accessible synthetically via condensation of the appropriate pyrrole with an aromatic aldehyde, followed by reaction with a suitable boron precursor to obtain the target fluorophore.[458,459] Many BODIPY fluorophores can be made water soluble via substitution with oligoethylene glycol chains or other solubilizing groups.[460] Higher order BODIPY architectures, including dimers,[461] trimers,[462] and polymers,[463] have been reported, and many BODIPY constructs maintain high quantum yields even in the solid state.[464] As a result of their favorable properties, BODIPY fluorophores have been used in a number of luminescent sensing schemes, including as high quantum yield energy acceptors from aromatic toxicant donors,[299,465] as part of white light-emitting constructs,[466,467] and as transducing elements for the detection of phosgene,[468] a toxic gas; mercury[469] and copper[470] cations; and many other analytes.[471-474]

3.1.2. Squaraines are a class of fluorophores characterized by an electron deficient cyclobutenone core, which is generally flanked by two electron rich aromatic moieties.[475] This donor-acceptor-donor (D-A-D) architecture gives rise to unique the photophysical properties of squaraines,[476] including: (a) extremely narrow absorption and emission bands, generally in the red- to near-infrared spectral region; (b) small Stokes shifts; (c) high quantum yields; (d) high extinction coefficients; and (e) often high two-photon absorption cross sections.[477] They are easily synthesized via the condensation of squaric acid with the appropriate aniline moieties,[478] and many squaraine compounds are commercially available.

Many of the photophysical properties of squaraines make them desirable components of luminescent sensors, and as a result they have been used extensively in a broad variety of detection schemes. Squaraines are effective energy acceptors when combined with energy donors,[465] including conjugated polymers.[479] They have also been used for the detection of cations,[480] anions,[481] gases,[482] and organic analytes.[483,484] Challenges associated with the use of squaraines include their propensity to aggregate into a variety of H-type and J-type aggregates,[485,486] and the fact that they often have only moderate aqueous stability. Attempts to improve squaraine stability in aqueous environments have focused on inclusion of the squaraine moiety inside the cavity of a rotaxane,[487] cyclodextrin,[488] or synthetic cavitand, which protects the squaraine from undesired degradation and limits uncontrolled squaraine aggregation. Of note, a broad variety of squaraine-derived compounds have been reported in the literature, including squaraine dimers,[489] oligomers,[490] and polymers.[491] Many of these squaraine derivatives have even stronger luminescent properties than the monomeric squaraine and have been used for high performance sensor applications.[492,493]

3.1.3. Cyanine dyes are near-infrared emitting, zwitterionic organic dyes characterized by a polymethine backbone capped by charged, conjugated end groups.[400] The high degree of conjugation and well-defined molecular symmetry of cyanine dyes allow for favorable optical properties including large extinction coefficients and high quantum yields.[400,401] Charge delocalization exists across the length of the polymethine backbone, often leading to red and near-infrared emission maxima. Moreover, zwitterionic salt dyes are often used because the hard counterion charges localize the charge density and distort the symmetry of the compound, leading to additional favorable properties for targeted sensing applications. Cyanine dyes are used extensively in medical imaging, as tumor markers[401,494] and nucleic acid labels,[402,495] due to their water solubility, nontoxic nature, and near-infrared emission;[494] and in all-optical switching applications due to their favorable non-linear optic properties[496,497,498] Supramolecular cyanine-G-quadruplex assemblies have been used for the detection of mercury(II)[499] and potassium,[500] and cyanine aggregates have been used for the detection of human serum albumin.[501]

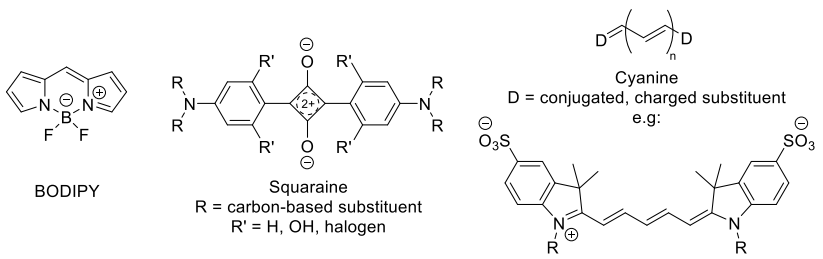

Figure 13. Zwitterionic dyes commonly used in luminescent detection schemes[451-501]

3.2. Xanthone- and Xanthylium-Derived. (Figure 14)

3.2.1. Fluorescein is a commercially available fluorophore that has been used extensively for biological imaging applications,[502,503] facilitated by the ability to modify the fluorescein structure to achieve aqueous solubility[504] and by the fact that aqueous-soluble fluorescein derivatives still have high quantum yields.[505] Fluorescein can act as an energy acceptor in Förster resonance energy transfer schemes for bioimaging and sensor applications.[506] Synthetic derivatives of fluorescein have also been reported,[507] including caged fluorescein variants that can be released via an external stimulus at targeted time points.[508] The use of fluorescein as a sensor for metal cations,[509] anions,[510] and small molecule toxicants[511] has also been reported.[512]

3.2.2. Eosin Y is a brominated derivative of fluorescein that has been used as a photoredox catalyst.[513] It has also been used for many of the same applications as fluorescein, including for fluorescence spectroscopy,[514] photovoltaic applications,[515] and as a probe of enzymatic activity.[516] In sensing applications, it has been used for the detection of active pharmaceutical agents,[517-519] organic toxicants,[520] biological macromolecules,[521] and whole cells.[522]

3.2.3. Pyronine Y is a cationic, commercially available dye which has been used primarily for the binding of anionic moieties including oligonucleotides,[523] anionic peptides,[524] and other anionic macromolecules.[525] It has found usage in sensing applications, including in the detection of fungicides,[526] transition metal cations,[527] nitrite anion,[528] and glucose.[529]

3.2.4. Rhodamines refer to a group of related compounds, including Rhodamine B, Rhodamine 6G, Rhodamine 800, and Rhodamine 123.[530] The core structure of rhodamine consists of a tricyclic heterocyclic conjugated core connected to another aromatic ring via a central biphenyl linkage.[531] Rhodamine dyes generally have high quantum yields, strong two-photon absorption cross sections,[532] and good photostability, all of which are advantageous in luminescent sensing schemes.[533] Rhodamine dyes are strong energy acceptors in both Förster[534,535] and non-Förster[536] energy transfer schemes. A variety of Rhodamine derivatives have been reported in the literature, and generally available via straightforward synthetic procedures.[537] Rhodamines and their derivatives have been used for the detection of multiple classes of analytes, including cations,[538] anions,[539] pesticides,[540] and have also been used in biological imaging applications.[541-543]

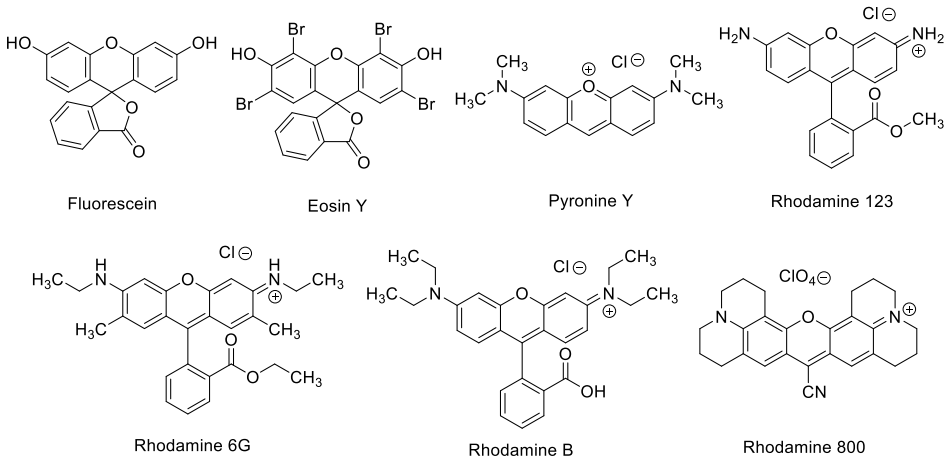

Figure 14. Common xanthone and xanthylium fluorescent dyes used for luminescent detection applications[502-543]

3.3. Acridine- and Acridinium-Derived. (Figure 15)

3.3.1. Acridine Orange is a water-soluble organic dye that has been reported in the literature to bind to a variety of oligonucleotides.[544] The amino groups can be protonated at low pH,[414] which provides opportunities to tune the polarity, solubility, and affinity of the dye for multiple analyte types.[545] Acridine orange is commercially available, and can be straightforwardly derivatized via synthetic procedures.[546,547] Both acridine orange and its derivatives have been used as components in sensors for biological macromolecules,[548] small molecules such as choline,[549] explosive analytes,[550] and others.[551,552]

3.3.2. *N*-Methylacridinium is a cationic organic dye. The anionic counterion is widely variable, and thus a number of different dye salts are commercially available, including a range of substituted derivatives.[553] This dye is redox active,[554] which means that it can participate in reversible redox reactions and as part of electron transfer processes.[555] As a sensor, *N*-methylacridinium can detect protons,[556] reactive oxygen species,[557] metal cations,[558] cyanide, and the herbicide paraquat.[559] *N*-Methylacridinium based compounds have also been used as tools to image and detect biological processes.[560-562]

3.3.3. Lucigenin is a commercially available compound that generates chemiluminescence in the presence of oxygen[563] and free radicals.[564] Lucigenin has been used extensively for the detection of these species in biological systems, as well as for the detection of hydrogen peroxide,[565] nitric oxide,[566] superoxide,[567] and chloride.[568] A variety of lucigenin derivatives have also been reported, and can have different photophysical properties[569] and propensities towards aggregation,[570] depending on the structure of the derivative in question.

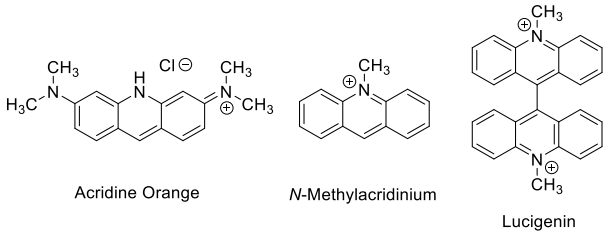

Figure 15. Acridine and acridinium dyes used for luminescent detection applications[544-570]

3.4. Phenoxazinium-, Phenothiazinium-, and Phenazine-Derived. (Figure 16)

3.4.1. Methylene Blue is a commercially available dye with an extremely high extinction coefficient, which has been used as a non-toxic surrogate for organic pollutants[571] and other non-polar analytes.[572] This dye has found additional usage in luminescent sensors for the detection of DNA,[573] Hg^{2+},[574] and a variety of

other analytes.[575-577] Of note, methylene blue is also a pharmaceutically active compound, with therapeutic roles as an antidepressant,[578] as a treatment for malaria,[579] and as an antidote for carbon monoxide poisoning.[580]

3.4.2. Thionine is a cationic, heterocyclic organic dye with a phenothiazine core[581] which is structurally related to methylene blue. A variety of thionine salts are commercially available, including thionine acetate and thionine chloride. Thionine and its derivatives are used most commonly for staining of biologically relevant anionic moieties,[582-584] as well as for photovoltaic[585] and solar cell applications.[586] Detection applications using thionine generally rely on electrochemical detection,[587-589] although isolated examples of luminescent sensing have also been reported.[590,591]

3.4.3. Neutral Red is a common pH indicator, specifically for the detection of basic pHs, that is highly water soluble due to its cationic charge.[592] Several patented uses of Neutral Red are as a colorimetric indicator of the lifetime of a protective glove,[593] as part of a humidity-responsive color-changing wallpaper,[594] and as a fluorescent dye for anti-counterfeiting measures.[595] In recent years, carbon dots[596,597] and gold nanoparticles[598] have been modified using Neutral Red to generate unique optical properties.

3.4.4. Nile Blue is a water soluble, cationic dye that is very fluorescent and photostable, even in aqueous solutions.[599] The fluorescence profile of Nile Blue is highly solvent dependent, with a propensity to form H-aggregates in aqueous solution. Nile Blue is used most often as a pH probe due to its high sensitivity toward changes in pH,[600] but it has also become a popular modifier for nanomaterials.[601,602] Additionally, the dye has unique thermochromic properties, which has facilitated its usage in temperature sensing applications.[599]

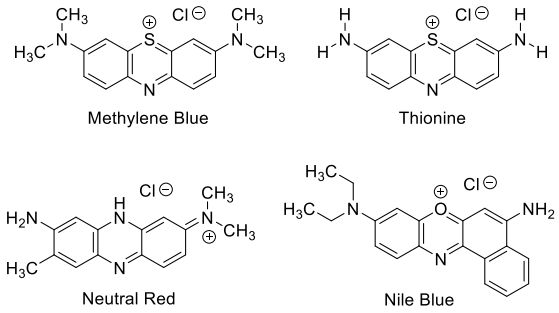

Figure 16. Phenoxazinium, phenothiazinium, and phenazine fluorescent dyes commonly used in luminescent detection schemes[571-602]

3.5. Isoquinolines. (Figure 17)

Isoquinolines refer to a class of fluorophores that are derived from the parent heterocyclic isoquinoline scaffold. Although isoquinoline itself is not fluorescent, many of its derivatives are highly fluorescent,[603] with absorption and emission maxima tunable throughout the visible region.[427,604] Additional tuning of the photophysical properties of isoquinoline derivatives can come from inclusion of the fluorophore in a supramolecular host,[605] which provides steric protection from degradation and leads to enhanced quantum yields.[606-608] Many isoquinoline derivatives are commercially available, and others can be synthesized via straightforward synthetic procedures.[609] Isoquinoline-derived turn-on fluorescent sensors have been used for the detection of a variety of cations,[610-612] and anions,[613] although concerns about the toxicity of isoquinoline derivatives have been noted.[614]

3.5.1. Berberine is a yellow-emitting organic fluorophore with a long history of usage in Chinese herbal medicine[615] and as a dye for ancient textiles.[616] As a fluorophore, berberine has been used for imaging protein conformations,[617] protein-protein interactions,[618] and other biochemical phenomena.[619] Berberine has also been used in a variety of high impact sensing applications,[620] including in the detection of nucleic acids,[621] the cancer medication oxaliplatin,[622] and tumor biomarkers,[623] and as part of method to monitor steroid depletion.[624]

3.5.2. Palmatine is a naturally occurring cationic alkaloid with strong anti-cancer,[625] anti-diabetic,[626] and anti-cardiovascular disease[627] therapeutic effects. Its cationic, highly planar structure facilitates its intercalation in DNA and intercalation-assisted binding.[628-630] Palmatine has been used for the imaging of biologically relevant targets,[631,632] and has also been used as a sensor for a variety of analytes, including a number of pharmaceutical agents, namely cetylpyridinium chloride, an antiseptic;[633] ambroxol, a decongestant;[634] phenformin hydrochloride, an antidiabetic agent;[635] coralyne, a potential cancer treatment;[636] and clorprenaline, a bronchodilator.[637]

3.5.3. Coptisine is another highly luminescent cationic alkaloid, with utility in Chinese herbal medicine as an anti-cardiovascular disease agent.[638] Its high extinction coefficient and strong fluorescence means that it can also be used for luminescent sensing applications, including in the detection of the cancer treatments oxaliplatin[622] and methotrexate,[639] and well as paraquat, an herbicide.[433] Its use in detecting certain DNA constructs has also been reported.[628,640,641]

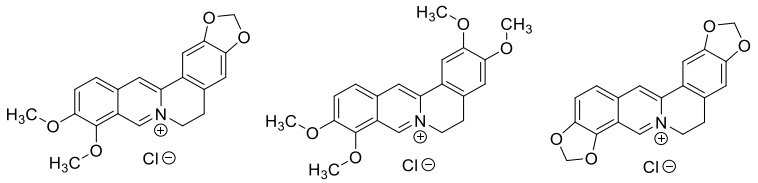

Figure 17. Isoquinoline dyes that have been used in luminescent detection schemes[603-641]

3.6. Rylene Luminophores. (Figure 18)

Rylenes are polycyclic aromatic hydrocarbons that are characterized by a *peri*-fused oligomeric naphthalene scaffold, which have high extinction coefficients and quantum yields, but in the unsubstituted forms suffer from limited solubility due to facile aggregation.[642] Rylene diimide dyes refer to rylenes that have been functionalized with terminal diimide groups, which provide enhanced solubility and a structural handle for synthetic manipulation,[643] maintain high extinction coefficients and quantum yields, and reduce the propensity for aggregation. Common applications of these dyes are in semiconductors[644] and as photosensitizers for reduced transition metals.[645]

3.6.1. Perylene Diimide is a high quantum yield fluorophore with absorption and emission maxima in the 500-600 nm range,[646] with the exact position of the peak maximum depending on the substitution on the imide nitrogen and on the perylene core structure.[647,648] While the parent diimide is not water soluble, perylene diimide can be made water soluble with the addition of solubilizing groups.[649] Perylene diimide has been incorporated into a variety of higher order architectures, including dimers,[650] oligomers,[651] polymers,[652] and nanoparticles,[653] which often results in aggregation-induced changes in the photophysical properties.[654] Higher order analogues of perylene diimide, including terrylene diimide[643] and quaterrylene diimide[655] have also been reported, as has the lower analogue naphthalene diimide.[656] Of note, all of these analogues demonstrate remarkable photostability to a broad range of environmental conditions,[657] making them particularly attractive for practical sensor applications.[658] Naphthalene diimide and perylene diimide are commercially available, and several synthetic derivatives of these architectures have been reported.[659,660] Terrylene diimide and quaterrylene diimide, by contrast, are not commercially available, but are accessible via straightforward synthetic pathways.[661]

The use of naphthalene diimide, perylene diimide, terrylene diimide, and quaterrylene diimide in luminescent sensors focuses largely on their usage as high quantum yield energy acceptors,[662,663] which can be used in combination with a variety of energy donors.[664] In order to ensure close proximity between the energy donor and diimide acceptor, the two components are often covalently linked,[665] or associated non-covalently in a thin film[666] or nanoparticle[667] to promote close interactions. Changes in the perylene diimide luminescence read-out signal have been used for the detection of anions[668] and cations,[669,670] as well as for achieving improved understanding of macromolecular dynamics[671] and biomolecule aggregation.[672]

3.6.2. *N*-Methyl-2,7-Diazapyrenium (MDAP$^+$) and *N,N*-Dimethyl-2,7-Diazapyrenium, while not strictly rylene species, can be characterized as reduced naphthalene diimide derivatives due to their highly related structures. Rather than bearing terminal diimide groups on the core naphthalene, these species are capped by pyridine and pyrenium moieties. These fluorophores are cationic heterocyclic compounds with strong extinction coefficients and quantum yields.[673] MDAP$^+$ is a known DNA intercalator,[674] and forms charge transfer complexes with the nucleobases upon such intercalation.[673] The utility of this fluorophore as a luminescent sensor centers mostly around its ability to detect certain DNA constructs.[675]

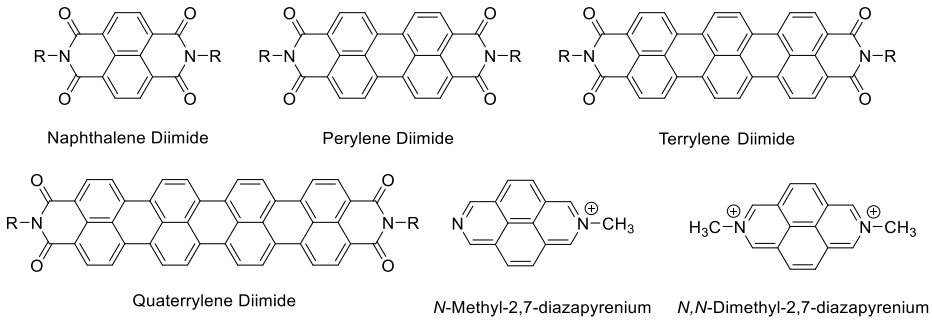

Figure 18. Rylene dyes that have been used for luminescent detection schemes[642-675]

3.7. Other Common Luminophores. (Figure 19)

3.7.1. Coumarins are a large class of organic fluorophores,[676] with absorption and emission maxima throughout the visible spectral region, depending on the molecular structure.[677] Many coumarins are commercially available, and a variety of other synthetic derivatives have been reported as well.[678] These functionalized derivatives can possess strong therapeutic properties,[679] high aqueous solubility[680] and/or other desirable properties such as improved photostability. Of note, the relatively small structure of coumarins compared to other high quantum yield fluorophores means that they can fit into relatively confined spaces,[681] such as small intracellular compartments[682] and inside organic macrocycles.[683] Such confinement generally leads to improved quantum yields and reduced degradation rates,[684] and can provide important information about detailed structural features in biological environments.[685] Coumarins have been used as sensors for broad varieties of analytes, including cations,[686] anions,[687] small molecule toxicants,[122] and biological macromolecules.[688] Their sensitive emission spectra with a strong dependence on the local microenvironment makes coumarins excellent sensors for such environments, and their favorable photophysical properties overall facilitate their usage in high performance luminescent sensing systems.[689,690]

3.7.2. Thiazole Orange is a commercially available, high quantum yield fluorophore that emits strong fluorescence upon binding to nucleic acids,[691] resulting in highly sensitive nucleic acid sensing[692] and DNA imaging.[693] This fluorophore has been conjugated to peptides,[10] DNA,[694] RNA,[695] and other oligonucleotide variants,[696] and its high cell permeability and intracellular stability means that these tagged macromolecules can be readily imaged in vivo.[697,698] Because the fluorescence of thiazole orange is highly sensitive to the presence of exogenous contaminants, it can be used for the detection of a broad variety of analytes, including tetracycline, an antibiotic,[699] cations,[700,701] melamine, a highly toxic comopound used in the production of plastics,[702] and other analytes of interest.[703,704]

3.7.3. Thioflavin T is a benzothiazole-based ultrafast molecular rotor, which means that in its excited state it exhibits non-radiative torsional motion and limited fluorescence emission.[379] When the torsional motion is hindered, radiative decay pathways occur, resulting in strong fluorescence emission. Such restricted rotation can occur when the fluorophore is in viscous solvents, intercalated in DNA,[705] or encapsulated in a macrocycle[706,707] or nanocavity.[708] Thioflavin T has been used to study the formation, aggregation, and inhibition of amyloid fibrils, which are linked to neurodegenerative diseases such as Alzheimer's disease.[709-711]

3.7.4. Luminol is used widely in forensic science for the detection of blood at very low concentrations and on a variety of surfaces,[712] and is a popular tool for explaining forensic science in chemical education.[713,714] Chemiluminescent detection strategies for small molecules using luminol as the photophysically active transducer have been developed, many of which use luminol in conjunction with nanomaterials.[715-718]

3.7.5. Bromothymol Blue is a sulfonphthalein dye with a highly sterically congested structure that has strongly pH-dependent optical properties, and as a result can be used for pH detection applications.[719] Bromothymol Blue has also been used as a dye for textile applications.[720] Recent applications include incorporation of bromothymol blue in a microgel for the colorimetric detection of metal cations,[721] inclusion of the dye in a paper-based microfluidic device,[722] and use of the dye in a thin film pH sensor.[723]

3.7.6. Diketopyrrolopyrrole dyes were first discovered in 1974 by Donald Farnum and coworkers[724] and are typically synthesized by the facile condensation of nitriles with succinic acid ethers or by other similar methods.[447] Simple modification of diketopyrrolopyrroles at the secondary amine position provides strong fluorescence intensity, and further reactions at the carbonyl carbon or carbon-carbon double bond are common.[725] The π-conjugated bicyclic dilactam core of these molecules is responsible for extremely strong intermolecular π-π stacking in the solid state that result in low solubility, excellent thermal and photostability, and high quantum yields.[447,725] Diketopyrrolopyrroles are efficient fluoride probes due to the ability of fluoride to easily form hydrogen bonds with, or deprotonate, the secondary amines,[725] and many such fluorescence-based detection schemes have been developed.[726,727,728] These species have also been used in bioimaging[729,730,731] and organic solar cells.[732,733]

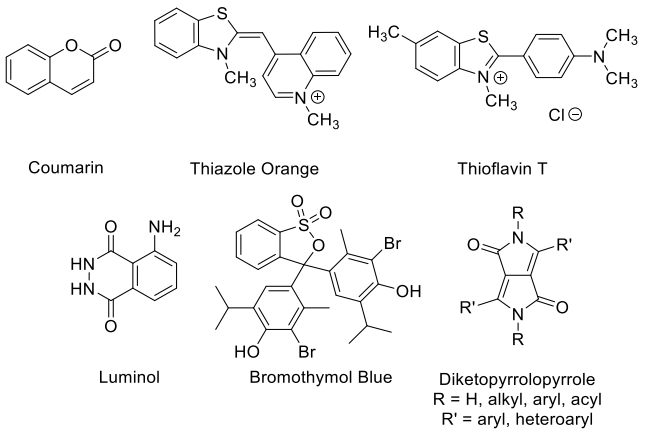

Figure 19. Other luminophores that have been used in luminescent detection applications[676-733]

4. Common Analytes

A broad variety of analytes, shown in Figures 20-26, are discussed in this review, and they can be divided into the following analyte classes:

4.1. Cations

Cations that are biologically relevant, highly toxic[734,735] and industrially useful[736] are important detection targets for luminescent chemical sensors. Biologically relevant cations refer to those that are found in living systems, and whose presence, within a tightly regulated concentration range, are essential for biological activity.[737] Included in this class are cationic enzyme cofactors, including molybdenum,[738] zinc,[739] and iron;[740] cations that are necessary for neuronal signaling pathways, including potassium[741] and sodium;[742] and cations that are involved in biologically necessary electrolyte homeostasis, including calcium[743] and magnesium.[744] Toxic cations include those that are radioactive, such as cesium which was released in the aftermath of the Fukushima nuclear disaster;[745] cations that contaminate the water supply, such as lead which contaminated the water in Flint, Michigan;[746] and transition metal cations that are often necessary

for effective syntheses[747] but need to be removed from commercial pharmaceutical drugs to avoid toxic effects,[748] such as platinum and palladium.

Methods for cation detection often rely on electrostatic complementarity of the cationic analytes with the anionic chemical sensor.[749] This is a particularly effective strategy for polycationic analytes, such as polyamines and cationic peptides,[750] because the cooperativity of multiple favorable electrostatic interactions can impart high sensitivity and selectivity.[751] Another strategy, especially for alkali and alkaline earth metal cations, is to use crown-ether type moieties to bind the target analytes.[752] Linking of these binding moieties with a luminescent transducer, through covalent linkage or through spatial proximity,[753] provides a mechanism by which cation binding is transduced into an optical signal response.[754]

The ability to develop detection schemes for cations depends on a number of variables, including the cationic charge state.[755] Cations with a +1 charge have markedly different solvation geometries and propensities compared to those with +2 or +3 (or occasionally +4) charged states.[756] These differences in solvation are attributed to differences in charge density as well as the relative sizes of the cations, and can have marked effects on energy transfer,[757,758] especially in biological systems,[759] and on the ability to develop effective supramolecular luminescent sensing schemes.[760]

4.2. Anions

Anion detection includes the sensing of both biologically relevant[761] and toxic[762] anions. Examples of biologically relevant anions include phosphate, which represents the anionic portion of DNA and RNA;[763] nitrate, which is converted in vivo to nitric oxide, a key cardiovascular signaling molecule;[764] oxalate, which develops in acidic urine and is a reliable indicator of kidney stones;[765] and acetate, which is a component of acetyl coenzyme A and is involved in ethanol metabolism pathways.[766] Toxic anions include cyanide, which can be highly toxic due to its disruption to the electron transport chain;[767] perchlorate, which is a component of many explosives;[768] fluoride, which is necessary in small quantities but in large quantities can lead to harmful fluorosis;[769] and arsenate, which is toxic and can lead to poisoning symptoms.[770]

Aqueous solution-state methods for anion detection are often complicated by the strong solubilization of the anions in aqueous solvents,[771] which leads to a tightly bound solvation sphere.[772] Nonetheless, highly sensitive and selective anion detection using supramolecular chemistry has been developed by the group of Amar Flood and coworkers using rationally designed supramolecular hosts.[773,774] The ability of anions to impart certain chemical reactivity that is translated into a luminescent read-out signal can also be used for selective anion detection. In one example of such a strategy, Swager and coworkers used fluoride-induced cyclization of moieties appended to a conjugated polymer backbone to change the polymer's fluorescence signal, resulting in effective fluoride detection.[775]

4.3. Toxicants

4.3.1. Polycyclic Aromatic Hydrocarbons (PAHs) (Figure 20) refer to a class of organic pollutants that contain multiple aromatic rings.[776-778] The toxicity of these pollutants varies widely, and includes highly toxic, carcinogenic,[779] and teratogenic[780] benzo[*a*]pyrene,[781] as well as naphthalene and fluorene, which have markedly lower toxicities and are used in commercial applications.[782] PAHs are known components of oil and fuel,[783] and have been found in the environment in the aftermath of the Deepwater Horizon oil spill[784] and other large-scale anthropogenic disasters.[785] The detection of PAHs in biological fluids has been reported,[786,787] in recognition of the fact that PAHs have been found in the blood,[788] breast milk,[789] and urine[790] of individuals living in oil spill-affected regions, and such detection provides a quantitative metric by which to assess such exposure.

Luminescent sensors for PAH analytes can detect the PAHs directly through monitoring their absorption[791] and/or fluorescence emission signals,[792] as many of these compounds have high extinction coefficients and quantum yields.[793] Indirect detection methods can provide additional advantages, including the ability to tune the fluorescence read-out signal to generate well-separated signals for PAH analytes with overlapping spectra.[794] Indirect detection methods include the use of PAHs as energy donors in combination

with high quantum yield energy acceptors, where the fluorescence read-out of the energy acceptor from excitation of the energy donor occurs only in the presence of the PAH analyte.[465,795,122] Other detection methods, including those that rely on π-π interactions between the PAH analytes and conjugated polymers,[796] those that require adsorption of the PAHs to carbon nanotube surfaces,[797] and those that bind PAHs in luminescent macrocycles,[297] have also been reported.

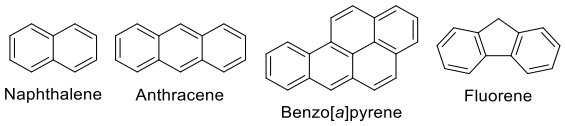

Figure 20. Common polycyclic aromatic hydrocarbon (PAH) analytes[776-797]

4.3.2. Pesticides (Figure 21) refer to several classes of compounds, where the main commercial usage of the compounds is to eliminate an undesired organism, and includes insecticides (for the elimination of certain insects),[798] fungicides (for the elimination of certain fungi),[799] and herbicides (for the elimination of certain plants).[800] Historically, DDT and DDT-related analogues were the most commonly used pesticides,[801] until toxicity studies demonstrated significant deleterious health effects to humans.[802] Newer pesticides have been developed and include a variety of aromatic and non-aromatic pesticides,[803] chlorinated[804] and non-chlorinated compounds,[805] and both metal-containing and non-metal containing variants.[806] Although the usage of many toxic pesticides has been banned, the environmental persistence of these pesticides means that they are still found in significant quantities in a variety of real-world environments.[807]

Detection methods for pesticides vary widely, largely because of their significant structural variability, and include electrochemical,[808] mass spectral,[809] and photophysical (i.e. spectroscopic-based)[810] methods. Photophysically active pesticides can be detected via energy transfer-based methods, in which the pesticide transfers excited state energy to a high quantum yield energy acceptor, resulting in bright, turn-on fluorescence emission in the presence of the pesticide of interest.[121] Non-photophysically active pesticides (i.e. aliphatic organochlorine compounds such as chlordane and mirex) can also be detected via close proximity to a high quantum yield fluorophore, when such proximity is facilitated by a supramolecular cyclodextrin host.[811] In such systems, proximity of the pesticide to the fluorophore results in highly analyte-specific changes to the fluorophore emission, in a process termed fluorescence modulation.[812] Proximity of pesticides to conjugated fluorescent polymers has also been reported to result in sensitive, analyte-specific changes in the polymer emission signal.[813]

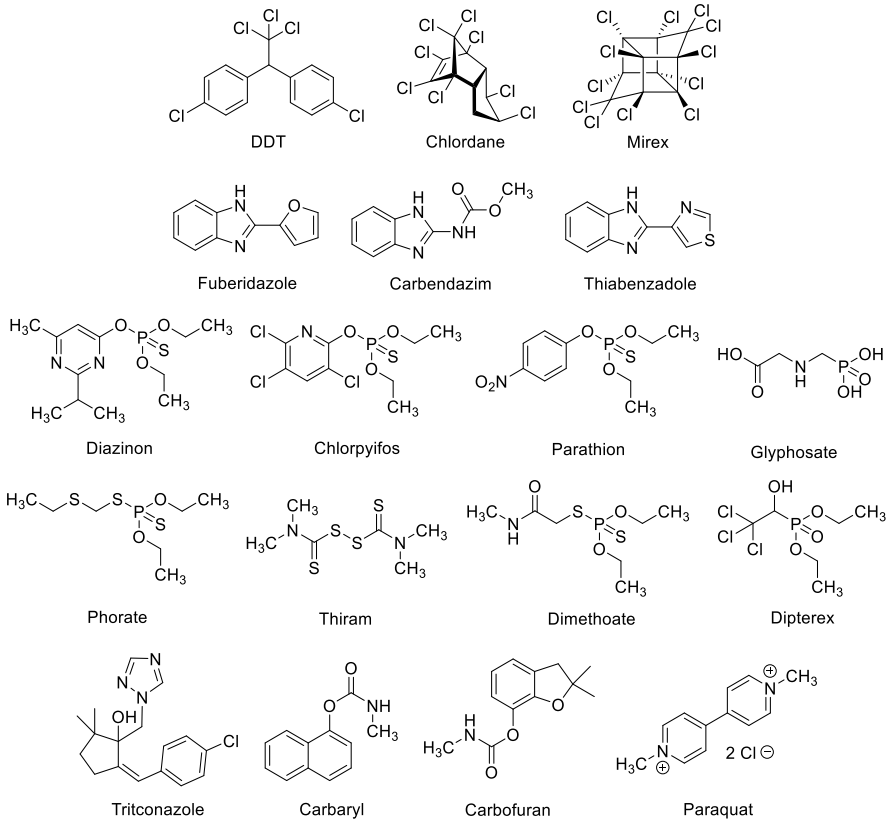

Figure 21. Pesticide analytes that have been detected via luminescence[798-813]

4.3.3. Industrially Relevant toxicants (Figure 22) are those that have common uses in industrial settings or are produced as a result of industrial processes. One example of such toxicants is nitrosamines, which are toxic and carcinogenic compounds that are commonly consumed by humans[814] and can be produced as a result of salting or curing foods.[815] Nitrosamines are also commonly found in tobacco products,[816] and are produced via the vulcanization of rubber. A recent study discovered these compounds in rubber baby bottle nipples and kitchen tools, though in concentrations below the regulatory limit.[817] Another example of an industrially relevant toxicant is bisphenol A (BPA), which has gained significant attention in recent years due to its common use in food packaging[818] and other plastic products, with about 4.5 million tons of BPA produced annually,[819] The prevalence of BPA is particularly concerning due to its suspected endocrine-disrupting properties and associated reproductive toxicities.[820] Other bisphenol derivatives, including bisphenol F and bisphenol S, are also of concern. Melamine is another industrially relevant toxicant that is connected to bladder cancer,[821] female reproductive toxicity,[822] and other serious health effects.[823] Its primary industrial application is in the synthesis of melamine formaldehyde resins, which are used for the production of laminates, coatings, adhesives, dishware, and flame retardants.[824,825] Melamine has also been used in the illegal adulteration of infant formulas and pet foods, dairy products and other consumables.[826] One final class of industrially relevant toxicants is polychlorinated biphenyls (PCBs), which were widely used in the industrial production of dielectric fluids[827] and in construction materials[828,829] until they were banned from the US in 1979 and worldwide after the Stockholm Convention in 2001.[830] PCBs are classified as persistent organic pollutants, meaning that they are toxic bio-accumulators which are prone to atmospheric transport.[831] Since the bans, both in the United States and world-wide, some PCBs have still been formed inadvertently through industrial processes,[832] further indicating the need for robust detection procedures. PCB have been linked to cardiovascular disease,[830] neurotoxicity,[832] viral infections,[833] and the disruption of endocrine and thyroid hormones.[834]

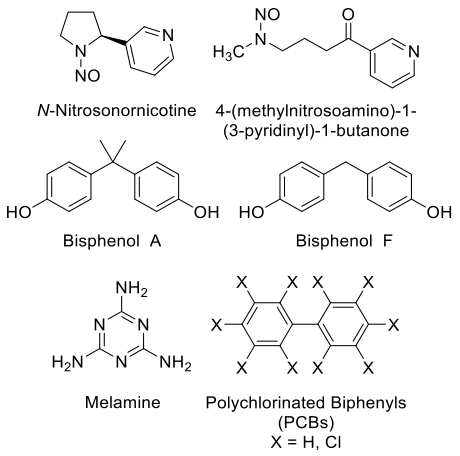

Figure 22. Industrially-related toxicants that can be detected with luminescent sensors.[814-834]

4.4. Explosives. (Figure 23)

The detection of aromatic explosives, including 2,4,6-trinitrotoluene (TNT), generally relies on both electronic complementarity between the electron deficient aromatic rings of the analytes and an electron rich chemical sensor,[835] as well as on favorable aromatic π-π stacking interactions between the aromatic analyte and an aromatic chemical sensor.[836] Examples of detection systems that fit into this category include the detection of TNT based on analyte-induced amplified quenching of a conjugated fluorescent polymer reported by Swager and coworkers, [837,838,17] as well as the detection of TNT using conjugated polymer nanoparticles[839] and conjugated organosilole polymers.[840] Challenges in the practical detection of TNT relate to its low vapor pressure which complicates vapor-phase detection,[841] although methods to address this issue through the detection of commonly co-existing and higher vapor pressure impurities have been reported.[842,843]

The detection of non-aromatic explosives can be more challenging due to a lack of a clear spectroscopic signature for many of these compounds.[844,845] RDX and PETN, for example, are often detected through monitoring the products of reactions that these analytes induce, including analyte-promoted reductions.[846] In other cases, researchers have reported explosive detection via the detection of commonly co-existing analytes including cyclohexanone,[479] which is a highly volatile additive used in explosive packaging.[847] The detection of other explosives and components of explosives, including hydrogen peroxide,[848] acetone,[849] nitrate-based fertilizer,[850] and picric acid,[851] have also been reported.

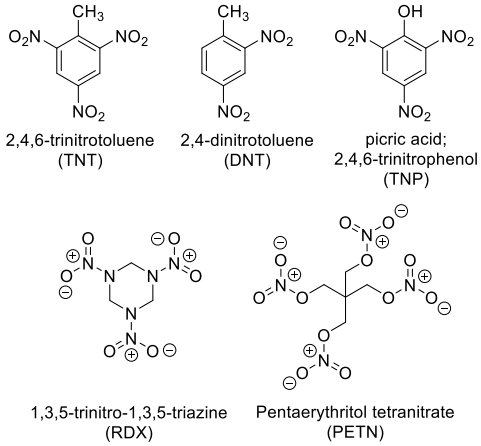

Figure 23. Explosives commonly detected using luminescent sensors[835-851]

4.5. Pharmaceutical Agents. (Figure 24)

The detection of active pharmaceutical agents, including over–the-counter drugs, is particularly important due to the increasing usage of these compounds in developed countries,[852] combined with their strong environmental persistence[853] that leads to their prolonged presence in water,[854] soil and sediment,[855] and air.[856] Because inadvertent exposure to such compounds correlates with deleterious health effects in fish[857] and other organisms,[858] as well as in people who consume such organisms,[859] detection methods that operate in complex environments are sorely needed. Detection methods are also needed that can differentiate real drugs from counterfeit[860] or contaminated ones[861] to prevent inadvertent exposure of consumers to undesired contaminants, adulterated substances, or ineffective drugs.[862]

Detection methods for such compounds vary widely due to significant variability in the compound structures. Opioid detection methods tend to rely on detecting the effects of the opioids,[863] in binding to a receptor target,[864] in inducing a noticeable change in the presence of metal cations,[865] or in facilitating chemiluminescent reactions.[866] The detection of over-the-counter drugs such as acetaminophen (paracetamol) and ibuprofen can be accomplished via electrochemical,[867] photophysical,[868] and mass spectral methods,[869] and many of these methods can also detect commonly occurring impurities in these products.[870] The detection of antibiotics in complex environments has been reported using Raman spectroscopy, aptamer-based sensors,[871] and photophysical methods.[872] Luminescent sensors for opioids,[873] over the counter drugs,[874] and antibiotics[875] have also been reported.

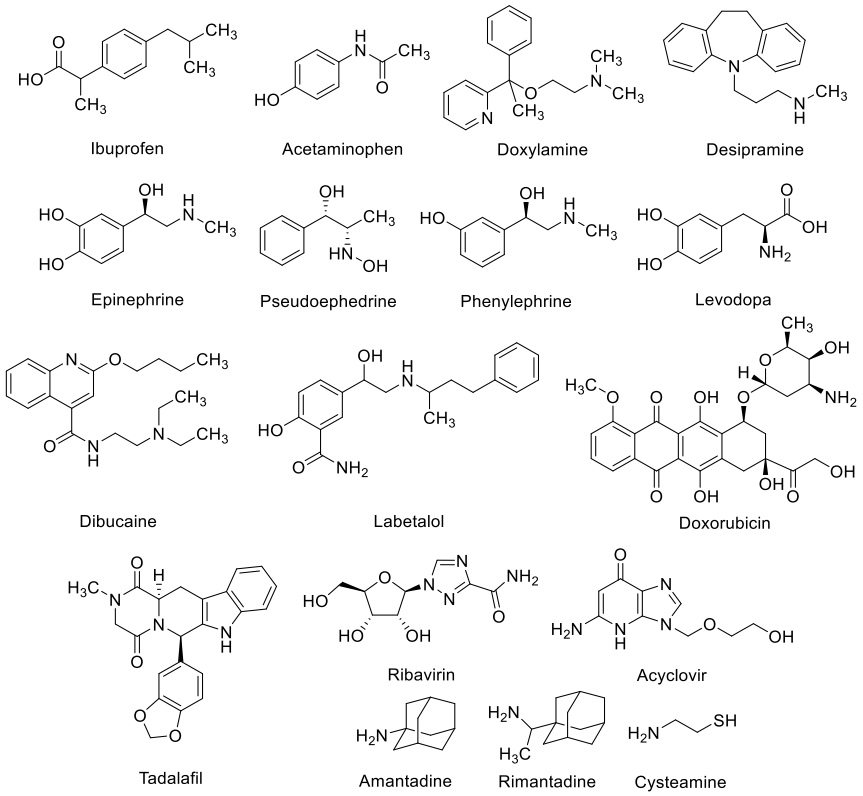

Figure 24. Pharmaceutically active compounds that have been detected with luminescent sensors[852-875]

4.6. Biologically Relevant. (Figures 25 and 26)

4.6.1. Adenosine Triphosphate (ATP) (Figure 25) is the main source of energy for intracellular processes,[876] due to the high energy stored in its terminal phosphate group, which is released upon the hydrolysis to form adenosine diphosphate (ADP).[877] Large concentrations of ATP in living systems indicate areas of robust intracellular activities;[878] conversely, depleted ATP concentrations are associated with less active systems.[879] As such, the detection and quantification of ATP in living systems provides an important benchmark of the system's overall health, and indicate areas of the system that are of particular biological

concern.[880] Methods to detect ATP rely on interactions of the triphosphate groups[881] and/or of the adenine base with the sensor.[882] Selectivity for ATP vs. ADP can often be achieved via straightforward tuning of the sensor structure, and is particularly important to distinguish a source of energy (ATP) from the structure after the energy has been released (ADP).[883] Electrochemical,[884] mass spectral,[885] and photophysical[886] (including luminescent)[887] methods for ATP detection have been reported. The detection of guanosine triphosphate (GTP), an important building block in RNA synthesis[888] and a source of intracellular energy for specialized metabolic processes,[889] has also been reported.[890]

4.6.2. Nicotine Adenine Dinucleotide, or NADH, (Figure 25) is a ubiquitous molecule which is involved in intracellular electron transfer processes[891] that are key components of cellular metabolism.[892] The presence of NADH or its reduced form, NAD^+, can be used to indicate relevant phenomena including alcohol intoxication,[893] liver disease,[894] and ketamine toxicity.[895] Many detection methods for NADH rely on the interaction of the analyte with NADH-dependent enzymes,[896] and use detection of that enzymatic activity (via Raman spectroscopy,[897] electrochemical sensors,[898] or fluorescent sensing)[899] as an indicator of the presence of NADH.

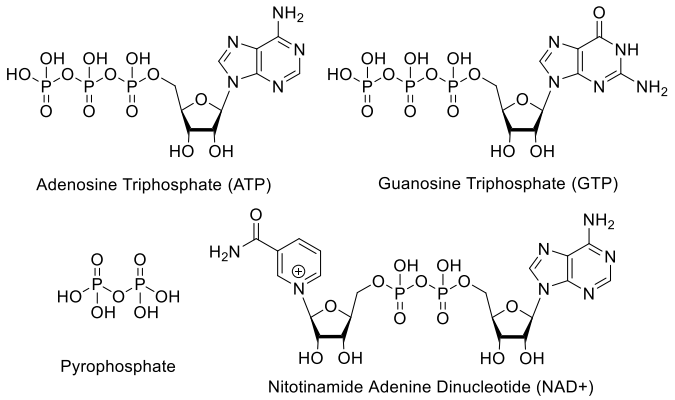

Figure 25. Examples of biologically relevant analytes for detection with luminescent chemosensors[876-899]

4.6.3. Amino Acids are ubiquitous and indispensable[900] in living systems as the building blocks of enzymes and other proteins,[901] and many amino acids and amino acid-derived molecules are also signaling molecules for biochemical processes.[902] For example, dopamine and serotonin, two amino acid-derived molecules, are key neurotransmitters,[903] and their aberrant expression has been implicated in a variety of neurological diseases,[904] including Parkinson's[905] and Alzheimer's disease.[906] Homocysteine, a non-naturally occurring amino acid, is involved in vascular regulation[907] with aberrantly high levels of homocysteine, termed hyperhomocysteinaemia, indicating vascular disease.[908] Among the 20 naturally occurring amino acids, leucine is a signaling molecule for muscle contraction and movement.[909] Sulfur-containing amino acids, such as cysteine and homocysteine, also play key roles in antioxidant processes and in the detoxification of heavy metals.[910]

Methods for the detection of amino acids vary widely depending on the identity of the amino acid, with aromatic amino acids detectable via UV-visible[911] or fluorescence spectroscopy.[912] Other amino acids generally lack clear spectroscopic signatures but can be detected via non-covalent interactions with a chemosensor. For example, fluorescent chemosensors bind with and detect a broad variety of amino acids,[913] Raman-active metal nanoparticles bind and detect amino acids via changes in the Raman spectral signals,[914] and electrochemical sensors detect the presence of amino acids via changes in their electrochemical signals.[915]

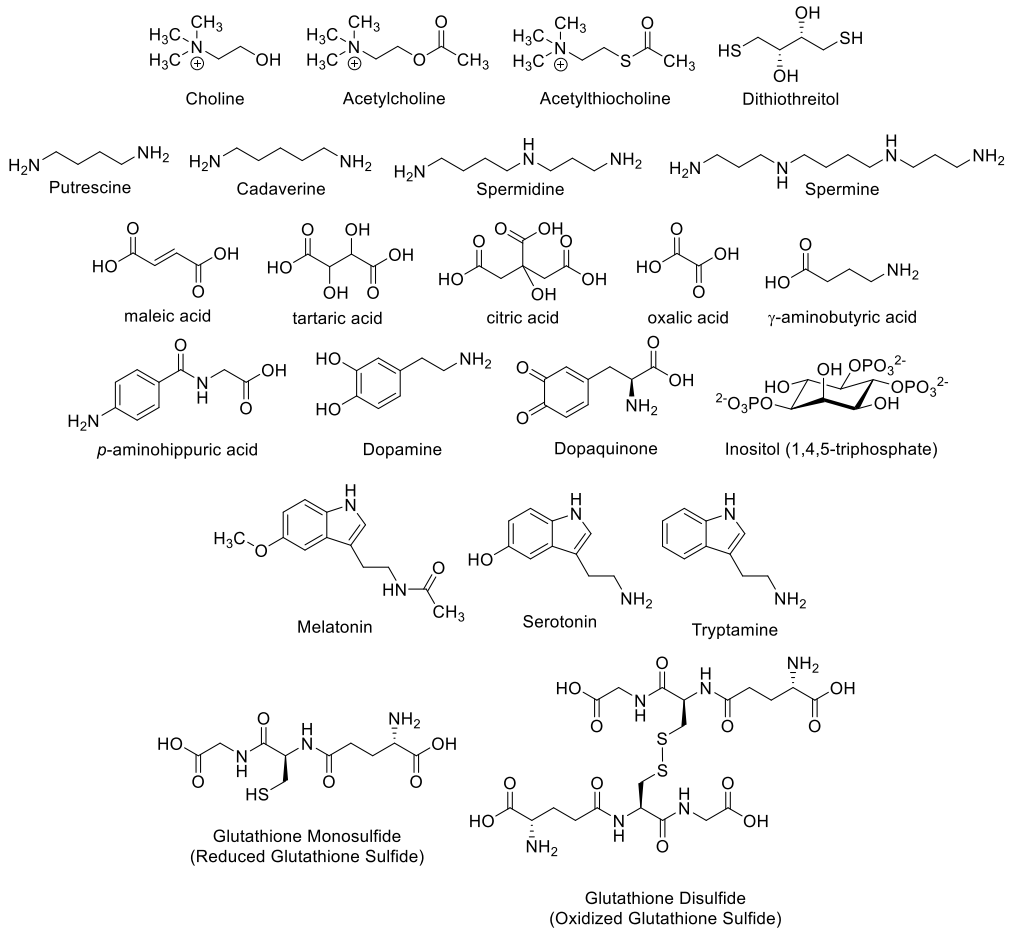

Figure 26. Examples of biologically relevant analytes for detection by luminescent chemosensors[900-915]

4.7. Other Detection Targets

4.7.1. Chirality sensing and the determination of chiral purity are extremely important in a number of applications, including pharmaceutical development. Often, one enantiomer of a compound is therapeutically active, while the other enantiomer is inactive or can lead to deleterious health outcomes.[916,917] Traditional methods for determining enantiomeric excesses of molecules include high performance liquid chromatography (HPLC),[918] mass spectrometry,[919] optical rotation measurements,[920] and circular dichroism spectroscopy.[919] While these methods provide highly accurate information, they are generally time-consuming and require expensive instrumentation and/or highly trained instrument operators. The use of optical probes for chirality instead of, or in complement to, these more traditional methods can provide markedly faster read-out results with less expense required.

4.7.2. Gases can be sensed directly in the air,[921] albeit with difficulty due to their low concentrations and rapid movement of all system components. More commonly, volatile analytes are detected by bubbling an analyte-containing gaseous mixture through a solution containing the sensor.[922,923] Differentiating certain gases, especially hydrocarbon gases, to achieve selective sensing is inherently difficult due to structural similarities and lack of functional groups.[925] Hydrocarbon gases are important detection targets because they are prevalent in the atmosphere due to the production and treatment of fossil fuels,[924] and are potentially harmful to human health.[925] Additionally, methane is one of the major greenhouse gases that contribute to global warming.[926] Ethylene is also an important detection target due to its relevance in fruit ripening and food spoilage, and in the agricultural industry.[927,928]

Other important gaseous detection targets include oxygen and hydrogen sulfide. Oxygen detection is critical in medical environments, due to the dangers of hypoxemia, defined as low oxygen in blood, and hypoxia, defined as low oxygen in tissues, and the diagnoses associated with such conditions;[929-931] in industrial settings in food packaging;[932,933] and in research laboratories where asphyxiants and compressed or cryogenic gases are commonly used.[934] Oxygen detection is complicated by the fact that oxygen itself has limited spectroscopic signals, and therefore oxygen sensors often rely on detecting oxygen-induced reaction products.[935] Multiple instances of oxygen detection using supramolecular chemosensors have been reported, including the use of a terbium-based macrocyclic host[921] and several fluorescent conjugated polymers.[936,937] Hydrogen sulfide is a poison,[938] an olfactory irritant,[923] and a serious atmospheric pollutant that is produced as an industrial byproduct.[939] It is also a natural gas and crude oil contaminant that, in concentrations greater than 2%, can lead to a faster combustion of these fuel sources.[938] Fluorescent macrocycle,[940,941] polymer,[942] and nanocluster[923] hosts have been used for H_2S detection in solution[923] and in vivo.[940,941]

4.7.3. VOCs. The detection of volatile organic compounds (VOCs) is of significant interest from a variety of perspectives. Some VOCs, such as formaldehyde,[943] are known to cause significant deleterious health effects.[944] Exposure to such VOCs can occur through a variety of routes, including through the use of commercial products,[945] through proximity to urban areas,[946] and through occupational exposure.[947] Other VOCs, including acetone,[948] aliphatic aldehydes,[949] and short chain aliphatic alkanes[950] have been found in human breath and can be used as a hallmark of a variety of diseases.[951,952,953] This research area of using human breath analysis for disease diagnostics has received significant attention in recent years,[954] with the exciting potential for the development of personalized medicine based on analysis of the human breath metabolome.[955]

Challenges in developing methods for the detection of VOC analytes include their volatility, which makes it difficult to isolate significant quantities for analysis; the fact that they often occur as mixtures of analytes, which complicates identification of any one analyte in the mixture;[956] and the general dearth of functional groups that provide clear spectroscopic signatures, especially for aliphatic alkanes and organic solvents. Nonetheless, a variety of detection methods have been reported in the chemical literature,[957,958] with the vast majority using gas chromatography-mass spectrometry (GC-MS) to accomplish such detection.[959,960,961] The use of luminescent sensors,[962] including supramolecular luminescent sensors,[963,964,965] has been reported as well.

4.7.4. Whole Cells[966] and bacterial organisms[967] as target analytes for detection have unique associated challenges that are not found in the detection of small molecules, anions, or cations. Of note, detection of cells and bacteria generally relies on strategies to detect the cell membrane and/or cell wall,[968] and in particular to detect the presence of compounds or other structural features[969] displayed on or near the cell surface. Challenges in such surface detection arise from the heterogeneity of the cell surface,[970971] which means that an effective sensor must bind its target among a variety of other unrelated targets, or, alternatively, the sensor must be designed so as to interact favorably with the heterogeneity itself. The latter strategy, while more challenging to design and execute, can lead to markedly improved targeting efficacy due to the potential for positive cooperativity.[972] Even within one cellular sub-type, different cells often display slightly different exterior surfaces;[973,974] a sensor with flexibility to recognize this degree of variability is therefore sorely needed.

Moreover, the detection of cells and bacteria almost always occurs in biological environments and therefore requires compatibility of the sensor with the biological matrix, which includes aqueous solubility and stability, temperature stability at physiologically relevant temperatures, and efficacy in the presence of high total ion concentrations.[975] Biological matrices also contain large numbers of potentially interfering analytes, often present in concentrations noticeably higher than the concentration of the target analyte.[976] Thus, effective sensors for whole cells and bacteria must be able to find their target analyte even in the presence of these interfering components, and to transduce that binding into a detectable change in signal to enable effective detection.

Luminescent sensors for whole cell detection have been reported by a number of research groups, including the groups of Bunz[977] and Rotello,[978] in which statistical analyses of the interactions of conjugated polymer sensors with the cell surface membranes enabled selectivity in distinguishing cancer cells from non-cancer cells, and in differentiating cancer cells based on their metastatic potential.[979] Of note, other, non-luminescent methods for cellular and bacteria detection have been reported as well, including electrochemical,[980] Raman-based,[981] and mechanochemical[982] methods.

5. Luminescent Macrocycle Sensors

In general, many classes of macrocycles are particularly amenable to binding small molecule organic compounds, which can associate with the macrocycle host via a variety of non-covalent interactions. These non-covalent host-guest interactions are particularly strong in cases where the macrocycle is rigid, such as for cucurbiturils (vide infra),[130] but also operate with reasonable strength and concomitant binding affinities in more flexible macrocycles such as cyclodextrin.[983] Compared to other luminescent supramolecular sensors, macrocycles offer the ability to accomplish binding and detection that is highly tailored for the particular analyte of interest. The oftentimes straightforward nature of synthetic modifications for the macrocycle provides an additional advantage to further tailor the system components in order to achieve optimal sensor performance. [984,985]

In contrast to many other macrocycle hosts that bind small molecule organic analytes with high affinities, crown ethers and crown ether-derived macrocycle hosts are particularly well suited for the binding of metal cations.[986] Such binding and concomitant detection relies on strong interactions between the cation and the chelating heteroatoms, including oxygen, nitrogen, and sulfur (vide infra).[987]

5.1. Cavitands

Cavitands are cyclic molecules with enforced nanometer-sized cavities large enough to bind small molecule guests.[988,989] In general, these molecules are basket- or container-shaped, either comprised of a wide upper rim and a narrower lower rim, like cyclodextrins and calixarenes; or with a symmetrical inner cavity, like cucurbiturils and pillararenes. Rational design of cavitand supramolecular hosts allows for sophisticated control over intermolecular host-guest interactions and enables selective small molecule recognition.[990] The relative rigidity of these structures compared to acyclic molecules promotes highly selective guest binding, although different classes of cavitands have widely disparate rigidities, binding strengths, and binding selectivities.[988] A variety of macrocycle classes are discussed below.

5.1.1. Cyclodextrins. Cyclodextrins are cyclic oligoamyloses[991,992] composed of glucose monomers, that adopt toroidal three-dimensional structures,[993,994] with a narrow upper rim and a wider lower rim. A broad variety of cyclodextrin isomers occur naturally in corn and other starch sources,[995] with the most common structural isomers being α-cyclodextrin,[996] β-cyclodextrin,[997] and γ-cyclodextrin,[998] with six, seven, and eight glucose moieties, respectively (Figure 27). The internal cavities of the cyclodextrins have hydrophobic character,[999] whereas the hydroxyl moieties on the exterior of the cavity confer relative hydrophilicity and reasonable aqueous solubilities.[1000] Interestingly, the solubility of β-cyclodextrin is markedly lower than that of the other two commonly occurring isomers, due the fact that strong intramolecular hydrogen bonds in the β-cyclodextrin create a relatively rigid structure that is poorly solvated.[1001,1002]

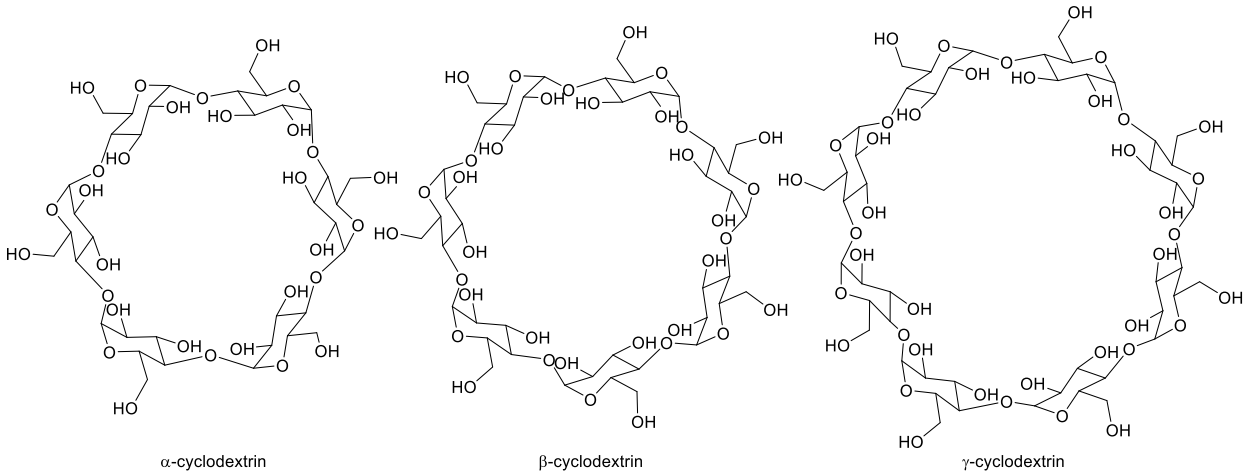

Figure 27. The α-,[996] β-,[997] and γ-[998] isomers of cyclodextrin

Compared to other macrocycle hosts (such as cucurbiturils[1003,1004] and synthetic cavitands[1005]), cyclodextrins have relatively flexible structures.[1006] This flexibility can complicate spectral analysis of their molecular structures and host-guest complexation behaviors, with many of the key structural components undergoing rapid motion on the experimental time scale.[1007,1008] Attempts to obtain X-ray crystal structures of cyclodextrin complexes suffer from similar challenges, with the high flexibility of the molecule leading to relatively poor structural resolution.[1009] Finally, computational work involving cyclodextrin host-guest complexes is also complicated by having to account for cyclodextrin structural flexibility, although more recent efforts in the development of novel computational methods have demonstrated promising success.[1010]

Covalently attached cyclodextrin-fluorophore conjugates can obviate many of the challenges associated with non-covalent complexes,[1011] mostly around the ambiguity of complexation structure and the distances between the fluorophore and analyte. Moreover, in non-covalent cyclodextrin-fluorophore-analyte systems, the analyte requires stronger binding affinities than the fluorophore in order to bind in cyclodextrin and displace the fluorophore, which can be a challenging condition to meet.[1037] Covalent cyclodextrin-fluorophore constructs, by contrast, contain a fluorescent transducer moiety at a relatively well-defined location relative to the cyclodextrin cavity, with the flexibility of the linker between the cyclodextrin and the fluorophore affecting the fluorophore mobility.[1012] Such covalently-linked architectures have been made with both β-cyclodextrin[1013] and γ-cyclodextrins,[1014] with single fluorophores and multiple fluorescent moieties covalently attached to the cyclodextrin hosts, and with both monomeric cyclodextrin hosts as well as higher order cyclodextrin architectures (dimers,[1015] trimers,[1016] and polymers).[1017] Cyclodextrins can be modified via a broad variety of chemical reactions,[1018] and many of the synthetic derivatives are commercially available, including randomly methylated β-cyclodextrin, with an average of 1.8 methyl groups per monomer unit, permethylated β-cyclodextrin, and 2-hydroxypropyl-β-cyclodextrin.[1019] Selective synthetic modification to access non-commercially available derivatives often begins with full protection of all the hydroxyl groups,[1020] followed by selective deprotection[1021] and further reaction at the target sites of interest.[1022] Other protecting group strategies are also available.[1023,1024] Using these methods, selective mono-functionalized,[1025] di-functionalized,[1026-1028] tri-functionalized,[1029] and tetra-functionalized cyclodextrins[1030,1031] have been synthesized. Synthetic modifications to the cyclodextrin structure have the ability to dramatically change the sterics,[1032] hydrophobicity,[1033] and charge density[1034] of the cyclodextrins, and have enabled the installation of covalently-linked aromatic moieties.[1035] Of interest for purposes of this review, photophysically active (usually fluorescent) transducer moieties [1036,1037] have been attached to cyclodextrin via covalent modification.[1038,1039] The functionalization of the larger secondary face[1040-1042] of cyclodextrins, so named because it contains secondary hydroxyl groups, is more challenging than the functionalization of the narrow primary face,[1043,1044] which contains more reactive, more sterically accessible primary alcohols. Thus, secondary face modifications typically begin with the protection of the

primary face. Several advances[1045] in secondary face modification strategies have been reported, including total functionalization by epoxidation[1041] or copper catalysis,[1042] and selective modification of the secondary face by mechanochemical means.[1046]

Cyclodextrins are well-known for their ability to bind a variety of non-polar small molecule guests in their hydrophobic interiors.[1047-1049] In the absence of any guest molecules, the cavity of cyclodextrin is filled with high-energy water molecules,[1050] so named because their inability to form a full complement of hydrogen bonding results in water molecules that are of higher energy compared to the bulk solvent.[1051] This water is typically displaced by a small molecule guest upon binding, which results in a thermodynamically favored process as the water returns to the lower energy bulk solvent state. Such cyclodextrin host-guest binding has been used for a broad variety of applications, including in the solubilization of pharmaceutically active agents for effective drug delivery,[1052-1054] in the environmental remediation of toxic chemicals,[1055,1056] fuel,[1057] and oil[1058,1059] through binding the toxicants in the cyclodextrin, in odor neutralization[1060,1061] in functionalized filters[1062] and membranes,[1063] and in chiral chromatography.[1064]

Cyclodextrin host-guest complexes have been used as fluorescent chemosensors, and these chemosensors can be divided into two categories: (a) covalently modified cyclodextrins, with covalently tethered fluorescent moieties that respond to binding of the analyte with a change in the fluorescence signal;[1065] and (b) cyclodextrin association complexes, with non-covalently attached fluorophores that respond to the presence of the analyte with non-covalent, analyte-specific interactions.

5.1.2. Modified Cyclodextrins.[1066] Major challenges in the covalent modification of cyclodextrin focus on the synthesis and purification of these complex supramolecular architectures, with singly functionalized cyclodextrin moieties generally accessible via global protection of the hydroxyl moieties,[1067] followed by selective deprotection to reveal a single site for functionalization.[1021] Doubly functionalized cyclodextrins can also be realized by judicious choice of deprotection agent; using diisobutyl aluminum hydride (DIBAL), for example, results in a di-deprotected β-cyclodextrin analogue with the sites of deprotection on opposite sides of the cyclodextrin host.[1068-1071] Other di-deprotected isomers have also been reported.[1072] Selective functionalization of a cyclodextrin host with more than two fluorophore appendages requires complex syntheses as well as often tedious purification procedures.[1] Of note, particular challenges of cyclodextrin purification result from their large size, highly polar functionalities, and plethora of hydroxyl groups that can complicate chromatographic purification.[1073-1075]

Efforts in the Levine group have enabled the synthesis of monomeric β-cyclodextrin moieties with covalently attached fluorophores, either with one (compound **1**) or two (compound **2**) appended fluorophore units (Figure 28).[1] Compared to the non-covalent cyclodextrin-fluorophore system, the covalently linked architectures had significantly improved selectivity in response to a broad range of isomeric and analogous hydrophobic toxicants, including aliphatic alcohols, DDT and related analogues, and PCB congeners, with 100% differentiation via array-based analysis observed. Micromolar detection limits were found for the majority of analytes, and the discrimination of 1:1 binary mixtures of aromatic alcohols was achieved. This improved selectivity was evident in the significant changes in fluorophore emission that occurred upon analyte introduction for the covalently linked adducts, which were markedly higher than the changes observed for the non-covalent adducts.

Further efforts by the same group led to the synthesis of covalently linked cyclodextrin dimers, where the fluorophore moieties were incorporated as part of the linker backbone.[488] These photophysically active cyclodextrin dimers (Figure 28), bearing pyridine,[1076] **3**, naphthalene,[1077] **4**, or anthracene,[1078] **5**, linkers, formed inclusion complexes with squaraine fluorophores, resulting in notable fluorescence changes. Displacement of the squaraine following analyte introduction resulted in significant changes in fluorescence emission as well as notable color changes, observed through naked eye detection, UV-visible spectroscopy, and quantitative RGB (red-green-blue) analyses.[1079]

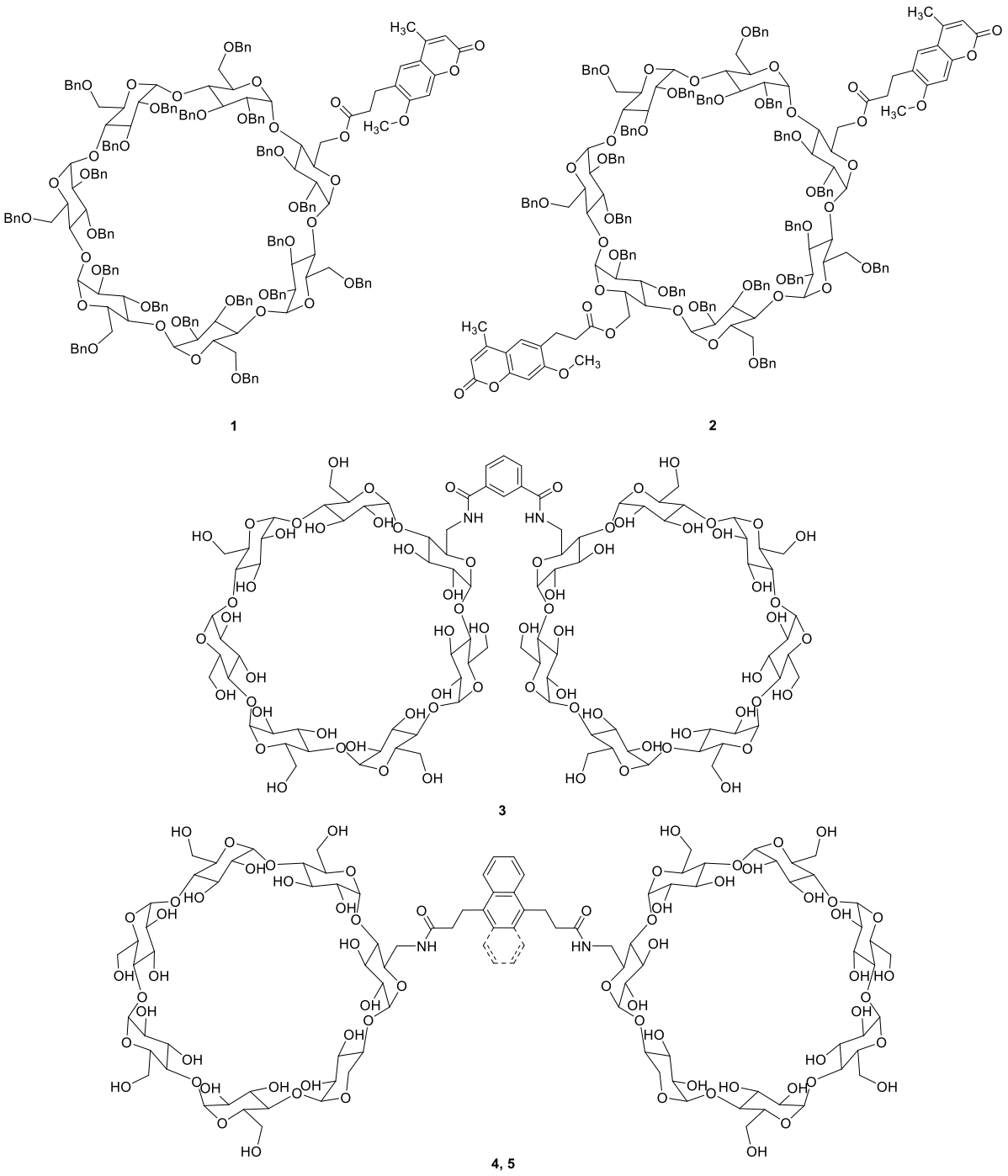

Figure 28. Cyclodextrin hosts modified to bear fluorescent appendages, **1** and **2**,[1] or fluorescent linkers, **3**, **4**, and **5**[488]

Another noteworthy application of covalently-linked cyclodextrin constructs is in the detection of biologically relevant analytes. Yang et al. functionalized an adenosine aptamer fragment with β-cyclodextrin and the complementary aptamer fragment with a dansyl fluorophore, which is known to form a strong inclusion complex with β-cyclodextrin (Figure 29).[1080] The presence of adenosine, the essential nucleoside for energy production in cells, brings the two nucleic acid fragments, and thus the dansyl and cyclodextrin fragments, into close proximity, leading to the association of the dansyl and β-cyclodextrin

functionalities and a subsequent increase in dansyl fluorescence emission. The estimated detection limit for adenosine using this system was calculated to be 1 μM. The authors surmised that changing the aptamer could enable detection of a variety of additional analytes.

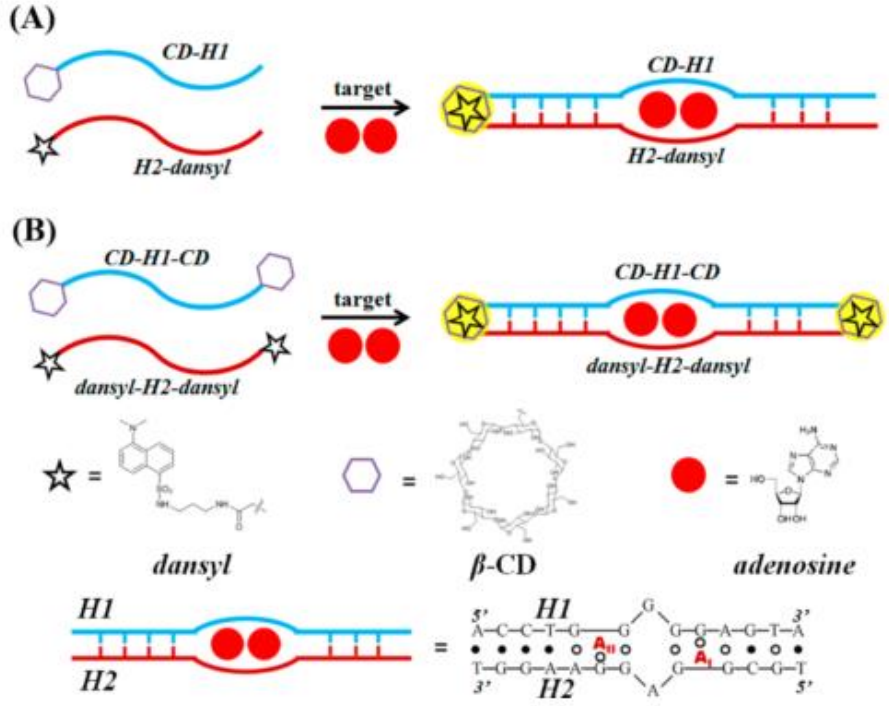

Figure 29. Representation of the ability of dansyl- and β-cyclodextrin appended aptamer fragments to encapsulate adenosine and lead to a fluorescence response using A) mono-functionalized and B) di-functionalized adenosine aptamer fragments. Reproduced from Ref. 1080. Copyright 2015 American Chemical Society.

The modification of β-cyclodextrin to include negatively charged pendant arms led to the selective detection of cationic amino acids by Pettiwala et al. (Figure 30).[1034] An association complex of Thioflavin-T and the polyanionic cyclodextrin allowed for the ratiometric sensing of lysine and arginine, with detection limits of 40 μM and 50 μM, respectively. It was hypothesized that the cationic ends of the amino acids associated with the anionic side chains of the macrocycle, allowing for the inclusion of the neutral segment of the analyte in the cyclodextrin cavity. In addition to detecting lysine and arginine in purified buffer solution, this detection system also operated efficiently in fetal bovine serum.

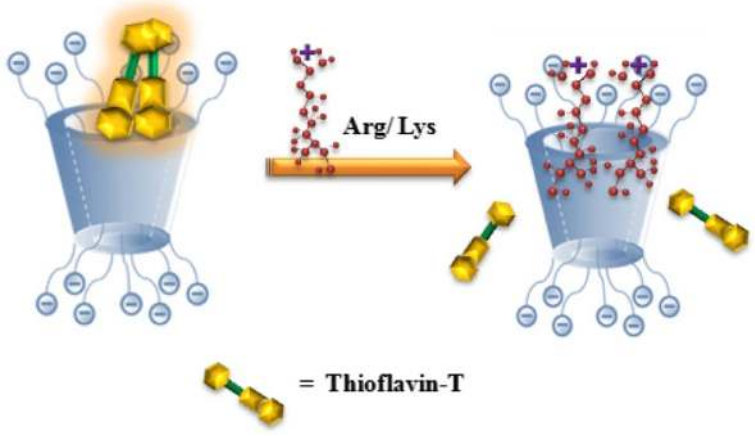

Figure 30. Representation of the use of a β-cyclodextrin modified with cationic pendant arms for the encapsulation and detection of arginine and lysine by indicator displacement. Reproduced from Ref. 1034. Copyright 2017 American Chemical Society.

Click chemistry has been used to synthesize several fluorophore-modified cyclodextrins, including tetraphenylethylene-functionalized **6**,[1081] pyrene-functionalized **7** and **8**,[1082] and cyclodextrin dimer **9** (Figure 31).[1083] Compound **6** was used for the selective detection of cadmium by Zhang et al., where the addition of Cd^{2+} led to the formation of **6** aggregates through cadmium-induced π-π stacking of the terphenylene moieties, resulting in fluorescence enhancements.[1081] The system demonstrated a low detection limit for Cd^{2+} (0.01 μM), and high levels of selectivity, with only Ag^{+} impeding effective cadmium detection. He et al. used modified macrocycles **7** and **8** in combination with fluorophores **10** and **11** for the detection of lectins, proteins found in legumes and grains that display strong binding to sugars. Such lectins include soybean agglutinin (SGA) and wheat germ agglutinin (WGA), both of which can be detected with nanomolar detection limits.[1082] The **8** host and **10** fluorophore combination led to the lowest detection limit, 260 nM, of SGA via fluorescence enhancement. Similar lectins, including WGA, concanavalin A, lentil lectin, and pea lectin had no effect on the SGA-induced fluorescence increases. Similarly, a combination of **7** and **11** could detect WGA at concentrations as low as 735 nM without interference from the aforementioned species. An array of cyclodextrin dimers, including **9**, was used by Martos-Maldonado et al. for the detection of bile salts, namely sodium chlorate and sodium deoxycholate, through salt-induced fluorescence increases of the dimer in aqueous media.[1083]

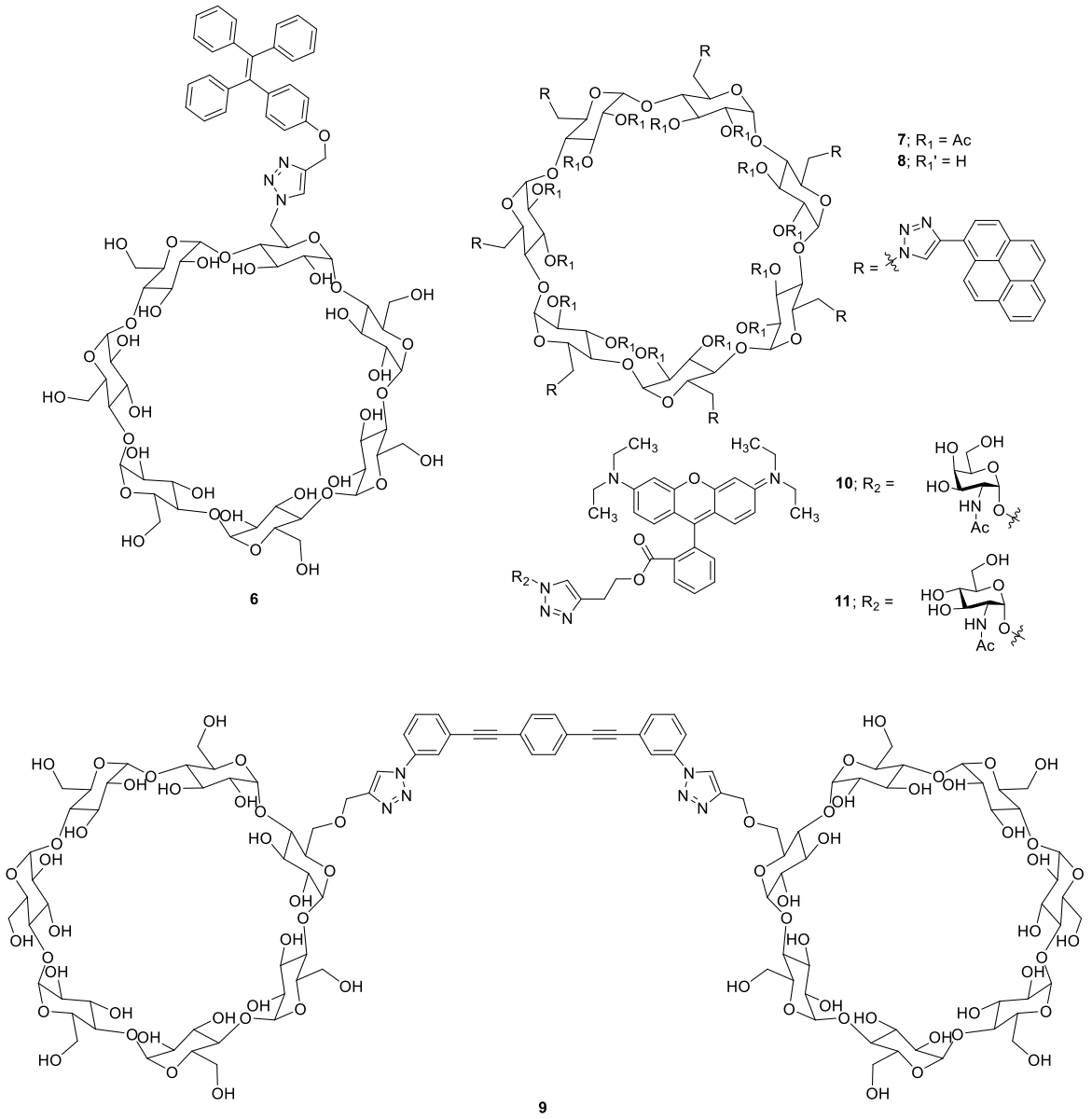

Figure 31. A series of modified cyclodextrins, **6**,[1081] **7**,[1082] **8**,[1082] and **9**,[1083] that were synthesized using click chemistry, and two novel fluorophores, **10** and **11**,[1082] with glucose-like appendages

Another example of a cyclodextrin modified with a signaling unit was reported by Feng et al.[1084] In this case, fluorescein-bound **12** (Figure 32), was used for the sensitive detection of TNT, a nitroaromatic explosive, in aqueous media (20 nM detection limit). The inclusion of TNT in the cyclodextrin cavity decreased the fluorescence of the system through TNT-induced fluorescence quenching with a Stern-Volmer constant of 3.79 x 10^5 M^{-1}. In one final example, a series of cyclodextrin-based ruthenium complexes were synthesized by Zhang et al. and were used for highly selective detection of lysozyme, an antimicrobial enzyme, through the binding of a lysozyme aptamer to the metallacyclodextrin host (Figure 33).[1085] The higher order cyclodextrin-ruthenium complex, containing six cyclodextrin moieties, enabled a limit of detection (48 pM) several orders of magnitude lower than its three-cyclodextrin and one-cyclodextrin analogues (27 nM and 239 nM, respectively).

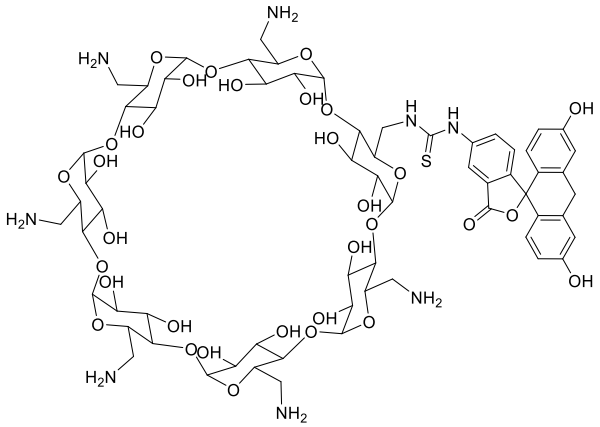

12

Figure 32. Fluorescein modified **12** used for the detection of TNT[1084]

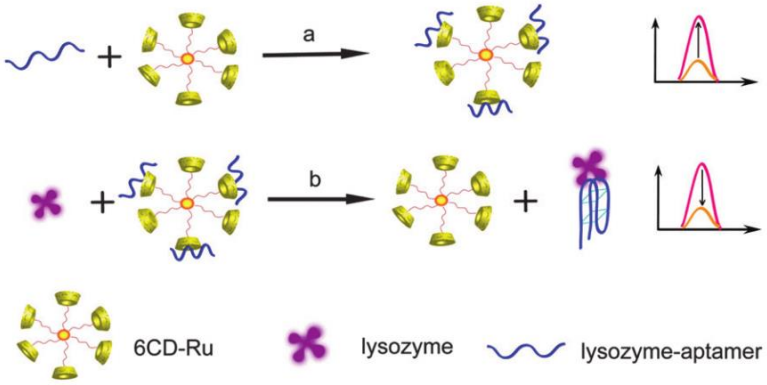

Figure 33. Ruthenium metallacyclodextrin complexes used by Zhang et al. for the detection of lysozyme through the favorable binding of the complex to the lysozyme aptamer. Reproduced with permission from Ref. 1085. Copyright 2015 Royal Society of Chemistry.

5.1.3. Ternary Cyclodextrin Association Complexes. Non-covalent cyclodextrin-fluorophore association complexes rely on the binding of a fluorophore in or around the cyclodextrin cavity. The introduction of an analyte to the system then causes either the displacement of the fluorophore from the cavity, co-binding of the fluorophore and analyte in the cavity to create a ternary (i.e. three-component complex),[1086] or another permutation of the environment around the fluorophore[1087] that results in a measurable change in the fluorophore emission signal, either in its intensity, position, or signal spectral shape.[1088]

Challenges around the use of non-covalent cyclodextrin-fluorophore complexes include ambiguity about the geometry of the guest(s) in the cavity. Moreover, ternary complexes are common only for γ-cyclodextrin (and larger) isomers, which have cavity sizes that can readily accommodate two small molecule guests simultaneously.[1089-1091] The use of the more common β-cyclodextrin generally utilizes analyte-induced displacement of the fluorophore from the cavity. This competitive displacement requires the analyte to have a stronger affinity for the hydrophobic cyclodextrin cavity than the fluorophore, which is only true in some cases. Isolated cases of ternary complexation inside a β-cyclodextrin cavity have been reported, although generally only for small analytes.[1092,1093]

The Levine group has developed non-covalent cyclodextrin sensors based on ternary complexation between γ-cyclodextrin, a high quantum yield fluorophore, and a target analyte, with binding of the photophysically active analyte resulting in highly efficient, cyclodextrin-promoted analyte-to-fluorophore

energy transfer.[465] The resulting fluorophore emission via analyte excitation was used as a highly sensitive and selective signal for analyte detection. Even in cases where the analyte was not photophysically active, binding of the analyte in the cyclodextrin cavity resulted in proximity-induced, analyte-specific changes in the fluorophore emission signal that were used for sensitive and selective detection.[812,811]

In particular, γ-cyclodextrin was used by the Levine group to promote energy transfer from five common polycyclic aromatic hydrocarbons (PAHs) to near-infrared emitting squaraine dyes, as illustrated in Figure 34, with a detection limit of 1.1 μM for the anthracene analyte.[795] Fluorescent dyes Rhodamine 6G and BODIPY were also found to act as efficient energy acceptors in combination with PAHs and polychlorinated biphenyl (PCB) energy donors, with ppm detection levels observed.[465] The system was successfully employed for the sequential cyclodextrin-promoted extraction and detection of PAHs from a variety of oils, including motor oil, pump oil, and vegetable oil, as well as from oil-contaminated seawater samples.[1059] Additionally, BODIPY and Rhodamine 6G acted as efficient energy acceptors, inducing analyte-specific fluorescence responses, in a broad variety of complex media, including coconut water,[1094] complex oils,[1095,1096] samples from environmental contamination scenarios,[1057] samples collected from oil spill sites,[1097] human plasma,[1094] human urine,[786] and human breast milk,[787] all with mid- to low- micromolar detection limits. These techniques rely on unique fluorescence modulation by each analyte and the use of multiple analyte-fluorophore combinations for the creation of array-based detection schemes. Notably, this array-based detection was used for the 96% accurate discrimination of 30 organic pollutants in purified buffer solution and 92% accurate discrimination in human urine.[122]

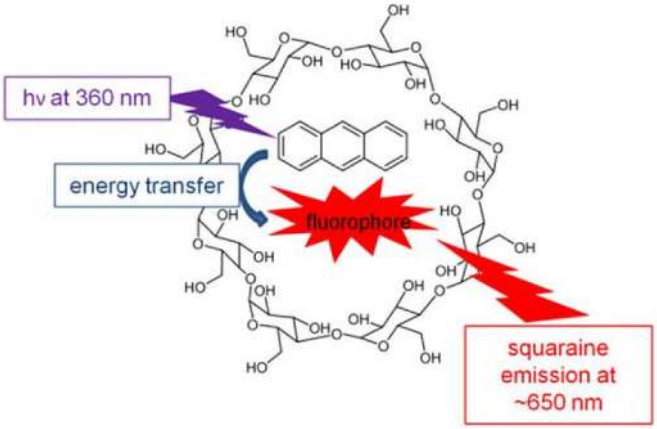

Figure 34. Illustration of a ternary complex in which energy transfer between the electron-rich analyte and electron-deficient fluorophore is promoted by cyclodextrin encapsulation. Reproduced with permission from Ref. 795. Copyright 2012 Taylor & Francis.

In addition to PAH detection using cyclodextrin-based ternary complexes, the Levine group also demonstrated the detection of pesticides and alcohols via analogous methods. The array-based detection of aromatic pesticides using BODIPY as an energy acceptor and a variety of cyclodextrins as supramolecular hosts allowed for the 100% successful discrimination of structurally analogous pesticide analytes.[804] Aliphatic analytes, including aliphatic pesticides and alcohols, could be detected using cyclodextrin-promoted fluorescence modulation, with high sensitivity and selectivity obtained.[812,811,121]

A ternary complex similar to that shown in Figure 29[1080] (vide supra) was reported by Jin et al., in which two fragments of an adenosine binding aptamer were functionalized with pyrene.[1098] As shown in Figure 35, in the presence of adenosine triphosphate (ATP), the aptamer fragments were brought in close proximity. This facilitated the formation of a pyrene excimer inside the γ-cyclodextrin cavity, leading to the observed excimer emission. In the absence of cyclodextrin, by contrast, only weak excimer fluorescence emission was observed. This ratiometric scheme detected ATP with an 0.08 μM detection limit. Of note,

structurally similar triphosphates did not produce analogous fluorescence changes, nor did they interfere with the detection of adenosine, and the system was effective in both Tris-HCl buffer and in human serum.

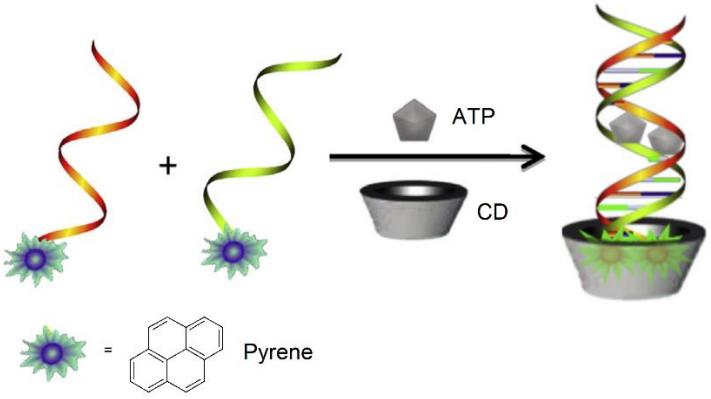

Figure 35. Pyrene appended to ATP aptamer fragments in conjunction with γ-cyclodextrin for the detection of ATP. Adapted with permission from Ref. 1098. Copyright 2013 Elsevier.

Murudkar et al. used the ultrafast molecular rotor Thioflavin-T (ThT), in combination with γ-cyclodextrin, for the fluorescence detection of surfactants containing long alkyl chains.[379] Binding of the surfactant alkyl chain in the cyclodextrin cavity led to the formation of a ternary complex and provided sufficient steric hindrance to ThT to prevent its non-emissive torsional motion, resulting in surfactant-induced fluorescence enhancement.

Ternary cyclodextrin complexes with metal cations have also been reported for cation sensor applications. In one example, 80% of the fluorescence emission of a 1,2-dihydroxyanthraquinone: β-cyclodextrin association complex was quenched upon addition of Co^{2+} to form a ternary complex in aqueous solution,[114] leading to a 22.7 nM detection limit. The ternary host-dye-cobalt system was then used to detect nitrate with a 2.4 nM detection limit, which the authors propose occurred via quaternary complex formation. Exogenous Co^{2+} and NO_3^- could also be detected following incubation of the host in HeLa cells. In a report by Khan et al., copper was detected with an association complex of β-cyclodextrin and novel coumarin derivative **13** (Figure 36).[1099] The addition of Cu^{2+} to the system resulted in formation of a ternary complex and quenching of the coumarin fluorophore. Of note, all other metal cations studied resulted in fluorescence emission increases, and the presence of these cations did not interfere with sensitive (ca. 25 nM) copper detection. Because the association complex was non-toxic to HeLa cells, in vivo Cu^{2+} detection was also obtained. Moreover, Jullian et al. reported that, in the absence of a supramolecular host, the emission of fluorophore **14** decreased only slightly in the presence of Cu^{2+}.[1100] Yet, when dimethyl-β-cyclodextrin was present, the fluorescence of **14** was decreased by both Cu^{2+} and Ni^{2+}, and the system could thus be used for the detection of both cations, with extremely low detection limits for nickel (65 ppb) obtained. Finally, Pd^{2+} was detected by Stalin and coworkers using an inclusion complex of β-cyclodextrin and **15**, with a detection limit of 1.0 μM obtained.[1101]

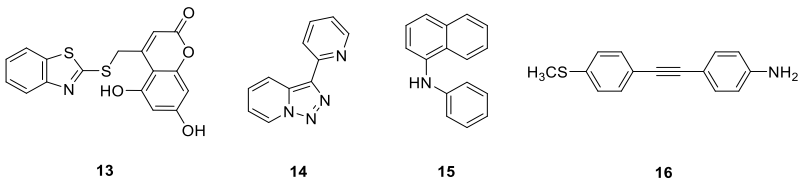

Figure 36. Various novel fluorophores used in ternary (compounds **13**,[1099] **14**,[1100] and **15**[1101]) and binary (compound **16**)[1102] cyclodextrin detection schemes

5.1.4. Binary Cyclodextrin Association Complexes. Binary cyclodextrin complexes have also been used as sensing platforms. For example, an indicator displacement assay was used for the detection of salicylaldehyde, a commonly used precursor in industrial processes, by Liu et al.[1102] The target analyte displaced **16** from the cavity of β-cyclodextrin, resulting in analyte-induced fluorescence quenching. A sensitive detection limit of 10 nM was reported, although selectivity for salicylaldehyde compared to other analytes was not discussed. Cyclodextrins have also been used for the detection of photophysically active analytes without the use of fluorescent dye transducers, such as in the detection of desipramine, an antidepressant,[1103] and *p*-aminohippuric acid, a kidney diagnostic agent.[1104] In the presence of β-cyclodextrin, Jalili et al. were able to detect 70 nM of desipramine,[1103] and Alremrithi et al. achieved the detection of *p*-aminohippuric acid at concentrations as low as 1 μM.[1104] Similarly, Abdel-Aziz et al. were able to detect nanomolar amounts of benzo[*a*]pyrene, a highly carcinogenic and photophysically active PAH, using both β-cyclodextrin and calix[8]arene as supramolecular hosts.[1105]

Additionally, Martínez-Tomé et al.[1106] and Ning et al.[1107] reported that 2-hydroxypropyl-β-cyclodextrin increased the fluorescence emission of napthotriazole and benzotriazole, respectively. Such systems were used for nitrite detection, in which the reaction of nitrite with 1,2-diaminonapthalene[1106] or 1,2-diaminobenzene[1107] formed the corresponding triazole that bound in the cyclodextrin, resulting in fluorescence increases only in the presence of the nitrite reactant. Detection limits of 13 nM and 2.0 nM were observed for naphthotriazole and benzotriazole, respectively. The derivatizing agents, 1,2-diaminonaphthalene and 1,2-diaminobenzene, were also found to react with Se^{4+}, leading to some erroneous results in the presence of this interferent.[1106] In a final example of binary complex formation for analyte detection, the encapsulation of fluorescent 2-hydroxy-1,4-napthoquinone in β-cyclodextrin increased the solubility and stability of the dye, and facilitated its use as a fluorescent pH sensor.[1108]

An interesting sensing application of cyclodextrins is in their employment as organic modifiers for capillary electrophoresis coupled with laser-induced fluorescence detection. The premise of this technique is that a mixture of analytes can be separated chromatographically by their differential complexation with cyclodextrin modifiers, and subsequently identified using fluorescence detection.[1109] Delaunay and coworkers have used cyclodextrin-modified capillary electrophoresis for the separation and identification of PAHs.[1109,1110] In this case, 19 PAHs could be separated and identified with ppb level detection limits in aqueous solution[1109] and in complex edible oils.[1109,1110] In another example, amino acids were derivatized with fluorescein isothiocyanate, **17** (Figure 37), and detected using cyclodextrin-modified capillary electrophoresis by Liang et al. with detection limits in the low pM levels.[1111] Derivatization with a different fluorescent modifier, naphthalene-2,3-dicarboxaldehyde, **18** (Figure 37), resulted in pM limits of detection,[1112] and in selectivity in separating of the D- and L- enantiomers of aspartic acid.

In a separate example, the enantiomeric purity of magnesium bis(L-hydrogenaspartate) dihydrate, a pharmaceutical agent, was determined through derivatization with *o*-phthaldialdehyde, **19** (Figure 37), followed by cyclodextrin-modified capillary electrophoresis.[1113] Trace levels of both L-aspartic acid and D-aspartic acid can contaminate this drug, although only the latter has deleterious effects on the human body. The authors were able to detect the presence of D-aspartic acid in levels as low as 0.003%, with full differentiation from its enantiomer observed. Liu et al. also detected amino acids using analogous methods and a rhodamine-based derivatizing agent.[1114] Stephen et al. reported the detection of the nucleosides adenosine and inosine with detection limits of 1.6 μM and 4.0 μM, respectively, using derivatization with 2,4,6-trinitrobenzene sulfonic acid **20** (Figure 37),[1115] in the complex media of frozen rat brain tissue. Moreover, inhibitory neurotransmitter γ-aminobutyric acid was derivatized with 4-chloro-7-nitro-2,1,3-benzoxadiazole **21** (Figure 37), by Shi et al. and detected by laser-induced fluorescence.[1116] Of note, capillary electrophoresis was used to separate the functionalized derivative from the heads of houseflies and moths, with low detection limits (16 nM) reported. In a final example of the use of cyclodextrin-modified capillary electrophoresis coupled with laser-induced fluorescence detection, berberine, an established herbal remedy, could be identified in solution with a 15.7 ppb detection limit.[1117]

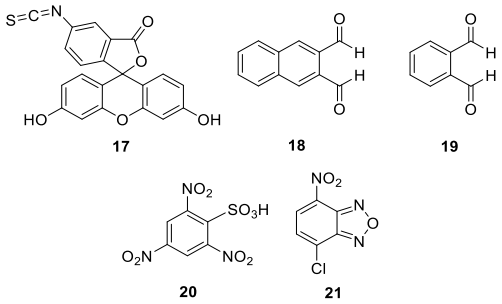

Figure 37. Derivatizing agents that have been used for the separation and identification of similar analytes by cyclodextrin-modified capillary electrophoresis coupled with laser-induced fluorescence detection[1111-1113,1115,1116]

5.1.5. Calix[*n*]arenes. Calixarenes[1118] are cyclic oligomers that are readily synthesized[1119] from the hydroxyalkylation reaction of a phenol and an aldehyde,[1120] resulting in the preferential formation of the thermodynamically favored, four benzene ring-containing product.[1121] These molecules adopt vase conformations, with a wide upper rim and narrow lower rim.[1122] Although unsubstituted calixarenes suffer from significant insolubility in organic solvents,[1123] the inclusion of *tert*-butyl substituents confer reasonable solubility.[1124] Alternatively, the addition of hydrophilic substituents can be used to lend enhanced water solubility to these species,[1125] and amphiphilic calixarenes have been used for drug delivery applications.[1126] Calixarenes are generally used in sensing applications as scaffolds on which transducing elements are appended.[1127-1129]

A common use of calixarenes as supramolecular hosts for fluorescence detection is as receptors for metal cations such as copper, zinc, mercury, and lead. Chawla and coworkers developed a series of calixarenes with fluorescent appendages derived from fluorescein,[1130] coumarin,[350] and hydroquinoline[1131] for the fluorescence detection of copper. Copper binding to photophysically active supramolecular sensors in general, and calixarene sensors in particular, can result in fluorescence enhancement, fluorescence quenching, and/or more complex changes to the fluorescence emission spectrum of the host, depending on the host structure and the mechanism of electronic interaction between the host and the copper analyte. The majority of calixarene-based copper sensors respond to the presence of copper with a noticeable quenching of the fluorescence emission.[11321133] This behavior is in line with other reports where the presence of copper induces fluorescence quenching, in both biological[1134] and non-biological systems,[1135] and is thought to be a result of energy transfer from the fluorescent energy donor to the non-fluorescent metal-ligand bonds,[1136] or charge-transfer type interactions.[1137] Less common copper-induced fluorescence enhancement, such as seen using host **23**,[350] can occur via copper-induced aggregation, in cases where such aggregates display aggregation-induced emission;[1138] copper-induced formation of a metal-to-ligand charge transfer band, for the right combination of copper salt and copper-chelating ligand;[1139] and copper-induced structural rigidification of an already existing fluorophore, resulting in potentially significant fluorescent enhancements.[1140] While other metal cations can display similar behaviors, the effects of copper on either fluorescence quenching or fluorescence enhancements are highly pronounced and can have potentially significant applications in biochemically-relevant sensing schemes.

Fluorescein-bearing species **22** (Figure 38) responded to the presence of Cu^{2+} with an increase in fluorescence emission, resulting in sensitive (10 nM) Cu^{2+} detection.[1130] Of note, this method was sensitive for copper ions in the presence of a variety of other potentially interfering species. The addition of copper to coumarin-appended **23** (Figure 38) was also characterized by an emission increase, as well as by a 90 nm bathochromic shift in the position of the emission maximum.[350] In a third report, **24** (Figure 38) was able to detect Cu^{2+} in tetrahydrofuran with a 0.5 μM detection limit.[1131] However, this system was not fully selective, as Ni^{2+}, Zn^{2+} and Mn^{2+} interfered with effective detection. Emission of pyrene-appended **25** (Figure 38), synthesized by Maher et al., was fully quenched upon the addition of Cu^{2+}perchlorate, leading to an 0.22 μM detection limit and a Stern-Volmer constant of 4.5×10^4 M^{-1}.[1141] In a final example, bis-

calix[4]arene tetra-triazole macrocycle **26** (Figure 38) formed a 1:3 host-guest complex with Cu^{2+}, resulting in 40 nM detection limits.[1142] Of note, slightly basic pH conditions were required to produce the optimal response, and the macrocycle could cross T-cell membranes without leading to cell death, indicating potential biocompatibility and future biological applications.

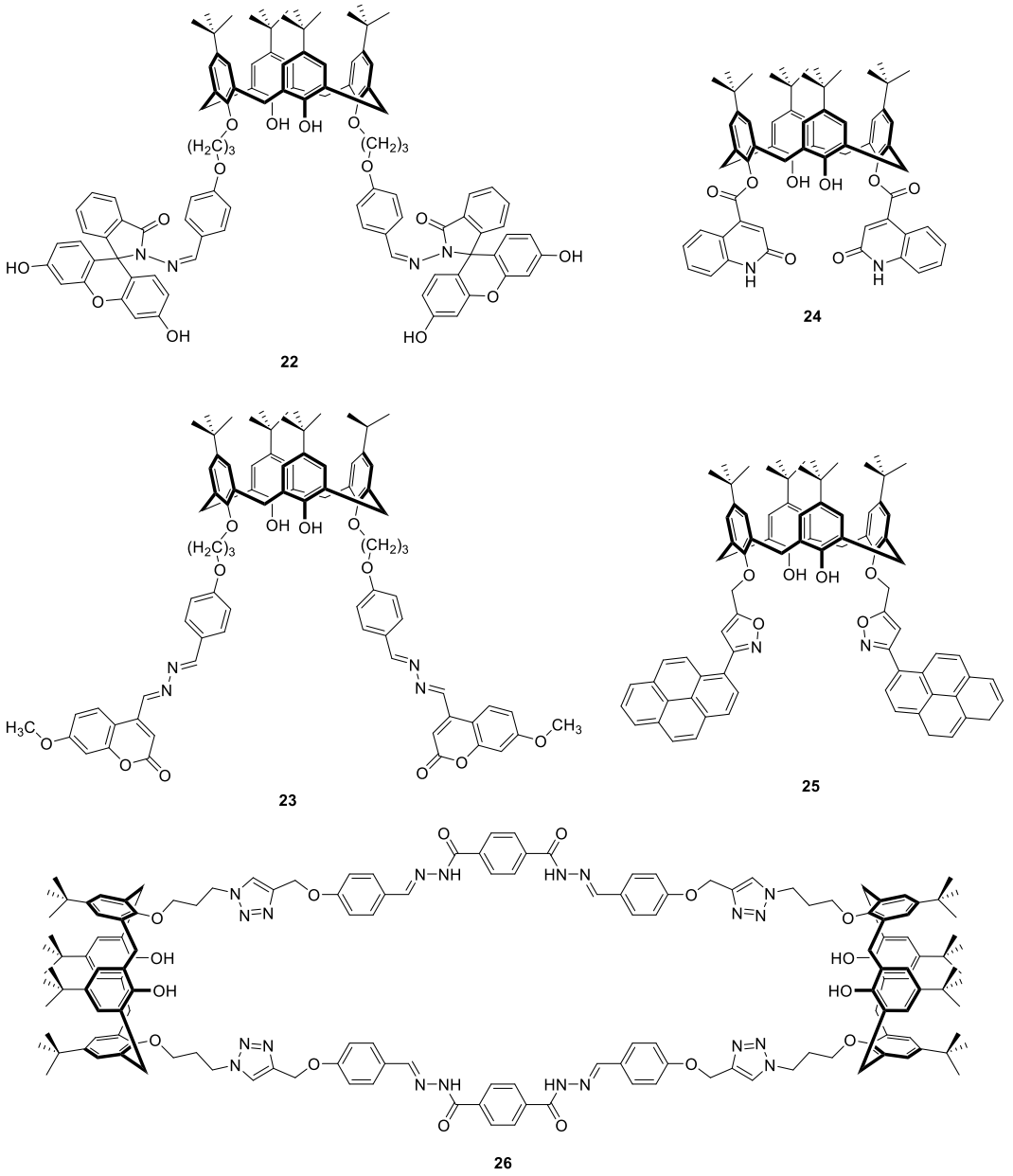

Figure 38. Calixarenes that have been employed for Cu^{2+} detection[350,1130,1131,1141,1142]

Rao and coworkers developed two fluorescence-based systems for the detection of copper with benzothiazole-appended calixarene **27**[1143] and benzimidazole-bearing **28**[1144] (Figure 39). An 8-fold decrease of the emission of **27** was observed in the presence of 10 equivalents of Cu^{2+}, and the quenching was not affected by the presence of up to 50 equivalents of other metal cations.[1143] A detection limit for copper of 403 ppm was achieved in acetonitrile. Compound **28** was found to produce a selective ratiometric response to Cu^{2+}, with no other cation leading to the formation of a new emission band.[1144] A 1:1 host-guest complex was the predominant species at lower concentrations of Cu^{2+}, and a 1:2 host-guest binding mode predominated at higher Cu^{2+} concentrations, with association constants of 7.24 x 10^9 M^{-1} and 1.80 x 10^{10}

M^{-1} for the first and second binding event, respectively. Competition experiments in methanol indicated that moderate fluorescence perturbations could occur in the presence of other metal cations, with the addition of Hg^{2+} leading to a full fluorescence quenching of both the excimer and monomer peaks. However, in HEPES-buffered water, mercury did not perturb the system fluorescence. Xie et al. developed calixarene **29**[1145] (Figure 39), which was semi-selective for the detection of copper, and Sahin and coworkers synthesized **30**[1146] and **31**[1147] (Figure 39), which exhibited good and moderate selectivities for copper, respectively. A final example of Cu^{2+} detection was published by Maity et al. in which pyrenyl-bearing **32** (Figure 39) was selectively quenched by Cu^{2+} in a 4:1 THF/H_2O solvent mixture.[1148]

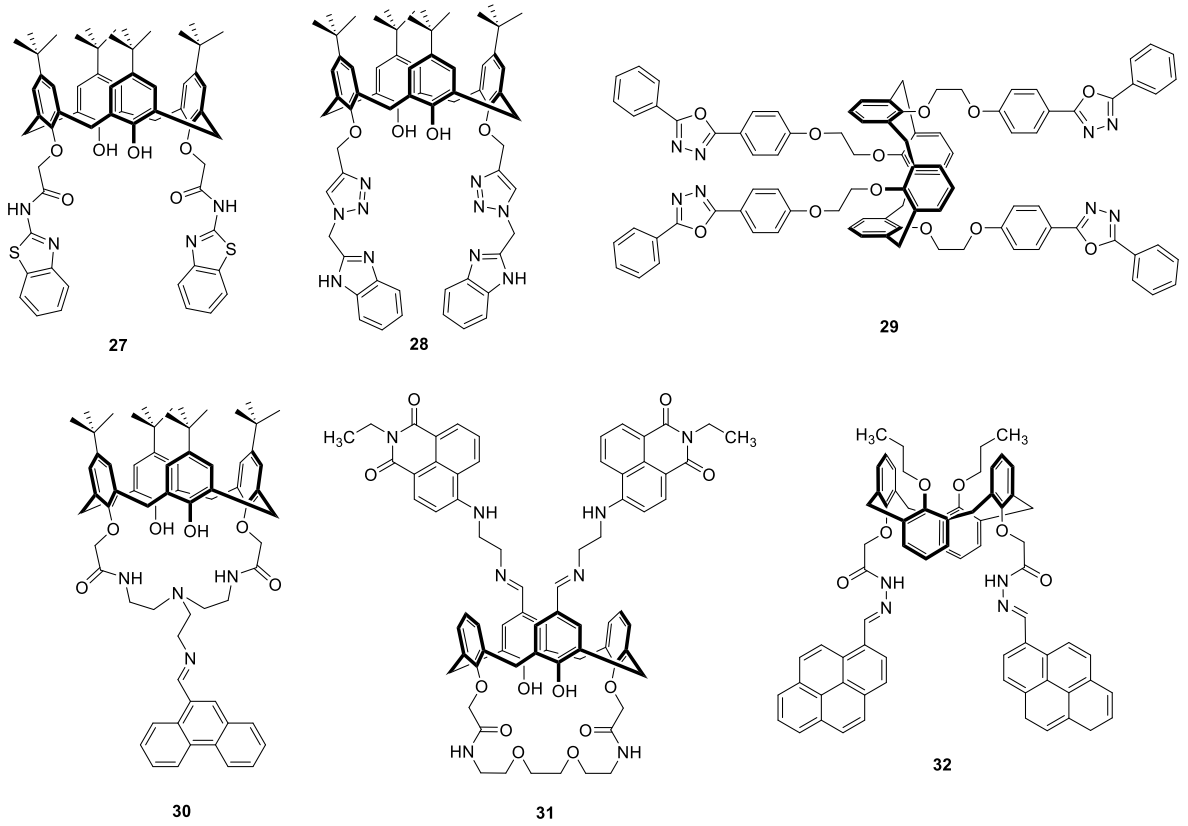

Figure 39. Calixarenes that have been used for Cu^{2+} detection[1143-1148]

Rao and coworkers developed a system for the fluorescent detection of zinc in human blood serum using **33** (Figure 40).[1149] Of 17 metal ions tested, zinc was the only species that increased the fluorescence emission, with a ten-fold increase in quantum yield observed in the Zn-complexed species. Compound **33** was able to detect Zn^{2+} in a buffer-methanol mixture with a detection limit of 36 ppb. A 1:1 binding stoichiometry was calculated along with a Benesi-Hildebrand binding constant of 1.49 x 10^5 M^{-1}. Of note, strong sensitivity was maintained in human blood serum, with a 332 ppb detection limit observed (corresponding to approximately 1.2 μM). Sutariya et al., using host **34** (Figure 40), were able to detect zinc in human blood serum at a level of 8.7 μM, which decreased to 33 nM in acetonitrile solvent.[1150] In another example, trioxacalix[3]arene **35** bearing anthracenyl units was synthesized by Jiang et al (Figure 40).[1151] Although this macrocycle demonstrated inherently weak fluorescence in the uncomplexed state due to PET, it was able to detect Cd^{2+} and Zn^{2+} via fluorescence increases, with a detection limit of 0.38 μM for the latter in acetonitrile. 1:1 binding stoichiometries were observed for both systems, and Benesi-Hildebrand binding constants of **35** with Cd^{2+} and Zn^{2+} were reported to be 4.06 x 10^4 M^{-1} and 1.44 x 10^4 M^{-1}, respectively. However, competing metal cations, including Cu^{2+} and Fe^{3+}, hindered the zinc-induced emission enhancement.

Compound **36** (Figure 40), a biscalixarene species with iminophenolate linkers developed by Ullman et al., selectively detected Zn^{2+} and Mg^{2+} in organic solvents.[1152] The two analytes increased the emission of the macrocycle by inhibiting PET from the imines to the fluorescent phenols. Of note, each analyte caused a unique fluorescence emission signal, with a 15 nm difference between the emission maxima, which enabled accurate differentiation between the two cations. The reported detection limit for Zn^{2+} was 0.15 ppb, which is two to three orders of magnitude smaller than previously reported limits using mono-calixarenes with iminophenolate pendant arms.[1153-1155] Naphthyl-bearing thiacalix[4]arene, **37** (Figure 40) was found by Darjee et al. to be a selective sensor for zinc, even in the presence of other metal cations.[1156] The 1:1 host-guest system enabled a broad linear detection range for Zn^{2+} (1 to 740 nM), and a binding constant was determined by Stern-Volmer analysis to be $3.16 \times 10^5\ M^{-1}$. Additional calixarene-based zinc sensors containing bispyridine and terpyridine units were developed by Zhang et al[1157] and Li et. al.[1158] The bispyridine-modified calixarenes **38** and **39** (Figure 40) formed 1:2 host-guest complexes with zinc, leading to unique emission changes.[1157] Terpyridine-appended **40** (Figure 40) formed 1:1 host-guest complexes with Zn^{2+} and Cd^{2+} with a relatively high binding constant of $>10^6\ M^{-1}$ for the former.[1158]

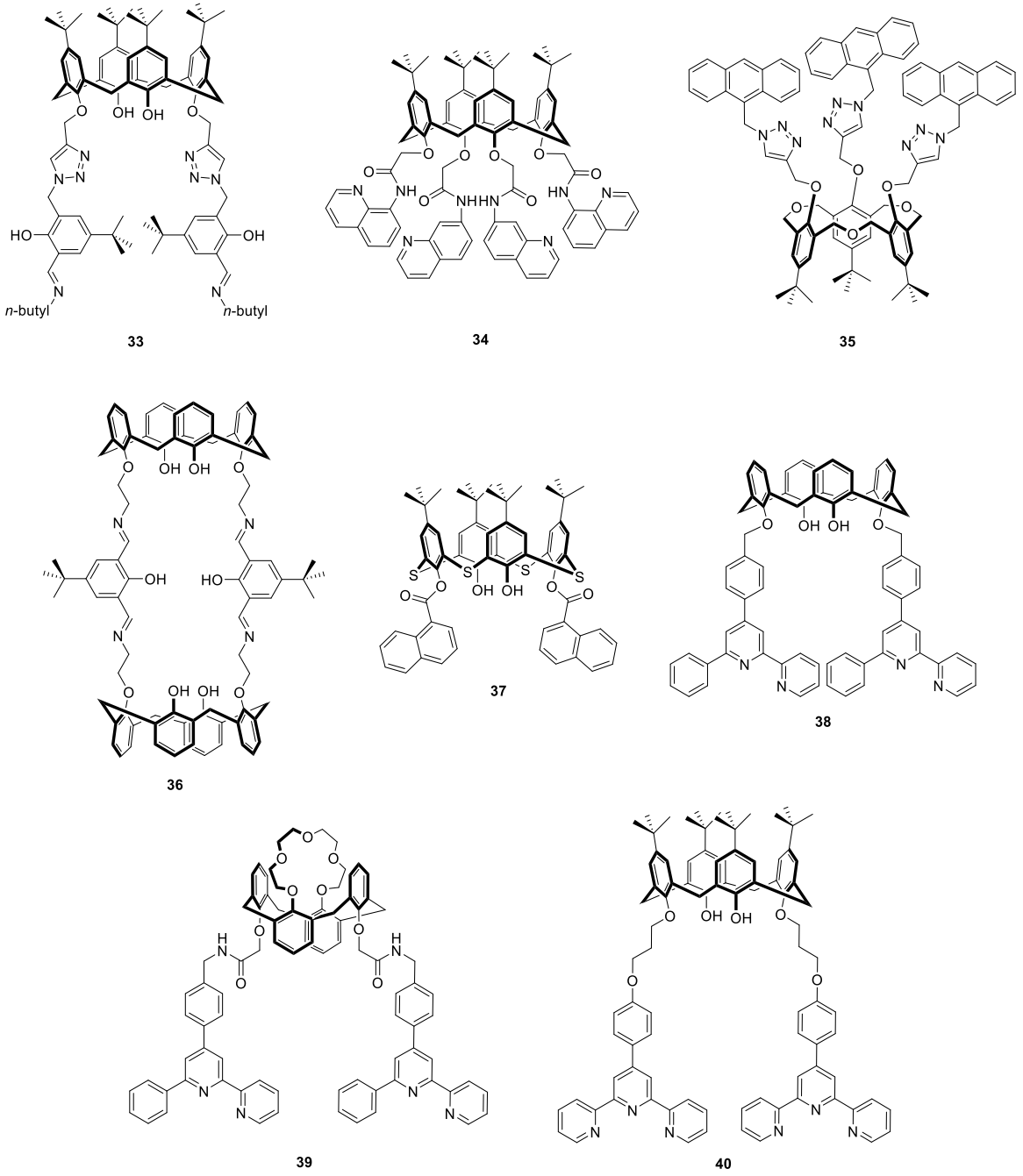

Figure 40. Calixarenes that have been used for the detection of zinc[1149-1152,1156-1158]

Calixarenes with covalently attached fluorescent units have also been used for the detection of toxic heavy metals such as mercury, lead, and cesium. In one example, BODIPY-modified calixarene host **41** (Figure 41) responded to the presence of as little as 28 μM of Hg^{2+} by fluorescence quenching, with a Stern-Volmer quenching constant of 3.42 x 10^7 M^{-1}, as a result of the formation of a 1:1 host-guest complex.[1159] Of note, the recognition ability of **41** toward mercury in a 9:1 methanol/water mixture was not significantly hindered by other metal cations. Arena et al. developed host **42** (Figure 41), whose fluorescence was quenched in acetonitrile by the addition of Hg^{2+}, Cd^{2+}, and Pb^{2+}, with a 60% to 70% quenching efficiency.[1160] When a 1:1 mixture of acetonitrile and water was employed as the solvent, however, only mercury effectively quenched the emission of **42** and a relatively low 1.6 μM detection limit was observed.

This system was also sensitive to pH, with acidic conditions decreasing the quantum yield of the complex, and basic conditions leading to displacement of the bound analyte and an increase in fluorescence. In another example, fluorescence quenching was observed during the titration of dansyl-bearing calixarenes, such as **43** (Figure 41), with metal cations. Although not selective, the quenching ability of the metal cations increased in the following order: alkali metals < alkaline earth metals < transition and heavy metals.[1161] Sulfonated, water-soluble, dansyl-bearing calixarenes **44** and **45** (Figure 41) could sense the presence of Hg^{2+}, with detection limits of 11.4 μM and 34.2 μM, respectively,[1162] and the sensing ability was maintained in live cells. Benesi-Hildebrand binding constant values were calculated to be 666.7 M^{-1} and 733.3 M^{-1} for hosts **44** and **45**, respectively. One shortcoming of this research is that the response of the calixarenes to other metal cations was not reported. In one final example, Erdemir and coworkers found that triphenylamine-bearing calixarene **46** (Figure 41), was moderately selective for the FRET-based fluorescence detection of mercury over other cations with a Benesi-Hildebrand binding constant of 7.52 x 10^4 M^{-1}.[1163]

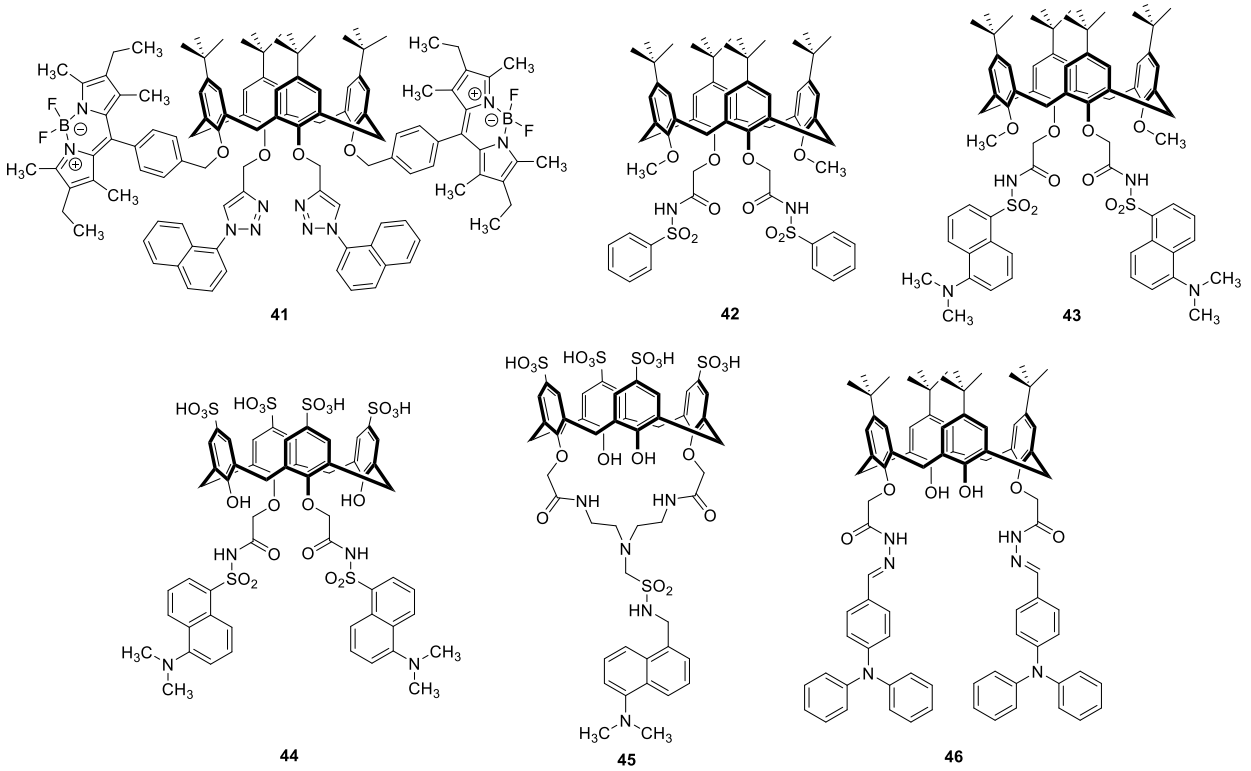

Figure 41. Calixarenes that have been reported for the sensing of mercury and other metals[1159-1163]

Pyrene-affixed calixarenes have been reported for the detection of Pb^{2+} by the Kumar[1164] and Sahin[1165] research groups. Kumar and coworkers developed **47** and **48** (Figure 42), for the ratiometric (for **47**) and "turn-off" (for **48**) fluorescence detection of Pb^{2+}.[1164] Ratiometric detection of Pb^{2+} with **47** occurred through lead-induced disruption of the pyrene excimer, resulting in a decrease in the excimer emission and concomitant increase in monomer emission, and a detection limit of 0.49 μM. In competition experiments with other metal cations, Hg^{2+} was the only other metal cation to induce ratiometric fluorescence changes, although of substantially lower magnitude than the lead-induced changes. For the quenching-based detection of lead using sensor **48**, nearly complete fluorescence quenching was observed in the presence of 10 equivalents of lead cation. Again, some Hg^{2+} interference was observed, although 100 equivalents of mercury were required to reach only a 25% fluorescence quench. Of note, the detection limit of sensor **48** towards Pb^{2+} was 0.29 μM, and reversibility was demonstrated through using EDTA to remove and sequester Pb^{2+} from the **48** cavity. Compounds **49** and **50** (Figure 42), were used for semi-selective Pb^{2+}

detection, with fluorescence quenching of **49** caused by Pb^{2+} and Zn^{2+}, and quenching of **50** caused by Pb^{2+} and Cu^{2+}.[1165] The fluorescence response of these hosts was thought to proceed through a PET mechanism, with metal coordination inhibiting charge transfer from the pyrene moieties to the amine nitrogen atoms, leading to the observed fluorescence decreases. Stern-Volmer quenching constants of **49** with Pb^{2+} and Zn^{2+} were found to be 3.15 x 10^4 M^{-1} and 3.15 x 10^5 M^{-1}, respectively, while the Stern-Volmer constants of **50** with Cu^{2+} and Pb^{2+} were 1.49 x 10^4 M^{-1} and 8.15 x 10^3 M^{-1}.

Cesium was successfully detected by several calixarene-crown ether macrocycles.[1166,1167] In one example, BODIPY-bearing species **51** and **52** (Figure 42) bound to both K^+ and Cs^+, with a stronger binding to Cs^+ observed due to steric complementarity between the size of the host cavity and the cesium atomic radius. The complexation of Cs^+ with **51** led to a bathochromic shift and small increase in emission, whereas complexation with **52** led to a hypsochromic shift and slightly larger emission increase.[1166] In a later publication, coumarin-containing **53** (Figure 42) was integrated into a microfluidic device that detected Cs^+ with a 1.4 μM detection limit.[1167] Competition experiments indicated that 0.02 equivalents of other cations (relative to cesium) did not compromise the **53** detection sensitivity.

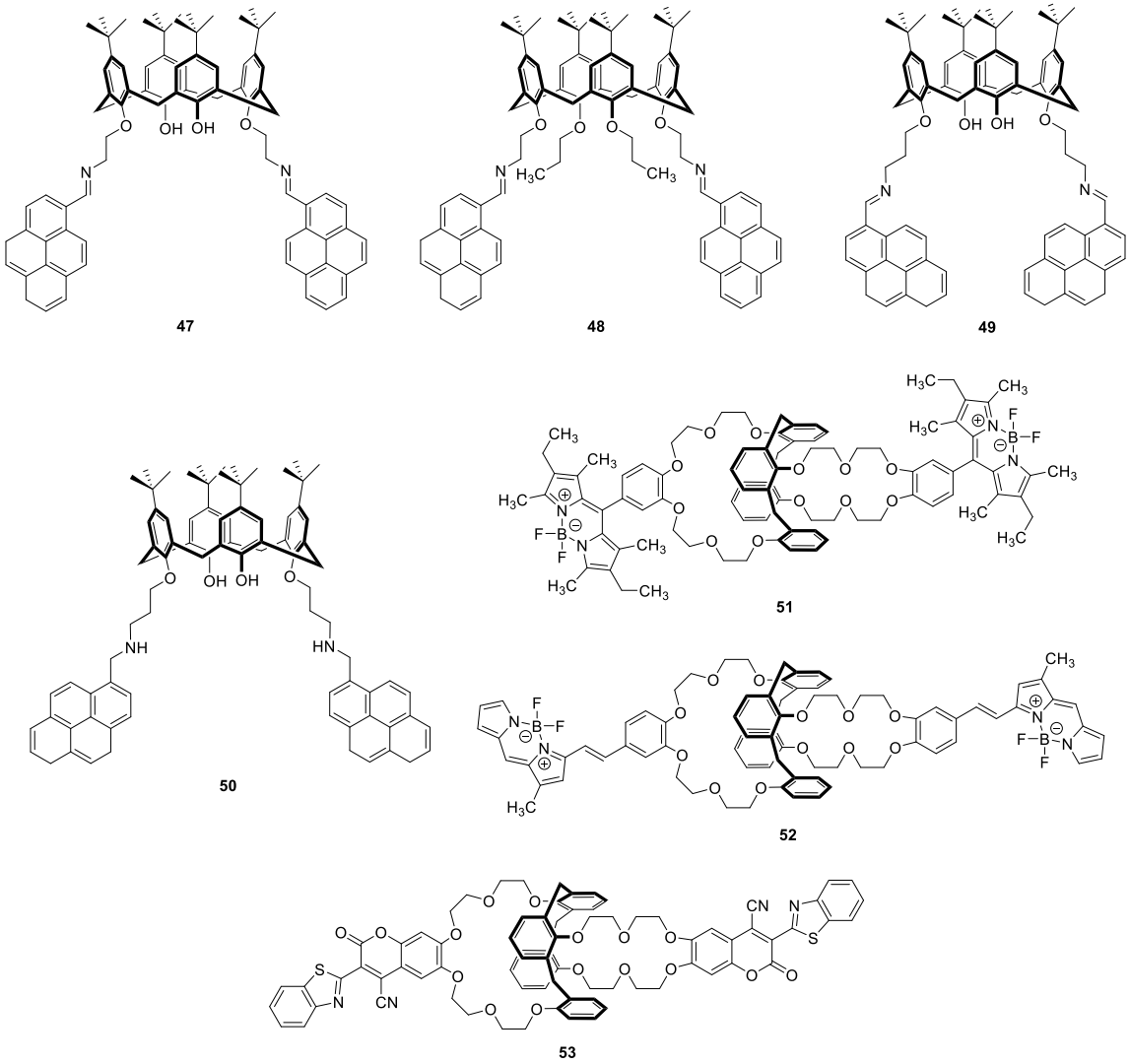

Figure 42. Pyrene-bearing calixarenes and crown-ether-modified calixarenes that have been used for heavy metal detection[1164-1167]

Other metal cations that have been detected by calixarenes include iron, chromium, gold, silver, and aluminum. In one example, Zhan et al. used a calixarene with pyridine-containing arms, **54** for the sensitive (0.5 μM detection limit) and selective detection of Fe^{3+} by iron-induced fluorescence quenching, with the proposed mechanism of quenching due to the reversal of PET.[1168] An association contant of 1.76 x 10^4 M^{-1} was calculated using the Benesi-Hildebrand equation for the binding of **54** with Fe^{3+}. Using nanoparticles of **54** rather than the monomeric calixarene caused an increase in the fluorescence detection limit, to 125 μM. Zheng et al. discovered that Fe^{3+} could also be detected by **55**, a rhodamine-armed thiacalixarene, although with some loss of selectivity observed, as evident by signal changes in the presence of Cr^{3+}.[1169] The addition of these metal cations to **55** leads to the ring opening of the spirolactam and a concomitant increase in fluorescence emission due to increased conjugation. This transformation was reversible with the addition of diethylenetriamine, which sequestered the cations and re-formed the spirolactam. Detection limits for Fe^{3+} and Cr^{3+} were 35 nM and 160 nM, respectively, and the system maintained high detection performance even in tap water samples.

Lotfi et al. discovered that, upon the addition of Ag^+ to **56**, a unique hypsochromic shift in emission occurred, allowing for selective detection that was minimally affected by competing cations (Figure 43).[1170] In simulated physiological conditions ([Na^+] = 145 mM, [K^+] = 5 mM, [Mg^{2+}] = 2 mM, and [Ca^{2+}] = 5 mM), the detection limit of Ag^+ was 23 μM, somewhat higher than the 6.3 μM observed in a 3:7 HEPES buffer/methanol mixture. In another example, Memon et al. developed systems for the detection of Au^{3+}[1171] and Al^{3+}[1172] using calixarenes **57** and **58**, respectively (Figure 43). The addition of Au^{3+} to **57** led to moderate quenching of the system, and allowed for a detection limit of 15 μM and a quantification limit of 52 μM.[1171] The addition of 32 potential interfering cations had no effect on the detection ability of the system. Compound **58** was found to detect Al^{3+} at concentrations as low as 2.8 μM via an increase in fluorescence emission.[1172] Other cations did not perturb the emission spectrum of **58** or interfere with Al^{3+} detection.

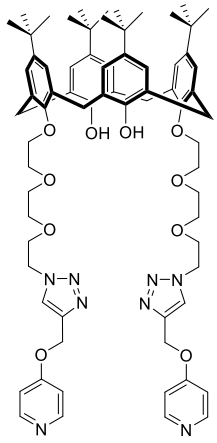

54

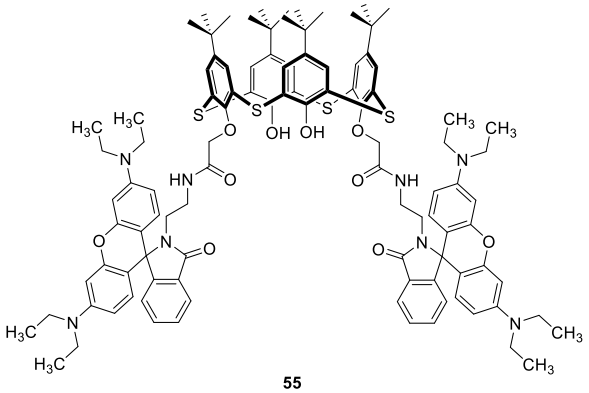

55

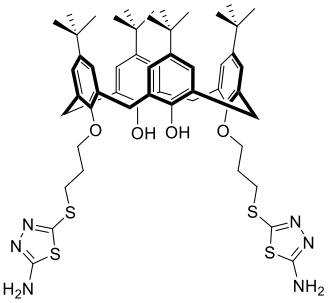

56

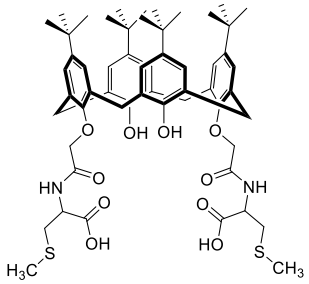

57

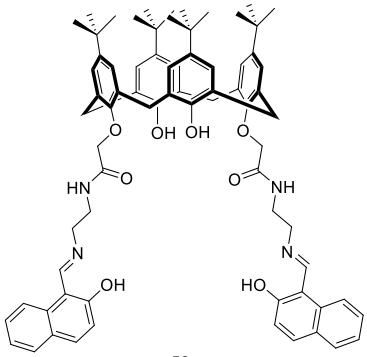

58

Figure 43. Calixarenes that have been used as sensors for metal cations[1168-1172]

Several of the systems discussed above for the detection of metal cations have also been used for the detection of anions, especially of fluoride, an anion with significant public health relevance.[769] Compound **24** (Figure 38), was reported as a ratiometric sensor for F^-, which responded to the presence of fluoride anion with a quenching of the excimer peak and enhancement of the monomer peak.[1131] The system allowed for the detection of F^- with a limit of 0.7 μM, and other anions were found to have limited interference with the detection ability toward F^-. Compound **34** (Figure 40) was sensitive to the presence of F^-, with a detection limit of 22 nM in wastewater samples and 8 nM in acetonitrile.[1150] However, the system was not selective for F^-. Fluoride ions could also be detected by the fluoride-induced fluorescence quenching of **30** (Figure 39), reported by Sahin and coworkers, although other anions (NO_3^- and $H_2PO_4^-$) interfered with the fluorescence response.[1146] Compound **46** (Figure 41), was quenched in the presence of F^-. The authors propose a quenching mechanism that includes fluoride-induced deprotonation of the amide NH and phenolic OH of the host. Although other basic conditions are expected to lead to the same deprotonations, such conditions were not examined.[1163] The emission of fluorenone-bearing **59** (Figure 44), was quenched in the presence of F^-, as reported by Nemati et al.[1173] The same group also reported the ratiometric sensing of F^- by **60** (Figure 44). Other anions induced similar effects on the emission profiles of both calixarenes, and the detection limit for F^- in the presence of **59** was calculated to be 32 nM.

Previously mentioned **57** (Figure 43) was fully quenched in the presence of 10 equivalents of iodide, with a low detection limit of 1.6 μM and a quantification limit of 4.5 μM, and no observed effects by any other anion investigated.[1170] In another report, Gómez-Machuca et al. reported the use of calixarenes **61**-**63** (Figure 44), for the semi-selective detection of I^-, with fluorescence quenching also observed for NO_2^-, SCN^-, NO_3^-, and N_3^-.[1174] Iodide detection limits of 1.81 ppm, 0.23 ppm, and 0.22 ppm were found for **61**, **62**, and **63**, respectively. Kim et al. reported that the inherent PET present between the pendant amine donor and pyrene acceptor units of calixarene **64**, (Figure 44) which resulted in excimer emission in the absence of analyte, was disrupted by iodide and bromide, allowing for their detection via the analyte-induced quenching of that emission.[1175] In another example of anion detection by calixarenes, dihydrogen phosphate anion was ratiometrically detected by Chen et al. using naphthol-armed hosts **65** and **66** (Figure 44).[1176] Ratiometric responses were also observed upon the addition of F^-, yet these hosts were much more sensitive toward $H_2PO_4^-$ (1.5-2.5 equivalents of $H_2PO_4^-$ required to induce a fluorescence response; 6-9 equivalents of F^- anion for the same effect). Benesi-Hildebrand constants were calculated to be $2.13 \times 10^3\ M^{-1}$ and $2.70 \times 10^3\ M^{-1}$ for the binding of $H_2PO_4^-$ with hosts **65** and **66**, respectively; and constants of $1.61 \times 10^3\ M^{-1}$ and $4.16 \times 10^2\ M^{-1}$ were reported for the binding of F^- with **65** and **66**, respectively. The emission of **58** (Figure 43) was increased in the presence of disulfate anion but quenched in the presence of all other anions examined, with a calculated detection limit of 0.26 μM for the $H_2PO_4^-$ observed.[1172] In a final example of anion detection, **67** (Figure 44), responded to the presence of HSO_4^- with an increase in fluorescence, even in the presence of competing anions.[1177] The observed fluorescence increases were due to the hydrolysis of **67** by the anion, which led to a detection limit of 0.98 μM.

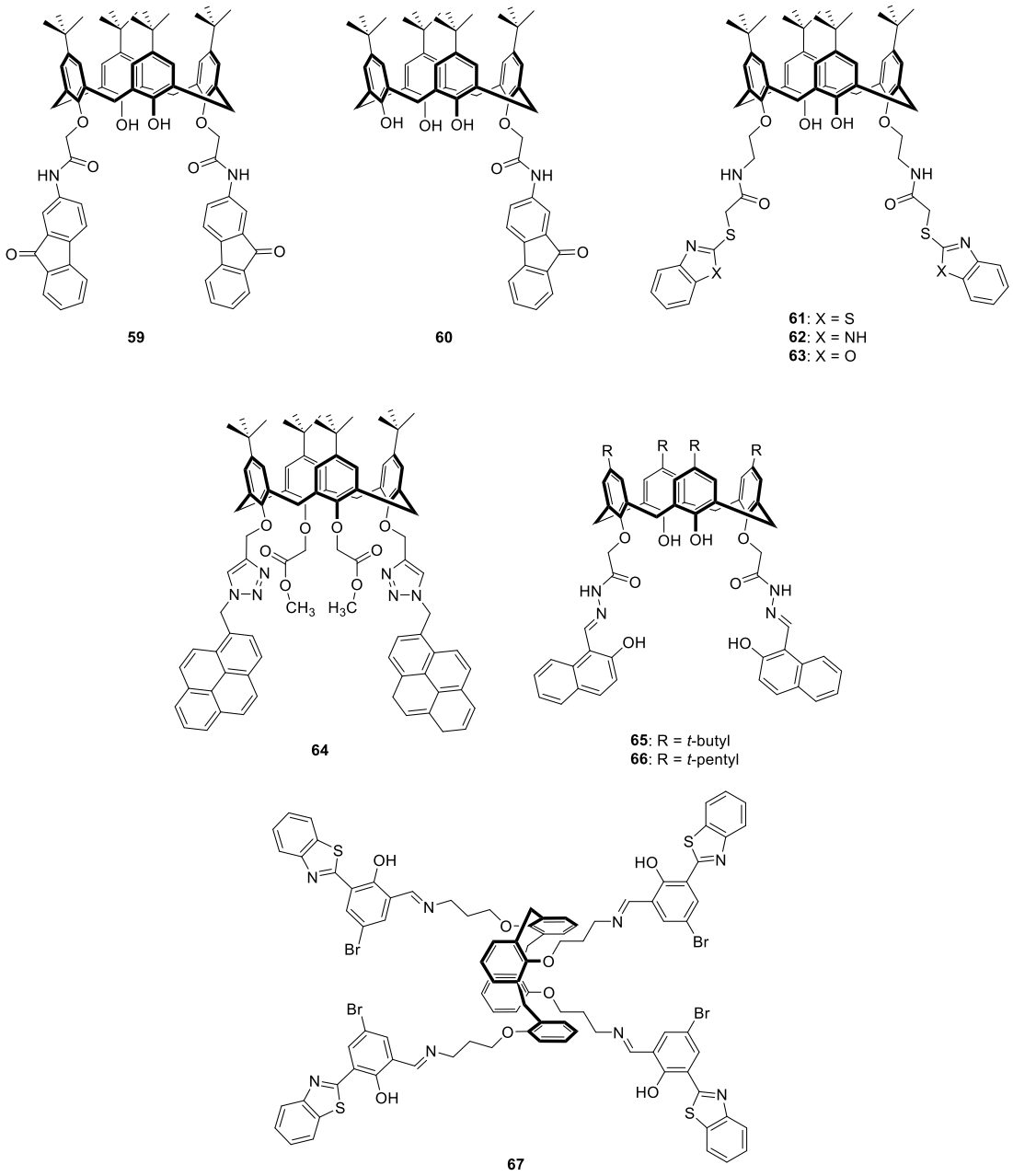

Figure 44. Calixarenes that have been used for the detection of anions[1173-1177]

Many dual-detection calixarene systems that detect both cations and anions have been developed in recent years. The premise of these systems is that a macrocyclic host is initially used for the detection of a cation, and the resulting host-cation species is subsequently used for the detection of an anion that sequesters the cation, allowing for the regeneration of the initial emission profile of the system. Many of these systems have been shown to have good reusability. Due to the high affinity of phosphates for zinc, several techniques for the detection of phosphate and zinc have been developed by Rao and coworkers using salicylyl-imine bearing calixarenes.[1178-1183] In 2010, the group synthesized **68** (Figure 45), and the addition of three equivalents of Zn^{2+} to this host promoted a 30-fold increase in emission, due to the analyte-induced disruption of PET between the phenolic oxygen and imine nitrogen, allowing for a minimum detection level of 192 ppb.[1178] A Benesi-Hildebrand binding constant of 2.7 x 10^4 M^{-1} was calculated, and competition experiments revealed that Fe^{2+}, Cu^{2+}, and Hg^{2+} all completely negated the Zn^{2+}-promoted

fluorescence enhancement, leading to no fluorescence changes compared to the uncomplexed macrocycle host, while Mn^{2+}, Na^{+}, K^{+}, Ca^{2+}, and Mg^{2+} had moderate deleterious effects. The titration of Zn-**68** with various anions revealed that the zinc was successfully sequestered by inorganic phosphate anions $H_2PO_4^-$, HPO_4^{2-}, and PO_4^{3-}; as well as by biologically relevant analytes: AMP, ADP, ATP, cysteine, and aspartic acid. A minimum detectable concentration of HPO_4^{2-} was established to be 426 ppb. The same group then developed host **69**, which could detect Zn^{2+} at levels as low as 45 ppb, with only the presence of Fe^{2+} and Cu^{2+} leading to significant changes in the detection ability of **69** (Figure 45) toward Zn^{2+}.[1179] A relatively high Benesi-Hildebrand constant of 4.93×10^5 M^{-1} was calculated for this interaction. In a similar fashion to the Zn-**68** association complex, the Zn-**69** association complex was disrupted by the addition of inorganic phosphates, $H_2PO_4^-$, HPO_4^{2-}, and $P_2O_7^{4-}$; with the sequestration of Zn^{2+} leading to regeneration of the fluorescence emission of **69**. The minimum detectable concentration of HPO_4^{2-} was found to be 247 ppb.

Rao and coworkers then modified their salicylyl-imine containing hosts by inserting triazole moieties into the pendant arms, forming **70** (Figure 45).[1180] The detection limit for zinc using **70** was 47 ppm, which was similar to the limit found when using **69**. The addition of thiols to the Zn^{2+}-**70** complex led to fluorescence quenching, due to interference of the thiols with PET, with the greatest degree of fluorescence quenching observed in the presence of the thiol-containing small molecules cysteine, dithiothreitol, and glutathione monosulfide. Of note, mercaptopropionic acid led to minimal quenching of the system; and homocysteine, mercaptoethanol, and cysteamine led to no fluorescence quenching. Reversibility of the system via the release of Zn^{2+} from the thiol was achieved by either oxidizing the thiol with H_2O_2 or by sequestering the thiol with Cd^{2+} or Hg^{2+}, allowing the zinc to rebind to **70**. This same Zn^{2+}-host adduct was used for the detection of pyrophosphate anion, with a reported detection limit of 340 ppb.[1181] Unlike **68** and **69**, this host was selective for pyrophosphate, with $H_2PO_4^-$, ATP, ADP, and AMP leading to very minimal quenching of the Zn^{2+}-**70** emission. In another report, the emission of Zn^{2+}-**70** was also found to be quenched by histidine and cysteine.[1182] Upon treatment of HeLa cells with **70**, zinc and pyrophosphate could be detected *in vitro*. However, no study was conducted comparing the affinity of Zn^{2+}-**70** to pyrophosphate, histidine, and the aforementioned thiols. In a later publication, Rao and coworkers ascertained that pyrophosphate could be detected selectively by zinc-bound-**71** (Figure 45).[1183] The unassociated **71** could detect Zn^{2+} with a limit of 112 ppb and a Benesi-Hildebrand constant of 7.2×10^4 M^{-1}, while the subsequent association complex could detect pyrophosphate with a limit of 278 ppb. While ATP was also found to sequester zinc, quenching was much less effective with ATP than with pyrophosphate. Successive additions of Zn^{2+} and pyrophosphate to **71** allowed for moderate reversibility.

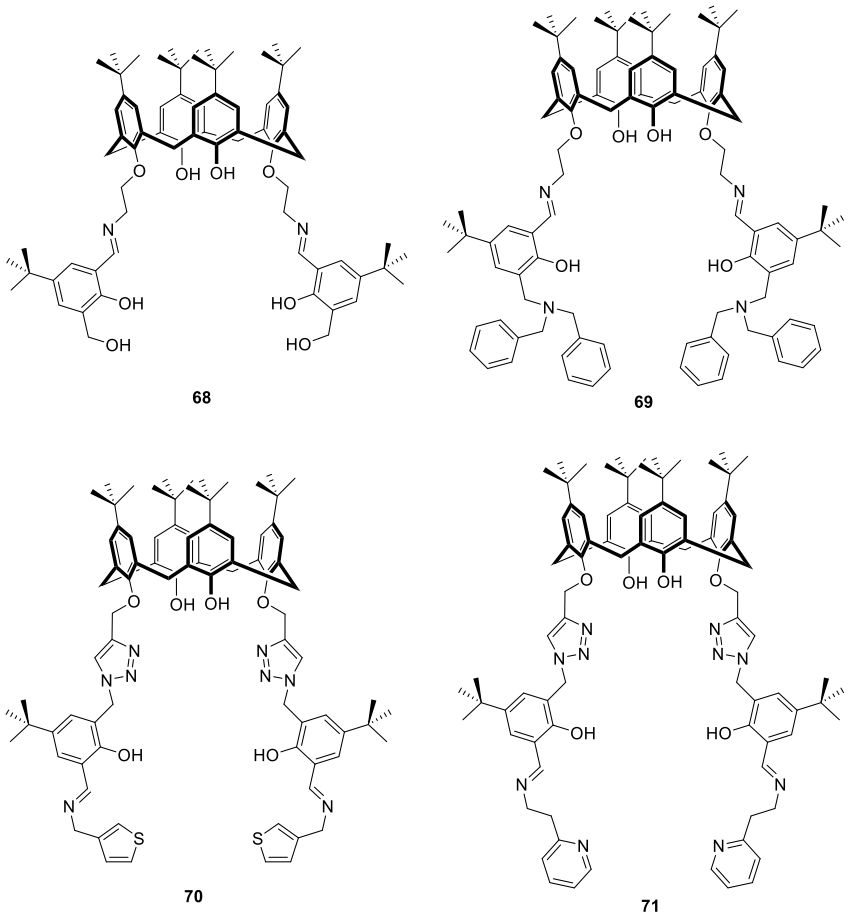

Figure 45. Calixarenes employed in the dual detection of zinc and phosphates[1178-1183]

Rao and coworkers developed other salicylyl-imino-bearing calixarenes that were selective for metals other than Zn^{2+}. In one example, a 1:2 host-guest complex of **72** (Figure 46) with cadmium was employed for the detection of phosphate-containing species by fluorescence quenching.[1184] $H_2PO_4^-$ was the most effective at quenching the emission of the association complex, which allowed for a detection limit of 20 ppb. HPO_4^-, ATP, ADP, AMP, and $P_2O_7^{4-}$ also quenched the emission, with reported detection limits between 50 and 580 ppb. Salicylyl-imine-containing calix[6]arene **73** (Figure 46), with a larger cavity size than calix[4]arene (7.6 Å vs. 3.0 Å cavity diameters),[1185] was able to bind La^{3+}, a cation with a relatively large atomic radius.[1186] The binding of La^{3+} to **73** was selective over other lanthanide metals and led to a ca. 70-fold increase in fluorescence emission upon the addition of eight equivalents of the analyte, translating into a 65 ppb minimal detectable La^{3+} concentration. Upon the addition of F^- to the La^{3+}-**73** association complex, a quenching of emission was observed. No other halide was found to promote the same behavior, and successive additions of La^{3+} and F^- led to excellent reversibility of the fluorescence emission signal. Although Zn^{2+} also bound to **73**, leading to observable fluorescence enhancements, the addition of F^- had no effect on the Zn-based association complex. Leray, Reinaud and coworkers also developed a calix[6]arene that has potential as a dual-sensing platform for multiple analytes.[1187] The macrocycle, **74** (Figure 46), bound to Zn^{2+} to form a complex that was responsive to the presence of primary alkylamines.

Rao and coworkers developed an extensive multiple sensor array system, using **75** (Figure 46), for the detection of a variety of metal cations and amino acids.[1153] **75** bound to Zn^{2+}, Mn^{2+}, Fe^{2+}, Co^{2+}, Ni^{2+}, Cu^{2+}, forming 1:2 host-metal complexes and resulting in a hypsochromic shift in the fluorescence emission peak. Response limits for these metal ions were found to be 0.76 μM, 1.8 μM, 1.0 μM, 1.99 μM, 1.99 μM, and

1.05 μM, respectively. All of the complexes formed had unique responses to amino acids, which enabled the creation of an array-based detection scheme. Mn^{2+}-**75** was able to sense aspartic acid and glutamic acid with detection limits of 20.2 μM and 19.0 μM, respectively; whereas complexes of **75** with Cu^{2+} and Zn^{2+} could detect cysteine at limits of 3.45 μM and 2.15 μM, respectively. Co^{2+}-**75** could detect 5.65 μM of cysteine, 3.44 μM of histidine, and 2.50 μM of aspartic acid. Ni^{2+}-**75** was found sensitive to 3.00 μM of histidine and 7.90 μM of aspartic acid. While all 20 natural amino acids were examined, only aspartic acid, glutamic acid, histidine, and cysteine effected a change in the emission profile of the metal-**75** complexes.

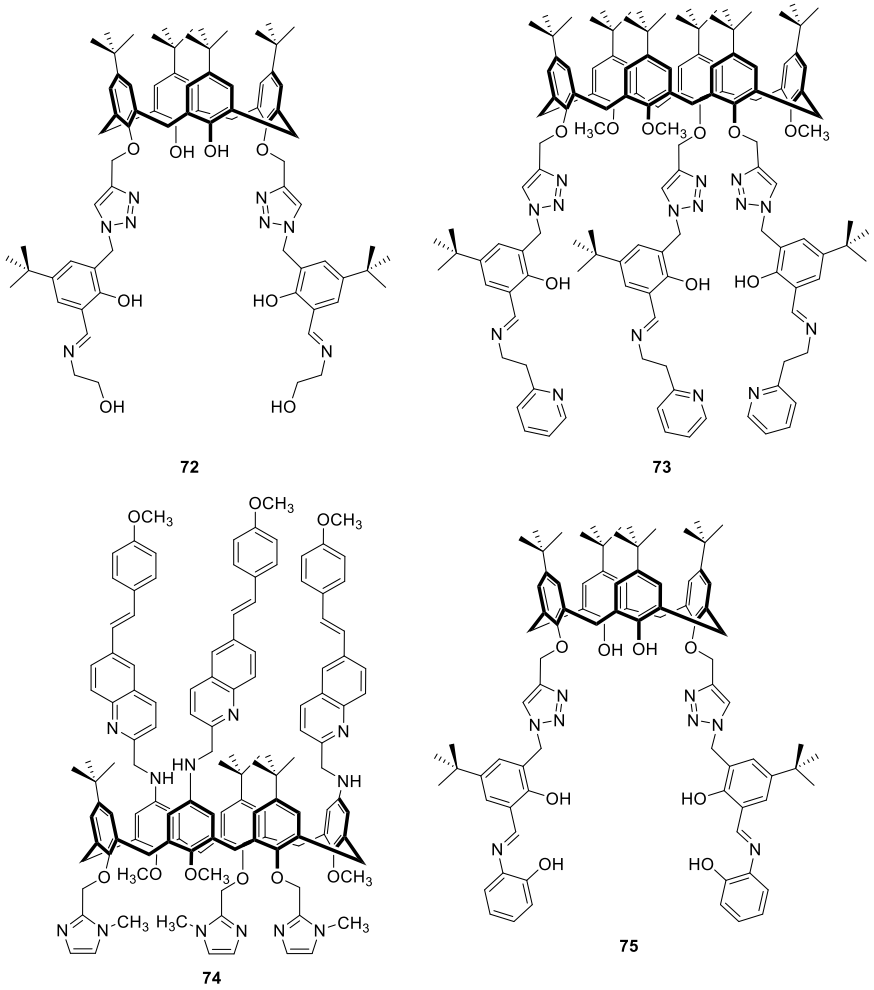

Figure 46. Calixarenes used as dual detection scaffolds[1153,1184,1185,1187]

Erdemir and coworkers developed perylene-linked bis-calix[4]arene **76** (Figure 47) for the dual detection of Hg^{2+} and I^-.[1188] Upon binding of Hg^{2+} to the macrocycle, a 1:2 host-guest complex formed with a Benesi-Hildebrand binding constant of 1.66 x 10^9 M^{-2}, resulting in an order of magnitude increase in quantum yield due to the disruption of PET between the pseudo-azacrown ether and perylene diimide fluorophore. The system could detect mercury at concentrations as low as 556 nM, and the addition of potentially interfering cations had little effect on this detection ability. Of a variety of anions examined, only I^- was able to effectively sequester Hg^{2+} from the system. Human colon cancer cells were incubated with Hg^{2+} and the host sequentially, leading to the detection of mercury in live cells. A detection limit of the system for I^- was not reported, and a relatively narrow optimal pH range of 5.5 to 7.5 was determined. Erdemir and coworkers also established that previously mentioned **67** (Figure 44) was a selective sensor for the detection of Cu^{2+} through fluorescence quenching, with a limit of 1.05 μM, and that other cations did not interfere with the detection capabilities of the system.[1177] The authors found, via Job's plot analysis, that a 1:2 host-guest

association complex was formed between **67** and Cu^{2+}. The resulting Cu^{2+}-**67** complex was used for the detection of S^{2-}, with the anion effectively sequestering Cu^{2+} and promoting fluorescence enhancement. No other anion sequestered the copper, and a detection limit of 1.54 μM for sulfide was achieved.

A copper-cyanide dual detection scheme using **77** (Figure 47) was created by Chawla and coworkers.[1189] In this scheme, a 1:1 host-guest complex of Cu^{2+} and **77** was formed, resulting in an emission decrease compared to the free calixarene. Upon the addition of CN^-, the fluorescence of the host was restored as the copper selectively bound to the anion and was removed from proximity to the host. Other cations and anions had little effect on this system, and detection limits of 0.4 μM and 1.26 μM were determined for Cu^{2+} and CN^-, respectively. The Stern-Volmer constant for binding of **77** with Cu^{2+} was reported to be 1.472 x 10^5 M^{-1}. Zhang et al. were able to selectively sense Ag^+ in aqueous media using **78** (Figure 47), through the generation of a new, bathochromically shifted emission peak for the Ag^+-**78** complex.[1190] This analyte could be detected with high sensitivity (detection limit of 0.62 μM) and selectivity (no other cations induced analogous fluorescence responses). Of note, the addition of formaldehyde, a toxicant widely used in industrial processes, to the system sequestered the silver cation, leading to the regeneration of the emission spectrum of free **78**. A detection limit for formaldehyde was calculated to be 0.66 μM in THF, and successful formaldehyde detection was demonstrated in doped tap water samples. In a final example of dual-detection schemes, Qazi et al. found that the addition of Pb^{2+} to **79** (Figure 47) led to a six-fold increase in emission, while other cations only led to moderate fluorescence changes.[1191] Subsequent addition of chromate caused a significant decrease in the fluorescence emission due to the sequestration of lead, in a phenomenon that other anions did not replicate.

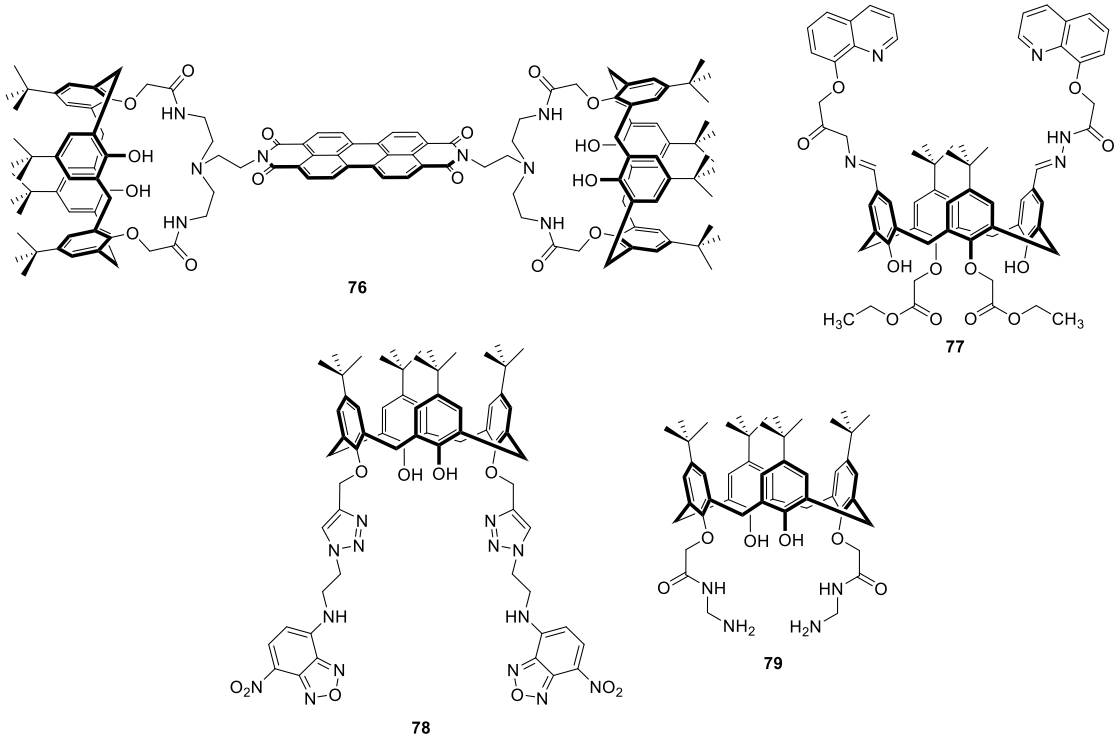

Figure 47. Calixarenes exploited for dual-detection systems[1188-1191]

The sensing of organic molecules by calixarenes has been pursued by several groups in recent years, especially for the detection of nitroaromatics. Each of these nitroaromatic detection schemes involved a fluorescent, electron rich calixarene donor transferring energy to a non-fluorescent, electron-deficient nitroaromatic guest. Thus, the fluorescence response of all such calixarenes upon complexation of the analyte was an emission quench. For example, Boonkitpatarakul et al. developed phenylethynylene calixarene **80** (Figure 48) for the detection of TNT in both solution and in the vapor phase.[1192] The addition

of one equivalent of TNT to **80** led to a 7.5-fold emission quench, though this technique was not fully selective, as the same amount of DNT led to a 4-fold emission quench. As little as 0.3 μM of TNT could be detected in aqueous solution over a wide pH range of 3 to 10. A solid-state device was fabricated for the detection of TNT in the vapor phase by dipping filter paper in a solution of the **80** and allowing it to dry in open air, and then using the functionalized paper for effective vapor-phase detection. Additionally, Rao and coworkers were able to detect TNT with **81** (Figure 48).[1193] A fluorescence quench of the macrocycle was also seen with the addition of similar nitroaromatic species dinitrobenzene and *m*- and *p*-nitrotoluene. Of note, in solution phase, concentrations as low as 3.03 μM of TNT could be detected.

Rao and coworkers also found that trinitrophenol (TNP) was selectively detected using **82** (Figure 48) with a detection limit of 300 nM and a Stern-Volmer quenching constant of 4.51×10^5 M^{-1}.[31] No other analogous electron-deficient analytes led to comparable quenching efficiencies nor did they interfere with TNP detection. Filter paper was soaked with a solution of the macrocycle to create a solid-state device, allowing for the naked eye detection of as low as 10 nM TNP under a UV-light irradiation. In another example, calix[4]arene **83** (Figure 48) was found by Lee et al. to be strongly quenched by the presence of trinitrobenzene and trinitrotoluene and moderately quenched by dinitrotoluene, dinitrobenzene, and nitrobenzene.[1194] Concentrations as low as 1.1 ppb TNT could be detected by this method. The authors propose that the emission quench observed was due to charge-transfer complexes forming between the electron rich pyrene units of **83** and the electron deficient nitroaromatic analyte. Several reports of calixarenes used for the detection of nitroaromatics have been published by Li and coworkers in recent years. In one example, the emission of **84** (Figure 48) was significantly quenched by the presence of *p*-nitrophenol, with other nitroaromatics leading to only minimal quenching.[1195] **85** (Figure 48) was used for the detection of trinitrophenol where dinitro- and mononitro- aromatics had minimal effect on the emission of **85**.[1196] The group was also able to detect *p*-nitroaniline over other nitroaromatic species using **86** (Figure 48).[1197] A final example of nitroaromatic detection was reported by Teixeira et al. using **87** (Figure 48) for the detection of nitroanilines.[1198]

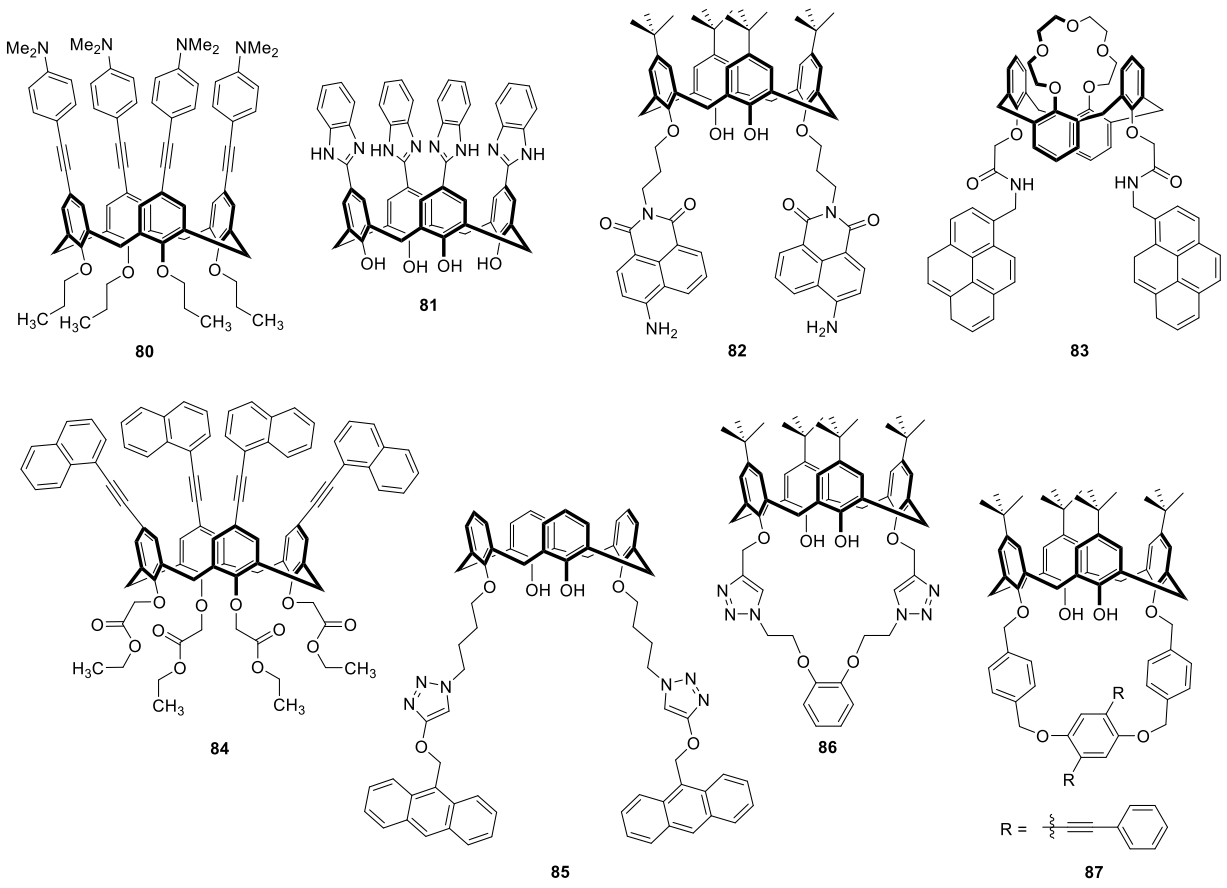

Figure 48. Calixarenes used for the detection of electron-deficient nitroaromatics[31,1192-1198]

Choline, an essential nutrient, and acetylcholine, a neurotransmitter, have been detected by two different schemes in recent years. Acetylcholine was found by Jin to displace Rhodamine 800 that was encapsulated in the cavity of thiacalix[8]arene **88** (Figure 49).[1199] Using this method, acetylcholine could be detected in concentrations as low as 0.5 mM. Structurally similar neurotransmitters, dopamine and γ-aminobutyric acid, led to no change in the emission of **88**, yet choline was found to enhance the emission to a lesser extent than acetylcholine, reflecting a lower degree of fluorophore displacement from the cavity. Guo et al. developed a system using calixarenes **89-91** (Figure 49) for the detection of acetylcholine via an indicator displacement assay, which was used for the real-time monitoring of acetylcholinesterase.[1200] As acetylcholine was converted to choline by the enzyme, lower concentrations of acetylcholine were available for binding in the macrocycle and inducing fluorophore displacement, which provided more opportunities for association of the host with lucigenin, a fluorescent dye. Although encapsulated lucigenin displayed only weak fluorescence, displacement of the dye by acetylcholine led to a pronounced increase in emission. Thus, the conversion of acetylcholine to choline resulted in a marked emission decrease. In two final examples, Xu et al. found that the emission of **92** (Figure 49) was quenched in the presence of acidic amino acids[1201] and enhanced in the presence of basic amino acids, and Han et al. used BODIPY-tethered **93** (Figure 49) for the monitoring of intracellular pH between 6.3 and 7.9.[1202]

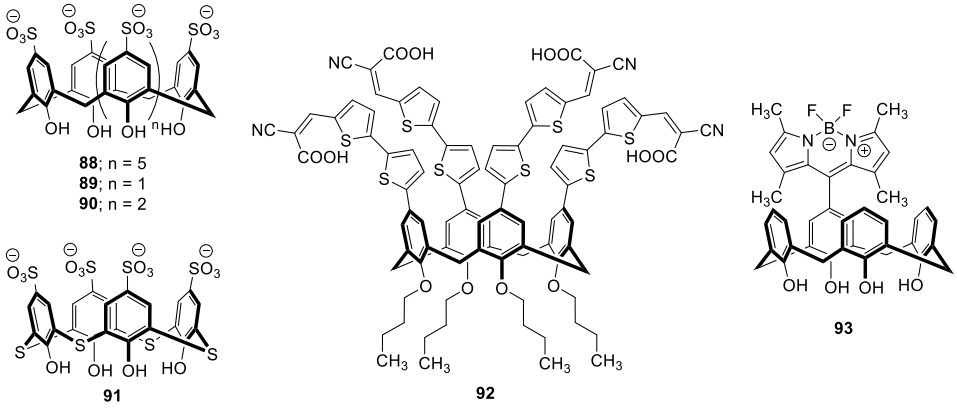

Figure 49. Calixarenes used for the detection of biomolecules in recent years[1199-1202]

5.1.6. Resorcin[*n*]arenes. Resorcin[*n*]arenes are a class of calixarenes that bear upper-rim hydroxyl groups and substitution at the methylene bridges. Other calixarenes, by contrast, are characterized by lower-rim hydroxyl groups and unfunctionalized methylene linkers. Often, resorcinarenes have additional methylene linkages between the hydroxyl substituents on the aromatic rings, as shown in Figure 50.[1203] The condensation of resorcinol and aldehydes to form resorcinarenes was first reported in the literature in 1940[1204] and, like calixarenes, the four-membered resorcinarene macrocycle, termed resorcin[4]arene, is the thermodynamically favored product under most reaction conditions.[1205] The majority of publications that report the use of resorcinarene-containing fluorescent chemosensors use resorcinarenes in the context of resorcinarene-based coordination polymers (CPs) and metal-organic frameworks (MOFs). While both of these terms describe crystalline structures comprised of infinite arrays of metal nodes and organic linkers, the term coordination polymer is much broader, encompassing a wide range of these structures, while the term 'metal-organic framework' is used to describe three-dimensional networks.[1206] The research group of Jian-Fang Ma has reported the synthesis of a number of resorcinarene-based CPs and MOFs and their use as fluorescent chemosensors, noting that these structures benefit from high tunability, enhanced sensitivity, and unique photophysical properties compared to free macrocycles.[1207] Aside from their use as fluorescent chemosensors, resorcinarenes have shown promise as ligands for metal-based catalysis,[1205] in chemical separations,[1208] and in other, non-luminescent molecular recognition schemes.[1209]

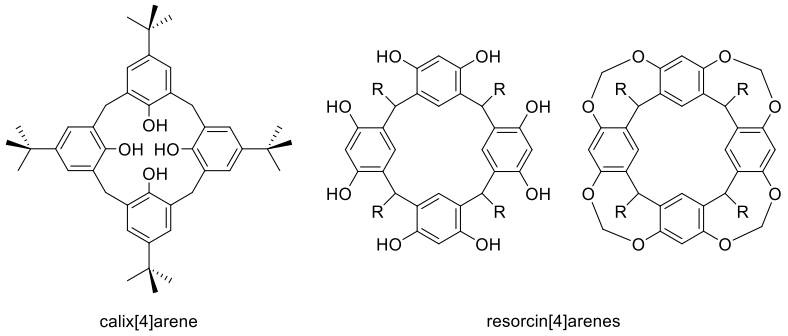

Figure 50. Typical core structures of calix[4]arenes and resorcin[4]arenes[1203]

Ma and coworkers have described several MOFs formed from resorcin[4]arenes shown in Figure 51, for the detection of cations, anions, and small molecules.[1207,1210-1212] Luminescent zinc, europium, and terbium MOFs were created using **94** (Figure 51), whose emission was almost fully quenched by the presence of Fe^{3+} in aqueous solution.[1210] Stern-Volmer quenching constants of 1.519 x 10^3 M^{-1}, 3.81 x 10^2 M^{-1} and 4.749 x 10^3 M^{-1} were reported for the binding of Fe^{+} with the Eu, Zn, and Tb MOFs, respectively, with a detection limit of 50 μM reported for the Tb-MOF sensor. While no other metal cations effected MOF luminescence, a number of polyoxometalates were also shown to quench emission. In a subsequent publication by the same research group, the ethyl groups of the resorcin[4]arene backbone were replaced with aromatic moieties to create **95** and **96** (Figure 51), which were used to form zinc MOFs.[1211] In the presence of metal cations in aqueous solution, hypsochromic shifts of the fluorescence of the zinc MOF were observed along with various degrees of fluorescent enhancement or quenching, with Fe^{3+}, Fe^{2+}, and Cu^{2+} leading to the most significant quenching. The addition of small amounts of acetone to aqueous solutions of **95** and **96** also quenched the emission, and acetone concentrations as low as 0.5 % and 10 % by volume could be detected, respectively. Additionally, fluorescence quenching was reported in the presence of vapor phase amines. Cadmium and zinc MOFs made from **97** (Figure 51), were also used for the detection of amine vapors, and comparison plots of quenching efficiency vs. wavelength shift allowed for nearly complete differentiation of seven different primary, secondary, and tertiary amines.[1207] Aldehyde vapors also led to fluorescence quenching of the supramolecular sensor, with the presence of benzaldehyde leading to approximately 80 % quenching of both MOFs after 10 minutes. Finally, the emission of a fluorescent cadmium-**98** MOF, (Figure 51), was completely quenched in the presence of Fe^{3+} and chromate anion, with Stern-Volmer constants for these analytes of 2.67 x 10^5 M^{-1} and 9.19 x 10^5 M^{-1}, respectively.[1212]

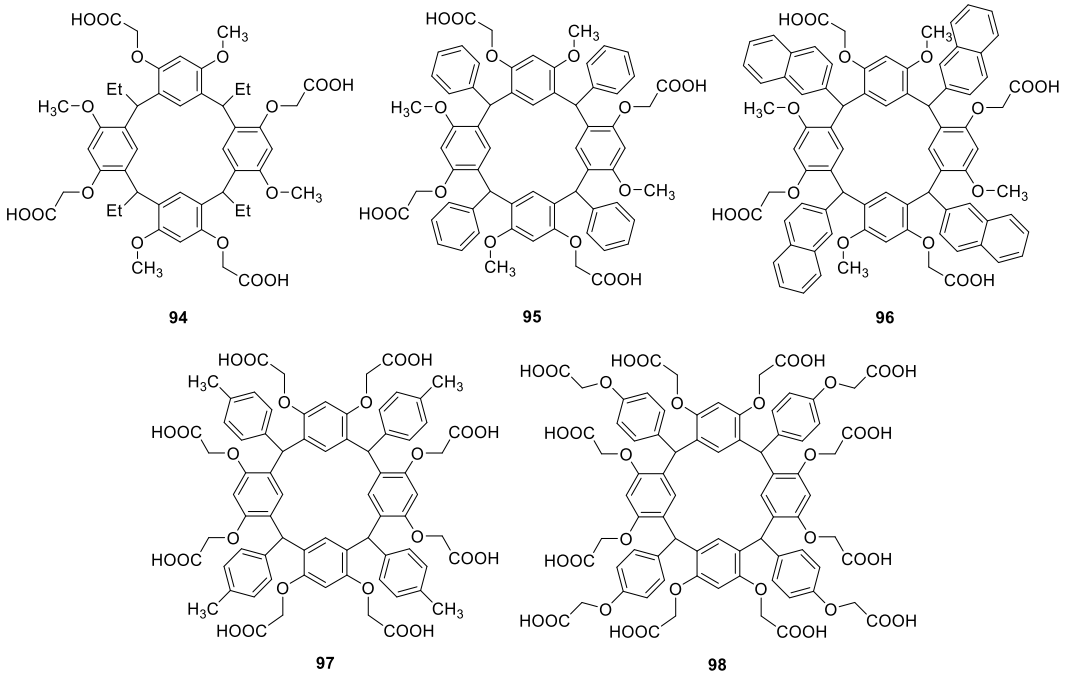

Figure 51. Resorcin[4]arenes used in metal-organic frameworks for the detection of cations, anions, and small molecules[1207,1210-1212]

The Ma group also developed a series of coordination polymers based on resorcin[4]arenes, some of which are shown in Figure 52.[1213-1215] Zinc and cadmium CPs of **99** (Figure 52) were treated with aqueous solutions of chromate, and significant fluorescence quenching was observed, as well as a bathochromic emission shift of the cadmium-**99** CP.[1213] Fe^{3+} was also able to quench the emission of both CPs with minimal interference from other cations. The Stern-Volmer quenching constants for the interaction of chromate and Fe^{3+} with the Zn-**99** CP were found to be 5.98 x 10^4 M^{-1} and 2.048 x 10^5 M^{-1}, respectively.

The fluorescence emission of zinc CPs of **100** and **101** (Figure 52) was also quenched by chromate anion, with Stern-Volmer constants of 4.303 x 10^4 M^{-1} obtained using **100** and 3.879 x 10^4 M^{-1} obtained with **101**.[1214] Furthermore, the replacement of aqueous solution with nitrobenzene was found to quench both CPs by several orders of magnitude. The presence of nitrobenzene was also found to quench cadmium and zinc CPs of **102** (Figure 52).[1215]

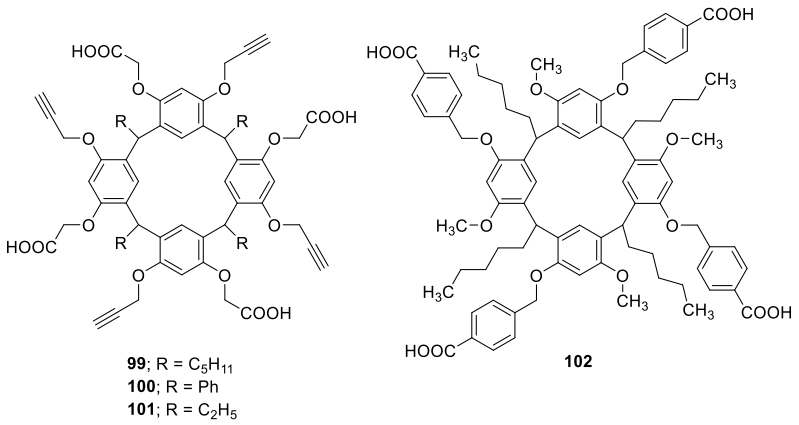

Figure 52. Resorcin[4]arenes used in coordination polymers for the fluorescent detection of cations, anions, and solvents[1213-1215]

Boron-based fluorescent appendages have been installed on the upper-rim of resorcin[4]arenes by Kubo et al. and used for the detection of alkyl ammonium cations.[1216,1217] Ratiometric sensing of hexyltrimethylammonium, tetramethylammonium, and acetylcholine cations was achieved in 9:1 methylene chloride: dimethylsulfoxide solution using **103** (Figure 53), with high association constants of 3.8 x 10^8 M^{-1} and 1.6 x 10^7 M^{-1} reported for the latter two, respectively.[1216] Interestingly, bulkier quaternary ammonium salts did not induce a fluorescence response. In a later publication, when resorcin[4]arene **104** (Figure 53) was treated with hexyltrimethylammonium hexafluorophosphate in methylene chloride solution, no changes in fluorescence were observed.[1216] However, with the addition of 5 % dimethylsulfoxide, a fluorescence quench and hypsochromic shift of the fluorescence emission occurred. It was posited by the authors that in purely methylene chloride solution, the resorcin[4]arene exists in an open "kite-like" structure, whereas the presence of dimethylsulfoxide facilitates and stabilizes strong non-covalent binding between the arms of the cavitand, pulling the cavity closed into a "vase-like" structure. This more closed cavity shape is ideal for binding the long alkyl chain of hexyltrimethylammonium hexafluorophosphate, with the cation of the analyte held tightly in the electron-rich macrocycle center. Indeed, a high association constant of 1.44 x 10^7 M^{-1} was observed in a 95:5 methylene chloride: dimethylsulfoxide solvent mixture. Mettra et al. functionalized the upper rim of phosphonate resorcin[4]arenes with fluorene appendages to form structures including **105** and **106** (Figure 53).[1218] In the presence of acetylcholine, a neurotransmitter, in chloroform solvent, dramatic quenching of the host's fluorescence was observed. Notably, the binding of acetylcholine and *cis*-fluorene-bearing host **106** had a higher association constant, 9.28 x 10^7 M^{-1} than the *trans*-fluorene-bearing host **105** and species containing one and four fluorene substituents, whose association constants fell in the range of 1.07-1.82 x 10^7 M^{-1}.

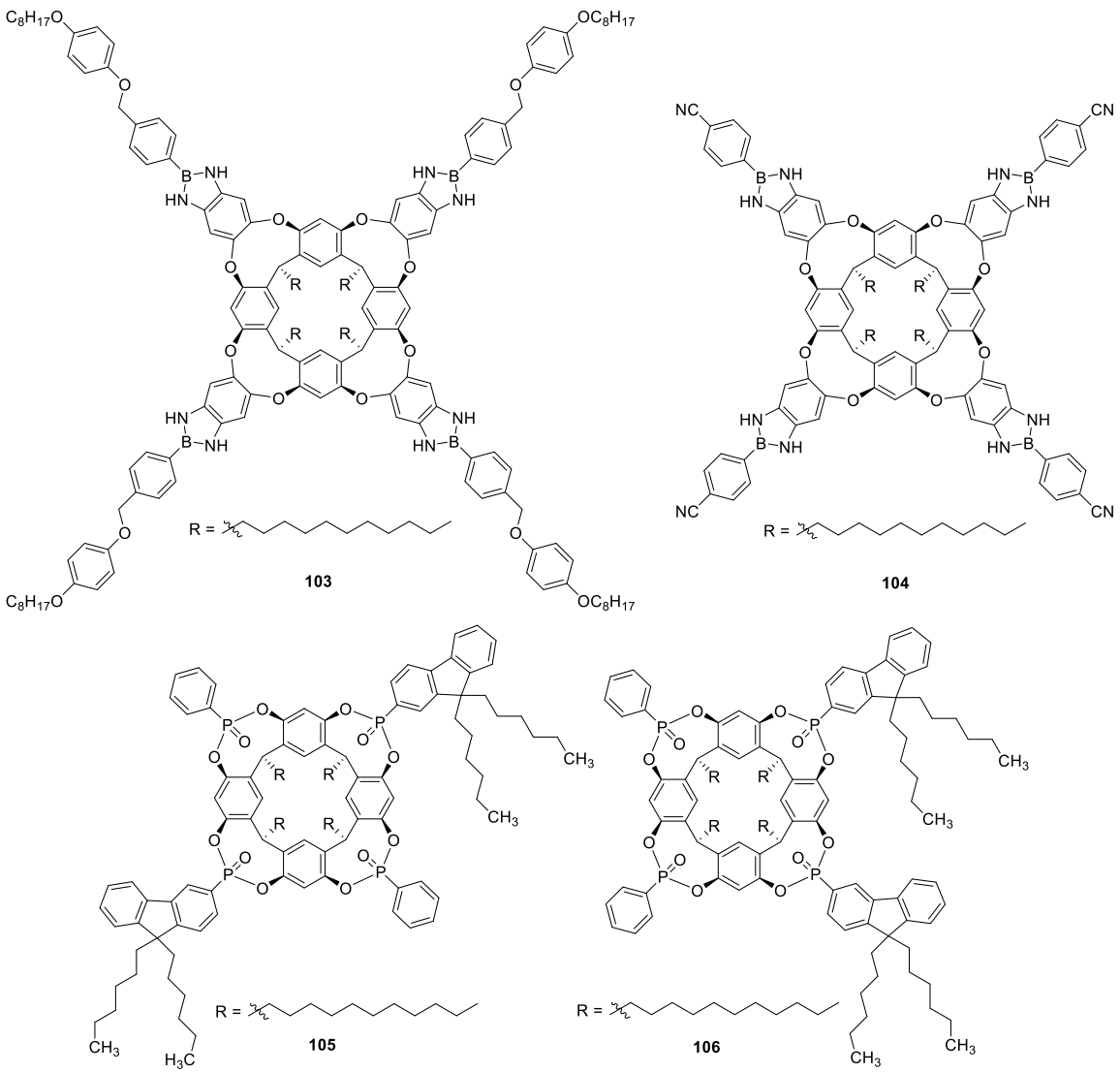

Figure 53. Resorcin[4]arenes bearing fluorescent tags that have been used for the detection of quaternary ammonium cations[1216-1218]

5.1.7. Calix[*n*]pyrroles. Calixpyrroles, also known as *meso*-octamethylporphyrinogens, are macrocycles which are formed from the condensation of pyrrole with acetone in acidic media, with the acetone forming covalent bonds to the alpha positions of the pyrrole.[1219-1221] While first synthesized by Baeyer in 1886,[1222] the utility of these species as supramolecular hosts was not realized until over a century later in 1996 by Sessler and coworkers.[1223] Sessler showed that in the uncomplexed state, methyl- and cyclohexyl-*meso*-substituted calix[4]pyrroles exist in a 1,3-alternate conformation, yet when complexed with a chloride or fluoride anion, the hosts adopted "cone-like" structures with all pyrrole units oriented in the same direction and with the nitrogen atoms non-covalently bound to the halide. Substitution at the *meso*-position of calixpyrroles prevents the spontaneous oxidation of these species to form porphyrins, and while methyl-substitution at this position is ubiquitous, more highly functionalized moieties including fluorescent groups[1224,1225] and highly polar solubility-enhancing groups[1226] are also common.[1220] Additionally, calixpyrroles with substitution at the pyrrole carbon backbone, or carbon-rim, have also been reported.[1227,1228] Functionalized at the nitrogens of the calixpyrroles has also been described, although such substituted variants are rarely used as chemosensors due to disruption of the main binding site of the compounds.[1220] Hybrid calixpyrroles that have one or two pyrrole units replaced with other units, such as

pyrene[1229,1230] or phenol[1231] have been reported, as well as extended calixpyrroles in which other units are interspersed between the four pyrrole units to form larger cavity sizes.[1232] Strapped or capped calixpyrroles contain a strap over the main binding pocket that aid in the preorganization of the binding pocket and can be tuned to enhance selectivity of the host system for target guests.[1221] These straps often contain additional handles for analyte binding and fluorescent units for chemosensing purposes.[1233,1234] Like calixarenes and resorcinarenes, the 4-membered calixpyrrole macrocycle, termed calix[4]pyrrole, is the most thermodynamically favored product under the vast majority of reaction conditions.[1221]

Calix[4]pyrroles show preferential binding toward halides in general, and fluoride in particular, due to its small size and hydrogen-bonding capabilities. Of note, several BODIPY-tagged calix[4]pyrroles have been developed for fluoride binding and concomitant fluoride detection.[1224,1235,1236] For example, **107** (Figure 54) was found to be a selective F^- sensor as binding of the fluoride to **107** resulted in a ratiometric change in fluorescence emission.[1224] A high Stern-Volmer constant of 5.48 x 10^7 M^{-1} was established. Similar species **108** (Figure 54) was found to be less selective for F^- based on changes in the host's fluorescence properties, with fluorescence quenching observed upon binding of OAc^-, Cl^-, and $H_2SO_4^-$ in addition to quenching in the presence of F^-.[1235] However, fluoride was the only species that also produced a colorimetric change, and coupling these signal outputs led to a dual-responsive sensor that was selective for fluoride. Job's plot analysis indicated a 1:1 stoichiometry for all anions, with a Stern-Volmer constant for fluoride of 7.34 x 10^4 M^{-1} reported. All of the fluorescence studies were conducted in acetonitrile and adding water to these systems was found to release the guest from the calixpyrrole cavity. The fluorescence emission of BODIPY-tagged dicalix[4]pyrrole species **109** (Figure 54) was quenched by the presence of F^-, Cl^-, Br^-, OAc^-, and $H_2PO_4^-$, with F^- providing the greatest amount of quenching with a ca. 10 nm hypsochromic shift reported.[1236] Job's plot analysis indicated a 1:1 binding stoichiometry with all anions, indicating that a sandwich-like complex forms with the anion bound to both macrocyclic moieties.

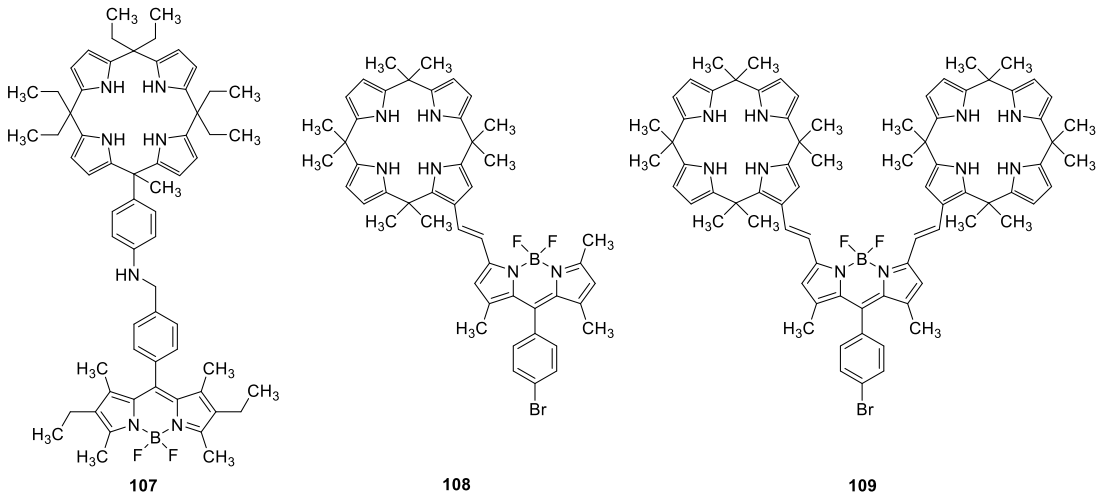

Figure 54. BODIPY-tagged calix[4]pyrroles used for the detection of fluoride anion[1224,1235,1236]

Coumarin-tagged calix[4]pyrrole **110** (Figure 55), was found, in the deprotonated form, to exist with the coumarin appendage bound inside the calix[4]pyrrole cavity, with the binding resulting in effective quenching of the coumarin fluorescence.[1225] With the addition of fluoride, which binds more strongly to the **110** cavity than the coumarin appendage the coumarin was released, leading to notable fluorescence increases. The presence of other anions did not affect the fluorescence of the host, but the introduction of lithium cation sequestered fluoride, prevented the fluoride from displacing the coumarin moiety, and led to quenching of the system fluorescence. Of note, a sensitive detection limit of 0.4 nM for fluoride was reported. Similarly, anthracene-bearing dicalix[4]pyrrole **111** (Figure 55) was found to be weakly emissive in acetonitrile until the addition of fluoride, which enhanced the emission significantly.[1237] High selectivity for fluoride was observed in this system, with a variety of other inorganic and organic mono- and multi-

anionic species having no effect on the fluorescence emission. 1:2 host-guest stoichiometry was confirmed by Job's Plot analysis and isothermal titration calorimetry, and fluorescence titration showed association constants of 1.91 x 10^5 M^{-1} for the first binding event and 5.95 x 10^7 M^{-1} for the second.

One way to achieve selectivity is through the use of steric differences between the target analyte and related structures. For example, Samanta et al. developed a series of strapped calix[4] pyrroles with very short straps, including **112**-**114** (Figure 55), with the goal of creating a binding pocket small enough to bind fluoride and no other anions.[1238] As expected, only fluoride was found to bind inside the cavities of the hosts, with no other anions causing notable spectral changes. Despite this high selectivity, **112**-**114** did not bind fluoride as well as other, larger homologues, with association constants generally an order of magnitude lower for the new hosts, suggesting that larger cavities are preferential for fluoride binding.

In contrast to the systems described above, the strong binding of fluoride to **115** (Figure 55) was used to modulate the response of the host to other analytes.[1229] The cone-shaped cavity created through binding of **115** with fluoride created an electron-rich binding pocket that was used by Lee and coworkers to bind the electron-deficient, sphere-shaped fullerene species C_{70} and C_{60}, resulting in fluorescence quenching of the host. With fluoride present, a 1:1 host-guest stoichiometry was formed between the host and either guest, and association constants were found to be 9.4 x $10^5 M^{-1}$ for C_{60} binding and 5.4 x 10^6 M^{-1} for C_{70} binding. In the absence of fluoride to modulate the cavity shape, 2:1 host-guest stoichiometries were observed with slightly lower association constants of 2.7 x 10^5 M^{-1} for C_{60} and 2.0 x 10^6 M^{-1} for C_{70}. Of note, the detection limit for C_{70} was found to be in the nanomolar range.

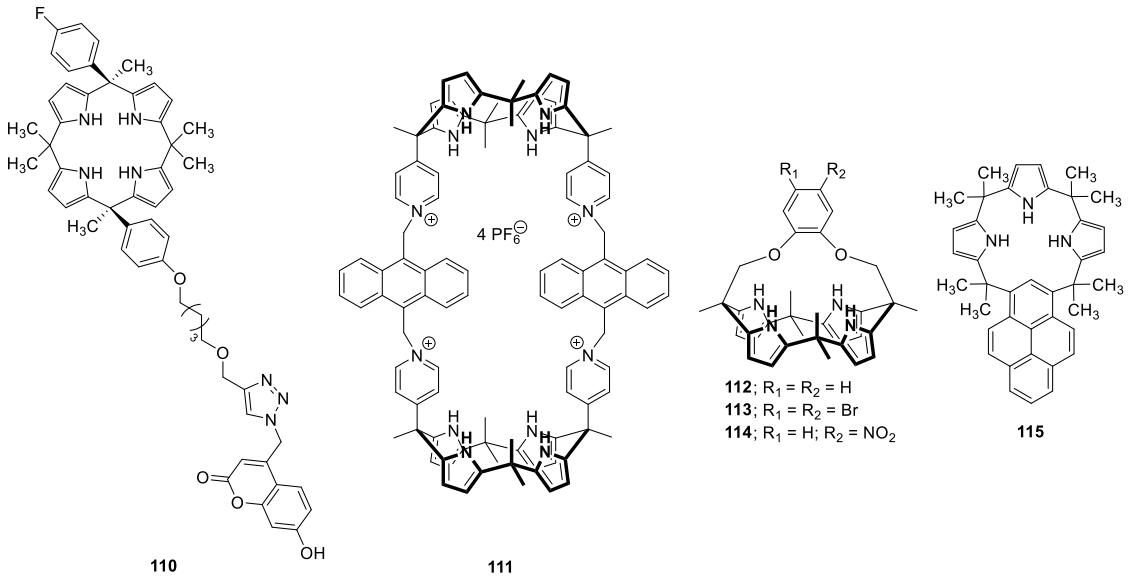

Figure 55. Calix[4]pyrrole hosts for the fluorescent detection of fluoride (**110**-**114**) or the fluoride-modulated detection of fullerenes(**115**)[1225,1229,1237,1238]

Strapped calix[4]pyrroles with pyrene fluorescent tags, **116** and **117** (Figure 56), were developed by Lee and coworkers. Upon titrating these macrocycles with anions in a 5% acetonitrile in toluene solvent system, fluorescence quenching was observed.[1233] In this instance, chloride, rather than fluoride, exhibited the strongest binding, with chloride binding to **116** and **117** with association constants of 4.9 x 10^6 M^{-1} and 4.6 x $10^6 M^{-1}$, respectively, and fluoride binding to the hosts with association constants of 3.0 x 10^6 M^{-1} with **116** and 2.7 x 10^6 M^{-1} with **117**. Competition studies were not conducted to determine whether fluoride or other anions had an effect on chloride binding and the subsequent emission quench. Naphthalene-strapped **118** and **119** (Figure 56) also bound most strongly to chloride, with association constants similar to those of **116** and **117**.[1234]

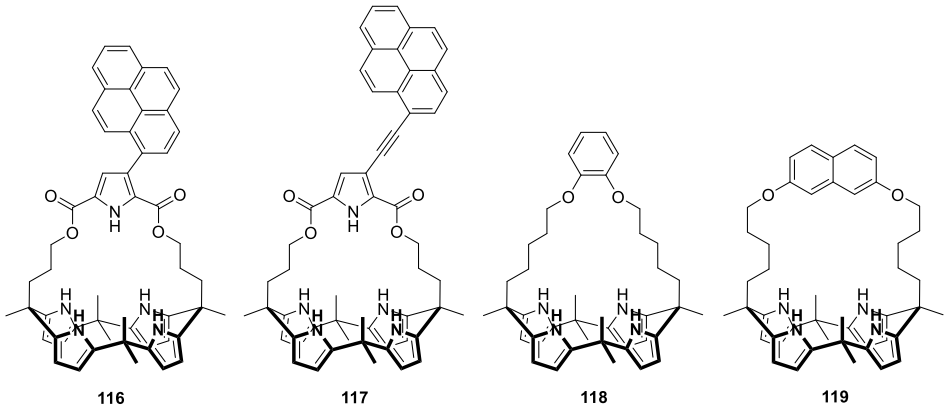

Figure 56. Fluorescent, strapped calix[4]pyrroles used for the recognition of chloride and other anions[1233,1234]

Calix[4]pyrrole **120** (Figure 57), bearing fluorescent pyrene appendages, was found to form 1:1 host-guest complexes with halides, which resulted in fluorescence quenching.[1239] Chloride bound to **120** with an association constant of 3.2 x 10^5 M^{-1}, which was only slightly higher than that of fluoride, 1.1 x 10^5 M^{-1}. Hosts **121** and **122** (Figure 57) underwent a fluorescence quench in the presence of several halides and oxoanions.[1240] Iodide was found to quench the system most effectively compared to bromide and chloride, although the effect of fluoride was not examined. Stern-Volmer constants for iodide, bromide, and chloride with **121** were found to be 3.36 x 10^2 M^{-1}, 2.28 x 10^2 M^{-1}, and 1.92 x 10^2 M^{-1}, respectively. A dye displacement assay for the detection of pyrophosphate, a biologically relevant anion, was accomplished using supramolecular complex **123** (Figure 57).[1226] The fluorescent dye, 7-hydroxy-4-(trifluoromethyl) coumarin, was quenched when held inside the calix[4]pyrrole cavity using a combination of hydrogen-bonding and cation-π interactions. Upon addition of pyrophosphate anion, the dye was released from the cavity and replaced with pyrophosphate, resulting in significant fluorescence enhancements. Good selectivity over fluoride, phosphate and other anions was found, with each of those species binding at least two orders of magnitude weaker than pyrophosphate, which had an extremely strong binding constant of 2.55 x 10^7 M^{-1} in acetonitrile. The authors hypothesize that this strong binding is facilitated through a combination of several intermolecular forces: hydrogen-bonding between the oxygen atoms of pyrophosphate and the pyrrole hydrogens; electrostatic interactions between the anion guest and pyridinium cation components of the host; and anion-pi interactions between the anionic guest and the aromatic core of the calix[4]pyrrole. Using this system, a nanomolar detection limit for pyrophosphate was obtained.

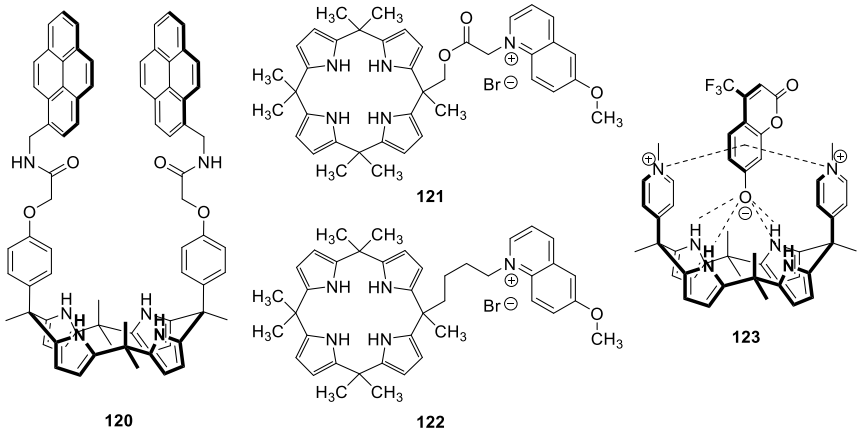

Figure 57. Calix[4]pyrroles used for the fluorescent detection of a variety of anions[1226,1239,1240]

A variety of carboxylate species, including non-steroidal anti-inflammatory drugs (NSAIDs) have been detected using calix[4]pyrroles.[1227,1228,1232,1241] A number of fluorophore-tagged calix[4]pyrroles, shown in Figure 58a, were developed by Anzenbacher and coworkers for the fluorimetric and colorimetric differentiation of 14 analytes, including six NSAIDs, several other drugs, and other biologically relevant compounds.[1228] Using the fluorescent and colorimetric responses of eight sensors to the analytes, an array-based detection scheme was developed. Principal component analysis (PCA) of the response patterns led to 95 % discrimination of analytes and linear discriminant analysis (LDA) enabled 89.4 % discrimination. When a cross-validation LDA method was used, however, 100% correct classification of the 14 analytes was achieved in both pure water and in human urine. PCA also allowed for quantitative detection of the six NSAIDs, with detection limits near 0.1 ppm and full discrimination at concentrations between 0.5 and 100 ppm, which includes typical NSAID urinary concentrations. In a later publication by the same authors, a series of fluorophore-tagged calix[4]pyrroles and hybrid, extended calixpyrroles, including those shown in Figure 58b, were used for the fluorescent detection of 18 analytes, including halides, oxoanions, carboxylates, and NSAIDs.[1232] LDA utilizing five fluorescent calixpyrroles allowed for 100 % correct classification of all analytes. Accurate quantitative recognition of oxalate, malonate, glutamate, aspartate, and phthalate was also achieved. In addition, Anzenbacher and coworkers have reported the use of poly(ether-urethane) hydrogel-encapsulated **124** (Figure 58a) for the array-based detection of several different anionic guests.[1241] Rather than using a variety of fluorescent hosts, the authors used ten different polymer matrices for the encapsulation of **124**. These matrices varied by comonomer ratio, which resulted in differences in matrix hydrophilicity, and also varied based on the environmental polarity of the hydrogel probe. LDA analysis using these hydrogels allowed for 100% correct classification of the eight anions examined and the quantitative detection of the NSAIDs ibuprofen and diclofenac, both in water and in human saliva with detection limits of 0.1 ppm obtained. Additionally, different concentrations of mixtures of chloride and phosphate were accurately quantified in human urine. A final dicarboxylate fluorescent detection scheme was reported by Gotor et al., in which BODIPY-tagged mono- and di-calix[4]pyrroles, similar to **108** and **109** (Figure 54) yet without bromine substitution on the BODIPY tag, were used for the sensing of aliphatic and aromatic carboxylates via fluorescence quenching and/or fluorescence modulation.[1227]

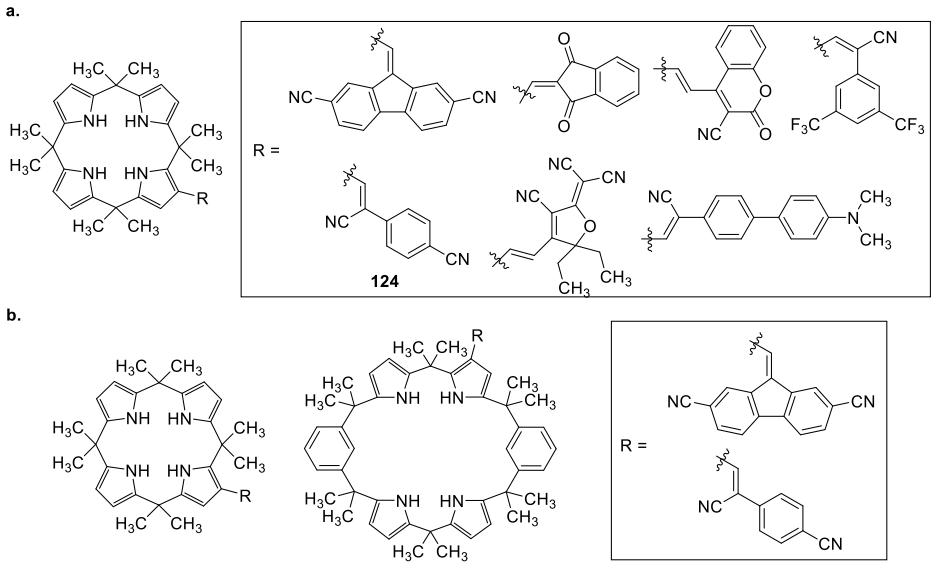

Figure 58. Calix[4]pyrroles and hybrid, extended calixpyrroles used for the array-based detection of carboxylates and NSAIDs[1228,1232,1241]

Sensing of metal cations can also be achieved using calix[4]arenes, such as those shown in Figure 59.[1242,1243,1244] Dansyl-tagged calix[4]pyrrole, **125** (Figure 59), was found to undergo fluorescence

quenching in the presence of uranium(IV), thorium(IV) and iron(III) cations in methanol solution.[1242] Additional metal cations, including alkali metals, alkaline earth metals, and other heavy metals, had no effect on the fluorescence of **125**. The authors propose that the mechanism of fluorescence quenching by cation inclusion is the disruption of ICT from the dimethylamino nitrogen to the naphthalene moiety by the presence of a metal cation. All three cations were found to bind in a 1:1 stoichiometry with binding constants of 1.90 x 10^4 M^{-1} for U^{4+}, 1.50 x 10^4 M^{-1} for Th^{4+}, and 1.40 x 10^4 M^{-1} for Fe^{3+}. Quinoline-bearing **126** (Figure 59) has been shown to bind to Cu^{2+} and Pb^{2+} with association constants of 2.42 x 10^4 M^{-1} and 2.91 x 10^4 M^{-1}, respectively.[1243] The significant fluorescence quenching observed is also hypothesized to be a result of ICT disruption of the fluorescent appendages. Despite the known affinity of calix[4]pyrroles toward anions, neither of these hosts were evaluated for anion detection applications. **127** (Figure 59), however, was found to undergo fluorescence enhancement in the presence of Cu^{2+} and Pb^{2+} with no interference from anions that were added after the initial complexation event.[1244] Association constants of the host with these species were found to be 6.6 x 10^5 M^{-1} for Cu^{2+} and 5.90 x 10^5 M^{-1} for Pb^{2+}. 1:2 host-guest binding stoichiometries identified by Job's plot analyses indicated that the metal cations were likely binding to the carbonyl groups of the fluorescent appendages, leaving the central calix[4]pyrrole cavity open to anion binding. However, addition of chloride or bromide to Pb-complexed or uncomplexed **127** resulted in no changes in fluorescence. Conversely, treatment of **127** with Cl^- before the addition of Pb^{2+} prevented the binding of Pb^{2+}, likely due to a chloride-mediated conformational change in the host.

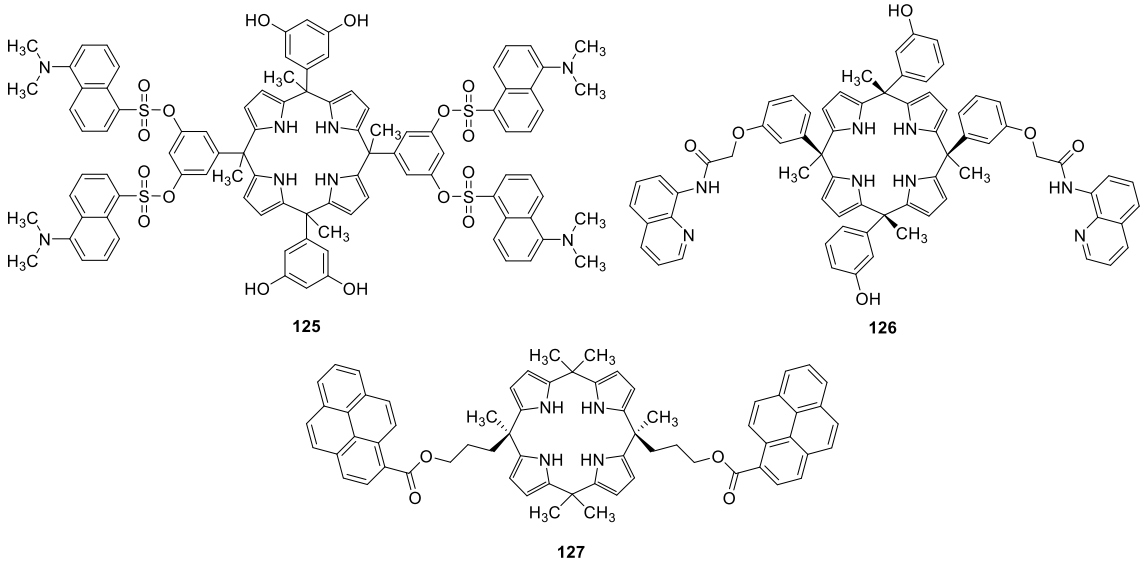

Figure 59. Calix[4]pyrroles used for the fluorescent detection of metal cations[1242-1244]

Like with **127**, while the central cavity of a calixpyrrole is generally used for anion binding, appendages can be installed on a calixpyrrole rim that allow for cation binding, resulting in multi-functional hosts for ion pair detection.[3,1245] For example, **128** (Figure 60) underwent fluorescence enhancement with the addition of iron difluoride in aqueous solution, as a result of dual binding of the cation and anions.[3] Upon addition of an Fe^{2+} source with a non-coordinating counteranion, no fluorescence enhancement was observed; similarly, no change in fluorescence occurred with the addition of F^- with a non-coordinating countercation. Thus, **128** is an efficient host for the selective detection of the FeF_2 ion pair upon the coordination of F^- to the central calix[4]pyrrole cavity and Fe^{2+} to the triazole moiety of the fluorescent appendages. Gotor et al. synthesized **129** (Figure 60), in which a calix[4]pyrrole anion-binding unit and a azo-crown ether cation-binding unit were linked together by a BODIPY fluorophore.[1245] Hypsochromic fluorescence emission shifts were observed with the addition of cations, with NH_4^+ and K^+ leading to the most significant shifts; while bathochromic shifts and quenches of fluorescence emission were observed in the presence of anions, with F^- leading to the most significant change. A three-dimensional comparison of

emission intensity, emission wavelength, and the ratio of absorbance at 680 nm and 625 nm allowed for the discrimination of nine different salts comprised of K^+, Li^+, Na^+, Cl^-, Br^-, and F^- ions. Seven zwitterionic amino acids were also examined, all of which were successfully differentiated using the same analysis. Notably, γ-butyric acid showed the most significant fluorescence response, indicating optimal matching of the distance between the host cavities with the size of the analyte.

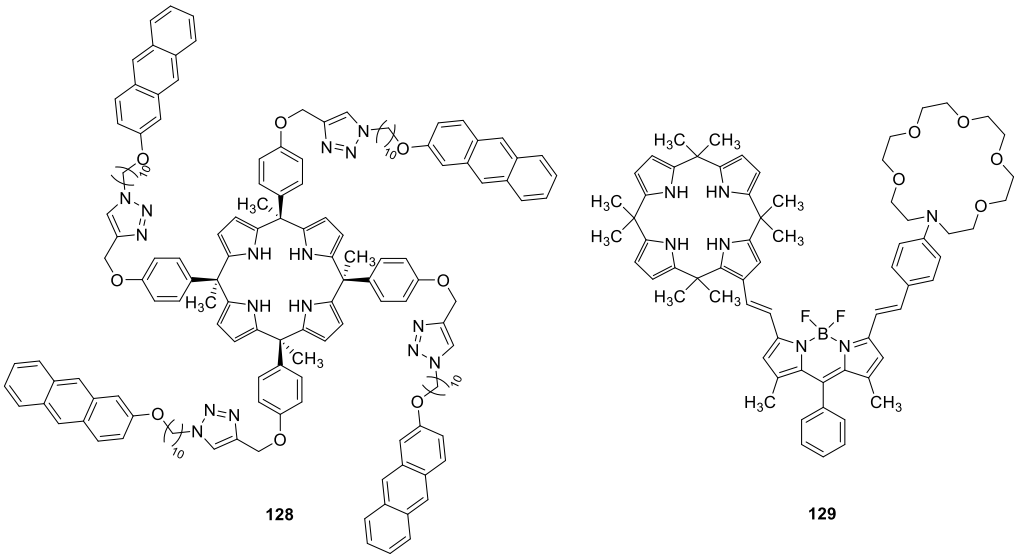

Figure 60. Calix[4]pyrroles used for the fluorescent detection of ion pairs[3,1245]

Certain calixpyrroles, shown in Figure 61, have been used for the detection of electron-deficient nitroaromatic analytes.[1230,1246,1247] Supramolecular complex **130** (Figure 61), comprised of a chloresterol-functionalized calix[4]pyrrole and a perylene bisimide diacid fluorophore was formed in solution, after treatment with ammonia resulted in diacid deprotonation.[1246] Once formed, this complex was shown to be efficient for the detection of TNT in ethanol, with a detection limit of 80 nM. The mechanism of this detection was via analyte-induced fluorescence quenching, due to the disruption of the supramolecular complex that occurred through TNT-calix[4]pyrrole association. Although some nitroaromatic species, specifically nitrobenzene and 2,5-dinitrobenzene, had no effect on the system's fluorescence, 2,4-dinitrotoluene exhibited some fluorescence quenching. Additionally, the fluorescence of a **130** film was quenched by phenol vapor, with a 1 ppb detection limit for phenol obtained. More substituted phenols were also shown to quench the system fluorescence, albeit with lower efficiencies. The fluorescence emission of hybrid calixpyrrole **131** (Figure 61) was also quenched in the presence of nitroaromatics, with 8000 equivalents of nitrobenzene and 3000 equivalents of TNT leading to a 5-fold and 10-fold quenching, respectively.[1230] A 1:1 binding stoichiometry was determined by Job's plot analysis, and the binding constant of **131** with TNT was found to be 1.1 x 10^6 M^{-1}. In a final example, oligomeric supramolecular complexes formed from calix[4]pyrrole **132** and fluorophore **133** (Figure 61) were used to detect trinitrobenzene.[1247] Upon oligomer formation, the fluorescence of **133** was quenched; subsequent addition of trinitrobenzene disrupted the supramolecular aggregates, resulting in restoration of the **133** fluorescence emission. Because aggregation is highly dependent on the concentration of the aggregating species, significant fluorescence enhancement was only seen with high concentrations of **132** and **133** that formed effective aggregates.

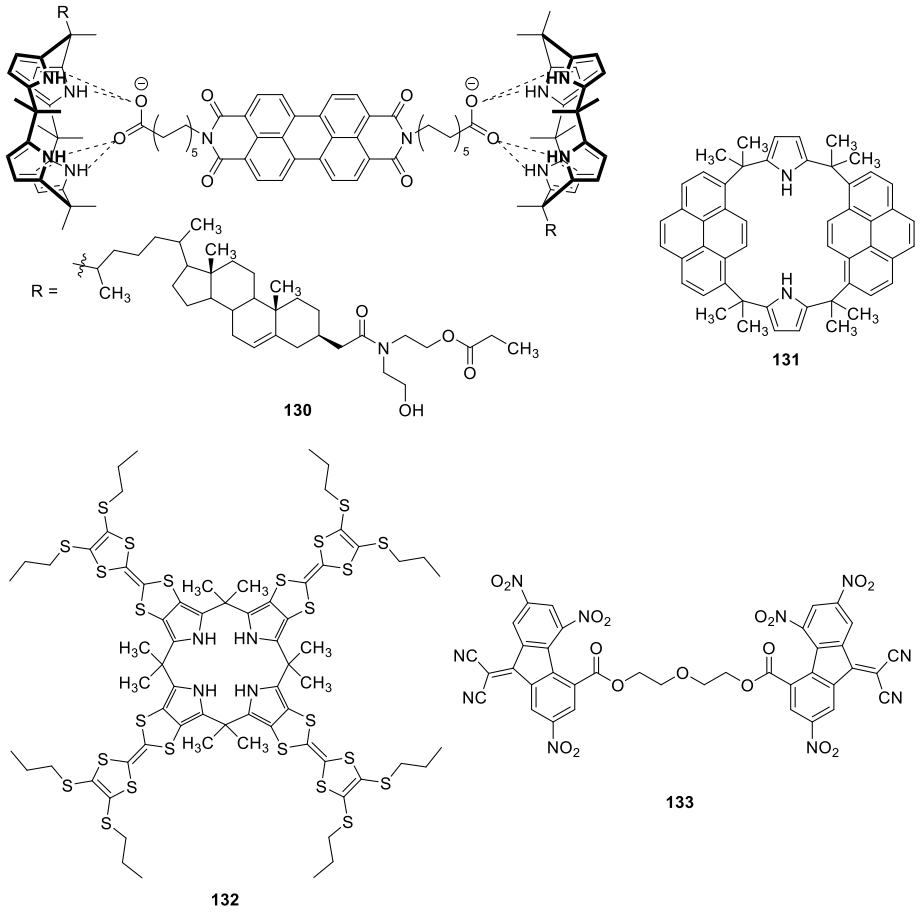

Figure 61. Calixpyrroles used for the fluorescent detection of nitroaromatics[1230,1246,1247]

5.1.8. Pillar[*n*]arenes. Pillar[*n*]arenes are a recently developed class of macrocycles, first reported by Ogoshi and coworkers in 2008,[1248] which are generally formed through the facile and versatile condensation of phenols with paraformaldehyde.[1249] Pillararenes are structurally similar to calixarenes, with both composed of aromatic repeating units, with the former having methylene bridges at the 2 and 5 positions of the repeat unit, and the latter bound at the 1 and 3 positions of the aromatic rings. Thus, whereas calixarenes are characterized by a wide upper rim and narrow lower rim, leading to a basket-like shape, the rims of traditional pillararenes are identical, allowing for a rigid, pillar-shaped cavity.[48] Pillararenes have been employed as supramolecular hosts for the encapsulation of a variety of guests, with such binding promoted by charge-transfer interactions, cation-π interactions, hydrophobic/hydrophilic interactions, electrostatic interactions or hydrogen bonding.[1249] More complex architectures have been formed from pillararenes, including self-inclusion complexes,[1250,1251] rotaxanes,[1252-1254] polyrotaxanes,[1255,1256] catenanes,[1257,1258] micelles,[1259] microtubes,[1260] liquid crystals,[1261,1262] and metal organic frameworks (MOFs).[1263]

Metal cations are common analytes for pillararene-based detection, and a number of modified pillararenes have been employed in such schemes in recent years. In one example, Yao et al. encapsulated a fluorescent dye, perylene diimide, in the cavity of **134** (Figure 62), leading to quenching of the dye emission through a PET mechanism.[1264] The PET was disrupted by the addition of Fe^{3+}, which led to an almost 100-fold increase in emission. Among all cations investigated, only Fe^{3+} was found to enhance the fluorescence emission of the system, leading to a detection limit of 0.21 μM. Although researchers reported that sodium pyrophosphate could sequester Fe^{3+} and "turn-off" the fluorescent probe, comparative

behaviors of other anions were not reported, and competition experiments with other metal cations were not conducted.

Zhang, Wei, and coworkers provided two additional schemes for the detection of Fe^{3+} by pillararene complexation. In the first example, fluorescent pillararene **135** (Figure 62) was synthesized, which displayed strong fluorescence in the absence of guest due to binding of the covalently appended benzothiazole unit in its own hydrophobic cavity.[1265] Introduction of Fe^{3+} led to its binding inside the cavity of **135**, displacing the benzothiazole moiety and quenching the macrocycle's fluorescence. A detection limit of 0.90 μM was found, and of all other metal cations examined, only Hg^{2+} also led to fluorescence quenching. Competition experiments showed little effect on the quenching ability of Fe^{3+} in the presence of 1 equivalent of a second metal cation. The addition of F^- regenerates the emission profile of **135**, with a fluoride detection limit of 26 nM. Other anions led to moderate fluorescence enhancement, and competition experiments revealed that the effect of F^- was altered somewhat in the presence of other species. Similarly, **136** (Figure 62) was found to complex both Fe^{3+} and Cu^{2+} with a detection limit for iron of 0.14 μM.[1266] The Fe^{3+}-**136** adduct was then used to detect F^- at concentrations as low as 0.25 μM. Other transition metal-**136** complexes did not have a pronounced affinity for F^-, and the iron complex was only moderately selective for fluoride over other anions.

Thorium was detected using **137** (Figure 62), with selectivity over a variety of other metals, including lanthanides, actinides, transition metals, and base metals, as reported by Fang et al.[1267] Upon the addition of one equivalent of Th^{4+} to **137**, the emission of the macrocycle was almost completely quenched. In the presence of 10 equivalents of potentially interfering metal cations, no disruption of the quenching was observed. Similar to previously discussed systems, the addition of fluoride sequestered the heavy metal, allowing the fluorescence of **137** to be regenerated, even in the presence of 100 equivalents of competing anion. Detection limits of 0.54 μM and 3.0 μM were observed for Th^{4+} and F^-, respectively.

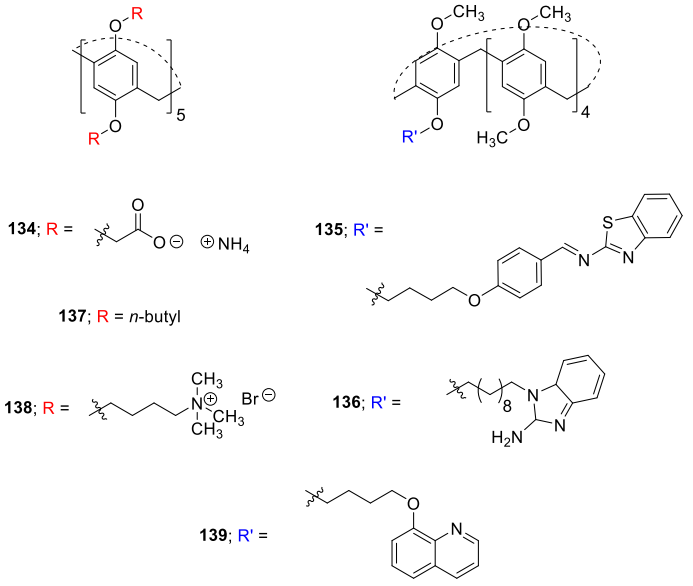

Figure 62. A series of pillararenes that have been reported for the detection of metal cations[1264-1269]

A 1:2 supramolecular complex of **138** (Figure 62) and fluorophore **140** (Figure 63) was employed by Wei and coworkers for the sequential detection of Al^{3+} and CN^- in aqueous media.[1268] Fluorescence enhancement unique to Al^{3+} was seen, with a detection limit of 99 nM. Notably, the addition of CN^- to the **138**-**140**-Al^{3+} system did not sequester the Al^{3+} and decrease the fluorescence, as with the aforementioned dual-detection systems, but instead led to another significant emission enhancement. The authors attribute emission enhancement to the formation of a highly fluorescent 1:2:1:1 **138**-**140**-Al^{3+}-CN^- quaternary complex. The further addition of Al^{3+} equivalents, however, re-formed the **138**-**140**-Al^{3+} complex, thus

regenerating its emission profile, allowing for reversible switching between the moderately and highly fluorescence states. No other anion was found to produce a response similar to that of CN^-, nor were any found to quench the emission of the **138**-**140**-Al^{3+} complex. Furthermore, a detection limit of 2.3 μM was found for CN^-. The group also discovered that **139** could be used for the detection of CN^-,[1269] where the addition of CN^- to the macrocycle led to a significant fluorescence enhancement along with a bathochromic shift that was unique to the presence of CN^-. Although no other anion caused enhancement of the fluorescence of **139** (Figure 62), a variety of anions, including F^-, AcO^-, $H_2PO_4^-$, HSO_4^-, as well as Ca^{2+}, interfered with the enhancement ability of CN^- and led to less fluorescence enhancement. A CN^- detection limit of 10.8 nM was observed, and the system maintained detection efficacy in a complex system, namely the detection of CN^- in sprouting potatoes. Compound **134** (Figure 62) was also used for both the detection of cyanide and of paraquat, an herbicide, as reported by Wang et al.[559] At pH 7.4, paraquat was found to displace *N*-methylacridinium iodide, a fluorophore, from the cavity of **134**, leading to significant emission enhancement. Of note, other substrates were not examined and so the detection selectivity could not be determined. When the solution was acidified to pH 6.0, protonation of the carboxylic acid pendant arms of the macrocycle led to the displacement of the acridinium dye. In this uncomplexed form, the dye readily reacted with CN^- and water, leading to oxidation in the 9-position of the molecule and a consequent fluorescence quench and hypsochromic shift in emission, allowing for the detection of CN^-.

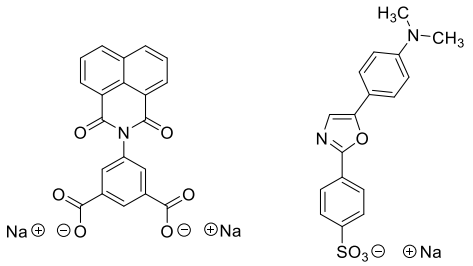

140 **141**

Figure 63. Novel fluorophores that have been used in pillararene-based detection schemes[1268,1273]

Wang et al. synthesized a dissymmetric pillararene that spontaneously formed fluorescent daisy chains in solution, leading to the application of the material as a fluorescent chemosensor for temperature, pH, solvent, and the presence of certain anions (Figure 64).[1270] Cation-π interactions between the ammonium and anthracene moiety governed the formation of the fluorescent daisy chains, thus changes in pH and subsequent deprotonation of the ammonium to form an amine led to decomplexation and fluorescence quenching. Moreover, because cation-π interactions are much weaker in polar solvents than in non-polar solvents, daisy chain formation was also solvent dependent. Anions were hypothesized to form ion pairs with the ammonium cation, blocking the cation from interactions with the anthracene and providing a mechanism for anion detection. Finally, heat was found to lead to decomplexation of the daisy chain and fluorescence quenching, by reducing the binding affinities of the macrocycles to one another. Of note, all of these supramolecular interactions were found to be reversible.

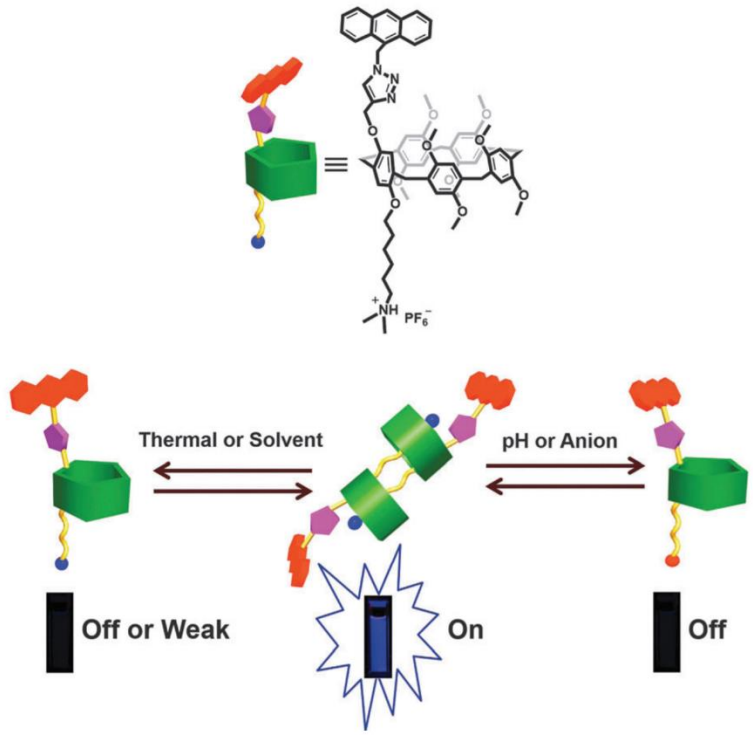

Figure 64. A pillararene daisy chain and its responses to temperature, solvent, pH, and the presence of anions. Adapted with permission from Ref. 1270. Copyright 2014 Royal Society of Chemistry.

Certain biologically relevant molecules have also been sensed by pillararene constructs in recent years. For example, L-tryptophan[1271] and L-methionine[1272] were detected by Wei and coworkers with hosts **142** (Figure 65) and **138** (Figure 62), respectively. In the former case, all 20 naturally-occurring amino acids were investigated, and only L-tryptophan successfully quenched the emission of **142**.[1271] A limit of detection of 0.28 μM was found, and competition experiments showed that the system was highly selective for L-tryptophan. Additionally, glass slides were dip-coated in a solution of **142**, and treatment of the dried slide with a solution of the analyte led to a noticeable quenching of fluorescence under a UV lamp. The detection of L-methionine with **138** was less selective than with **142**, with only 0.20 equivalents of interfering amino acids leading to significant decreases in the emission enhancement induced by L-methionine.[1272] The detection limit of L-methionine was 0.55 μM when no interfering species were present, and increased to 2.0 μM in the presence of 10 equivalents of histidine.

Host **143** (Figure 65) was found to be selective for the detection of ATP via the ATP-induced displacement of fluorophore **141** (Figure 63).[1273] ATP bound strongly to **143**, with an association constant an order of magnitude higher than GTP, ADP, and AMP, allowing for a much greater fluorescence quenching by the target analyte compared to other structurally similar substances. While these reported results were promising, competition experiments were not conducted, and a detection limit was not calculated. In another example, Hua et al. realized the ability of **134** (Figure 62) as a probe of enzymatic activity.[549] In this system, choline bound strongly in the cavity of **134**, displacing a previously encapsulated fluorophore, acridine orange, which resulted in an increased emission. By monitoring this fluorescence, the activity of the enzyme choline oxidase was measured via the enzymatic-induced transformation of the choline reactant into a betaine product, which does not bind in the **134** cavity.

144 (Figure 65) was shown by Hua et al. to encapsulate salicylaldehyde, promoting deprotonation of the guest and leading to a highly fluorescent supramolecular complex.[1274] Salicylaldehyde could then be displaced by chlorophenols, which are ubiquitous, toxic environmental contaminants. While mono- and di-chlorophenols were found to decrease the emission of the complex somewhat by binding in the cavity and

displacing salicylaldehyde, 2,4,6-trichlorophenol quenched the emission of the host-dye complex to the largest extent, most likely due to a binding constant two orders of magnitude higher than salicylaldehyde and the other guests. A final report by Strutt et al. described the synthesis of **145** (Figure 65) and its application in the detection of moderately toxic alkyldiamines via fluorescence quenching.[1252]

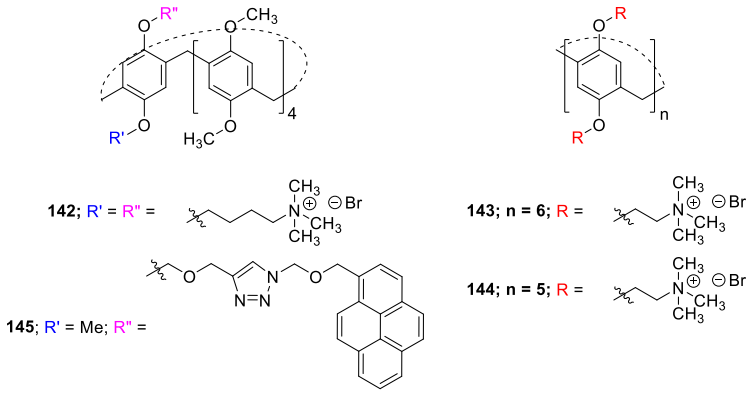

Figure 65. A series of pillararenes that have been used as scaffolds for detection schemes[1252,1271,1273,1274]

5.1.9. Cucurbiturils. Cucurbiturils, or CBs,[1275,1276] are pumpkin-shaped structures (cucurbituril is derived from the Latin word for "pumpkin"), and three of the most common cucurbituril architectures are shown in Figure 66, below.[1277,1278] Unlike cyclodextrins, cucurbiturils are not naturally occurring, and their syntheses can involve relatively harsh conditions,[985] typically involving a condensation reaction between glycouril and formaldehyde. [1279] The interior cavities of cucurbiturils are hydrophobic, much like the cyclodextrin hydrophobic cavities, but there are two main differences when comparing these classes of macrocycles: First, cucurbiturils are much more rigid structures, and their binding affinities for small molecule guests are much stronger.[1280] Cyclodextrin binding affinities for small molecule guests usually have binding constants between 100 and 1000 M^{-1}. Cucurbiturils, by contrast, can have binding affinities as high as 10^{14} or 10^{15} M^{-1},[1,1281,1282] which rivals the binding of avidin and biotin, which is among the strongest interactions known.[1283,1284] Secondly, cucurbiturils have a ring of carbonyls pointed at each entrance to the cavity.[1285-1287] These carbonyls are polarized to have negative electron charge density, and therefore cucurbiturils are much stronger cation binders than are cyclodextrins. Cucurbiturils show the strongest binding affinities in cases where they can bind molecules that are both cationic (in one portion),[1288] and hydrophobic (in a different portion),[1289] such as biogenic amines,[1290] which take full advantage of the structural features of the cucurbiturils.

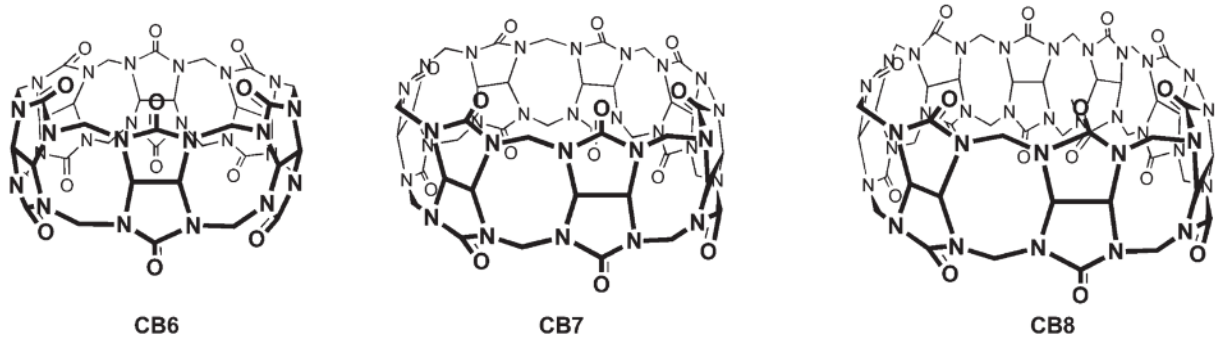

Figure 66. The most common cucurbituril architectures, CB6, CB7, and CB8. Reproduced from Ref. 1277. Copyright 2011 American Chemical Society.

Applications of cucurbiturils as chemosensors have emerged in recent years, with many examples of cucurbiturils used for the detection of over-the-counter (OTC) or prescription drugs, pesticides and toxicants. One example by Anzenbacher and coworkers used CB derivative **146** and acyclic analogue **147**

(Figure 67) for the detection of addictive OTC drugs, such as doxylamine, pseudoephedrine, and phenylephrine, that are found in common cold and flu medications such as NyQuil and Sudafed.[1291] Each analyte provided a unique fluorescence quench or enhancement, with the enhanced fluorescence a result of rigidification of the photophysically active moieties and elimination of undesired non-radiative decay pathways. Linear discriminant analyses (LDA) of the response patterns allowed for the 100% correct classification of individual analytes as well as three component mixtures of doxylamine, pseudoephedrine, and phenylephrine at a variety of concentrations. The calculated detection limits of doxylamine, pseudoephedrine, and phenylephrine were 1.0 ppm, 0.7 ppm, and 0.8 ppm, respectively, and doxylamine was accurately detected in undoped and doped human urine samples. Notably, fluctuations of electrolyte levels in solution had no effect on the detection ability of the system.

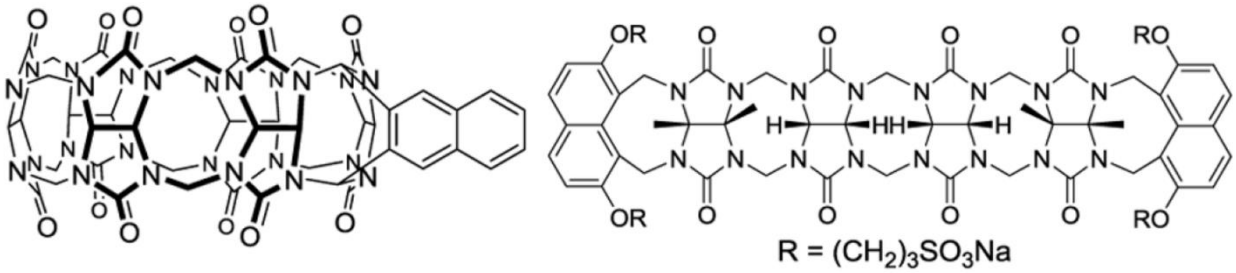

146 **147**

Figure 67. CB6 derivative **146** and acyclic derivative **147** used by Anzenbacher for the detection of over-the-counter drugs. Adapted from Ref. 1291. Copyright 2013 American Chemical Society.

Amantadine, a drug for the treatment of Parkinson's disease, was successfully detected by del Pozo et al.[1292] and Yang et al.[1293] In the former report, fluorescent dye thionine was displaced from the cavity of CB7 or CB8 by adamantadine, leading to a decrease in fluorescence for the CB7 host and an increase in fluorescence for the CB8 host.[1292] Structurally similar drugs rimantadine, ribavirine, and acyclovir, were examined, and only rimantadine was found to lead to perturbations of the CB/dye emission spectra; allowable concentrations of the potential interferents were found to be 4.5 nM, 36 μM, and 3.6 μM, respectively. A detection limit of 0.16 μM was found and the system was then applied to doped human serum samples and pharmaceutical capsules containing adamantadine with high accuracy. Notably, the binding studies occurred in a flow reactor with the analyte and host mixing in flow before being analyzed by the detector, which facilitated quick and automated results. The report by Yang et al. utilized CB7 with a different fluorophore, 1,1'-butane(1,4-diyl)bis(2-aminopyridine)bromide (DPAD), for the detection of adamantadine by fluorescence quenching.[1293] A very high binding constant of 4.23×10^{12} M^{-1} was reported,[1294] which allowed for the low analyte detection limit, 1.3 μM, and moderate selectivity observed.

An assay of CB7 with three fluorophores, palmatine, berberine, and coptisine, was used by Li and coworkers for the detection of both labetalol hydrochloride,[1295] a performance-enhancing drug, and dibucaine,[1296] a cocaine-related local anesthetic. Labetalol hydrochloride was detected with limits ranging from 4.9 nM to 12.0 nM,[1295] and dibucaine was detected with limits of 6.0 nM to 25.0 nM.[1296] In both instances, common components of urine were analyzed as potential system interferents, and it was found that only the amino acids cysteine, alanine, phenylalanine, and valine led to any quenching of the system. Of note, although the same system was used to test both dibucaine and labetalol hydrochloride, the analytes were not compared against one another.

Aryal and coworkers found that certain therapeutic drugs were able to displace a naphthalimide-derived dye from the cavity of CB7 leading to an observed quench in the fluorescence emission signal.[1297] The therapeutic drugs *N*-(aminophenyl)-piperidine, doxorubicin, and adamantyl-carboxamido-benzenesulfonamide all exhibited high affinity for CB7, with association constants of 1.0×10^7 M^{-1}, 2.5×10^6 M^{-1}, and 1.3×10^9 M^{-1}, respectively. Competition studies between the wide array of analytes were not conducted, and no method was employed for the discrimination of one analyte from another. In a report by

Lazer et al., displacement of a fluorescent dye (perylene diimide, berberine chloride, or methylene blue) from the cavity of CB8 was caused by a number of steroids, allowing for effective steroid detection.[1298] Strong binding constants between 10^5 and 10^9 M^{-1} were found for the steroid analytes, and the steroids could be detected at low micromolar concentrations. LDA analysis enabled the successful differentiation of 10 of the 12 steroids examined, and the assay was used to monitor the activity of steroid-producing enzymes.

Two reports of the detection of pesticides and fungicides by CB encapsulation were reported by Huang and coworkers in recent years. In the first report, three different cucurbiturils, CB6, CB7, and tetramethyl-CB6 were screened as potential sensors for the fungicide thiabendazole.[1299] Upon encapsulation of thiabendazole by a cucurbituril, its fluorescence was enhanced, enabling low nanomolar limits of detection for this toxic pesticide. In 2018, the group published the use of a pyronine Y-CB8 supramolecular complex for the detection of thiabendazole, fuberidazole, and carbendazim.[526] Initially, a weakly fluorescent 1:2 host-dye complex formed, from which one of the two pyronine Y molecules was displaced upon introduction of the analyte. A ternary complex between the host, dye, and analyte was formed that exhibited a large increase in fluorescence emission along with a slight bathochromic shift. Detection limits of approximately 100 nM were calculated, and it was found that other pesticides, including paraquat and tritconazole, did not show the same fluorescence-increasing behavior. The host-dye complex had low cytotoxicity, and was used to detect exogenous thiabendazole, fuberidazole, and carbendazim in PC3 cells. A similar report by del Pozo et al. also described the detection of carbendazim by encapsulation with CB7.[1300] Detection and quantification limits of 5.0 nM and 26 nM were observed, and the technique was applied to the sensing of carbendazim in orange peels.

Compounds **146** and **147** (Figure 67) were again used by Anzenbacher and coworkers, this time for the detection of the toxic nitrosamines *N*-nitrosonornicotine and (4-methylnitrosamino)-1-(3-pyridul)-1-butanone, along with a range of other toxicants.[1301] In this report, the cyclic and acyclic analogues were first complexed with metal cations, including Zn^{2+}, Eu^{3+}, Yb^{3+}, and Hg^{2+}, which were subsequently displaced by the analytes of interest, resulting in appreciable changes in fluorescence emission. The authors use statistical analyses of the differences in the signal responses of **146**, heavy metal-containing **146**, and acyclic analogue **147** to each analyte to create array-based detection schemes. LDA allowed for 100% classification of all 12 guests, and a support vector machine (SVM) regression method allowed for quantification of analytes, even in the presence of nicotine, which was a strong interferent. Detection limits of *N*-nitrosonornicotine and (4-methylnitrosamino)-1-(3-pyridul)-1-butanone were found to be 0.05 ppm and 0.27 ppm, respectively.

Cucurbiturils have been employed for the detection of biologically relevant molecules, including the detection of cadaverine, a naturally occuring toxic diamine, by Wang et al.[1302] In this system, the addition of cadaverine to a highly fluorescent supramolecular complex of CB7 with acridine orange led to the displacement of the dye and a subsequent decrease in fluorescence. The activity of lysine decarboxylase, which converts lysine into cadaverine, was monitored by observing the differential fluorescence responses of the enzymatic reactant and its product. The presence of lysine did not affect the fluorescence intensity of the system as lysine cannot displace the fluorophore from the host cavity. As lysine was converted to cadaverine, the system fluorescence decreased accordingly as acridine orange was displaced. The inhibition of the enzyme by several organophosphate esters was examined using this system. Enzyme inhibition was monitored in a similar manner by Biedermann et al. where a fluorophore, either MDAP+ or perylene diimide, was displaced from the cavity of CB8 by an analyte that was either a substrate or product of an enzymatic reaction.[1303] The key for this detection to be successful was that the substrate and product need to have complementary association constants, meaning that one species will bind preferentially to the macrocyclic cavity whereas the other species will not, resulting in differential response signals.

Ye et al. synthesized a modified bispyridinium fluorene, **148** (Figure 68), which acted as a fluorescent guest for CB8 encapsulation and enabled ATP detection.[1304] The long chain fluorophore threaded through the CB8 cavity, and the authors hypothesize that electrostatic interactions between the positively charged fluorophore and negatively charged ATP induced aggregation of the supramolecular complex, which led to

a decrease in fluorescence emission. ADP, AMP, and carbonate were also found to quench the emission of the supramolecular host, and all other anions led to negligible changes in emission.

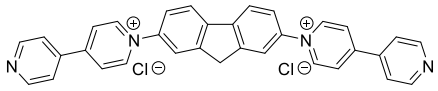

148

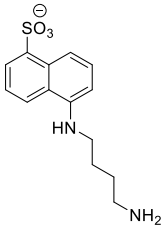

149

Figure 68. Novel fluorophores that have been involved in cucurbituril-based detection schemes[1304,922]

Synthetically accessible twisted CB14[1305] (Figure 69) was used by Zhang et al. for the detection of metal cations.[1306] In this scheme, thiazole orange was encapsulated in CB14, and the additions of Ba^{2+} and Pb^{2+} led to a decrease in the fluorescence and hypsochromic shift of emission signal. Conversely, the addition of one equivalent of Hg^{2+} led to an increase in emission, and further Hg^{2+} aliquots led to fluorescence quenching. The authors hypothesized that in the presence of one equivalent or less of mercury, a highly fluorescent ternary complex was formed, whereas at higher concentrations of the analyte, binary Hg-CB14 and Hg-thiazole orange complexes were formed, both of which are minimally fluorescent. The detection limit of Hg^{2+} at neutral pH was found to be 78 nM, with only Ba^{2+} and Pb^{2+} disturbing the emission profile. Notably, in acidic media, Hg^{2+} does not increase emission, and only Ba^{2+} and Pb^{2+} were shown to affect the CB14-thiazole orange complex, again leading to decreases and hypsochromic shifts in emission. Under these conditions, the detection limits of Ba^{2+} and Pb^{2+} were found to be 0.46 μM and 3.6 μM, respectively.

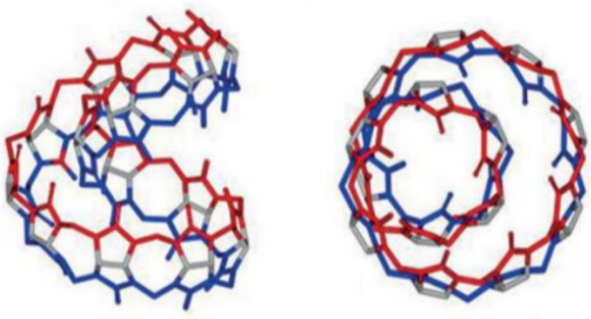

Figure 69. Side (left) and top (right) view of twisted CB14 that was used by Zhang et al. for the detection of metal cations.[1306] Reproduced with permission from Ref. 1305. Copyright 2013 Wiley.

Sinha et al. were able to sense copper ions via displacement of 4-aminobipyridine from the cavity of CB6.[1307] The fluorescence quenching observed was readily reversed by the addition of EDTA to sequester the metal cation. CB6 was also used to monitor enzymatic reactions in which 4-aminobipyridine was produced, due to the significant fluorescence of the 4-aminobipyridine-CB6 complex. A final notable example of the applicability of CB sensors was the detection of hydrocarbon gases encapsulated by CB6, published by Florea et al. (Figure 70).[922] Volatile hydrocarbons, such as isobutane and cyclopentane, bound strongly to CB6, with association constants on the order of 10^6 M^{-1}. In acidic aqueous solution with hydrocarbon gas bubbled through, fluorescent dye **149** (Figure 68) was displaced from the cavity of CB6 by the hydrocarbon, leading to a drastic decrease in the dye emission. Upon bubbling air into the solution,

the hydrocarbon was released, and the dye reentered the CB6 cavity, allowing the restoration of fluorescence. This cycle could be repeated several times without a loss of efficiency. Notably, non-hydrocarbon gases Ar, Kr, and N_2 did not bind in CB6.

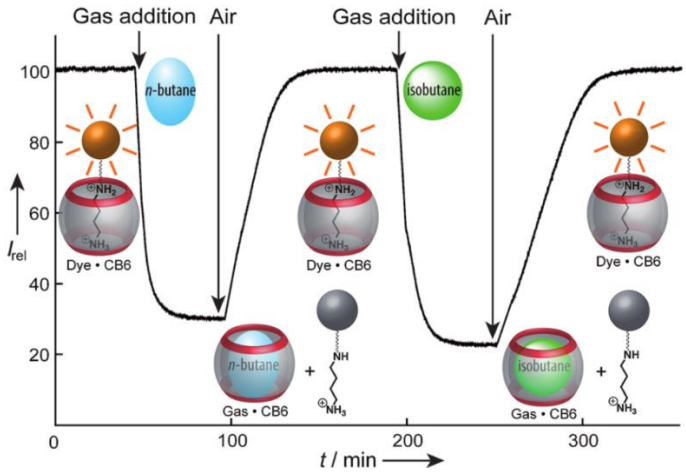

Figure 70. Illustration of the ability of CB6 to capture hydrocarbon gases and provide an emission response via analyte-induced dye displacement. Reproduced with permission from Ref. 922. Copyright 2011 Wiley.

5.2. Cryptands

Cryptands are cyclic molecules comprised of ether, amine, or thiol units. Crown ethers, first developed by Charles J. Pederson in 1967, may be the most well-known cryptand class.[1308-1310] The ability of these species to coordinate to alkali and alkaline earth metals, which are normally difficult to separate from solution and differentiate from each other, has allowed for the solubilization, complexation, and detection of such cations.[1311] One notable early example of such coordination was the 18-crown-6-ether-mediated dissolution of $KMnO_4$ in benzene, allowing for the oxidation of organic species using the $KMnO_4$-dissolved species.[1312] The discovery of crown ethers is widely acknowledge to have brought about the advent of supramolecular host-guest chemistry as it is known today,[1313,1314,1311] and had led to the use of a variety of cryptand-like structures for detection applications.[1315]

While crown ethers are characterized as being cyclic, oxygen-containing macrocycles that coordinate to hard metals, the development of "hetero crown ethers," containing nitrogen or sulfur moieties, has expanded this field for the coordination of softer metal cations that coordinate to nitrogen and/or sulfur preferentially.[1316] In one example, cyclens and tacns (1,4,7-triazacyclononanes), containing nitrogen coordination nodes (see Figure 80 in section **5.2.3**), coordinate to a variety of transition-, lanthanide-, and actinide metals.[1316] These polyamines are easily functionalized at nitrogen, with very versatile syntheses allowing for the fine-tuning of macrocycle selectivity and photophysical activity. Furthermore, nitrogen-containing crown structures can readily mimic metal binding that occurs in biological systems between nitrogen-containing enzymes and metal cation cofactors.[1317] A popular application of cyclens, is as MRI contrast agents,[1318] in which the chelation of lanthanide metal ions in the crown cavity produces strong luminescence, without allowing for the leaching of the lanthanide metal into biological systems.[1319] Like nitrogen-containing crowns, the use of sulfur-containing crowns allows for the selective binding of softer metals than traditional crowns allow.[1320] In many instances, combinations of oxygen, nitrogen, and sulfur binding nodes are employed for the selective binding of desired metal species (vide infra).[314,1321]

5.2.1. Crown Ethers. Several fluorescence detection schemes utilizing crown ethers have been used to detect alkali and alkaline earth metals. The emission of the macrocycle shown in Figure 71, was shown by Sinn et al. to exhibit a significant hypsochromic shift in the presence of K^+.[316] The hypothesized mechanism for the hypsochromic shift is that the luminescent platinum-containing pendant arms aggregate in the absence of K^+, leading to an excimer emission peak at 585 nm. The aggregation was disrupted by

complexation with K^+, causing a decrease in excimer emission and reemergence of monomer emission at 464 nm, allowing for ratiometric sensing and an overall hypsochromic shift.

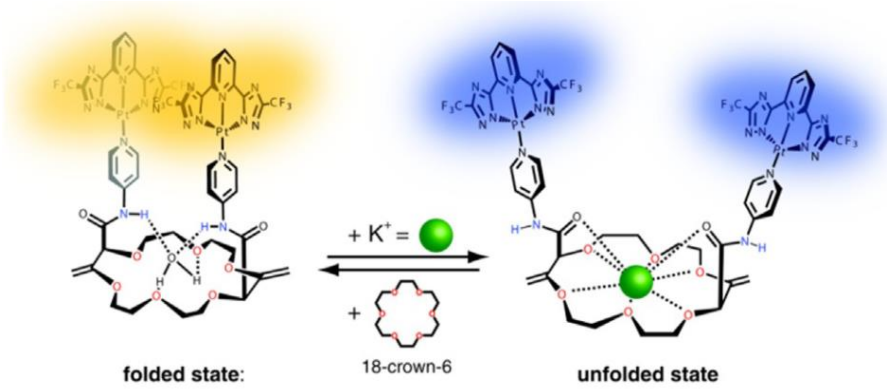

Figure 71. A crown ether with luminescent platinum-containing pendant arms used for potassium detection by Sinn et al. Reproduced with permission from Ref. 316. Copyright 2015 Elsevier.

Hosts **150** and **151** (Figure 72) were found by Li et al.[1322] and Safin et al.,[1323] respectively, to detect the presence of K^+ only after an initial binding event with Zn^{2+}. Compound **150** bears two bispyridyl binding sites distal to the central crown ether that acts as the zinc binding site.[1322] A ratiometric change in emission along with an increase in quantum yield from 0.36 to 0.75 was observed upon the formation of the 1:2 host-Zn^{2+} complex. The addition of the K^+ analyte to the ternary species led to the near-full quenching of excimer emission that was not seen when adding K^+ to free **150**. The authors hypothesized that the detection ability of the host toward Zn^{2+} was derived from ICT, whereas the fluorescence response to K^+ was due to the disruption of PET between the aromatic fluorophores. Upon addition of Zn^{2+} to **151**, a 2:1 host-guest complex was formed, with zinc ligating to the imine and phenol moieties of both hosts. As a result of such binding, the quantum yield of the complex increased from 0.1% to 23.7% and the emission had a slight bathochromic shift.[1323] The crown ether portions of the hosts then bound to K^+, and the solution fluorescence decreased as K^+-induced aggregates precipitated from solution. Compounds **152**[1324] and **153**,[1325] shown in Figure 72, both bearing two crown ether units linked to a central fluorophore, formed 1:2 host-guest complexes with potassium. These methods were not fully selective, however, as the emission of **152** increased in the presence of Rb^+ as well as K^+,[1324] and the emission of **153** increased when complexed with either K^+ or Pb^{2+}.[1325] Coumarin-appended crown ethers **154** and **155** (Figure 72) underwent hypsochromic shifts in emission when treated with Na^+, potentially due to disruption of PET; however, no other cations were investigated and so selectivity could not be ascertained.[1326] Alkaline earth metal barium was found to promote a noticeable fluorescence enhancement upon complexation with **156** (Figure 72).[1327] While no other cation produced the same response as Ba^{2+}, many cations interfered with Ba^{2+}-promoted fluorescence; potassium, which is known to bind crown ethers most strongly, was not examined.

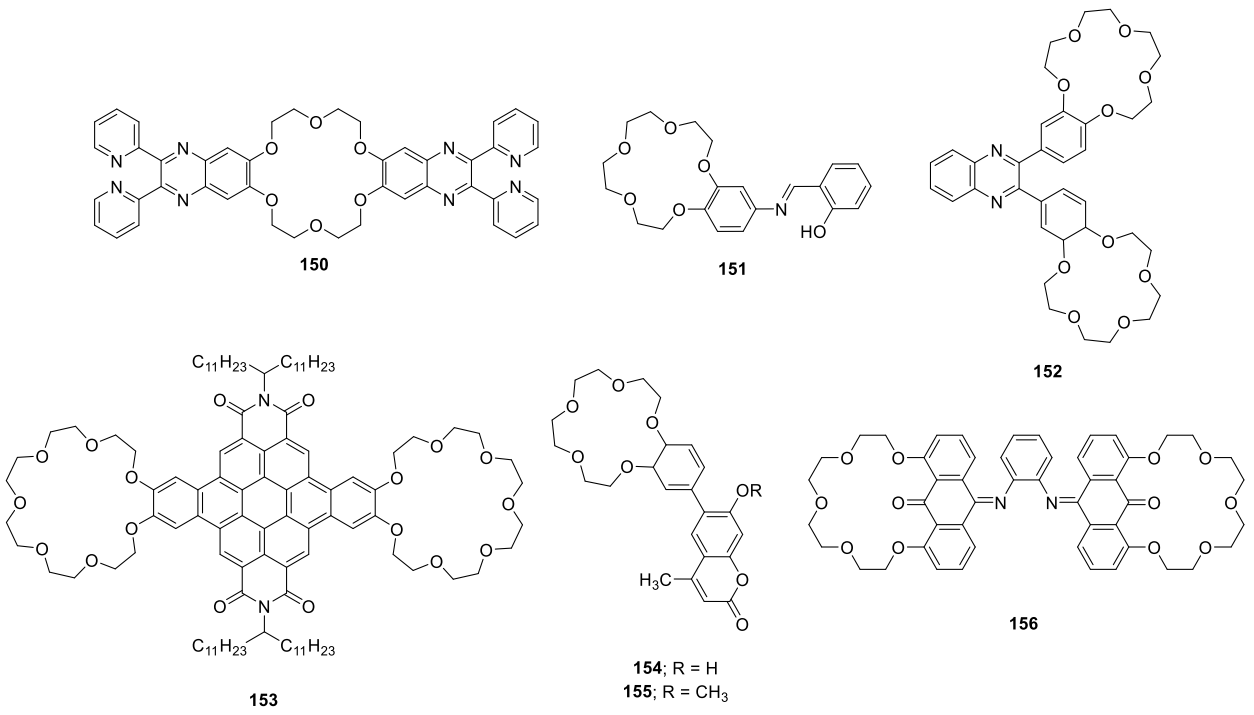

Figure 72. Modified crown ethers that have been used for the detection of alkali or alkaline earth metals[1322-1326]

Transition metals have also been detected using modified crown ethers. Azo dye-appended **157** (Figure 73) bound to Hg^{2+} and Cu^{2+} with 80% and 40% quenches of emission, and Stern-Volmer constants of 1.18 x 10^5 M^{-1} and 3.85 x 10^4 M^{-1}, respectively, whereas neither K^+ nor Na^+ produced notable emission changes.[1328] A detection limit of 12.5 nM for mercury was found, and this technique was applied for mercury detection in industrial water runoff from a coal-fired power plant, in which a mercury concentration of 1.64 μM was determined. BODIPY-linked bis-crown ether **158** (Figure 73) was employed for the ratiometric sensing of Al^{3+} and Fe^{3+} due to the cation-induced hypsochromic shifts of 65 nm and 67 nm, respectively.[1329] Finally, the emission of terpyridine-appended crown ether **159** (Figure 73) was significantly quenched upon the addition of Zn^{2+}.[1330]

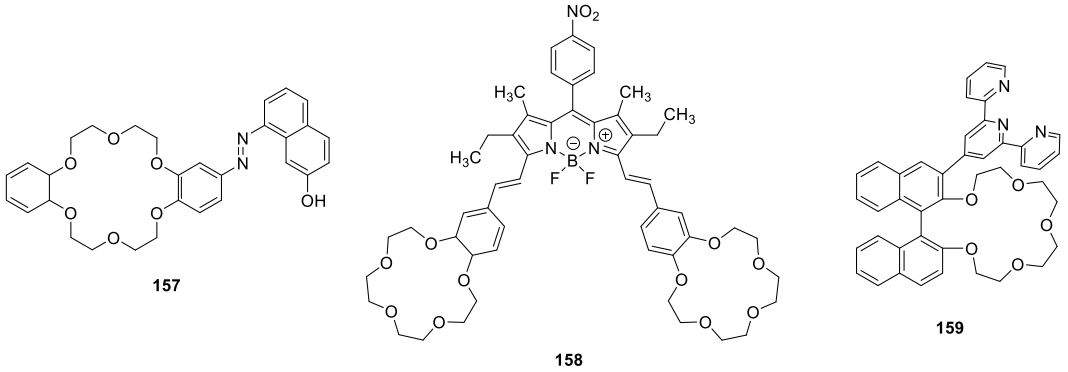

Figure 73. Crown ethers that have been used for the sensing of transition metal cations.[1328-1330]

5.2.2. Oxygen- and Nitrogen- Mixed Crowns. Many supramolecular cryptand hosts are comprised mainly of oxygen nodes with one or two nitrogen nodes present as attachment points for fluorescent pendant arms. For example, host 18-crown-6-ether **160** (Figure 74) contains one nitrogen moiety that connects the macrocycle to a coumarin derivative.[1331] This macrocycle, developed by Ast et al., was sensitive to the

presence of K^+, allowing for a detection limit of 29 mM for K^+ in an aqueous environment. While Na^+ did not lead to any changes in the emission of **160**, additional cations were not investigated. Additionally, **160** was found to rapidly permeate into cells without cytotoxic effects, allowing for in vivo K^+ detection. Yetisen and coworkers used fluorophore appended **161** and **162** (Figure 74) for the detection of Na^+ and K^+, respectively, with detection limits of 2.7 mM and 1.4 mM observed.[1332] These macrocycles, along with Ca^{2+} and pH sensors, were incorporated into a multi-analyte microfluidic device that was used for the analysis of the electrolytes present in human tears. Potassium was detected by rhodamine-appended **163** (Figure 74), and computational studies indicated that **163** was a PET-based sensor, in which complexation with K^+ destabilized the charge transfer state, leading to the observed signal changes.[1333] **164** (Figure 74), containing a europium luminophore appendage, was used to detect potassium in synthetic human blood serum.[314]

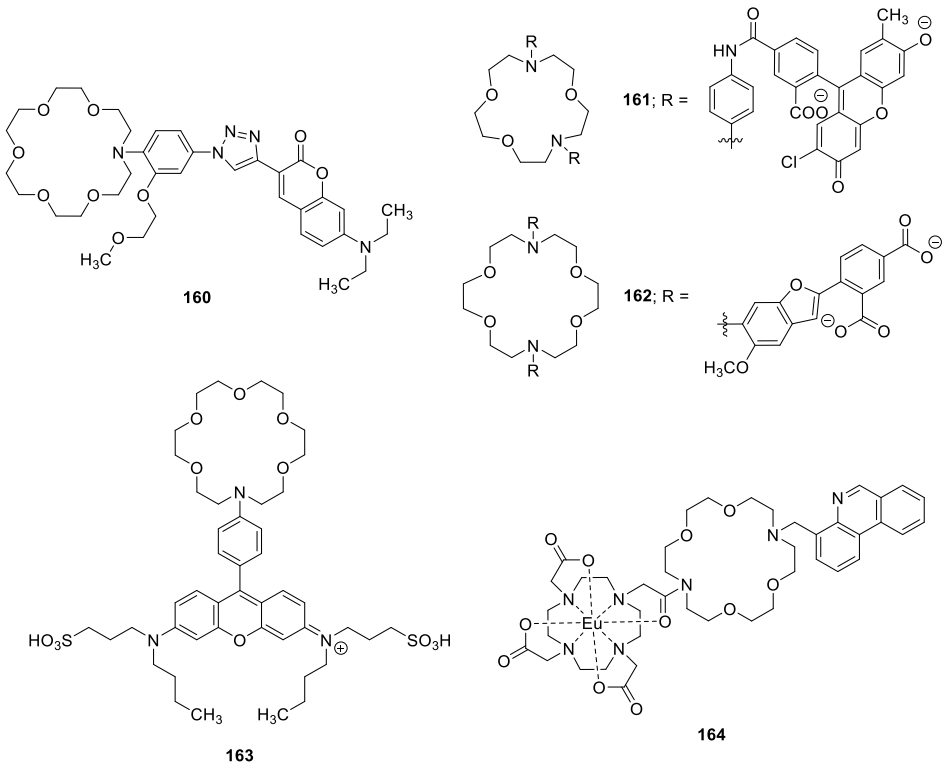

Figure 74. Nitrogen-containing crown ethers that have been employed for the detection of potassium and sodium[314,1331-1333]

Calcium and magnesium cations have also been detected by mixed oxygen/nitrogen crown ether sensors. Mono- and bis-crown ether hosts **165** and **166** (Figure 75) bearing naphthalene diimide fluorescent appendages, were found to selectively detect the presence of Ca^{2+} in acetonitrile, with the quantum yield of **166** increasing 5-fold in the presence of three equivalents of calcium due to the disruption of PET between the azacrown and naphthalene diimide.[1334] The Benesi-Hildebrand equation was used to calculate binding constants for Ca^{2+} with **165** and **166** of 3.33 x 10^3 M^{-1} and 9.13 x 10^6 M^{-1}, respectively. **167** (Figure 75) with pendant pyrene arms could also sense Ca^{2+}, due to analyte-induced PET disruption, at Ca^{2+} concentrations between 0.25 and 1.25 μM and in the presence of typical biological amounts of sodium, potassium, and magnesium.[1335] A detection limit of 0.25 nM was achieved for Mg^{2+} using **168** (Figure 75), with only moderate interference from Ca^{2+} and certain transition metals.[1336] This host was successfully used for the bioimaging of magnesium in embryonic mouse fibroblasts. Other alkali and alkaline earth metal have been detected by xanthenone-appended **169**[1337] (Figure 75) and simple benzaldehyde derived azacrown ethers **170** and **171** (Figure 75).[1338] In the former case, fluorescence enhancement was observed upon metal chelation, because chelation disrupted PET from the nitrogen lone pair of the azacrown to the HOMO of the xanthenone fluorophore.[1337]

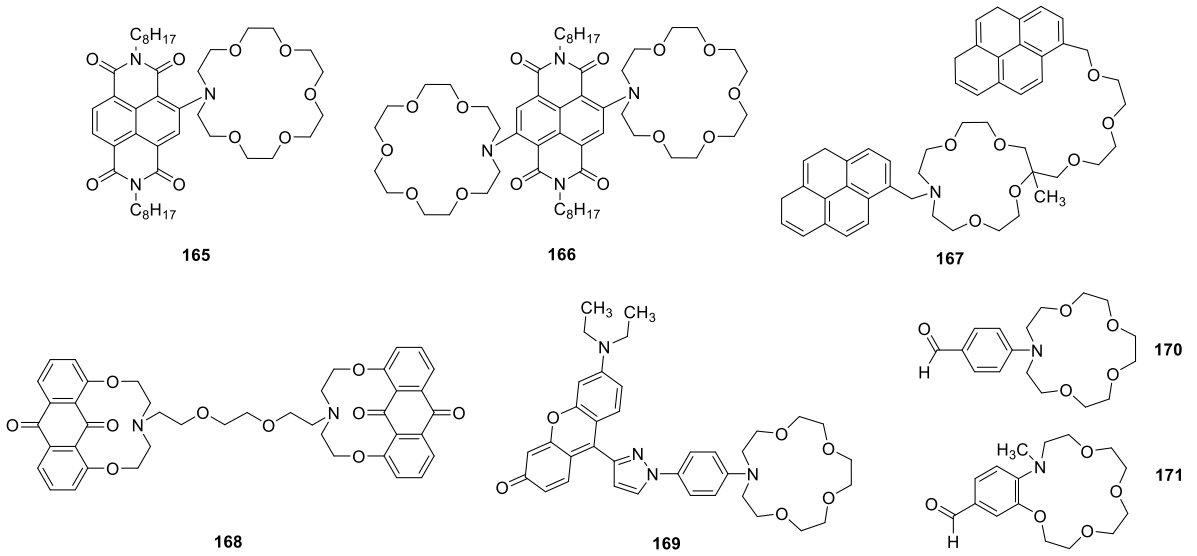

Figure 75. Nitrogen-containing crown ethers that have been used for the detection of calcium and magnesium[1334-1338]

Azacrown ethers have also been used for the detection of transition metal cations. In one example, Goswami et al. used **172** (Figure 76) for the selective detection of Zn^{2+} in a 1:1 mixture of acetonitrile and HEPES buffer at physiological pH.[1339] No other cations decreased the Zn^{2+}-enhanced emission, including Cd^{2+} which is expected to have similar binding properties. A 1:1 **172**-Zn^{2+} stoichiometry was determined, a limit of detection of 5.4 μM was calculated, and a Benesi-Hildebrand binding constant of 1 x 10^4 M^{-1} was reported. The Zn^{2+}-**172** adduct was treated with a variety of anions, and it was found that one equivalent of dihydrogen phosphate ($H_2PO_4^-$) fully quenched the Zn^{2+}-enhanced emission, and that one equivalent of phosphate (PO_4^{3-}) led to moderate fluorescence quenching. The group then tested the efficacy of the system in vitro by sequential incubation of human lung cancer cells with zinc and **172**. Through fluorescence imaging, the presence of the exogenous zinc was observed in the cells and, upon the addition of monopotassium phosphate (KH_2PO_4), the fluorescence was successfully quenched. Furthermore, cytotoxicity studies indicated that the host was relatively nontoxic to cells.

Bhanja et al. also developed a system that was used for in vitro detection studies.[1340] The combination of **173** (Figure 76), which initially exhibited negligible fluorescence emission, with Zn^{2+} led to a significant emission enhancement. The addition of Al^{3+} also increased the emission of **173**, but with a pronounced bathochromic shift in peak maximum, allowing for the full differentiation of these two cations. The response of the host to the cations was optimal at pH 9, with effective cation detection in a wide pH range (pH 2-12). Detections limits of 1.2 μM and 21 nM were found for Al^{3+} and Zn^{2+}, respectively, and no other metal cations led to emission enhancement. However, the addition of a variety of transition metal cations, including Co^{2+}, Mn^{2+}, Ni^{2+}, or Cu^{2+} to the **173**-Zn^{2+} and **173**-Al^{3+} systems hindered the system performance. The host was employed for cation detection in human oral carcinoma cells by consecutive doping of the cells with analyte, Al^{3+} or Zn^{2+}, and **173**, which was found to be cell permeable and non-toxic up to 150 μg/mL.

Hosts **174** and **175** (Figure 76) showed increased emission when PET was hindered by Zn^{2+} complexation, but were not fully selective, as other cations showed significant perturbations of the emission spectrum as well.[1341] Ghanbari et al. found that the emission of **176** and **179** (Figure 76) were enhanced by Zn^{2+}, and similar macrocycles **177** and **178** (Figure 76) were quenched by the addition of Cu^{2+}.[1342] However, only moderate selectivity was achieved, and significant competition with interferent cations was observed. Ambrosi et al. synthesized three macrocycles, **180**-**182** (Figure 76) that interacted with metal cations in

aqueous solution at physiological pH.[1343] Cu^{2+} led to emission quenching of all three hosts, while Zn^{2+} led to emission enhancement of **182**. Competition experiments were not conducted in this case.

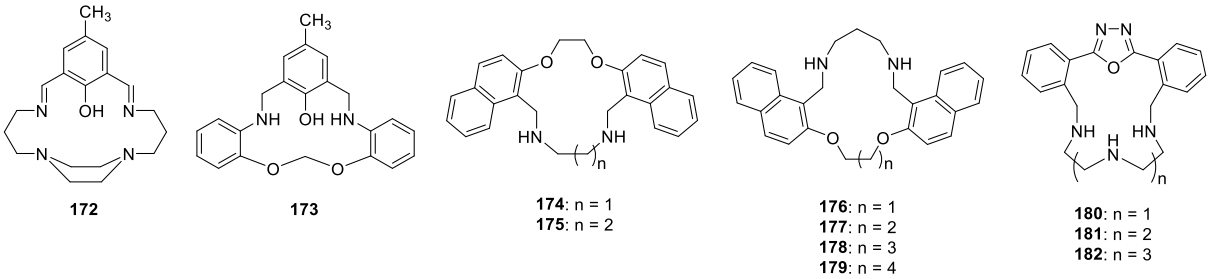

Figure 76. Nitrogen-containing crown ethers that have been utilized for the detection of biologically relevant transition metal cations[1339-1343]

Toxic mercury cations were detected with sugar-based crown ether **183** (Figure 77) by a large mercury-induced emission increase, leading to a detection limit of 12.6 μM.[1344] The fluorescent pyrene appendages were initially minimally fluorescent due to PET from the nitrogen atoms; however, they became strongly fluorescent upon mercury-induced disruption of PET. Cu^{2+} was also found to promote a fluorescence response from this host, albeit with a much lower magnitude than the mercury-induced response, and with a higher detection limit of 130 μM. Stern-Volmer constants of the two analytes with **183** were found in methanol to be 4.4×10^3 M^{-1} for mercury and 7.4×10^1 M^{-1} for copper. Hou and coworkers determined that the ICT of naphthalimide-containing **184** (Figure 77) was interrupted by the presence of Hg^{2+}, allowing for a analyte-induced 22 nm hypsochromic shift.[1345] Li et al. appended a phosphorescent $iridium^{3+}$ complex to aza-18-crown-6-ether, and the emission of the resulting macrocycle, **185** (Figure 77) was significantly quenched in the presence of Hg^{2+} and mildly quenched in the presence of Cu^{2+}.[1346] Mercury could be detected at concentrations of 10 – 700 μM using this method, and the Benesi-Hildebrand equation was used to determine an association constant of 2.00×10^3 M^{-1}. Similarly, Abel et al. functionalized an azacrown ether with a ruthenium bipyridyl moiety to form **186** (Figure 77) that was used for the detection of copper by fluorescence quenching.[1347] The addition of all other cations to **186** led to only small perturbations of its fluorescent profile, and competition experiments indicated that Cu^{2+} could effectively be detected in the presence of other species. The emission of BODIPY-affixed **187** (Figure 77) was nearly completely quenched by the presence of Cu^{2+}, allowing for the detection of the analytes at concentrations as low as 2.4 μM with no interference from other cations.[1348] The Stern-Volmer constant for the interaction of **187** with Cu^{2+} was found to be 1.43×10^5 M^{-1}.

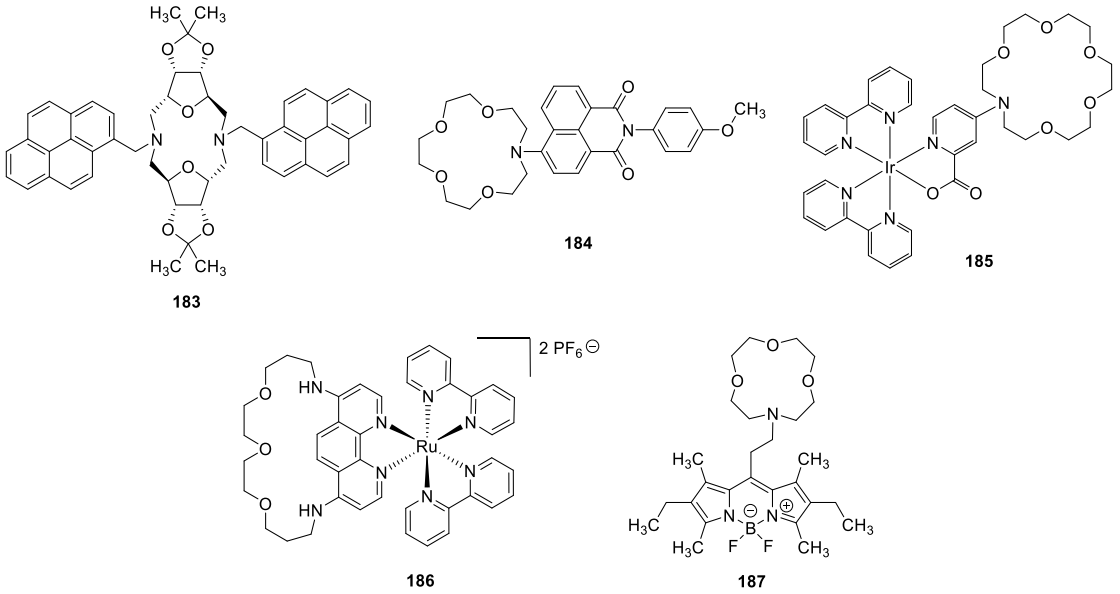

Figure 77. Nitrogen-containing crown ethers that have been used for the determination of mercury or copper[1344-1348]

Qiu et al. developed a macrocycle, **188** (Figure 78) that experienced a substantial increase in emission (5.6-fold) upon the addition of Fe^{3+} in a 1:1 methanol:tris-HCl buffer solution, due to an impedance of PET.[1349] Although Al^{3+} led to a 2.5-fold enhancement, no biologically relevant metal cations impacted the emission enhancement caused by Fe^{3+}. In the same 1:1 methanol:buffer solvent system, a detection limit of 0.58 μM was calculated. However, as the percentage of water content increased, so did the detection limit, indicating that this system was less effective in purely aqueous solutions. To further the study, SKOV-3 and HeLa cells were doped with Fe^{3+}, then incubated with **188**, revealing bright fluorescence in the cytosol of the cells where **188** spontaneously congregates. Of note, despite the strong response of **188** to Fe^{3+}, **188** showed no fluorescence response to Fe^{2+}, and thus the system could be used for monitoring Fe^{2+}/Fe^{3+} oxidation and reduction reactions. Coumarin-based **189** (Figure 78) selectively detected the presence of Fe^{3+} by emission quenching with a detection limit of 0.31 μM, within a wide pH range, and in the presence of a variety of other cations.[1350] System reversibility was obtained through the use of EDTA to remove the iron from the host cavity, allowing for the reuse of the macrocycle.

Azadbakht and coworkers developed two similar macrocycles for the detection of Al^{3+}. Compound **190** (Figure 78) was significantly fluorescent at acidic pH's, whereas at neutral and basic pH, the fluorescence emission was inhibited by PET.[1351] Thus, at neutral pH, **190** was an ideal host for a PET-based detection scheme. The addition of Al^{3+} under these experimental conditions led to almost a 14-fold emission increase, whereas all other ions led to little to no emission changes. However, the addition of Cs^{+}, Pb^{2+}, Fe^{2+}, Cu^{2+}, and Ag^{+} greatly negated the ability of Al^{3+} to interrupt PET and induce the luminescent response. The second study by Azadbakht used similar species **191** (Figure 78) which was found to be less selective for Al^{3+} than **190** was, with Zn^{2+} and Cd^{2+} also inducing significant emission increases.[1352] Nanoparticles formed from **191** had moderately increased sensitivity for Al^{3+} over other metal cations, yet competition experiments indicated that the detection of Al^{3+} was sensitive to the presence of other metal cations, including Cs^{+}, Fe^{2+}, Fe^{3+}, and Ag^{+}. In a final report of transition metal detection, a strong fluorescence increase was seen by Liu et al. when Cr^{3+} was added to host **192** (Figure 78).[1353] Although many other cations were also examined, none produced a significant optical response. A 7.5 ppb detection limit was established, and the host was successfully employed for the detection of Cr^{3+} in normal human liver cells, with no observed toxicity over a 24-hour time window.

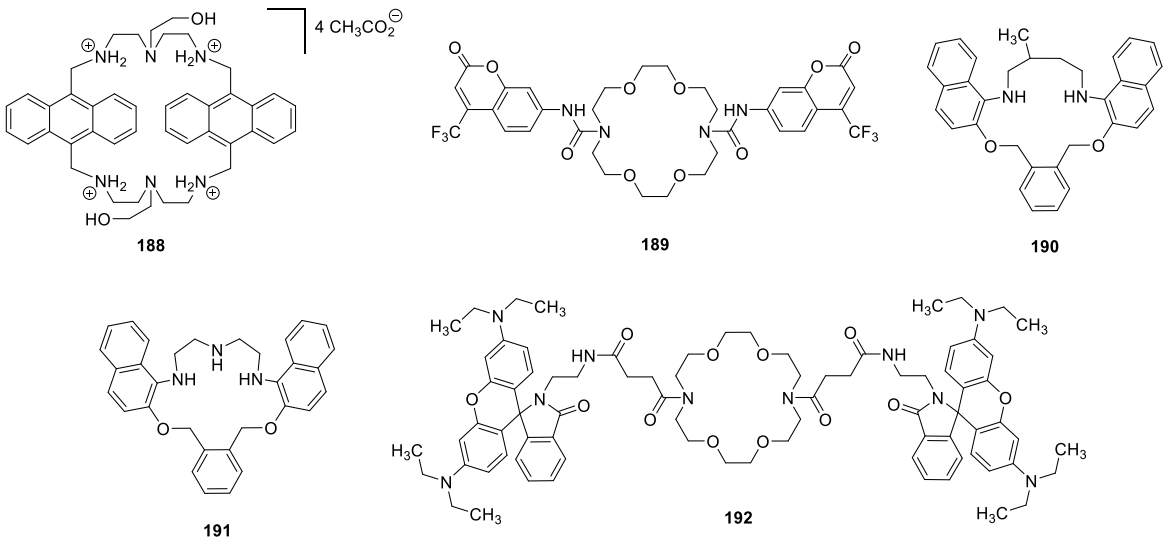

Figure 78. Nitrogen-containing crown ethers that were employed as sensors for transition metal cations[1349-1353]

One mixed oxygen-nitrogen crown system recently published by Yang reports the detection of HSO_4^- anion.[1354] Addition of HSO_4^- to this macrocycle, shown in Figure 79, led to a unique 6-fold emission increase that the authors hypothesized was due to an increase in the rigidity of the host upon guest binding. The detection scheme was applicable in a wide pH range, with a detection limit of 1.36 μM obtained. Although no other anions studied affected the ability of the system to detect hydrogen sulfate, no other sulfur-containing anions were examined.

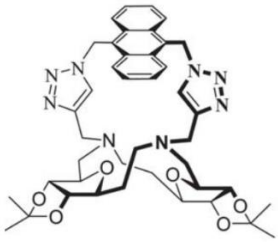

Figure 79. Nitrogen-containing bridged crown ether that was employed by Yang et al. for the detection of HSO_4^-. Reproduced with permission from Ref. 1354. Copyright 2012 Royal Society of Chemistry.

5.2.3. Nitrogen-Containing Crowns. Nitrogen-containing species analogous to crown ethers are a popular choice of host for the detection of transition metal cations. These species, shown in Figure 80, colloquially known as tacn, cyclen, cyclam, and pentacyclen, are softer bases than their oxygen-containing analogues and therefore show preferential binding to softer metal acids.

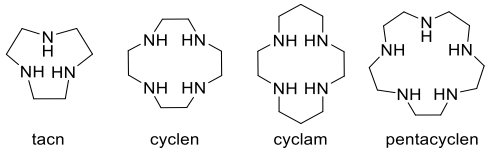

Figure 80. Common cyclic polyamines

Copper is a common target for these nitrogen-containing hosts, and due to the strong interactions between copper cations and sulfur-containing species, a number of dual-detection systems for copper and sulfur have been established. For example, BINOL-appended cyclen **193** could detect Cu^{2+} with high selectivity by fluorescence quenching, with a 4.0 μM detection limit, and a Benesi-Hildebrand binding constant of 3 x

10^2 M^{-1}.[367] Job's plot analysis confirmed the formation of a 2:1 host-guest complex, and the authors hypothesize the binding mode shown in Figure 81, where the single copper cation was held between the internal faces of the two cyclen moieties. The addition of S^{2-} to this system led to the recovery of the initial macrocycle emission, due to removal of the copper from the cavity. Minimal interference from other anions was observed, and sulfide could be detected in concentrations as low as 16 μM. Li and coworkers affixed ruthenium tris(bipyridine) to cyclen to afford host **194** (Figure 81), which was also shown to successively detect Cu^{2+} and S^{2-} with detection limits of 5.4 μM and 37 μM, respectively.[1355] Only minimal changes in the fluorescence signal were seen when potentially interfering cations and anions were added to the system, or when the pH was varied between 5 and 11. The complex formed upon treating anthracenyl cyclen **195** (Figure 81) with Cu^{2+} could detect H_2S in solution with a detection limit of 205 nM, and was used for the detection of this analyte in live cells.[940] The system showed good reversibility upon successive Cu^{2+} – H_2S additions, and was effective between pH 5 and 10. The sensing of copper was also accomplished using **196** (Figure 81), which contains a rhodamine-based fluorescent arm, with a detection limit of 2.0 μM.[1356] Minimal interference from several other metal cations was observed.

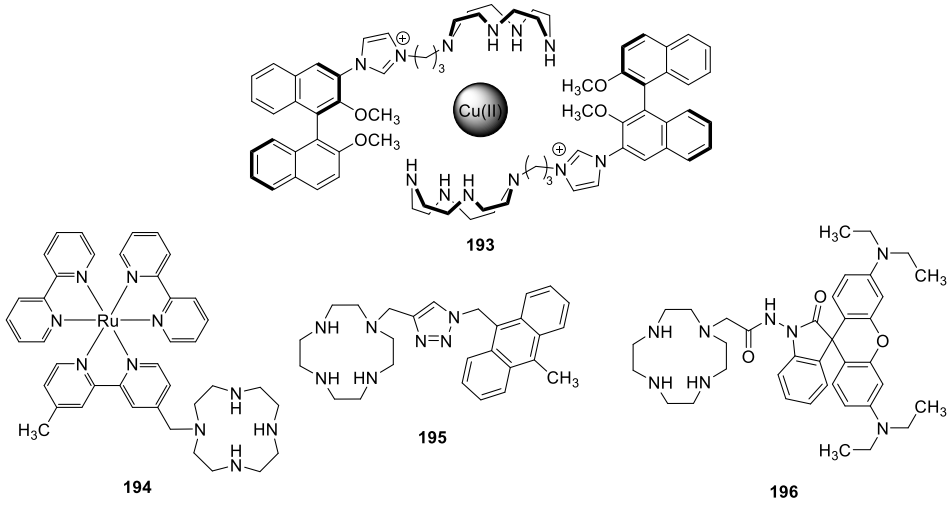

Figure 81. Modified cyclen species used for the detection of copper[367,1355-1356]

The four aforementioned systems all exhibited emission quenching with copper addition, as did methylbenzimidazolium-cyclam conjugate **197** (Figure 82).[1357] However, **197** was responsive to Zn^{2+}, with a dramatic Zn-induced increase in emission due to zinc binding with the amine moieties of the cyclam and hindering PET. The detection limit for zinc was 4.5 nM; however, the presence of copper completely negated the macrocycle's response to zinc, resulting in a near complete fluorescence quench. Nouri et al. used modified cyclen **198** (Figure 82) for zinc sensing, discovering that the addition of one equivalent of zinc led to an emission quench, followed by an emission increase as more than one equivalent of zinc was added.[366,363] The first equivalent of zinc was thought to bind inside the cyclen cavity, turning off the emission of the appended fluorescent azaxanthone derivative. The second equivalent of zinc was hypothesized to bind to the hydrazone moiety of the fluorophore, interrupting PET and restoring the fluorescence. Density functional theory (DFT) and time-dependent density functional threory (TD-DFT) calculations supported the existence of a PET mechanism for this system. Other metal cations were found to interfere with effective zinc detection. Wang et al. reported a cyclen-derived species, **199** (Figure 82) containing a pyridine ring, to which an anthracenyl fluorophore was appended.[1358] This macrocycle selectively bound Zn^{2+} in aqueous solution with 1:1 stoichiometry, leading to a 14-fold increase in fluorescence emission. Not only was Zn^{2+} the only metal cation that induced a fluorescence change, but the addition of other cations to a solution of zinc and macrocycle had very little effect on emission. The host-guest association constant was relatively high, at 1.96 x 10^5 M^{-1}, and a detection limit of 1.1 μM was calculated. Pyrophosphate anion ($P_2O_7^{4-}$) sequestered zinc from the macrocycle cavity, and thus, the Zn^{2+}-

199 adduct was used for pyrophosphate detection, with a detection limit of 0.11 μM. This system was used to monitor the enzymatic conversion of adenosine triphosphate (ATP) to pyrophosphate by tracking fluorescent enhancement, with potential future applications in monitoring enzyme inhibition.

With many macrocycle hosts, especially those that have functionalities that are readily protonated or deprotonated, the pH of the system can have a dramatic effect on the detection schemes. This pH effect was exemplified by a study conducted by Bazzicalupi et al. where potentiometric studies elucidated the fluorescence profiles, at various pH values, of two cyclen-like hosts, **200** and **201** (Figure 82), bearing acridine moieties in the macrocycle core.[1359] Further potentiometric studies of the hosts with various cations were conducted, and the authors concluded that zinc exhibited optimal fluorescence enhancement of **200** at pH values between 5 and 8, whereas all other cations tested, Cu^{2+}, Cd^{2+}, and Pb^{2+}, led to insignificant changes in emission intensity at all pH values investigated. In both acidic and basic solutions, no enhancement of emission by Zn^{2+} was observed, outlining important limitations of the system. This group also conducted potentiometric studies with a similar macrocycle that was subsequently used for pH detection.[1360]

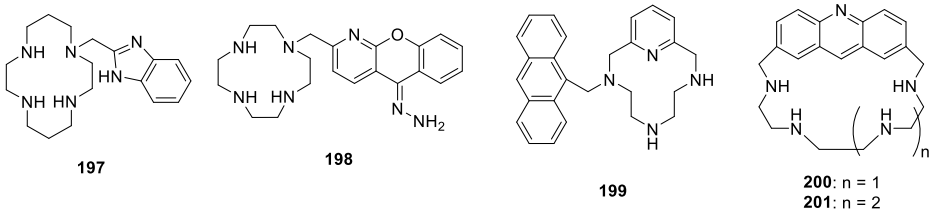

Figure 82. Cyclic polyamine species that were used to sense various transition metal cations[363,366,1357-1360]

Several years prior to the use of **195** (Figure 81) for the detection of copper (vide supra),[940] this host, along with the analogous **202** (Figure 83) bearing two fluorescent appendages, were examined by Xu et al. for the detection of lead.[365] The addition of Pb^{2+} to **202** increased the quantum yield from 4.9% to 13.8%, resulting in a high binding constant, log $K_{binding}$ = 10.7. The host was able to permeate cell membranes efficiently and could detect the lead analyte in vitro¸ but the response of **202** to lead in fetal bovine serum was low, likely due to matrix proteins interfering with the formation of the desired host-guest complex. Wang et al. appended a 7-nitrobenz-2-oxa-1,3-diaole (NBD) fluorophore to a cyclen-like macrocycle to produce species **203** (Figure 83).[1361] The fluorescence emission of this host was preferentially quenched by the addition of Cu^{2+} in aqueous solution at physiological pH. Other biologically relevant cations Ca^{2+}, Na^{+}, and Mg^{2+} did not affect the Cu^{2+}-induced quenching, and a detection limit of 0.84 μM was calculated. In vitro studies were conducted in which it was found that **203** effectively permeated the cell membrane and accumulated in the lysosomes of HeLa cells. When the cells were doped with Cu^{2+}, its presence was observable by fluorescence imaging due to intracellular copper-macrocycle binding and the resulting binding-induced fluorescence increases. A perylene diimide functionalized with two cyclen moieties, **204** (Figure 83), was examined by Zhou et al., and the emission of the host increased in the presence of Pb^{2+} but decreased in the presence of Hg^{2+} and Cu^{2+}.[1362] Similar mono-cyclen host **205** (Figure 83) was more selective to Pb^{2+}, with minimal perturbations of the spectrum by other cations. Compound **205** demonstrated more versatility in intracellular detection and a wider effective pH range than **204**.

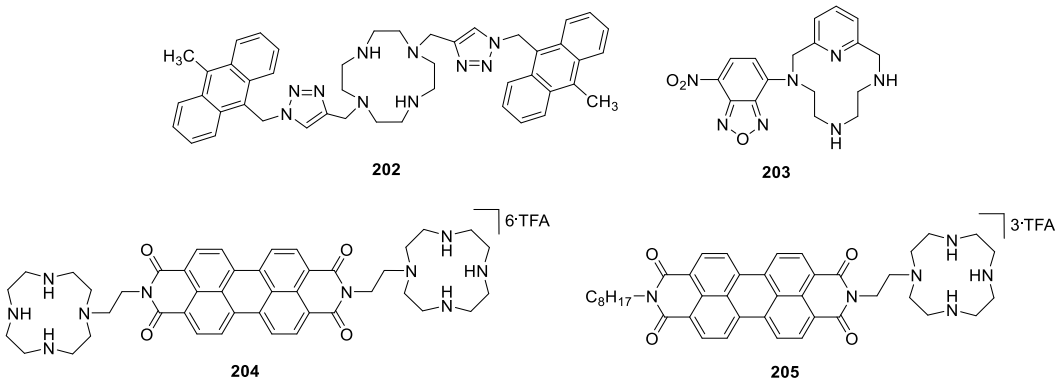

Figure 83. Cyclic polyamine hosts that have been used for the detection of transition metal cations.[365,1361,1362]

Rhodamine-appended cyclen **206** (Figure 84) was used by Shim et al. for the sensing of cadmium via analyte-induced fluorescence enhancement.[1363] A detection limit of 25 nM was calculated, however, Hg^{2+}, Zn^{2+}, Pb^{2+}, Cu^{2+}, and Pd^{2+} interfered with the detection ability of the system. In a final example of cation detection with cyclic polyamines, two pentacyclen hosts with BODIPY-containing pendant arms, **207** and **208** (Figure 84), underwent 52-fold and 28-fold emission increases, respectively, upon treatment with Mn^{2+} and concomitant disruption of internal PET.[1364] **208**, with four ester groups attached to the pentacyclen ring, formed a 1:2 host-guest complex with Mn^{2+}, with one cation bound in the cavity and the other bound to the pendant arms outside the cavity, whereas **207**, with only two ester groups, formed a 1:1 host-guest complex. The authors hypothesized that the additional binding sites of **208** made it a less selective host for Mn^{2+} sensing, because other cations bound to those sites and interfered with detection. Both hosts were able to permeate cell membranes, thus enabling in vivo manganese detection.

An organic phosphate, inositol(1,4,5-triphosphate), which acts as a signaling molecule in biological systems, was detected by Do-Thanh et al. using cyclen-containing tweezer compound with an acridine-based fluorescent unit **209** (Figure 84).[1365] The analyte bound between the two cyclen motifs via electrostatic interactions, with an association constant of $K = 1.0 \times 10^6\ M^{-1}$. However, this host was not selective for inositol (1,4,5-triphosphate) over structurally related analytes including *D*-fructose, 1,6-bisphosphate trisodium salt, cyanoethyl phosphate barium salt, and sodium dihydrogen phosphate, which all led to analogous fluorescence changes.

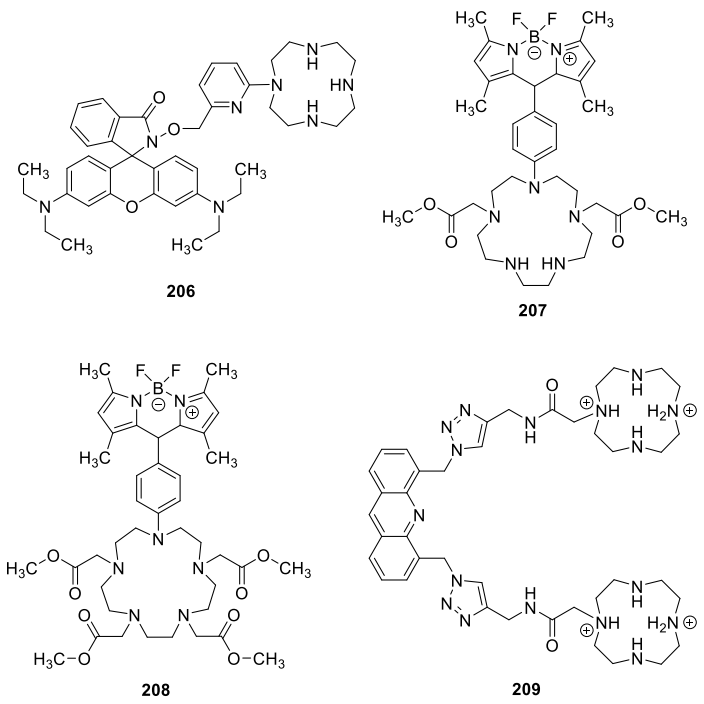

Figure 84. Cyclen and pentacyclen species that have been used for various detection schemes.[1363-1365]

5.2.4. Sulfur-Containing Crowns. Due to the high affinity of sulfur for transition metals such as copper and mercury, sulfur-containing crowns are ideal detection platforms for such analytes. In one example, Tian et al. used host **210** to sense Hg^{2+} in the presence of DNA.[1321] The genotoxic effects of mercury are associated with the ability of mercury to bind strongly to DNA, and thus the authors designed a Hg^{2+} sensing platform that can also ensure close proximity to DNA strands. Compound **210** was designed with a fluorescent benzo[*b*]quinolizinium appendage which, due to its planar nature, intercalates into DNA strands (Figure 85). The supramolecular complex of DNA, **210**, and mercury was highly fluorescent, whereas in the absence of any one of these components, the fluorescence was minimal. It was hypothesized by the authors that two emission inhibiting pathways are operational in the free host that must be deactivated before emission of the fluorescent appendage can occur:[1366] PET between the aminophenyl and the benzo[*b*]quinolizinium of **210** was hindered by complexation with mercury, and the fluorescence-deactivating C-N bond rotation that is characteristic of such species was prohibited by intercalation into DNA strands. A mercury detection limit of 39 nM was established.

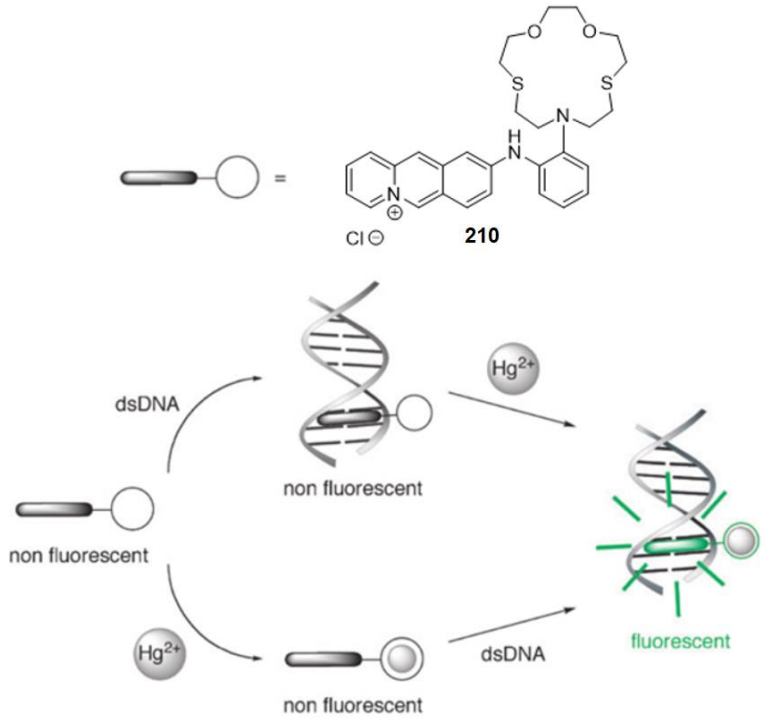

Figure 85. The use of intercalator-bound azathiacrown ether **210** for the detection of Hg^{2+} in close proximity to DNA. Adapted with permission from Ref. 1321. Copyright 2016 Royal Society of Chemistry.

A four-coordinate, dansyl-bearing, azathiacrown ether **211** (Figure 86), was used by Dai et al. for the selective detection of mercury with a detection limit of 0.1 μM and was applied to drinking water and river water samples.[1367] This method was effective from pH 2.0 to 8.0, with no other cations perturbing the detection scheme. A series of anthracenyl sulfur-containing crowns **212** – **215** (Figure 86) were synthesized by Mameli et al., all of which were shown to have a high affinity for mercury, allowing for micromolar detection levels of Hg^{2+} with moderate perturbations by interfering cations.[1368] The fluorescence emission of mixed crown **216** (Figure 86) was also quenched in the presence of Hg^{2+}, and the subsequent addition of anions regenerated the macrocycle emission as mercury was removed from the macrocycle core.[387] **217** (Figure 86) bearing two azathiacrown ethers linked by a fluorescein unit, was able to sense copper with a limit of 87 nM in slightly acidic conditions.[1369] The ICT between the heterocrown ether moieties and fluorescein was hindered by the presence of Cu^{2+} or Ag^{+}, leading to a quench of emission, though the quenching effect was more pronounced with copper than with silver.

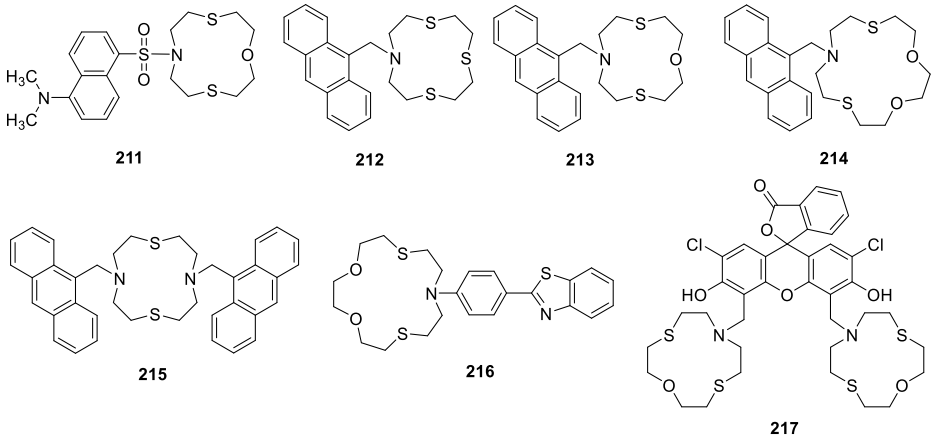

Figure 86. Azathiacrowns and azathiacrown ethers that have been employed for cation sensing[387,1367-1369]

Similar to the aforementioned crowns appended with ruthenium tris(bipyridine), (**186**,[1347] Figure 77, and **194**,[1355] Figure 81) **218** (Figure 87), and its sulfur-containing analogues **219** and **220** (Figure 87) were investigated for metal cation sensing abilities by Boricha et al.[1370] **218** was selectively quenched by Cu^{2+}, and analogous sulfur-containing species **219** was quenched by both Cu^{2+} and Fe^{2+}. The emission of bis(hetero crown ether) host **220** was predominantly quenched by Pb^{2+}, but Ce^{2+}, Fe^{2+}, and Hg^{2+} all promoted some degree of emission quenching. Anions F^- and $H_2PO_4^-$ also acted to quench the host emission through interactions with the aromatic protons of the luminophore.

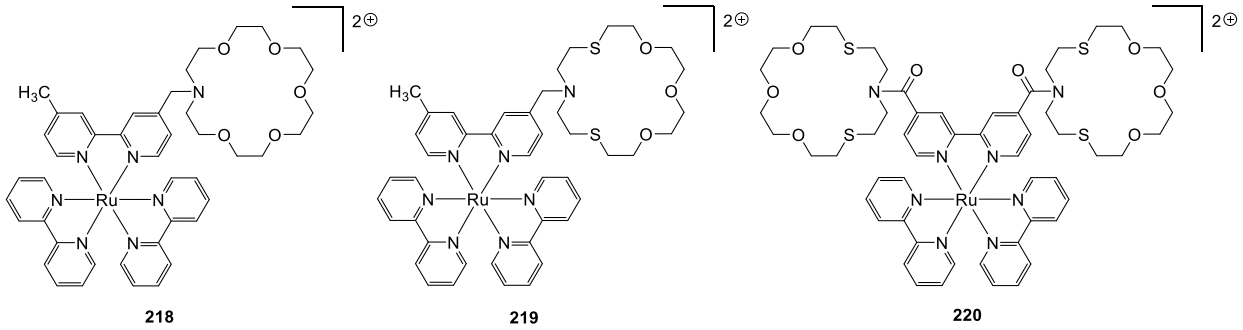

Figure 87. Ruthenium tris(bipyridine) bound crowns that were used by Boricha et al. for transition metal cation detection[1370]

A ratiometric dual detection system for the presence of Ag^+ and I^- was developed by Wang et al. utilizing **221** (Figure 88).[1371] The addition of silver to the host provided an analyte-specific 84 nm hypsochromic emission shift with an increase in quantum yield from 0.05 to 0.28. The addition of I^- led to the precipitation of AgI from the aqueous solution, and the decreases in the intensity of the emission spectrum as the silver was removed allowed for the detection of I^- with a detection limit of 7.2 μM. BODIPY-modified azathiacrown ether **222** (Figure 88) was responsive to the presence of both Pd^{2+} and Hg^{2+}, as evident by an increase in the emission of the host upon guest-induced hampering of PET, the mechanism of which was elucidated by DFT and TD-DFT studies.[1372] Although Pd^{2+} bound more strongly to **222** than Hg^{2+} did, the presence of the latter impacted the detection ability of **222** towards the former. In order to circumvent this issue, the authors added cysteine to the solution, which bound to the interfering mercury cations and prevented their interaction with the host. This allowed for the selective detection of Pd^{2+} at concentrations as low as 1.2 ppb in the solution phase. Exogenous Pd^{2+} could also be identified in human breast cancer cells that were incubated with **222**.

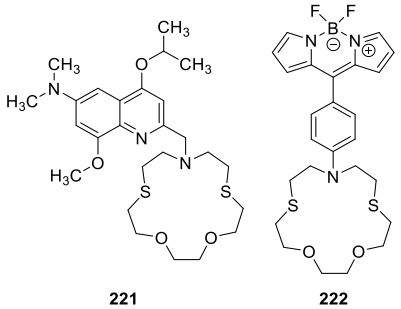

Figure 88. Azathiacrown ethers that have been employed for the detection of transition metal cations in solution.[1371,1372]

5.2.5. Transition Metal-Containing Crowns. Discussed in this sub-section are cyclens and cyclen derivatives coordinated to transition metal centers that are used to detect certain analytes, via either the formation of association complexes, the displacement of fluorescent indicators, or the removal of the

transition metal from the host cavity. This section focuses on reports in which metal-containing cyclens are synthesized, characterized, and treated as the supramolecular host, whereas earlier discussion focused on metal-free hosts that coordinated to specific transition metal cations for cation detection applications.

Five zinc-centered supramolecular hosts have been reported for the sensing of biologically relevant phosphates. Compound **223** (Figure 89) was shown by Mesquita et al. to selectively detect hydrogen pyrophosphate ($HPPi^{3-}$) in aqueous environments by analyte-induced fluorescence enhancement.[1373] No other mono-, di-, or trianions led to a change in macrocycle emission of the $HPPi^{3-}$-**223** complex emission, including hydrogen phosphate and all adenosine phosphates. A relatively low detection limit of 300 nM was calculated for this system. Similar macrocycle **224** (Figure 89) also exhibited a fluorescence response when treated with pyrophosphate, yet was not as selective as with **223**, with ATP and ADP also producing some degree of fluorescence changes.[364] The decrease of excimer emission and increase in monomer emission upon analyte addition implied that the initial π-π stacking of the anthracene appendages that led to excimer emission was disrupted by analyte coordination. A comparison between the two systems highlighted that **223** coordinated much more strongly to $HPPi^{3-}$ ($K_a = 1.66 \times 10^6\ M^{-1}$) than **224** does to PPi^{4-} ($K_a = 1.55 \times 10^3\ M^{-1}$). In a report by Joshi et al., thymidine mono-, di-, and triphosphate nucleotides promoted the formation of an excimer of **225** (Figure 89).[1317] The phosphate coordination promoted macrocycle folding, which allowed the pyrene moieties to stack and produced the new emission peak. A series of zinc-containing di- and tetra-cyclen hosts, including **226** and **227** (Figure 89) responded to the presence of pyrophosphate with notable emission changes.[1374] **226**, containing two cyclen units each coordinated to a zinc cation, underwent a 3.4-fold increase in emission upon the addition of one equivalent of pyrophosphate. The emission of **227**, with four zinc-cyclen moieties, increased by 5.5-fold, whereas a similar species with a benzene linker, rather than an anthracene linker, experienced a 10-fold emission decrease. Complicated stepwise binding modes were elucidated, and the tetra-zinc complexes also bound to tetraaspartate and tetraglutamate peptides with high binding constants (ca. $10^7\ M^{-1}$). Non-fluorescent copper-ligated polyamine **228** (Figure 89) relied on an indicator displacement assay to achieve the luminescent detection of dihydrogen phosphate.[1375] In water buffered at physiological pH, the emission of Eosin Y was quenched upon binding inside the cavity of **228**. Of the anions examined, only $H_2PO_4^-$ displaced the dye from the macrocycle cavity, turning on the fluorescence emission of Eosin Y. However, no other phosphate anions were analyzed.

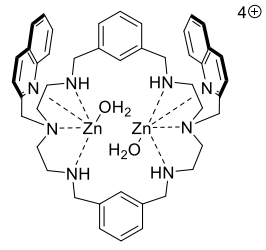

223

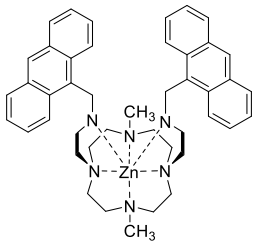

224

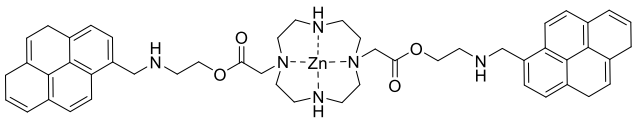

225

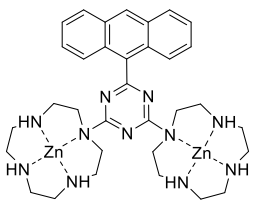

226

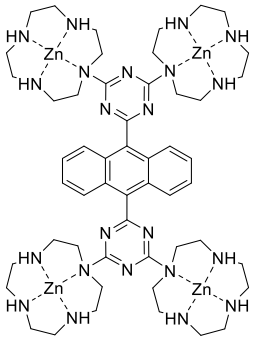

227

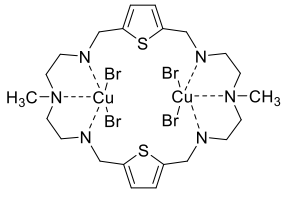

228

Figure 89. Zinc and copper centered cyclic polyamines that have been used for the detection of various phosphates[364,1317,1373-1375]

Two metal-containing cyclen-like hosts have been found to be selective for the binding and detection of oxalate, a dicarboxylic acid that is linked to the formation of kidney stones, using indicator displacement strategies. When Eosin Y was treated with nickel-containing macrocycle **229** (Figure 90) in water buffered at pH 7.4, a substantial hypsochromic shift in the emission spectrum was observed.[1376] Subsequently, upon treatment of the **229**-Eosin Y complex with oxalate, the indicator was displaced and the emission peak underwent a bathochromic shift, enabling an oxalate detection limit of 5 μM. Notably, none of the other anions examined were found to displace Eosin Y, however, anions similar to oxalate, such as citrate and tartrate, were not examined. For copper-ligated species **230** (Figure 90), the displacement of Eosin Y by oxalate led to an increase in fluorescence emission.[1377] A detection limit of 79 nM was calculated, much lower than that obtained using **229**. The system was found to be only somewhat selective, as the presence of other anions led to moderate displacement of Eosin Y from the cavity of **230**. The anions examined by this study, however, were much more similar to oxalate than those anions tested with **229**, which may account for the apparent differences in selectivity. A final difference between the two systems was that **229** formed a 1:2 host guest complex with oxalate whereas **230** formed a 1:1 complex. With the former host, one oxalate anion coordinated to each of the nickel centers and was oriented outside of the cavity, whereas **230** binds one oxalate anion between the two copper centers, localizing it inside the host cavity.

BODIPY-appended **231** (Figure 90) was synthesized by Wu et al. and used for the detection of S^{2-}.[941] The host selectively detected this analyte over thiol-containing amino acids and other small anions. Concentrations as low as 80 nM could be detected, and the probe was incubated into RAW264.7 cells, after first being dispersed into a DOTAP liposome to aid in intracellular probe delivery. Following the successful detection of H_2S in these cells, **231** was injected into a live mouse, and fluorescence imaging was used to detect the analyte therein. Certain H_2S donors, such as the enzyme cystathionine-γ lysase and a compound extracted from garlic, diallyl trisulfide, were indirectly detected in solution due to their ability to release H_2S into solution. Another BODIPY-derived host, copper bis(tacn) **232** (Figure 90) reported by Li et al. was exposed to a number of amino acids, leading to the discovery that the host was a selective sensor for homocysteine, with a Benesi-Hildebrand constant of 3.41×10^4 M^{-1}.[1378] A detection limit of 0.24 μM was achieved, and the host was used for monitoring the activity of cystathionine β-synthase, which converts homocysteine to cystathionine in vitro. Additionally, Amatori and et al. developed three metal-containing cyclen-like molecules, represented by **233** (Figure 90) where M = Zn, Cd, or Cu, that underwent changes in emission upon the addition of halides.[362] For each combination of **233** with halide, a different fluorescence response was observed, allowing for the creation of a preliminary array that effectively discriminated the analytes. No anions other than halides were examined with this system.

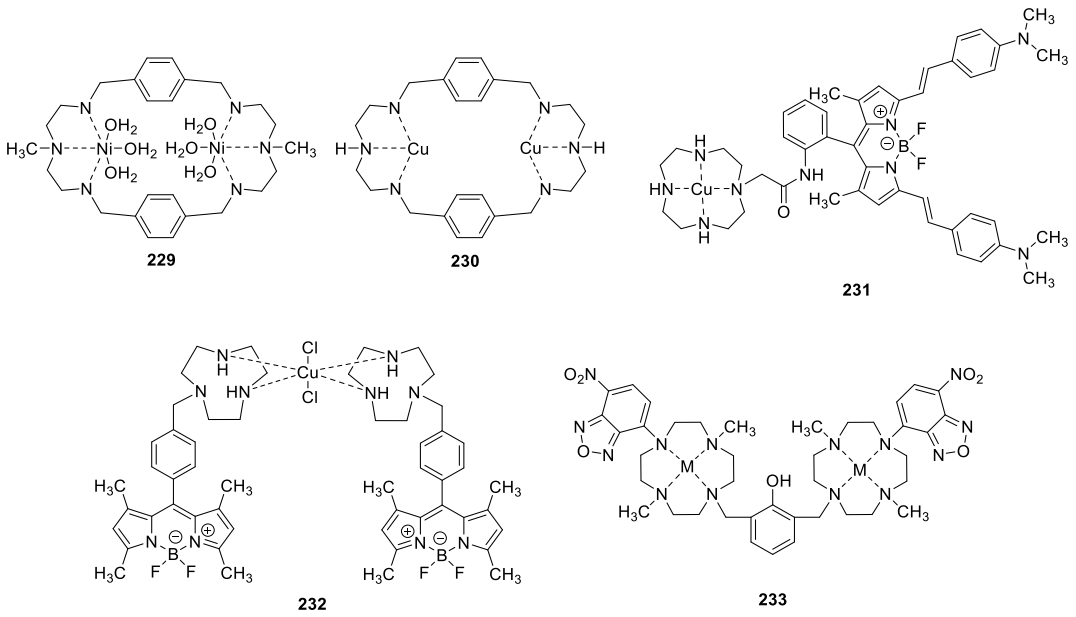

Figure 90. Metal ligated cyclic polyamine species used for the detection of anions[362,941,1376-1378]

5.2.6. Lanthanide Metal-Containing Crowns. Lanthanide metal-containing cyclen hosts have unique structural and optical properties that make them exciting candidates for supramolecular luminescent sensors. The inherent phosphorescence of such species facilitates time-resolved detection schemes, in which the luminescence lifetime of the host is altered in response to association with a guest analyte. In such systems, background biological fluorescence, which is normally a strong interferent, is not part of the detected signal because it typically occurs on much shorter time scales than the phosphorescence.[313] In one example of a lanthanide metal-containing crown, terbium-containing **234** (Figure 91) was used for the detection of adenosine nucleotides in aqueous conditions.[313] The complexation of **234** with ATP induced PET from the purine base to the phenanthridine fluorophore of **234**, leading to a quench of emission. ADP and AMP could also be detected in this manner, although the quenching efficiency was lower for these analytes compared to ATP-induced quenching. Stern-Volmer constants for ATP, ADP, and AMP with this host were found to be 1.28 M^{-1}, 0.85 M^{-1}, and 0.397 M^{-1}, respectively. The system was most effective in the analyte range of 1 to 10 mM, which is within the typical intracellular concentration range for these analytes. Another terbium complex, in this case containing an azaxanthone fluorophore, **235** (Figure 91), was utilized by Urano and coworkers for the detection of NADH. NADH association was shown to have a Stern-Volmer constant of 1.9 x 10^5 M^{-1}, and led to a decrease of luminescence intensity and luminescence lifetime of the host, whereas NAD^+ had minimal effects on both of these properties. This differential analyte response was applied to the monitoring of the NADH-dependent enzymes lactate dehydrogenase, alcohol dehydrogenase, and malate dehydrogenase. In a report by Ito et al., chiral europium and terbium containing species, **(*R*)-236** and **(*S*)-236** (Figure 91) were able to differentiate amino acid anions based on both the chirality and steric size of the analyte.[1379] Azab and coworkers found that the complex formed in situ from europium hydrate, cyclen, and a fluorophore, 4,4,4-trifluoro-1-(2-naphthyl)-1,3-butanedione, responded to the presence of DNA, nucleosides, and nucleotides.[1380]

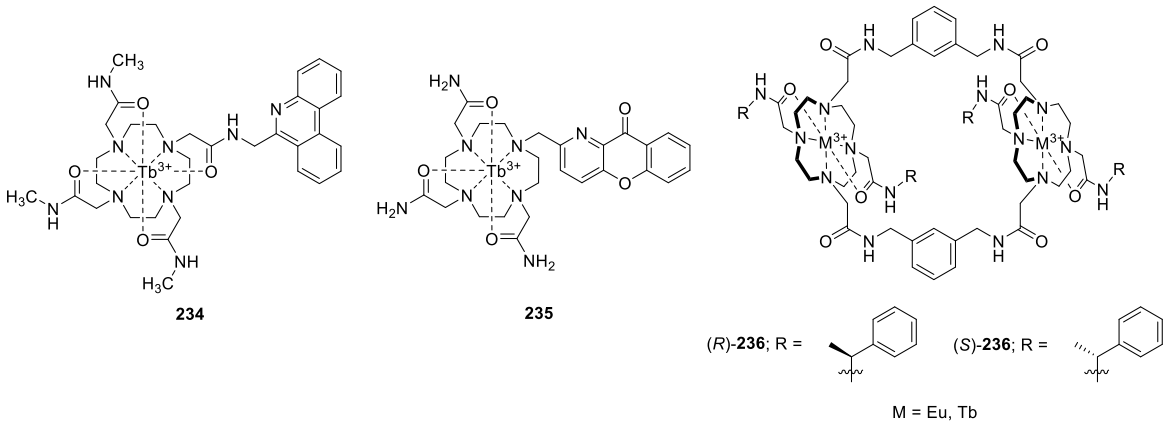

Figure 91. Terbium and europium containing cyclen complexes used for the detection of biologically relevant molecules[313,1379,1380]

Cations are also targets for sensing with lanthanide metal-containing luminophores. For example, ytterbium-centered cyclen, **237** (Figure 92) formed an association complex with 8-hydroxyquinoline sulfate, and that complex was used for the detection of zinc by Gunnlaugsson and coworkers.[1381] Strong phosphorescent emission of the initial host was hypothesized to be due to the sensitization of Yb^{3+} by the triplet excited state of 8-hydroxyquinoline sulfonate via a Dexter (i.e. electron exchange) energy transfer mechanism. Zinc quenched the emission of the supramolecular complex by displacing 8-hydroxyquinoline sulfate, thus enabling zinc detection at concentrations as low as 68 μM. Rhodamine-appended gadolinium complex **238** (Figure 92) was also able to detect zinc, with increased fluorescence emission occurring upon zinc complexation.[1382] This complex also was used for monitoring pH due to the ring opening of the spirolactam under acidic conditions and concomitant emission changes. Gunnlaugsson and coworkers reported two more instances of cation sensing by these types of complexes. The first, terbium-based **239** (Figure 92), experienced a decrease in fluorescence emission upon complexation with both Cu^{2+} and Hg^{2+}.[1383] In the second report, a europium-bound cyclen associated with a phenanthroline fluorophore to form complex **240** (Figure 92), which was used for the detection of Fe^{2+}.[1384] By monitoring changes in the luminescence emission that occurred as Fe^{2+} sequestered the fluorophore from the europium host, a detection limit of 10 pM Fe^{2+} was reached. This technique was not selective however, and other transition metals disturbed the emission profile of the host as well. Terbium crown ether complex **241** (Figure 92) was reported by Leonenko et al. to form a 1:2 host-guest complex, with Tb^{3+} residing in the crown ether cavity and coordinating to the carboxylic acid moiety.[1385] As crown ethers bind more strongly to alkali metals than to softer metals, the addition of Na^{+} and K^{+} displaced Tb^{3+} from the cavity, but not from the carboxylic acid, leading to a decrease in emission. Detection limits were observed for NaCl and KCl at 1.50 ppm and 25 ppm, respectively.

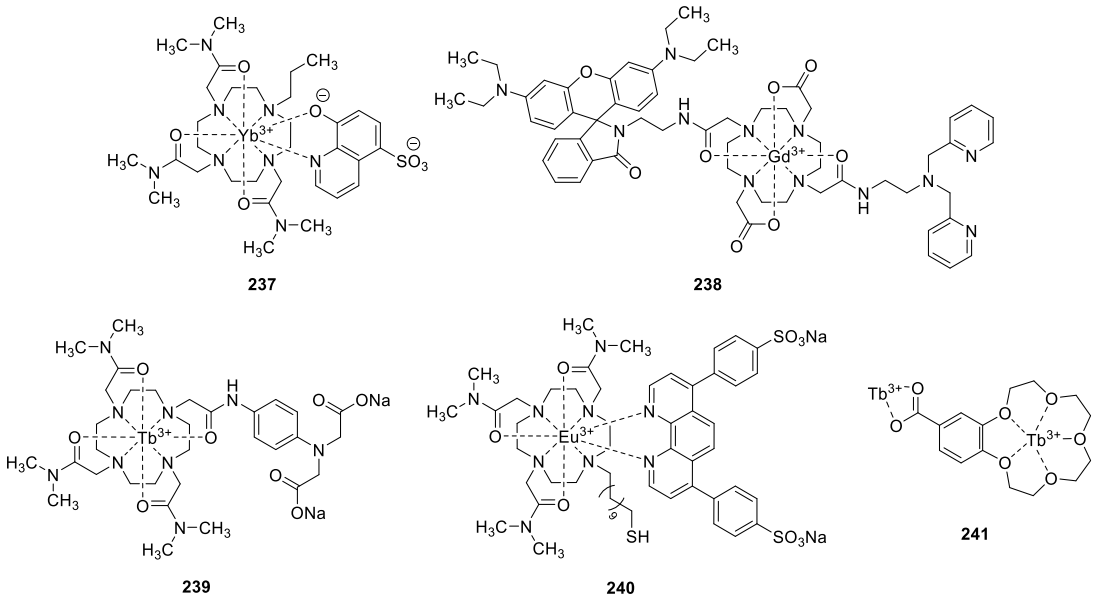

Figure 92. Lanthanide-metal cyclen complexes used for the detection of cations.[1381-1385]

Gunnlaugsson and coworkers have also developed supramolecular terbium complexes for the detection of anions. Terbium association complex **242** (Figure 93) underwent emission quenching in the presence of phosphates and nitrates, because these anions associated with the terbium center and displaced the pseudo crown ether linkages. Pyrophosphate bound most strongly to terbium, leading to a complete quench of emission, with dihydrogen phosphate, nitrate, chloride, and acetate leading to weaker binding and lesser degrees of emission quenching.[1386] In a final report of such complexes, Nakai and coworkers utilized terbium-based **243** (Figure 93) as an oxygen sensor.[921] Under a nitrogen atmosphere, the quantum yield of **243** was found to be 0.91, as opposed to 0.031 in oxygen-containing open-air conditions, and a Stern-Volmer quenching constant of 1.26×10^4 M^{-1} was calculated. Successive additions of nitrogen atmospheres and open-air atmospheres switched the emission profile of **243**, indicating the high reversibility of the system.

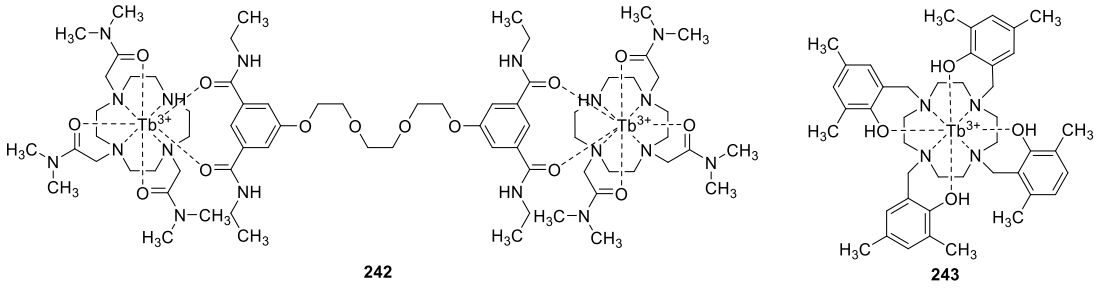

Figure 93. Terbium-based cyclen sensors for the detection of phosphate, **242**,[1386] and oxygen, **243**[921]

5.2.7. Cyclotriveratrylenes. Cyclotriveratrylenes are a class of trimeric cryptand macrocyclic hosts typically formed from the condensation of veratrole alcohol, which often occurs under acidic conditions.[1387] Whereas pillararenes and calixarenes are formed from repeating aromatic units that are joined in the 2,5 and 1,3 positions, respectively, cyclotriveratrylenes are joined in the 1 and 2 positions, resulting in their shallow, bowl-like cavity. Like these two similar macrocycle classes, cyclotriveratrylenes can be easily functionalized at the upper rim, effectively extending the size of the cavity, often in an alternating pattern to form C_3-symmetric cyclotriveratrylenes. In addition to their use in detection schemes, cyclotriveratrylenes have also been used for materials applications and in separation chemistry.[1387,1388]

Gosse and coworkers have developed several cyclotriveratrylene hosts for the complexation of choline, an essential nutrient, and acetylcholine, a neurotransmitter, both of which are present in mammalian brains.[1389] In 2009, the group developed a cyclotriveratrylene bearing alternating electron-donating methoxy groups and electron-acceptor phosphonate groups, **244** (Figure 94).[1390] While this is the first reported example of a fluorescent detection method using a cyclotriveratrylene, acetylcholine was only found to bind to **244** with association constants of 63 M^{-1} in water and 23 M^{-1} in physiological media, and no other analytes were examined. In a subsequent publication, the group developed **245** (Figure 94), a similar host, which was found to bind to choline more effectively than acetylcholine in HEPES buffer with association constants of 66 M^{-1} and 23.4 M^{-1}, respectively, with a 1:1 host-guest stoichiometry assumed.[1391] Additionally, trimethylpentylammonium, tetramethylammonium, and methoxycholine were found to bind less effectively than choline, leading the authors to conclude that the hydrogen bonding abilities of choline coupled with electrostatic and cation-π interactions drive the host-guest binding of choline in this instance. Improving upon these two systems, **246** (Figure 94) was found to bind to acetylcholine and choline with association constants of 5.39 x 10^2 M^{-1} and 2.40 x 10^2 M^{-1}, respectively.[1389] In contrast to the selectivity observed with **245**, **246** was more selective for acetylcholine than choline, and other, less polar quaternary amines, trimethylpentylammonium and methylcholine, demonstrated a higher binding affinity than either target analyte, indicating strong contributions from intermolecular hydrophobic interactions. Limits of detection were found to be 0.25 mM for acetylcholine and 0.5 for choline, which are lower concentrations than the 1 mM amounts typically found in the human brain.

The emission of **247** (Figure 94), a cyclotriveratrylene bearing quinolinyl appendages, was found by Moriuchi-Kawakami et al. to be enhanced by the presence of Cu^{2+} in acetonitrile.[1392] A 12-fold increase in emission was observed, with Mg^{2+} and K^+ only leading to 4-fold and 2-fold increases, respectively. A poly(vinyl chloride) polymer membrane was then used to encapsulate the cyclotriveratrylene host and used for the detection of concentrations of Cu^{2+} as low as 10 μM. The detection of metal cations, anions, and small molecules was also probed with a series of cyclotriveratrylene-lanthanide metal coordination polymers by Ma et al.[1393] Due to their electron-rich nature and bowl-shaped shallow cavity, cyclotriveratrylenes can act as electron exchange donors to enhance the luminescence of lanthanide metals through sensitization (section 2.2.3). The emission profiles of both Eu^{3+}-**248** and Tb^{3+}-**248** (Figure 94) coordination polymers were quenched by the presence of Fe^{3+}, MnO_4^-, and nitromethane. Stern-Volmer constants of the host-guest interaction of Fe^{3+} with the Eu^{3+} and Tb^{3+} coordination polymers were found to be 3.697 x 10^3 M^{-1} and 8.005 x 10^3 M^{-1}, respectively. In contrast, the Stern-Volmer constants for binding with MnO_4^- were found to be 5.989 x 10^3 M^{-1} with the Eu^{3+}-**248** coordination polymer and 1.460 x 10^3 M^{-1} with the Tb^{3+}-**248** coordination polymer. While no other anion or cation was found to similarly quench the systems, other iron species, M^{3+} species, or anions with similar oxidizing properties as MnO_4^- were not examined. Nitromethane also quenched the emission of these coordination polymers, with quenching efficiencies of approximately 90 %. However, no other nitro-organic compounds were examined, and so the system selectivity could not be determined.

Cyclotriveratrylenes have been found to be effective for the binding and detection of C_{60} due to electronic complementarity between the electron rich cavity of cyclotriveratrylene and the electron accepting capabilities of fullerenes, which leads to photoinduced electron transfer.[1394,1395] Fullerenes, which are carbon nanomaterial cages with extended π-systems, are of interest due to their redox-active properties, potential use in photodynamic therapy, and antimicrobial activity.[1396] Yang et al. developed two cyclotriveratrylenes, **249** and **250** (Figure 94), bearing sugar-derived lactopyranosyl and glucopyranosyl appendages, respectively, which extend the cyclotriveratrylene cavity and enhance the water solubility of the host and the host-guest complex.[1394] In the presence of C_{60} in a 1:1 toluene-DMSO mixture, the fluorescence of both cyclotriveratrylene hosts decreased, with an 80 % quenching of the **250** fluorescence observed with the addition of 5 equivalents of C_{60}. Association constants of the **249** and **250** host-guest complexes were found to be 5.09 x 10^4 M^{-1} and 1.38 x 10^5 M^{-1}, respectively, with the bulkier lactopyranosyl chains of **249** slightly hindering the binding of C_{60}. In contrast to the mixed organic solvent, fluorescence changes in aqueous solution were only observed after an extended time period of 30 hours, with significant

differences observed after 20 days. Deschamps et al. synthesized cyclotriveratrylenes with zinc(II) porphyrin appendages which bound moderately well to C_{60} and led to fluorescence quenching.[1395] **251** (Figure 94), which bears a single zinc(II) porphyrin appendage, was found to bind to C_{60} with an association constant of 4000 M^{-1} and a Stern-Volmer constant of 2.86 M^{-1}. Increasing the number of appendages led to dimerization of the zinc(II) porphyrin moieties, thus blocking off the binding pocket and hindering binding.

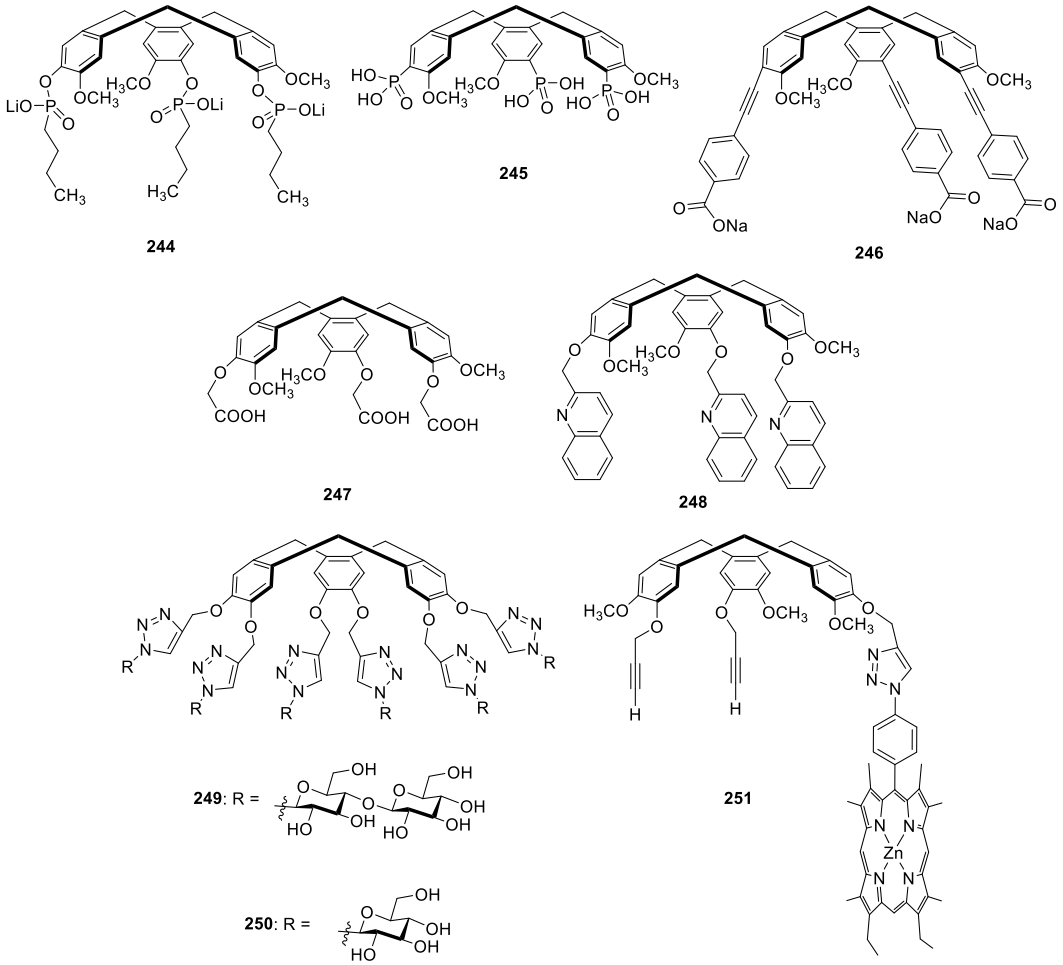

Figure 94. Cyclotriveratrylene hosts used for the fluorescence detection[1389-1395]

5.3. Metallamacrocycles.

Metallamacrocycles, also known as metallacages and metallacycles, are supramolecular hosts which are formed spontaneously by metal-ligand coordination-driven self-assembly.[1397,1398] Because transition metals have well-defined and predictable coordination spheres and ligand interactions, they can be used for rational and predictable metallamacrocycle design. The presence of a metal node in the macrocycle leads to unique photophysical properties, and often higher selectivities for certain analytes compared to analogous non-metallic hosts. Due to the spontaneous and straightforward nature of the self-assembly process, the use of tunable ligands allows for highly modular syntheses, in which libraries of these compounds can be rapidly produced and their sensor ability can be rapidly screened.[1399]

Two tetracoordinate platinum-based metallamacrocycles have been reported by Mukherjee and coworkers for the detection of pyrophosphate, a biologically relevant anion,[1400] and maleic acid, a commonly used raw material for industrial processes,[378] by analyte-induced fluorescence enhancement. The emission profile of metallamacrocycle **252** (Figure 95) underwent a 3.5-fold increase in intensity upon the

addition of one equivalent of pyrophosphate, with a Stern-Volmer constant of 2.4 x 10^4 M^{-1}, and no other anions, including dihydrogen phosphate, promoted such enhancement.[1400] However, no other biological sources of phosphate were examined, nor were analyte competition experiments conducted. **253** (Figure 95) bound maleic acid with a 1:2 host-guest stoichiometry, a Stern-Volmer constant of 1.4 x 10^4 M^{-1}, and a resultant 2.5-fold fluorescence enhancement.[378] Other dicarboxylic acids, by contrast, induced only minimal changes in the fluorescence spectrum. Despite the similarities between **253** and **252**, there are no reports of anions being examined as guests for **253** nor dicarboxylic acids being examined for possible binding with **252**. Stang and coworkers synthesized ruthenium-based metallamacrocycles **254** and **255** (Figure 95) that were also used for the detection of multi-carboxylate species.[1401] 9-fold, 7-fold, and 5-fold increases in emission of **255** were observed upon the addition of four equivalents of citrate, tartrate, and oxalate, respectively, and with Stern-Volmer constants of 1.9 x 10^4 M^{-1} with tartrate and 2.7 x 10^4 M^{-1} with citrate. Other anions investigated interacted only minimally with both macrocycles.

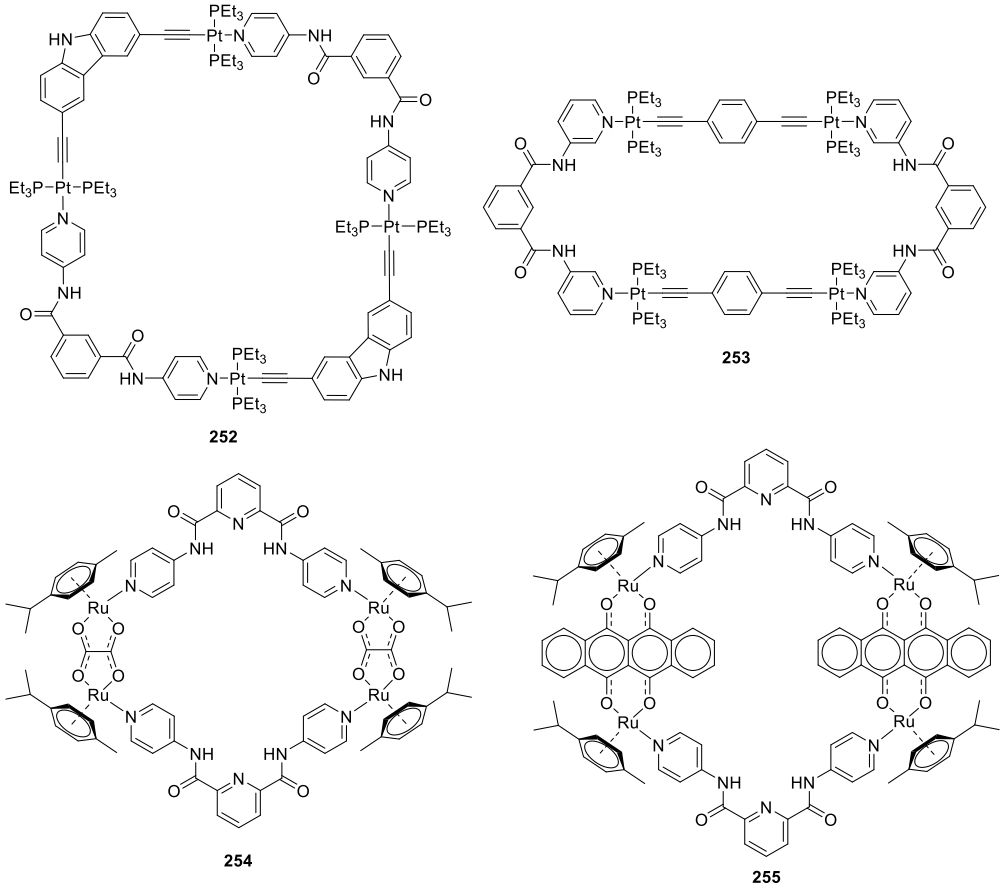

Figure 95. Platinum- and ruthenium-based metallamacrocycles that have been used for the detection of organic anions[378,1400,1401]

Wu et al. reported the synthesis of cobalt-based **256** (Figure 96) and its use for the selective detection of ATP, with no other biological phosphate leading to an emission change.[1402] Although the technique was selective, the fluorescence of **256** did not change until 20 equivalents of ATP were added, and while there was a linear change in fluorescence between 30 and 40 equivalents, there were no further changes at higher ATP concentrations. Thus, this system was only viable in a small range of ATP concentrations, with lower, biologically-relevant concentrations being undetectable. The Stang group produced bi- and tri-metallic macrocycles **257** and **258** (Figure 96) that were used for the detection of the nitroaromatics picric acid and trinitrobenzene.[1403] The authors hypothesized that strong π-π interactions facilitated energy transfer from the electron-rich metallamacrocycles to the electron-deficient analytes, leading to decreases in emission.

Finally, Guzmán-Percástegui et al. developed a series of macrocycles of the general form **259** (Figure 96) for the detection of trinitrophenol.[1404] Higher quenching efficiencies were seen with macrocycles containing tetrahedral metal ions (i.e. n = 2), and approximately 700 μM of trinitrophenol was sufficient to quench 90% of the emission of the majority of macrocycles produced.

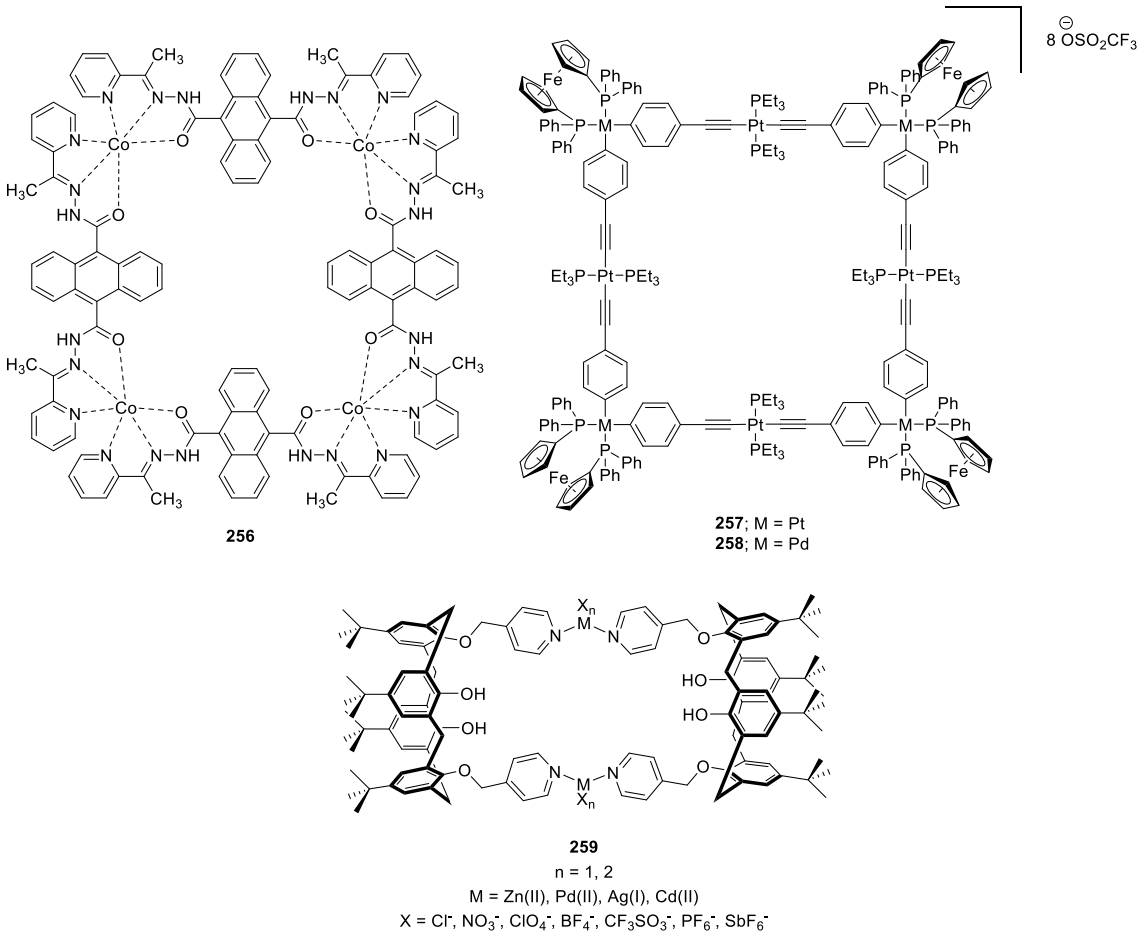

Figure 96. Metallamacrocycles that have been used for the detection of ATP and nitroaromatics[1402-1404]

5.4. Additional Macrocycle Hosts.

5.4.1. Peptide Macrocycles. Peptide-containing macrocycles have been reported extensively in the chemical literature, and their use in drug discovery,[1405] in the elucidation of biologically-relevant supramolecular interactions,[1406] and in achieving understanding of disease mechanisms and progression[1407] has been described in several excellent reviews. Compared to other classes of macrocycles, those that contain peptides tend to be more polar, due to the highly polar amide backbone; have greater varieties of three-dimensional configurations, based on the ability of the peptides to adopt α-helices, β-sheets, and other tertiary structures;[1408] and contain significantly greater structural diversity, as a result of the ability to incorporate all 20 natural amino acids as well as a variety of non-natural variants.[1409] Advantages of peptide macrocycles include synthetic accessibility of a broad range of architectures,[1410] through the use of solid-phase peptide synthesis[1411] and other synthetic techniques[1412] to access the targets, as well as the ability to access peptoids,[1413] foldamers,[1414] and other non-natural peptide-like architectures[1415] through similar synthetic techniques.

Peptide-containing macrocycles have also been used as chemical sensors, with binding of a target analyte resulting in measurable signal changes for either the analyte guest and/or the macrocycle host. These signal changes encompass changes in the ^{1}H NMR spectral signals, in the UV-visible signals, and in the

luminescence (fluorescence and/or phosphorescence) spectral properties.[1416] In one example, Iwasaki et. al. designed a peptide-containing macrocycle with photophysically active units (fluorescein or Alexa Fluor 633) covalently attached to the side chain of a lysine residue.[1417] These fluorescent macrocycles bound to the extracellular domains of a particular MCF7 cell line, with the optimal thioether-containing macrocycles identified using four rounds of guided selection. Notably, an extremely strong association complex between the macrocycle and the cell membrane was observed, with a 1.7 nM dissociation constant reported.

Fully synthetic peptide-based macrocycles were synthesized by the Harran group using a highly efficient synthetic sequence, using a chiral, orthogonally functionalized ω-octynoic acid as the key intermediate (Figure 97).[1418] The optimized synthetic sequence was used to generate a mimic of a mitochondria-derived caspase activator, with the ability to rapidly generate fully synthetic architectures critical for identifying high performance products. The use of a wide variety of other macrocyclic peptides for biologically-relevant applications, including targeted cellular sensing,[1419] the inhibition of protein-protein interactions,[1420] the targeting of telomeric repeat binding Factor 2 (TRF2) and Apollo interactions,[1421] and the detection of highly curved membrane surfaces[1422] have also been reported.

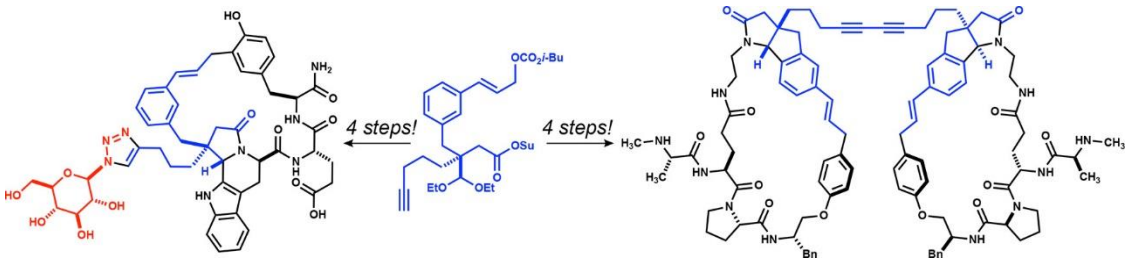

Figure 97. Schematic illustration of the use of a complex ω-octynoic acid as a scaffold for the assembly of complex, peptide-derived macrocycles. Reproduced from Ref. 1418. Copyright 2018 American Chemical Society.

An interesting example of peptide-based macrocycles for biologically relevant sensing was reported by Penas et. al., who used solid-phase synthesis with F-moc protected amino acids to rapidly assemble a 20-mer oligopeptide.[1423] A terbium-chelating macrocycle was appended to the peptide while it was still on the solid support, with subsequent cleavage from the resin, followed by incubation with a terbium salt to form the target heavy-metal containing acyclic peptide variant. Binding of this peptide to an RNA hairpin structure resulted in folding of the peptide into an ordered, α-helical structure, with concomitant increases in the terbium luminescence enabling selective sensing of the target RNA hairpin. A detection limit for this system of approximately 1 nM was reported, based on strong binding between the peptide and the RNA structure (ca. 12 nM dissociation constant). In related work, Li et. al. synthesized a gadolinium-binding peptide-based chemical sensor, which was used for the effective molecular imaging of prostate cancer via highly selective sensor-prostate tumor interactions.[1424] Other lanthanide-containing, peptide-based chemical sensors have also been reported.[1425,1426]

A combination of a macrocyclic peptide and carbon-based materials was reported as a highly sensitive and selective chemical sensor by Wang et. al.[1427] This hybrid sensor detected cyclin A_2,[1428] a protein that indicates early-stage cancer,[1429] with detection limits as low as 0.5 nM reported. Both graphene oxide and single-walled carbon nanotubes quenched the fluorescence of the terbium-chelating, peptide-derived macrocycle (Figure 98). Addition of cyclin A_2 resulted in strong binding between the cyclin protein and the macrocyclic sensor, removing the macrocycle from proximity to the carbon nanomaterials and restoring the terbium luminescence.

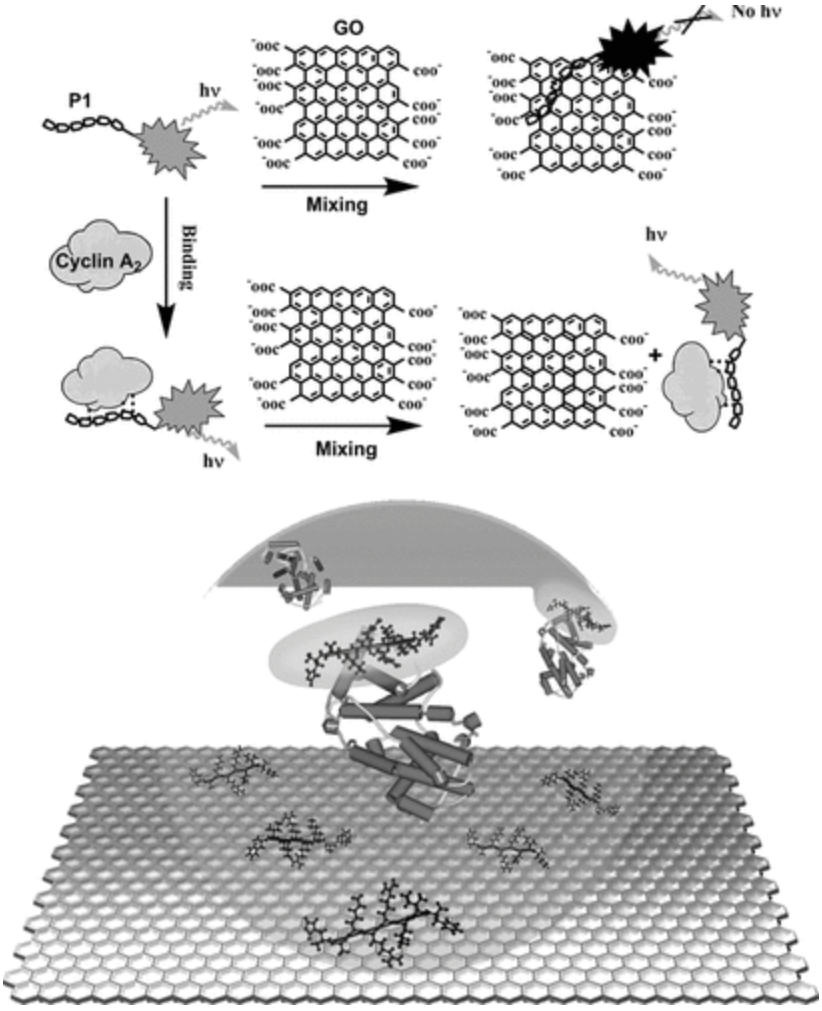

Figure 98. Schematic illustration of how a terbium-binding peptide-derived sensor can be used as a highly selective sensor for cyclin A_2 based on the restoration of the sensor's luminescence. Reproduced with permission from Ref. 1427. Copyright 2010 Wiley.

5.4.2. Other Macrocycles. The macrocyclic hosts discussed in this section are those that do not fall into any of the previously discussed categories. While the classes of macrocycles previously discussed have demonstrated favorable performance as supramolecular luminescent sensors, designing new classes of macrocycles has notable advantages, including the ability to manipulate the intermolecular forces that govern host-guest interactions, leading to the creation of hosts that are highly suited to bind specific targets.[299] For example, highly conjugated tetra-cationic cyclophane, ExBox was designed by Stoddart to form strong inclusion complexes with PAHs[292] based to π-π stacking and electrostatic (cation-π) interactions.[1430] Additionally, the Levine group has rationally designed a series of macrocycles bearing electron-rich and electron-deficient aromatic units, which they used to elucidate the effect that small changes in host structure and configuration have on the ability to bind small molecule guests.[299]

Biologically important transition metal cations, such as zinc, copper, and iron, including those with negative biological effects such as mercury and cadmium, are common target analytes for supramolecular detection schemes. An intriguing series of helical macrocycles were synthesized by Nakatani et al. for zinc detection, wherein the helical structure was held together by a salt bridge in the center of the molecule.[1431] Upon disturbance of the salt bridge, the macrocycle helical structure was disrupted, leading to measurable changes in photophysical properties. Three variations of this system were synthesized, with the only differences being whether the ester linkages were bound to the *ortho*-, *meta*-, or *para* position (**260**, **261**,

262, respectively, Figure 99) of the phenylacetylene moiety of the macrocycle core. Zn^{2+} was shown to effectively disrupt the helical structure of all three hosts, leading to zinc-induced changes in the photophysical properties. The addition of Zn^{2+} to **260** or **261** caused a significant bathochromic shift in the emission signal, with the signal intensity of **261** significantly enhanced. Conversely, the addition of Zn^{2+} to **262** led to almost full quenching of the macrocycle emission. With three different hosts leading to different fluorescence responses upon analyte introduction, this system could potentially be used as an effective array-based system. No other metal cations were examined, and the performance of this system in fully aqueous media was not examined. Moreover, the addition of trifluoroacetic acid also disrupted the helical nature of the macrocycle. Another example of zinc detection used calixarene-like "calixsalene" species **263** (Figure 99).[1432] Upon addition of Zn^{2+} to the macrocycle, a unique hypsochromic shift in emission occurred. Some transition metal ions, including Fe^{3+}, Hg^{2+}, and Cu^{2+} slightly interfered with the system's ability to detect zinc, whereas even up to 100 equivalents of Na^{+}, K^{+}, Ca^{2+}, and Mg^{2+} had no effect on the observed emission enhancement. Successful incubation of HeLa cells with **263** allowed for the detection of exogenous zinc in vitro by confocal fluorescence imaging, suggesting that this technique has potential for biological applications.

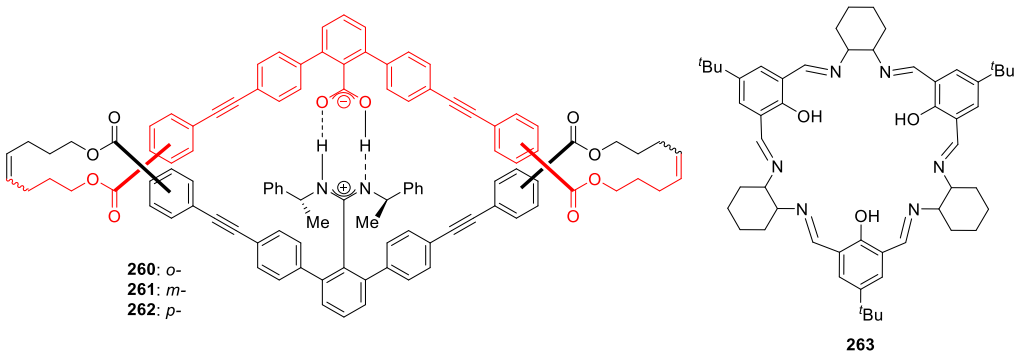

Figure 99. Several macrocycles that have been used for the detection of metal cations[1431,1432]

A fully conjugated macrocycle, **264**, provided a colorimetric and fluorescent sensor for Cu^{2+}, as reported by Feng et al.[369] In solution, this planar molecule spontaneously aggregated into nanofibers. The formation of a 1:2 host-guest complex with copper led to the full quenching of the emission spectrum due to disruption of the nanofiber structure, with other metal cations leading to only mild signal alterations. The detection limit for Cu^{2+} was 1.1 nM, and the system was effectively employed in complex environmental systems, including lake, river, and pork juice-containing samples. Moderate changes in quenching efficiency were observed in the presence of competing metal cations.

Porphyrin-like molecule **265** (Figure 100) synthesized by Ishida et al., exhibited a strong enhancement of emission upon the addition of Mg^{2+}, along with a bathochromic shift of the emission maximum from 572 nm to 639 nm.[1433] Notably, there was a negligible fluorescence response of the macrocycle to other biologically relevant cations, including Na^{+}, K^{+}, and Ca^{2+}. Transition metal species did affect macrocycle emission; however, the concentrations of transition metals are much lower than the concentration of Mg^{2+} in biological systems. Goswami et al. employed **266** (Figure 100) as a PET probe for both cadmium and zinc.[1434] Although responsive to both species, the host bound to Cd^{2+} more strongly than to Zn^{2+}, with a Benesi-Hildebrand constant of 1.14×10^{5} M^{-1} for the former and 4.08×10^{4} M^{-1} for the latter, and no perturbation of Cd^{2+}-enhanced emission was seen by the addition of Zn^{2+}. Dai et al. found that Hg^{2+} could successfully quench the emission of host **267** (Figure 100) in acetonitrile or an acetonitrile/water mixture.[1435] No other metal cations quenched or enhanced the emission of **267**, nor did they impact the quenching of the macrocycle by Hg^{2+}. The detection limit of Hg^{2+} was 0.15 μM in acetonitrile, which increased to 3.6 μM in an 8:2 acetonitrile: water solvent mixture. Likewise, the binding constant of Hg^{2+} and **267** decreased from 2.55×10^{4} M^{-1} to 5.86×10^{3} M^{-1} with the addition of water to the solvent mixture. Baxter and coworkers reported two systems in which the strained acetylenic hosts exhibited photophysical

changes upon complexation with Hg^{2+}. However, the hosts in these systems were either non-selective toward Hg^{2+} or not compared against other, potentially interfering, heavy metal cations.[1436,1437] Ganapathi et al. synthesized two S- and N-containing porphyrin-like macrocycles with BODIPY or BODIPY-like fluorophore appendages, **268** and **269** (Figure 100) which bound selectively to Hg^{2+} to produce increases in emission intensity.[1438] A final example of cation sensing reported the synthesis of three phenyl-urea based macrocycles that were shown to complex a range of cation and anion analytes.[1439]

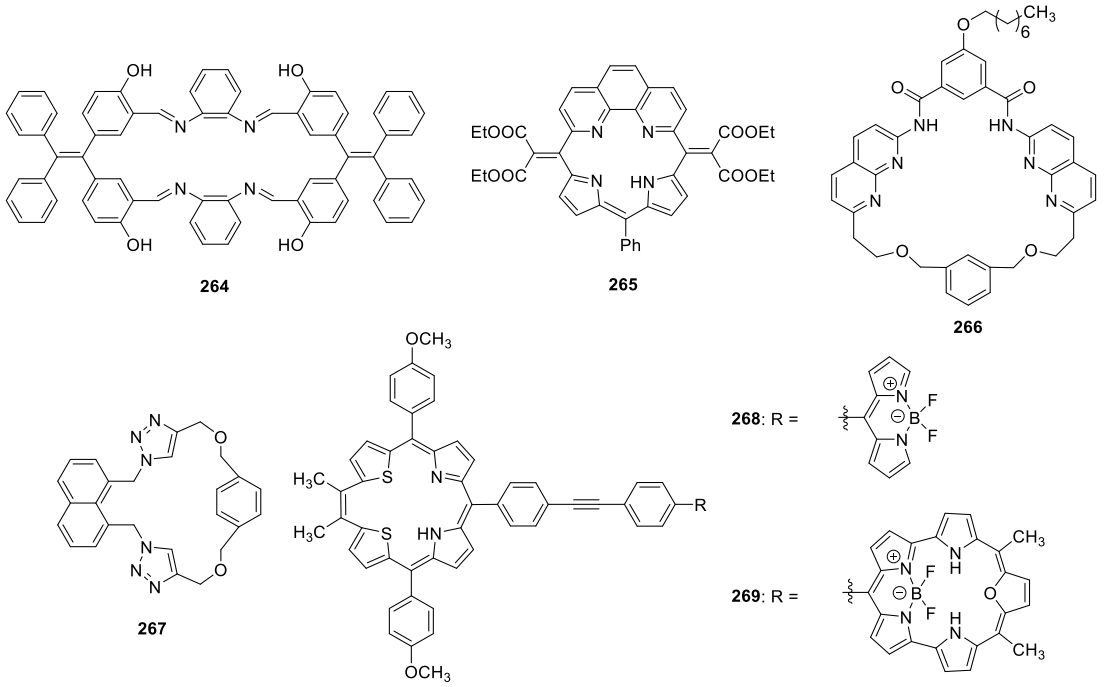

Figure 100. Synthetic macrocycles that have been employed as sensors for metal cations[1433-1435,1438]

There have been several examples of anion-sensing platforms with fully synthetic macrocycles reported since 2010, focused mainly on the detection of anions commonly found in biological systems, including phosphates, halides, and sulfates. In 2013, Martinez, Gao, and coworkers synthesized a series of acridine- and anthracene-based benzimidazolium macrocycles as selective sensors for $H_2PO_4^-$, enabling comparisons of the effects of macrocyclic structure and rigidity on the host sensing ability. In one report, acridine-containing macrocycles **270**-**273** (Figure 101) were developed, and the addition of four equivalents of $H_2PO_4^-$ caused all macrocycles to undergo substantial bathochromic shifts, which allowed for ratiometric sensing of the target anion.[1440] Notably, no other anions led to any shift in the emission wavelength maximum, and only F^- led to a noticeable decrease in emission, however, competition experiments were not conducted. It was hypothesized that $H_2PO_4^-$ promoted the assembly of excimers between two acridine moieties, whereas other anions could not. Comparing the results of the four macrocycles led to the conclusion that increased ring size decreased the magnitude of the bathochromic shift: although all macrocycles initially emitted at 430 nm, with the addition of $H_2PO_4^-$, the excimer peaks of **270**, **271**, and **272** appeared at 556 nm, 544 nm, and 503 nm, respectively. The addition of $H_2PO_4^-$ to the smallest ring macrocycle, **270**, also quenched the excimer peak so that it was less intense than that of **271** and significantly smaller than that of **272**. An increase in macrocycle rigidity decreased the extent of the bathochromic shift; rigid benzene ring-containing **273**, for example, demonstrated a smaller shift than the hosts containing flexible alkyl chains, with an excimer peak for **273** appearing at 466 nm. In the second report, acridine- and anthracene-containing benzimidazolium macrocycles with and without urea moieties, **274**-**276** (Figure 101) were synthesized and compared to **272**.[1441] The effect of the urea unit was clear, as **274** (with urea) showed almost a four-fold increase in excimer emission compared to **272**, which is urea-free. Moreover, acridine units promoted greater detection ability than the analogous anthracenyl species.

Indeed, the detection limits toward phosphate of acridine-containing **274** and anthracene-containing **275** were found to be 1.0 μM and 6.5 μM, respectively, when measured in acetonitrile solution. Competition experiments with additional anions confirmed that **274** and **272** are selective for $H_2PO_4^-$ even in the presence of 10 equivalents of competing anions.

A third example of the sensing of dihydrogen phosphate anion was reported by Ghosh and Saha in which host **277** (Figure 101) was synthesized and used as a supramolecular sensor.[1442] In acetonitrile, the addition of three equivalents of $H_2PO_4^-$ to **277** deactivated an internal PET mechanism and led to an almost seven-fold increase in emission. However, the probe was not completely selective, as three equivalents of fumarate led to a nearly three-fold fluorescence increase. Additionally, in a 1:1 mixture of acetonitrile in water, four equivalents of dihydrogen phosphate led to a negligible fluorescence enhancement, whereas the addition of ATP, ADP and pyrophosphate led to noticeable emission enhancements.

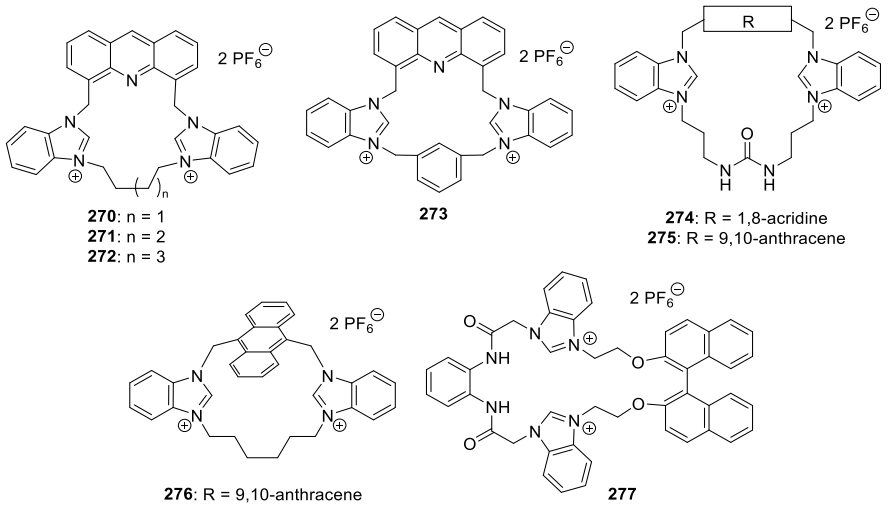

Figure 101. Synthetic macrocycles that have been used for anion detection[1440-1442]

Zapata et al. discovered that species **278** and **279** (Figure 102) were able to selectively detect bromide and iodide ions via halogen-bond promoted complexation in an aqueous environment.[390] **278**, which contains bromo-imidazolium functionalities, bound more strongly to I^- ($K_a = 6.31 \times 10^5\ M^{-1}$) than Br^- ($K_a = 2.88 \times 10^4\ M^{-1}$), leading to 5.8-fold and 2.0-fold emission intensity increases, respectively. Conversely, **279**, containing iodo-imidazolium units, bound more strongly to Br^- ($K_a = 9.55 \times 10^5\ M^{-1}$) than I^- ($K_a = 3.71 \times 10^4\ M^{-1}$), with a 6.4-fold increase in emission for the former compared to a 1.6-fold increase with the latter analyte. These findings exemplified that halogen-bonding was the predominant driving force of the host-guest binding in this system that resulted in luminescent spectral changes. No other halide or oxo-anions were shown to have an effect on the emission spectrum of either macrocycle.

Disulfide-containing macrocycle **280** (Figure 102), synthesized by Vonnegut et al., underwent discernable bathochromic shifts, when the macrocycle was fabricated into thin films and soaked in hydrochloric acid or trifluoroacetic acid.[1443] In solution phase, by contrast, no emission shift was observed. Zhou et al. developed tetrakisimidazolium host **281** (Figure 102) for the selective detection of SO_4^{2-}.[1444] The formation of a 2:1 host-guest sandwich-like complex, with a high association constant of $8.6 \times 10^9\ M^{-1}$ in aqueous solution, led to a dramatic emission enhancement. Competition experiments with up to 20 equivalents of other anions led to only small changes in the fluorescence enhancement. However, the effects of other oxygen and sulfur containing species, such as HSO_3^- or HSO_4^-, on the emission properties of the free host or of the 2:1 host-guest complex were not reported. Finally, a porphyrin-like molecule was synthesized by Do-Thanh et al. which underwent fluorescence changes upon binding to a range of ions.[1445]

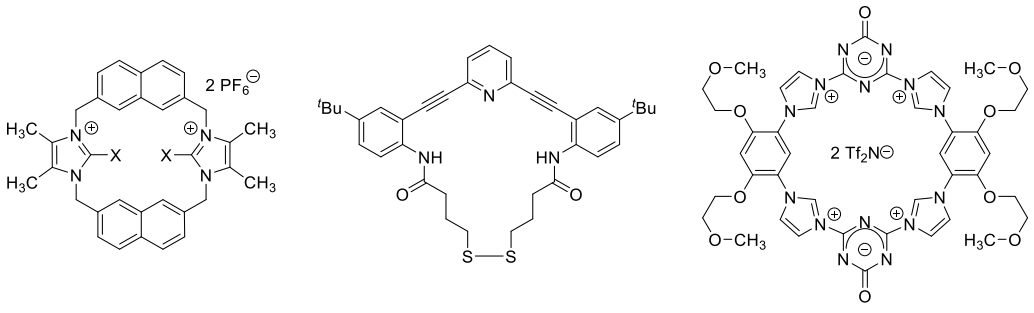

278: X = Br
279: X = I

280

281

Figure 102. Macrocycles that have been shown to sense anions[390,1443,1444]

Feng et al. were able to detect minute amounts of explosive trinitrotoluene (TNT) by analyte-induced fluorescence quenching in 95% aqueous solution, with detection limits of 1 nM, 10 nM, and 20 nM, using macrocycles **282**, **283**, and **284** (Figure 103), respectively.[1446] Although dinitrotoluene (DNT) could also be detected by this method, albeit with reduced quenching efficiency, other nitroaromatic compounds showed little effect on the emission of **282** and **283**. Compound **284** was less selective than the other hosts, with moderate fluorescence quenching induced by nitrobenzene and dinitrobenzene. This method was shown to effectively detect TNT in a complex environmental sample of a soil-water mixture, indicating that the method was not hampered by the presence of other materials, such as metal ions and organic material, that exist in such media. Furthermore, the detection scheme was translated to solid state detection, through dipping pieces of filter paper in a solution of macrocycle, and then allowing the paper to dry. Upon addition of 10 μL of aqueous solutions of varying concentrations of TNT, analyte-induced quenching was observed with UV light-irradiation, even at a low analyte concentration of 0.1 pM.

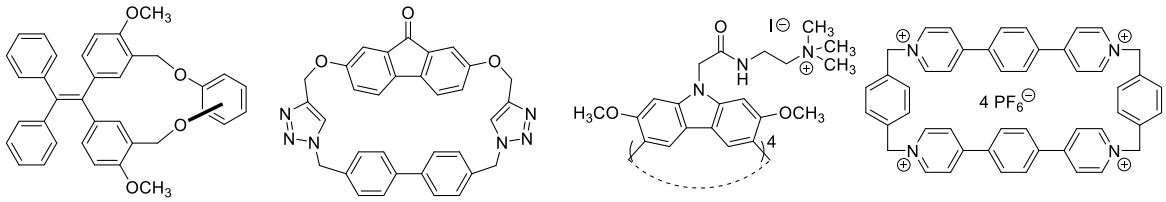

282: *o*-
283: *m*-
284: *p*-

285

286

287

Figure 103. Conjugated macrocycles that have been used for the detection of various analytes[297,1446-1448]

The Levine group has synthesized a variety of macrocycle hosts with electron-rich and electron-poor aromatic units connected by biphenyl linkers, with the general structure shown in Figure 104.[299] The macrocycles formed ternary complexes with benzo[*a*]pyrene, which is an example of a highly toxic PAH analyte, and BODIPY fluorophore, resulting in proximity-induced energy transfer from the analyte to the fluorophore. The BODIPY emission peak could be enhanced nearly 4-fold by energy transfer from the benzo[*a*]pyrene energy donor, with the particular energy transfer performance intimately dependent on the structure of the macrocycle used. The group also synthesized a fluorenone-based fluorescent macrocycle, **285** (Figure 103) that encapsulatedpolycyclic aromatic hydrocarbons (PAHs) with 2.2 nM to 37.2 nM detection limits, depending on analyte identity.[297] The same host also formed a 2:1 complex with fluoride that was detectable by changes in ^{1}H NMR chemical shifts. Another fluorenone-like macrocycle, **286** (Figure 103) was found by Li et al. to encapsulate bisphenol F, an industrially relevant toxicant, in a 1:1 ratio with a detection limit of 157 nM.[1447] In this report, one potentially interfering analyte, *p*-cresol, was found not to interfere with the detection of bisphenol F, but no other potential interfering species were examined. Scherman and coworkers employed ExBox, **287** (Figure 103) originally designed by Stoddart,[292] as a host for the detection of melatonin, a sleep hormone, via the displacement of a perylene diimide dye.[1448]

A 46% quench of emission of the dye was seen upon the addition of 1 equivalent of melatonin, and other, similar neurotransmitters had no effect on the luminescence of the ExBox:perylene diimide complex.

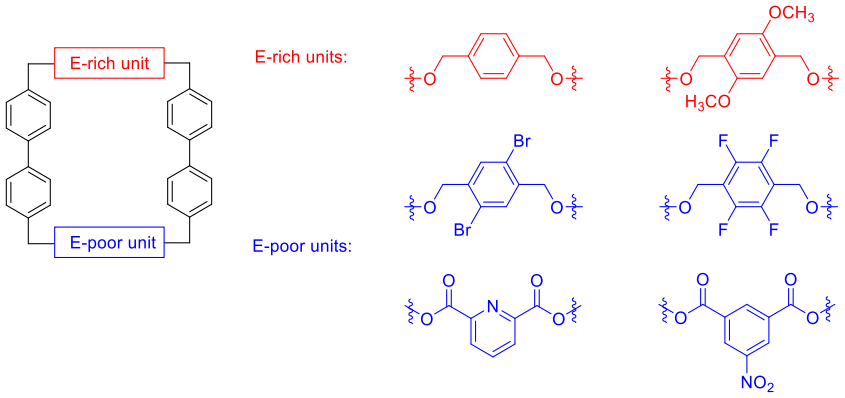

Figure 104. A series of macrocycles synthesized by the Levine group that bear electron-rich and electron-deficient units for the detection of PAHs[299]

Both (*R*)- and (*S*)- enantiomers of **288** and **289** (Figure 105) were synthesized by Ema, Anzenbacher, and coworkers and were able to differentiate between the enantiomers of cytidine monophosphate, an anionic nucleotide, with moderate selectivity.[1449] The hosts also provided unique responses to other anionic nucleotides, regardless of chirality, and a linear discriminant analysis (LDA) using the four-sensor array was constructed that allowed for 100% correct classification of the analytes. A subsequent paper by the same group found that hosts **290**-**293** (Figure 105) could be used to determine the enantiomeric excess of five different pharmaceutical agents with only a 1.6% prediction error.[1450] LDA was used to differentiate ibuprofen (IBP), ketoprofen (KTP), 2-phenylpropionic acid (2-PPA), mandelic acid (MA), and phenylalanine (Phe) and to provide semi-quantitative analysis (Figure 106). Additionally, a support vector machine (SVM) algorithm was used to fully quantify the enantiomeric excess of individual mixtures. Interestingly, the presence of non-chiral carboxylates and phosphates did not hinder chirality determination of the analytes of interest. In another example, the axial chirality of triazine-based binaphthyl host **294** (Figure 105) and similar species, were found by Xu et al. to promote the selective chiral detection of the amino acid alanine.[1451] The emission of the *R*-enantiomer of **294** increased in the presence of *R*-alanine but was unaffected by the presence of *S*-alanine. The authors proposed that mechanism of such emission increases was that the oxygen and nitrogen moieties of the macrocycle quench the fluorescence of the binaphthyl groups by PET, and analyte binding interrupts that PET.

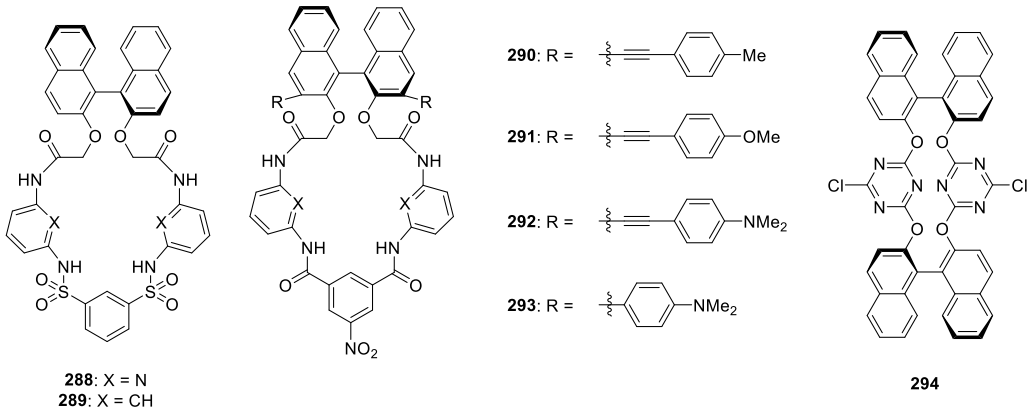

Figure 105. BINAP-containing macrocycles used for the chiral differentiation of analytes[1449-1451]

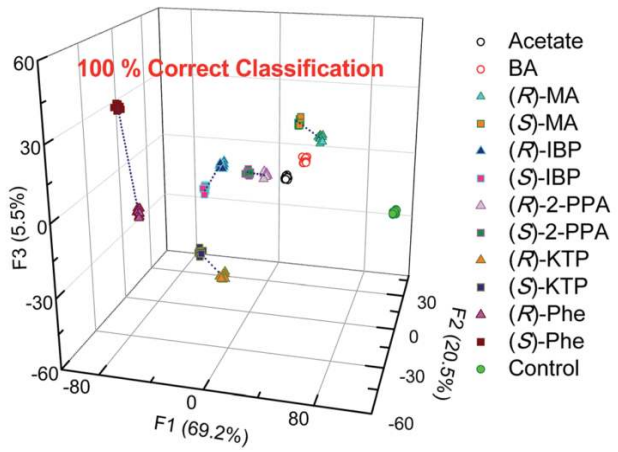

Figure 106. LDA analysis of achiral – acetate, benzoic acid (BA) - and chiral analytes –mandelic acid (MA), ibuprofen (IBP), 2-phenylpropionic acid (2-PPA), ketoprofen (KTP), and phenylalanine (Phe) - using **290-293** as luminescent sensors. Fluorescence response was dependent on enantiomeric composition, providing linear trends (dotted lines) that were used for the 100% correct classificaition of the enantiomeric excesses of mixtures. Reproduced with permission from Ref. 1450. Copyright 2016 Royal Society of Chemistry.

A series of peptidomimetic macrocycles that were designed by Burguete et al. (Figure 107), enabled the detection of aliphatic, unreactive amino acids, which are particularly challenging targets for detection.[1452] Introduction of carboxybenzyl (CBZ)-protected L-phenylalanine led to a decrease in the emission of an exciplex formed from PET between the naphthalene fluorophore and secondary amines of the host **295**. This ratiometric behavior of the host was observed in the presence of CBZ-L-valine, CBZ-L-alanine, or BOC-L-phenylalanine, with highly analyte-specific responses observed. The authors used **295** to identify the excess or deficiency of phenylalanine that would be produced from phenylketonuria (PKU) or maple sugar urine disease (MSUD), respectively. Solutions containing CBZ-L-phenylalanine, CBZ-L-leucine, and CBZ-L-valine that were comparable to those found in healthy conditions and under simulated disease conditions were added to host **295**, and the ratiometric emission output was used to differentiate the samples. Results indicated that the sample containing normal concentrations of the three amino acids gave a monomer to excimer ratio of 1-2, the sample with PKU conditions showed a ratio of 2-3, and the MSUD sample conditions produced a ratio of 0-1. Although this technique shows promise for future applications, the sensing technique was not attempted in biological conditions or aqueous media, and variations in the molar ratio of host to guest were not reported.

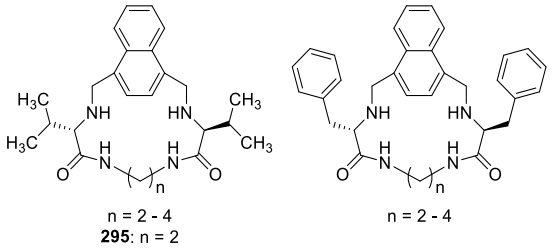

Figure 107. Peptidomimetic hosts used for the detection of amino acids[1452]

The capsule-like host shown in Figure 108 was applied to the detection of monoterpenes, fragrant compounds found in essential oils, by Suzuki et al. in 2016.[1453] The addition of an analyte led to the formation of a 2:1 host-guest system with two molecules of **296** forming a capsule-like structure around the guest and leading to changes in the emission spectrum of the host. Furthermore, the shape of the guest led to differing spatial rearrangements of the capsule, causing highly guest-specific perturbations of the

fluorescence spectra (Figure 108). The quantum yield of each host-guest system along with the fluorescence color tone (CIE chromaticity) were used to create a three-dimensional fluorescence map to be used for the identification of unknown guests.

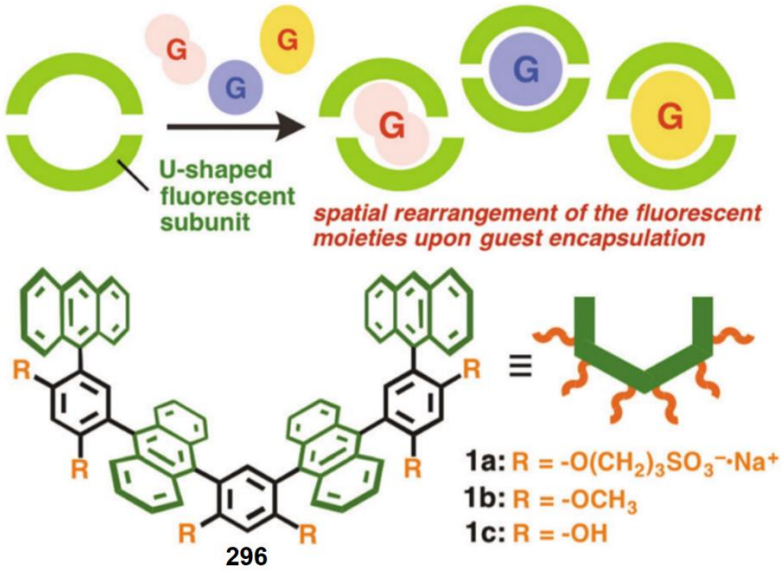

Figure 108. 2:1 host-guest system used for the detection of monoterpenes. Adapted with permission from Ref. 1453. Copyright 2016 Royal Society of Chemistry.

A final example of the design of a macrocyclic sensor was reported by Smith and coworkers in 2017.[1454] Tetralactam macrocycle **297** (Figure 109) was employed in a detection scheme for an influenza-indicative viral neuraminidase by encapsulating a guest that had been altered by the neuraminidase, thereby enhancing its fluorescent signal. Upon addition of squaraine fluorophore **298** to a solution containing the neuraminidase, the sialic acid blocking groups of **298** were cleaved to form **299** which readily threaded into host **297**. Upon encapsulation, energy transfer from the macrocycle to the squaraine led to squaraine-specific fluorescence emission at 720 nm (via 390 nm excitation of the macrocycle). This system was also used to test drug inhibition of viral neuraminidases, with potential future applications in identifying proper treatments for specific viruses.

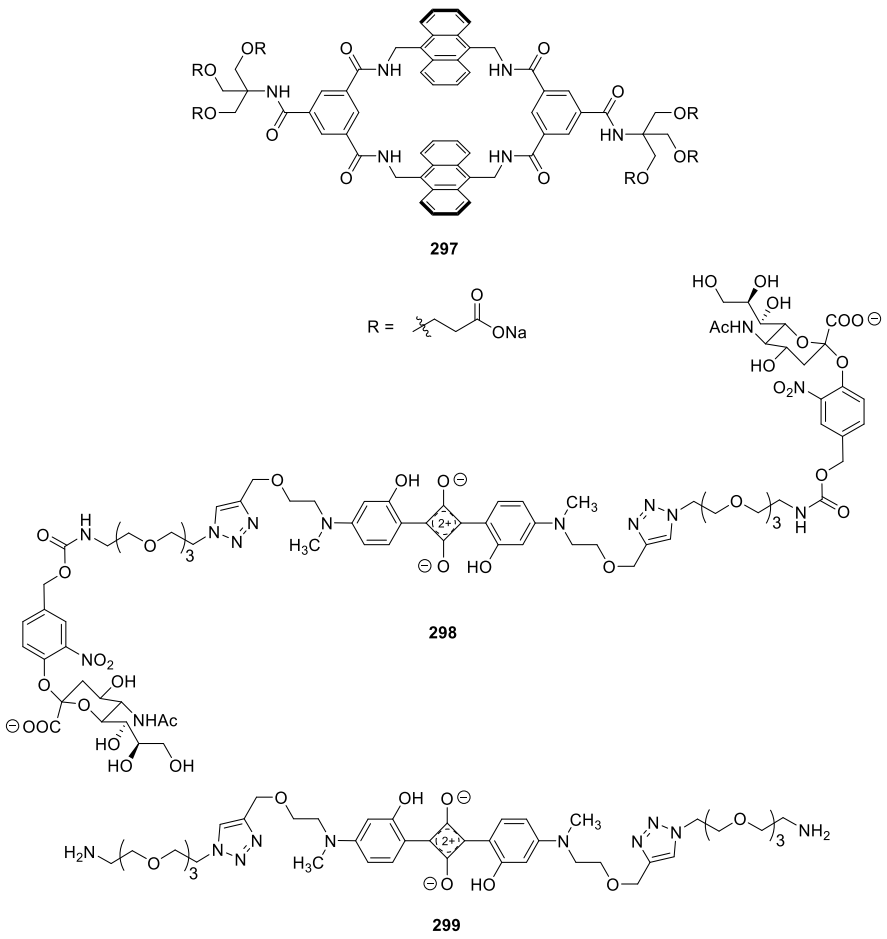

Figure 109. Host and guest species used for the detection viral neuraminidase as reported by Smith and coworkers[1454]

5.5. Mechanically Interlocked Hosts.

Mechanically interlocked hosts are those in which two or more system components are prevented from separating by steric blocking, that hinders movement between the two components, or by interlocking, that makes it physically impossible for the two components to separate.[1455] Two such architectures, catenanes and rotaxanes, are shown in Figure 110.

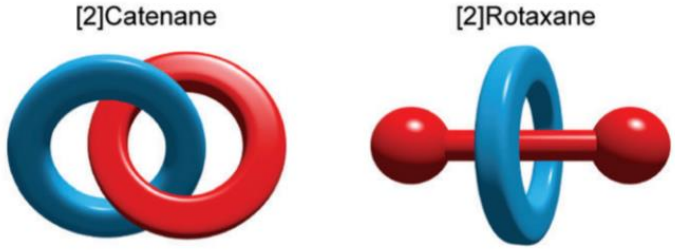

Figure 110. Representation of a [2]catenane and [2]rotaxane. Reproduced with permission from Ref. 1455. Copyright 2017 Royal Society of Chemistry.

5.5.1. Catenanes. Catenanes are composed of two or more interlocked, but not covalently linked, macrocyclic rings, and are almost always fabricated via templation of the components prior to assembly.[1456] The first allusion to the possibility of catenane structures was put forth by 1915 Nobel Laureate Richard

Willstätter in the early 1900's,[1457] however, the first published evidence of such a system was reported by Wasserman in 1960.[1458,1459] Schill and Lüttringhaus published the first directed catenane synthesis in 1964,[1460] which was improved with a metal-templation method shown by Sauvage and coworkers in 1984.[1461] Other templation methods use π-π stacking,[1462-1464] hydrogen bonding,[1465,1466] and halogen bonding to prearrange the components prior to system formation.[1456] Common applications of catenanes are in the formation of molecular machines and motors,[1467-1470] and the high profile development of catenated DNA rings was first realized by Vinograd and coworkers in 1967.[1471,1472]

Four examples of catenane hosts used for fluorescence detection of anions have been published by Beer and coworkers in the past several years, all synthesized via halogen bond templation. The first, reported in 2012, utilized catenane **300** (Figure 111) to selectively bind Cl^- and Br^- with 1:1 host-guest stoichiometries.[1473] These anions promoted a ratiometric fluorescence response, likely due to the formation of an excimer species, and no other anions perturbed the emission of the catenane. The high selectivity was attributed by the authors to the formation of a host cavity of complementary size to the analytes along with intra-ring halogen bonding between the two bromoimidazolium moieties. In 2015, the same group synthesized a zinc-porphyrin-containing catenane, **301** (Figure 111).[1474] This host underwent very slight changes in emission upon titration with Cl^-, yet no changes were seen with the addition of any other halide species. In the same year, the group found that catenane **302** (Figure 111) exhibited significant changes in emission upon treatment with $H_2PO_4^-$ and OAc^-, contrary to what was observed with **300** and **301** where no oxoanion binding was observed.[1475] Although Cl^-, Br^-, and I^- also led to changes in fluorescence emission, the differences in ratiometric response of the catenane to each anion allowed for successful differentiation, albeit not in cases where multiple analytes were in the same solution.

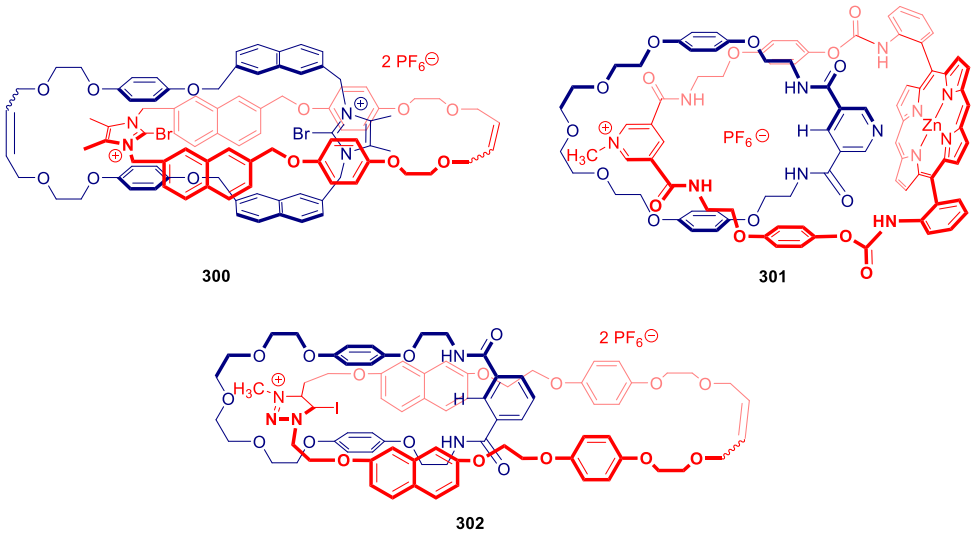

Figure 111. A series of catenanes developed by Beer and coworkers for the fluorescence detection of anions[1473-1475]

A [3]catenane was developed that was shown to undergo circumrotary motion of the two pendant rings, **303**, about the central ring, **304** (Figure 112) upon treatment with certain anions, leading to noticeable changes in emission as well as in the visible color of the solution.[1476] The central ring of the catenane (red, Figure 112) contains a fluorophore (perylene diimide, Figure 112) and two positively charged imidazolium (orange, Figure 112) units. When the counteranion of the imidazolium units was bulky, such as PF_6^- (brown, Figure 112), preferential π-π stacking between the fluorophore and the pendant rings of the catenane (blue, Figure 112) occurred, promoting strong fluorescence emission. When this complex was treated with Cl^- (green, Figure 112), which replaces PF_6^-, dual halogen- and hydrogen- bonding facilitated by Cl^- pulled both of the **303** rings from the fluorophore to the imidazolium functionalities, leading to a decrease in emission. Titration experiments with NO_3^-, $H_2PO_4^-$, OAc^-, and SO_4^{4-} showed that these anions promoted the

same behavior as Cl^- in the catenane. Notably, this system was highly solvent dependent, as protic solvents also induced circumrotary motion; thus, anion detection was only feasible in aprotic solvents.

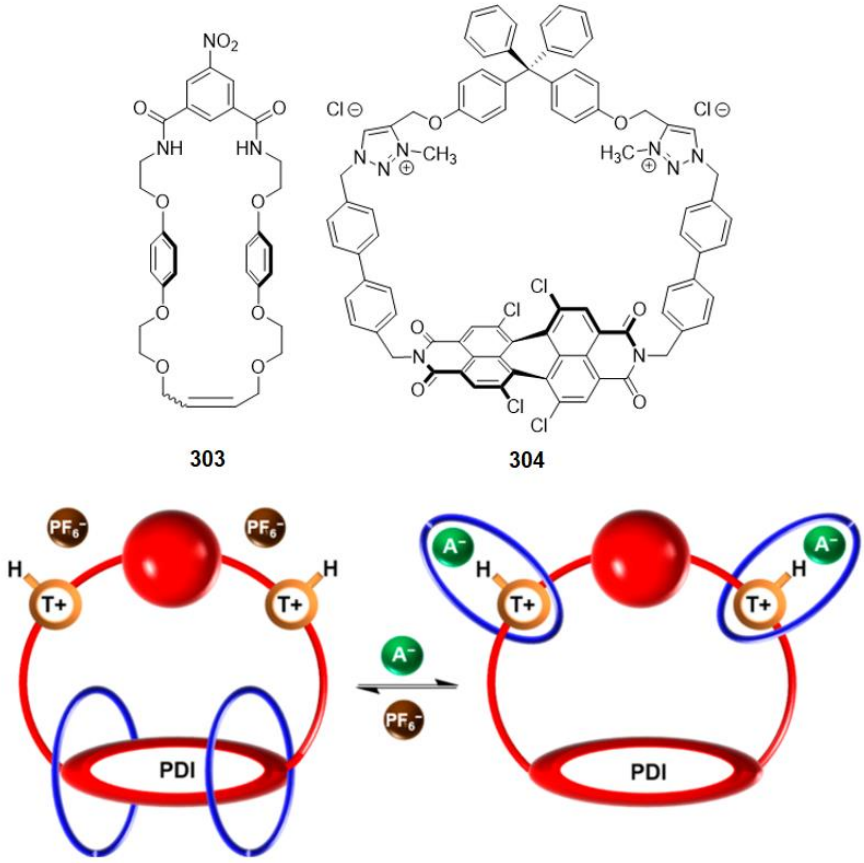

Figure 112. A [3]catenane developed by Beer and coworkers that undergoes circumrotary motion and a concomitant change in fluorescence upon complexation with different anions. Adapted from Ref. 1476. Copyright 2017 American Chemical Society.

5.5.2. Rotaxanes. Originally disclosed by Harrison and coworkers in 1967, rotaxanes are characterized by a rod-like guest, or axle, which is encapsulated by a macrocyclic species, or wheel.[1477] Noncovalent forces promote the encapsulation of the guest, whose ends are then capped with bulky groups that prevent its dethreading from the macrocycle cavity.[1478] Often, the axle precursor is encapsulated using a noncovalent template via π-π stacking,[1479] hydrogen bonding,[1480] anion binding,[1481] hydrophobic interactions,[1482] or metal ion coordination,[1483] then capped using click chemistry[1484] to form the final rotaxane. Most common are [2]rotaxanes, in which one thread and one macrocycle are present,[1485] but [3]rotaxanes[308,1486,1487] and [4]rotaxanes,[1488,1489] involving two and three wheels, respectively, have also been developed, along with higher order systems such as polymers,[1486,1490] supramolecular gels,[1491] and daisy chains.[1492,1493] Rotaxanes have been incorporated into nanovalves[1494] and MOFs,[1495,1496] and have been assembled onto surfaces.[1497,1498]

The majority of research on the use of rotaxanes for fluorescence detection applications has been published by the groups of Paul D. Beer from Oxford University, Bradley D. Smith of the University of Notre Dame, and Hong-Chen Lin from National Chiao Tung University of Taiwan. Beer and coworkers have focused much of their work on rotaxanes containing fluorescent threads capped by tetraphenylmethane moieties.[308,1487,1499] Complexation of these rotaxanes with different anions led to anion-specific fluorescence responses. For example, the addition of small anions, such as Cl^-, to [3]rotaxane system **305**, shown in Figure 113, displaced the larger PF_6^- anions, leading to small amounts of emission enhancement.[1487]

Alternatively, in the presence of small amounts of sulfate anion, the conformation of the rotaxane was altered, and the fluorescence was quenched. In the presence of larger amounts of sulfate, the fluorescence was restored. A similar [2]rotaxane system containing a indolocarbazole-bearing axle, **306** (Figure 113) was shown to detect sulfate by a moderate, sulfate-induced bathochromic shift.[1499] Most recently, the Beer group reported the enantioselective binding of dicarboxylate anions with **307** (Figure 113).[308] Installing 3,5-bis(iodotriazole)pyridinium functionalities on the axle promoted halogen-bonding with dicarboxylate anions glutamate, maleate, fumarate, and oxalate; and an (*S*)-BINOL motif was utilized for enantiorecognition of (*R*)- and (*S*)-glutamate. Complete quenching of rotaxane emission was observed, albeit in the presence of large excesses of analyte.

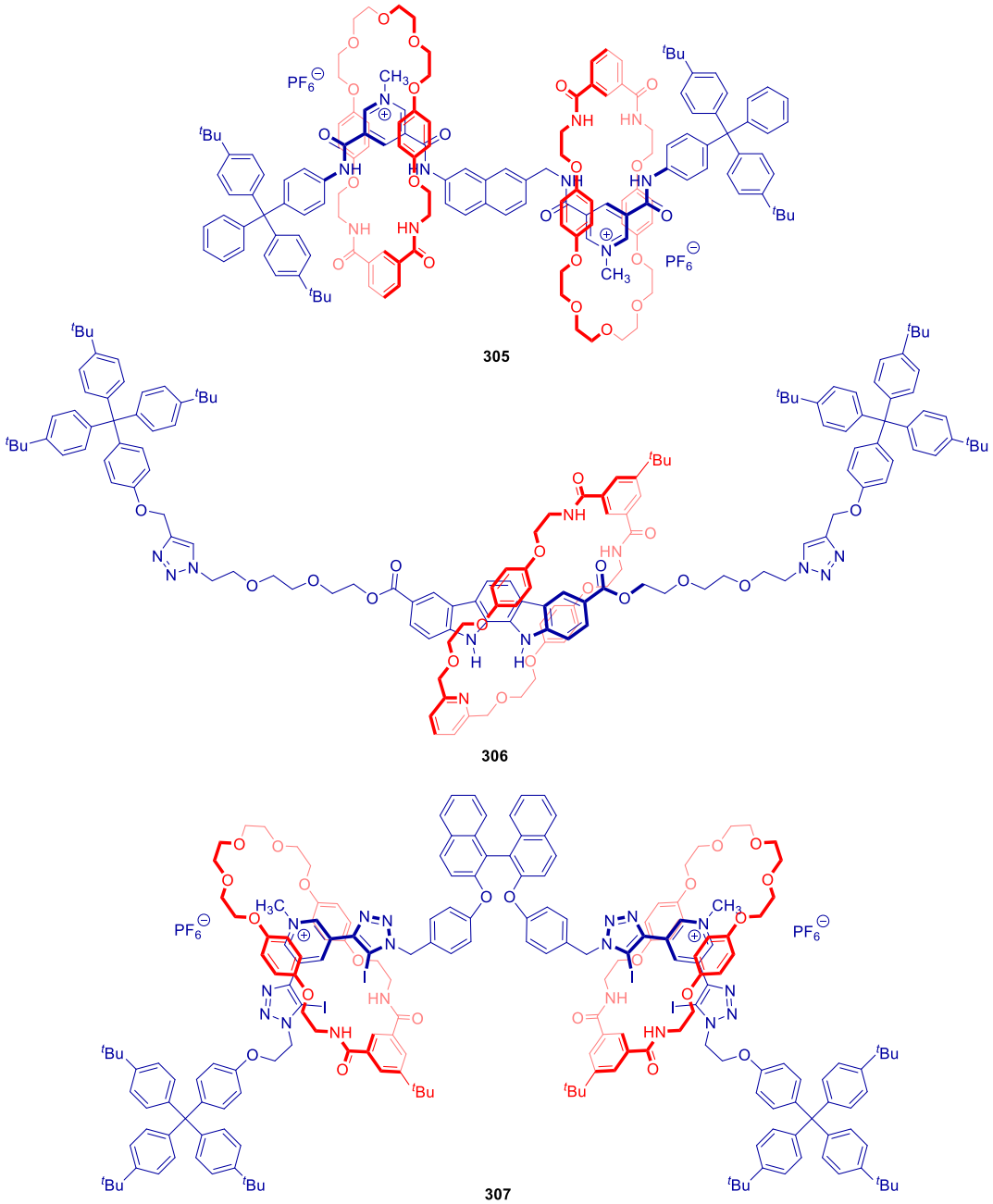

Figure 113. A series of rotaxanes developed by Beer and coworkers for the detection of anions[308,1487,1499]

The Beer group has also developed a number of rotaxanes with optically-active heavy-metal containing macrocycle components. The emission of osmium-containing **308** (Figure 114) was increased with the addition of Cl^-, $H_2PO_4^-$, and AcO^- and moderately strong host-guest associations constants were observed.[1498] Rhenium-containing **309** (Figure 114) bound to Cl^-, Br^-, and I^- via halogen bonding, with the fluorescence emission of the rotaxane enhanced by the former two anions and quenched by the latter.[1500] Additionally, lanthanide rotaxanes of the form **310** (Figure 114) were found to be semi-selective sensors for F^-,[1501] and ruthenium-containing **311** (Figure 115), bearing a cyclodextrin-capped thread, was shown to preferentially bind to I^- over other ions.[1502]

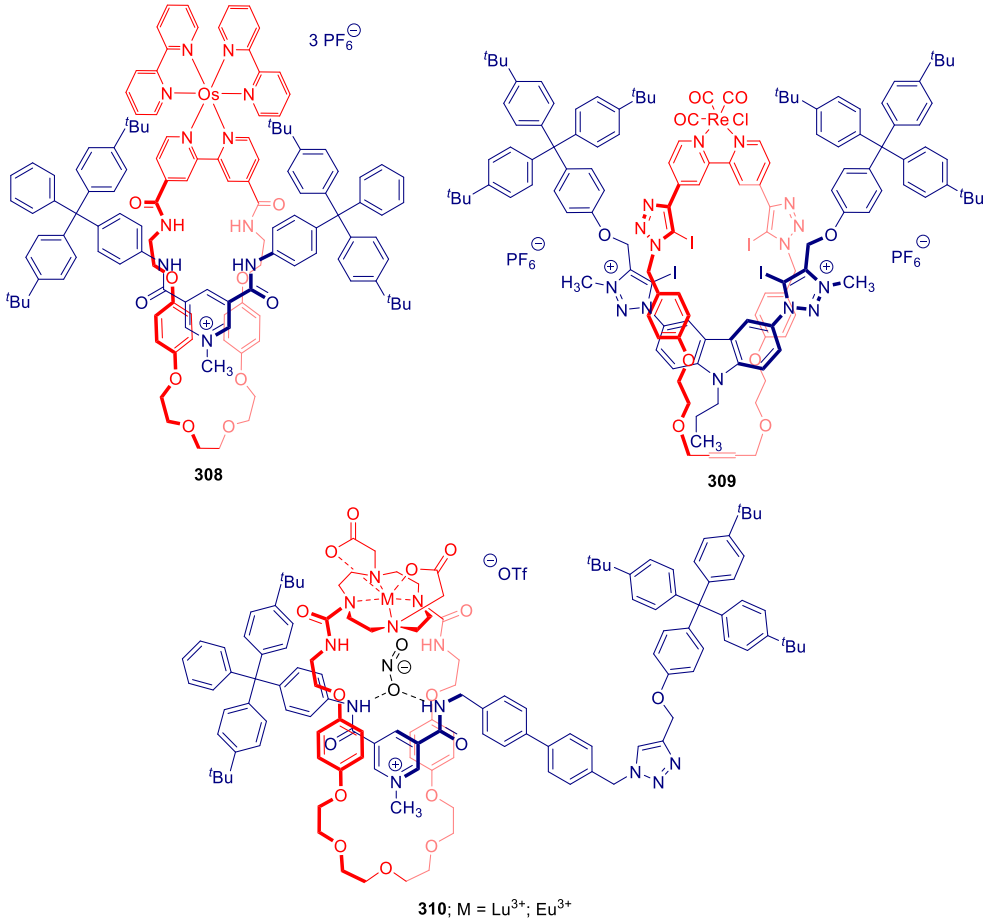

Figure 114. Heavy metal containing rotaxanes developed by Beer and coworkers for anion detection.[1498,1500-1502]

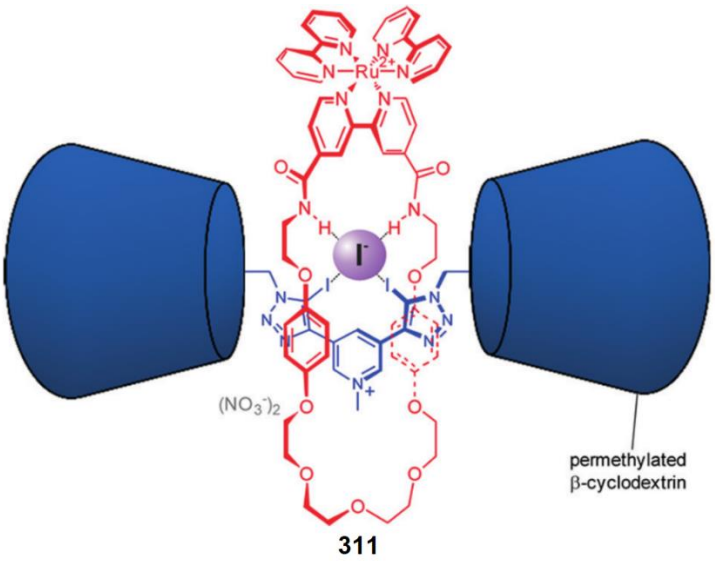

Figure 115. Ruthenium-containing rotaxane developed by Beer and coworkers for anion detection. Reproduced with permission from Ref. 1502. Copyright 2016 Wiley.

The Smith group has focused on the use of fluorescent squaraine axles (Figure 116). In the presence of Cl^-, the quenched squaraine thread of **312** (Figure 116) was displaced and fluorescence enhancement was observed in solution and on a rotaxane-soaked C18-coated silica gel plate.[1503] The group developed a set of "second-generation" ratiometric detection rotaxanes, which contained a squaraine axle that was more easily displaced by Cl^- and was less susceptible to solvent-promoted degradation and systemic artifacts.[1504] Although these systems were effective for the detection of Cl^- in the form of TBACl, the addition of more hydrophilic salts, such as NaCl and KCl, had no effect on the fluorescence emission.

The use of rotaxanes containing fluorophore-capped axles has been employed by the Lin group in recent years. Compound **313** (Figure 116) bearing a diketopyrrolopyrrole cap, was shown to be selective for the detection of F^- by fluoride-induced emission quenching.[1505] The fluoride anion could be displaced, and thus the emission regenerated, by the addition of trifluoroacetic acid. The addition of base to BODIPY-capped [2]rotaxane **314** (Figure 116) deprotonated the central amine of the axle, and the crown ether wheel shifted from the central amine to one of the imidazolium moieties, inducing PET and leading to an emission quench.[1506] The addition of $H_2PO_4^-$ also led to fluorescence quenching by causing a conformational change of the rotaxane. Of note, the emission of the thread alone was also quenched by the addition of phosphate, with a detection limit of 18 μM, as compared to 20 μM for the rotaxane, and with Stern-Volmer quenching constants of the thread and rotaxane toward $H_2PO_4^-$ of 4.80 x 10^4 M^{-1} and 3.75 x 10^4 M^{-1}. The presence of the axle of the rotaxane blocked the binding sites on the thread and slightly hindered interactions with phosphate. In a final report by the group, rotaxane **315** (Figure 116) selectively bound to Fe^{3+}, leading to an emission quench, with a Stern-Volmer constant of 3.7 x 10^4 M^{-1}, and bathochromic shift in the position of the emission spectrum.[370] No other cation induced spectral changes, and even when Fe^{3+} was introduced in the form of hemin, effective fluorescence quenching was observed.

Sun et al. developed a pillar[5]arene with a BODIPY-capped axle for the detection of pH, temperature, and solvent,[1491] while Shi et al. employed a [2]rotaxane with a Rhodamine B cap for the detection of pH.[1507] Finally, Wu et al. developed squaraine rotaxane **316** (Figure 116) for the detection of electric current.[1508] The rotaxane was spin coated onto a glass slide and exposed to electric current, with fluorescence monitoring using scanning confocal microscopy. Upon exposure of the sensor to 1000 V/mm of current, the fluorescence emission was completely quenched. When the electric current was removed, the emission was restored to its original intensity, and good reversibility between the 'on' and 'off' state was observed.

While all of the rotaxane systems discussed show significant promise as detection schemes for anions, pH, or other analytes, further studies are required for the full realization of the potential of such motifs.

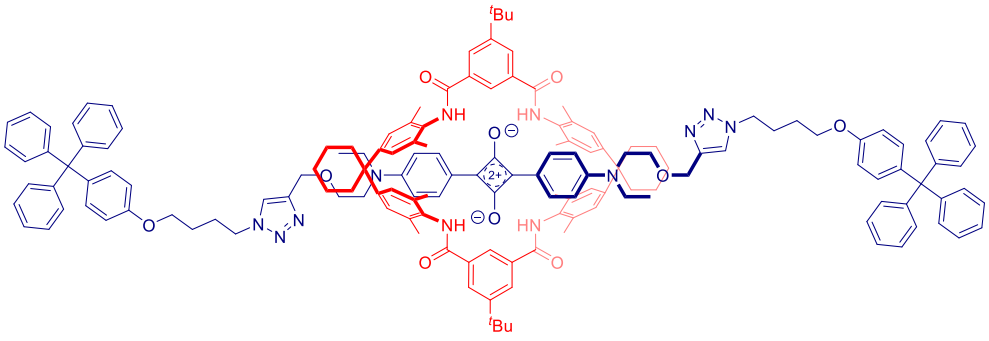

312

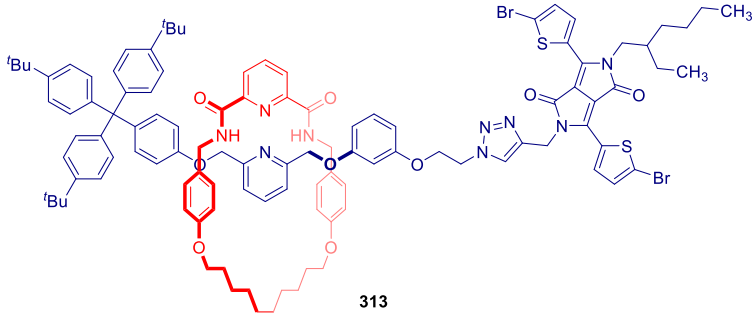

313

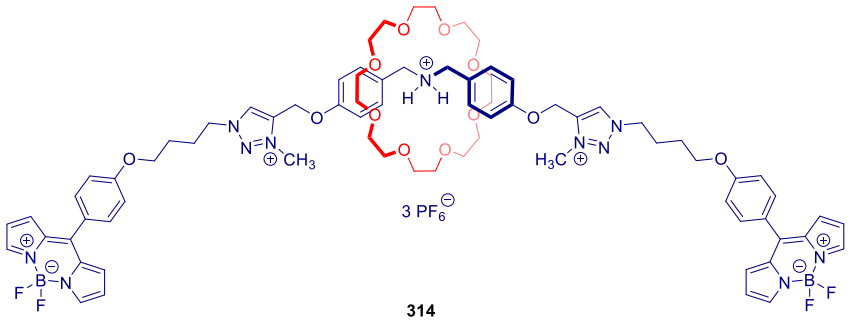

314

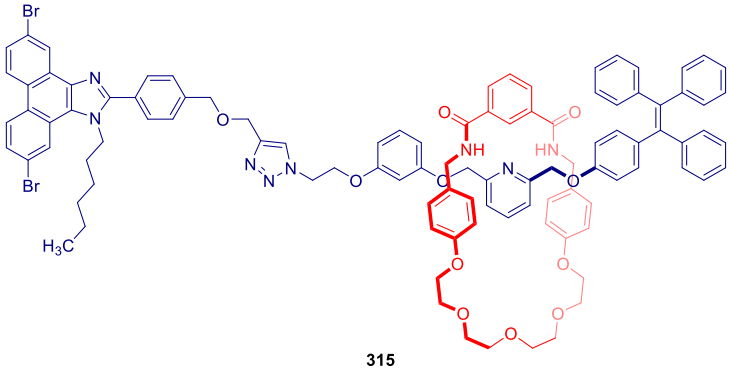

315

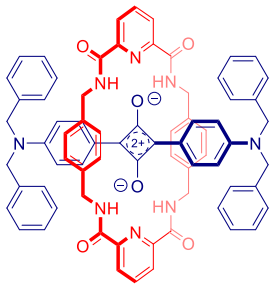

316

Figure 116. Rotaxanes containing fluorescent threads that have been employed as supramolecular hosts for detection schemes[1503,1505-1508]

6. Luminescent Polymer Sensors

The use of polymers as chemical sensors requires the existence of a transducing, or signaling element, in or around the polymer, which can respond to the presence of the analyte with a measurable change in signal. For luminescent sensors in particular, the measurable change occurs in a luminescent signal, i.e. either fluorescence or phosphorescence. Fluorescent polymer sensors are by far the more common of these two categories and can be divided into those that are conjugated in the backbone to achieve fluorescence,[86] and those that contain luminescent moieties appended from or around the main polymer chain. Of note for purposes of this review, the interactions between the target analyte and the luminescent polymer sensor are almost always through non-covalent association, which requires significant structural, spectral, and/or electronic complementary to enable efficient detection. These non-covalent analyte-polymer systems that result in luminescent read-out signals will be discussed herein as highly relevant categories of supramolecular luminescent sensors.

Because fluorescent polymer sensors rely on changes to the fluorescence signal in order to accomplish detection, they are particularly well-suited for the detection of analytes that lead to significant fluorescence changes. Such fluorescence-disrupting analytes include strongly electron-deficient fluorescence quenchers, such as 2,4,6-trinitrotoluene (TNT) and 2,4-dinitrotoluene (DNT).[1509] It also includes a variety of metal cations that cause fluorescence disruption, such as lead,[1510] palladium,[1511] and iron.[1512] Analyte-induced enhancements to the polymer fluorescence intensity can also occur,[1513] as can the detection of photophysically active analytes that interact with the polymer to enable fluorescence energy transfer from the polymer to the small molecule analytes.[1514]

6.1. Fluorescent Conjugated Polymers

Polymers that exhibit fluorescence through conjugation in the main chain of the backbone were popularized in the late 1990s by Swager and co-workers,[838] who demonstrated that the conjugated polymer backbone could act as a molecular wire.[1515] In such a wire, excitons generated at any point along the polymer backbone are able to migrate freely throughout the length of the polymer backbone before relaxing to ground state,[85] with a single binding event sufficient, in theory, to trigger a response throughout the length of the entire polymer chain, and to turn on or off the fluorescence of the entire polymer.[1514]

In practice, however, exciton migration is limited by a number of factors,[1516] including: (a) defects in the polymer chain that break the conjugation length;[1517] (b) the lifetime of the exciton which limits its ability to sample multiple receptor sites prior to relaxation to the ground state;[1518,1519] and (c) the fact exciton migration occurs through “random walk” pathways which are inefficient and are likely to lead to repeat sampling of the same sites during the exciton lifetime.[1520,1521] As a result of these limitations on the number of receptor sites sampled by a single exciton, researchers have found, using both experimental[1522,1523] and computational tools,[1524,1525] that conjugated oligomers can have remarkably similar photophysical properties and sensor performance to larger conjugated polymers.

The efficiency of exciton migration can be increased by addressing each of the factors that contribute to their general inefficiencies:

(a) Defects in the polymer chain can be minimized through the development of new and/or improved methods for conjugated polymer syntheses which limit the defects present. Such synthetic methods overwhelmingly rely on metal-catalyzed cross coupling polymerization reactions, including Sonogashira,[1526] Suzuki,[1527] Heck,[1528] and Kumada[1529] polymerizations. Although higher performing reaction conditions have been developed recently,[1530] a certain number of defects are still expected in each polymer, especially for those of higher molecular weights which are statistically more likely to contain defects. Other synthetic methods,[1531] including C-H activation polymerizations[1532-1534] and decarboxylative cross-coupling for polymerization,[1535] have numerous potential advantages, and some have shown reduced prevalence of decreases as well. Of note, the existence of polymer defects can be measured by a variety of NMR spectral analyses. In one example, Byers and co-workers reported that $^{1}H\{^{1}H\}$ NMR and $^{13}C\{^{1}H\}$ spectroscopy provided important structural information about polymer tacticity and in particular for that case, information about polymer chirality.[1536]

(b) Longer lived excitons can be generated through modifications to the polymer that increase the band gap between the HOMO and LUMO and reduce the propensity for facile exciton relaxation.[1537] Such long-lived excited states are particularly prevalent in cases where the excitation is associated with a structural change in the polymer,[1538,1539] such as a planarization/deplanarization event.[1540] The time required to reverse that structural modification and relax to the ground state results in increases to the average exciton lifetime.

(c) Random walks of the exciton in a polymer backbone can be minimized in cases where the polymer is synthesized with a gradient of electron density, or with other structural features that bias the direction of exciton migration. Such cases have been realized, for example, in polymers with low energy anthracenyl traps dispersed within a poly(phenyleneethynylene) (PPE) conjugated polymer (Figure 117).[1541,1542] Gradients throughout the polymer chain are more difficult to access synthetically, but have been reported in isolated cases[1543] as well as in dendrimers, which can be thought of as non-linear polymers.[1544] The inefficiencies associated with random walk migration can also be reduced through increasing the dimensionality of the available migration space.[1545] In particular, ensuring close proximity between polymer chains through inclusion in thin films[1546] or nanoparticles[1547] facilitates inter-chain exciton migration, which provides more effective pathways for exciton movement, and enhances the efficacy of sensors based on such constructs.[1548]

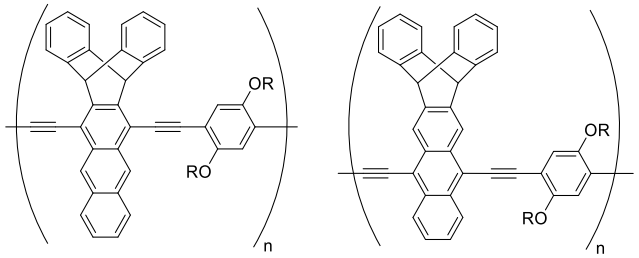

Figure 117. Poly(phenyleneethynylene) conjugated polymers containing low energy anthracenyl traps[1541]

Analyte-induced responses of such polymers include both amplified quenching[1549] and amplified turn-on[1550] fluorescence responses. Researchers working in this field have debated the relative advantages/disadvantages of a turn-on vs. a turn-off response. In principle, turn-on responses have the ability to enable enhanced sensitivities;[1551] however, in practice, challenges in obtaining a completely dark background for such systems mitigates the system-wide sensitivity.[1552] Selectivity (i.e. the ability to generate unique signals for unique analytes) is also enhanced with turn-on fluorescence sensors.[1553] In practice, however, turn-off sensors have been markedly more reported in the scientific literature, due to easier pathways to access such sensors[1554-1556]

One example of amplified quenching-based detection using conjugated fluorescent polymers is the detection of 2,4,6-trinitrotoluene (TNT).[837] In this example, the fluorescent conjugated polymer synthesized by Swager and co-workers contained bulky iptycene moieties around the polymer backbone, which resulted in significant empty space (Figure 118).[1557] These cavities were of appropriate size to enable single aromatic ring-containing molecules to diffuse inside, and the electron rich nature of the polymer backbone favored the inclusion of complementary electron deficient aromatic guests, including TNT and 2,4-dinitrotoluene (DNT). The fluorescent polymer responded to such analytes with highly efficient analyte-induced quenching of the fluorescence signal.[1558] Further sensitivity enhancements were demonstrated when the polymer was fabricated into a spin-coated thin film or coated in the interior of a capillary tube.[1559] Other fluorescent conjugated polymers systems have demonstrated strong quenching in the presence of these nitroaromatic analytes as well,[1560-1563] including in cases where the polymers have been aggregated in nanoparticles.[1564,1565,839]

Several examples of amplified fluorescence energy transfer using conjugated polymers have been reported by the groups of Swager,[1566] McNeill,[1567] and others,[1568,1569] with energy transfer occurring from a conjugated polymer to a small molecule fluorophore,[667] as well as occurring between two conjugated

polymers.[1570] Understanding the mechanism of energy transfer in these systems is key to further developments and improvements. Although Förster resonance energy transfer is the most prevalent energy transfer mechanism discussed in the scientific literature, evidence suggests that Dexter energy transfer is also operative in conjugated polymer systems.[1571] As mentioned previously (section 2.2, vide supra), the existence of a FRET mechanism can be determined by examining the fluorescence and absorbance spectra of the donor and acceptor, respectively, to determine spectral overlap, which is a prerequisite for effective FRET. If the ratio of energy transfer efficiency to spectral overlap is constant or nearly constant, FRET can be presumed. The fact that this ratio was nowhere near constant in a report from the Swager group investigating conjugated polymer energy transfer indicates that at least in that system, non-Förster based mechanisms (i.e. Dexter energy transfer) are likely predominant.[1566]

The phenomena that drive interactions between the analytes of interest and the fluorescent conjugated polymers vary significantly depending on the structure of the analyte(s) and of the polymer system.[1572] Many conjugated polymers rely on π-π stacking between the aromatic analytes and the conjugated backbone of the polymer to enable close-range interactions and drive effective sensing.[1573] These interactions have been used successfully for the detection of TNT and related nitroaromatics,[1574,1575] polycyclic aromatic hydrocarbons,[796] and nucleic acids.[1576]

While methods based on aromatic ring association generally work well, such methods are inherently limited to analytes that contain aromatic moieties capable of interacting with the aromatic polymer backbone, which precludes large classes of non-aromatic analytes (i.e. non-aromatic explosives and pesticides)[1577] from participating in such interactions. Moreover, conjugated polymers with large, flat aromatic surfaces that are optimal for π-π stacking interactions often suffer from aggregation[1578] and limited solubility;[1579] increasing solubility by incorporating bulky side chains[1580] can limit the accessibility of the surfaces to the target analytes. Architectures such as those that contain iptycene around the polymer backbone directly address the challenge of reducing aggregation while ensuring accessibility of the analytes to the polymer (Figure 118):[32] undesired aggregation is limited by the presence of bulky moieties, whereas enforced free space around the polymer backbone provides ample space for the diffusion of target analytes, such as TNT and DNT (vide supra).[1581]

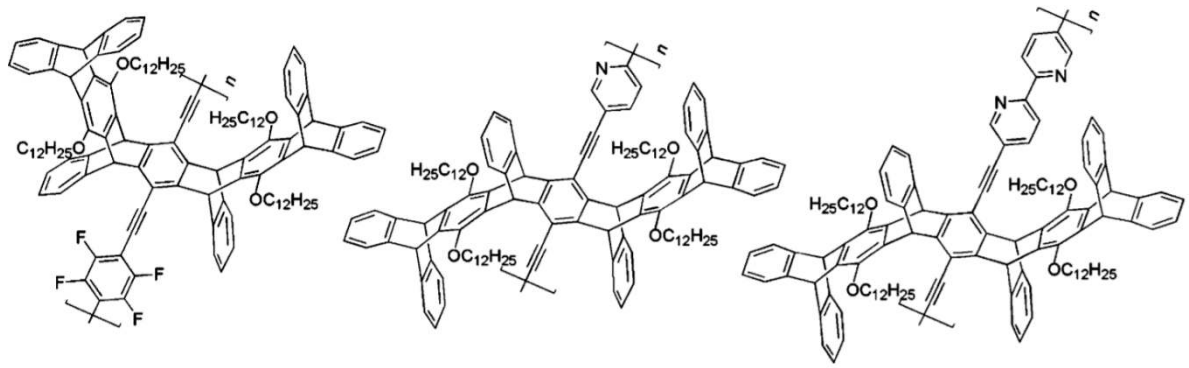

Figure 118. Bulky iptycene containing polymers that prohibit aggregation of the polymer chains. Reproduced from Ref. 32. Copyright 2005 American Chemical Society.

Solubility challenges can also be addressed through the incorporation of charged moieties,[1582] either as part of the main polymer backbone or as charged side chains.[1583] Charged polymers are almost always water soluble,[1584] and bind analytes using non-covalent electrostatic complementarity between the polymer and the target analyte to accomplish effective detection.[1585] One example of the use of electrostatic conjugated polymers, termed conjugated polyelectrolytes, is the reported binding between conjugated cationic polyfluorene and anionic, fluorophore-labeled single-stranded DNA for the detection of adenosine deaminase (ADA), the enzyme that converts adenosine to inosine (Figure 119).[1568,1586] The presence of adenosine caused the DNA aptamer to form a hairpin-like complex around adenosine. Upon hydrolysis of

adenosine to inosine in the presence of ADA, the free aptamer formed a FRET complex with the PFP polymer, leading to an increase in fluorescence. Other cationic polyelectrolyte-anionic DNA interactions have been reported by a number of research groups, including Bazan[188] and Liu.[1587] Of note, a significant concern around the use of conjugated polyelectrolytes is the possibility of nonspecific interactions with any complementary charged moiety, not only with the target analyte. Methods to reduce nonspecific binding and increase the interactions between the target analyte and the charged polymer sensor include using cooperativity of multiple favorable electrostatic interactions,[1584] incorporating an additional recognition element that facilitates the desired analyte-polymer interactions,[1588] and adding a separation step prior to detection to remove common interferents prior to binding and analysis.[1589]

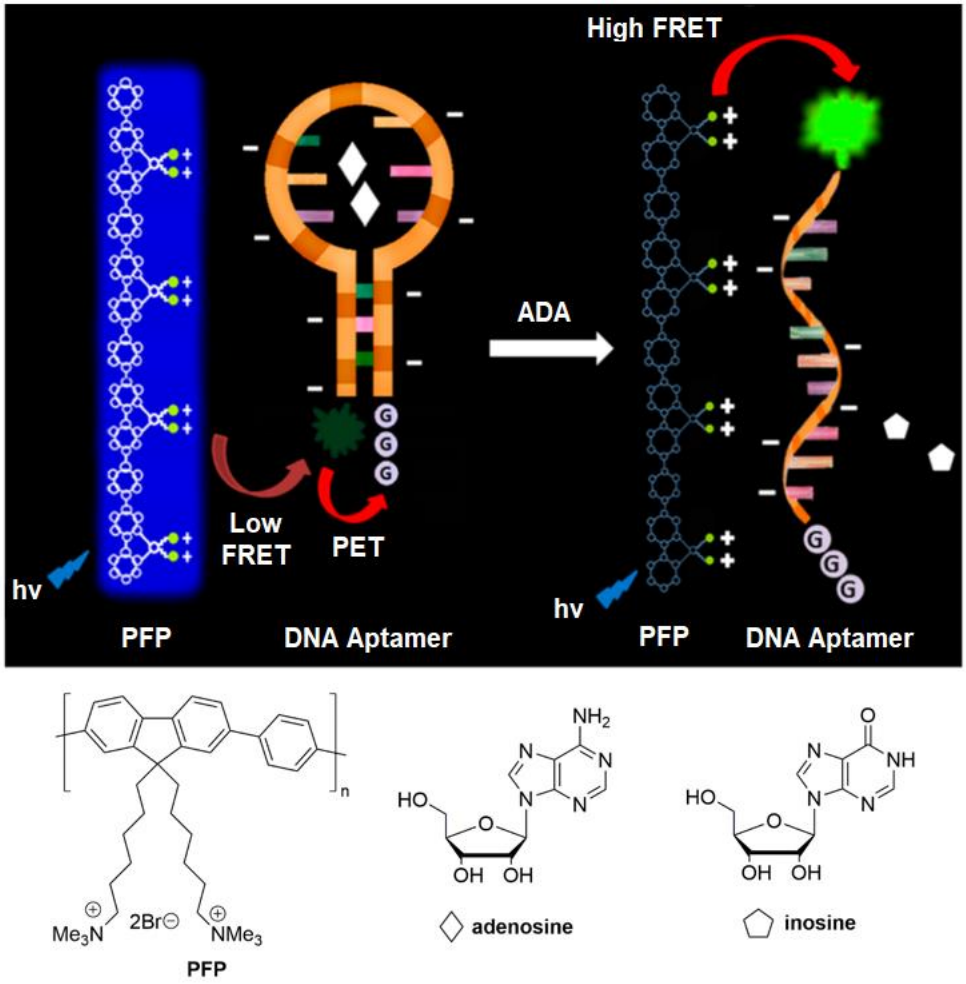

Figure 119. Conjugated cationic polyfluorene (PFP) used for the detection of adenosine deaminase (ADA) through binding with a fluorophore-labeled, anionic DNA aptamer. Adapted from Ref. 1568. Copyright 2014 Americal Chemical Society.

Hydrophobic association between conjugated polymers and target analytes can also facilitate strong non-covalent association that leads to noticeable changes in the transducing signal of the polymer.[1590] Such association has been reported, in combination with electrostatic interactions, for the detection of proteins and DNA via conjugated polyelectrolytes.[178,1591,1592] Of note, fully or completely aqueous solvent systems are required to enable favorable hydrophobic interactions between the two non-polar moieties,[1593] and the generally limited solubility of conjugated polymers in aqueous environments limits the overall application of such methods. Non-ionic methods of imparting aqueous solubility to polymers, including through the use of oligoethylene glycol chains and other highly polar substituents,[1594-1596] have also been reported.[1597]

Metal-ligand binding between a conjugated polymer and target analyte can also facilitate strong association that translates into spectroscopically detectable signals.[1598] In one example, Swager and co-workers reported the detection of ethylene gas through competitive binding to a Cu^+ complex that removed the copper from proximity to a conjugated fluorescent polymer (Figure 120).[1599] Because the proximity of the copper quenched the polymer emission, removal of the copper from the polymer proximity resulted in a concomitant fluorescence increase.[1600] In addition to utilizing metal-ligand binding for detection of non-metallic analytes, the detection of metals cations including potassium, sodium, and lithium through cation binding to crown ether appended to the backbone of a conjugated fluorescent polymer has also been reported.[754,1601-1603]

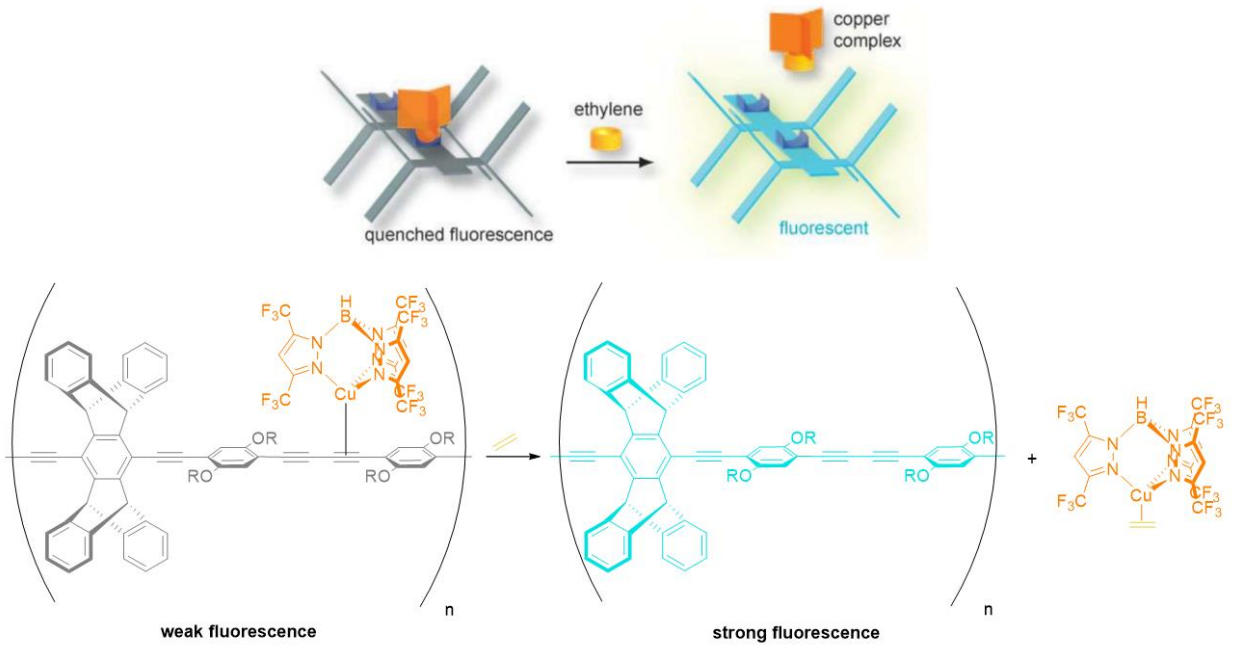

Figure 120. Detection of ethylene gas by displacement of a copper-based quenching agent from a conjugated fluorescent polymer. Adapted with permission from Ref. 1599. Copyright 2010 Wiley.

Metal-ligand binding was also the key intermolecular force in a conjugated polymer-derived potassium sensor, in which the potassium analyte was bound in a crown ether moiety appended to the polymer backbone. In this system, selectivity for potassium was achieved by the fact that it was the only metal cation that bound two crown ethers in a 2:1 crown ether: cation stoichiometry. The resulting cation-induced aggregation of the polymer resulted in a bathochromic shift of the emission maximum and decrease in the fluorescence intensity.[1604-1606] Although polymer aggregation is often deleterious to sensor performance due to a commonly observed reduction in fluorescence intensity, aggregation that occurs only in the presence of a target analyte, such as in the system reported herein and in an analogous thiol detection system,[1607] can enable turn-off fluorescence sensing of that analyte. Moreover, in some cases aggregation of a conjugated polymer can lead to enhanced fluorescence emission, in a process known as aggregation-induced emission (AIE).[1608,1609] Such aggregation-enhanced emission has been used for the detection of mercury cations, silver cations,[1610] lead cations,[1611] and explosives.[1612]

Intermolecular hydrogen bonding is another example of an intermolecular interaction that has been used in fluorescent conjugated polymers for sensing applications, including in the detection of nucleosides,[1613] nitroaromatic compounds,[1614] ammonia gas,[1615] and tamoxifen, a cancer treatment.[1616] In one example, researchers were interested in the detection of the volatile organic compound (VOC) cyclohexanone because of its prevalence in explosive packaging materials.[1617] Non-volatile explosives such as TNT, which are not easily detectable using standard vapor-phase methods, can therefore be detected indirectly by monitoring the presence of cyclohexanone. To accomplish cyclohexanone detection, Swager and co-

workers used a squaramide-containing fluorophore acceptor, relying on the known ability of squaramide to act as a strong hydrogen bond donor.[1618] In the absence of the target analyte, strong polymer-to-fluorophore energy transfer was observed. Introduction of the cyclohexanone resulted in slight movement of the squaramide from its close proximity to the polymer backbone due to the interfering hydrogen bond acceptor cyclohexanone, which decreased the energy transfer signal with high selectivity and sensitivity (Figure 121).[479]

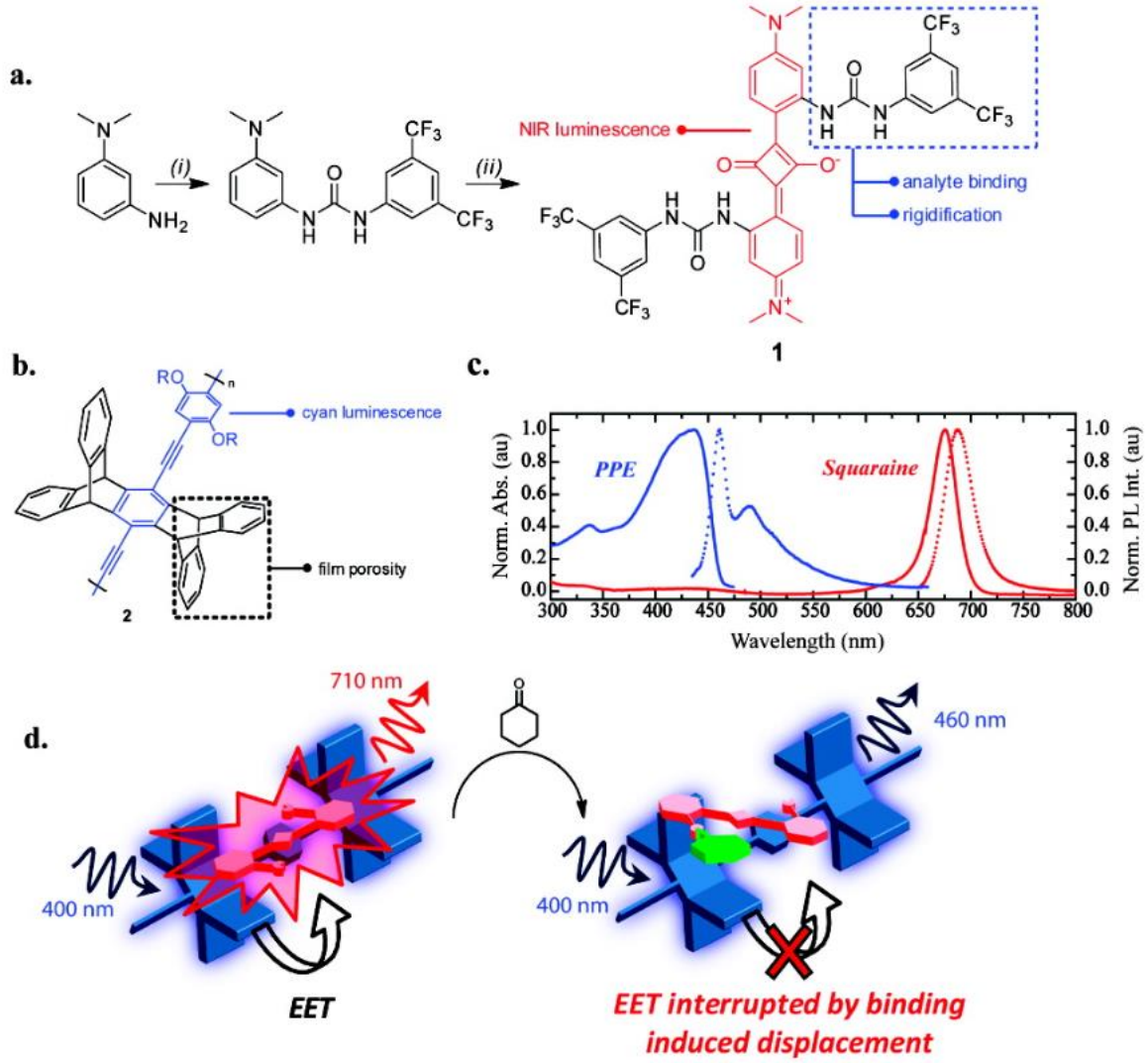

Figure 121. The use of a conjugated fluorescent polymer in conjunction with a squaramide fluorophore for the detection of cyclohexanone. (a) The synthesis of the squaramide fluorophore; (b) The structure of the conjugated fluorescent polymer; (c) The absorbance and photoluminescent profiles of the polymer and squaramide; and (d) The mechanism of cyclohexanone sensing via analyte-induced disruption of polymer-to-squaramide energy transfer. Reproduced from Ref. 479. Copyright 2011 American Chemical Society.

The use of conjugated polymers as fluorescent supramolecular sensors has a myriad of high impact applications, and readers are directed to a number of relevant review articles on this topic.[83,346,1619-1621] We review three main classes of sensing applications herein.

6.1.1. Military and National-Security Related Sensor Applications: The detection of TNT and other small molecule explosives has significant relevance for national security applications, as such explosives

are used in the fabrication of improvised explosive devices (IEDs) and in terror attacks, such as in the case of the "Underwear Bomber" in 2009[1622] and the "Shoe Bomber" in 2001.[16231624] Challenges in the detection of TNT in military settings include its extremely low vapor pressure,[842] which make the detection of buried explosives by monitoring the air above the explosive site particularly challenging.[1625] Selectivity for TNT relative to other nitroaromatics with higher vapor pressures is also challenging,[1626] although many of these nitroaromatics are found in such explosives as well and can serve as reasonable proxies for TNT detection. Military applications also require stand-off detection systems,[1627] i.e. detection that can be accomplished at a distance, to ensure the safety of the system operator, as well as systems that can withstand extreme environmental conditions without compromising system performance.[1628] The Swager group at MIT has demonstrated strong success in this field,[18] as have the groups of Trogler,[1509] Dichtel,[1629] and others.[1630]

6.1.2. Biological Detection Applications: Biologically-relevant detection applications tend to occur in aqueous environments,[1631] which requires that the polymers be soluble in such environments.[1632] Methods to impart aqueous solubility include the incorporation of charged moieties to generate conjugated polyelectrolytes or the incorporation of polar, charge-neutral side chains (vide supra).[1633] However, in some cases water-insoluble polymers can be used for detection in aqueous environments, such as in conjugated polymer thin film sensors that were dipped into an analyte-containing aqueous solution and respond to the presence of that analyte with a change in spectral signal.[1634]

Conjugated polymers can also be fabricated into conjugated polymer nanoparticles using a variety of methods, including via the hydrophobically-induced collapse of the polymer chains upon introduction of a well-solubilized polymer solution to an aqueous environment.[1635] This reprecipitation method has been used with high levels of success by Jason McNeill and co-workers, who have demonstrated strong control over the size[1636] and functionality[1637] of the nanoparticles through varying the experimental conditions used for reprecipitation. Such particles are made from conjugated polymers that are not water soluble; however, once fabricated, they are relatively stable in aqueous environments[1638] and can be used for aqueous-phase sensing,[1639] including in biological applications.[1640]

Many biologically relevant small molecule analytes are relatively electron rich, including aromatic amino acids,[1641] small molecule neurotransmitters,[1642] and pharmaceutically active compounds,[1643] which means that electron deficient conjugated polymers provide the most effective sensing platform.[1644-1646] Examples of such polymer-analyte combinations include the use of a highly fluorinated conjugated polyphenylene ethynylene for the detection of dopamine, tryptamine, and tryptophan;[1647] the use of anthryl-doped polyelectrolytes for the detection of the naturally occurring polyamines spermine, spermidine, and putrescine;[1648] the use of a porous conjugated polymer for silver (I) binding and hydrogen sulfide detection (Figure 122);[942] and the detection of other physiologically relevant anions in complex biological environments.[1649]

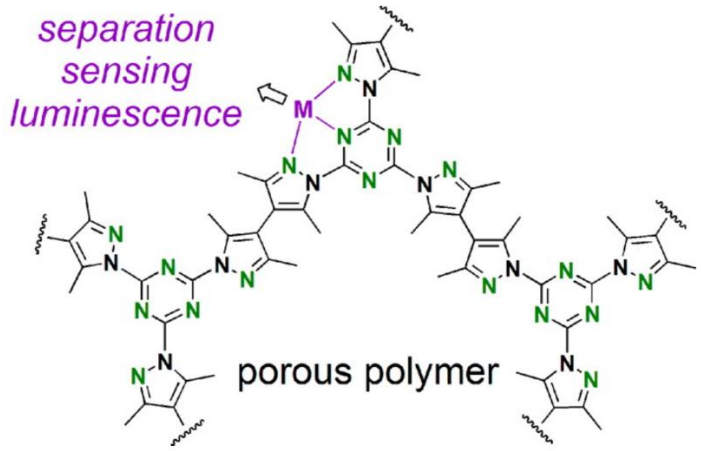

Figure 122. A porous conjugated polymer used for the subsequent detection of Ag^+ and H_2S. Reproduced from Ref. 942. Copyright 2014 American Chemical Society.

The detection of biological macromolecules such as oligonucleotides,[1650] proteins,[1651] and tumor biomarkers[1652] generally relies on conjugated polyelectrolytes binding to the macromolecular targets via electrostatically-driven complementarity.[1653] This binding is often used in conjunction with an additional system component that facilitates purification, sequestration, or detection of the target analyte, including: (a) the attachment of the polymer[1654] and/or analyte to a surface,[1655] which facilitates site isolation of the detection event; (b) the addition of a metallic nanoparticle to enhance the luminescence response;[1656] and (c) the inclusion of a nanopore[1657] and/or chromatographic method to purify the complex system and isolate the target analyte prior to luminescence detection. [1658-1660]

The sensitive and selective detection of certain cell types can also be achieved using conjugated polymer fluorescent sensors, such as in the case of selectively detecting cancer cells through sensing cell surface molecules that are specific to cancer cells but are not on that of normal cells.[978] In the reported example by Rotello, Bunz, and co-workers, cancer cells were detected selectively using an array of conjugated fluorescent polymers.[11,979] Each cell type interacted with each polymer with the interactions highly specific to each polymer-cell combination. By subjecting the results obtained from each interaction to statistical analyses, selective response patterns for each cancer type were obtained.[1661,1662] Moreover, the array was also able to distinguish cells from the same cancer type but with different degrees of metastatic potential (determining the likelihood of metastasis and correlating strongly with overall cancer prognosis).[1663] A ratiometric version of the sensor was reported as well.[1664]

In addition to sensing whole cells, conjugated polymers can also be used for bacteria sensing, which is particularly important for understanding the conditions under which a quorum of bacteria forms,[1665] and for detecting the presence of bacteria before deleterious health effects are observed.[1666] In one example of such detection, a fluorescent polymer was designed with carbohydrate substituents that are known substrates for bacterial consumption (Figure 123).[13] Bacteria that consumed these carbohydrates caused noticeable changes in the spectroscopic signal of the conjugated polymers, resulting in a sensitive and selective bacterial detection system.[1667]

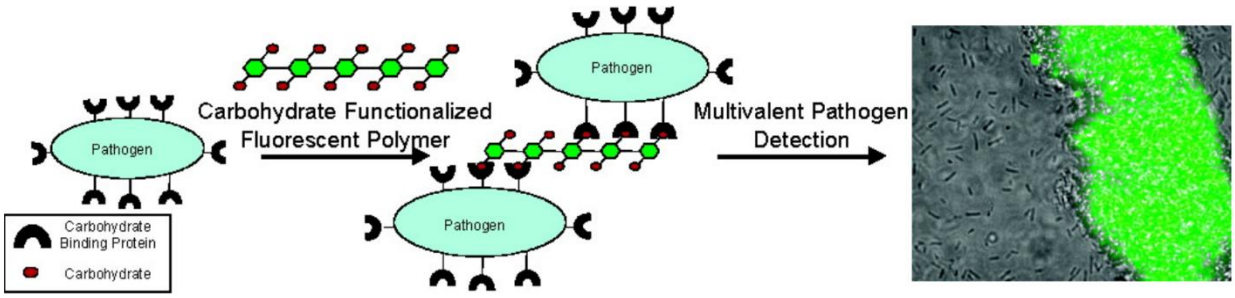

Figure 123. A Fluorescent conjugated polymer for the detection of pathogens. Reproduced from Ref. 13. Copyright 2014 American Chemical Society.

6.1.3. Food-Related Applications: The detection of analytes that can compromise food safety[1668] and/or quality is particularly important from a variety of public health objectives,[1669] including ensuring the health of the population that consumes the food,[1670] developing methods to transport food safely from the point of origin to the point of consumption,[1671] and reducing the waste of food in developed countries[1672] and the food shortages in developing ones.[1673] Analytes that are of interest for such detection include a variety of pathogenic bacteria such as salmonella[1674] and E. coli[1675] that can contaminate the food supply; small molecule analytes such as ethylene that are indicators of fruit ripening;[927] and oxygen that can indicate that a sealed container has been opened and that food spoilage will be accelerated.[932] All of these analytes have been detected using conjugated fluorescent polymers, with the bacterial testing occurring via a

carbohydrate-containing conjugated polymer, and ethylene gas detected by displacement of a copper (I)-scorpionate complex from the conjugated polymer backbone (vide supra).

Oxygen detection using conjugated polymer sensors is complicated by the fact that oxygen itself has limited spectroscopic signals,[935] and therefore detection methods need to be designed to detect something that is an effect of oxygen's presence, such as an oxygen-accelerated reaction product.[1676] Swager and co-workers demonstrated that oxygen detection could be accomplished through the synthesis of a sulfide-containing conjugated fluorescent polymer which displayed a strong increase in fluorescence with addition of oxygen, due to oxygen-induced conversion of the sulfide moieties to sulfones.[936] This transformation dramatically increased the fluorescence of the conjugated polymer, due to a reduction in the non-radiative decay pathways and to greater spatial overlap of the orbitals required for effective conjugation. Other research groups have reported analogous oxygen detection methods as well, including that shown in Figure 124.[937,1677]

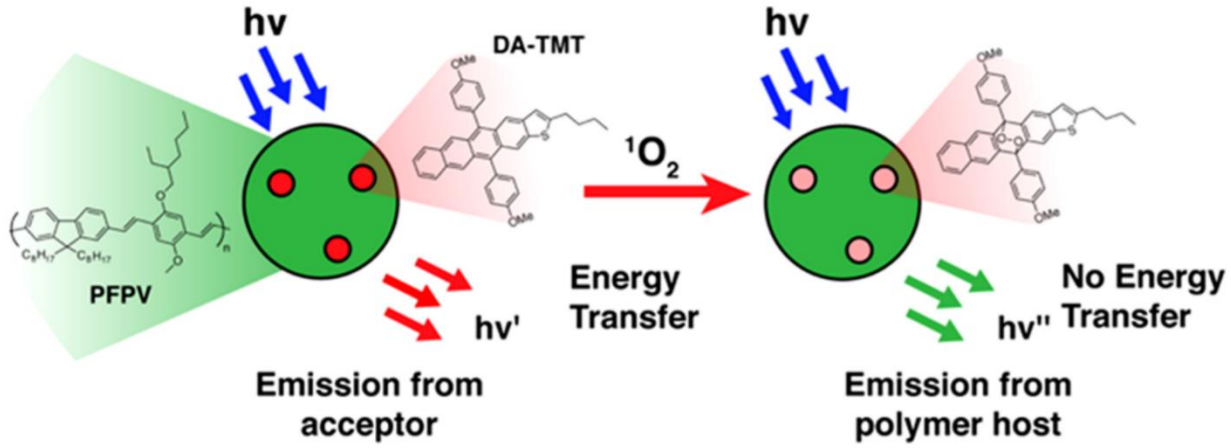

Figure 124. Ratiometric detection of singlet oxygen by a conjugated fluorescent polymer. Reproduced from Ref. 937. Copyright 2017 American Chemical Society.

6.2. Fluorescent Non-Conjugated Polymers

These include polymers that have fluorescent moieties appended to the non-conjugated polymer backbone,[1678] as well as those that are composed of fluorescent backbone segments linked by non-conjugated, non-fluorescent linkers.[1679] Advantages of using non-conjugated polymers include the fact that there are more synthetic pathways available to access the broader variety of non-conjugated polymer backbones, including free radical polymerization,[1680-1682] step-growth polymerization,[1683] and ring-opening metathesis polymerization.[1684] Moreover, the non-conjugated backbone can have unique responsiveness to external stimuli, such as pH[1685] or temperature changes,[1686] which provides an additional handle for performance tunability and additional opportunities for sensing applications.[1687] Disadvantages include the lack of facile exciton migration and the resultant sensitivity that are promoted by conjugation.[1688] Non-conjugated polymer backbones, by contrast, do not have facile exciton migration and are therefore unable to access the resulting gains in sensitivity and performance.

The synthesis of polymers with pendant luminescent groups can occur either through attaching the luminescent group before the polymerization step,[1689] or by doing so after the polymer is formed via post-polymerization functionalization.[1690] Advantages to functionalizing prior to polymerization is that greater control over the degree of functionalization is available, with each monomeric unit containing the chemosensor of interest. Disadvantages include the fact that polymerization of a more functionalized monomer and/or a particularly large monomer (i.e. macromonomer) can come with significant synthetic challenges, leading to less than ideal molecular weights and polydispersities of the resulting polymer

product. Advantages of functionalizing after polymerization focus on the ease of polymerizing an unfunctionalized monomer, whereas disadvantages include the limited control over functionalization density using post-polymerization functionalization methods.[1691]

In one example of a non-conjugated polymer with pendant fluorescent groups, Mama et al. synthesized a coumarin-appended vinyl monomer using a 3+2 Huisgen cycloaddition (i.e. click chemistry).[1692] The monomer underwent free radical polymerization in the presence of radical initiator AIBN to yield a fluorescently-appended polymer with an average molecular weight of 2.17 x 10^3 kDa and a polydispersity index (PDI) of 1.92. The fluorescent polymer was used for the detection of Cu^{2+}, with the introduction of the analyte resulting in a hypsochromic shift in the emission maximum and a significant decrease in emission intensity. The response was somewhat selective, although the presence of Hg^{2+} also led to a moderate fluorescence decrease, albeit with no change in the position of the emission maximum. The proposed mechanism by which Cu^{2+} induces such spectral changes is through bidentate binding of the copper to the triazole nitrogen and coumarin carbonyl, which planarizes the coumarin moiety and leads to facile, copper-induced aggregation.

Another example of metal cation detection using a non-conjugated fluorescent polymer was reported for the detection of Ca^{2+} in extracellular environments.[1693] In this example, tetraphenylethene (TPE), which is known to undergo aggregation-induced emission,[1694] was attached to an acrylate monomer, which then underwent free radical polymerization to yield a polyacrylic acid-derived gel. Introduction of Ca^{2+} to this system resulted in significant increases in the fluorescence intensity, with the fluorescence increasing linearly with Ca^{2+} concentration in a broad concentration range (0.1 to 10 mM). Importantly, the system response could be reversed upon addition of EDTA to sequester the Ca^{2+} cations, and good selectivity for Ca^{2+} in the presence of other physiologically relevant cationic analytes was also observed. The authors hypothesize that aggregation induced by the presence of Ca^{2+} is responsible for the observed emission enhancements (Figure 125). Of note, the underlying intermolecular interactions that enabled such detection include metal-ligand coordination between the calcium and the tetraphenylethene, as well as aromatic π-π stacking between the TPE units to enable aggregation-induced emission to occur. In a related polyacrylate system, nitro containing compounds were detected via aggregation-induced emission of TPE pendant groups.[1695] Other polymers with luminescent pendant groups that display aggregation-induced emission have been reported as well, including a triblock copolymer with carbazole-derived pendants,[1696] hetero-functionalized polymers that contain both TPE and a spiroxazine pendant group,[1697] and a non-conjugated polymer with a tetraphenylthiophene pendant group, which was also AIE-active.[1698]

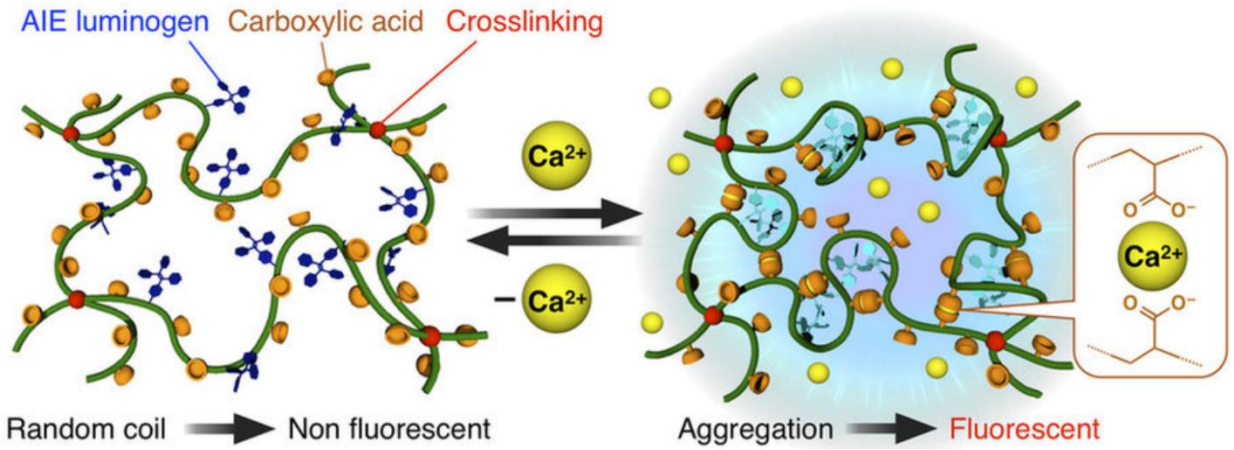

Figure 125. Illustration of a non-conjugated polymer with pendant tetraphenylene units and the proposed mechanism by which Ca^{2+} induces fluorescence enhancement. Reproduced with permission from Ref. 1693. Copyright 2016 Nature Publishing Group.

Detection of dopamine, a neurotransmitter, and the sugars glucose and fructose could also be accomplished using analogous constructs, in which a phenylboronic acid substituent was added to the acrylate monomer prior to free radical polymerization.[1699] The resulting fluorescent polymer reacted with dopamine, glucose, and fructose to form boronate esters,[1700] via the robust dynamic covalent chemistry of such functionalities.[1701] The authors propose that dopamine induced fluorescence decreases via dynamic quenching processes, analogous to literature reports,[1702] whereas the stable complexes formed with glucose and fructose demonstrated enhanced luminescence. This system also displayed slightly different read-out signals for the glucose and fructose complexes, indicating the potential for generating selective saccharide sensors. Detection limits of 0.3-0.4 mM were reported for all three of the analytes investigated.

An interesting combination of polymer and macrocycle chemistry was reported by Zhang and co-workers, who synthesized a thermoresponsive oligoethylene glycol-derived polymer with pendant cyclodextrin units (Figure 126).[1703] This polymer was synthesized from the free radical polymerization of a cyclodextrin-appended acrylate macromonomer, with final molecular weights in the range of 1.4-2.2 x10^4 g/mol and moderate polydispersities obtained. The resulting polymers demonstrated thermoresponsive behavior within a relatively narrow temperature range, with well dissolved and hydrated species at lower temperatures, and dehydrated, aggregated polymeric species at elevated temperatures. Changes in the hydration level around the polymer and the resulting aggregation states could be monitored using a variety of spectroscopic methods, including ^{1}H NMR spectroscopy and dynamic light scattering (DLS) measurements.[1704] Moreover, the inclusion of a small molecule dye, 6-(p-tolylamino)naphthalene-2-sulfonate in the cyclodextrin cavity resulted in a luminescent supramolecular construct, where the dye bound in cyclodextrin with a calculated binding affinity on the order of 10^3 M^{-1} at room temperature. Increasing the system temperature resulted in ejection of the dye from the cyclodextrin cavity, with concomitant changes in the fluorescence emission signal. The resulting system could thus be used as a luminescent temperature sensor for the determination of highly local temperature fluctuations,[1705] with significant potential applications envisioned.[1706,1707]

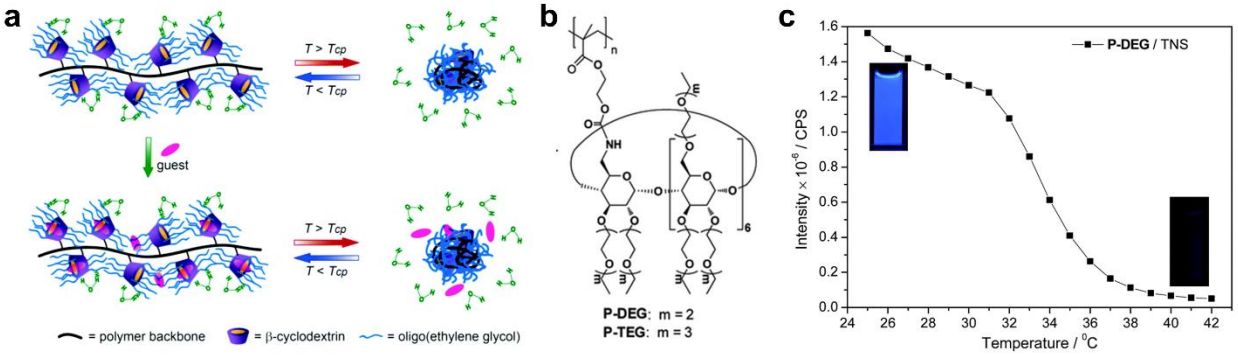

Figure 126. A supramolecular cyclodextrin-polymer construct that acts as a luminescent temperature sensor: (A) Schematic illustration of how cyclodextrin-appended polymers respond to temperature changes with changes in host-guest complexation and/or changes in supramolecular structure; (B) Structure of the cyclodextrin-appended oligoethylene glycol polymers; (C) Illustration of fluorescence changes of an oligoethylene glycol/cyclodextrin/fluorescent dye constructs as a function of increasing temperature. Reproduced with permission from Ref. 1703. Copyright 2015 Royal Society of Chemistry.

6.3. Fluorescent Non-Conjugated Polymers with Conjugated Segments.

The second class of fluorescent non-conjugated polymers discussed herein are those that contain conjugated segments covalently attached via non-conjugated, non-photophysically active linkers. Although these are less common than both of the other polymer classes discussed herein, fully conjugated fluorescent polymers and non-conjugated polymers with pendant fluorescent groups, they have unique practical advantages in sensor development. In a sense, such polymers reap the benefits of both of their component parts: they have

amplified fluorescence responses in the presence of a target analyte due to the interaction of the analyte with the conjugated segments, and they have a broader range of possible synthetic pathways and stimuli-responsive components via their non-conjugated components.

In one example, Fang and co-workers reported the synthesis of a co-polymer in which conjugated polyphenylene ethynylene (PPE) subunits containing cholesterol appendages were covalently attached via ethylene diamine linkers.[1708] The cholesterol side chains facilitated the formation of robust thin films of these polymers via drop-casting or spin-coating, following literature precedent on the use of cholesterol moieties in analogous systems. Significant fluorescence quenching of these films was induced by the addition of HCl gas, with 140 ppb of HCl sufficient to induce 80% luminescence quenching, which corresponds to a vapor phase detection limit of 0.9 ppb. Moderate selectivity for HCl was demonstrated, with other acids inducing smaller (albeit non-zero) fluorescence changes. The authors propose that protonation of the amino groups in the non-conjugated linker segments alters the HOMO-LUMO band gap and provides a site for highly efficient fluorescence quenching. The preference for HCl compared to other acids is hypothesized to be a result of the small size of the HCl analyte, which allows for facile diffusion through the thin film to reach the transducing polymer sensor.

In another example, distyrylbenzene conjugated segments were linked by isopropylene spacers to generate a segmented conjugated polymer that responded to nitroaromatic analytes with a strong decrease in fluorescence (Figure 127a).[1709] Of note, distyrylbenzene as a chromophore has been reported as a key component of luminescent amine sensors[1710] and as part of proton sensing for pH detection schemes.[1711] In this system, the styrylbenzene units were electronically isolated from each other due to the saturated linkers, which caused a highly rigid kinked structure (Figure 127b) and photophysical properties of the polymer that were essentially indistinguishable from the monomer distyrylbenzene unit. Of note, the fluorescence quenching observed in the presence of nitroaromatic analytes, including trinitrotoluene (TNT), trinitrophenol (TNP), and dinitrotoluene (DNT) was highly reversible upon washing the film with water, leading to near-complete recovery of fluorescence over six cycles (Figure 127c). One caveat in this system is that the model monomeric compounds were more effective sensors compared to the polymer architectures, although the polymers displayed enhanced stability to a variety of experimental conditions. Other examples of segmented conjugated polymers as sensors for nitroaromatics[1712-1714] and anions[1715] have also been reported.

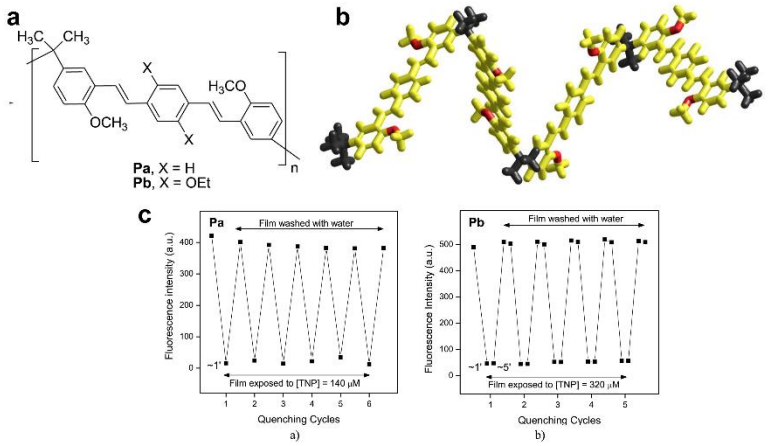

Figure 127. An example of a segmented conjugated polymer reported as a nitroaromatic sensor: (a) Structure of the segmented conjugated polymers Pa and Pb; (b) Computed structure of a four-repeat unit segment of the polymer, showing the highly kinked structure; and (c) Illustration of the reversibility of the sensor for TNP detection, where washing with water resulted in restoration of the film's fluorescence for up to six cycles. Reproduced with permission from Ref. 1709. Copyright 2017 Elsevier.

7. Luminescent Nanomaterial Sensors

Nanomaterials are defined as materials with dimensions between 1 and 100 nm.[1716] The design, synthesis, and applications of nanomaterials in a broad range of areas has received significant attention in recent years, including in the areas of drug delivery,[1717] catalysis,[1718] energy storage,[1719] and chemical sensing.[1720] The small size of nanomaterials results in a number of properties that are beneficial for chemosensing applications, including a high surface area-to-volume ratio,[1721] high signal-to-noise ratio,[1722] high signal amplification,[1723] and size-dependent optical properties.[1716] They can be fabricated from a number of substances to form metal-containing[1724] or metal-free materials,[1725] with the ability to add stabilizing external ligands[1726] and/or surface coatings.[1727] Additionally, targeting moieties can be attached to nanomaterials to enable a variety of biological applications, including the delivery of pharmaceutical agents (through targeting the diseased biological area)[1728] and the accurate demarcation of tumor boundaries (through including a tumor-targeting moiety).[1729]

Nanoparticles, the most common type of nanomaterial, are typically characterized by a spherical shape and 2-30 nm radius, and often exhibit intense, size-dependent colors.[1716] The development of nanomaterials with unique luminescent properties, including semiconductor quantum dots, lanthanide-doped nanoparticles, coinage metal nanoparticles and nanoclusters, carbon-based nanomaterials and organic dye-based nanomaterials has opened up new horizons for the detection of various analytes. In this section, developments in luminescent nanomaterial sensors will be discussed, focused on those that have been reported since 2014. This is not an exhaustive account of all luminescent nanomaterial sensors, and the authors would like to direct interested readers to several other reviews on this subject.[1730-1737]

Nanomaterials have been used most frequently for the detection of anions[762] and cations,[1738] which can be detected via electrostatically driven complementarity between the luminescent sensor and the charged analyte of interest. While small organic analytes have also been detected via nanomaterial-based sensors (vide supra),[1720] such detection generally requires more complex sensor architectures and/or schemes in order to accomplish such detection.

Nanomaterial sensors, like the other categories of sensors discussed herein, rely heavily on a broad variety of non-covalent supramolecular interactions.[1739] These interactions govern the relationship between the analyte and the sensor, determine how the analyte's presence leads to a detectable signal, and underlie the sensitivity and selectivity of the nanomaterial sensor.[1740] Although not traditionally thought of in the category of 'supramolecular luminescent sensors,' the strong similarities to other sensor categories discussed herein and the reliance on a broad range of supramolecular interactions to accomplish effective sensor performance leads us to include this category of sensors herein.

7.1. Quantum Dots

A quantum dot is a semiconductor crystal that is characterized by its small size (1-10 nm) and size-dependent UV-visible absorption and fluorescent properties.[1741,1732] The dots are most often composed of a CdSe or CdTe core, with a ZnS outer shell (written as "CdSe/ZnS" and "CdTe/ZnS," respectively) that confers substantial stability.[1742] Quantum dots have 10-100 times higher molar extinction coefficients compared to conventional fluorophores, and are the most commonly used nanomaterial for fluorescence-based sensing applications.[1743,1744] Quantum dots also have better photostability than small-molecule organic fluorophores, due to their markedly decreased susceptibility to photobleaching.[1745] Silica coatings are commonly used for the surface modification of quantum dots, particularly when biological applications are targeted, because the coating decomposes into silicic acid, which is readily cleared from the body without accumulating toxicity.[1746,1747]

Highly fluorescent quantum dot-embedded silica particles have been widely reported as detection platforms for metal cations and anions. For example, Sung et al. developed a sensor for Cu^{2+} based on monodispersed hydrophobic CdSe/ZnS quantum dots encapsulated within a silica shell.[1748] The porous silica shell of the nanostructure prevented nanoparticle aggregation. Additionally, the silica shell promoted Cu^{2+} adsorption, resulting in a strong reduction in luminescence intensity due to the displacement of Zn^{2+} from the quantum dot core. In a related report, Zhao et al. used silicon-containing quantum dots for the

selective and sensitive detection of hydroxyl radicals produced from the Fenton reaction between H_2O_2 and Cu^+, which was reduced from Cu^{2+} by ascorbic acid.[1749] Hydroxyl radicals were produced in an equimolar amount to Cu^+ in this reaction, and the interactions of the radicals with the quantum dots caused strong radical-induced fluorescence quenching. Using this radical quenching in combination with an understanding of the equimolar ratios between radical production and Cu^+ generation led to a sensor for Cu^{2+} with an 8 nM detection limit.

Other transition metals, including lead and mercury, are also popular detection targets for nanomaterial chemosensors. Xu et al. used CdTe quantum dots as well as Yb^{3+} and Tm^{3+} co-doped $NaYF_4$ nanoparticles for the detection of lead ions in human serum.[1750] The sensor was based on a FRET interaction between Yb^{3+} and Tm^{3+} doped $NaYF_4$ and CdTe quantum dots, with a reported detection limit of 80 nM. Furthermore, a fluorescence nanoprobe based on metal-enhanced fluorescence combined with FRET was developed by Liu et al. for the detection of nitrite.[1751] The probe was composed of CdTe quantum dots and gold nanoparticles, as well as denatured bovine serum albumin (BSA), which provided a binding site for Neutral Red which interacts with nitrite to effect fluorescence quenching.[1752] The fluorescence intensity of the CdTe quantum dots was optimized by varying the size of the gold nanoparticles and the distance between the two particle types. Neutral Red was bound on the quantum dot surface, resulting in a quench of the green emission of CdTe quantum dots as a result of FRET to the Neutral Red fluorophore acceptor. Green emission was recovered with the addition of nitrite, due to the disruption of the energy transfer between Neutral Red and the CdTe quantum dots. The sensor showed selectivity for nitrite compared to other ions and maintained high performance in real-world samples including tap water and lake water.

In addition to detecting anions and cations, quantum dots have also been utilized for the detection of small organic analytes. For example, a silicon quantum dot-based sensor was reported by Yi et al. for the detection of pesticides via monitoring of the activity of enzymes that are negatively affected by the presence of such toxicants.[1753] One example of such an enzyme is acetylcholinesterase, which converts acetylcholine, a neurotransmitter, to choline, an essential nutrient which in turn is converted to betaine, another essential nutrient, and H_2O_2 by a second enzyme, choline oxidase. H_2O_2 as an analyte was able to selectively quench the luminescence of the silicon quantum dots. With the addition of pesticides, the activity of acetylcholinesterase was inhibited, preventing the generation of H_2O_2 and the H_2O_2-induced fluorescence quenching (Figure 128). The pesticide-induced inhibition and concomitant reduction in H_2O_2 production was directly related to the pesticide concentration, and a variety of pesticides, including carbaryl, parathion, diazinon and phorate, could be detected with LODs of 0.00725 ppb, 0.0325 ppb, 0.0676 ppb, and 0.190 ppb, respectively. Additionally, carbaryl concentrations were analyzed in several fruits, including apples, tomatoes and cucumbers, and showed results that were consistent with those obtained using standard HPLC analysis, indicating that the quantum dot system is a promising strategy for pesticide detection. Gold nanoparticles in combination with CdTe quantum dots have also been applied for the detection of bisphenol A (BPA), an industrially relevant toxicant, utilizing an inner filter effect-based fluorescence method, as reported by Ying et al.[1754]

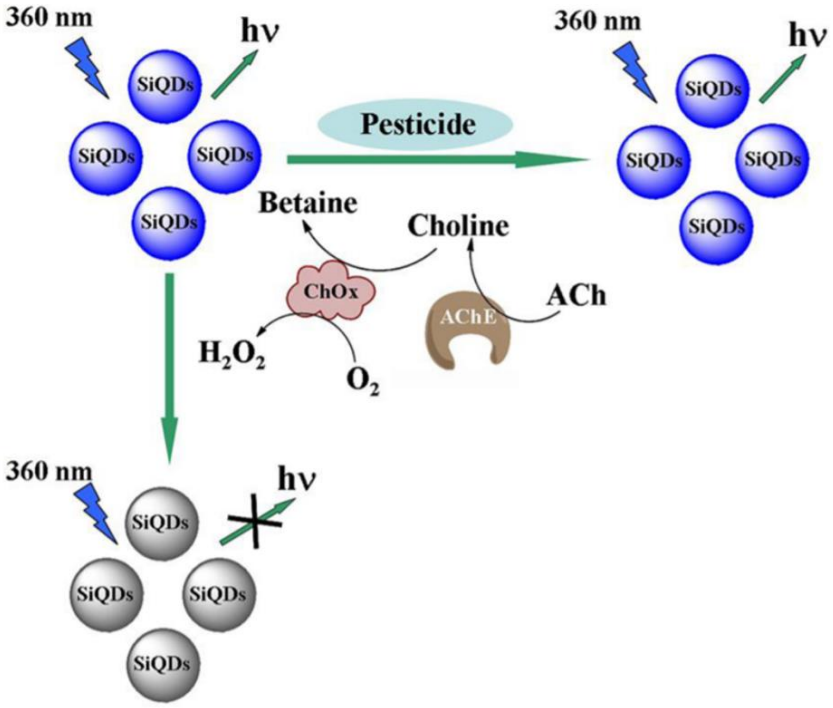

Figure 128. The sensing mechanism of silicon quantum dots for the detection of various pesticides through the inhibition of acetylcholinesterase. Reproduced from Ref. 1753. Copyright 2013 American Chemical Society.

In order to avoid the toxic effects of cadmium, a commonly used substance in quantum dots, alternative transition metal-derived quantum dots have been developed, including manganese, copper and chromium.[1755] Among these, Mn-doped quantum dots have been studied for the detection of various analytes including cadmium,[1756] TNT,[1757] and glucose.[1758] A method for the detection of thiram, a fungicide, was developed by Zhang et al. using phosphorescent Mn-doped ZnS quantum dots and Ag^+.[1759] The phosphorescence of the quantum dots was quenched by the addition of Ag^+; however, the presence of both thiram and Ag^+ caused the formation of a stable Ag-thiram complex bound to the nanoparticle surface, which enhanced the phosphorescence of the system (Figure 129). The sensor selectively detected thiram over other pesticides and was successfully applied to the analysis of thiram in fruit peel samples.

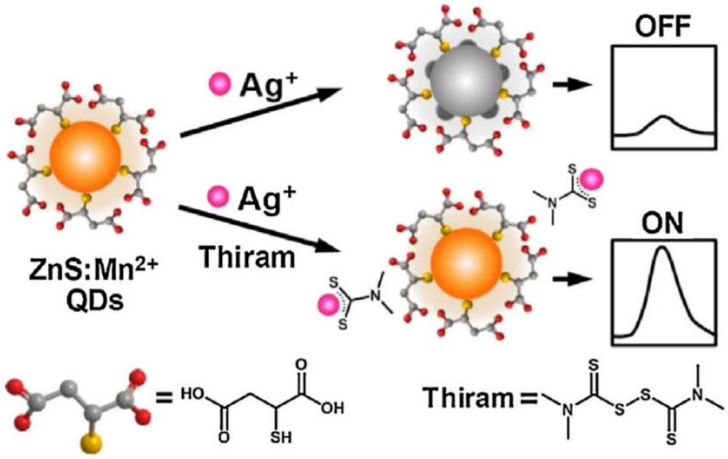

Figure 129. The sensing mechanism of Mn-doped ZnS quantum dots for the detection of thiram. Reproduced with permission from Ref. 1759. Copyright 2017 Elsevier.

7.2. Lanthanide-Doped Nanomaterials

Lanthanide metal-based, or rare-earth metal-based, luminescent sensors have several advantages over traditional luminescent sensors including strong luminescence, long fluorescence lifetimes (μs-ms range), large Stokes shifts, and enhanced photostability, due to the unique inner shell configurations of lanthanide metal ions.[1760,1761] Luminescent Ln-doped nanomaterial sensors can be categorized as either downconversion or upconversion nanoparticles: downconversion nanoparticles convert two or more high energy photons to low energy photons, and upconversion nanoparticles convert two or more low energy photons into high energy photons.[1760] Downconversion nanomaterials are more prevalent and more closely related to conventional organic dyes, and follow Stokes' law, which states that compounds absorb short-wave light and emit long-wave light. Upconversion nanoparticles often require the presence of rare-earth metals, and allow near-infrared excitation wavelengths to result in visible or UV emission. The use of near-infrared excitation facilitates both greater biocompatibility, because near-infrared light is less harmful to biological organisms than typical UV excitation; and deeper sample penetration,[1762] because near-infrared light can travel further through tissue and other biological samples. As a result of this enhanced biocompatibility, upconversion nanoparticle sensors have gained considerable attention in recent years.[1763,1764] However, the relatively weak luminescent intensity of lanthanide metals alone do not allow for sensitive analyte detection and therefore the lanthanide metal ions are often incorporated into host materials such as polymer beads[1765] or inorganic nanoparticles[1766] to improve luminescent intensity, selectivity, and sensitivity.[1764] Alternatively, lanthanide system luminescence can be improved through the incorporation of cofactor ligands, which bind to the metal and lead to enhanced luminescence via the "antenna effect," in which the peripheral, "antenna" ligands transfer their excited state energy to lanthanide ions following UV light excitation.[1767] In one example, Tan et al. prepared an adenine-based terbium coordination polymer nanoparticle for the fluorescent detection of mercury.[33] The polymer nanoparticle was composed of adenine and Tb^{3+} moieties with a dipicolinic acid linker. Initially, the fluorescence of the nanoparticle was very weak due to the presence of PET from adenine to dipicolinic acid, but the addition of Hg^{2+} significantly enhanced the fluorescence intensity of the system due to the suppression of PET, resulting in the augmentation of energy transfer from dipicolinic acid to Tb^{3+} (Figure 130).

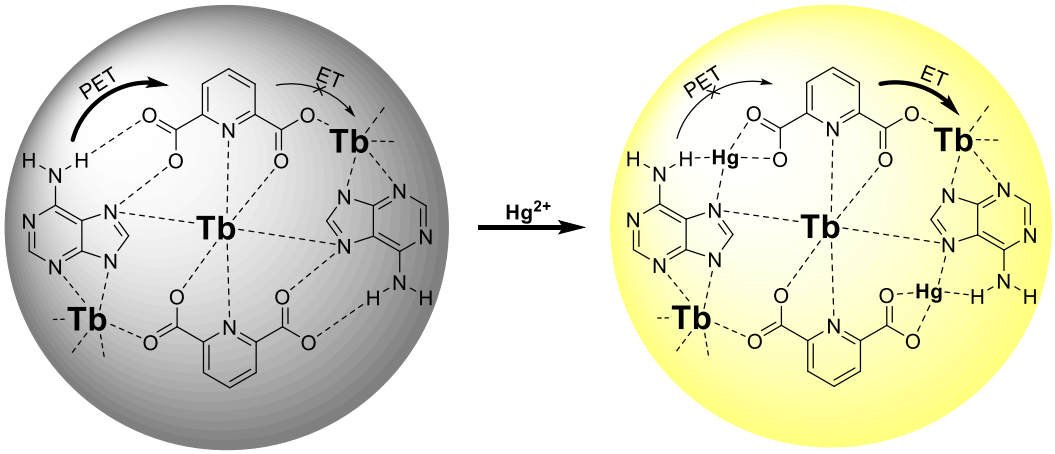

Figure 130. Coordination polymer nanoparticle for sensing of Hg(II) by PET.[33]

Analogously, Huang developed a method for sensing Cu^{2+} using a lanthanide coordination polymer nanoparticle constructed from adenosine monophosphate (AMP) and Tb^{3+}.[1767] 5-sulfosalicylic acid was used as a cofactor ligand and resulted in an enhanced luminescence due to energy transfer from the ligand to Tb^{3+}. The system fluorescence was quenched by the addition of Cu^{2+}, which strongly coordinated to 5-sulfosalicylic acid, due to favorable electrostatic interactions. The sensor was combined with in vivo

microdialysis and successfully used in the detection of cerebral Cu^{2+} in rat brains. Of note, the calculated LOD of 300 nM is lower than the concentration of cerebral Cu^{2+} typically found in rats.

Sarkar et al. synthesized a Cu^{2+} sensor that used poly(acrylic acid)-coated Eu^{3+}-doped $KZnF_3$ nanoparticles.[1768] The nanoparticles exhibited a strong red emission upon UV excitation that was selectively quenched upon the addition of Cu^{2+}. Another Ln-doped sensor was developed by Han et al., which used selective ratiometric fluorescence switching for the detection of nitrite in water and in real-world, cured meat samples.[1769] The detection relied on green-emitting Eu^{3+} and Yb^{3+} doped $NaYF_4$ nanoparticles that were quenched by Neutral Red, a fluorescent dye, due to a FRET mechanism. However, when nitrite was present, the green emission of the doped $NaYF_4$ nanoparticles was recovered due to the reaction between nitrite and Neutral Red to form a diazonium group, which was no longer able to participate in the FRET scheme. Of note, the system was selective for nitrite over other ions and had a reported LOD of 0.7 ppm.

Ln-doped materials have also been applied as pH sensors for biological applications. Xie et al. developed a plasticized poly(vinyl chloride) matrix that included Er^{3+} and Yb^{3+} doped $NaYF_4$ upconverting nanorods and a Nile Blue derivative, 9-dimethyl-amino-5-[4-(15-butyl-1,13-dioxo-2,14-dioxanonadecyl)-phenylimino] benzo[a]phenoxazine (ETH 5418). This system was used to measure the presence and concentration of metal cations in human blood samples along with the sample pH.[1770] Spectral overlap between the absorbance region of chromoionophore and the luminescence of the nanorods was observed and induced an inner filter effect, whereby the chromoionophore absorbed some of the excited state energy and filtered the amount that reached the nanorods. The degree of the inner filter effect depended on both the pH of the system and on the metal ions present, with more acidic pH or the presence of Na^{+} or Ca^{2+} resulting in increased inner filter effects and a lower overall emission. Similarly, Chu et al. used europium-doped silicon nanorods for ratiometric pH sensing.[1771] The nanorods exhibited blue fluorescence emission at 470 nm from the silicon nanorods and red fluorescence emission at 620 nm from the doped Eu^{3+}. With an increase in pH values, the fluorescence intensity at 470 nm decreased while the intensity at 620 nm remained unchanged, producing a ratiometric signal. The probe was able to measure the pH in a range of pH 3 to pH 9, and exhibited low cytotoxicity, enabling its use as an in vivo pH sensor. Additionally, Ln-doped nanoparticles have been used to detect a variety of other analytes, including glucose,[1772] TNT,[1773,1774] DNA,[1775] and cocaine.[1776]

7.3. Coinage Metal Nanoparticles

The term coinage metal nanoparticles refers to particles made from gold, silver or copper and are of interest due to the fact that they are easily synthesized and can be readily functionalized with analyte-responsive ligands such as phosphines, amines and thiolates.[1716,1745] Often, the binding of analytes to the ligands results in aggregation of the nanoparticles and aggregation-induced emission (AIE) changes. Metal nanoparticles are excellent fluorescence quenchers for FRET-based assays due to their high molar extinction coefficients and broad energy bandwidths, which facilitate strong spectral overlap, a known prerequisite for efficient FRET.[1734] Coinage metal nanoparticles have better biocompatibility and lower toxicity compared to many cadmium-derived quantum dots, and are therefore promising alternatives for biological applications.

Gold nanoparticles have been developed for the detection of various cations and anions, including mercury, lead, and nitrite. Huang et al. used a time-gated FRET sensing strategy for the detection of mercury in aqueous solution.[1777] In this system, complementary single DNA strands were affixed to energy-donating quantum dots and energy-accepting gold nanoparticles. With the addition of Hg^{2+}, a stable thymine-Hg^{2+}-thymine complex formed, bringing the two DNA strands, and thus the quantum dot and nanoparticle, into closer proximity, and resulting in energy transfer from the quantum dots to the gold nanoparticles. The gold nanoparticles quenched the fluorescence of the quantum dots and the decrease in fluorescence intensity observed was proportional to the concentration of Hg^{2+} ions with a detection limit of 0.49 nM. In another example, Li et al. developed luminol-capped gold nanoparticles that reacted with silver nitrate under alkaline conditions to generate a strong chemiluminescence emission.[1778] The subsequent addition of Hg^{2+} caused significant chemiluminescent quenching, allowing for an LOD of 1 nM. General applicability of

this probe was demonstrated through its use in real-world complex water and soil samples. Wu et al. developed a catechin-functionalized gold nanoparticle probe for the detection of lead in both real-world water and urine samples.[1779] Even in such complex environments, the probe was highly selective for lead in the presence of other metal ions and had a LOD of 1.5 nM. A unique fluorescent and colorimetric sensor was developed by Li et al. for the detection of nitrite using *p*-aminothiophenol-capped gold nanorods and 1,8-diaminonaphthalene-modified gold nanoparticles.[1780] In the presence of nitrite, the *p*-aminothiophenol and 1,8-diaminonaphthalene functionalities reacted to form azo-dye bridged nanorod-nanoparticle hybrid assemblies. The formation of these supramolecular architectures resulted in an increase in coloration and a decrease in fluorescence, allowing for both naked-eye and fluorescent detection of nitrite.

Additionally, coinage metal nanoparticles have been used to detect biologically relevant compounds and other small molecules. For example, FRET between upconversion nanoparticles and gold nanoparticles was used for melamine detection, as reported by Wu et al.[1781] The positively charged upconversion nanoparticles and negatively charged gold nanoparticles formed electrostatically-driven association complexes, leading to strong fluorescence quenching. Melamine, an industrially relevant toxicant, caused aggregation of the gold nanoparticles due to a strong interaction between amino groups of melamine and Au, disrupting the initial electrostatic interactions and leading to recovery of the upconversion nanoparticles' fluorescence. This nanosensor was used for melamine detection in raw milk samples and showed high selectivity over other common ions, amino acids and organic molecules. Dai et al. also used gold nanoparticles for the FRET-based detection of melamine using amino-functionalized carbon dots as energy donors and gold nanoparticles as energy acceptors.[1782] The fluorescence of the gold nanoparticles was quenched upon addition of carbon dots but could be recovered with the addition of melamine (Figure 131). As with Wu's system, the fluorescence restoration was due to the preferential binding of the amino groups on melamine to the gold nanoparticles, displacing the amino-functionalized carbon dots. The system was used for the detection of melamine in raw milk and milk powder and showed selectivity over other commonly occurring species, including calcium ions, vitamin C and lactose.

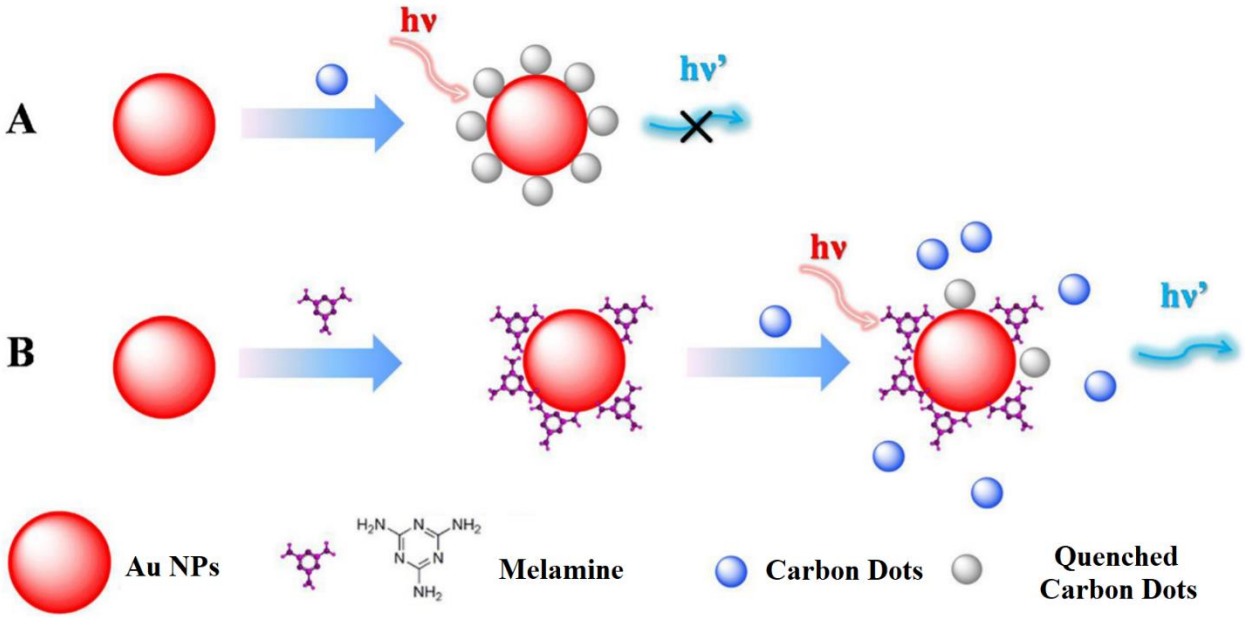

Figure 131. The FRET based mechanism for the detection of melamine using gold nanoparticles and carbon dots: (A) The fluorescence of carbon dots was quenched by gold nanoparticles; and (B) The fluorescence was restored with addition of melamine. Adapted with permission from Ref. 1782. Copyright 2014 Elsevier.

Similarly, Guo et al. developed a quantum dot-nanoparticle assembly for the FRET-based detection of glyphosate,[1783] a common pesticide with significant biochemical relevance. Quantum dots were used as the

energy-transfer donors, while gold nanoparticles were used as the energy-transfer acceptors. Positively charged cysteamine moieties stabilized the gold nanoparticles and effectively quenched the fluorescence intensity of the CdTe quantum dots through disrupting the predominant energy transfer pathway. However, the addition of glyphosate induced aggregation of the gold nanoparticles and recovered the fluorescence of the quantum dot donors (Figure 132). This FRET-based fluorescent method was applied for the detection of glyphosate in apples.

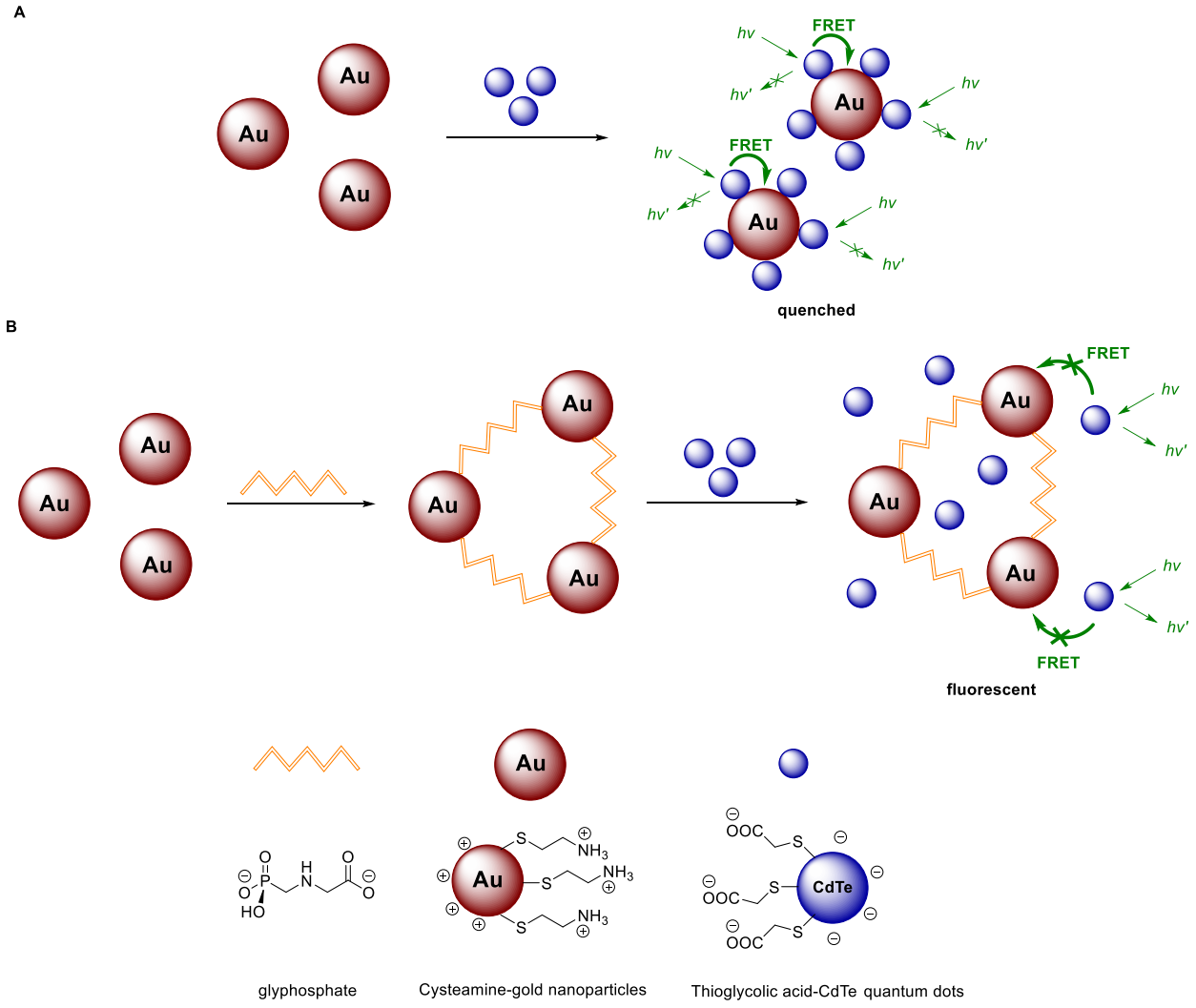

Figure 132. Schematic illustrations of FRET in a nanoparticle-quantum dot system: (A) Illustration of the FRET mechanism between thioglycolic acid-CdTe-quantum dots and cysteamine-gold nanoparticles in the absence of the target analyte; and (B) Illustration of the fluorescence quenching that occurs with the addition of glyphosate[1783]

Silver nanoparticles have been used for luminescent detection applications and show several advantages compared to gold nanoparticles, including sharper extinction bands and higher extinction coefficients.[1784] They have been used for the detection of dopamine, as shown by Biswel et al., who synthesized polymethacrylate-stabilized silver nanoparticles through in situ reduction of Ag^+ in the presence of polymethacrylate using gamma irradiation.[1785] The detection limit for dopamine was found to be 0.527 µM. Furthermore, a unique array-based sensor was developed by He et al. for the detection of five organophosphate- and carbamate-containing pesticides using luminol-functionalized silver nanoparticles.[1786] The chemiluminescence of luminol is typically produced via oxidation with hydrogen

peroxide; similarly, chemiluminescence of the luminol-functionalized nanoparticles was generated upon the addition of H_2O_2, although at a slower rate than the free luminol fluorophore. When pesticide analytes were adsorbed onto the nanoparticle surface before the addition of hydrogen peroxide, changes in the chemiluminescence intensity, time required to generate chemiluminescence, and time required to reach the chemiluminescence peak value were observed. Principle component analysis (PCA) using these changes in spectral features generated an array-based detection scheme (Figure 133), which successfully distinguished between various pesticides including dimethoate, dipterex, carbaryl, chlorpyrifos and carbofuran.

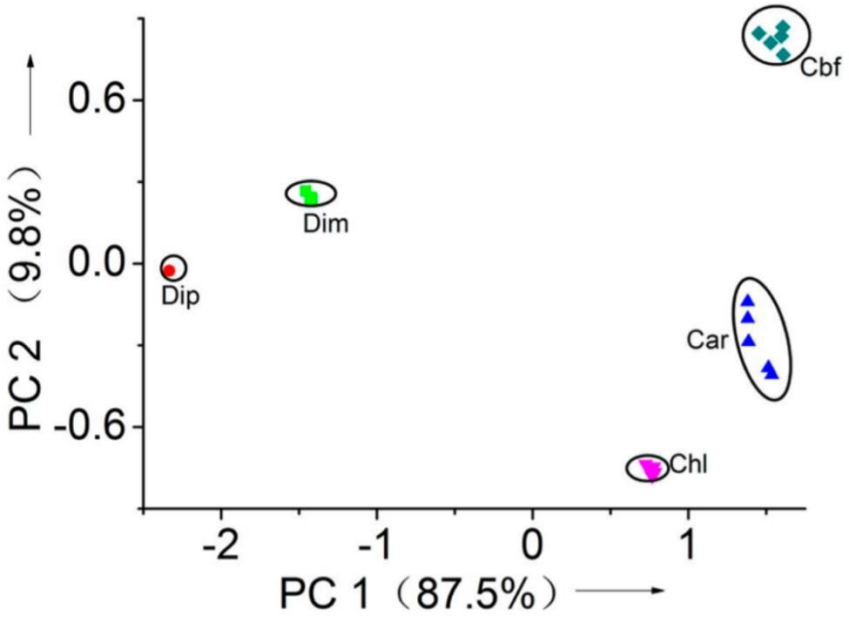

Figure 133. Sensor array based on multi-component analysis of the analyte-induced fluorescence responses for the detection of various pesticides – dimethoate (Dim), dipterex (Dip), carbaryl (Car), chlorpyrifos (Chl) and carbofuran (Cbf). Structures of these compounds can be found in Figure 21. Reproduced from Ref. 1786. Copyright 2015 American Chemical Society.

7.4. Coinage Metal Nanoclusters

Coinage metal nanoclusters, which are distinct from nanoparticles and quantum dots because of their ultra-small size (<1 nm)[1787] and low toxicity,[1788] have also been widely exploited for sensing applications. The luminescent features of gold and silver nanoclusters are highly tunable based on their size and the identity of the surface-coating agents and these nanoclusters can act as signal amplifiers and energy donors for FRET-based systems.[1789] Similar to the capping ligands on nanoparticles, capping ligands on the surfaces of gold nanoclusters significantly affect system emission properties. Many gold and silver nanoclusters have been used for the detection of metal cations such as copper and mercury. In one example, Deng et al. reported the synthesis of water-soluble, monodispersed gold nanoclusters that used methionine both as a reductant and as a nanocluster stabilizer.[1790] The methionine-functionalized gold nanoclusters displayed an intense yellow fluorescence emission at 530 nm that was quenched by the addition of Cu^{2+}. The intensity linearly decreased as the copper concentration increased from 50 nM to 8 μM, leading to a limit of detection for Cu^{2+} of 7.9 nM. More recently, Chen reported gold nanoclusters that were synthesized by an electrostatically induced phase transfer method and used for the detection of Cu^{2+}.[1791] The nanoclusters displayed red fluorescence emission at 700 nm that was quenched due to the aggregation induced by Cu^{2+}. Silver nanoclusters have also been used for metal cation detection as shown by Yuan et al. who reported a highly luminescent silver nanocluster sensor for the detection of mercury ions.[1792] The silver nanoclusters

were protected by glutathione and showed desirable sensor features including fast detection time (<1 min), high selectivity, and a low LOD of 5 nM.

Copper nanoclusters are also desirable detection platforms due to their high conductivity and relatively low cost.[1798] However, they are more difficult to synthesize than gold and silver nanoclusters owing to their susceptibility to surface oxidation when exposed to air. As a result, copper nanoclusters are typically prepared in an inert atmosphere under nitrogen[1793] or argon[1794] gas. Stabilizing and protecting ligands such as glutathione[1795], hydrazine[1796] and $NaBH_4$[1797], can also be used to avoid undesired copper oxidation. In one example of a copper nanocluster-based detection scheme, Xiaoqing et al. synthesized copper nanoclusters using hydrogen peroxide as a stabilizing additive, and used them for the detection of mercury.[1798] The copper nanoclusters showed better photostability compared with those formed by other preparation methods, and had a limit of detection of 4.7 pM. Luo et al. also used copper nanomaterials for the detection of mercury, in which glutathione served as a protecting ligand and ascorbic acid was used as a reducing agent.[1799] The nanomaterials thus formed displayed good water solubility and photostability. Bimetallic nanoclusters have been shown to have better performance compared to monometallic nanoclusters due to positive synergies between the metal components. In one example of a bimetallic sensor, a series of bovine serum albumin-protected Au-Ag bimetallic nanoclusters were prepared by Zhai et al., and they found that the electrochemiluminescence emission of Ag-doped gold nanoclusters was approximately five times higher than those of monometallic gold nanoclusters.[1800] The nanoclusters were used as Hg^{2+} sensors, based on the analyte-induced quenching of the electrochemiluminescence signal due to the binding of Hg^{2+} to Au or Ag atoms.

Several dual-detection fluorescent sensors have been developed for the sequential detection of more than one analyte. An example of such a sensor was reported by Niu et al. who developed a ratiometric fluorescence sensor for the detection of both melamine, an industrially relevant toxicant, and mercury ions.[1801] The red fluorescence of the gold nanoclusters was quenched by the addition of mercury cations due to the affinity of Hg^{2+} toward Au. Melamine was able to sequester the bound Hg^{2+} due to the stronger affinity of mercury toward amines, which allowed for near-complete emission recovery. Furthermore, a naked-eye visible color change from red to green was observed with increasing concentrations of Hg^{2+}, with the original red color restored after the addition of melamine. The ratiometric nanoprobe was biocompatible and therefore was used for cell imaging. More recently, Qu et al. also developed a dual-emission fluorescence sensor for the detection of both Hg^{2+} and melamine.[1802] This fluorescent probe used carbon nanodots as an internal reference (defined as a species in a ratiometric detection scheme whose emission remains consistent) and glutathione-stabilized gold nanoclusters as the sensing probe. As in the previous example, the red emission of the glutathione-stabilized gold nanoclusters was quenched with addition of Hg^{2+} and recovered with addition of melamine. The fluorescent probe had a detection limit of 29.3 nM and showed selectivity over other potentially interfering substances, including other metal cations and nitrogen-containing organic molecules. Furthermore, Bian et al. developed a simple and portable test paper that used glutathione-functionalized gold nanoclusters for the fluorometric detection of both Hg^{2+} and Pb^{2+}.[1803] The nanoclusters responded to the presence of the target analytes by aggregating, resulting in aggregation-induced fluorescence quenching and enhancement for analytes Hg^{2+} and Pb^{2+}, respectively. The sensor could be reused up to three times by immersing the test paper in a saturated solution of ethylenediamine tetraacetic acid (EDTA) between each sensor use to remove the bound metal analytes. Lin et al. developed bovine serum albumin-coated gold nanoparticles that were quenched by the presence of Cu^{2+}, which could be sequestered by histidine to enable fluorescence recovery.[1804] It was found that the presence of Hg^{2+} interfered with the effective detection of Cu^{2+} in this system; moreover, the Hg^{2+}-induced fluorescence quenching was irreversible and therefore could not be recovered by the addition of histidine. This sensor was applied to Cu^{2+} detection in drinking tap water and displayed detection results that were consistent with data obtained by Atomic Absorption Spectrometry (AAS). The sensor had a lifetime of more than 6 months and could be used more than 20 times, making it a stable and recyclable sensor for Cu^{2+}detection.

Coinage metal nanoclusters have been used for pH sensing as shown by Ali et al., who used gold nanoclusters for the fluorescent sensing of physiological pH.[719] Bovine serum albumin was used as both a reducing agent and capping agent for the gold nanoclusters, which showed red luminescence at 640 nm emission. The sensing system was capable of detecting pH changes from a starting pH of 5 to a pH of 9, which is a common pH change that occurs in the extracellular matrix after the death of red blood cells. In another example, silver nanoclusters were used to detect changes in pH, as shown by Lu et al.[1805] The yellow-green emitting silver nanoclusters were functionalized with a copolymer ligand containing *N*-heterocyclic groups of 8-hydroxyquinoline and *N*-isopropylacrylamide. The system was moderately reversible and could be reused up to 6 times within a detectable pH range of 3.04-5.25. Additionally, copper nanoclusters were utilized as bifunctional sensors for the detection of dopamine, a neurotransmitter, and for pH sensing, as shown by Miao et al.[1806] Bovine serum albumin was used as a capping agent for these fluorescent copper nanoclusters, which showed a linear decrease in fluorescence proportional to a decrease in pH from 12 to 4, and a linear increase in fluorescence proportional to an increase in dopamine concentration from 0.5 to 50 μM. The sensor was used for pH determination of tap, river and drinking water samples as well as for dopamine detection in urine samples.

Gold nanoclusters were used as fluorescent sensors for the selective and sensitive detection of hydrogen sulfide, as shown by Zhang et al.[1807] Acetylcysteine was used as a nanoparticle stabilizing agent, with the thiol group binding to the surface of the gold nanoclusters due to strong thiol-gold affinity. The presence of H_2S led to the formation of Au_2S, leading to an increase in the size of the clusters, and causing fluorescence quenching of the acetylcysteine-modified gold nanoclusters (Figure 134). The sensor showed selectivity for hydrogen sulfide over anions, amino acids and thiol-containing compounds, and practical applicability of the sensor was demonstrated through the detection of hydrogen sulfide in tap water, river water, human serum and mouse serum. Additionally, silver nanoclusters embedded with quantum dots were used for hydrogen sulfide detection by Yan and coworkers.[923] The silver nanoclusters self-assembled onto the thiol-functionalized surface of colloidal silica nanospheres, which encapsulated red fluorescent CdTe quantum dots. Mercaptopropyltrimethoxysilane was functionalized onto the silica shell, where it induced the self-assembly of the silver nanoclusters through interaction between thiols and the surface Ag atoms of adjacent nanoparticles. The silver nanoclusters were extremely reactive with hydrogen sulfide, forming Ag_2S-derived surface defects; these defects, in turn, resulted in fluorescence quenching of the blue-emitting nanoclusters. The red-emitting quantum dots were not affected by the presence of hydrogen sulfide, and therefore acted as a reference signal for the ratiometric nanohybrid probe. The detection of gaseous H_2S was accomplished by bubbling the gas into bottles containing the nanocluster sensor and exciting the samples via UV light irradiation. The solution-state fluorescence color change from violet to blue was directly proportional to the concentration of H_2S present and showed significant potential in the development of on-site detection schemes.

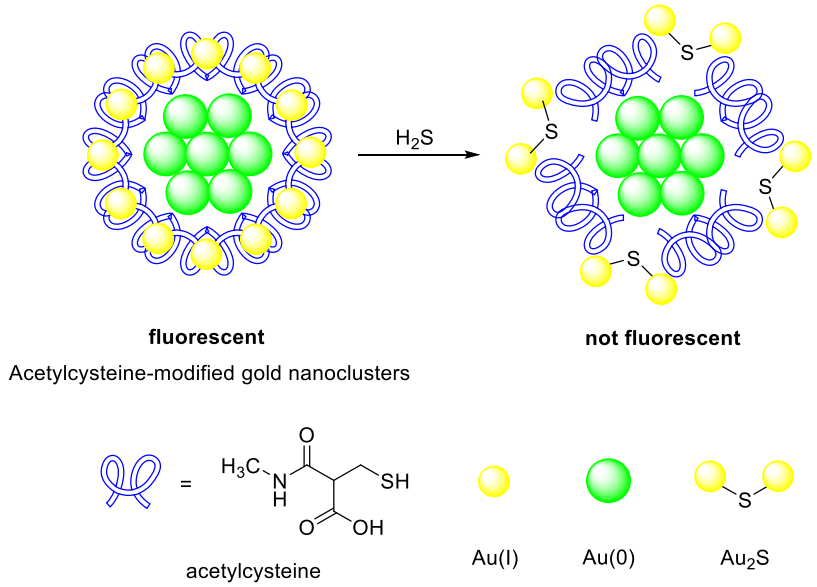

Figure 134. Schematic illustration of an acetylcysteine-modified gold nanocluster as a fluorescent sensor for the detection of H_2S[1807]

Coinage nanoclusters have also been used for the detection of small organic molecules such as bisphenol A (BPA), an industrially relevant toxicant, and dopamine, a neurotransmitter. In one example, Deng et al. developed a sensor for the detection of BPA by anchoring a molecularly imprinted polymer layer onto the surface of fluorescent silver nanoclusters.[1808] The fluorescence of the silver nanoclusters was quenched by the addition of BPA and was selective for BPA in the presence of other structurally related analytes, including tetrabromobisphenol A, biphenol and hydroquinone. Even in real-world milk and juice samples, the sensor was still able to detect BPA with an LOD of 0.02 ppb. In another example, Devi et al. developed a fluorescent probe for dopamine detection using aminophenyl boronic acid-conjugated gold nanoclusters.[1809] The fluorescence of the probe was initially quenched due to interactions of the functionalized nanoclusters with lactose, which caused the formation of boronate esters between the boronic acid coating and the lactose moieties. Introduction of dopamine caused dissociation of the labile boronate esters and the formation of new, dopamine-containing boronate esters with the probe, which led to a fluorescence recovery. The probe was highly selective for dopamine compared to other catechol amines, including adrenaline and noradrenaline, which had no effect on the emission of the probe.

Electron-rich luminescent nanomaterials can easily be quenched via PET or FRET in the presence of electron-deficient nitroaromatic compounds, facilitating the development of sensors for explosives and explosive-like compounds.[1810] In one example, copper nanoclusters were used for the detection of TNT by Yang et al.[1811] The L-cystine-modified copper nanoclusters emitted a faint fluorescence when dispersed in aqueous solution, but with addition of TNT, the fluorescence intensity was significantly enhanced due to analyte-induced nanocluster aggregation, caused by donor-acceptor interactions between the nanoclusters and the analyte molecules (Figure 135). The sensor displayed selectivity for TNT over other nitro-containing, structurally related analytes, and had a detection limit of 9.1 nM. More recently, Aparna et al. also used copper nanoclusters for the detection of TNT by both fluorescence and colorimetric detection.[1812] The polyethylene imine-capped copper nanoclusters were adsorbed onto paper strips for solid-state detection, and detected TNT vapors with an LOD of 10 nM.

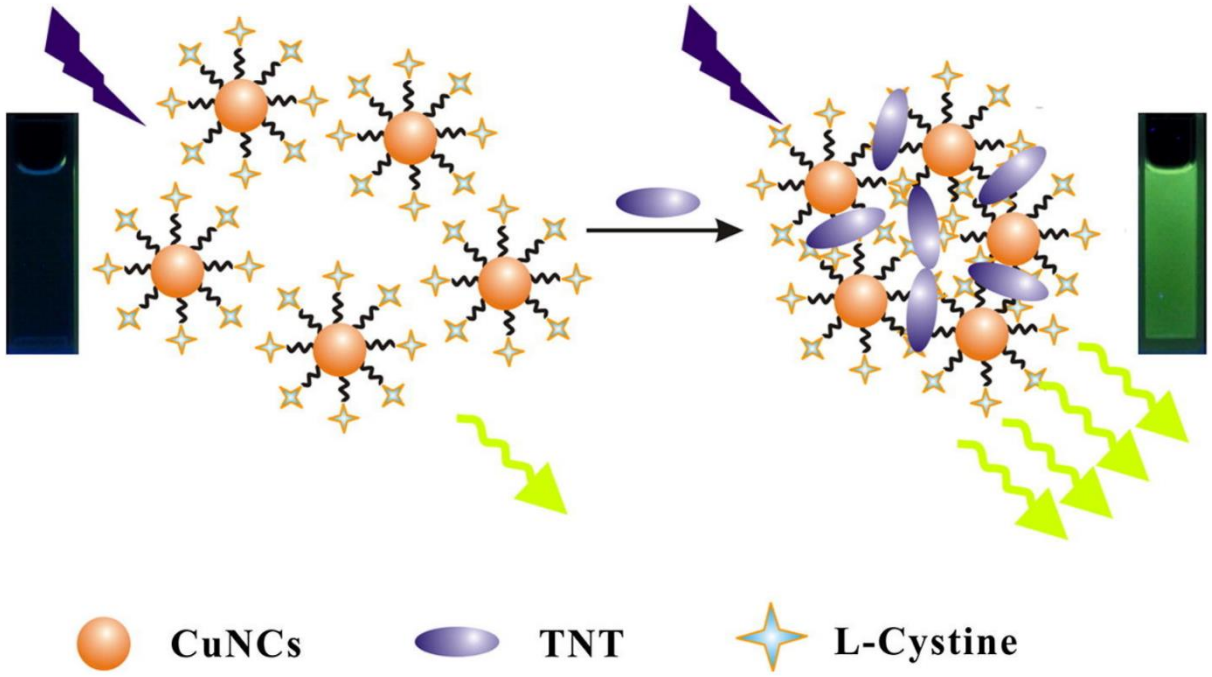

Figure 135. L-cysteine modified copper nanoclusters for the detection of TNT through fluorescence enhancement. Reproduced with permission from Ref. 1811. Copyright 2017 Elsevier.

7.5. Fluorescent Dye-Doped Nanomaterials

Fluorescent dye-doped nanomaterials are produced by encapsulating, doping, or capping fluorescent dyes in and around nanomaterials.[1813] By dispersing fluorescent dyes into nanofibers or other matrices, the quantum efficiency of the dye increases due to reduced aggregation and limits of undesired FRET between dye molecules.[1814] An example of this phenomenon was reported by Wang et al., who developed two 1,4-dihydroxyanthraquinone (1,4-DHAQ)-doped cellulose microporous nanofiber films that could detect Cu^{2+} and Cr^{3+} sequentially in aqueous solution.[1814] The sensing mechanism for Cu^{2+} was due to the binding of copper with the phenolate of 1,4-DHAQ (Figure 136), which enabled linear decreases in the fluorescence intensity of the system with increasing concentrations of copper, for [Cu^{2+}] between 2.5 nM and 37.5 nM. Interestingly, the fluorescence of the 1,4-DHAQ could be recovered by the addition of Cr^{3+}, which displaced Cu^{2+} and bound to the 1,4-DHAQ phenolate moiety, resulting in fluorescence restoration. The Cu^{2+}-containing 1,4-DHAQ nanofiber film was therefore used for the fluorescence detection of Cr^{3+}, with the fluorescence intensity of the co-doped 1,4-DHAQ-Cu^{2+} nanofiber film linearly increasing in the Cr^{3+} concentration range between 2.5 nM and 25 nM. The detection of Cu^{2+} and Cr^{3+} was successfully accomplished in polluted lake water samples, where good selectivity over other metal cations was demonstrated. In another report Tyagi et al. used silver nanorods that were coated with Rhodamine 6G for the detection of lead in aqueous solution.[1815] Upon the addition of lead to the sample, the fluorescence of Rhodamine 6G turned on, resulting in a sensor with a detection limit of 50 ppb.

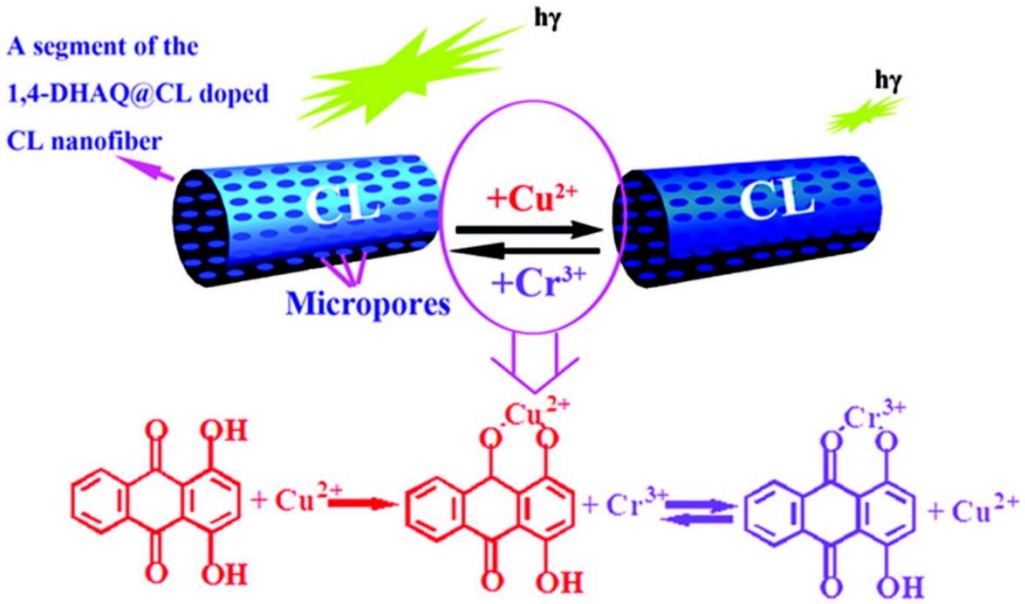

Figure 136. Illustration of the sensing mechanism of the 1,4-DHAQ doped cellulose (CL) microporous nanofiber films for Cu^{2+} and Cr^{3+} detection. Reproduced from Ref. 1814. Copyright 2012 American Chemical Society.

Chromophore-gold nanoparticle composites are also very advantageous for sensing applications, due to the strongly quenching nature of gold nanoparticles which facilitates the development of a system that is "off" in the absence of the target analyte. Recently, Xu et al. developed a gold nanoparticle-based sensor that incorporated a meso-(4-pyridinyl)-substituted BODIPY dye for the detection of thiols in aqueous solution.[1816] The coordination of the dye to the gold nanoparticle surface occurred through strong N-Au interactions, efficiently quenching the fluorescence of the BODIPY moiety (Figure 137). The addition of biologically relevant thiols, including cysteine, homocysteine and glutathione, led to displacement of the chromophore and a near-complete restoration of fluorescence. The sensor had an LOD of 30 nM and was successfully used in the intracellular imaging of thiols in living HeLa cells.

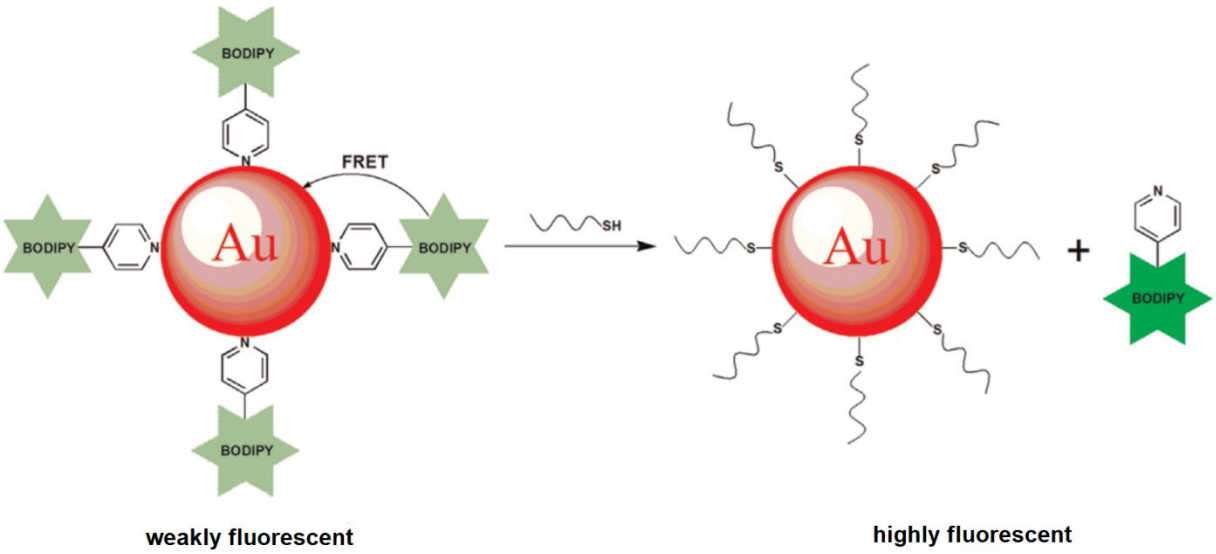

Figure 137. Thiol sensor based on the fluorescence quenching of BODIPY by gold nanoparticles. Adapted with permission from Ref. 1816. Copyright 2016 Elsevier.

Additionally, Cao et al. presented a method for detecting melamine, an industrially relevant toxicant utilizing FRET between Rhodamine B and citrate-stabilized gold nanoparticles.[1817] The emission of Rhodamine B was quenched when it was electrostatically adsorbed to the surface of the gold nanoparticles. The addition of melamine caused aggregation of the gold nanoparticles and release of the adsorbed Rhodamine B, leading to recovery of the fluorescence emission. The method was applied to real-world samples of milk and powdered infant formula, and a detection limit of 0.18 ppb was obtained. The incorporation of fluorescent dyes on the surface of nanomaterials has also been applied for nitroaromatic sensing using fluorescein[1818] or pyridine derivatives.[1819] Ma et. al. developed a fluorescent nanoparticle that encapsulated tris-(8- hydroxyquinoline) aluminum and was used for the detection of the nitroaromatic trinitrophenol (TNP).[1820] The fluorescence emission of the nanoparticle at 499 nm was quenched with the addition of TNP, with a TNP detection limit of 32.3 ppb reported.

7.6. Carbon-Based Nanomaterials

Carbon nanomaterials have attracted much attention in recent years due to their high mechanical strength, good chemical and physical stability, ease of functionalization and relatively low cost.[1789,1821] Additionally, fluorescent carbon dot sensors are becoming attractive materials for biological applications, due to their low toxicity and good biocompatibility.[1734] Zhao et al. developed a strategy for synthesizing carbon dots with differentially functionalized surfaces using various ionic liquids as solvents and microwave treatment procedures for effective sample preparation. [1822] The carbon dots obtained via these methods were highly luminescent and showed differential, analyte-specific selectivities for Cu^{2+} and Fe^{3+} (Figure 138).

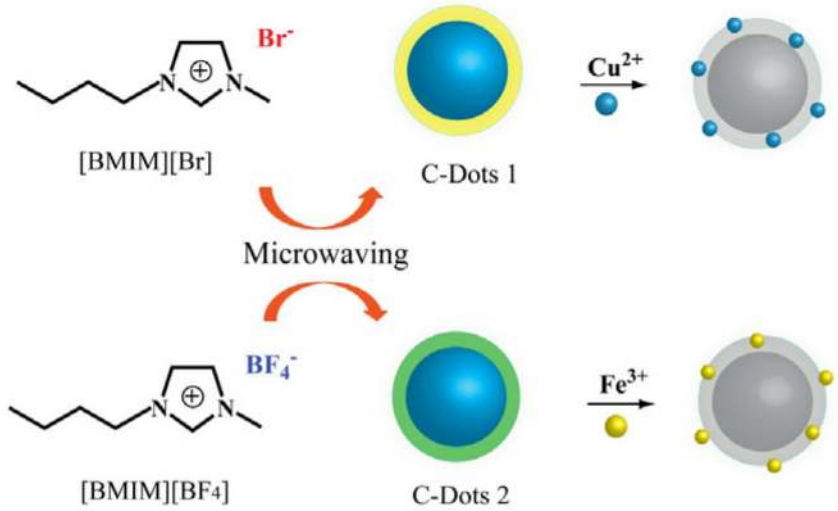

Figure 138. Surface-different carbon dots synthesized using different ionic liquids and applied for the detection of Cu^{2+} and Fe^{3+}. Reproduced with permission from Ref. 1822. Copyright 2014 Elsevier.

Additionally, a novel nanohybrid fluorescent probe was developed by Cao et al. for the ratiometric detection of mercury.[1823] The probe was composed of red-emitting carboxylmethyldithiocarbamate-modified CdSe/ZnS quantum dots and a form of carbon nanomaterials, blue-emitting carbon dots (vide infra), and exhibited dual peak emissions at 436 nm and 629 nm from a single excitation wavelength. In the presence of Hg^{2+}, the fluorescence of the carboxymethyldithiocarbamate-modified CdSe quantum dots was quenched while that of the carbon dots was unaffected, resulting in a visible color change of the system from red to blue.

A dual-emission carbon dot was reported by Qu et al. for the detection of dopamine and the monitoring of the activity of tyrosinase, an enzyme that converts tyrosine into melanin.[1824] The carbon dot's fluorescence emission was quenched by gold nanoparticles and could rapidly be restored by addition of dopamine. With the addition of tyrosinase, dopamine was oxidized to dopaquinone and the emission of the

carbon dots returned to the off state. The sensor was selective for dopamine over other structurally similar compounds, including levodopa, epinephrine, L-phenylalanine and catechol.

7.7. Graphene Oxide-Based Nanomaterials

Graphene oxide is a material characterized by a single graphene sheet, or "monolayer," that displays unique electronic and mechanical properties that are advantageous for sensing applications.[1825] Of note, graphene oxide can be functionalized using a variety of straightforward methods, and numerous functional groups, including epoxy, carboxy and hydroxy, can be appended onto the surface.[1827] Graphene has a higher quenching efficiency compared to other quenching agents, due to its enhanced electrical conductivity and 2D planar structure,[70] and therefore is a great energy transfer acceptor for FRET-based luminescent sensors.[1826] In one example, graphene oxide was used as a sensing platform for the detection of amantadine as demonstrated by Li et al.[1827] This probe was based on the host-guest interaction of mono-[6-(2-aminoethylamino)-6-deoxy]-β-cyclodextrin (EDA-CD) functionalized graphene oxide with amantadine and Rhodamine 6G. In the absence of analyte, the emission of Rhodamine 6G was quenched by addition to the cyclodextrin-modified graphene oxide layer; however, introduction of amantadine, a pharmaceutical agent,displaced Rhodamine 6G from the surface and led to significant fluorescence increases (Figure 139). The addition of compounds that are likely to co-exist in real-world environmental samples, such as sugars, starches, vitamin C, and amino acids, did not affect the detection of amantadine. The sensor had a limit of detection of 5 μM and was used for amantadine detection in variety of complex environments, including in pharmaceutical capsule formulations.

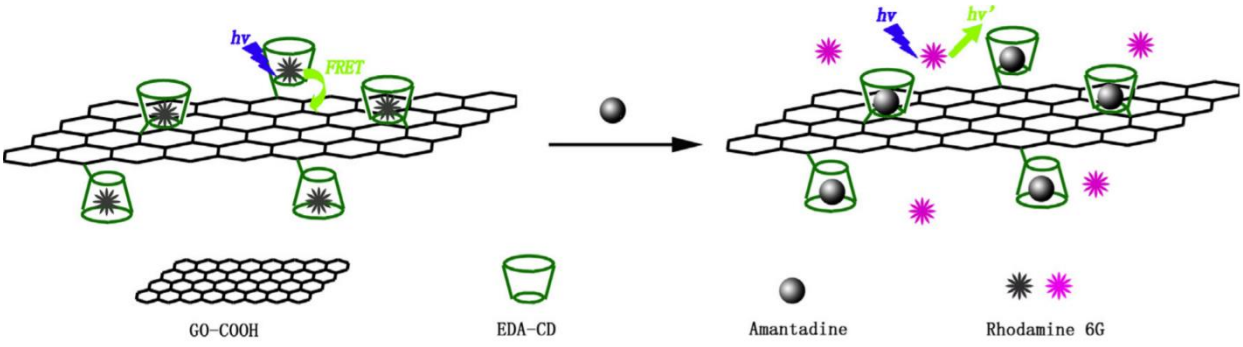

Figure 139. Mono-[6-(2-aminoethylamino)-6-deoxy]-β-cyclodextrin (EDA-CD)-modified graphene oxide used for the detection of amantadine based on competitive host-guest interactions. Reproduced with permission from Ref. 1827. Copyright 2014 Elsevier.

Bao et al. also developed a sensor that was based on the advantageous quenching capabilities of graphene oxide.[1828] A [2]rotaxane bearing a thread functionalized with both pyrene and Rhodamine B moieties (Figure 140) adsorbed on the surface of graphene oxide using π-π interactions and intermolecular hydrogen bonding, leading to FRET-induced luminescence quenching of the rotaxane. The addition of doxorubicin, a pharmaceutical agent, displaced the rotaxane from the graphene oxide surface, resulting in an increased fluorescence emission. The sensor was selective toward doxorubicin over other commonly occurring pharmaceutical agents, with a doxorubicin detection limit of 18.5 nM and a Benesi-Hildebrand binding constant of $3.63 \times 10^4\ M^{-1}$. Similarly, a sensor for the detection of the amino acid L-methionine was reported by Zor et al. based on the host-guest interactions between L-methionine and reduced graphene oxide/α-cyclodextrin hybrid materials.[1829] The addition of luminol to the reduced graphene oxide/α-cyclodextrin sheets led to a 90% quenching of the luminol emission, with emission restoration occurring with the addition of L-methionine. This system was able to detect concentrations of L-methionine as low as 1.7 mM. Furthermore, Mondal et al. also used a graphene-bound β-cyclodextrin as a cholesterol sensor based on the competitive host-guest interaction between Rhodamine 6G and cholesterol.[1830] The emission of Rhodamine 6G was quenched by encapsulation in the cavity of the graphene-bound β-cyclodextrin. Cholesterol selectively displaced the Rhodamine 6G, freeing it from the quenching agent and turning the fluorescence

back on. (Figure 141). Of note, little interference occurred with the addition of anionic surfactants such as sodium dodecyl sulfate, however, neutral surfactants such as Tween 80 displaced Rhodamine 6G, resulting in emission enhancement.

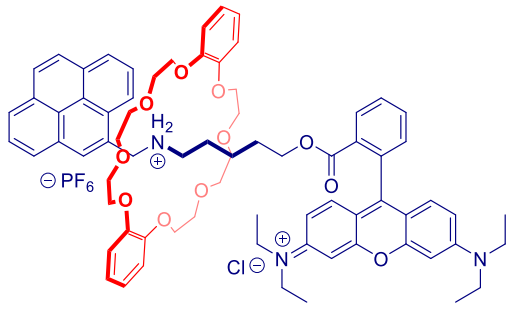

Figure 140. [2]Rotaxane with a pyrene- and Rhodamine B-functionalized thread that had been used in the fluorescent detection of doxorubicin[1828]

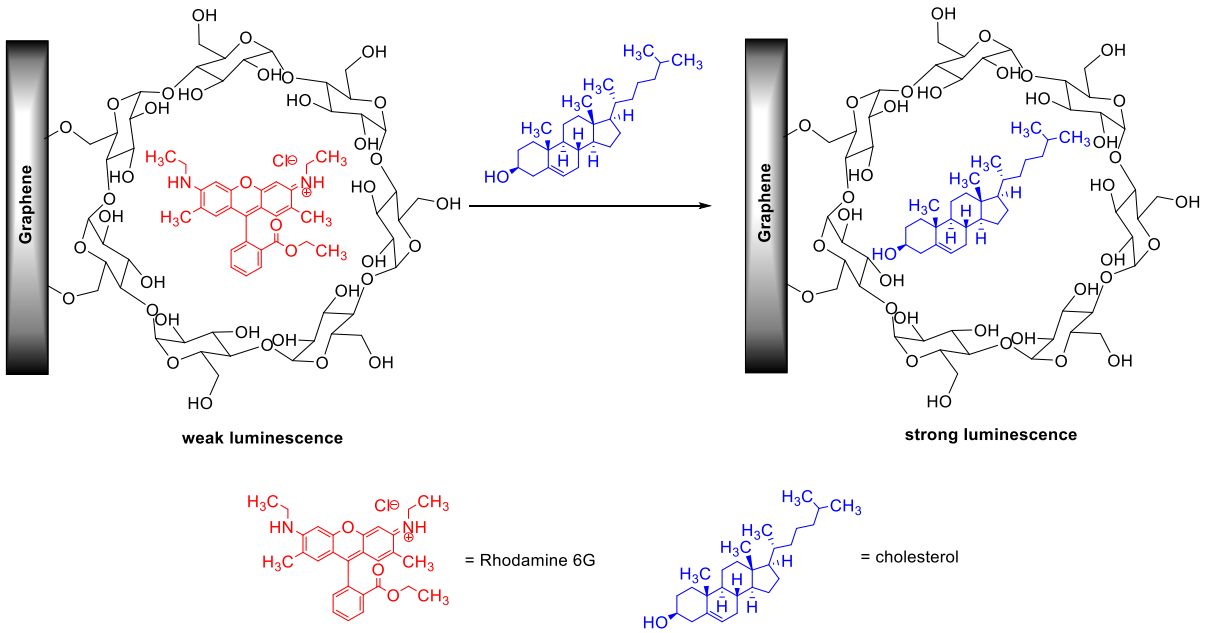

Figure 141. β-cyclodextrin-modified graphene for the detection of cholesterol via competitive host-guest interaction[1830]

Similarly, Hu et al. used a β-cyclodextrin-functionalized graphene-based fluorescent probe for the detection of tetrahydrofuran (THF), a VOC.[1831] This sensor was based on the competitive interactions of Rhodamine B and the analyte for binding in the cyclodextrin cavity. Prior to analyte addition, the emission of Rhodamine B was quenched due to its close proximity to the graphene oxide monolayer as a result of binding in the cyclodextrin cavity. With the addition of (THF), increased Rhodamine B emission was observed due to the displacement of Rhodamine B from the cyclodextrin cavity and its concomitant removal from proximity to the graphene oxide. An increase in emission was also observed when the system was dissolved in water-miscible solvents, indicating limited selectivity in this sensor system, but strong sensitivity for THF was seen, with a 1.7 ppm detection limit calculated. Sensors have also been developed by grafting cyclodextrin onto silica beads with a fluorogenic linker, such as in the example reported by Becuwe et al., in which toluene, another VOC, was detected through pyridinoindolizin-functionalized cyclodextrin binding near a nanomaterial surface (Figure 142).[1832] 1000 ppm of toluene led to a 19% decrease in fluorescence emission intensity in this system, compared to only 10% that was observed in the presence of free pyridinoindolizin-modified β-cyclodextrin.

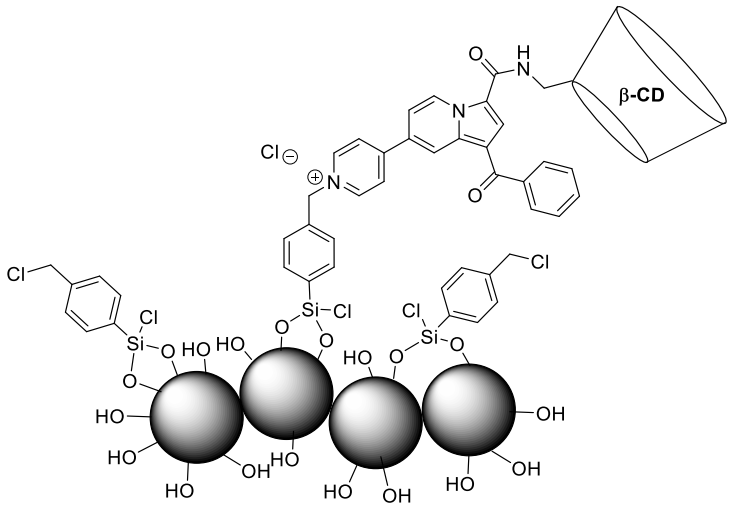

Figure 142. β-cyclodextrin grafted onto chlorobenzylated silica by a fluorescent linker[1832]

Silylated quartz modified with a calix[5]arene has been used for the detection of linear alkylammonium ions, as reported by Cristaldi et al.[1833] In the absence of analyte, the calix[5]arene adhered strongly to the silylated quartz substrate, however, with the addition of *n*-dodecylammonium chloride, *n*-butylammonium chloride or cadaverine, a naturally occurring toxic diamine, the macrocycle was released from the surface and an increase in emission was observed. The sensor had a detection limit of 10 ppm for *n*-dodecylammonium chloride, and the initial fluorescence could be fully restored by washing the analyte with basic THF. Additionally, Zhoa et al. developed an amphiphillic pillar[5]arene covalently attached to reduced graphene oxide as a sensor for acetaminophen, a pharmaceutical agent, with the key intermolecular interactions in this system including hydrogen bonding, hydrophobic interactions and π- π interactions.[1834] In the absence of analyte, an acridine orange fluorophore bound in the pillar[5]arene cavity, leading to a quenching of fluorescence due to its proximity to the reduced graphene oxide. Introduction of acetaminophen to the system resulted in displacement of acridine orange from the cavity and a resultant increase in fluorescence intensity. The sensing system showed selectivity for acetaminophen over a variety of potentially interfering species including 4-aminophenol, amino acids, surfactants, sugars, and salts. In complex matrices such as human serum samples, the system still maintained efficacy and had a detection limit of 0.05 μM. In another example, a selective sensor for tadalafil, a pharmaceutical agent for the treatment of erectile dysfunction, was developed by Yang et al. using a calix[6]arene bound to reduced graphene oxide.[1835] In the absence of analyte, Rhodamine B emission was quenched by the calix[6]arene-reduced graphene oxide, however, the addition of tadalafil released the Rhodamine B and regenerated the fluorescence emission (Figure 143). Of note, the binding constant for tadalafil was an order of magnitude stronger than the binding constant of Rhodamine B (10^5 vs. 10^4 M^{-1}), and the sensor was selective for tadalafil over other similar drugs, surfactants, sugars and ions, with a detection limit of 0.32 μM. In another example, Sun et al. developed a fluorescent sensor for the detection of carbaryl, a commonly used pesticide, at nanomolar concentrations, with a Benesi-Hildebrand binding constant of 4.2 x 10^5 M^{-1}.[1836] The sensor was fabricated by the non-covalent association of graphene oxide with a triazole-linked pyrenyl calix[4]arene, and the presence of carbaryl led to 75% quenching of the system fluorescence emission.

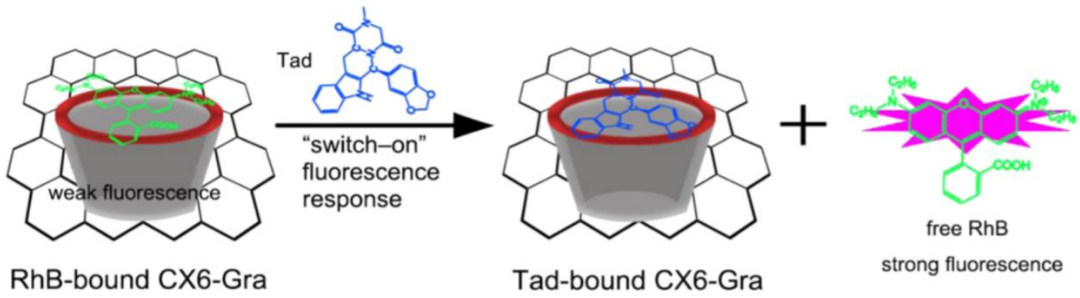

Figure 143. Calix[6]arene-reduced graphene oxide for the detection of tadalafil by fluorescent indicator displacement. Reproduced with permission from Ref. 1835. Copyright 2015 American Chemical Society.

Graphitic carbon nitride is a material similar to graphene oxide that is typically composed of heptazine or triazine sheets, both of which are produced from melamine (Figure 144).[1837] Graphitic carbon nitride is a promising photocatalyst[1838] and displays good biocompatibility, high fluorescence quantum yields, and strong electrochemiluminescence.[1839] Wang et al. deposited β-cyclodextrin onto the surface of graphitic carbon nitride to form a luminescent nanocomposite that was used for organophosphate detection.[1840] In the absence of the organophosphate analyte, the graphitic carbon nitride host was highly luminescent due to the presence of a triethylamine additive. Acetylcholinesterase was then immobilized on the surface of the nanocomposite, through binding to ferrocenecarboxylic acid encapsulated in the β-cyclodextrin cavity, and the system was treated with acetylthiocholine. Treatment with acetylthiocholine produced acetic acid, which reacted with the triethylamine and effectively quenching the triethylamine-promoted emission of the nanocomposite. When the enzyme was inhibited by the addition of organophosphates, triethylamine was not consumed by acetic acid, and the host remained highly luminescent. Thus, the activity of the enzyme could be monitored by changes in luminescence. Organophosphate concentrations as low as 0.3 pM were found to lead to enough enzyme inhibition to produce emission enhancement.

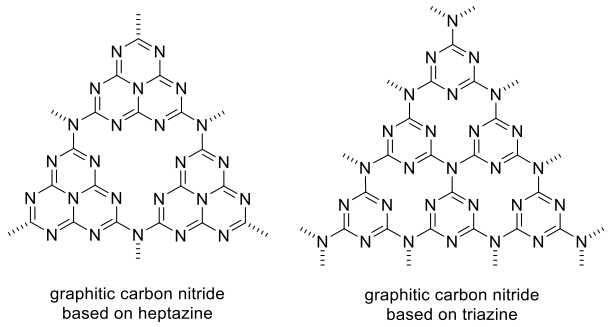

Figure 144. Typical graphitic carbon nitride constructs[1837]

8. Conclusions and Outlook

This review article covers a broad variety of supramolecular luminescent sensors that have been developed for an extremely diverse range of analytes based on supramolecular associations. These sensors are based on supramolecular architectures, including macrocycles, polymers, and nanomaterials and respond to the presence of the target analyte with a measurable change in their luminescence signal, including a change in luminescence intensity or a shift in the spectral position of the luminescence read-out signal. Low limits of detection have been reported in numerous cases, including pM level sensitivities,[1841] and high levels of selectivity for the target analyte have been demonstrated, even in the presence of large numbers of potentially interfering analytes.

Despite these significant advances and the enormity of the intellectual effort that has been spent in this field, unsolved problems in the area of chemical detection remain. Many of these problems relate to detection in complex systems, such as in the remediation of large-scale environmental disasters (i.e. oil

spills,[1842] industrial chemical contamination,[1843] etc). In such cases, a priori knowledge of the main chemical contaminant(s) is still necessary in order to accomplish practical detection/screening, especially of large numbers of potentially contaminated samples in a rapid time frame. This knowledge is necessary because state-of-the-art detection methods still rely overwhelmingly on mass spectral-based detection, which generates a signal for every one of the uniquely massed species in the complex environment. In order to screen for a particular compound with a particular mass, therefore, a priori knowledge is required.

While such knowledge is usually available, there are multiple reported cases in which inaccurate or incomplete knowledge delayed accurate detection and was responsible for inadvertent toxicant exposure. In the 2014 Elk River chemical spill in West Virginia, for example, first responders were initially unaware of the presence of a secondary contaminant in addition to the primary 4-methylcyclohexylmethanol (4-MCHM) contaminant.[1844] The first responders in this case relied on the chemical company responsible for the spill to accurately disclose the nature of the contamination, and then screened large numbers of samples only for the reported contaminant. When accurate information was not forthcoming until several days after the initial contamination event, residents were inadvertently exposed to additional contaminants, first responders were unable to develop effective remediation strategies, and the development of an effective containment response was delayed.[1845] Similar gaps in current state-of-the art detection methods explain why consumers were initially unaware of the presence of bisphenol A (BPA) analogues, including bisphenol S (BPS) and bisphenol F (BPF), in the presence of products labeled "BPA-free," and were inadvertently exposed to these BPA derivatives.[1846] Detection methods for BPA relied on mass spectral methods;[1847] because the BPA analogues have slightly different molar masses, they remained undetected in the products for an as-yet undetermined amount of time.

Array-based luminescent sensors that are not specific for a single analyte but display patterns of interactions with broader varieties of analytes can provide some knowledge of the nature of an unknown contaminant, especially if the statistical analyses of such signals can be tuned to identify certain structural features of the analyte. Rotello discusses some of the challenges of unknown analyte identification in his 2015 review article on selectivity vs. specificity in chemical sensors,[34] and highlights the potential of luminescent chemical sensors to address these challenges. Currently used commercial sensors still do not have the ability to accomplish completely unguided analyte identification, however, and numerous practical and technical challenges remain before such powerful commercial devices become a reality. In the interim, the large numbers of chemists working in this extremely active research area are developing and reporting significant research advances in luminescent chemical sensors, and numerous practical applications of such sensors in airport security screening, fluorescence-guided surgery, cancer diagnostics, and other areas have been, and continue to be, reported. There is great need for stand-alone luminescence-based sensors that encompass selectivity, sensitivity, and applicability that overcome the aforementioned challenges, and the chemistry described herein exemplifies the significant advances that have been taken toward that goal from numerous research groups in recent years.

Supramolecular luminescent sensors have solved significant problems in a broad variety of research areas, including in biological imaging,[1848] medical diagnostics,[1849] national security,[346] and food and agricultural safety.[1850] Among the classes of luminescent sensors discussed herein, supramolecular polymer-based sensors have significant system advantages due to their ability to amplify chemical signals that are generated as a result of interactions with the target analyte.[83] This signal amplification occurs due to the fact that conjugated polymers act as molecular wires, with uninterrupted electron communication throughout the length of the conjugated polymer chain.[1688] As a result, interaction with an analyte that occurs anywhere along the chain can be detected spectroscopically as a result of facile exciton migration throughout the chain. Cavitand and cryptand-based sensors, by contrast, lack the capability for signal amplification; as a result, sensitivity for a target analyte is often lowered in these sensors compared to the conjugated polymer-based ones, although selectivity due to specific binding is often enhanced.[1851]

Despite the significant advances that have been made in solving sensor-related problems, a number of unsolved challenges still remain. Such challenges include:

(a) Achieving selectivity in anion detection in aqueous environments: The high degree of solvation of anions means that anion-specific binders often are binding a highly solvated anionic analyte.[1852] Such solvated anions often have less structural differences than the unsolvated anions, and as a result, achieving selectivity in the detection of solvated anions remains challenging.[1853] Efforts to address this lack of selectivity including the use of array-based analysis to generate unique response patterns,[1854] the development of methods to desolvate anions prior to binding,[1855] and the ability to generate sensors that can accurately distinguish between solvated anions, despite their small structural differences.[1856]

(b) Demonstrating robust performance in biological environments: Chemical sensing in biological environments is inherently complex, due to the large numbers of potentially interfering analytes as well as the highly polar aqueous environment.[1857] Although significant progress has been made in this area, there is still a significant need for sensors that operate with high sensitivity, selectivity, and robust performance within the complex biological milieu.[1858]

(c) Accomplishing unguided chemical detection: Although the chemistry community has made significant progress in detecting an analyte when the identity of the analyte is known, detecting analytes whose identity is unknown remains a largely unsolved challenge. The need for such unguided detection occurs in a number of real-world scenarios, including in the 2014 Elk River chemical spill in West Virginia, in which the identity of the contaminants was not initially disclosed;[1859] when an unconscious patient comes into the emergency room as a result of a chemical exposure event that is unknown to the physician; and when food is contaminated with an unknown pathogen that needs to be detected accurately. Progress in achieving such unguided detection has been reported, although significantly more work remains to be accomplished before this problem is solved.[34]

9. References

(1) Chaudhuri, S.; DiScenza, D. J.; Smith, B.; Yocum, R.; Levine, M. Array-Based Detection of Isomeric and Analogous Analytes Employing Synthetically Modified Fluorophore Attached β-Cyclodextrin Derivatives. *New J. Chem.* **2017**, *41*, 14431-14437.

(2) Beyeh, N. K.; Jo, H. H.; Kolesnichenko, I.; Pan, F.; Kalenius, E.; Anslyn, E. V.; Ras, R. H. A.; Rissanen, K. Recognition of Viologen Derivatives in Water by N-Alkyl Ammonium Resorcinarene Chlorides. *J. Org. Chem.* **2017**, *82*, 5198-5203.

(3) Chi, X.; Peters, G. M.; Hammel, F.; Brockman, C.; Sessler, J. L. Molecular Recognition Under Interfacial Conditions: Calix[4]pyrrole-Based Cross-Linkable Micelles for Ion Pair Extraction. *J. Am. Chem. Soc.* **2017**, *139*, 9124-9127.

(4) Fatila, E. M.; Twum, E. B.; Sengupta, A.; Pink, M.; Karty, J. A.; Raghavachari, K.; Flood, A. H. Anions Stabilize Each Other Inside Macrocyclic Hosts. *Angew. Chem. Int. Ed.* **2016**, *55*, 14057-14062.

(5) Harding Lepage, P.; Peytavi, R.; Bergeron, M. G.; Leclerc, M. Amplification Strategy Using Aggregates of Ferrocene-Containing Cationic Polythiophene for Sensitive and Specific Electrochemical Detection of DNA. *Anal. Chem.* **2011**, *83*, 8086-8092.

(6) Boonkitpatarakul, K.; Wang, J.; Niamnont, N.; Liu, B.; Mcdonald, L.; Pang, Y.; Sukwattanasinitt, M. Novel Turn-On Fluorescent Sensors with Mega Stokes Shifts for Dual Detection of Al3+ and Zn2+. *ACS Sensors* **2016**, *1*, 144-150.

(7) Yuan, Y.; Zhang, R.; Cheng, X.; Xu, S.; Liu, B. A FRET Probe with AIEgen as the Energy Quencher: Dual Signal Turn-On for Self-Validated Caspase Detection. *Chem. Sci.* **2016**, *7*, 4245-4250.

(8) Zhang, R.; Sung, S. H. P.; Feng, G.; Zhang, C.-J.; Kenry; Tang, B. Z.; Liu, B. Aggregation-Induced Emission Probe for Specific Turn-On Quantification of Soluble Transferrin Receptor: An Important Disease Marker for Iron Deficiency Anemia and Kidney Diseases. *Anal. Chem.* **2018**, *90*, 1154-1160.

(9) Woo, H. Y.; Nag, O. K.; Kim, J.; Kang, M.; Bazan, G. C. Water-Soluble Polyelectrolytes for FRET-based DNA Detection. *Molec. Crystals Liq. Crystals* **2008**, *486*, 244-249.

(10) Gade, A. M.; Meadows, M. K.; Ellington, A. D.; Anslyn, E. V. Differential Array Sensing for Cancer Cell Classification and Novelty Detection. *Org. Biomol. Chem.* **2017**, *15*, 9866-9874.

(11) Le, N. D. B.; Yesilbag Tonga, G.; Mout, R.; Kim, S.-T.; Wille, M. E.; Rana, S.; Dunphy, K. A.; Jerry, D. J.; Yazdani, M.; Ramanathan, R.; Rotello, C. M.; Rotello, V. M. Cancer Cell Discrimination Using Host-Guest "Doubled" Arrays. *J. Am. Chem. Soc.* **2017**, *139*, 8008-8012.

(12) Zhang, Q.; Savagatrup, S.; Kaplonek, P.; Seeberger, P. H.; Swager, T. M. Janus Emulsions for the Detection of Bacteria. *ACS Central Sci.* **2017**, *3*, 309-313.

(13) Disney, M. D.; Zheng, J.; Swager, T. M.; Seeberger, P. H. Detection of Bacteria with Carbohydrate-Functionalized Fluorescent Polymers. *J. Am. Chem. Soc.* **2004**, *126*, 13343-13346.

(14) Fang, Y.; Ramasamy, R. P. Current and Prospective Methods for Plant Disease Detection. *Biosensors* **2015**, *5*, 537-561.

(15) Pieczywek, P. M.; Cybulska, J.; Szymanska-Chargot, M.; Siedliska, A.; Zdunek, A.; Nosalewicz, A.; Baranowski, P.; Kurenda, A. Early Detection of Fungal Infection of Stored Apple Fruit with Optical Sensors - Comparison of Biospeckle, Hyperspectral Imaging and Chlorophyll Fluorescence. *Food Control* **2018**, *85*, 327-338.

(16) Rose, A.; Zhu, Z.; Madigan, C. F.; Swager, T. M.; Bulovic, V. Sensitivity Gains in Chemosensing by Lasing Action in Organic Polymers. *Nature* **2005**, *434*, 876-879.

(17) Narayanan, A.; Varnavski, O. P.; Swager, T. M.; Goodson, T., III Multiphoton Fluorescence Quenching of Conjugated Polymers for TNT Detection. *J. Phys. Chem. C* **2008**, *112*, 881-884.

(18) Williams, V. E.; Yang, J. S.; Lugmair, C. G.; Miao, Y. J.; Swager, T. M. Design of Novel Iptycene-Containing Fluorescent Polymers for the Detection of TNT. *Proc. SPIE* **1999**, *3710*, 402-408.

(19) Prince, A. C.; Jani, A.; Korb, M.; Tipirneni, K. E.; Kasten, B. B.; Rosenthal, E. L.; Warram, J. M. Characterizing the Detection Threshold for Optical Imaging in Surgical Oncology. *J. Surgical Oncology* **2017**, *116*, 898-906.

(20) Bruno, J. G.; Sivils, J. C.; Phillips, T. Aptamer-Magnetic Bead Quantum Dot Sandwich Assays for Foodborne Pathogen Detection: Pros, Cons, and Lessons Learned. *J. AOAC Int.* **2017**, *110*, 895-899.

(21) Zhang, H.; Yang, S.; Beier, R. C.; Beloglazova, N. V.; Lei, H.; Sun, X.; Ke, Y.; Zhang, S.; Wang, Z. Simple, High Efficiency Detection of Microcystins and Nodularin-R in Water by Fluorescence Polarization Immunoassay. *Anal. Chim. Acta* **2017**, *992*, 119-127.

(22) Chauhan, B.; Jalalpure, S. Analysis of Amikacin in Human Serum by UHPLC with Fluorescence Detector Using Chloro-formate Reagent with Glycine. *Pharmaceutical Methods* **2016**, *7*, 99-103.

(23) Kundu, A.; Anthony, S. P. Triphenylamine Based Reactive Coloro/Fluorimetric Chemosensors: Structural Isomerism and Solvent Dependent Sensitivity and Selectivity. *Spectrochim. Acta A* **2018**, *189*, 342-348.

(24) Ball, P.; Hallsworth, J. E. Water Structure and Chaotropicity: Their Uses, Abuses and Biological Implications. *Phys. Chem. Chem. Phys.* **2015**, *17*, 8297-8305.

(25) Potyrailo, R. A. Toward High Value Sensing: Monolayer-Protected Metal Nanoparticles in Multivariable Gas and Vapor Sensors. *Chem. Soc. Rev.* **2017**, *46*, 5311-5346.

(26) Calvo, N. L.; Maggio, R. M.; Kaufman, T. S. Characterization of Pharmaceutically Relevant Materials at the Solid State Employing Chemometrics Methods. *J. Pharmaceutical Biomed. Anal.* **2018**, *147*, 538-564.

(27) Huang, L.; Wang, Z.; Zhu, X.; Chi, L. Electrical Gas Sensors Based on Structured Organic Ultra-Thin Films and Nanocrystals on Solid State Substrates. *Nanoscale Horizons* **2016**, *1*, 383-393.

(28) Shi, W.; Friedman, A. K.; Baker, L. A. Nanopore Sensing. *Anal. Chem.* **2017**, *89*, 157-188.

(29) Holmstrom, E. D.; Nesbitt, D. J. Biophysical Insights from Temperature-Dependent Single-Molecule Forster Resonance Energy Transfer. *Ann. Rev. Phys. Chem.* **2016**, *67*, 441-465.

(30) Aylward, L. L.; Hays, S. M.; Zidek, A. Variation in Urinary Spot Sample, 24 h Samples, and Longer-Term Average Urinary Concentrations of Short-Lived Environmental Chemicals: Implications for Exposure Assessment and Reverse Dosimetry. *J. Exposure Sci. Environ. Epidemiology* **2017**, *27*, 582-590.

(31) Bandela, A. K.; Bandaru, S.; Rao, C. P. A Fluorescent 1,3-Diaminonaphthalimide Conjugate of Calix[4]arene for Sensitive and Selective Detection of Trinitrophenol: Spectroscopy, Microscopy, and Computational Studies, and its Applicability Using Cellulose Strips. *Chem. Eur. J.* **2015**, *21*, 13364-13374.

(32) Zhao, D.; Swager, T. M. Conjugated Polymers Containing Large Soluble Diethynyl Iptycenes. *Org. Lett.* **2005**, *7*, 4357-4360.

(33) Tan, H.; Liu, B.; Chen, Y. Lanthanide Coordination Polymer Nanoparticles for Sensing Mercury(II) by Photoinduced Electron Transfer. *ACS Nano* **2012**, *6*, 10505-10511.

(34) Peveler, W. J.; Yazdani, M.; Rotello, V. M. Selectivity and Specificity: Pros and Cons in Sensing. *ACS Sensors* **2016**, *1*, 1282-1285.

(35) Zeng, X.; Mernaugh, R. Single-Chain Fragment Variable Recombinant Antibodies and Their Applications in Biosensors for Cancer Diagnosis. *Ed.* Preedy, V. R.; Patel, V B in *Biosensors and Cancer* **2012**, 337-358.

(36) Barr, J. R.; Kalb, S. R.; Pirkle, J. L. Detection, Differentiation and Subtyping of Botulinum Neurotoxins in Clinical Samples with Mass Spectrometry. *ACS Symposium Series* **2011**, *1065*, 83-97.

(37) McGhee, C. E.; Loh, K. Y.; Lu, Y. DNAzyme Sensors for Detection of Metal Ions in the Environment and Imaging Them in Living Cells. *Curr. Opinion Biotechnol.* **2017**, *45*, 191-201.

(38) Nigam, V. K.; Shukla, P. Enzyme Based Biosensors for Detection of Environmental Pollutants-A Review. *J. Microbiol. Biotechnol.* **2015**, *25*, 1773-1781.

(39) Verdian, A. Apta-Nanosensors for Detection and Quantitative Determination of Acetamiprid - A Pesticide Residue in Food and Environment. *Talanta* **2018**, *176*, 456-464.

(40) de Franciscis, V. A Theranostic "SMART" Aptamer for Targeted Therapy of Prostate Cancer. *Molec. Therapy* **2014**, *22*, 1886-1888.

(41) Mak, W. C.; Beni, V.; Turner, A. P. F. Lateral-Flow Technology: From Visual to Instrumental. *TrAC, Trends Anal. Chem.* **2016**, *79*, 297-305.

(42) Braunstein, G. D. The Long Gestation of the Modern Home Pregnancy Test. *Clinical Chem.* **2014**, *60*, 18-21.

(43) Tavakoli, A.; Karbalaie Niya, M. H.; Keshavarz, M.; Ghaffari, H.; Asoodeh, A.; Monavari, S. H.; Keyvani, H. Current Diagnostic Methods for HIV. *Future Virology* **2017**, *12*, 141-155.

(44) Mauk, M.; Song, J.; Bau, H. H.; Gross, R.; Bushman, F. D.; Collman, R. G.; Liu, C. Miniaturized Devices for Point of Care Molecular Detection of HIV. *Lab on a Chip* **2017**, *17*, 382-394.

(45) Kim, J.; Campbell, A. S.; Wang, J. Wearable Non-Invasive Epidermal Glucose Sensors: A Review. *Talanta* **2018**, *177*, 163-170.

(46) Scirica, B. M. Use of Biomarkers in Predicting the Onset, Monitoring the Progression, and Risk Stratification for Patients with Type 2 Diabetes Mellitus. *Clinical Chem.* **2017**, *63*, 186-195.

(47) Diehl, K. L.; Anslyn, E. V. Array Sensing Using Optical Methods for Detection of Chemical and Biological Hazards. *Chem. Soc. Rev.* **2013**, *42*, 8596-8611.

(48) Chen, J.-F.; Lin, Q.; Zhang, Y.-M.; Yao, H.; W., T.-B. Pillararene-Based Fluorescent Chemosensors: Recent Advances and Perspectives. *Chem. Commun.* **2017**, *53*, 13296-13311.

(49) Kaur, N.; Kaur, G.; Fegade, U. A.; Singh, A.; Sahoo, S. K.; Kuwar, A. S.; Singh, N. Anion Sensing with Chemosensors Having Multiple -NH Recognition Units. *TrAC, Trends Anal. Chem.* **2017**, *95*, 86-109.

(50) Wang, Q.; Li, Z.; Tao, D.-D.; Zhang, Q.; Zhang, P.; Guo, D.-P.; Jiang, Y.-B. Supramolecular Aggregates as Sensory Ensembles. *Chem. Commun.* **2016**, *52*, 12929-12939.

(51) Liu, J.; Xu, M.; Wang, B.; Zhou, Z.; Wang, L. Fluorescence Sensor for Detecting Protamines Based on Competitive Interactions of Polyacrylic Acid Modified with Sodium 4-Amino-1-Naphthalenesulfonate with Protamines and Aminated Graphene Oxide. *RSC Adv.* **2017**, *7*, 1432-1438.

(52) Shumilova, T. A.; Rueffer, T.; Lang, H.; Kataev, E. A. Straightforward Design of Fluorescent Receptors for Sulfate: Study of Non-Covalent Interactions Contributing to Host-Guest Formation. *Chem. Eur. J.* **2018**, *24*, 1500-1504.

(53) Kaifer, A. E. Toward Reversible Control of Cucurbit[n]uril Complexes. *Acc. Chem. Res.* **2014**, *47*, 2160-2167.

(54) Kreno, L. E.; Leong, K.; Farha, O. K.; Allendorf, M.; Van Duyne, R. P.; Hupp, J. T. Metal-Organic Framework Materials as Chemical Sensors. *Chem. Rev.* **2012**, *112*, 1105-1125.

(55) Cui, Y.; Chen, B.; Qian, G. Lanthanide Metal-Organic Frameworks for Luminescent Sensing and Light-Emitting Applications. *Coord. Chem. Rev.* **2014**, *273-274*, 76-86.

(56) Hu, Z.; Deibert, B. J.; Li, J. Luminescent Metal-Organic Frameworks for Chemical Sensing and Explosive Detection. *Chem. Soc. Rev.* **2014**, *43*, 5815-5840.

(57) Yan, B. Lanthanide-Functionalized Metal-Organic Framework Hybrid Systems to Create Multiple Luminescent Centers for Chemical Sensing. *Acc. Chem. Res.* **2017**, *50*, 2789-2798.

(58) Zhang, Y.; Yuan, S.; Day, G.; Wang, X.; Yang, X.; Zhou, H.-C. Luminescent Sensors Based on Metal-Organic Frameworks. *Coord. Chem. Rev.* **2018**, *354*, 28-45.

(59) Sriram, G.; Bhat, M. P.; Patil, P.; Uthappa, U. T.; Jung, H.-Y.; Altalhi, T.; Kumeria, T.; Aminabhavi, T. M.; Pai, R. K.; Madhuprasad; Kurkuri, M. D. Paper-Based Microfluidic Analytical Devices for Colorimetric Detection of Toxic Ions: A Review. *TrAC, Trends Anal. Chem.* **2017**, *93*, 212-227.

(60) Tang, L.; Li, J. Plasmon-Based Colorimetric Nanosensors for Ultrasensitive Molecular Diagnostics. *ACS Sensors* **2017**, *2*, 857-875.

(61) Ajay, P. V. S.; Printo, J.; Kiruba, D. S. C. G.; Susithra, L.; Takatoshi, K.; Sivakumar, M. Colorimetric Sensors for Rapid Detection of Various Analytes. *Materials Sci. Engineering C* **2017**, *78*, 1231-1245.

(62) Pu, H.; Xiao, W.; Sun, D.-W. SERS-Microfluidic Systems: A Potential Platform for Rapid Analysis of Food Contaminants. *Trends Food Sci. Technol.* **2017**, *70*, 114-126.

(63) Xi, W.; Shrestha, B. K.; Haes, A. J. Promoting Intra- and Intermolecular Interactions in Surface-Enhanced Raman Scattering. *Anal. Chem.* **2018**, *90*, 128-143.

(64) Arif, S.; Qudsia, S.; Urooj, S.; Chaudry, N.; Arshad, A.; Andleeb, S. Blueprint of Quartz Crystal Microbalance Biosensor for Early Detection of Breast Cancer Through Salivary Autoantibodies Against ATP6AP1. *Biosensors Bioelectronics* **2015**, *65*, 62-70.

(65) Kabir, K. M. M.; Ippolito, S. J.; Kandjani, A. E.; Sabri, Y. M.; Bhargava, S. K. Nano-Engineered Surfaces for Mercury Vapor Sensing: Current State and Future Possibilities. *TrAC, Trends Anal. Chem.* **2017**, *88*, 77-99.

(66) Skladal, P. Piezoelectric Biosensors. *TrAC, Trends Anal. Chem.* **2016**, *79*, 127-133.

(67) Wu, J.; Kwon, B.; Liu, W.; Anslyn, E. V.; Wang, P.; Kim, J. S. Chromogenic/Fluorogenic Ensemble Chemosensing Systems. *Chem. Rev.* **2015**, *115*, 7893-7943.

(68) Liemburg-Apers, D. C.; Imamura, H.; Forkink, M.; Nooteboom, M.; Swarts, H. G.; Brock, R.; Smeitink, J. A. M.; Willems, P. H. G. M.; Koopman, W. J. H. Quantitative Glucose and ATP Sensing in Mammalian Cells. *Pharmaceutical Res.* **2011**, *28*, 2745-2757.

(69) Zhao, C.; Montaseri, M. H.; Wood, G. S.; Pu, S. H.; Seshia, A. A.; Kraft, M. A Review on Coupled MEMS Resonators for Sensing Applications Utilizing Mode Localization. *Sensors Actuators A: Phys.* **2016**, *249*, 93-111.

(70) Zheng, P.; Wu, N. Fluorescence and Sensing Applications of Graphene Oxide and Graphene Quantum Dots: A Review. *Chem. Asian J.* **2017**, *12*, 2343-2353.

(71) Gupta, A.; Kumar, N. A Review of Mechanisms for Fluorescent "Turn-On" Probes to Detect Al3+ Ions. *RSC Adv.* **2016**, *6*, 106413-106434.

(72) Hu, F.; Liu, B. Organelle-Specific Bioprobes Based on Fluorogens with Aggregation-Induced Emission (AIE) Characteristics. *Org. Biomol. Chem.* **2016**, *14*, 9931-9944.

(73) Li, D.; Yu, J. AIEgens-Functionalized Inorganic-Organic Hybrid Materials: Fabrications and Applications. *Small* **2016**, *12*, 6478-6494.

(74) He, L.; Dong, B.; Liu, Y.; Lin, W. Fluorescent Chemosensors Manipulated by Dual/Triple Interplaying Sensing Mechanisms. *Chem. Soc. Rev.* **2016**, *45*, 6449-6461.

(75) Chapin, B. M.; Anslyn, E. V. Physical Organic Chemistry by Any Other Name Would Smell as Sweet. *Israel J. Chem.* **2016**, *56*, 38-45.

(76) You, L.; Zha, D.; Anslyn, E. V. Recent Advances in Supramolecular Analytical Chemistry Using Optical Sensing. *Chem. Rev.* **2015**, *115*, 7840-7892.

(77) Rotello, V. M. Organic Chemistry Meets Polymers, Nanoscience, Therapeutics and Diagnostics. *Beilstein J. Org. Chem.* **2016**, *12*, 1638-1646.

(78) Creran, B.; Bunz, U. H. F.; Rotello, V. M. Polymer - Nanoparticle Assemblies for Array Based Sensing. *Curr. Org. Chem.* **2015**, *19*, 1054-1062.

(79) Murray, J.; Kim, K.; Ogoshi, T.; Yao, W.; Gibb, B. C. The Aqueous Supramolecular Chemistry of Cucurbit[n]urils, Pillar[n]arenes and Deep-Cavity Cavitands. *Chem. Soc. Rev.* **2017**, *46*, 2479-2496.

(80) Jordan, J. H.; Gibb, B. C. Molecular Containers Assembled Through the Hydrophobic Effect. *Chem. Soc. Rev.* **2015**, *44*, 547-585.

(81) Ajami, D.; Rebek, J. Reversibly Expanded Encapsulation Complexes. *Topics Curr. Chem.* **2012**, *319*, 57-78.

(82) Ajami, D.; Rebek, J., Jr. More Chemistry in Small Spaces. *Acc. Chem. Res.* **2013**, *46*, 990-999.

(83) Wu, W.; Bazan, G. C.; Liu, B. Conjugated-Polymer-Amplified Sensing, Imaging, and Therapy. *Chem.* **2017**, *2*, 760-790.

(84) Zhan, R.; Pan, Y.; Manghnani, P. N.; Liu, B. AIE Polymers: Synthesis, Properties, and Biological Applications. *Macromol. Bioscience* **2017**, *17*; DOI: 10.1002/mabi.201600433

(85) Thomas, S. W.; Joly, G. D.; Swager, T. M. Chemical Sensors Based on Amplifying Fluorescent Conjugated Polymers. *Chem. Rev.* **2007**, *107*, 1339-1386.

(86) Swager, T. M. 50th Anniversary Perspective: Conducting/Semiconducting Conjugated Polymers. A Personal Perspective on the Past and the Future. *Macromolecules* **2017**, *50*, 4867-4886.

(87) Fennell, J. F. Jr.; Liu, S. F.; Azzarelli, J. M.; Weis, J. G.; Rochat, S.; Mirica, K. A.; Ravnsbaek, J. B.; Swager, T. M. Nanowire Chemical/Biological Sensors: Status and a Roadmap for the Future. *Angew. Chem. Int. Ed.* **2016**, *55*, 1266-1281.

(88) Song, C.; Swager, T. M. Reactive Conducting Thiepin Polymers. *J. Org. Chem.* **2010**, *75*, 999-1005.

(89) Eersels, K.; Lieberzeit, P.; Wagner, P. A Review on Synthetic Receptors for Bioparticle Detection Created by Surface-Imprinting Techniques-From Principles to Applications. *ACS Sensors* **2016**, *1*, 1171-1187.

(90) Balaz, M.; Tannir, S.; Varga, K. Chiral Multichromophoric Supramolecular Nanostructures Assembled by Single Stranded DNA and RNA Templates. *Coordination Chem. Rev.* **2017**, *349*, 66-83.

(91) Prochowicz, D.; Kornowicz, A.; Lewinski, J. Interactions of Native Cyclodextrins with Metal Ions and Inorganic Nanoparticles: Fertile Landscape for Chemistry and Materials Science. *Chem. Rev.* **2017**, *117*, 13461-13501.

(92) Amendola, V.; Bergamaschi, G.; Miljkovic, A. Azacryptands as Molecular Cages for Anions and Metal Ions. *Supramol. Chem.* **2018**, *30*, 236-242.

(93) Kim, S. K.; Sessler, J. L. Calix[4]pyrrole-Based Ion Pair Receptors. *Acc. Chem. Res.* **2014**, *47*, 2525-2536.

(94) Lauko, J.; Kouwer, P. H. J.; Rowan, A. E. 1H-1,2,3-Triazole: From Structure to Function and Catalysis. *J. Heterocyclic Chem.* **2017**, *54*, 1677-1699.

(95) Umadevi, D.; Panigrahi, S.; Sastry, G. N. Noncovalent Interaction of Carbon Nanostructures. *Acc. Chem. Res.* **2014**, *47*, 2574-2581.

(96) Giese, M.; Albrecht, M.; Rissanen, K. Experimental Investigation of Anion-π Interactions - Applications and Biochemical Relevance. *Chem. Commun.* **2016**, *52*, 1778-1795.

(97) D'Souza, F.; Ito, O. Supramolecular Donor-Acceptor Hybrids of Porphyrins/Phthalocyanines with Fullerenes/Carbon Nanotubes: Electron Transfer, Sensing, Switching, and Catalytic Applications. *Chem. Commun.* **2009**, 4913-4928.

(98) Anzenbacher, P.; Mosca, L.; Palacios, M. A.; Zyryanov, G. V.; Koutnik, P. Iptycene-Based Fluorescent Sensors for Nitroaromatics and TNT. *Chem. Eur. J.* **2012**, *18*, 12712-12718.

(99) Chen, Y.; Huang, F.; Li, Z.-T.; Liu, Y. Controllable Macrocyclic Supramolecular Assemblies in Aqueous Solution. *Sci. China Chem.* **2018**, *61*, 979-992.

(100) Rest, C.; Mayoral, M. J.; Fucke, K.; Schellheimer, J.; Stepanenko, V.; Fernández, G. Self-Assembly and Hydro(gelation) Triggered by Cooperative π-π and Unconventional C-H…X Hydrogen Bonding Interactions. *Angew. Chem. Int. Ed.* **2014**, *53*, 700-705.

(101) Nowroozi, A.; Edrahimi, A.; Rad, O. R. Mutual Effects of the Cation-π, Anion-π and Intermolecular Hydrogen Bond in the Various Complexes of 1,3,5-Triamino-2,4,6-Trinitrobenzene with Some Cations (Li+, Na+, K+, Mg2+, Ca2+) and Anions (F-, Cl-, Br-). *Struct. Chem.* **2018**, *29*, 129-137.

(102) Jiang, M.; Li, M.; Liu, L.; Xiang, M. L.; Zhu, L. Macromolecular Aggregation. Complexation Due to Hydrogen Bonding and Hydrophobic Association. *Macromol. Symposia* **1997**, *124*, 135-146.

(103) Fisicaro, E.; Compari, C.; Braibanti, A. Hydrophobic Hydration Processes: General Thermodynamic Model by Thermal Equivalent Dilution Determinations. *Biophys. Chem.* **2010**, *151*, 119-138.

(104) Cerdeirina, C. A.; Debenedetti, P. G. Water Anomalous Thermodynamics, Attraction, Repulsion, and Hydrophobic Hydration. *J. Chem. Phys.* **2016**, *144*, 164501/1-164501/11.

(105) Ekwall, P.; Aminoff, C. F. Interaction of Paraffin Chain Alcohols and Association Colloids. VI. Sodium Caprate Concentration Where Interaction with Long-Chain Alcohols Begins and Its Dependence on the Chain Length of the Alcohol. *Acta Chem. Scandinavica* **1956**, *10*, 237-243.

(106) Gershfeld, N. L. Influence of Structure on the Orientation of Veratrum Alkaloids at the Air-Water Interface. *Biochim. Biophys. Acta* **1960**, *42*, 282-289.

(107) Winther, Chr. The First Step in the Swelling of Gelatin with Water. IV. *Acta Chem. Scandinavica* **1958**, *12*, 1643-1651.

(108) Baker, B. R.; Kawazu, M. Irreversible Enzyme Inhibitors. LXXVIII. Inhibitors of Thymidine Phosphorylase. 4. Hydrophobic Bonding by Uracils Substituted at the 5 and 6 Position. *J. Med. Chem.* **1967**, *10*, 311-313.

(109) Ringold, H. J.; Graves, J. M. H.; Clark, A.; Bellas, T. E. 3α-Hydroxysteroid Dehydrogenase from Pseudomonas testosteroni. Enzyme-Substrate Complementarity as the Basis of Selectivity and Steric Specificity. *Recent Progress Hormone Res.* **1967**, *23*, 349-369.

(110) McEwen, C. M., Jr.; Sober, A/ J. Rabbit Serum Monoamine Oxidase. II. Determinants of Substrate Specificity. *J. Biol. Chem.* **1967**, *242*, 3068-3078.

(111) Breslow, E.; Abrash, L. The Binding of Oxytocin and Oxytocin Analogs by Purified Bovine Neurophysins. *Proc. Natl. Acad. Sci. U.S.A.* **1966**, *56*, 640-646.

(112) Breslow, R.; Overman, L. E. "Artificial Enzyme" Combining a Metal Catalytic Group and a Hydrophobic Binding Cavity. *J. Am. Chem. Soc.* **1970**, *92*, 1075-1077.

(113) Breslow, R.; Campbell, P. Selective Aromatic Substitution by Hydrophobic Binding of a Substrate to a Simple Cyclodextrin Catalyst. *Bioorganic Chem.* **1971**, *1*, 140-156.

(114) Mohandoss, S.; Stalin, T. A New Fluorescent PET Sensor Probe for Co2+ Ion Detection: Computational, Logic Device and Living Cell Imaging Applications. *RSC Adv.* **2017**, *7*, 16581-16593.

(115) Zengin, A.; Tamer, U.; Caykara, T. SERS Detection of Polyaromatic Hydrocarbons on a β-Cyclodextrin Containing Polymer Brush. *J. Raman Spectroscopy* **2018**, *49*, 452-461.

(116) Chakraborty, S.; Kumar, H.; Dasgupta, C.; Maiti, P. K. Confined Water: Structure, Dynamics, and Thermodynamics. *Acc. Chem. Res.* **2017**, *50*, 2139-2146.

(117) Galia, A.; Scialdone, O.; Spano, T.; Valenti, M. G.; Grignard, B.; Lecomte, P.; Monflier, E.; Tilloy, S.; Rousseau, C. Ring Opening Polymerization of ε-Caprolactone in the Presence of Wet β-Cyclodextrin: Effect of the Operative Pressure and of Water Molecules in the β-Cyclodextrin Cavity. *RSC Adv.* **2016**, *6*, 90290-90299.

(118) Tao, Y.; Gu, X.; Deng, L.; Qin, Y.; Xue, H.; Kong, Y. Chiral Recognition of D-Tryptophan by Confining High-Energy Water Molecules Inside the Cavity of Copper-Modified β-Cyclodextrin. *J. Phys. Chem. C* **2015**, *119*, 8183-8190.

(119) Zhou, X.; Liang, J. F. A Fluorescence Spectroscopy Approach for Fast Determination of β-Cyclodextrin-Guest Binding Constants. *J. Photochem. Photobiol. A* **2017**, *349*, 124-128.

(120) Maniyazagan, M.; Rameshwaran, C.; Mariadasse, R.; Jeyakanthan, J.; Premkumar, K.; Stalin, T. Fluorescence Sensor for Hg2+ and Fe3+ ions using 3,3'-Dihydroxybenzidine:α-Cyclodextrin

Supramolecular Complex: Characterization, In-Silico and Cell Imaging Study. *Sensors Actuators B: Chem.* **2017**, *242*, 1227-1238.

(121) Serio, N.; Roque, J.; Badwal, A.; Levine, M. Rapid and Efficient Pesticide Detection via Cyclodextrin-Promoted Energy Transfer. *Analyst* **2015**, *140*, 7503-7507.

(122) Serio, N.; Moyano, D. F.; Rotello, V. M.; Levine, M. Array-Based Detection of Persistent Organic Pollutants via Cyclodextrin Promoted Energy Transfer. *Chem. Commun.* **2015**, *51*, 11615-11618.

(123) Samanta, S. K.; Quigley, J.; Vinciguerra, B.; Briken, V.; Isaacs, L. Cucurbit[7]uril Enables Multi-Stimuli-Responsive Release from the Self-Assembled Hydrophobic Phase of a Metal Organic Polyhedron. *J. Am. Chem. Soc.* **2017**, *139*, 9066-9074.

(124) Rabbani, R.; Masson, E. Probing Interactions between Hydrocarbons and Auxiliary Guests inside Cucurbit[8]uril. *Org. Lett.* **2017**, *19*, 4303-4306.

(125) Liu, W.; Samanta, S. K.; Smith, B. D.; Isaacs, L. Synthetic Mimics of Biotin/(Strept)avidin. *Chem. Soc. Rev.* **2017**, *46*, 2391-2403.

(126) Shcherbakova, E. G.; Zhang, B.; Gozem, S.; Minami, T.; Zavalij, P. Y.; Pushina, M.; Isaacs, L. D.; Anzenbacher, P. Supramolecular Sensors for Opiates and Their Metabolites. *J. Am. Chem. Soc.* **2017**, *139*, 14954-14960.

(127) Masson, E.; Ling, X.; Joseph, R.; Kyeremeh-Mensah, L.; Lu, X. Cucurbituril Chemistry: A Tale of Supramolecular Success. *RSC Adv.* **2012**, *2*, 1213-1247.

(128) Masson, E.; Lu, X.; Ling, X.; Patchell, D. L. Kinetic vs Thermodynamic Self-Sorting of Cucurbit[6] uril, Cucurbit[7]uril, and a Spermine Derivative. *Org. Lett.* **2009**, *11*, 3798-3801.

(129) Nau, W. M.; Florea, M.; Assaf, K. I. Deep Inside Cucurbiturils: Physical Properties and Volumes of their Inner Cavity Determine the Hydrophobic Driving Force for Host-Guest Complexation. *Israel J. Chem.* **2011**, *51*, 559-577.

(130) Barrow, S. J.; Kasera, S.; Rowland, M. J.; del Barrio, J.; Scherman, O. A. Cucurbituril-Based Molecular Recognition. *Chem. Rev.* **2015**, *115*, 12320-12406.

(131) Liu, L.; Zhao, Z.; Hao, C. 3D Fluorescent Cucurbit[7]uril Framework Linked by Anion Fluorophore. *J. Inclusion Phenom. Macrocyclic Chem.* **2017**, *88*, 247-252.

(132) Bockus, A. T.; Smith, L. C.; Grice, A. G.; Ali, O. A.; Young, C. C.; Mobley, W.; Leek, A.; Roberts, J. L.; Vinciguerra, B.; Isaacs, L.; Urbach, A. R. Cucurbit[7]uril-Tetramethylrhodamine Conjugate for Direct Sensing and Cellular Imaging. *J. Am. Chem. Soc.* **2016**, *138*, 16549-16552.

(133) Thomas, S. S.; Tang, H.; Gaudes, A.; Baggesen, S. B.; Gibb, C. L. D.; Gibb, B. C.; Bohne, C. Tuning the Binding Dynamics of a Guest-Octaacid Capsule through Noncovalent Anchoring. *J. Phys. Chem. Lett.* **2017**, *8*, 2573-2578.

(134) Tang, D.; Barnett, J. W.; Gibb, B. C.; Ashbaugh, H. S. Guest Controlled Nonmonotonic Deep Cavity Cavitand Assembly State Switching. *J. Phys. Chem. B* **2017**, *121*, 10717-10725.

(135) Purse, B. W.; Rebek, J., Jr. Functional Cavitands: Chemical Reactivity in Structured Environments. *Proc. Natl. Acad. Sci. U.S.A.* **2005**, *102*, 10777-10782.

(136) Biros, S. M.; Rebek, J., Jr. Structure and Binding Properties of Water-Soluble Cavitands and Capsules. *Chem. Soc. Rev.* **2007**, *36*, 93-104.

(137) Lee, J.; Choi, K.; Paek, K. Conformational Study of a Rigid-Structured Octathiabiscavitand from [2 + 2] Coupling of Caps and Bridging Units. *Tetrahedron Lett.* **1997**, *38*, 8203-8206.

(138) Schroeder, T.; Sahu, S. N.; Mattay, J. Molecular Capsules Derived From Resorcin[4]arenes by Metal-Coordination. *Topics Curr. Chem.* **2012**, *319*, 99-124.

(139) Chakraborty, S.; Kuman, H. Dasgupta, C.; Maiti, P. K. Confined Water: Structure, Dynamics, and Thermodynamics. *Acc. Chem. Res.* **2017**, *50*, 2139-2146.

(140) Das, S.; Chatterjee, D. P.; Ghosh, R.; Nandi, A. K. Water Soluble Polythiophenes: Preparation and Applications. *RSC Adv.* **2015**, *5*, 20160-20177.

(141) Bandyopadhyay, P.; Ghosh, A. K. Recent Developments in Micelle-Induced Fluorescent Sensors. *Sensor Lett.* **2011**, *9*, 1249-1264.

(142) Shin, S.; Lim, J.; Gu, M.-L.; Yu, C.-Y.; Hong, M.; Char, K.; Choi, T.-L. Dimensionally Controlled Water-Dispersible Amplifying Fluorescent Polymer Nanoparticles for Selective Detection of Charge-Neutral Analytes. *Polym. Chem.* **2017**, *8*, 7507-7514.

(143) Wu, X.; Hang, H.; Li, H.; Chen, Y.; Tong, H.; Wang, L. Water-Dispersible Hyperbranched Conjugated Polymer Nanoparticles with Sulfonate Terminal Groups for Amplified Fluorescence Sensing of Trace TNT in Aqueous Solution. *Mater. Chem. Frontiers* **2017**, *1*, 1875-1880.

(144) Dong, W.; Ma, Z.; Duan, Q.; Fei, T. Crosslinked Fluorescent Conjugated Polymer Nanoparticles for High Performance Explosive Sensing in Aqueous Media. *Dyes Pigments* **2018**, *159*, 128-134.

(145) van der Vegt, N. F. A.; Nayar, D. The Hydrophobic Effect and the Role of Cosolvents. *J. Phys. Chem. B* **2017**, *121*, 9986-9998.

(146) Buschmann, H.-J.; Schollmeyer, E. Influence of the Solvation Upon the Reaction of α-Cyclodextrin with Carboxylic Acids, Their Methyl Esters, and Their Sodium Salts in Aqueous Solution Studied by Calorimetric Measurements. *J. Solution Chem.* **2005**, *34*, 731-737.

(147) Liu, P.; Chipot, C.; Shao, X.; Cai, W. Solvent-Controlled Shuttling in a Molecular Switch. *J. Phys. Chem. C* **2012**, *116*, 4471-4476.

(148) Leontidis, E. Chaotropic Salts Interacting with Soft Matter: Beyond the Lyotropic Series. *Curr. Opinion Colloid Interface Sci.* **2016**, *23*, 100-109.

(149) Moelbert, S.; Normand, B.; De Los Rios, P. Kosmotropes and Chaotropes: Modelling Preferential Exclusion, Binding and Aggregate Stability. *Biophys. Chem.* **2004**, *112*, 45-57.

(150) Bonn, M.; Nagata, Y.; Backus, E. H. G. Molecular Structure and Dynamics of Water at the Water-Air Interface Studied with Surface-Specific Vibrational Spectroscopy. *Angew. Chem. Int. Ed.* **2015**, *54*, 5560-5576.

(151) Minofar, B. Self Assembly of Ionic Liquids at the Air/Water Interface. *J. Self-Assembly Molec. Electronics* **2015**, *3*, 27-40.

(152) Saha, A.; Sen Gupta, S.; Kumar, A.; Naik, P. D. Interaction of L-Phenylalanine with Lipid Monolayers at Air-Water Interface at Different pHs: Sum-Frequency Generation Spectroscopy and Surface Pressure Studies. *J. Phys. Chem. C* **2018**, *122*, 3875-3884.

(153) Zhang, J.; Li, Y.; Wang, J.; Zhang, Y. Interfacial Behavior of Alkaline Protease at the Air-Water and Oil-Water Interfaces. *Appl. Surface Sci.* **2018**, *433*, 1128-1136.

(154) Cui, X.; Shi, C.; Zhang, S.; Xie, L.; Liu, J.; Jiang, D.; Zeng, H. Probing the Effect of Salinity and pH on Surface Interactions between Air Bubbles and Hydrophobic Solids: Implications for Colloidal Assembly at Air/Water Interfaces. *Chem. Asian J.* **2017**, *12*, 1568-1577.

(155) Lakshmanan, M.; Dhathathreyan, A. Langmuir and Langmuir-Blodgett Films of Proline-Rich N-Terminal Domain Peptide of γ-Zein. *Colloids Surf., B* **2007**, *55*, 185-191.

(156) Xu, W.; Zhang, Q.; Wei, H.; Qin, J.; Yu, L. Self-Aggregation of Catanionic Surface Active Ionic Liquids in Aqueous Solutions. *J. Surfactants Detergents* **2015**, *18*, 421-428.

(157) Wick, C. D.; Chang, T.-M.; Slocum, J. A.; Cummings, O. T. Computational Investigation of the n-Alkane/Water Interface with Many-Body Potentials: The Effect of Chain Length and Ion Distributions. *J. Phys. Chem. C* **2012**, *116*, 783-790.

(158) Rissanen, K. Crystallography of Encapsulated Molecules. *Chem. Soc. Rev.* **2017**, *46*, 2638-2648.

(159) Nguyen, N. N.; Nguyen, A. V. Hydrophobic Effect on Gas Hydrate Formation in the Presence of Additives. *Energy & Fuels* **2017**, *31*, 10311-10323.

(160) Sharon, M.; Robinson, C. V. A Quantitative Perspective on Hydrophobic Interactions in the Gas-Phase. *Curr. Proteomics* **2011**, *8*, 47-58.

(161) Nasief, N. N.; Hangauer, D. Influence of Neighboring Groups on the Thermodynamics of Hydrophobic Binding: An Added Complex Facet to the Hydrophobic Effect. *J. Med. Chem.* **2014**, *57*, 2315-2333.

(162) Yaminsky, V.; Ohnishi, S. Physics of Hydrophobic Cavities. *Langmuir* **2003**, *19*, 1970-1976.

(163) Paul, B. K.; Ghosh, N.; Mukherjee, S. Interaction of Bile Salts with β-Cyclodextrins Reveal Nonclassical Hydrophobic Effect and Enthalpy-Entropy Compensation. *J. Phys. Chem. B* **2016**, *120*, 3963-3968.

(164) Smithrud, D. B.; Wyman, T. B.; Diederich, F. Enthalpically Driven Cyclophane-Arene Inclusion Complexation: Solvent Dependent Calorimetric Studies. *J. Am. Chem. Soc.* **1991**, *113*, 5420-5426.

(165) Biela, A.; Sielaff, F.; Terwesten, F.; Heine, A.; Steinmetzer, T.; Klebe, G. Ligand Binding Stepwise Disrupts Water Network in Thrombin: Enthalpic and Entropic Changer Reveal Classical Hydrophobic Effect. *J. Med. Chem.* **2012**, *55*, 6094-6110.

(166) Graves, A. P.; Wall, I. D.; Edge, C. M.; Woolven, J. M.; Cui, G.; Le Gall, A.; Hong, X.; Raha, K.; Manas, E. S. A Perspective on Water Site Prediction Methods for Structure Based Drug Design. *Current Topics Med. Chem.* **2017**, *17*, 2599-2616.

(167) Raffaini, G.; Ganazzoli, F.; Malpezzi, L.; Fuganti, C.; Fronza, G.; Panzeri, W.; Mele, A. Validating a Strategy for Molecular Dynamics Simulations of Cyclodextrin Inclusion Complexes through Single-Crystal X-Ray and NMR Experimental Data: A Case Study. *J. Phys. Chem. B* **2009**, *113*, 9110-9122.

(168) Minh, D. D. L.; Chang, C.-e.; Trylska, J.; Tozzini, V.; McCammon, J. A. The Influence of Macromolecular Crowding on HIV-1 Protease Internal Dynamics. *J. Am. Chem. Soc.* **2006**, *128*, 6006-6007.

(169) Chen, W.; Chang, C.-e.; Gilson, M. K. Concepts in Receptor Optimization: Targeting the RGD Peptide. *J. Am. Chem. Soc.* **2006**, *128*, 4675-4684.

(170) Minh, D. D. L.; Bui, J. M.; Chang, C.-e.; Jain, T.; Swanson, J. M. J.; McCammon, J. A. The Entropic Cost of Protein-Protein Association: A Case Study on Acetylcholinesterase Binding to Fasciculin-2. *Biophys. J.* **2005**, *89*, L25-L27.

(171) Shityakov, S.; Broscheit, J.; Forster, C. α-Cyclodextrin Dimer Complexes of Dopamine and Levodopa Derivatives to Assess Drug Delivery to the Central Nervous System: ADME and Molecular Docking Studies. *Int. J. Nanomedicine* **2012**, *7*, 3211-3219.

(172) Ambrosetti, A.; Alfe, D.; DiStasio, R. A.; Tkatchenko, A. Hard Numbers for Large Molecules: Toward Exact Energetics for Supramolecular Systems. *J. Phys. Chem. Lett.* **2014**, *5*, 849-855.

(173) Collins, K. D. Why Continuum Electrostatics Theories Cannot Explain Biological Structure, Polyelectrolytes or Ionic Strength Effects in Ion-Protein Interactions. *Biophys. Chem.* **2012**, *167*, 43-59.

(174) Anslyn, E. V.; Dougherty, D. A. *Modern Physical Organic Chemistry*; University Science Books: USA, 2006.

(175) Duarte, A.; Chworos, A.; Flagan, S. F.; Hanrahan, G.; Bazan, G. C. Identification of Bacteria by Conjugated Oligoelectrolyte/Single-Stranded DNA Electrostatic Complexes. *J. Am. Chem. Soc.* **2010**, *132*, 12562-12564.

(176) Wang, Y.; Liu, B.; Mikhailovsky, A.; Bazan, G. C. Conjugated Polyelectrolyte-Metal Nanoparticle Platforms for Optically Amplified DNA Detection. *Adv. Mater.* **2010**, *22*, 656-659.

(177) Xia, F.; Zuo, X.; Yang, R.; Xiao, Y.; Kang, D.; Vallee-Belisle, A.; Gong, X.; Yuen, J. D.; Hsu, B. B. Y.; Heeger, A. J.; Plaxco, K. W. Colorimetric Detection of DNA, Small Molecules, Proteins, and Ions Using Unmodified Gold Nanoparticles and Conjugated Polyelectrolytes. *Proc. Natl. Acad. Sci. U.S.A.* **2010**, *107*, 10837-10841.

(178) Xia, F.; Zuo, X.; Yang, R.; Xiao, Y.; Kang, D.; Vallee-Belisle, A.; Gong, X.; Heeger, A. J.; Plaxco, K. W. On the Binding of Cationic, Water-Soluble Conjugated Polymers to DNA: Electrostatic and Hydrophobic Interactions. *J. Am. Chem. Soc.* **2010**, *132*, 1252-1254.

(179) Charlebois, I.; Gravel, C.; Arrad, N.; Boissinot, M.; Bergeron, M. G.; Leclerc, M. Impact of DNA Sequence and Oligonucleotide Length on a Polythiophene-Based Fluorescent DNA Biosensor. *Macromol. Biosci.* **2013**, *13*, 717-722.

(180) Wang, Y.; Zhan, R.; Li, T.; Pu, K.-Y.; Wang, Y.; Tan, Y. C.; Liu, B. Fluorescence and Visual Detection of Single Nucleotide Polymorphism Using Cationic Conjugated Polyelectrolyte. *Langmuir* **2012**, *28*, 889-895.

(181) Wang, C.; Zhan, R.; Pu, K.-Y.; Liu, B. Cationic Polyelectrolyte Amplified Bead Array for DNA Detection with Zeptomole Sensitivity and Single Nucleotide Polymorphism Selectivity. *Adv. Functional Mater.* **2010**, *20*, 2597-2604.

(182) Butler, S. J.; Parker, D. Anion Binding in Water at Lanthanide Centres: From Structure and Selectivity to Signalling and Sensing. *Chem. Soc. Rev.* **2013**, *42*, 1652-1666.

(183) Buehlmann, P.; Aoki, H.; Xiao, K. P.; Anemiya, S.; Tohda, K.; Umezawa, Y. Chemical Sensing with Chemically Modified Electrodes that Mimic Gating at Biomembranes Incorporating Ion-Channel Receptors. *Electroanalysis* **1998**, *10*, 1149-1158.

(184) Su, Q.; Feng, W.; Yang, D.; Li, F. Resonance Energy Transfer in Upconversion Nanoplatforms for Selective Biodetection. *Acc. Chem. Res.* **2017**, *50*, 32-40.

(185) Wang, X.; He, F.; Tang, F.; Li, L. Optically Amplified DNA Detection on Self-Assembled Solid Films Using Conjugated Polyelectrolytes. *J. Mater. Chem.* **2012**, *22*, 15303-15308.

(186) Li, K.; Liu, B. Conjugated Polyelectrolyte Amplified Thiazole Orange Emission for Label Free Sequence Specific DNA Detection with Single Nucleotide Polymorphism Selectivity. *Anal. Chem.* **2009**, *81*, 4099-4105.

(187) Zheng, C.; Niu, L.; Pan, W.; Zhou, J.; Lv, H.; Cheng, J.; Liang, D. Long-Term Kinetics of DNA Interacting with Polycations. *Polym.* **2014**, *55*, 2464-2471.

(188) Feng, X.; Lv, F.; Liu, L.; Yang, Q.; Wang, S.; Bazan, G. C. A Highly Emissive Conjugated Polyelectrolyte Vector for Gene Delivery and Transfection. *Adv. Mater.* **2012**, *24*, 5428-5432.

(189) Weinhold, F.; Klein, R. A. Anti-Electrostatic Hydrogen Bonds. *Angew. Chem. Int. Ed.* **2014**, *126*, 11214-11217.

(190) Fatila, E. M.; Pink, M.; Twum, E. B.; Karty, J. A.; Flood, A. H. Phosphate-Phosphate Oligomerization Drives Higher Order Co-Assemblies with Stacks of Cyanostart Macrocycles. *Chem. Sci.* **2018**, *9*, 2863-2872.

(191) Qiao, B.; Anderson, J. R.; Pink, M.; Flood, A. H. Size-Matched Recognition of Large Anions by Cyanostar Macrocycles is Saved When Solvent-Bias is Avoided. *Chem. Commun.* **2016**, *52*, 8683-8686.

(192) Delisavva, F.; Mountrichas, G.; Pispas, S. Quaternized Poly[3,5-bis(dimethylaminomethylene) hydroxystyrene]/DNA Complexes: Structure Formation as a Function of Solution Ionic Strength. *J. Phys. Chem. B* **2013**, *117*, 7790-7796.

(193) Ghosh, R.; Chatterjee, D. P.; Das, S.; Mukhopadhyay, T. K.; Datta, A.; Nandi, A. K. Influence of Hofmeister I- on Tuning Optoelectronic Properties of Ampholytic Polythiophene by Varying pH and Conjugating with RNA. *Langmuir* **2017**, *33*, 12739-12749.

(194) Ren, P.; Chun, J.; Thomas, D. G.; Schnieders, M. J.; Marucho, M.; Zhang, J.; Baker, N. A. Biomolecular Electrostatics and Solvation: A Computational Perspective. *Quarterly Rev. Biophysics* **2012**, *45*, 427-491.

(195) Kelley, M. P.; Yang, P.; Clark, S. B.; Clark, A. E. Structural and Thermodynamic Properties of the CmIII Ion Solvated by Water and Methanol. *Inorganic Chem.* **2016**, *55*, 4992-4999.

(196) Pruitt, S. R.; Brorsen, K. R.; Gordon, M. S. Ab Initio Investigation of the Aqueous Solvation of the Nitrate Ion. *Phys. Chem. Chem. Phys.* **2015**, *17*, 27027-27034.

(197) Radhakrishnan, M. L. Designing Electrostatic Interactions in Biological Systems via Charge Optimization or Combinatorial Approaches: Insights and Challenges with a Continuum Electrostatic Framework. *Theoretical Chem. Accounts* **2012**, *131 (8)*, 1-24.

(198) Kitahara, A. Nonaqueous Systems. *Surfactant Sci. Series* **1998**, *76*, 135-150.

(199) Creighton, T. E. Stability of Folded Conformations. *Curr. Opinion Structural Biol.* **1991**, *1*, 5-16.

(200) Iyer, M. A.; Oza, G.; Velumani, S.; Maldonado, A.; Romero, J.; Munoz, M. de L.; Sridharan, M.; Asomoza, R.; Yi, J. Scanning Fluorescence-Based Ultrasensitive Detection of Dengue Viral DNA on ZnO Thin Films. *Sensors Actuators B: Chem.* **2014**, *202*, 1338-1348.

(201) Harris, B. C.; Korampally, V.; Weilbaecher, C.; Polo-Parada, L.; Grant, S.; Gangopadhyay, S. Protease Biosensing on Novel High Surface Area Organosilicate Nanoporous Films. *Sensors Actuators B: Chem.* **2013**, *176*, 351-359.

(202) Bhattacherjee, A.; Wategaonkar, S. Nature and Hierarchy of Noncovalent Interactions in Gas-Phase Binary Complexes of Indole and Benzimidazole with Ethers. *J. Phys. Chem. A* **2017**, *121*, 8815-8824.

(203) Warnke, S.; Hoffmann, W.; Seo, J.; De Genst, E.; von Helden, G.; Pagel, K. From Compact to String - The Role of Secondary and Tertiary Structure in Charge-Induced Unzipping of Gas-Phase Proteins. *J. Am. Soc. Mass Spectrom.* **2017**, *28*, 638-646.

(204) Pairas, G. N.; Tsoungas, P. G. H-Bond: The Chemistry-Biology H-Bridge. *ChemistrySelect* **2016**, *1*, 4520-4532.

(205) Ajitha, M. J.; Huang, K.-W. Non-Classical C-H···X Hydrogen Bonding and Its Role in Asymmetric Organocatalysis. *Synthesis* **2016**, *48*, 3449-3458.

(206) Garzon-Tovar, L.; Duarte-Ruiz, A.; Wurst, K. Non-Classical Hydrogen Bond (C-H···I) Directed Self-Assembly Formation of a Novel 1D Supramolecular Polymer, Based on a Copper Complex [Cu{(CH3) 2SO}6]I4. *Inorganic Chem. Commun.* **2013**, *32*, 64-67.

(207) Hascall, T.; Baik, M.-H.; Bridgewater, B. M.; Shin, J. H.; Churchill, D. G.; Friesner, R. A.; Parkin, G. A Non-Classical Hydrogen Bond in the Molybdenum Arene Complex [η6-C6H5C6H3(Ph)OH]

Mo(PMe3)3: Evidence that Hydrogen Bonding Facilitates Oxidative Addition of the O-H Bond. *Chem. Commun.* **2002**, 2644-2645.

(208) Yokoyama, T.; Mido, T.; Takahara, G.; Ogata, K.; Chwojnowska, E.; Yonezawa, N.; Okamoto, A. Crystal Structure of 1-Benzoyl-2,7-dimethoxy-8-(3,5-dimethylbenzoyl) Naphthalene: Head-to-Head Fashioned Molecular Motif for Accumulating Weak Non-Classical Hydrogen Bonds. *Eur. J. Org. Chem.* **2017**, *8*, 188-194.

(209) Zou, W.; Zhang, X.; Dai, H.; Yan, H.; Cremer, D.; Kraka, E. Description of an Unusual Hydrogen Bond Between Carborane and a Phenyl Group. *J. Organometallic Chem.* **2018**, *865*, 114-127.

(210) Li, H.; Han, J.; Zhao, H.; Liu, X.; Ma, L.; Sun, C.; Yin, H.; Shi, Y. Investigation of the Intermolecular Hydrogen Bonding Effects on the Intermolecular Charge Tranfer Process of Coumarin 340 in Tetrahydrofuran Solvent. *J. Cluster Sci.* **2018**, *29*, 585-592.

(211) Chauhan, P.; Mahajan, S.; Kaya, U.; Hack, D.; Enders, D. Bifunctional Amine-Squaramides: Powerful Hydrogen-Bonding Organocatalysts for Asymmetric Domino/Cascade Reactions. *Adv. Synth. Catal.* **2015**, *357*, 253-281.

(212) Yamanaka, M. Urea Derivatives as Low-Molecular-Weight Gelators. *J. Inclusion Phenom. Macrocyclic Chem.* **2013**, *77*, 33-48.

(213) Limnios, D.; Kokotos, C. G. Ureas and Thioureas as Asymmetric Organocatalysts. *RSC Green Chem. Series* **2016**, *41*, 196-255.

(214) Ma, L.; Zhou, C.; Yang, Q.; Yang, X.; Zhang, C.; Liao, L. Polymeric Supramolecular Materials and Their Biomedical Applications. *Curr. Org. Chem.* **2014**, *18*, 1937-1947.

(215) Han, Y.; Jiang, Y.; Chen, C.-F. Cryptand-Based Hosts for Organic Guests. *Tetrahedron* **2015**, *71*, 503-522.

(216) Shimizu, L. S.; Salpage, S. R.; Korous, A. A. Functional Materials from Self-Assembled Bis-Urea Macrocycles. *Acc. Chem. Res.* **2014**, *47*, 2116-2127.

(217) Gibb, C. L. D.; Stevens, E. D.; Gibb, B. C. The Self-Assembly of Benzyl Alcohol Derived Deep-Cavity Cavitands: A New, Highly Efficient Moiety for Irreversible Assemblies? *Chem. Commun.* **2000**, 363-364.

(218) Gibb, C. L. D.; Gibb, B. C. Straight-Chain Alkanes Template the Assembly of Water-Soluble Nano-Capsules. *Chem. Commun.* **2007**, 1635-1637.

(219) Tang, H.; Santos de Oliveira, C.; Sonntag, G.; Gibb, C. L. D.; Gibb, B. C.; Bohne, C. Dynamics of a Supramolecular Capsule Assembly with Pyrene. *J. Am. Chem. Soc.* **2012**, *134*, 5544-5547.

(220) Gan, H.; Gibb, B. C. ITC Analysis of Guest Binding to a Deep-Cavity Cavitand. *Supramol. Chem.* **2010**, *22*, 808-814.

(221) Gibb, C. L. D.; Stevens, E. D.; Gibb, B. C. C-H···X-R (X = Cl, Br, and I) Hydrogen Bonds Drive the Complexation Properties of a Nanoscale Molecular Basket. *J. Am. Chem. Soc.* **2011**, *123*, 5849-5850.

(222) Murray, T. J.; Zimmerman, S. C. New Triply Hydrogen Bonded Complexes with Highly Variable Stabilities. *J. Am. Chem. Soc.* **1992**, *114*, 4010-4011.

(223) Kuykendall, D. W.; Anderson, C. A.; Zimmerman, S. C. Hydrogen-Bonded DeUG·DAN Heterocomplex: Structure and Stability and a Scalable Synthesis of DeUG with Reactive Functionality. *Org. Lett.* **2009**, *11*, 61-64.

(224) Zimmerman, S. C.; Mrksich, M.; Baloga, M. Highly Efficient Complexation of a π-Acceptor by a Molecular Tweezer Containing Two π-Donors: The Role of Preorganization. *J. Am. Chem. Soc.* **1989**, *111*, 8528-8530.

(225) Quinn, J. R.; Zimmerman, S. C. Structure-Function Studies on a Synthetic Guanosine Receptor That Simultaneously Binds Watson-Crick and Hoogsteen Sites. *J. Org. Chem.* **2005**, *70*, 7459-7467.

(226) Park, T.; Todd, E. M.; Nakashima, S.; Zimmerman, S. C. A Quadruply Hydrogen Bonded Hetero-Complex Displaying High-Fidelity Recognition. *J. Am. Chem. Soc.* **2005**, *127*, 18133-18142.

(227) Zimmerman, S. C.; Wu, W.; Zeng, Z. Complexation of Nucleotide Bases by Molecular Tweezers with Active Site Carboxylic Acids: Effects of Microenvironment. *J. Am. Chem. Soc.* **1991**, *113*, 196-201.

(228) Muñoz, E. M.; de la Paz, M. L.; Jiménez-Barbero, J.; Ellis, G.; Pérez, M.; Vicent, C. The Relevance of Carbohydrate Hydrogen-Bonding Cooperativity Effects: A Cooperative 1,2-*trans*-Diaxial Diol and Amido Alcohol Hydrogen-Bonding Array as an Effective Carbohydrate-Phosphate Binding Motif in Nonpolar Media. *Chem. Eur. J.* **2002**, *8*, 1908-1914.

(229) Leung, M.-k.; Mandal, A. B.; Wang, C.-C.; Lee, G.-H.; Peng, S.-M.; Cheng, H.-L.; Her, G.-R.; Chao, I.; Lu, H.-F.; Sun, Y.-C.; Shiao, M.-Y.; Chou, P.-T. Self-Complementarity of Oligo-2-Aminopyridines: A New Class of Hydrogen-Bonded Ladders. *J. Am. Chem. Soc.* **2002**, *124*, 4287-4297.

(230) Ross, P. D.; Subramanian, S. Thermodynamics of Protein Association Reactions: Forces Contributing to Stability. *Biochemistry* **1981**, *20*, 3096-3102.

(231) van der Spoel, D.; van Maaren, P. J.; Larsson, P.; Tîmneanu, N. Thermodynamics of Hydrogen Bonding in Hydrophilic and Hydrophobic Media. *J. Phys. Chem. B* **2006**, *110*, 4393-4398.

(232) Ivasenko, O.; Perepichka, D. F. Mastering Fundamentals of Supramolecular Design with Carboxylic Acids. Common Lessons from X-Ray Crystallography and Scanning Tunneling Microscopy. *Chem. Soc. Rev.* **2011**, *40*, 191-206.

(233) Butcher, S. E.; Pyle, A. M. The Molecular Interactions That Stabilize RNA Tertiary Structure: RNA Motifs, Patterns, and Networks. *Acc. Chem. Res.* **2011**, *44*, 1302-1311.

(234) Langan, P.; Chen, J. C.-H. Seeing the Chemistry in Biology with Neutron Crystallography. *Phys. Chem. Chem. Phys.* **2013**, *15*, 13705-13712.

(235) Inokuma, Y.; Fujita, M. Visualization of Solution Chemistry by X-Ray Crystallography Using Porous Coordination Networks. *Bull. Chem. Soc. Japan* **2014**, *87*, 1161-1176.

(236) Meisburger, S. P.; Thomas, W. C.; Watkins, M. B.; Ando, N. X-ray Scattering Studies of Protein Structural Dynamics. *Chem. Rev.* **2017**, *117*, 7615-7672.

(237) Charisiadis, P.; Kontogianni, V. G.; Tsiafoulis, C. G.; Tzakos, A. G.; Siskos, M.; Gerothanassis, I. P. 1H-NMR as a Structural and Analytical Tool of Intra- and Inter-Molecular Hydrogen Bonds of Phenol-Containing Natural Products and Model Compounds. *Molecules* **2014**, *19*, 13643-13682.

(238) Kottke, T.; Lorenz-Fonfria, V. A.; Heberle, J. The Grateful Infrared: Sequential Protein Structural Changes Resolved by Infrared Difference Spectroscopy. *J. Phys. Chem. B* **2017**, *121*, 335-350.

(239) El Khoury, Y.; Hellwig, P. Far Infrared Spectroscopy of Hydrogen Bonding Collective Motions in Complex Molecular Systems. *Chem. Commun.* **2017**, *53*, 8389-8399.

(240) Sunner, J.; Nishizawa, K.; Kebarle, P. Ion-Solvent Molecule Interactions in the Gas Phase. The Potassium Ion and Benzene. *J. Phys. Chem.* **1981**, *85*, 1814-1820.

(241) Shepodd, T. J.; Petti, M. A.; Dougherty, D. A. Tight, Oriented Binding of Aliphatic Guest by a New Class of Water-Soluble Molecules with Hydrophobic Binding Sites. *J. Am. Chem. Soc.* **1986**, *108*, 6085-6087.

(242) Dougherty, D. A. The Cation-π Interaction. *Acc. Chem. Res.* **2013**, *46*, 885-893.

(243) Daze, K. D.; Hof, F. The Cation-π Interaction at Protein-Protein Interaction Interfaces: Developing and Learning from Synthetic Mimics of Proteins That Bind Methylated Lysines. *Acc. Chem. Res.* **2013**, *46*, 937-945.

(244) Schneider, H.-J. Interactions in Supramolecular Complexes Involving Arenes: Experimental Studies. *Acc. Chem. Res.* **2013**, *46*, 1010-1019.

(245) Sherrill, C. D. Energy Component Analysis of π Interactions. *Acc. Chem. Res.* **2013**, *46*, 1020-1028.

(246) Yang, D.; Wang, Y.; Liu, D.; Li, Z.; Li, H. Luminescence Modulation via Cation-π Interaction in a Lanthanide Assembly: Implications for Potassium Detection. *J. Mater. Chem. C* **2018,** *6*, 1944-1950.

(247) Lin, Q.; Mao, P.-P.; Fan, Y.-Q.; Liu, L.; Liu, J.; Zhang, Y.-M.; Yao, H.; Wei, T.-B. A Novel Supramolecular Polymer Gel Based on Naphthalimide Functionalized-Pillar[5]arene for the Fluorescence Detection of Hg2+ and I- and Recyclable Removal of Hg2+ via Cation-π Interactions. *Soft Matter* **2017**, *13*, 7085-7089.

(248) Ahn, J.; Lim, N. Y.; Choi, Y.; Choi, M. Y.; Jung, J. H. Highly Selective Chromogenic Probe for Cesium Ions Prepared from an Electrospun Film of Self-Assembled Benzenetricarboxyamide Nanofibers. *Sensors Actuators B: Chem.* **2018**, *255*, 325-331.

(249) Kumar, J.; Bhattacharyya, P. K.; Das, D. K. New Dual Fluorescent "On-Off" and Colorimetric Sensor for Copper(II): Copper(II) Binds Through N Coordination and pi Cation Interaction to Sensor. *Spectrochim. Acta A* **2015**, *138*, 99-104.

(250) Maner, J. A.; Mauney, D. T.; Duncan, M. A. Imaging Charge Transfer in a Cation-π System: Velocity-Map Imaging of Ag+(benzene) Photodissociation. *J. Phys. Chem. Lett.* **2015**, *6*, 4493-4498.

(251) Rodriguez-Sanz, A. A.; Cabaleiro-Lago, E. M.; Rodriguez-Otero, J. On the Interaction Between the Imidazolium Cation and Aromatic Amino Acids. A Computational Study. *Org. Biomol. Chem.* **2015**, *13*, 7961-7972.

(252) Yamada, S.; Yamamoto, N.; Takamori, E. A Molecular Seesaw Balance: Evaluation of Solvent and Counteranion Effects on Pyridinium-π Interactions. *Org. Lett.* **2015**, *17*, 4862-4865.

(253) Arias, S.; Bergueiro, J.; Freire, F.; Quinoa, E.; Riguera, R. Chiral Nanostructures from Helical Copolymer-Metal Complexes: Tunable Cation-π Interactions and Sergeants and Soldiers Effect. *Small* **2016**, *12*, 238-244.

(254) Ito, R.; Nakada, C.; Hoshino, T. β-Amyrin Synthase from Euphorbia tirucalli L. Functional Analyses of the Highly Conserved Aromatic Residues Phe413, Tyr259 and Trp257 Disclose the Importance of the Appropriate Steric Bulk, and Cation-π and CH-π Interactions for the Efficient Catalytic Action of the Polyolefin Cyclization Cascade. *Org. Biomol. Chem.* **2017**, *15*, 177-188.

(255) Neel, A. J.; Hilton, M. J.; Sigman, M. S.; Toste, F. D. Exploiting Non-Covalent π Interactions for Catalyst Design. *Nature* **2017**, *543*, 637-646.

(256) Halder, R.; Manna, R. N.; Chakraborty, S.; Jana, B. Modulation of the Conformational Dynamics of Apo-Adenylate Kinase through a π-Cation Interaction. *J. Phys. Chem. B* **2017**, *121*, 5699-5708.

(257) Stefancic, A.; Klupp, G.; Knaflic, T.; Yufit, D. S.; Tavcar, G.; Potocnik, A.; Beeby, A.; Arcon, D. Triphenylide-Based Molecular Solid - A New Candidate for a Quantum Spin-Liquid Compound. *J. Phys. Chem. C* **2017**, *121*, 14864-14871.

(258) Zhong, J.; Li, Z.; Guan, W.; Lu, C. Cation-π Interaction Triggered-Fluorescence of Clay Fillers in Polymer Composites for Quantification of Three-Dimensional Macrodispersion. *Anal. Chem.* **2017**, *89*, 12472-12479.

(259) Shen, J.; Ren, C.; Zeng, H. Tuning Cation-Binding Selectivity and Capacity via Side Chain-Dependent Molecular Packing in the Solid State. *Chem. Commun.* **2016**, *52*, 10361-10364.

(260) Shailaja, J.; Lakshminarasimhan, P. H.; Pradhan, A. R.; Sunoj, R. B.; Jockusch, S.; Karthikeyan, S.; Uppili, S.; Chandrasekhar, J.; Turro, N. J.; Ramamurthy, V. Alkali Ion-Controlled Excited-State Ordering of Acetophenones Included in Zeolites: Emission, Solid-State NMR, and Computational Studies. *J. Phys. Chem. A* **2003**, *107*, 3187-3198.

(261) Breugst, M.; von der Heiden, D.; Schmauck, J. Novel Noncovalent Interactions in Catalysis: A Focus on Halogen, Chalcogen, and Anion-π Bonding. *Synthesis* **2017**, *49*, 3224-3236.

(262) Giese, M.; Albrecht, M.; Rissanen, K. Anion-π Interactions with Fluoroarenes. *Chem. Rev.* **2015**, *115*, 8867-8895.

(263) Quinonero, D.; Garau, C.; Frontera, A.; Ballester, P.; Costa, A.; Deya, P. M. Counterintuitive Interaction of Anions with Benzene Derivatives. *Chem. Phys. Lett.* **2002**, *359*, 486-492.

(264) Kozuch, S. Should "Anion-π Interactions" Be Called "Anion-σ Interactions"? A Revision of the Origin of Some Hole-Bonds and Their Nomenclature. *Phys. Chem. Chem. Phys.* **2016**, *18*, 30366-30369.

(265) Quinonero, D.; Garau, C.; Rotger, C.; Frontera, A.; Ballester, P.; Costa, A.; Deya, P. M. Anion-π Interactions: Do They Exist? *Angew. Chem. Int. Ed.* **2002**, *114*, 3539-3542.

(266) Demeshko, S.; Dechert, S.; Meyer, F. Anion-π Interactions in a Carousel Copper(II)-Triazine Complex. *J. Am. Chem. Soc.* **2004**, *126*, 4508-4509.

(267) Berryman, O. B.; Hof, F.; Hynes, M. J.; Johnson, D. W. Anion-π Interaction Augments Halide Binding in Solution. *Chem. Commun.* **2006**, 506-508.

(268) Bagheri, S.; Masoodi, H. R. Theoretical Study of the Influence of Cation-π and Anion-π Interactions on Some NMR Data of Borazine Complexes. *Chem. Phys. Lett.* **2015**, *629*, 46-52.

(269) Zhang, D.; Chatelet, B.; Serrano, E.; Perraud, O.; Dutasta, J.-P.; Robert, V.; Martinez, A. Insights into the Complexity of Weak Intermolecular Interactions Interfering in Host-Guest Systems. *ChemPhysChem* **2015**, *16*, 2931-2935.

(270) Collings, J. C.; Roscoe, K. P.; Robins, E. G.; Batsanov, A. S.; Stimson, L. M.; Howard, J. A. K.; Clark, S. J.; Marder, T. B. Arene-Perfluoroarene Interactions in Crystal Engineering. 8: Structures of 1:1 Complexes of Hexafluorobenzene with Fused-Ring Polyaromatic Hydrocarbons. *New J. Chem.* **2002**, *26*, 1740-1746.

(271) Tsuzuki, S.; Uchimaru, T.; Mikami, M. Intermolecular Interaction between Hexafluorobenzene and Benzene: Ab Initio Calculations Including CCSD(T) Level Electron Correlation Correction. *J. Phys. Chem. A* **2006**, *110*, 2027-2033.

(272) Berryman, O. B.; Bryantsev, V. S.; Stay, D. P.; Johnson, D. W.; Hay, B. P. Structural Criteria for the Design of Anion Receptors: The Interaction of Halides with Electron-Deficient Arenes. *J. Am. Chem. Soc.* **2007**, *129*, 48-58.

(273) Albrecht, M.; Wessel, C.; de Groot, M.; Rissanen, K.; Lüchow, A. Structural Versatility of Anion-π Interactions in Halide Salts with Pentafluorophenyl Substituted Cations. *J. Am. Chem. Soc.* **2008**, *130*, 4600-4601.

(274) Dhillon, A.; Nair, M.; Kumar, D. Analytical Methods for Determination and Sensing of Fluoride in Biotic and Abiotic Sources: A Review. *Anal. Methods* **2016**, *8*, 5338-5352.

(275) Lasagna, M.; De Luca, D. A. The Use of Multilevel Sampling Techniques for Determining Shallow Aquifer Nitrate Profiles. *Environ. Sci. Pollution Res.* **2016**, *23*, 20431-20448.

(276) Zapata, F.; Lopez-Lopez, M.; Garcia-Ruiz, C. Detection and Identification of Explosives by Surface Enhanced Raman Scattering. *Appl. Spectroscopy Rev.* **2016**, *51*, 227-262.

(277) Beer, P. D.; Gale, P. A. Anion Recognition and Sensing: The State of the Art and Future Perspectives. *Angew. Chem. Int. Ed.* **2001**, *40*, 486-516.

(278) Bieske, E. J. Spectroscopic Studies of Anion Complexes and Clusters: A Microscopic Approach to Understanding Anion Solvation. *Chem. Soc. Rev.* **2003**, *32*, 231-237.

(279) Custelcean, R.; Moyer, B. A. Anion Separation with Metal-Organic Frameworks. *Eur. J. Inorganic Chem.* **2007**, *2007*, 1321-1340.

(280) Shchegolev, B. F.; McKee, M. L.; Zhuravlev, A. V.; Savvateeva-Popova, E. V. Analysis of Intermolecular Interaction Energy Inputs in Benzene-Imidazole and Imidazole-Imidazole Systems in Parallel Displaced and T-Configuration. *Biophysics* **2013**, *58*, 355-360.

(281) Garcia, A. M.; Determan, J. J.; Janesko, B. G. Tunable Fictitious Substituent Effects on the π-π Interactions of Substituted Sandwich Benzene Dimers. *J. Phys. Chem. A* **2014**, *118*, 3344-3350.

(282) Zhou, P.-P.; Yang, X.; Zhou, D.-G.; Liu, S. T-Shaped Phenol-Benzene Complexation Driven by π-Involved Noncovalent Interactions. *Theoretical Chem. Acc*. **2016**, *135 (4)*, 1-11.

(283) Gao, X.-C.; Hao, Q.; Wang, C.-S. Improved Polarizable Dipole-Dipole Interaction Model for Hydrogen Bonding, Stacking, T-Shaped, and X-H···π Interactions. *J. Chem. Theory Computation* **2017**, *13*, 2730-2741.

(284) Kumar Tummanapelli, A.; Vasudevan, S. Communication: Benzene Dimer - The Free Energy Landscape. *J. Chem. Phys*. **2013**, *139*, 201102/1-201102/4.

(285) Chipot, C.; Jaffe, R.; Maigret, B.; Pearlman, D. A.; Kollman, P. A. Benzene Dimer: A Good Model for π-π Interactions in Proteins? A Comparison between the Benzene and the Toluene Dimers in the Gas Phase and in an Aqueous Solution. *J. Am. Chem. Soc.* **1996**, *118*, 11217-11224.

(286) Williams, J. H. Modeling the Vibrational Dynamics of Solid Benzene: Hexafluorobenzene. The Anatomy of a Phase Transition. *Chem. Phys.* **1993**, *172*, 171-186.

(287) Patrick, C. R.; Prosser, G. S. A Molecular Complex of Benzene and Hexafluorobenzene. *Nature* **1960,** *187***,** 1021.

(288) Mackie, I. D.; DiLabio, G. A. Interactions in Large, Polyaromatic Hydrocarbon Dimers: Application of Density Functional Theory with Dispersion Corrections. *J. Phys. Chem. A* **2008**, *112*, 10968-10976.

(289) Antony, J.; Alameddine, B.; Jenny, T. A.; Grimme, S. Theoretical Study of the Stacking Behavior of Selected Polycondensed Aromatic Hydrocarbons with Various Symmetries. *J. Phys. Chem. A* **2013**, *117*, 616-625.

(290) Wheeler, S. E. Understanding Substituent Effects in Noncovalent Interactions Involving Aromatic Rings. *Acc. Chem. Res.* **2013**, *46*, 1029-1038.

(291) Li, C.; Shi, G. Polythiophene-Based Optical Sensors for Small Molecules. *ACS Appl. Mater. Interfaces* **2013**, *5*, 4503-4510.

(292) Barnes, J. C.; Juricek, M.; Strutt, N. L.; Frasconi, M.; Sampath, S.; Giesener, M. A.; McGrier, P. L.; Bruns, C. J.; Stern, C. L.; Sarjeant, A. A.; Stoddart, J. F. ExBox: A Polycyclic Aromatic Hydrocarbon Scavenger. *J. Am. Chem. Soc.* **2013**, *135*, 183-192.

(293) Hayakawa, K. Environmental Behaviors and Toxicities of Polycyclic Aromatic Hydrocarbons and Nitropolycyclic Aromatic Hydrocarbons. *Chem. Pharmaceutical Bull.* **2016**, *64*, 83-94.

(294) Verma, R.; Vinoda, K. S.; Papireddy, M.; Gowda, A. N. S. Toxic Pollutants from Plastic Waste- A Review. *Procedia Environ. Sci.* **2016**, *35*, 701-708.

(295) Minguez-Alarcon, L.; Hauser, R.; Gaskins, A. J. Effects of Bisphenol A on Male and Couple Reproductive Health: A Review. *Fertility and Sterility* **2016**, *106*, 864-870.

(296) Jaacks, L. M.; Staimez, L. R. Association of Persistent Organic Pollutants and Non-Persistent Pesticides with Diabetes and Diabetes-Related Health Outcomes in Asia: A Systematic Review. *Environ. Int.* **2015**, *76*, 57-70.

(297) Tamgho, I.-S.; Chaudhuri, S.; Verderame, M.; DiScenza, D. J.; Levine, M. A Highly Versatile Fluorenone-Based Macrocycle for the Sensitive Detection of Polycyclic Aromatic Hydrocarbons and Fluoride Anions. *RSC Adv.* **2017**, *7*, 28489-28493.

(298) Radaram, B.; Potvin, J.; Levine, M. Highly Efficient Non-Covalent Energy Transfer in All-Organic Macrocycles. *Chem. Commun.* **2013**, *49*, 8259-8261.

(299) Radaram, B.; Levine, M. Rationally Designed Supramolecular Organic Hosts for Benzo[a]pyrene Binding and Detection. *Eur. J. Org. Chem.* **2015**, *2015*, 6194-6204.

(300) Tepper, R.; Schubert, U. S. Halogen Bonding in Solution: Anion Recognition, Templated Self-Assembly, and Organocatalysis. *Angew. Chem. Int. Ed.* **2018**, *57*, 6004-6016.

(301) Cavallo, G.; Metrangolo, P.; Milani, R.; Pilati, T.; Priimagi, A.; Resnati, G.; Terraneo, G. The Halogen Bond. *Chem. Rev.* **2016**, *116*, 2478-2601.

(302) Montana, A. M. The σ and π Holes. The Halogen and Tetrel Bondings: Their Nature, Importance and Chemical, Biological and Medicinal Implications. *ChemistrySelect* **2017**, *2*, 9094-9112.

(303) Eskandari, K.; Zariny, H. Halogen Bonding: A Lump-Hole Interaction. *Chem. Phys. Lett.* **2010**, *492*, 9-13.

(304) Wolters, L. P.; Schyman, P.; Pavan, M. J.; Jorgensen, W. L.; Bickelhaupt, F. M.; Kozuch, S. The Many Faces of Halogen Bonding: A Review of Theoretical Models and Methods. *Wiley Interdisciplinary Rev: Computational Molecular Sci.* **2014**, *4*, 523-540.

(305) Dumele, O.; Trapp, N.; Diederich, F. Halogen Bonding Molecular Capsules. *Angew. Chem. Int. Ed.* **2015**, *54*, 12339-12344.

(306) Gropp, C.; Quigley, B. L.; Diederich, F. Molecular Recognition with Resorcin[4]arene Cavitands: Switching, Halogen-Bonded Capsules, and Enantioselective Complexation. *J. Am. Chem. Soc.* **2018**, *140*, 2705-2717.

(307) Abdelbar, M. F.; El-Sheshtawy, H. S.; Shoeir, K. R.; El-Mehasseb, I.; Ebeid, E.-Z. M.; El-Kemary, M. Halogen Bond Triggered Aggregation Induced Emission in an Iodinated Cyanine Dye for Ultra Sensitive Detection of Ag Nanoparticles in Tap Water and Agricultural Wastewater. *RSC Adv.* **2018**, *8*, 24617-24626.

(308) Lim, J. Y. C.; Marques, I.; Felix, V.; Beer, P. D. A Chiral Halogen-Bonding [3]Rotaxane for the Recognition and Sensing of Biologically Relevant Dicarboxylate Anions. *Angew. Chem. Int. Ed.* **2018**, *57*, 584-588.

(309) Danelius, E.; Andersson, H.; Jarvoll, P.; Lood, K.; Graefenstein, J.; Erdelyi, M. Halogen Bonding: A Powerful Tool for Modulation of Peptide Conformation. *Biochem.* **2017**, *56*, 3265-3272.

(310) Engel, T. *Quantum Chemistry & Spectroscopy,* 2nd Ed.; Pearson Education, Inc.: New York, 2010; pp 295-320.

(311) Lakowicz, J. R. *Principles of Fluorescence Spectroscopy*, 3rd Ed.; Springer: New York, 2006.

(312) Zhang, K.; Dou, W.; Tang, X.; Yang, L.; Ju, Z.; Cui, Y.; Liu, W. Selective and Sensitive Time-Gated Luminescence Detection of Hydrogen Sulfide. *Tetrahedron Lett.* **2015**, *56*, 2707-2709.

(313) Weitz, E. A.; Chang, J. Y.; Rosenfield, A. H.; Pierre, V. C. A Selective Luminescent Probe for the Direct Time-Gated Detection of Adenosine Triphosphate. *J. Am. Chem. Soc.* **2012**, *134*, 16099-16102.

(314) Weitz, E. A.; Pierre, V. C. A Ratiometric Probe for the Selective Time-Gated Luminescence Detection of Potassium in Water. *Chem. Commun.* **2011**, *47*, 541-543.

(315) Jiang, L.; Tang, K.; Ding, X.; Wang, Q.; Zhou, Z.; Xiao, R. Arginine-Responsive Terbium Luminescent Hybrid Sensors Triggered by Two Crown Ether Carboxylic Acids. *Mater. Sci. Eng., C* **2013**, *33*, 5090-5094.

(316) Sinn, S.; Biedermann, F.; Vishe, M.; Aliprandi, A.; Besnard, C.; Lacour, J.; De Cola, L. A Ratiometric Luminescent Switch Based on Platinum Complexes Tethered to a Crown-Ether Scaffold. *Chem. Phys. Chem.* **2016**, *17*, 1829-1834.

(317) Hestand, N. J.; Spano, F. C. Molecular Aggregate Photophysics beyond the Kasha Model: Novel Design Principles for Organic Materials. *Acc. Chem. Res.* **2017**, *50*, 341-350.

(318) Patlolla, P. R.; Das Mahapatra, A.; Mallajosyula, S. S.; Datta, B. Template-Free H-Dimer and H-Aggregate Formation by Dimeric Carbocyanine Dyes. *New J. Chem.* **2018**, *42*, 6727-6734.

(319) Wuerthner, F.; Kaiser, T. E.; Saha-Moeller, C. R. J-Aggregates: From Serendipitous Discovery to Supramolecular Engineering of Functional Dye Materials. *Angew. Chem. Int. Ed.* **2011**, *50*, 3376-3410.

(320) Artyukhov, V. Y.; Mayer, G. V. Theoretical Study of the Effect of Orientation and Solvent on Energy Transfer in Bichromophore Systems. *Optics Spectroscopy* **2001**, *90*, 664-668.

(321) Khrenova, M.; Topol, I.; Collins, J.; Nemukhin, A. Estimating Orientation Factors in the FRET Theory of Fluorescent Proteins: the TagRFP-KFP Pair and Beyond. *Biophys. J.* **2015**, *108*, 126-132.

(322) Yang, H. The Orientation Factor in Single-Molecule Forster-Type Resonance Energy Transfer, with Examples for Conformational Transitions in Proteins. *Israel J. Chem.* **2009**, *49*, 313-321.

(323) Hummer, G.; Szabo, A. Dynamics of the Orientational Factor in Fluorescence Resonance Energy Transfer. *J. Phys. Chem. B* **2017**, *121*, 3331-3339.

(324) Loura, L. M. S. Simple Estimation of Forster Resonance Energy Transfer (FRET) Orientation Factor Distribution in Membranes. *Int. J. Molec. Sci.* **2012**, *13*, 15252-15270.

(325) Kobayashi, A.; Watanabe, S.; Yoshida, M.; Kato, M. Importance of the Molecular Orientation of an Iridium(III)-Heteroleptic Photosensitizer Immobilized on TiO2 Nanoparticles. *ACS Appl. Energy Mater.* **2018**, *1*, 2882-2890.

(326) Wang, D.; Ivanov, M. V.; Kokkin, D.; Loman, J.; Cai, J.-Z.; Reid, S. A.; Rathore, R. The Role of Torsional Dynamics on Hole and Exciton Stabilization in π-Stacked Assemblies: Design of Rigid Torsionomers of a Cofacial Bifluorene. *Angew. Chem. Int. Ed.* **2018**, *57*, 8189-8193.

(327) Kulkarni, R. U.; Yin, H.; Pourmandi, N.; James, F.; Adil, M. M.; Schaffer, D. V.; Wang, Y.; Miller, E. W. A Rationally Designed, General Strategy for Membrane Orientation of Photoinduced Electron Transfer-Based Voltage-Sensitive Dyes. *ACS Chem. Biol.* **2017**, *12*, 407-413.

(328) Frances-Monerris, A.; Segarra-Marti, J.; Merchan, M.; Roca-Sanjuan, D. Theoretical Study on the Excited-State π-Stacking Versus Intermolecular Hydrogen-Transfer Processes in the Guanine-Cytosine /Cytosine Trimer. *Theoretical Chem. Accounts* **2016**, *135*, 1-15.

(329) Toyoda, T.; Yindeesuk, W.; Kamiyama, K.; Katayama, K.; Kobayashi, H.; Hayase, S.; Shen, Q. The Electronic Structure and Photoinduced Electron Transfer Rate of CdSe Quantum Dots on Single Crystal

Rutile TiO2: Dependence on the Crystal Orientation of the Substrate. *J. Phys. Chem. C* **2016**, *120*, 2047-2057.

(330) Xie, L.-Q.; Ding, D.; Zhang, M.; Chen, S.; Qiu, Z.; Yan, J.-W.; Yang, Z.-L.; Chen, M.-S.; Mao, B.-W.; Tian, Z.-Q. Adsorption of Dye Molecules on Single Crystalline Semiconductor Surfaces: An Electrochemical Shell-Isolated Nanoparticle Enhanced Raman Spectroscopy Study. *J. Phys. Chem. C* **2016**, *120*, 22500-22507.

(331) Johansson, L. B.-A.; Bergstroem, F.; Edman, P.; Grechishnikova, I. V.; Molotkovsky, J. G. Electronic-Energy Migration and Molecular Rotation Within Bichromophoric Macromolecules. Part 1. Test of a Model Using Bis(9-anthrylmethylphosphonate) Bisteroid. *J. Chem. Soc. Faraday Trans.* **1996**, *92*, 1563-1567.

(332) Harriman, A.; Mallon, L. J.; Goeb, S.; Ulrich, G.; Ziessel, R. Electronic Energy Transfer to the S2 Level of the Acceptor in Functionalized Boron Dipyrromethene Dyes. *Chem. Eur. J.* **2009**, *15*, 4553-4564.

(333) Kitoh-Nishioka, H.; Yokogawa, D.; Irle, S. Förster Resonance Energy Transfer between Fluorescent Proteins: Efficient Transition Charge-Based Study. *J. Phys. Chem. C* **2017**, *121*, 4220-4238.

(334) Ma, J.; Cao, J. Forster Resonance Energy Transfer, Absorption and Emission Spectra in Multichromophoric Systems. I. Full Cumulant Expansions and System-Bath Entanglement. *J. Chem. Phys.* **2015**, *142*, 094106/1-094106/13.

(335) Misra, V.; Mishra, H. Effect of Polymer Microenvironment on Excitation Energy Migration and Transfer. *J. Phys. Chem. B* **2008**, *112*, 4213-4222.

(336) Allan, G.; Delerue, C. Energy Transfer Between Semiconductor Nanocrystals: Validity of Forster's Theory. *Phys. Rev. B* **2007**, *75*, 195311/1-195311/8.

(337) Scholes, G. D. Long-Range Resonance Energy Transfer in Molecular Systems. *Ann. Rev. Phys. Chem.* **2003**, *54*, 57-87.

(338) Kodaimati, M. S.; Wang, C.; Chapman, C.; Schatz, G. C.; Weiss, E. A. Distance-Dependence of Interparticle Energy Transfer in the Near-Infrared Within Electrostatic Assemblies of PbS Quantum Dots. *ACS Nano* **2017**, *11*, 5041-5050.

(339) Wei, W.; Xu, C.; Ren, J.; Xu, B.; Qu, X. Sensing Metal Ions with Ion Selectivity of a Crown Ether and Fluorescence Resonance Energy Transfer between Carbon Dots and Graphene. *Chem. Commun.* **2012**, *48*, 1284-1286.

(340) Didraga, C.; Malyshev, V. A.; Knoester, J. Excitation Energy Transfer between Closely Spaced Multichromophoric Systems: Effects of Band Mixing and Intraband Relaxation. *J. Phys. Chem. B* **2006**, *110*, 18818-18827.

(341) Zheng, J.; Swager, T. M. Biotinylated Poly(p-phenylene Ethynylene): Unexpected Energy Transfer Results in the Detection of Biological Analytes. *Chem. Commun.* **2004**, 2798-2799.

(342) Chen, S.; Yu, Y.-L.; Wang, J.-H. Inner Filter Effect-Based Fluorescent Sensing Systems: A Review. *Anal. Chim. Acta* **2018**, *999*, 13-26.

(343) Zu, F.; Yan, F.; Bai, Z.; Xu, J.; Wang, Y.; Huang, Y.; Zhou, X. The Quenching of the Fluorescence of Carbon Dots: A Review on Mechanisms and Applications. *Microchim. Acta* **2017**, *184*, 1899-1914.

(344) Tang, D.; Zhang, J.; Zhou, R.; Xie, Y.-N.; Hou, X.; Xu, K.; Wu, P. Phosphorescent Inner Filter Effect-Based Sensing of Xanthine Oxidase and its Inhibitors with Mn-Doped ZnS Quantum Dots. *Nanoscale* **2018**, *10*, 8477-8482.

(345) Shanmugaraj, K.; John, S. A. Inner Filter Effect Based Selective Detection of Picric Acid in Aqueous Solution using Green Luminescent Copper Nanoclusters. *New. J. Chem.* **2018**, *42*, 7223-7229.

(346) Sun, X.; Wang, Y.; Lei, Y. Fluorescence Based Explosive Detection: From Mechanisms to Sensory Materials. *Chem. Soc. Rev.* **2015**, *44*, 8019-8061.

(347) Brennaman, M. K.; Fleming, C. N.; Slate, C. A.; Serron, S. A.; Bettis, S. E.; Erickson, B. W.; Papanikolas, J. M.; Meyer, T. J. Distance Dependence of Intrahelix RuII* to OsII Polypyridyl Excited-State Energy Transfer in Oligoproline Assemblies. *J. Phys. Chem. B* **2013**, *117*, 6352-6363.

(348) Chen, J.; Kuss-Petermann, M.; Wenger, O. S. Distance Dependence of Bidirectional Concerted Proton-Electron Transfer in Phenol-Ru(2,2'-bipyridine)32+ Dyads. *Chem. Eur. J.* **2014**, *20*, 4098-4104.

(349) Sisido, M.; Hoshino, S.; Kusano, H.; Kuragaki, M.; Makino, M.; Sasaki, H.; Smith, T. A.; Ghiggino, K. P. Distance Dependence of Photoinduced Electron Transfer along α-Helical Polypeptides. *J. Phys. Chem. B* **2001**, *105*, 10407-10415.

(350) Chawla, H. M.; Goel, P.; Shukla, R. Calix[4]arene based molecular probe for sensing copper ions. *Tetrahedron Lett.* **2014**, *55*, 2173-2176.

(351) Ghosh, R.; Palit, D. K. Ultrafast Twisting Dynamics of Thioflavin-T: Spectroscopy of the Twisted Intramolecular Charge-Transfer State. *Chem. Phys. Chem.* **2014**, *15*, 4126-4131.

(352) Stsiapura, V. I.; Kurhuzenkau, S. A.; Kuzmitsky, V. A.; Bouganov, O. V.; Tikhomirov, S. A. Solvent Polarity Effect on Nonradiative Decay Rate of Thioflavin T. *J. Phys. Chem. A* **2012**, *120*, 5481-5496.

(353) Peckus, D.; Matulaitis, T.; Franckevičius, M.; Mimaitė, V.; Tamuelvičius, T.; Simokaitienė, J.; Volyniuk, D.; Gulbinas, V.; Tamuelvičius, S.; Gražulevičius, J. V. Twisted Intramolecular Charge Transfer States in Trinary Star-Shaped Triphenylamine-Based Compounds. *J. Phys. Chem. A* **2018**, *122*, 3218-3226.

(354) Li, Y.; Liu, T.; Liu, H.; Tian, M.-Z.; Li, Y. Self-Assembly of Intramolecular Charge-Transfer Compounds in Functional Molecular Systems. *Acc. Chem. Res.* **2014**, *47*, 1186-1198.

(355) De Silva, A. P.; Gunaratne, H. Q. N.; Gunnlaugsson, T.; Huxley, A. J. M.; McCoy, C. P.; Rademacher, J. T.; Rice, T. E. Signaling Recognition Events with Fluorescent Sensors and Switches. *Chem. Rev.* **1997**, *97*, 1515-1566.

(356) Hush, N. S.; Reimers, J. R. Solvent Effects on Metal to Ligand Charge Transfer Excitations. *Coord. Chem. Rev.* **1998**, *117*, 37-60.

(357) Chisholm, M. H.; Brown-Xu, S. E.; Spilker, T. F. Photophysical Studies of Metal to Ligand Charge Transfer Involving Quadruply Bonded Complexes of Molybdenum and Tungsten. *Acc. Chem. Res.* **2015**, *48*, 877-885.

(358) Garakyaraghi, S.; McCusker, C. E.; Khan, S.; Koutnik, P.; Bui, A. T.; Castellano, F. N. Enhancing the Visible-Light Absorption and Excited-State Properties of Cu(I) MLCT Excited States. *Inorg. Chem.* **2018**, *57*, 2296-2307.

(359) Harcourt, R. D.; Scholes, G. D.; Ghiggino, K. P. Rate Expressions for Excitation Transfer. II. Electronic Considerations of Direct and Through-Configuration Exciton Resonance Interactions. *J. Chem. Phys.* **1994**, *101*, 10521-10525.

(360) Antusch, L.; Gass, N.; Wagenknecht, H.-A. Elucidation of the Dexter-Type Energy Transfer in DNA by Thymine-Thymine Dimer Formation Using Photosensitizers as Artificial Nucleosides. *Angew. Chem. Int. Ed.* **2017**, *56*, 1385-1389.

(361) Nielsen, A.; Kuzmanich, G.; Garcia-Garibay, M. A. Quantum Chain Reaction of Tethered Diarylcyclopropenones in the Solid State and Their Distance-Dependence in Solution Reveal a Dexter S2-S2 Energy-Transfer Mechanism. *J. Phys. Chem. A* **2014**, *118*, 1858-1863.

(362) Amatori, S.; Ambrosi, G.; Borgogelli, E.; Fanelli, M.; Formica, M.; Fusi, V.; Giorgi, L.; Macedi, E.; Micheloni, M.; Paoli, P.; Rossi, P.; Tassoni, A. Modulating the Sensor Response to Halide Using NBD-Based Azamacrocycles. *Inorg. Chem.* **2014**, *53*, 4560-4569.

(363) Nouri, H.; Cadiou, C.; Lawson-Daku, L. M.; Hauser, A.; Chevreaux, S.; Déchamps-Olivier, I.; Lachaud, F.; Ternane, R.; Trabelsi-Ayadi, M.; Chuburu, F.; Lemercier, G. A Modified Cyclen Azaxanthone Ligand as a New Fluorescent Probe for Zn2+. *Dalton Trans.* **2013**, *42*, 12157-12164.

(364) Huang, X.-H.; Lu, Y.; He, Y.-B.; Chen, Z.-H. A Metal-Macrocycle Complex as a Fluorescent Sensor for Biological Phosphate Ions in Aqueous Solution. *Eur. J. Org. Chem.* **2010**, *2010*, 1921-1927.

(365) Xu, H.-R.; Li, K.; Liu, Q.; Wu, T.-M.; Wang, M.-Q.; Hou, J.-T.; Huang, Z.; Xie, Y.-M.; Yu, X.-Q. Dianthracene-Cyclen Conjugate: The First Equal-Equivalent Responding Fluorescent Chemosensor for Pb2+ in Aqueous Solution. *Analyst* **2013**, *138*, 2329-2334.

(366) Nouri, H.; Cadiou, C.; Henry, A.; Déchamps-Olivier, I.; Ternane, R.; Trabelsi-Ayadi, M.; Lemercier, G.; Chuburu, F. 1-(2-Methyl-5*H*-chromeno[2,3-b]pyridine-5-ylidene) Hydrazone as Fluorescent Probes for Selective Zinc Sensing in DMSO. *J. Luminescence* **2014**, *148*, 202-206.

(367) Wang, M.-Q.; Li, K.; Hou, J.-T.; Wu, M.-Y.; Huang, Z.; Yu X.-Q. BINOL-Based Fluorescent Sensor for the Recognition of Cu(II) and Sulfide Anion in Water. *J. Org. Chem.* **2012**, *77*, 8350-8354.

(368) Bhasikuttan, A. C.; Mohanty, J. Detection, Inhibition and Disintegration of Amyloid Fibrils: The Role of Optical Probes and Macrocyclic Receptors. *Chem. Commun.* **2017**, *53*, 2789-2809.

(369) Feng, H.-T.; Song, S.; Chen, Y.-C.; Shen, C.-H.; Zheng, Y.-S. Self-Assembled Tetraphenylethylene Macrocycle Nanofibrous Materials for the Visual Detection of Copper(II) in Water. *J. Mater. Chem. C* **2014**, *2*, 2353-2359.

(370) Shukla, T.; Dwivedi, A. K.; Arumugaperumal, R.; Lin, C.-M.; Chen. S.-Y.; Lin, H.-C. Host-Guest Interaction of Rotaxane Assembly Through Selective Detection of Ferric Ion: Insight into Hemin Sensing and Switching with Sodium Ascorbate. *Dyes and Pigments* **2016**, *131*, 49-59.

(371) Upadhyayula, S.; Nunez, V.; Espinoza, E. M.; Larsen, J. M.; Bao, D.; Shi, D.; Mac, J. T.; Anvari, B.; Vullev, V. I. Photoinduced Dynamics of a Cyanine Dye: Parallel Pathways of Non-Radiative Deactivation Involving Multiple Excited-State Twisted Transients. *Chem. Sci.* **2015**, *6*, 2237-2251.

(372) Kathayat, R. S.; Yang, L.; Sattasathuchana, T.; Zoppi, L.; Baldridge, K. K.; Linden, A.; Finney, N. S. On the Origins of Nonradiative Excited State Relaxation in Aryl Sulfoxides Relevant to Fluorescent Chemosensing. *J. Am. Chem. Soc.* **2016**, *138*, 15889-15895.

(373) El-Sayed, Y. S. Optical Properties and Inclusion of an Organic Fluorophore in Organized Media of Micellar Solutions and beta-Cyclodextrin. *Optics Laser Technol.* **2013**, *45*, 89-95.

(374) Hashemi, J.; Alizadeh, N. Investigation of Solvent Effect and Cyclodextrins on Fluorescence Properties of Ochratoxin A. *Spectrochim. Acta A* **2009**, *73A*, 121-126.

(375) DeDora, D. J.; Suhrland, C.; Goenka, S.; Mullick Chowdhury, S.; Lalwani, G.; Mujica-Parodi, L. R.; Sitharaman, B. Sulfobutyl Ether β-Cyclodextrin (Captisol) and Methyl β-Cyclodextrin Enhance and Stabilize Fluorescence of Aqueous Indocyanine Green. *J. Biomed. Mater. Res. B: Appl. Biomaterials* **2016**, *104*, 1457-1464.

(376) Benesi, H. A.; Hildebrand, J. H. Ultraviolet Absorption Bands of Iodine in Aromatic Hydrocarbons. *J. Am. Chem. Soc.* **1948**, *70*, 2832-2833.

(377) Benesi, H. A.; Hildebrand, J. H. A Spectrophotometric Investigation of the Interaction of Iodine with Aromatic Hydrocarbons. *J. Am. Chem. Soc.* **1949**, *71*, 2703-2707.

(378) Shanmugaraju, S.; Bar, A. K.; Jadhav, H.; Moon, D.; Mukherjee, P. S. Coordination Self-Assembly of Tetranuclear Pt(II) Macrocycles with an Organometallic Backbone for Sensing of Acyclic Dicarboxylic Acids. *Dalton Trans.* **2013**, *42*, 2998-3008.

(379) Murudkar, S.; Mora, A. K.; Singh, P. K.; Bandoypadhyay, T.; Nath, S. An Ultrafast Molecular Rotor Based Ternary Complex in a Nanocavity: A Potential "Turn On" Fluorescence Sensor for the Hydrocarbon Chain. *Phys. Chem. Chem. Phys.* **2015**, *17*, 5691-5703.

(380) Wang, M-Q.; Li, K.; Hou, J.-T.; Wu, M.-Y.; Huang, Z.; Yu, X.-Q. BINIOL-Based Fluorescent Sensor for Recognition of Cu(II) and Sulfide Anion in Water. *J. Org. Chem.* **2012**, *77*, 8350-8354.

(381) Periasamy, R.; Kothainayaki, S.; Sivakumar, K. Encapsulation of Dicinnamalacetone in β-Cyclodextrin: A Physicochemical Evaluation and Molecular Modeling Approach on 1:2 Inclusion Complex. *J. Macromol. Sci. A: Pure Appl. Chem.* **2016**, *53*, 546-556.

(382) Boaz, H.; Rollefson, G. K. The Quenching of Fluorescence. Derivations from the Stern-Volmer Law. *J. Am. Chem. Soc.* **1950**, *72*, 3435-3443.

(383) Ghosh, D.; Chattopadhyay, N. Gold and Silver Nanoparticles Based Superquenching of Fluorescence: A Review. *J. Lumin.* **2015**, *160*, 223-232.

(384) Gogoi, S.; Khan, R. Fluorescence Immunosensor for Cardiac Troponin T Based on Förster Resonance Energy Transfer (FRET) Between Carbon Dot and MoS2 Nano-Couple. *Phys. Chem. Chem. Phys.* **2018**, *20*, 16501-16509.

(385) Green, N. J. B.; Pimblott, S. M.; Tachiya, M. Generalizations of the Stern-Volmer Relation. *J. Phys. Chem.* **1993**, *97*, 196-202.

(386) Thordarson, P. Determining Association Constants from Titration Experiments in Supramolecular Chemistry. *Chem. Soc. Rev.* **2011**, *40*, 1305-1323.

(387) Ju, H.; Chang, D. J.; Kim, S.; Ryu, H.; Lee, E.; Park, I.-H.; Jung, J. H.; Ikeda, M.; Habata, Y.; Lee, S. S. Cation-Selective and Anion-Controlled Fluorogenic Behaviors of a Benzothiazole-Attached Macrocycle That Correlate with Structural Coordination Modes. *Inorg. Chem.* **2016**, *55*, 7448-7456.

(388) Wang, D.-X.; Fa, S.-X.; Liu, Y.; Hou, B.-Y.; Wang, M.-X. Anion-Directed Assembly of a Rectangular Supramolecular Cage in the Solid State with Electron-Deficient Phenoxylated Oxacalix[2]arene[2]triazine. *Chem. Commun.* **2012**, *48*, 11458-11460.

(389) Panchenko, P. A.; Fedorov, Y. V.; Fedorova, O. A.; Jonusauskas, G. Comparative Analysis of the PET and ICT Sensor Properties of 1,8-Naphthalimides Containing Aza-15-Crown-5 Ether Moiety. *Dyes Pigments* **2013**, *98*, 347-357.

(390) Zapata, F.; Caballero, A.; White, N. G.; Claridge, T. D. W.; Costa, P. J.; Félix, V.; Beer, P. B. Fluorescent Charge-Assisted Halogen-Bonding Macrocyclic Halo-Imidazolium Receptors for Anion Recognition and Sensing in Aqueous Media. *J. Am. Chem. Soc.* **2012**, *134*, 11533-11541.

(391) Job, P. Formation and Stability of Inorganic Complexes in Solution. *Annali di Chimica Applicata* **1928**, *9*, 113-203.

(392) Renny, J. S.; Tomasevich, L. L.; Tallmadge, E. H.; Collum, D. B. Method of Continuous Variations: Applications of Job Plots to the Study of Molecular Associations in Organometallic Chemistry. *Angew. Chem. Int. Ed.* **2013**, *52*, 11998-12013.

(393) Belter, M.; Sajnóg, A.; Barałkiewicz, D. Over a Century of Detection and Quantification Capabilities in Analytical Chemistry – Historical Overview and Trends. *Talanta* **2014**, *129*, 606-616.

(394) Qu, X.; Liu, Q.; Ji, X.; Chen, H.; Zhou, Z.; Shen, Z. Enhancing the Stokes' Shift of BODIPY Dyes Via Through-Bond Energy Transfer and its Application for Fe3+-Detection in Live Cell Imaging. *Chem. Commun.* **2012**, *48*, 4600-4602.

(395) Galangau, O.; Dumas-Verdes, C.; Meallet-Renault, R.; Clavier, G. Rational Design of Visible and NIR Distyryl-BODIPY Dyes from a Novel Fluorinated Platform. *Org. Biomol. Chem.* **2010**, *8*, 4546-4553.

(396) Ulrich, G.; Ziessel, R.; Harriman, A. The Chemistry of Fluorescent BODIPY Dye: Versatility Unsurpassed. *Angew. Chem. Int. Ed.* **2008**, *47,* 1184-1201.

(397) Paterno, G. M.; Moretti, L.; Barker, A. J.; D'Andrea, C.; Luzio, A.; Barbero, N.; Galliano, S.; Barolo, C.; Lanzani, G.; Scotognella, F. Near-Infrared Emitting Single Squaraine Dye Aggregates with Large Stokes Shift. *J. Mater. Chem. C* **2017**, *5*, 7732-7738.

(398) Ros-Lis, J. V.; Martinez-Manez, R.; Sancenon, F.; Soto, J.; Spieles, M.; Rurack, K. Squaraines as Reporter Units: Insights into their Photophysics, Protonation and Metal-Ion Coordination Behiavor. *Chem. Eur. J.* **2008**, *14*, 10101-10114.

(399) McNamara, L. E.; Rill, T. A.; Huckaba, A. J.; Ganeshraj, V.; Gayton, J.; Nelson, R. A.; Sharpe, E. A.; Dass, A.; Hammer. N. I.; Delcamp, J. H. Indolizine-Squaraines: NIR Fluorescent Materials with Molecularly Engineered Stokes Shifts. *Chem. Eur. J.* **2017**, *23*, 12494-12501.

(400) Li, Z.; Zhao, P.; Tofighi, S.; Sharma, R.; Ensley, T. R.; Jang, S. H.; Hagan, D. J.; Van Stryland, E. W.; Jen, A. K.-Y. Zwitterionic Cyanine-Cyanine Salt: Structure and Optical Properties. *J. Phys. Chem.* **2016**, *120*, 15378-15384.

(401) Sato, K.; Gorka, A. P.; Nagaya, T.; Michie, M. S.; Nani, R. R.; Nakamura, Y.; Coble, V. L.; Vasalatiy, O. V.; Swenson, R. E.; Choyke, P. L.; Schnermann, M. J.; Kobayashi, H. Role of Fluorophore Charge on the In Vivo Optical Imaging Properties of Near-Infrared Cyanine Dye/Monoclonal Antibody Conjugates. *Bioconjugate Chem.* **2016**, *27*, 404-413.

(402) Spitsyn, M. A.; Kuznetsova, V. E.; Shershov, V. E.; Emelyanova, M. A.; Guseinov, T. O.; Lapa, S. A.; Nasedkina, T. V.; Zasedatelev, A. S.; Chudinov, A. V. Synthetic Route to Novel Zwitterionic Pentamethine Indocyanine Fluorophores with Various Substitutiones. *Dyes Pigments* **2017**, *147*, 199-210.

(403) Chen, S.; Liu, J.; Liu, Y.; Su, H.; Hong, Y.; Jim, C. K. W.; Kwok, R. T. K.; Zhao, N.; Qin, W.; Lam, J. W. Y.; Wong, K. S.; Tang, B. Z. An AIE-Active Hemicyanine Fluorogen with Stimuli-Responsive Red/Blue Emission: Extending the pH Sensing Range by "Switch + Knob" Effect. *Chem. Sci.* **2012**, *3*, 1804-1809.

(404) De, S.; Girigoswami, A. Fluorescence Resonance Energy Transfer – A Spectroscopic Probe for Organized Surfactant Media. *J. Colloid Interface Sci.* **2004**, *271*, 485-495.

(405) Seybold, P.G.; Gouterman, M.; Callis, J. Calorimetric, Photometric, and Lifetime Determinations of Fluorescence Yields of Fluorescein Dyes. *Photochem. Photobiol.* **1969**, *9*, 229-242.

(406) Kondepudi, R.; Srinivasan, S. Optical Studies on Some Dyes for Liquid Solar Concentrations. *Sol. Energy Mater.* **1990**, *20*, 257-263.

(407) Taniguchi, M.; Lindsey, J. S. Database of Absorption and Fluorescence Spectra of >300 Common Compounds for use in PhotochemCAD. *Photochem. Photobiol.* **2018,** *94*, 290-327.

(408) Hari, D. P.; Koenig, B. Synthetic Applications of Eosin Y in Photoredox Catalysis. *Chem. Commun.* **2014**, *50*, 6688-6699.

(409) Chakraborty, M.; Panda, A. K. Spectra Behavior of Eosin Y in Different Solvents and Aqueous Surfactant Media. *Spectrochim. Acta A* **2011**, *81*, 458-465.

(410) Zhang, X.-F.; Zhang, J.; Xulin, L. The Fluorescence Properties of Three Rhodamine Dye Analogues: Acridine Red, Pyronin Y and Pyronin B. *J. Fluoresc*. **2015**, *25*, 1151-1158.

(411) Arik, M.; Onganer, Y. Molecular Excitons of Pyronin B and Pyronin Y in Colloidal Silica Suspension. *Chem. Phys. Lett.* **2003**, *375*, 126-133.

(412) Drexhage, K.H. Fluorescence Efficiency of Laser Dyes. *J. Res. Nat. Bur. Stand. A* **1976**, *3*, 421-428.

(413) Mottram, L. F.; Forbes, S.; Ackley, B. D.; Peterson, B. R. Hydrophobic Analogues of Rhodamine B and Rhodamine 101: Potent Fluorescent Probes of Mitochondria in Living C. Elegans. *Beilstein J. Org. Chem.* **2012**, *8*, 2156-2165.

(414) Thome, M. P.; Filippi-Chiela, E. C.; Villodre, E. S.; Migliavaca, C. B.; Onzi, G. R.; Felipe, K. B.; Lenz, G. Ratiometric Analysis of Acridine Orange Staining in the Study of Acidic Organelles and Autophagy. *J. Cell. Sci.* **2016**, *129*, 4622-4632.

(415) Feng, X.-Z.; Lin, Z.; Yang, L.-J.; Wang, C.; Bai, C.-L. Investigation of the Interaction Between Acridine Orange and Bovine Serum Albumin. *Talanta*, **1998**, *47*, 1223-1229.

(416) Sharma, V. K.; Sahare, P. D.; Rastogi, R. C.; Ghoshal, S. K.; Mohan, D. Excited State Characteristics of Acridine Dyes: Acriflavine and Acridine Orange. *Spectrochim. Acta A* **2003**, *59A*, 1799-1804.

(417) Czapkiewicz, J.; Dlugolecka, M.; Tutaj, B. 10- Methylacridinium Ion as a Fluorimetric Probe Measuring the Activity of Halide Anions in Aqueous Solutions of Cationic Surfactants. *J. Colloid Interface Sci.* **2004**, *276*, 227-230.

(418) Mooser, G.; Sigman, D. S. Ligand Binding Properties of Acetylcholinesterase Determined with Fluorescent Probes. *Biochemistry* **1974**, *13*, 2299-2307.

(419) Biwersi, J.; Tulk, B.; Verkman, A. S. Long-Wavelength Chloride-Sensitive Fluorescent Indicators. *Anal. Biochem.* **1994**, *219*, 139-143.

(420) Olmsted, J. Calorimetric Determinations of Absolute Fluorescence Quantum Yields. *J. Phys. Chem.* **1979**, *83*, 2581-2584.

(421) Zhang, G.; Shuang, S.; Dong, C.; Pan, J. Study on the Interaction of Methylene Blue with Cyclodextrin Derivatives by Absorption and Fluorescence Spectroscopy. *Spectrochim. Acta A* **2003**, *59A*, 2935-2941.

(422) Lewis, G. N.; Goldschmid, O.; Magel, T. T.; Bigeleisen, J. Dimeric and Other Forms of Methylene Blue: Absorption and Fluorescence in the Pure Monomer. *J. Am. Chem. Soc*. **1943**, *6*, 1150-1154.

(423) Krzyszkowska, E.; Walkowiak-Kulikowska, J.; Stienen, S.; Wojcik, A. Thionine-Graphene Oxide Covalent Hybrid and its Interaction with Light. *Phys. Chem. Chem. Phys.* **2017**, *19*, 14412-14423.

(424) Rodriguez-Serrano, A.; Rai-Constapel, V.; Daza, M. C.; Doerr, M.; Marian, C. M. A Theoretical Study of Thionine: Spin-Orbit Coupling and Intersystem Crossing. *Photochem. Photobiol. Sci.* **2012**, *11*, 1860-1867.

(425) Singh, M. K.; Pal, H.; Koti, A. S. R.; Sapre, A. V. Photophysical Properties and Rotational Relaxation Dynamics of Neutral Red Bound to β-Cyclodextrin. *J. Phys. Chem. A.* **2004**, *108*, 1465-1474.

(426) Tajalli, H.; Gilani, A. G.; Zakerhamidi, M. S.; Tajalli, P. The Photophysical Properties of Nile Red and Nile Blue in Ordered Anisotropic Media. *Dyes Pigments* **2008**, *78*, 15-24.

(427) Jana, A.; Manna, S. K.; Mondal, S. K.; Mandal, A.; Manna, S. K.; Jana, A.; Senapati, B. K.; Jana, M.; Samanta, S. An Efficient Synthesis of Pyrrole and Fluorescent Isoquinoline Derivatives Using NaN3 /NH4Cl Promoted Intramolecular Aza-Annulation. *Tetrahedron Lett.* **2016**, *57*, 3722-3726.

(428) Diaz, M. S.; Freile, M. L.; Gutierrez, M. I. Solvent Effect on the UV/Vis Absorption and Fluorescence Spectroscopic Properties of Berberine. *Photochem. Photobiol. Sci.* **2009**, *8*, 970-974.

(429) Wu, H.; Zhang, L.-b; Du, L.-m. Ionic Liquid Sensitized Fluorescence Determination of Four Isoquinoline Alkaloids. *Talanta* **2011**, *85*, 787-793.

(430) Li, J.; Shuang, S.; Dong, C. Study on the Phosphorescence Characterizations of Palmatine Chloride on the Solid Substrate and its Interaction with ctDNA. *Talanta* **2009**, *77*, 1043-1049.

(431) Chung, Y.-L.; Hong, R.-D.; Wu, H. W.; Hung, W.-H.; Lai, L.-J.; Wang, C. M. Fluorescence Enhancement for Alkaloids by Anions: Spectroscopic and Electrochemical Characterizations. *J. Electroanal. Chem*. **2007**, *610*, 85-89.

(432) Liu, H. L.; Zhao, Y.; Du, Q.; Du, L. M.; Pang, T. T.; Fu, Y. L. Suparmolecular Interactions of Ionic Liquids with P-Sulfonated Calix[4]arene Using a New Type of Fluorescent Probe. *J. Chem. Soc. Pak*. **2015**, *37*, 25-32.

(433) Yao, F.; Liu, H.; Wang, G.; Du, L.; Yin, X.; Fu, Y. Determination of Paraquat in Water Samples Using a Sensitive Fluorescent Probe Titration Method. *J. Environ. Sci.* **2013**, *25*, 1245-1251.

(434) Galban, J.; Mateos, E.; Cebolla, V.; Dominguez, A.; Delgado-Camon, A.; de Marcos, S.; Sanz-Vicente, I.; Sanz, V. The Environmental Effect on the Fluorescence Intensity in Solution. An Analytical Model. *Analyst* **2009**, *134*, 2286-2292.

(435) Margineanu, A.; Hofkens, J.; Cotlet, M.; Habuchi, S.; Stefan, A.; Qu, J.; Kohl, C.; Mullen, K.; Vercammen, J.; Engelborghs, Y.; et al. Photophysics of a Water-Soluble Rylene Dye: Comparison with Other Fluorescent Molecules for Biological Applications. *J. Phys. Chem. B* **2004**, *108*, 12242-12251.

(436) Bullock, J. E.; Vagnini, M. T.; Ramanan, C.; Co, D. T.; Wilson, T. M.; Dicke, J. W.; Marks, T. J.; Wasielewski, M. R. Photophysics and Redox Properties of Rylene Imide and Diimide Dyes Alkylated Ortho to the Imide Groups. *J. Phys. Chem. B,* **2010**, *114*, 1794-1802.

(437) Wang, K.-P.; Lei, Y.; Chen, J.-P.; Ge, Z.-H.; Liu, W.; Zhang, Q.; Chen, S.; Hu, Z.-Q. The Coumarin Conjugate: Synthesis, Photophysical Properties and the Ratiometric Fluorescence Response to Water Content of Organic Solvent. *Dyes Pigments* **2018**, *151*, 233-237.

(438) Jones, G.; Jackson, W. R.; Choi, C. Y.; Bergmark, W. R. Solvent Effects on Emission Yield and Lifetime for Coumarin Laser Dyes. Requirements for a Rotatory Decay Mechanism. *J. Phys. Chem*. **1985**, *89*, 294-300.

(439) Huang, D.; Chen, Y.; Zhao, J. Access to a Large Stokes Shift in Functionalized Fused Coumarin Derivatives by Increasing the Geometry Relaxation Upon Photoexcitation: An Experimental and Theoretical Study. *Dyes and Pigments* **2012**, *95*, 732-742.

(440) Fei, X.; Gu, Y.; Wang, Y.; Meng, Q.; Zhang, B. Targeted Thiazole Orange Derivative with Folate: Synthesis, Fluorescence and In Vivo Fluorescence Imaging. *Molecules* **2010**, *15*, 6983-6992.

(441) Nygren, J.; Svanvik, N.; Kubista, M. The Interactions Between the Fluorescent Dye Thiazole Orange and DNA. *Biopolymers* **1998**, *46*, 39-51.

(442) Lee, L. G.; Chen, C.; Chiu, L. A. Thiazole Orange: A New Dye for Reticulocyte Analysis. *Cytometry* **1986**, *7*, 508-517.

(443) Makler, M. T.; Lee, L. G.; Recktenwald, D. Thiazole Orange: A New Dye for *Plasmodium* Species Analysis. *Cytometry* **1987**, *8*, 568-570.

(444) Balduini, C. L.; Noris, P.; Spedini, P.; Belletti, S.; Zambelli, A.; Da Prada, G. A. Relationship Between Size and Thiazole Orange Fluorescence of Platelets in Patients Undergoing High-Dose Chemotherapy. *Br. J. Haematol.* **1999**, *106*, 202-207.

(445) Mitra, S.; Das, R.; Mukherjee, S. Complex Formation and Photophysical Properties of Luminol: Solvent Effects. *J. Photochem. Photobiol. A* **1995**, *87*, 225-230.

(446) Vellosa, J. C. R.; Khalil, N. M.; Fonseca, L. M.; Brunetti, I. L.; Oliveira, O. M. M. F. Does Cotinine Act Upon Reactive Oxygen Species and Peroxidases? *Eclet. Quím.* **2007**, 32, 65-70.

(447) Grzybowski, M.; Gryko, D. T. Diketopyrrolopyrroles: Synthesis, Reactivity, and Optical Properties. *Adv. Optical Mater.* **2015**, *3*, 280-320.

(448) Cui, W.; Tang, H.; Xu, L.; Wang, L.; Meier, H.; Cao, D. Pillar[5]arene-Diketopyrrolopyrrole Fluorescent Copolymer: A Promising Recognition and Adsorption Material for Adiponitrile by Selective Formation of Conjugated Polypseudorotaxane. *Macromol. Rapid Commun.* **2017**, *38*, 1700161/1-1700161/5.

(449) Alp, S.; Ertekin, K.; Horn, M.; Icli, S. Photostability Studies of Thermomesomorphic Derivative of 2,5-Dihydropyrrolo[3,4-c]pyrrole-1,4-dione. *Dyes Pigments* **2003**, *60*, 103-110.

(450) Deng, L.; Wu, W.; Guo, H.; Zhao, J.; Ji, S.; Zhang, X.; Yuan, X.; Zhang, C. Colorimetric and Ratiometric Fluorescent Chemosensor Based on Diketopyrrolopyrrole for Selective Detection of Thiols: An Experimental and Theoretical Study. *J. Org. Chem.* **2011**, *76*, 9294-9304.

(451) Zhang, L.; Chen, Y.; Jiang, J. Solid State Fluorescent Functionalized-Triphenylamine Bodipy Detector for HCl Vapor with High Stability and Absolute Fluorescent Quantum Yield. *Dyes Pigments* **2016**, *124*, 110-119.

(452) Boens, N.; Leen, V.; Dehaen, W. Fluorescent Indicators Based on BODIPY. *Chem. Soc. Rev.* **2012**, *41*, 1130-1172.

(453) Zhang, X.-F.; Zhang, Y.; Xu, B. Enhance the Fluorescence and Singlet Oxygen Generation Ability of BODIPY: Modification on the meso-Phenyl Unit with Electron Withdrawing Groups. *J. Photochem. Photobiol.* **2017**, *349*, 197-206.

(454) Sheng, W.; Cui, J.; Ruan, Z.; Yan, L.; Wu, Q.; Yu, C.; Wei, Y.; Hao, E.; Jiao, L. [a]-Phenanthrene-Fused BF2 Azadipyrromethene (AzaBODIPY) Dyes as Bright Near-Infrared Fluorophores. *J. Org. Chem.* **2017**, 82, 10341-10349.

(455) Wu, M.; Wu, X.; Wang, Y.; Gu, L.; You, J.; Wu, H.; Feng, P. Alkoxy Tetrazine Substitution at a Boron Center: A Strategy for Synthesizing Highly Fluorogenic Hydrophilic Probes. *ChemBioChem.* **2018**, *19*, 530-534.

(456) Jiang, X.-D.; Li, S.; Guan, J.; Fang, T.; Liu, X.; Xiao, L.-J. Recent Advances of the Near-Infrared Fluorescent aza-BODIPY Dyes. *Curr. Org. Chem.* **2016**, *20*, 1736-1744.

(457) Ni, Y.; Wu, J. Far-Red and Near Infrared BODIPY Dyes: Synthesis and Applications for Fluorescent pH Probes and Bio-Imaging. *Org. Biomol. Chem.* **2014**, *12*, 3774-3791.

(458) Boens, N.; Verbelen, B.; Dehaen, W. Postfunctionalization of the BODIPY Core: Synthesis and Spectroscopy. *Eur. J. Org. Chem.* **2015**, *2015*, 6577-6595.

(459) Loudet, A.; Burgess, K. BODIPY Dyes and their Derivatives: Syntheses and Spectroscopic Properties. *Chem. Rev.* **2007**, *107*, 4891-4932.

(460) Sui, B.; Tang, S.; Woodward, A. W.; Kim, B.; Belfield, K. D. A BODIPY-Based Water-Soluble Fluorescent Probe for Mitochondria Targeting. *Eur. J. Org. Chem.* **2016**, *2016*, 2851-2857.

(461) Montero, R.; Martinez-Martinez, V.; Longarte, A.; Epelde-Elezcano, N.; Palao, E.; Lamas, I.; Manzano, H.; Agarrabeitia, A. R.; Lopez Arbeloa, I.; Ortiz, M. J.; Garcia-Moreno, I. Singlet Fission Mediated Photophysics of BODIPY Dimers. *J. Phys. Chem. Lett.* **2018**, *9*, 641-646.

(462) Ozdemir, T.; Bila, J. L.; Sozmen, F.; Yildirim, L. T.; Akkaya, E. U. Orthogonal Bodipy Trimers as Photosensitizers for Photodynamic Action. *Org. Lett.* **2016**, *18*, 4821-4823.

(463) Yoshii, R.; Yamane, H.; Nagai, A.; Tanaka, K.; Taka, H.; Kita, H.; Chujo, Y. π-Conjugated Polymers Composed of BODIPY or Aza-BODIPY Derivatives Exhibiting High Electron Mobility and Low Threshold Voltage in Electron-Only Devices. *Macromolecules* **2014**, *47*, 2316-2323.

(464) Telore, R. D.; Jadhav, A. G.; Sekar, N. NLOphoric and Solid State Emissive BODIPY Dyes Containing N-Phenylcarbazole Core at Meso Position - Synthesis, Photophysical Properties of and DFT Studies. *J. Lumin.* **2016**, *179*, 420-428.

(465) Serio, N.; Miller, K.; Levine, M. Efficient Detection of Polycyclic Aromatic Hydrocarbons and Polychlorinated Biphenyls via Three-Component Energy Transfer. *Chem. Commun.* **2013**, *49*, 4821-4823.

(466) Kajiwara, Y.; Nagai, A.; Tanaka, K.; Chujo, Y. Efficient Simultaneous Emission from RGB-Emitting Organoboron Dyes Incorporated into Organic-Inorganic Hybrids and Preparation of White Light-Emitting Materials. *J. Mater. Chem. C* **2013**, *1*, 4437-4444.

(467) Neelakandan, P. P.; Jimenez, A.; Nitschke, J. R. Fluorophore Incorporation Allows Nanomolar Guest Sensing and White-Light Emission in M4L6 Cage Complexes. *Chem. Sci.* **2014**, *5*, 908-915.

(468) Sayar, M.; Karakus, E.; Guener, T.; Yildiz, B.; Yildiz, U. H.; Emrullahoglu, M. A BODIPY-Based Fluorescent Probe to Visually Detect Phosgene: Toward the Development of a Handheld Phosgene Detector. *Chem. Eur. J.* **2018**, *24*, 3136-3140.

(469) He, Y. W.; Feng, Y.; Kang, L. W.; Li, X. L. A Turn-On Fluorescent Sensor for Hg2+ Based on Graphene Oxide. *J. Chem.* **2017**, 9431605/1-9431605/5.

(470) He, S.-J.; Xie, Y.-W.; Chen, Q.-Y. A NIR-BODIPY Derivative for Sensing Copper(II) in Blood and Mitochondrial Imaging. *Spectrochim. Acta A* **2018**, *195*, 210-214.

(471) Cao, Y. W.; Li, X. L.; He, Y. W. A High Selective Fluorescent Sensor for Ni(II) Ion in Acetonitrile. *Eur. J. Chem.* **2017**, *8*, 314-316.

(472) Xia, S.; Shen, J.; Wang, J.; Wang, H.; Fang, M.; Zhou, H.; Tanasova, M. Ratiometric Fluorescent and Colorimetric BODIPY-Based Sensor for Zinc Ions in Solution and Living Cells. *Sens. Actuators B* **2018**, *258*, 1279-1286.

(473) Purdey, M. S.; McLennan, H. J.; Sutton-McDowall, M. L.; Drumm, D. W.; Zhang, X.; Capon, P. K.; Heng, S.; Thompson, J. G.; Abell, A. D. Biological Hydrogen Peroxide Detection with Aryl Boronate and Benzil BODIPY-Based Fluorescent Probes. *Sens. Actuators B* **2018**, *262*, 750-757.

(474) Prasannan, D.; Arunkumar, C. A "Turn-On-and-Off" pH Sensitive BODIPY Fluorescent Probe for Imaging E. Coli Cells. *New J. Chem.* **2018**, *42*, 3473-3482.

(475) Beverina, L.; Sassi, M. Twists and Turns Around a Square: The Many Faces of Squaraine Chemistry. *Synlett* **2014**, *25*, 477-490.

(476) Sreejith, S.; Carol, P.; Chithra, P.; Ajayaghosh, A. Squaraine Dyes: A Mine of Molecular Materials. *J. Mater. Chem.* **2008**, *18*, 264-274.

(477) Klein, M.; Majumdar, S.; Zassowski, P.; Stampor, W. Unravelling the Role of Electron-Hole Pair Spin in Exciton Dissociation in Squaraine-Based Organic Solar Cells by Magneto-Photocurrent Measurements. *J. Mater. Chem. C* **2018**, *6*, 482-490.

(478) Beverina, L.; Salice, P. Squaraine Compounds: Tailored Design and Synthesis towards a Variety of Material Science Applications. *Eur. J. Org. Chem.* **2010**, 1207-1225.

(479) Cox, J. R.; Muller, P.; Swager, T. M. Interrupted Energy Transfer: Highly Selective Detection of Cyclic Ketones in the Vapor Phase. *J. Am. Chem. Soc.* **2011**, *133*, 12910-12913.

(480) Radaram, B.; Mako, T.; Levine, M. Sensitive and Selective Detection of Cesium via Fluorescence Quenching. *Dalton Trans.* **2013**, *42*, 16276-16278.

(481) Liu, T.; Liu, X.; Valencia, M. A.; Sui, B.; Zhang, Y.; Belfield, K. D. Far-Red-Emitting TEG-Substituted Squaraine Dye: Synthesis, Optical Properties, and Selective Detection of Cyanide in Aqueous Solution. *Eur. J. Org. Chem.* **2017**, *2017*, 3957-3964.

(482) Sun, J.; Zheng, X.; Wu, X.; Li, D.; Xia, G.; Yu, S.; Yu, Q.; Wang, H. A Squaraine-Based Sensor for Colorimetric Detection of CO2 Gas in an Aqueous Medium Through an Unexpected Recognition Mechanism: Experiment and DFT Calculation. *Anal. Methods* **2017**, *9*, 6830-6838.

(483) Xiong, L.; Ma, J.; Huang, Y.; Wang, Z.; Lu, Z. Highly Sensitive Squaraine-Based Water-Soluble Far-Red/Near-Infrared Chromofluorogenic Thiophenol Probe. *ACS Sens.* **2017**, *2*, 599-605.

(484) Tu, J.; Sun, S.; Xu, Y. A Novel Self-Assembled Platform for the Ratiometric Fluorescence Detection of Spermine. *Chem. Commun*. **2016**, *52*, 1040-1043.

(485) Chen, G.; Sasabe, H.; Lu, W.; Wang, X.-F.; Kido, J.; Hong, Z.; Yang, Y. J-Aggregation of a Squaraine Dye and its Application in Organic Photovoltaic Cells. *J. Mater. Chem. C* **2013**, *1*, 6547-6552.

(486) Li, X.-H.; Zhang, B.-W.; Cao, Y. Aggregation of Bis(2,4,6-trihydroxyphenyl) Squaraine in Different Solutions. *Dyes Pigments* **2000**, *45*, 209-217.

(487) Gassensmith, J. J.; Baumes, J. M.; Smith, B. D. Discovery and Early Development of Squaraine Rotaxanes. *Chem. Commun*. **2009**, 6329-6338.

(488) Chaudhuri, S.; Verderame, M.; Mako, T. L.; Bandara, Y. M. N. D. Y.; Fernando, A. I.; Levine, M. Synthetic β-Cyclodextrin Dimers for Squaraine Binding: Effect of Host Architecture on Photophysical Properties, Aggregate Formation, and Chemical Reactivity. *Eur. J. Org. Chem.* **2018**, *2018*, 1964-1974.

(489) Karpenko, I. A.; Collot, M.; Richert, L.; Valencia, C.; Villa, P.; Mely, Y.; Hibert, M.; Bonnet, D.; Klymchenko, A. S. Fluorogenic Squaraine Dimers with Polarity-Sensitive Folding as Bright Far-Red Probes for Background-Free Bioimaging. *J. Am. Chem. Soc.* **2015**, *137*, 405-412.

(490) Kuster, S.; Geiger, T. Strategies and Investigations on Bridging Squaraine Dye Units. *Dyes Pigments* **2012**, *95*, 657-670.

(491) Ajayaghosh, A. Donor-Acceptor Type Low Band Gap Polymers: Polysquaraines and Related Systems. *Chem. Soc. Rev*. **2003**, *32*, 181-191.

(492) Block, M. A. B.; Hecht, S. Alternating (Squaraine-Receptor) Sensory Polymers: Modular One-Pot Synthesis and Signal Transduction via Conformationally Controlled Exciton Interaction. *Macromolecules* **2004**, *37*, 4761-4769.

(493) Chenthamarakshan, C. R.; Ajayaghosh, A. Enhanced Sensitivity and Selectivity in Lithium Ion Recognition Property of an Oligomeric Squaraine Dye Based Fluorescent Sensor. *Tetrahedron Lett.* **1998**, *39*, 1795-1798.

(494) Yang, Z.; Usama, S. M.; Li, F.; Burgess, K.; Li, Z. A Zwitterionic Near-Infrared Dye Linked TrkC Targeting Agent for Imaging Metastatic Breast Cancer. *MedChemComm* **2018**, *Ahead of Print*, DOI: 10.1039/C8MD00190A.

(495) Shershov, V. E.; Kuznetsova, V. E.; Lapa, S. A.; Spitsyn, M. A.; Guseinov, T. O.; Tkachev, Y. V.; Zasedatelev, A. S.; Chudinov, A. V. Synthesis and Characterization of Novel Zwitterionic Heptamethine Indocyanine Fluorophores. *Mendeleev Commun.* **2017**, *27*, 360-362.

(496) Shiring, S. B.; Gieseking, R. L.; Risko, C.; Brédas, J.-L. Assessment of Front-Substituted Zwitterionic Cyanine Polymethines for All-Optical Switching Applications. *J. Phys. Chem. C* **2017**, *121*, 14166-14175.

(497) Shi, Y.; Lou, A. J.-T.; Hu, G. S.; Baev, A.; Swihart, M. T.; Prasad, P. N.; Marks, T. J. Cooperative Coupling of Cyanine and Tictoid Twisted π-Systems to Amplify Organic Chromophore Cubic Nonlinearities. *J. Am. Chem. Soc.* **2015**, *137*, 4622-4625.

(498) Sainudeen, Z.; Ray, P. C. Nonlinear Optical Properties of Zwitterionic Merocyanine Aggregates: Role of Intermolecular Interaction and Solvent Polarity. *J. Phys. Chem. A* **2005**, *109*, 9095-9103.

(499) Chen, H.; Zhang, X.; Sun, H.; Sun, X.; Shi, Y.; Xu, S.; Tang, Y. Visual Detection of Mercury(II) Based on Recognition of the G-Quadruplex Conformational Transition by a Cyanine Dye Supramolecule. *Analyst* **2015**, *140*, 7170-7174.

(500) Sun, H.; Xiang, J.; Gei, W.; Shang, Q.; Li, Q.; Guan, A.; Yang, Q.; Liu, Y.; Tang, Y.; Xu, G. Visual Detection of Potassium by a Cyanine Dye Supramolecular Aggregate Responsive to G-Quadruplex Motif Transition. *Analyst* **2012**, *137*, 5713-5715.

(501) Sun, H.; Xiang, J.; Zhang, X.; Chen, H.; Yang, Q.; Li, Q.; Guan, A.; Shang, Q.; Tang, Y.; Xu, G. A Colorimetric and Fluorometric Dual-Modal Supramolecular Chemosensor and its Application for HSA Detection. *Analyst* **2014**, *139*, 581-584.

(502) Peveler, W. J.; Algar, W. R. More Than a Light Switch: Engineering Unconventional Fluorescent Configurations for Biological Sensing. *ACS Chem. Biol.* **2018**, *13*, 1752-1766.

(503) Heintzmann, R.; Huser, T. Super-Resolution Structured Illumination Microscopy. *Chem. Rev.* **2017**, *117*, 13890-13908.

(504) Li, X.; Gao, X.; Shi, W.; Ma, H. Design Strategies for Water-Soluble Small Molecular Chromogenic and Fluorogenic Probes. *Chem. Rev.* **2014**, *114*, 590-659.

(505) Urano, Y.; Kamiya, M.; Kanda, K.; Ueno, T.; Hirose, K.; Nagano, T. Evolution of Fluorescein as a Platform for Finely Tunable Fluorescence Probes. *J. Am. Chem. Soc.* **2005**, *127*, 4888-4894.

(506) Fan, J.; Hu, M.; Zhan, P.; Peng, X. Energy Transfer Cassettes Based on Organic Fluorophores: Construction and Applications in Ratiometric Sensing. *Chem. Soc. Rev.* **2013**, *42*, 29-43.

(507) Thielbeer, F.; Chankeshwara, S. V.; Bradley, M. Polymerizable Fluorescein Derivatives: Synthesis of Fluorescent Particles and Their Cellular Uptake. *Biomacromolecules* **2011**, *12*, 4386-4391.

(508) Kobayashi, T.; Urano, Y.; Kamiya, M.; Ueno, T.; Kojima, H.; Nagano, T. Highly Activatable and Rapidly Releasable Caged Fluorescein Derivatives. *J. Am. Chem. Soc.* **2007**, *129*, 6696-6697.

(509) Li, T.; Yang, Z.; Li, Y.; Liu, Z.; Qi, G.; Wang, B. A Novel Fluorescein Derivative as a Colorimetric Chemosensor for Detecting Copper(II) Ion. *Dyes Pigments* **2010**, *88*, 103-108.

(510) Swamy, K. M. K.; Lee, Y. J.; Lee, H. N.; Chun, J.; Kim, Y.; Kim, S.-J.; Yoon, J. A New Fluorescein Derivative Bearing a Boronic Acid Group as a Fluorescent Chemosensor for Fluoride Ion. *J. Org. Chem.* **2006**, *71*, 8626-8628.

(511) Grimme, J.; King, T.; Jo, K. D.; Cropek, D.; Timperman, A. T. Development of Fieldable Lab-on-a-Chip Systems for Detection of a Broad Array of Targets from Toxicants to Biowarfare Agents. *J. Nanotechnol. Eng. Med*. **2013**, *4*, 020904/1-020904/8.

(512) Kabessa, Y.; Korouma, V.; Ilan, H.; Yagur-Kroll, S.; Belkin, S.; Agranat, A. J. Simultaneous Quantification of the Fluorescent Responses of an Ensemble of Bacterial Sensors. *Biosens. Bioelectron.* **2013**, *49*, 394-398.

(513) Ghosh, I.; Marzo, L.; Das, A.; Shaikh, R.; Koenig, B. Visible Light Mediated Photoredox Catalytic Arylation Reactions. *Acc. Chem. Res.* **2016**, *49*, 1566-1577.

(514) Li, J.-F.; Li, C.-Y.; Aroca, R. F. Plasmon-Enhanced Fluorescence Spectroscopy. *Chem. Soc. Rev.* **2017**, *46*, 3962-3979.

(515) Hazebroucq, S.; Labat, F.; Lincot, D.; Adamo, C. Theoretical Insights on the Electronic Properties of Eosin Y as Organic Dye for Photovoltaic Applications. *J. Phys. Chem. A* **2008**, *112*, 7264-7270.

(516) Skou, J. C.; Esmann, M. Eosin as a Fluorescence Probe for Measurement of Conformational States of Sodium-Potassium ATPase. *Methods Enzymol.* **1988**, *156*, 278-281.

(517) Azmi, S. N. H.; Al-Fazari, A.; Al-Badaei, M.; Al-Mahrazi, R. Utility of Eosin Y as a Complexing Reagent for the Determination of Citalopram Hydrobromide in Commercial Dosage Forms by Fluorescence Spectrophotometry. *Luminescence* **2015**, *30*, 1352-1359.

(518) El-Masry, A. A.; Hammouda, M. E. A.; El-Wasseef, D. R.; El-Ashry, S. M. Validated Spectroscopic Methods for Determination of Anti-Histaminic Drug Azelastine in Pure Form: Analytical Application for Quality Control of its Pharmaceutical Preparations. *Spectrochim. Acta A* **2018**, *191*, 413-420.

(519) Bkhaitan, M. M.; Mirza, A. Z. Spectrophotometric Method for Determination of Meclizine in Pure and Dosage Form Via Ion Pair Complex Formation Using Eosin Y. *Curr. Pharm. Anal.* **2018**, *14*, 95-100.

(520) Zhu, X.; Zhang, K.; Wang, C.; Guan, J.; Yuan, X.; Li, B. Quantitative Determination and Toxicity Evaluation of 2,4-Dichlorophenol Using Poly(eosin Y)/Hydroxylated Multi-Walled Carbon Nanotubes Modified Electrode. *Sci. Rep.* **2016**, *6*, 38657.

(521) Ling, Y.; Gao, Z. F.; Zhou, Q.; Li, N. B.; Luo, H. Q. Multidimensional Optical Sensing Platform for Detection of Heparin and Reversible Molecular Logic Gate Operation Based on the Phloxine B /Polyethyleneimine System. *Anal. Chem.* **2015**, *87*, 1575-1581.

(522) Ma, X.-L.; Ye, J.-X.; Su, J.; Qi, F.-F.; Meng, Q.-Y.; Shi, X.-Y. A Modified GEWF Solution is Cost-Saving and Effective for Lymph Node Retrieval in Resected Colorectal Carcinoma Specimens. *Pathol. Res. Pract.* **2014**, *210*, 543-547.

(523) Li, F.; Xu, Y.; Li, H.; Wang, C.; Lu, A.; Sun, S. Discrimination of DNA from RNA with the Host-Guest Complexes of Tricyclic Basic Dyes and Cucurbit[8]uril. *New J. Chem*. **2014**, *38*, 1396-1400.

(524) Salci, A.; Toprak, M. Spectroscopic Investigations on the Binding of Pyronin Y to Human Serum Albumin. *J. Biomol. Struct. Dyn.* **2017**, *35*, 8-16.

(525) Vitagliano, V. Interaction between Cationic Dyes and Polyelectrolytes. *NATO Adv. Study Institute Series* **1975**, *18*, 437-466.

(526) Tang, Q.; Zhang, J.; Sun, T.; Wang, C.-H.; Huang, Y.; Zhou, Q.; Wei, G. A Turn-On Supramolecular Fluorescent Probe for Sensing Benzimidazole Fungicides and its Application in Living Cell Imaging. *Spectrochim. Acta A* **2018**, *191*, 372-376.

(527) Malek, A.; Thomas, T.; Prasad, E. Visual and Optical Sensing of Hg2+, Cd2+, Cu2+, and Pb2+ in Water and Its Beneficiation via Gettering in Nanoamalgam Form. *ACS Sustain. Chem. Eng.* **2016**, *4*, 3497-3503.

(528) Dagci, K.; Alanyalioglu, M. Electrochemical Preparation of Polymeric Films of Pyronin Y and its Electrocatalytic Properties for Amperometric Detection of Nitrite. *J. Electroanal. Chem.* **2013**, *711*, 17-24.

(529) Essawy, A. A.; Attia, M. S. Novel Application of Pyronin Y Fluorophore as High Sensitive Optical Sensor of Glucose in Human Serum. *Talanta* **2013**, *107*, 18-24.

(530) Lavis, L. D. Teaching Old Dyes New Tricks: Biological Probes Built from Fluoresceins and Rhodamines. *Annu. Rev. Biochem.* **2017**, *86*, 825-843.

(531) Beija, M.; Afonso, C. A. M.; Martinho, J. M. G. Synthesis and Applications of Rhodamine Derivatives as Fluorescent Probes. *Chem. Soc. Rev.* **2009**, *38*, 2410-2433.

(532) Pourtabrizi, M.; Shahtahmassebi, N.; Kompany, A.; Sharifi, S. Effect of Microemulsion Structure on Fluorescence and Nonlinear Optical Properties of Rhodamine 6G. *J. Fluorescence* **2018**, *28*, 323-336.

(533) Klymchenko, A. S. Solvatochromic and Fluorogenic Dyes as Environment-Sensitive Probes: Design and Biological Applications. *Acc. Chem. Res.* **2017**, *50*, 366-375.

(534) Shah, S.; Gryczynski, Z.; Chib, R.; Fudala, R.; Baxi, A.; Borejdo, J.; Synak, A.; Gryczynski, I. Demonstration of FRET in Solutions. *Methods Applications Fluorescence* **2016**, *4*, 015001/1-015001/9.

(535) Wang, Y.-Y.; Xiang, X.; Yan, R.; Liu, Y.; Jiang, F.-L. Förster Resonance Energy Transfer from Quantum Dots to Rhodamine B as Mediated by a Cationic Surfactant: A Thermodynamic Perspective. *J. Phys. Chem.* **2018**, *122*, 1148-1157.

(536) Zheng, J.; Swager, T. M. Biotinylated Poly(p-phenylene Ethynylene): Unexpected Energy Transfer Results in the Detection of Biological Analytes. *Chem. Commun.* **2004**, 2798-2799.

(537) Chen, X.; Sun, W.; Bai, Y.; Zhang, F.; Zhao, J.; Ding, X. Novel Rhodamine Schiff Base Type Naked-Eye Fluorescent Probe for Sensing Fe3+ and the Application in Cell. *Spectrochim. Acta A* **2018**, *191*, 566-572.

(538) Wang, H.; Kang, T.; Wang, X.; Feng, L. Design and Synthesis of a Novel Tripod Rhodamine Derivative for Trivalent Metal Ions Detection. *Sens. Actuators B* **2018**, *264*, 391-397.

(539) Li, X.; Ma, Y.; Yang, Y.; Wu, J.; Jiang, T.; Ren, H.; Mu, R.; Jia, X. Recyclable Nitrite Ion Sensing Nanocomposites Based on a Magnetic-Emissive Core-Shell Structure: Characterization and Performance. *Inorg. Chim. Acta* **2018**, *469*, 144-153.

(540) Luo, Q.; Yu, F.; Yang, F.; Yang, C.; Qiu, P.; Wang, X. A 3D-Printed Self-Propelled, Highly Sensitive Mini-Motor for Underwater Pesticide Detection. *Talanta* **2018**, *183*, 297-303.

(541) Chen, L.; Park, J.-S.; Wu, D.; Kim, C.-H.; Yoon, J. A Colorimetric and Fluorescent Probe for Rapid Detection of Glutathione and its Application to Tissue Specific Bio-Imaging in Living Cells and Zebrafish. *Sens. Actuators B* **2018**, *262*, 306-312.

(542) Li, L.; Wang, S.; Lan, H.; Gong, G.; Zhu, Y.; Tse, Y. C.; Wong, K. M.-C. Rhodol Derivatives as Selective Fluorescent Probes for the Detection of HgII Ions and the Bioimaging of Hypochlorous Acid. *ChemistryOpen* **2018**, *7*, 136-143.

(543) Ozdemir, M.; Zhang, Y.; Guo, M. A Highly Selective "Off-On" Fluorescent Sensor for Subcellular Visualization of Labile Iron(III) in Living Cells. *Inorg. Chem. Commun.* **2018**, *90*, 73-77.

(544) Bregadze, Vasil G.; Giorgadze, Tamar G.; Melikishvili, Zaza G. DNA and Nanophotonics: Original Methodological Approach. *Nanotechnol. Rev.* **2014**, 3, 445-465.

(545) Eisenhart, T. T.; Dempsey, J. L. Photo-Induced Proton-Coupled Electron Transfer Reactions of Acridine Orange and Comprehensive Spectral and Kinetics Analysis. *J. Am. Chem. Soc.* **2014**, *136*, 12221-12224.

(546) Zelenka, K.; Borsig, L.; Alberto, R. Metal Complex Mediated Conjugation of Peptides to Nucleus Targeting Acridine Orange: A Modular Concept for Dual-Modality Imaging Agents. *Bioconjugate Chem.* **2011**, *22*, 958-967.

(547) Bragagni, M.; Carta, F.; Osman, S. M.; Al Othman, Z.; Supuran, C. T. Synthesis of an Acridine Orange Sulfonamide Derivative with Potent Carbonic Anhydrase IX Inhibitory Action. *J. Enzyme Inhib. Med. Chem.* **2017**, *32*, 701-706.

(548) Zhu, W.; Xuan, C.; Liu, G.; Chen, Z.; Wang, W. A Label-Free Fluorescent Biosensor for Determination of Bovine Serum Albumin and Calf Thymus DNA Based on Gold Nanorods Coated with Acridine Orange-Loaded Mesoporous Silica. *Sens. Actuators B* **2015**, *220*, 302-308.

(549) Hua, B.; Shao, L.; Zhang, Z.; Sun, J.; Yang, J. Pillar[6]arene/Acridine Orange Host-Guest Complexes as Colorimetric and Fluorescence Sensors for Choline Compounds and Further Application in Monitoring Enzymatic Reactions. *Sens. Actuators B* **2018**, *255*, 1430-1435.

(550) Askim, J. R.; Li, Z.; La Gasse, M. K.; Rankin, J. M.; Suslick, K. S. An Optoelectronic Nose for Identification of Explosives. *Chem. Sci.* **2016**, *7*, 199-206.

(551) Li, Z.; Jang, M.; Askim, J. R.; Suslick, K. S. Identification of Accelerants, Fuels and Post-Combustion Residues Using a Colorimetric Sensor Array. *Analyst* **2015**, *140*, 5929-5935.

(552) Li, N.; Hao, X.; Kang, B. H.; Li, N. B.; Luo, H. Q. Sensitive and Selective Turn-On Fluorescence Method for Cetyltrimethylammonium Bromide Determination Based on Acridine Orange-Polystyrene Sulfonate Complex. *Luminescence* **2016**, *31*, 1025-1030.

(553) Suzuki, T.; Takeda, T.; Ohta, E.; Wada, K.; Katoono, R.; Kawai, H.; Fujiwara, K. Bis(10-methylacridinium)s as a Versatile Platform for Redox-Active Functionalized Dyes and Novel Structures. *Chem. Rec.* **2015**, *15*, 280-294.

(554) Li, Y.; Zhu, H.; Kuppusamy, P.; Roubaud, V.; Zweier, J. L.; Trush, M. A. Validation of Lucigenin (bis-N-Methylacridinium) as a Chemilumigenic Probe for Detecting Superoxide Anion Radical Production by Enzymic and Cellular systems. *J. Biol. Chem.* **1998**, *273*, 2015-2023.

(555) Fukuzumi, S.; Itoh, A.; Suenobu, T.; Ohkubo, K. Formation of the Long-Lived Charge-Separated State of the 9-Mesityl-10-methylacridinium Cation Incorporated into Mesoporous Aluminosilicate at High Temperatures. *J. Phys. Chem. C* **2014**, *118*, 24188-24196.

(556) Basili, S.; Del Giacco, T.; Elisei, F.; Germani, R. An Acridinium-Based Sensor as a Fluorescent Photoinduced Electron Transfer Probe for Proton Detection Modulated by Anionic Micelles. *Org. Biomol. Chem.* **2014**, *12*, 6677-6683.

(557) Yamaguchi, S.; Kishikawa, N.; Ohyama, K.; Ohba, Y.; Kohno, M.; Masuda, T.; Takadate, A.; Nakashima, K.; Kuroda, N. Evaluation of Chemiluminescence Reagents for Selective Detection of Reactive Oxygen Species. *Anal. Chim. Acta* **2010**, *665*, 74-78.

(558) del Giacco, T.; Carlotti, B.; De Solis, S.; Barbafina, A.; Elisei, F. Steady-State and Time-Resolved Investigations of a Crown Thioether Conjugated with Methylacridinium and its Complexes with Metal Ions. *Phys. Chem. Chem. Phys.* **2011**, *13*, 2188-2195.

(559) Wang, P.; Yao, Y.; Xue, M. A Novel Fluorescent Probe for Detecting Paraquat and Cyanide in Water Based on Pillar[5]arene/10-Methylacridinium Iodide Molecular Recognition. *Chem. Commun.* **2014**, *50*, 5064-5067.

(560) Fukuzumi, S.; Yukimoto, K.; Ohkubo, K. DNA Cleavage Induced by Thermal Electron Transfer from a Dimeric NADH Analogue to Acridinium Ions in the Presence of Oxygen. *J. Am. Chem. Soc.* **2004**, *126*, 12794-12795.

(561) Anderson, R. J.; Groundwater, P. W.; Huang, Y.; James, A. L.; Orenga, S.; Rigby, A.; Roger-Dalbert, C.; Perry, J. D. Synthesis and Evaluation of Novel Chromogenic Peptidase Substrates Based on 9-(4'-Aminophenyl)-10-Methylacridinium Salts as Diagnostic Tools in Clinical Bacteriology. *Bioorg. Med. Chem. Lett.* **2008**, *18*, 832-835.

(562) Kitaguchi, H.; Ohkubo, K.; Ogo, S.; Fukuzumi, S. Electron-Transfer Oxidation Properties of Unsaturated Fatty Acids and Mechanistic Insight into Lipoxygenases. *J. Phys. Chem. A* **2006**, *110*, 1718-1725.

(563) Reshetnyak, O. V.; Koval'chuk, E. P.; Blazejowski, J. Role of Molecular Oxygen and its Active Forms in Generation of Electrochemiluminescence. *Russian J. Electrochem.* **2011**, *47*, 1111-1118.

(564) Vladimirov, Y. A.; Proskurnina, E. V.; Izmailov, D. Y. Chemiluminescence as a Method for Detection and Study of Free Radicals in Biological Systems. *Bull. Exp. Biol. Med.* **2007**, *144*, 390-396.

(565) Segundo, M. A.; Castro, C.; Magalhaes, L. M.; Reis, S. Determination of Scavenging Capacity Against Hydrogen Peroxide: Recent Trends on Chemical Methods. Ed. Aguilar, G.; Guzman, R. A. in *Hydrogen Peroxide: Detection, Applications and Health Implications.* **2013**, 203-218.

(566) Rodriguez-Rodriguez, R.; Simonsen, U. Measurement of Nitric Oxide and Reactive Oxygen Species in the Vascular Wall. *Curr. Anal. Chem.* **2012**, *8*, 485-494.

(567) Muenzel, T.; Afanas'ev, I. B.; Kleschyov, A. L.; Harrison, D. G. Detection of Superoxide in Vascular Tissue. *Arterioscler. Thromb. Vasc. Biol.* **2002**, *22*, 1761-1768.

(568) Biwersi, J.; Tulk, B.; Verkman, A. S. Long-Wavelength Chloride-Sensitive Fluorescent Indicators. *Anal. Biochem.* **1994**, *219*, 139-143.

(569) Healy, E. F.; Manzer, S.; Gorman, J.; Jones, A.; Cristea, N. A Dramatic Heavy-Atom Effect in the Quenching of Dichlorosubstituted Lucigenin Fluorescence. *Chem. Phys. Lett.* **2010**, *485*, 258-261.

(570) Papadopoulos, K.; Spartalis, S.; Nikokavouras, J. Chemiluminescence in Organized Molecular Assemblies: Lucigenin Derivatives Containing Long Alkyl Chains in Micellar Media. *Anal. Chim. Acta* **1994**, *290*, 179-185.

(571) Hamitouche, A.; Haffas, M.; Boudjemaa, A.; Benammar, S.; Sehailia, M.; Bachari, K. Efficient Biosorption of Methylene Blue, Malachite Green and Methyl Violet Organic Pollutants on Biomass Derived from *Anethum graveolens*: An Eco-Benign Approach for Wastewater Treatment. *Desalin. Water Treat.* **2017**, *75*, 225-236.

(572) de Azevedo, A. C. N.; Vaz, M. G.; Gomes, R. F.; Pereira, A. G. B.; Fajardo, A. R.; Rodrigues, F. H. A. Starch/Rice Husk Ash Based Superabsorbent Composite: High Methylene Blue Removal Efficiency. *Iran. Polym. J*. **2017**, *26*, 93-105.

(573) Nejdl, L.; Zelnickova, J.; Vaneckova, T.; Hynek, D.; Adam, V.; Vaculovicova, M. Rapid Preparation of Self-Assembly CdTe Quantum Dots Used for Sensing of DNA in Urine. *New J. Chem.* 2018, *42*, 6005-6012.

(574) Hai, J.; Chen, F.; Su, J.; Xu, F.; Wang, B. Porous Wood Members-Based Amplified Colorimetric Sensor for Hg2+ Detection through Hg2+-Triggered Methylene Blue Reduction Reactions. *Anal. Chem.* **2018**, *90*, 4909-4915.

(575) Kumar, R.; Umar, A.; Rana, D. S.; Sharma, P.; Chauhan, M. S.; Chauhan, S. Fe-Doped ZnO Nanoellipsoids for Enhanced Photocatalytic and Highly Sensitive and Selective Picric Acid Sensor. *Mater. Res. Bull.* **2018**, *102*, 282-288.

(576) Roy, A.; Roy, S.; Pradhan, A.; Maiti Choudhury, S.; Ranjan Nayak, R. Gel-Emulsion Properties of Nontoxic Nicotinic Acid-Derived Glucose Sensor. *Ind. Eng. Chem. Res.* **2018**, *57*, 2847-2855.

(577) Zhou, X.; Zhao, G.; Chen, M.; Gao, W.; Zhou, X.; Xie, X.; Yang, L.; Du, G. Facile and Green Approach to Prepare Nanostructured Au@MnO2 and Its Applications for Catalysis and Fluorescence Sensing of Glutathione in Human Blood. *ACS Sustain. Chem. Eng.* **2018**, *6*, 3948-3956.

(578) Delport, A.; Harvey, B. H.; Petzer, A.; Petzer, J. P. Methylene Blue and its Analogues as Antidepressant Compounds. *Metab. Brain Dis.* **2017**, *32*, 1357-1382.

(579) van Schalkwyk, D. A.; Nash, M. N.; Shafik, S. H.; Summers, R. L.; Lehane, A. M.; Smith, P. J.; Martin, R. E. Verapamil-Sensitive Transport of Quinacrine and Methylene Blue via the *Plasmodium falciparum* Chloroquine Resistance Transporter Reduces the Parasite's Susceptibility to these Tricyclic Drugs. *J. Infect. Dis.* **2016**, *213*, 800-810.

(580) Tucker, D.; Lu, Y.; Zhang, Q. From Mitochondrial Function to Neuroprotection-an Emerging Role for Methylene Blue. *Molec. Neurobiol.* **2018**, *55*, 5137-5153.

(581) Kiernan, J. A. Classification and Naming of Dyes, Stains and Fluorochromes. *Biotech. Histochem.* **2001**, *76*, 261-278.

(582) Francois, J.; Germe, K.; Ferrandon, A.; Koning, E.; Nehlig, A. Carisbamate has Powerful Disease-Modifying Effects in the Lithium-Pilocarpine Model of Temporal Lobe Epilepsy. *Neuropharmacol*. **2011**, *61*, 313-328.

(583) Popp, A.; Jaenisch, N.; Witte, O. W.; Frahm, C. Identification of Ischemic Regions in a Rat Model of Stroke. *PLoS One* **2009**, *4*; DOI: 10.1371/journal.pone.0004764.

(584) Francois, J.; Koning, E.; Ferrandon, A.; Nehlig, A. The Combination of Topiramate and Diazepam is Partially Neuroprotective in the Hippocampus but not Antiepileptogenic in the Lithium-Pilocarpine Model of Temporal Lobe Epilepsy. *Epilepsy Res.* **2006**, 72, 147-163.

(585) Mahmoudzadeh, M. A.; Madden, J. D. W. A Vertical Architecture for Increasing Photogalvanic Solar Cell Efficiency: Theory and Modeling. *Electrochim. Acta* **2014**, *143*, 98-105.

(586) Jana, A. K. Solar Cells Based on Dyes. *J. Photochem. Photobiol. A* **2000**, *132*, 1-17.

(587) Zhang, M.; Li, G.; Zhou, Q.; Pan, D.; Zhu, M.; Xiao, R.; Zhang, Y.; Wu, G.; Wan, Y.; Shen, Y. Boosted Electrochemical Immunosensing of Genetically Modified Crop Markers Using Nanobody and Mesoporous Carbon. *ACS Sens.* **2018**, *3*, 684-691.

(588) Yu, H.; Han, J.; An, S.; Xie, G.; Chen, S. Ce(III, IV)-MOF Electrocatalyst as Signal-Amplifying Tag for Sensitive Electrochemical Aptasensing. *Biosens. Bioelectron.* **2018**, *109*, 63-69.

(589) Dong, H.; Zou, F.; Li, H.; Zhu, H.; Koh, K.; Yin, Y.; Chen, H. Thionine Mediated Para-Sulfonatocalix[4]arene Capped AuNPs Multilayers for Sensitive Electrochemical Detection of Acetylcholinesterase Activity. *Electrochim. Acta* **2018**, *267*, 206-212.

(590) Chiou, B.-H.; Tsai, Y.-T.; Wang, C. M. Phenothiazine-Modified Electrodes: A Useful Platform for Protein Adsorption Study. *Langmuir* **2014**, *30*, 1550-1556.

(591) del Pozo, M.; Fernandez, A.; Quintana, C. On-Line Competitive Host-Guest Interactions in a Turn-On Fluorometric Method to Amantadine Determination in Human Serum and Pharmaceutical Formulations. *Talanta* **2018**, *179*, 124-130.

(592) Singh, H. K.; Saquib, M.; Haque, M. M.; Muneer, M. Heterogeneous Photocatalysed Decolorization of Two Selected Dye Derivatives Neutral Red and Toluidine Blue in Aqueous Suspensions. *Chem. Eng. J.* **2008**, *136*, 77-81.

(593) Cobianu, C. Stratulat, A.; Serban, B.; Buiu, O.; Piesker, A.; Farin, E. Protective Glove with Indicator of Remaining Lifetime. EP Patent 3251533, Dec 06, 2017.

(594) Zhang, X.; Lu, Y.; Liu, Z. Humidity-Sensitive Color-Changing Wallpaper, and Preparation Method Thereof. CN Patent 107386009, Nov 24, 2017.

(595) Ling, Z. Fluorescent Dyes for Anti-Counterfeiting Color Printing and its Manufacturing Process. CN Patent 106675207, May 17, 2017.

(596) Yang, W.; Ni, J.; Luo, F.; Weng, W.; Wei, Q.; Lin, Z.; Chen, G. Cationic Carbon Dots for Modification-Free Detection of Hyaluronidase via an Electrostatic-Controlled Ratiometric Fluorescence Assay. *Anal. Chem.* **2017**, *89*, 8384-8390.

(597) Gao, W.; Song, H.; Wang, X.; Liu, X.; Pang, X.; Zhou, Y.; Gao, B.; Peng, X. Carbon Dots with Red Emission for Sensing of Pt2+, Au3+, and Pd2+ and Their Bioapplications in Vitro and in Vivo. *ACS Appl. Mater. Interfaces* **2018**, *10*, 1147-1154.

(598) Prakash, A.; Pathrose, B. P.; Mathew, S.; Nampoori, V. P. N.; Radhakrishnan, R.; Mujeeb, A. Variations in Thermo-Optical Properties of Neutral Red Dye with Laser Ablated Gold Nanoparticles. *Opt. Mater.* **2018**, *79*, 237-242.

(599) Martinez, V.; Henary, M. Nile Red and Nile Blue: Applications and Synthesis of Structural Analogues. *Chem. Eur. J.* **2016**, *22*, 13764-13782.

(600) Madsen, J.; Canton, I.; Warren, N. J.; Themistou, E.; Blanazs, A.; Ustbas, B.; Tian, X.; Pearson, R.; Battaglia, G.; Lewis, A. L.; Armes, S. P. Nile Blue-Based Nanosized pH Sensors for Simultaneous Far-Red and Near-Infrared Live Bioimaging. *J. Am. Chem. Soc.* **2013**, *135*, 14863-14870.

(601) Ensafi, A. A.; Afiuni, S. A. S.; Rezaei, B. NiO Nanoparticles Decorated at Nile Blue-Modified Reduced Graphene Oxide, New Powerful Electrocatalysts for Water Splitting. *J. Electroanal. Chem.* **2018**, *816*, 160-170.

(602) Jin, H.; Zhao, C.; Gui, R.; Gao, X.; Wang, Z. Reduced Graphene Oxide/Nile Blue/Gold Nanoparticles Complex-Modified Glassy Carbon Electrode used as a Sensitive and Label-Free Aptasensor for Ratiometric Electrochemical Sensing of Dopamine. *Anal. Chem. Acta* **2018**, *1025*, 154-162.

(603) Harabuchi, Y.; Saita, K.; Maeda, S. Exploring Radiative and Nonradiative Decay Paths in Indole, Isoindole, Quinoline, and Isoquinoline. *Photochem. Photobiol. Sci*. **2018**, *17*, 315-322.

(604) Rahmani, F.; Darehkordi, A.; Ramezani, M.; Bazmandegan-Shamili, A. Synthesis and Photophysical Properties of 3-(Trifluoromethyl)-2H-imidazo[5,1-a]isoquinolinium Chloride Derivatives. *Synlett* **2018**, *29*, 296-300.

(605) Yatsimirsky, A. K. Host-Guest Chemistry of Alkaloids. *Nat. Prod. Commun.* **2012**, *7*, 369-380.

(606) Maafi, M.; Aaron, J.-J.; Mahedero, M. C.; Salinas, F. Spectrofluorimetric Study of a 2-Hydroxypropyl-β-Cyclodextrin Benzo[a]phenothiazine Inclusion Complex. *J. Fluorescence* **1997**, *7*, 11S-13S.

(607) Mitra, A. K.; Ghosh, S.; Sarangi, M. K.; Chakraborty, S.; Saha, C.; Basu, S. Photophysics of a Solvent Sensitive Keto-Tetrahydrocarbazole Based Fluorophore and its Interaction with Triethylamine: A Spectroscopic Inquest Under Surfactant and β-CD Confinement. *J. Molec. Struct.* **2014**, *1074*, 617-628.

(608) Yong, G.; Zhang, X.; She, W. Phosphorescence Enhancement of Organic Dyes by Forming β-Cyclodextrin Inclusion Complexes: Color Tunable Emissive Materials. *Dyes Pigments* **2013**, *97*, 65-70.

(609) Gandeepan, P.; Cheng, C.-H. Advancements in the Synthesis and Applications of Cationic N-Heterocycles through Transition Metal-Catalyzed C-H Activation. *Chem. Asian J.* **2016**, *11*, 448-460.

(610) Wang, Y.; Liu, Z.; Sun, J.; Liu, X.; Pei, M.; Zhang, G. A Turn-On Fluorescence Probe for Fe3+ Based-on Benzimidazo[2,1-α]benz[de]isoquinoline-7-one Derivatives. *J. Photochem. Photobiol. A* **2017**, *332*, 515-520.

(611) Kho, Y.-M.; Shin, E. J. Spiropyran-Isoquinoline Dyad as a Dual Chemosensor for Co(II) and In(III) Detection. *Molecules* **2017**, *22*, 1569/1-1569/13.

(612) Wang, Y.; Ma, Z.-Y.; Zhang, D.-L.; Deng, J.-L.; Chen, X.; Xie, C.-Z.; Qiao, X.; Li, Q.-Z.; Xu, J.-Y. Highly Selective and Sensitive Turn-On Fluorescent Sensor for Detection of Al3+ Based on Quinoline-Base Schiff Base. *Spectrochim. Acta A* **2018**, *195*, 157-164.

(613) Meka, R. K.; Heagy, M. D. Selective Modulation of Internal Charge Transfer and Photoinduced Electron Transfer Processes in N-Aryl-1,8-Naphthalimide Derivatives: Applications in Reaction-Based Fluorogenic Sensing of Sulfide. *J. Org. Chem.* **2017**, *82*, 12153-12161.

(614) Cushnie, T. P. T.; Cushnie, B.; Lamb, A. J. Alkaloids: An Overview of Their Antibacterial, Antibiotic-Enhancing and Antivirulence Activities. *Int. J. Antimicrob. Agents* **2014**, *44*, 377-386.

(615) Liu, Q.; Zhu, L.; Cheng, C.; Hu, Y.-y.; Feng, Q. Natural Active Compounds from Plant Food and Chinese Herbal Medicine for Nonalcoholic Fatty Liver Disease. *Curr. Pharm. Des.* **2017**, *23*, 5136-5162.

(616) Zhang, L.; Tian, K.; Wang, Y.; Zou, J.; Du, Z. Characterization of Ancient Chinese Textiles by Ultra-High Performance Liquid Chromatography/Quadrupole-Time of Flight Mass Spectrometry. *Int. J. Mass Spectrom*. **2017**, *421*, 61-70.

(617) Jash, C.; Kumar, G. S. Binding of Alkaloids Berberine, Palmatine and Coralyne to Lysozyme: A Combined Structural and Thermodynamic Study. *RSC Adv.* **2014**, *4*, 12514-12525.

(618) Domingo, M. P.; Pardo, J.; Cebolla, V.; Galvez, E. M. Berberine, a Fluorescent Alkaloid with a Variety of Applications from Medicine to Chemistry. Mini-Rev. *Org. Chem*. **2010**, *7*, 335-340.

(619) Yang, C.-Z.; Liang, C.-Y.; Zhang, D.; Hu, Y.-J. Deciphering the Interaction of Methotrexate with DNA: Spectroscopic and Molecular Docking Study. *J. Molec. Liquids* **2017**, *248*, 1-6.

(620) Park, J.-H.; Byun, J.-Y.; Jang, H.; Hong, D.; Kim, M.-G. A Highly Sensitive and Widely Adaptable Plasmonic Aptasensor Using Berberine for Small-Molecule Detection. *Biosens. Bioelectron.* **2017**, *97*, 292-298.

(621) Zhao, Y.; Zhou, H.; Shen, J.; Wang, M.; Wu, X. Study on the Interaction of Berberine with Nucleic Acids in the Presence of Silver Nanoparticles, and the Fluorometric Determination of Nucleic Acids. *RSC Adv*. **2016**, *6*, 29612-29618.

(622) Chang, Y. X.; Duan, X. C.; Zhang, X. M.; Liu, F.; Du, L. M. A New Fluorometric Method for the Determination of Oxaliplatin Based on Cucurbit[7]uril Supramolecular Interaction. *Australian J. Chem.* **2017**, *70*, 677-682.

(623) Lu, S.; Li, G.; Lv, Z.; Qiu, N.; Kong, W.; Gong, P.; Chen, G.; Xia, L.; Guo, X.; You, J.; Wu, Y. Facile and Ultrasensitive Fluorescence Sensor Platform for Tumor Invasive Biomarker β-Glucuronidase Detection and Inhibitor Evaluation with Carbon Quantum Dots Based on Inner-Filter Effect. *Biosens. Bioelectron.* **2016**, *85*, 358-362.

(624) Stahl, A.; Lazar, A. I.; Muchemu, V. N.; Nau, W. M.; Ullrich, M. S.; Hennig, A. A Fluorescent, Supramolecular Chemosensor to Follow Steroid Depletion in Bacterial Cultures. Anal. Bioanal. Chem. 2017, 409, 6485-6494.

(625) Wang, Y.-X.; Pang, W.-Q.; Zeng, Q.-X.; Deng, Z.-S.; Fan, T.-Y.; Jiang, J.-D.; Deng, H.-B.; Song, D.-Q. Synthesis and Biological Evaluation of New Berberine Derivatives as Cancer Immunotherapy Agents Through Targeting IDO1. *Eur. J. Med. Chem.* **2018**, *143*, 1858-1868.

(626) Rios, J. L.; Francini, F.; Schinella, G. R. Natural Products for the Treatment of Type 2 Diabetes Mellitus. *Planta Medica* **2015**, *81*, 975-994.

(627) Zhang, Q.; Chen, C.; Wang, F.-Q.; Li, C.-H.; Zhang, Q.-H.; Hu, Y.-J.; Xia, Z.-N.; Yang, F.-Q. Simultaneous Screening and Analysis of Antiplatelet Aggregation Active Alkaloids from Rhizoma Corydalis. *Pharmacetical Biol.* **2016**, *54*, 3113-3120.

(628) Hu, Y.; Lin, F.; Wu, T.; Wang, Y.; Zhou, X.-S.; Shao, Y. Fluorescently Sensing of DNA Triplex Assembly Using an Isoquinoline Alkaloid as Selector, Stabilizer, Inducer, and Switch-On Emitter. *Chem. Asian J.* **2016**, *11*, 2041-2048.

(629) Padmapriya K.; Barthwal, R. Structural and Biophysical Insight into Dual Site Binding of the Protoberberine Alkaloid Palmatine to Parallel G-Quadruplex DNA Using NMR, Fluorescence and Circular Dichroism Spectroscopy. *Biochim.* **2018**, *147*, 153-169.

(630) Yang, H.; Yao, W.; Wang, Y.; Shi, L.; Su, R.; Wan, D.; Xu, N.; Lian, W.; Chen, C.; Liu, S. High-Throughput Screening of Triplex DNA Binders from Complicated Samples by 96-Well Plate Format in Conjunction with Peak Area-Fading UHPLC-Orbitrap MS. *Analyst* **2017**, *142*, 670-675.

(631) Wu, J.; Xiao, Q.; Zhang, N.; Xue, C.; Leung, A. W.; Zhang, H.; Xu, C.; Tang, Q.-J. Photodynamic Action of Palmatine Hydrochloride on Colon Adenocarcinoma HT-29 Cells. *Photodiagnosis Photodyn. Ther.* **2016**, *15*, 53-58.

(632) Wu, J.; Xiao, Q.; Zhang, N.; Xue, C.; Leung, A. W.; Zhang, H.; Tang, Q.-J.; Xu, C. Palmatine Hydrochloride Mediated Photodynamic Inactivation of Breast Cancer MCF-7 Cells: Effectiveness and Mechanism of Action. *Photodiagnosis Photodyn. Ther.* **2016**, *15*, 133-138.

(633) Jian-Hong, X.; Lin, S.; Li-Ming, D.; Cai-Ping, C.; Hao, W.; Yin-Xia, C. Determination of Cetylpyridinium Chloride Employing a Sensitive Fluorescent Probe. *Anal. Chem. Indian J.* **2016**, *16*, 1-16.

(634) Mao, Z.; Wang, X.; Di, X.; Liu, Y.; Zang, Y.; Ma, D.; Liu, Y. Quantitative Detection of Ambroxol in Human Plasma Using HPLC-APCI-MS/MS: Application to a Pharmacokinetic Study. *Anal. Sci.* **2017**, *33*, 1099-1103.

(635) Shi, L.; Xie, J.-H.; Du, L.-M.; Chang, Y.-X.; Wu, H. Determination of Phenformin Hydrochloride Employing a Sensitive Fluorescent Probe. *Spectrochim. Acta A* **2016**, *162*, 98-104.

(636) Huang, H.; Shi, S.; Zheng, X.; Yao, T. Sensitive Detection for Coralyne and Mercury Ions Based on Homo-A/T DNA by Exonuclease Signal Amplification. *Biosens. Bioelectron.* **2015**, *71*, 439-444.

(637) Zhang, C.-X.; Jing, X.; Du, L.-M.; Liu, H.-L.; You, J.-C.; Chang, Y.-F.; Bai, B.; Fu, Y.-L. A Fluorescent Probe for the Detection of Clorprenaline and its Analytical Application. *J. Indian Chem. Soc.* **2014**, *91*, 1817-1824.

(638) Tan, H.-L.; Chan, K.-G.; Pusparajah, P.; Duangjai, A.; Saokaew, S.; Khan, T. M.; Lee, L.-H.; Goh, B.-H. Rhizoma Coptidis: A Potential Cardiovascular Protective Agent. *Frontiers Pharmacol.* **2016**, *7*, 362/1-362/13.

(639) Chang, Y.-X.; Zhang, X.-M.; Duan, X.-C.; Liu, F.; Du, L.-M. Supramolecular Interaction of Methotrexate with Cucurbit[7]uril and Analytical Application. *Spectrochim. Acta A* **2017**, *183*, 131-137.

(640) Chen, W.-H.; Qin, Y.; Cai, Z.; Chan, C.-L.; Luo, G.-A.; Jiang, Z.-H. Spectrometric Studies of Cytotoxic Protoberberine Alkaloids Binding to Double-Stranded DNA. *Bioorganic Med. Chem.* **2005**, *13*, 1859-1866.

(641) Wang, Y.; Hu, Y.; Wu, T.; Zhang, L.; Liu, H.; Zhou, X.; Shao, Y. Recognition of DNA Abasic Site Nanocavity by Fluorophore-Switched Probe: Suitable for All Sequence Environments. *Spectrochim. Acta A* **2016**, *153*, 645-650.

(642) Zeng, W.; Qi, Q.; Wu, J. Toward Long Rylene Ribbons and Quinoidal Rylene Diradicaloids. *Eur. J. Org. Chem.* **2018**, *2018*, 7-17.

(643) Zhao, X.; Xiong, Y.; Ma, J.; Yuan, Z. Rylene and Rylene Diimides: Comparison of Theoretical and Experimental Results and Prediction for High-Rylene Derivatives. *J. Phys. Chem. A* **2016**, *120*, 7554-7560.

(644) Feng, J.; Jiang, W.; Wang, Z. Synthesis and Application of Rylene Imide Dyes as Organic Semiconducting Materials. *Chem. Asian J.* **2018**, *13*, 20-30.

(645) La Porte, N. T.; Martinez, J. F.; Hedström, S.; Rudshteyn, B.; Phelan, B. T.; Mauck, C. M.; Young, R. M.; Batista, V. S. Wasielewski, M. R. Photoinduced Electron Transfer from Rylenediimide Radical Anions and Dianions to Re(bpy)(CO)3 using Red and Near-Infrared Light. *Chem. Sci.* **2017**, *8*, 3821-3831.

(646) Soh, N.; Ueda, T. Perylene Bisimide as a Versatile Fluorescent Tool for Environmental and Biological Analysis: A Review. *Talanta* **2011**, *85*, 1233-1237.

(647) Jozeliunaite, A.; Striela, R.; Labanauskas, L.; Orentas, E. Practical Preparation of Octa- and Tetrabromoperylene Diimides and Derivatives Thereof. *Synthesis* **2017**, *49*, 5176-5182.

(648) Pasaogullari, N.; Icil, H.; Demuth, M. Symmetrical and Unsymmetrical Perylene Diimides: Their Synthesis, Photophysical and Electrochemical Properties. *Dyes Pigments* **2006**, *69*, 118-127.

(649) Alvino, A.; Franceschin, M.; Cefaro, C.; Borioni, S.; Ortaggi, G.; Bianco, A. Synthesis and Spectroscopic Properties of Highly Water-Soluble Perylene Derivatives. *Tetrahedron* **2007**, *63*, 7858-7865.

(650) Gao, G.; Liang, N.; Geng, H.; Jiang, W.; Fu, H.; Feng, J.; Hou, J.; Feng, X.; Wang, Z. Spiro-Fused Perylene Diimide Arrays. *J. Am. Chem. Soc.* **2017**, *139*, 15914-15920.

(651) Wang, H.; Chen, L.; Xiao, Y. Perylene Diimide Arrays: Promising Candidates for Non-Fullerene Organic Solar Cells. *J. Mater. Chem. C* **2017**, *5*, 12816-12824.

(652) Liu, Y.; Cole, M. D.; Jiang, Y.; Kim, P. Y.; Nordlund, D.; Emrick, T.; Russell, T. P. Chemical and Morphological Control of Interfacial Self-Doping for Efficient Organic Electronics. *Adv. Mater.* **2018**, *Ahead of Print*; DOI: 10.1002/adma.201705976.

(653) Villafiorita-Monteleone, F.; Kozma, E.; Giovanella, U.; Catellani, M.; Paolino, M.; Collico, V.; Colombo, M.; Cappelli, A.; Botta, C. Red and Deep-Red Emissive Polymeric Nanoparticles Based on Polybenzofulvene and Perylenediimide Derivatives. *Dyes Pigments* **2018**, *149*, 331-335.

(654) Tuerkmen, G.; Erten-Ela, S.; Icli, S. Highly Soluble Perylene Dyes: Synthesis, Photophysical and Electrochemical Characterizations. *Dyes Pigments* **2009**, *83*, 297-303.

(655) Oh, J. H.; Lee, W.-Y.; Noe, T.; Chen, W.-C.; Koenemann, M.; Bao, Z. Solution-Shear-Processed Quaterrylene Diimide Thin-Film Transistors Prepared by Pressure-Assisted Thermal Cleavage of Swallow Tails. *J. Am. Chem. Soc.* **2011**, *133*, 4204-4207.

(656) Jiang, W.; Li, Y.; Wang, Z. Tailor-Made Rylene Arrays for High Performance n-Channel Semiconductors. *Acc. Chem. Res.* **2014**, *47*, 3135-3147.

(657) Davies, M.; Jung, C.; Wallis, P.; Schnitzler, T.; Li, C.; Muellen, K.; Braeuchle, C. Photophysics of New Photostable Rylene Derivatives: Applications in Single-Molecule Studies and Membrane Labelling. *ChemPhysChem* **2011**, *12*, 1588-1595.

(658) Roy, B.; Noguchi, T.; Tsuchiya, Y.; Yoshihara, D.; Yamamoto, T.; Shinkai, S. Molecular Recognition Directed Supramolecular Control Over Perylene-Bisimide Aggregation Resulting in Aggregation Induced Enhanced Emission (AIEE) and Induced Chiral Amplification. *J. Mater. Chem. C* **2015**, *3*, 2310-2318.

(659) Kobaisi, M. A.; Bhosale, S. V.; Latham, K.; Raynor, A. M.; Bhosale, S. V. Functional Naphthalene Diimides: Synthesis, Properties, and Applications. *Chem. Rev.* **2016**, *116*, 11685-11796.

(660) Huang, C.; Barlow, S.; Marder, S. R. Perylene-3,4,9,10-Tetracarboxylic Acid Diimides: Synthesis, Physical Properties, and Use in Organic Electronics. *J. Org. Chem.* **2011**, *76*, 2386-2407.

(661) Chen, L.; Li, C.; Muellen, K. Beyond Perylene Diimides: Synthesis, Assembly and Function of Higher Rylene Chromophores. *J. Mater. Chem. C* **2014**, *2*, 1938-1956.

(662) Andrew, T. L.; Swager, T. M. Thermally Polymerized Rylene Nanoparticles. *Macromolecules* **2011**, *44*, 2276-2281.

(663) Liu, Z.; Wu, Y.; Zhang, Q.; Gao, X. Non-Fullerene Small Molecule Acceptors Based on Perylene Diimides. *J. Mater. Chem. A* **2016**, *4*, 17604-17622.

(664) Stappert, S.; Li, C.; Muellen, K.; Basche, T. Synthesis of an Acceptor-Donor-Acceptor Multichromophore Consisting of Terrylene and Perylene Diimides for Multistep Energy Transfer Studies. *Chem. Mater.* **2016**, *28*, 906-914.

(665) Yasarapudi, V. B.; Frazer, L.; Webb, J. E. A.; Gallaher, J. K.; Macmillan, A.; Falber, A.; Thordarson, P.; Schmidt, T. W. Competing Energy Transfer Pathways in a Five-Chromophore Perylene Array. *J. Phys. Chem. C* **2018**, *122*, 13937-13943.

(666) Park, H. J.; So, M. C.; Gosztola, D.; Wiederrecht, G. P.; Emery, J. D.; Martinson, A. B. F.; Er, S.; Wilmer, C. E.; Vermeulen, N. A.; Aspuru-Guzik, A.; Stoddart, J. F.; Farha, O. K.; Hupp, J. T. Layer-by-Layer Assembled Films of Perylene Diimide- and Squaraine-Containing Metal-Organic Framework-like Materials: Solar Energy Capture and Directional Energy Transfer. *ACS Appl. Mater. Interfaces* **2016**, *8*, 24983-24988.

(667) Wu, C.; Zheng, Y.; Szymanski, C.; McNeill, J. Energy Transfer in a Nanoscale Multichromophoric System: Fluorescent Dye-Doped Conjugated Polymer Nanoparticles. *J. Phys. Chem. C* **2008**, *112*, 1772-1781.

(668) Chen, C.-y.; Wang, K.; Gu, L.-l.; Li, H. The Study of Perylene Diimide-Amino Acid Derivatives for the Fluorescence Detection of Anions. *RSC Adv.* **2017**, *7*, 42685-42689.

(669) Makam, P.; Shilpa, R.; Kandjani, A. E.; Periasamy, S. R.; Sabri, Y. M.; Madhu, C.; Bhargava, S. K.; Govindaraju, T. SERS and Fluorescence-Based Ultrasensitive Detection of Mercury in Water. *Biosensors Bioelectronics* **2018**, *100*, 556-564.

(670) Yao, Q.; Lu, B.; Ji, C.; Cai, Y.; Yin, M. Supramolecular Host-Guest System as Ratiometric Fe3+ Ion Sensor Based on Water-Soluble Pillar[5]arene. *ACS Appl. Mater. Interfaces* **2017**, *9*, 36320-36326.

(671) Li, D.; Yang, J.; Zhao, J. Positioning a Fluorescent Probe at the Core of a Glassy Star Polymer for Detection of Local Dynamics. *Chinese Chem. Lett.* **2018**, *29*, 374-380.

(672) Guo, L.; Zhang, Z.; Tang, Y. Cationic Conjugated Polymers as Signal Reporter for Label-Free Assay Based on Targets-Mediated Aggregation of Perylene Diimide Quencher. *Chinese Chem. Lett.* **2018**, *29*, 305-308.

(673) Becker, H.-C.; Broo, A.; Norden, B. Ground- and Excited-State Properties of Molecular Complexes between Adenine and 2,7-Diazapyrene and Its N-Methylated Cations. *J. Phys. Chem. A* **1997**, *101*, 8853-8860.

(674) Malinge, J.-M.; Sip, M.; Blacker, A. J.; Lehn, J.-M.; Leng, M. Formation of a DNA Monofunctional cis-Platinum Adduct Cross-Linking the Intercalating Drug N-Methyl-2,7-Diazapyrenium. *Nucleic Acids Res.* **1990**, *18*, 3887-3891.

(675) Becker, H.-C.; Norden, B. DNA Binding Properties of 2,7-Diazapyrene and Its N-Methylated Cations Studied by Linear and Circular Dichroism Spectroscopy and Calorimetry. *J. Am. Chem. Soc.* **1997**, *119*, 5798-5803.

(676) Wagner, B. D. The Use of Coumarins as Environmentally-Sensitive Fluorescent Probes of Heterogeneous Inclusion Systems. *Molecules* **2009**, *14*, 210-237.

(677) Katerinopoulos, H. E. The Coumarin Moiety as Chromophore of Fluorescent Ion Indicators in Biological Systems. *Curr. Pharmaceutical Design* **2004**, *10*, 3835-3852.

(678) Zambare, A. S.; Kalam Khan, F. A.; Zambare, S. P.; Shinde, S. D.; Sangshetti, J. N. Recent Advances in the Synthesis of Coumarin Derivatives via Pechmann Condensation. *Curr. Org. Chem.* **2016**, *20*, 798-828.

(679) Klenkar, J.; Molnar, M. Natural and Synthetic Coumarins as Potential Anticancer Agents. *J. Chem. Pharmaceutical Res.* **2015**, *7*, 1223-1238.

(680) Camur, M.; Durmus, M.; Bulut, M. Highly Singlet Oxygen Generative Water-Soluble Coumarin Substituted Zinc(II) Phthalocyanine Photosensitizers for Photodynamic Therapy. *Polyhedron* **2012**, *41*, 92-103.

(681) Ethiraj, A. S.; Kharrazi, S.; Hebalkar, N.; Urban, J.; Sainkar, S. R.; Kulkarni, S. K. Highly Photostable Dye Entrapped Core-Shell Particles. *Mater. Lett.* **2007**, *61*, 4738-4742.

(682) Plajnsek, K. T.; Pajk, S.; Govedarica, B.; Pecar, S.; Srcic, S.; Kristl, J. A Novel Fluorescent Probe for More Effective Monitoring of Nanosized Drug Delivery Systems Within the Cells. *Int. J. Pharmaceutics* **2011**, *416*, 384-393.

(683) Aliaga, M. E.; Garcia-Rio, L.; Pessego, M.; Montecinos, R.; Fuentealba, D.; Uribe, I.; Martin-Pastor, M.; Garcia-Beltran, O. Host-Guest Interaction of Coumarin-Derivative Dyes and Cucurbit[7]uril: Leading to the Formation of Supramolecular Ternary Complexes with Mercuric Ions. *New. J. Chem.* **2015**, *39*, 3084-3092.

(684) Gupta, M.; Maity, D. K.; Nayak, S. K.; Ray, A. K. Modulation of Photophysics and Photostability of Cationic Coumarin 1 Dye Upon Inclusion with Macrocyclic Host Cucurbit[7]uril. *J. Photochem. Photobiol. A: Chem.* **2015**, *300*, 15-21.

(685) Tang, S.; Zhang, Y.; Thapaliya, E. R.; Brown, A. S.; Wilson, J. N.; Raymo, F. M. Highlighting Cancer Cells with Halochromic Switches. *ACS Sensors* **2017**, *2*, 92-101.

(686) Wu, G.; Gao, Q.; Li, M.; Tang, X.; Lai, K. W. C.; Tong, Q. A Ratiometric Probe Based on Coumarin-Quinoline for Highly Selective and Sensitive Detection of Zn2+ Ions in Living Cells. *J. Photochem. Photobiol. A: Chem.* **2018**, *355*, 487-495.

(687) Babur, B.; Seferoglu, N.; Seferoglu, Z. A Coumarin-Pyrazolone Based Fluorescent Probe for Selective Colorimetric and Fluorimetric Fluoride Detection: Synthesis, Spectroscopic Properties and DFT Calculations. *J. Molec. Structure* **2018**, *1161*, 218-225.

(688) Yan, J.-w.; Tian, Y.-g.; Tan, J.-h.; Huang, Z.-s. Colorimetric and Fluorescence Detection of G-Quadruplex Nucleic Acids with a Coumarin-Benzothiazole Probe. *Analyst* **2015**, *140*, 7146-7149.

(689) Sonu; Tiwari, A. K.; Kumari, S.; Saha, S. K. Study on Intramolecular Charge Transfer Processes, Solvation Dynamics and Rotational Relaxation of Coumarin 490 in Reverse Micelles of Cationic Gemini Surfactant. *RSC Adv.* **2014**, *4*, 25210-25219.

(690) Ruiz, C. C.; Hierrezuelo, J. M.; Molina-Bolivar, J. A. Analysis of the Photophysical Behavior and Rotational-Relaxation Dynamics of Coumarin 6 in Nonionic Micellar Environments: The Effect of Temperature. *Molecules* **2015**, *20*, 19343-19360.

(691) Okamoto, A. Excitonic Interaction: Another Photophysical Process for Fluorescence-Controlled Nucleic Acid Sensing. *Chem. Record* **2010**, *10*, 188-196.

(692) Okamoto, A. Thiazole Orange-Tethered Nucleic Acids and ECHO Probes for Fluorometric Detection of Nucleic Acids. *Nucleic Acids Molec. Biol.* **2016**, *31*, 63-81.

(693) Okamoto, A. ECHO Probes: A Concept of Fluorescence Control for Practical Nucleic Acid Sensing. *Chem. Soc. Rev.* **2011**, *40*, 5815-5828.

(694) Liang, M.; Liu, X.; Cheng, D.; Nakamura, K.; Wang, Y.; Dou, S.; Liu, G.; Rusckowski, M.; Hnatowich. D. J. Optical Antisense Tumor Targeting in Vivo with an Improved Fluorescent DNA Duplex Probe. *Bioconjugate Chem.* **2009**, *20*, 1223-1227.

(695) Hoevelmann, F.; Gaspar, I.; Loibl, S.; Ermilov, E. A.; Roeder, B.; Wengel, J.; Ephrussi, A.; Seitz, O. Brightness Through Local Constraint-LNA-Enhanced FIT Hybridization Probes for in Vivo Ribonucleotide Particle Tracking. *Angew. Chem. Int. Ed.* **2014**, *53*, 11370-11375.

(696) Kam, Y.; Rubinstein, A.; Nissan, A.; Halle, D.; Yavin, E. Detection of Endogenous K-ras mRNA in Living Cells at a Single Base Resolution by a PNA Molecular Beacon. *Molec. Pharmaceutics* **2012**, *9*, 685-693.

(697) Fei, X.; Gu, Y.; Wang, Y.; Meng, Q.; Zhang, B. Targeted Thiazole Orange Derivative with Folate: Synthesis, Fluorescence and in Vivo Fluorescence Imaging. *Molecules* **2010**, *15*, 6983-6992.

(698) Robinson, M.; Machin, S.; Mackie, I.; Harrison, P. In Vivo Biotinylation Studies: Specificity of Labelling of Reticulated Platelets by Thiazole Orange and Mepacrine. *British J. Haematology* **2000**, *108*, 859-864.

(699) Sun, C.; Su, R.; Bie, J.; Sun, H.; Qiao, S.; Ma, X.; Sun, R.; Zhang, T. Label-Free Fluorescent Sensor Based on Aptamer and Thiazole Orange for the Detection of Tetracycline. *Dyes Pigments* **2018**, *149*, 867-875.

(700) Qiu, H.; Pu, F.; Ran, X.; Ren, J.; Qu, X. A DNA-Based Label-Free Artificial Tongue for Pattern Recognition of Metal Ions. *Chem. Eur. J.* **2017**, *23*, 9258-9261.

(701) Zhang, B.; Wei, C. A Label-Free Fluorescent Sensor Based on Structure-Switching Oligonucleotides for the Detection of Ag+, Biothiols and Acetylcholinesterase Activity. *ChemistrySelect* **2017**, *2*, 6844-6849.

(702) Gu, C.; Xiang, Y.; Guo, H.; Shi, H. Label-Free Fluorescence Detection of Melamine with a Truncated Aptamer. *Analyst* **2016**, *141*, 4511-4517.

(703) Leung, K.-H.; He, H.-Z.; He, B.; Zhong, H.-J.; Lin, S.; Wang, Y.-T.; Ma, D.-L.; Leung, C.-H. Label-Free Luminescence Switch-On Detection of Hepatitis C Virus NS3 Helicase Activity Using a G-Quadruplex-Selective Probe. *Chem. Sci.* **2015**, *6*, 2166-2171.

(704) Hashim, S. N.; Tsuchiya, A.; Kamiya, N.; Sando, S. A Single Fluorophore-Labeled Aptamer Sensor for the Detection of Interferon Gamma. Chem. Lett. 2015, 44, 1670-1672.

(705) Murudkar, S.; Mora, A. K.; Jakka, S.; Singh, P. K.; Nath, S. Ultrafast Molecular Rotor Based DNA Sensor: An Insight into the Mode of Interaction. *J. Photochem. Photobiol., A* **2014**, *295*, 17-25.

(706) Bhasikuttan, A. C.; Choudhury, S. D.; Pal, H.; Mohanty, J. Supramolecular Assemblies of Thioflavin T with Cucurbiturils: Prospects of Cooperative and Competitive Metal Ion Binding. *Isr. J. Chem.* **2011**, *51*, 634-645.

(707) Zhang, Y.-M.; Zhang, X.-J.; Xu, X.; Fu, X.-N.; Hou, H.-B.; Liu, Y. Rigid Organization of Fluorescence-Active Ligands by Artificial Macrocyclic Receptor to Achieve the Thioflavin T-Amyloid Fibril Level Association. *J. Phys. Chem. B* **2016**, *120*, 3932-3940.

(708) Singh, P. K.; Kumbhakar, M.; Pal, H.; Nath, S. Confined Ultrafast Torsional Dynamics of Thioflavin-T in a Nanocavity. *Phys. Chem. Chem. Phys.* **2011**, *13*, 8008-8014.

(709) Gestwicki, J. E.; Crabtree, G. R.; Graef, I. A. Harnessing Chaperones to Generate Small-Molecule Inhibitors of Amyloid β Aggregation. *Science* **2004**, *306*, 865-869.

(710) Gilead, S.; Gazit, E. Inhibition of Amyloid Fibril Formation by Peptide Analogues Modified with α-Aminoisobutyric Acid. *Angew. Chem. Int. Ed.* **2004**, *116*, 4133-4136.

(711) Ban, T.; Yamaguchi, K.; Goto, Y. Direct Observation of Amyloid Fibril Growth, Propagation, and Adaption. *Acc. Chem. Res.* **2006**, *39*, 663-670.

(712) Saferstein, R. *Criminalistics: An Introduction to Forensic Science*, 9th ed.; Pearson Education, Inc.: New Jersey, 2007.

(713) Jones, P.; Frew, J. E.; Scowen, N. Inorganic Fireflies – A Chemiluminescent Clock Reaction. *J. Chem. Educ.* **1987**, *64*, 70-71.

(714) Chalmers, J. H.; Bradbury, M. W.; Fabricant, J. D. A Multicolored Luminol-Based Chemiluminescence Demonstration. *J. Chem. Educ.* **1987**, *64*, 969-970.

(715) Tian, K.; Li, D.; Tang, T.; Nie, F.; Zhou, Y.; Du, J.; Zheng, J. A Novel Electrochemiluminescence Resonance Energy Transfer System of Luminol-Graphene Quantum Dot Composite and its Applications in H2O2 Detection. *Talanta* **2018**, *185*, 446-452.

(716) Ouyang, H.; Wang, M.; Wang, W.; Fu, Z. Colorimetric/Chemiluminescent Immunochromatographic Test Strip by Using Luminol-Reduced Gold Nanoparticles as Dual-Response Probes. *Sens. Actuators B* **2018**, *266*, 318-322.

(717) Ouyang, H.; Li, Q.; Wang, W.; Song, Y.; Tu, X.; Zhu, C.; Smith, J. N.; Du, D.; Fu, Z.; Lin, Y. Dual-Readout Immunochromagraphic Assay by Utilizing MnO2 Nanoflowers as the Unique Colorimetric/Chemiluminescent Probe. *Anal. Chem.* **2018**, *1018*, 94-103.

(718) Li, F.; Zhang, Y.; Liu, J.; He, J. Luminol, Horseradish Peroxidase and Antibody Ternary Codified Gold Nanoparticles for a Label-Free Homogenous Chemiluminescent Immunoassay. *Anal. Methods* **2018**, *10*, 722-729.

(719) Ali, R.; Saleh, S. M.; Aly, S. M. Fluorescent Gold Nanoclusters as pH Sensors for the pH 5 to 9 Range and for Imaging of Blood Cell pH Values. *Microchim. Acta* **2017**, *184*, 3309-3315.

(720) Van der Schueren, L.; De Clerck, K. The Use of pH-Indicator Dyes for pH-Sensitive Textile Materials. *Textile Res. J.* **2010**, *80*, 590-603.

(721) Zhou, X.; Nie, J.; Du, B. Functionalized Ionic Microgel Sensor Array for Colorimetric Detection and Discrimination of Metal Ions. *ACS Appl. Mater. Interfaces* **2017**, *9*, 20913-20921.

(722) Grancia, M.; Fiedoruk-Pogrebniak, M.; Koncki, R.; Tymecki, Ł. Flow Injection Analysis in Lab-on-Paper Format. *Sens. Actuators B* **2018**, *257*, 16-22.

(723) Dhara, P.; Singh, V. K. Improved Mesostructure by Incorporating Surfactant on Thin Film to Develop an Advanced Optical Fiber pH Sensor with a Temperature Cross Sensitivity Feature. *Laser Phys.* **2017**, *27*, 035101/1-035101/6.

(724) Farnum, D. G.; Mehta, G.; Moore, G. G. I.; Siegal, F. P. Attempted Reformatskii Reaction of Benzonitrile. 1,4-Dioxo-3,6-diphenylpyrrolo[3,4-c]pyrrole, a Lactam Analog of Pentalene. *Tetrahedron Lett.* **1974**, *29*, 2549-2552.

(725) Kaur, M.; Choi, D. H. Diketopyrrolopyrrole: Brilliant Red Pigment Dye-Based Fluorescent Probes and Their Applications. *Chem. Soc. Rev.* **2015**, *44*, 58-77.

(726) Yang, X.; Zheng, L.; Xie, L.; Liu, Z.; Li, Y.; Ning, R.; Zhang, G.; Gong, X.; Gao, B.; Liu, C.; Cui, Y.; Sun, G.; Zhang, G. Colorimetric and On-Off Fluorescent Chemosensor for Fluoride Ion Based on Diketopyrrolopyrrole. *Sens. Actuators B* **2015**, *207*, 9-24.

(727) Yang, X.; Xie, L.; Ning, R.; Gong, X.; Liu, Z.; Li, Y.; Zheng, L.; Zhang, G.; Gao, B.; Cui, Y.; Sun, G.; Zhang, G. A Diketopyrrolopyrrole-Based Near-Infrared Sensor for Selective Recognition of Fluoride Ion. *Sens. Actuators B* **2015**, *210*, 784-794.

(728) Yang, X.; Zhang, G.; Li, Y.; Liu, Z.; Gong, X.; Gao, B.; Zhang, G.; Cui, Y.; Sun, G. Colorimetric and Fluorogenic Signalling for Fluoride Ions by Diketopyrrolopyrrole-Based Chemosensor. *RSC Adv.* **2015**, *5*, 22455-22462.

(729) Shou, K.; Tang, Y.; Chen, H.; Chen, S.; Zhang, L.; Zhang, A.; Fan, Q.; Yu, A.; Cheng, Z. Diketopyrrolopyrrole-Based Semiconducting Polymer Nanoparticles for In Vivo Second Near-Infrared Window Imaging and Image-Guided Tumor Surgery. *Chem. Sci.* **2018**, *9*, 3105-3110.

(730) Du, C.; Fu, S.; Ren, X.; Wang, X.; Wang, Z.; Zhou, J.; Wang, H. A Diketopyrrolopyrrole-Based Fluorescent Probe for Investigating Mitochondrial Zinc Ions. *New J. Chem.* **2018**, *42*, 3493-3502.

(731) Liang, P.; Wang, Y.; Wang, P.; Zou, J.; Xu, H.; Zhang, Y.; Si, W.; Dong, X. Triphenylamine Flanked Furan-Diketopyrrolopyrrole for Multi-Imaging Guided Photothermal/Photodynamic Cancer Therapy. *Nanoscale* **2017**, *9*, 18890-18896.

(732) Tang, A.; Zhan, C.; Yao, J.; Zhao, E. Design of Diketopyrrolopyrrole (DPP)-Based Small Molecules for Organic-Solar-Cell Applications. *Adv. Mater.* **2017**, *29*(2), 1600013/1-1600013/39.

(733) Li, W.; Hendriks, K. H.; Wienk, M. M.; Janssen, R. A. J. Diketopyrrolopyrrole Polymers for Organic Solar Cells. *Acc. Chem. Res.* **2016**, *49*, 78-85.

(734) Spiller, H. A. Rethinking Mercury: The Role of Selenium in the Pathophysiology of Mercury Toxicity. *Clinical Toxicol.* **2018**, *56*, 313-326.

(735) Melnikov, P.; Zanoni, L. Z. Clinical Effects of Cesium Intake. *Biol. Trace Element Res.* **2010**, *135*, 1-9.

(736) Suganya, S.; Kayalvizhi, K.; Senthil Kumar, P.; Saravanan, A.; Vinoth Kumar, V. Biosorption of Pb(II), Ni(II) and Cr(VI) Ions from Aqueous Solution Using *Rhizoclonium tortuosum*: Extended Application to Nickel Plating Industrial Wastewater. *Desalination Water Treatment* **2016**, *57*, 25114-25139.

(737) Gohara, D. W.; Di Cera, E. Molecular Mechanisms of Enzyme Activation by Monovalent Cations. *J. Biol. Chem.* **2016**, *291*, 20840-20848.

(738) Rothery, R. A.; Weiner, J. H. Shifting the Metallocentric Molybdoenzyme Paradigm: The Importance of Pyranopterin Coordination. *J. Biol. Inorganic Chem.* **2015**, *20*, 349-372.

(739) O'Halloran, T. V.; Kebede, M.; Philips, S. J.; Attie, A. D. Zinc, Insulin, and the Liver: A Menage a Trois. *J. Clinical Investigation* **2013**, *123*, 4136-4139.

(740) Seo, J.; Ali, A. K.; Rose, M. J. Novel Ligand Architectures for Metalloenzyme Modeling: Anthracene-Based Ligands for Synthetic Modeling of Mono-[Fe] Hydrogenase. *Comments Inorganic Chem.* **2014**, *34*, 103-113.

(741) Magura, I. S.; Bogdanova, N. A.; Dolgaya, E. V. Potassium Channels and Signal Transduction Pathways in Neurons. *Neurophysiol.* **2015**, *47*, 71-76.

(742) Bhutia, Y. D.; Kopel, J. J.; Lawrence, J. J.; Neugebauer, V.; Ganapathy, V. Plasma Membrane Na+-Coupled Citrate Transporter (SLC13A5) and Neonatal Epileptic Encephalopathy. *Molecules* **2017**, *22*, 378/1-378/15.

(743) Yano, S.; Brown, E. M.; Chattopadhyay, N. Calcium-Sensing Receptor in the Brain. *Cell Calcium* **2004**, *35*, 257-264.

(744) San-Cristobal, P.; Dimke, H.; Hoenderop, J. G. J.; Bindels, R. J. M. Novel Molecular Pathways in Renal Mg2+ Transport: A Guided Tour Along the Nephron. *Current Opinion Nephrology Hypertension* **2010**, *19*, 456-462.

(745) Mathieu, A.; Kajino, M.; Korsakissok, I.; Perillat, R.; Quelo, D.; Querel, A.; Saunier, O.; Sekiyama, T. T.; Igarashi, Y.; Didier, D. Fukushima Daiichi-Derived Radionuclides in the Atmosphere, Transport and Deposition in Japan: A Review. *Appl. Geochem.* **2018**, *91*, 122-139.

(746) Laidlaw, M. A. S.; Ball, A. S.; Filippelli, G. M.; Sadler, R. C.; Gonzales, C. R.; Mielke, H. W. Children's Blood Lead Seasonality in Flint, Michigan (USA), and Soil-Sourced Lead Hazard Risks. *Int. J. Environ. Res. Public Health* **2016**, *13*, 358.

(747) Busacca, C. A.; Fandrick, D. R.; Song, J. J.; Senanayake, C. H. The Growing Impact of Catalysis in the Pharmaceutical Industry. *Adv. Synth. Catal.* **2011**, *353*, 1825-1864.

(748) Vural Guersel, I.; Noel, T.; Wang, Q.; Hessel, V. Separation/Recycling Methods for Homogeneous Transition Metal Catalysts in Continuous Flow. *Green Chem.* **2015**, *17*, 2012-2026.

(749) Li, Z.; Wang, Y.; Ni, Y.; Kokot, S. A Rapid and Label-Free Dual Detection of Hg (II) and Cysteine with the Use of Fluorescence Switching of Graphene Quantum Dots. *Sensors Actuators B: Chem.* **2015**, *207*, 490-497.

(750) Katano, H.; Kuroda, Y.; Taira, S.; Maruyama, C.; Hamano, Y. Colorimetric Microtiter Plate Assay of Polycationic Aminoglycoside Antibiotics in Culture Broth Using Amaranth. *Anal. Sci.* **2017**, *33*, 499-504.

(751) Wu, W.; Chen, A.; Tong, L.; Qing, Z.; Langone, K. P.; Bernier, W. E.; Jones, W. E., Jr. Facile Synthesis of Fluorescent Conjugated Polyelectrolytes Using Polydentate Sulfonate as Highly Selective and Sensitive Copper(II) Sensors. *ACS Sensors* **2017**, *2*, 1337-1344.

(752) Pauric, A. D.; Jin, S.; Fuller, T. J.; Balogh, M. P.; Halalay, I. C.; Goward, G. R. NMR Determination of the Relative Binding Affinity of Crown Ethers for Manganese Cations in Aprotic Nonaqueous Lithium Electrolyte Solutions. *J. Phys. Chem. C* **2016**, *120*, 3677-3683.

(753) Demeter, D.; Blanchard, P.; Grosu, I.; Roncali, J. Poly(thiophenes) Derivatized with Linear and Macrocyclic Polyethers: From Cation Detection to Molecular Actuation. *J. Inclusion Phenom. Macrocyclic Chem.* **2008**, *61*, 227-239.

(754) Kim, J.; McQuade, D. T.; McHugh, S. K.; Swager, T. M. Ion-Specific Aggregation in Conjugated Polymers: Highly Sensitive and Selective Fluorescent Ion Chemosensor. *Angew. Chem. Int. Ed.* **2000**, *39*, 3868-3872.

(755) Liu, C.-L.; Zhang, R.-L.; Lin, C.-S.; Zhou, L.-P.; Cai, L.-X.; Kong, J.-T.; Yang, S.-Q.; Han, K.-L.; Sun, Q.-F. Intraligand Charge Transfer Sensitization on Self-Assembled Europium Tetrahedral Cage Leads to Dual-Selective Luminescent Sensing toward Anion and Cation. *J. Am. Chem. Soc.* **2017**, *139*, 12474-12479.

(756) Bogatko, S. A. Ion Solvation Structure and Dynamical Information via Deviations from the Solvent-Berg Diffusion Model. *Chem. Phys. Lett.* **2013**, *565*, 148-150.

(757) Rosenholm, J. B. Critical Evaluation of Dipolar, Acid-Base and Charge Interactions II. Charge Exchange Within Electrolytes and Electron Exchange with Semiconductors. *Adv. Colloid Interface Sci.* **2017**, *247*, 305-353.

(758) Xue, J.; Wang, X.; Jeong, J. H.; Yan, X. Spectral and Energy Transfer in Bi3+-Ren+ (n = 2, 3, 4) Co-Doped Phosphors: Extended Optical Applications. *Phys. Chem. Chem. Phys.* **2018**, *20*, 11516-11541.

(759) Papageorgiou, G. C.; Kalosaka, K.; Lagoyanni, T.; Sotiropoulou, G. The Role of Cations in the Photoinduced Electron Transport of Cyanobacteria. *NATO ASI Series A* **1985**, *91*, 369-391.

(760) Beneto, A. J.; Siva, A. A Pyridine - Containing Fluorescent Probe for the Detection of Trivalent Cations in Aqueous Medium and in the Solid State. *ChemistrySelect* **2016**, *1*, 3548-3554.

(761) Kumar, R.; Sandhu, S.; Singh, P.; Kumar, S. Imidazolium Based Probes for Recognition of Biologically and Medically Relevant Anions. *Chem. Record* **2017**, *17*, 441-471.

(762) Fang, C.; Dharmarajan, R.; Megharaj, M.; Naidu, R. Gold Nanoparticle-Based Optical Sensors for Selected Anionic Contaminants. *TrAC, Trends Anal. Chem.* **2017**, *86*, 143-154.

(763) Ermert, S.; Marx, A.; Hacker, S. M. Phosphate-Modified Nucleotides for Monitoring Enzyme Activity. *Topics Curr. Chem.* **2017**, *375*, 1-25.

(764) Su, J. B. Role of Bradykinin in the Regulation of Endothelial Nitric Oxide Synthase Expression by Cardiovascular Drugs. *Curr. Pharmaceutical Design* **2017**, *23*, 6215-6222.

(765) Ivanovski, O.; Drueeke, T. B. A New Era in the Treatment of Calcium Oxalate Stones? *Kidney Int.* **2013**, *83*, 998-1000.

(766) Israel, Y.; Quintanilla, M. E.; Karahanian, E.; Rivera-Meza, M.; Herrera-Marschitz, M. The "First Hit" Toward Alcohol Reinforcement: Role of Ethanol Metabolites. *Alcoholism: Clinical Experimental Res.* **2015**, *39*, 776-786.

(767) DeLeon, S. M.; Downey, J. D.; Hildenberger, D. M.; Rhoomes, M. O.; Booker, L.; Rockwood, G. A.; Basi, K. A. DMTS is an Effective Treatment in Both Inhalation and Injection Models for Cyanide Poisoning Using Unanesthetized Mice. *Clinical Toxicol.* **2018**, *56*, 332-341.

(768) Ma, H.; Bonnie, N. A.; Yu, M.; Che, S.; Wang, Q. Biological Treatment of Ammonium Perchlorate-Contaminated Wastewater: A Review. *J. Water Reuse Desalination* **2016**, *6*, 82-107.

(769) Goodarzi, F.; Mahvi, A. H.; Hosseini, M.; Nodehi, R. N.; Kharazifard, M. J.; Parvizishad, M. Fluoride Concentration of Drinking Water and Dental Fluorosis: A Systematic Review and Meta-Analysis in Iran. *Dental Hypotheses* **2016**, *7*, 81-87.

(770) Cubadda, F.; Jackson, B. P.; Cottingham, K. L.; Van Horne, Y. O.; Kurzius-Spencer, M. Human Exposure to Dietary Inorganic Arsenic and Other Arsenic Species: State of Knowledge, Gaps and Uncertainties. *Sci. Total Environ.* **2017**, *579*, 1228-1239.

(771) Ou, S.-C.; Cui, D.; Patel, S. Molecular Modeling of Ions at Interfaces: Exploring Similarities to Hydrophobic Solvation Through the Lens of Induced Aqueous Interfacial Fluctuations. *Phys. Chem. Chem. Phys.* **2016**, *18*, 30357-30365.

(772) Fisicaro, G.; Genovese, L.; Andreussi, O.; Mandal, S.; Nair, N. N.; Marzari, N.; Goedecker, S. Soft-Sphere Continuum Solvation in Electronic-Structure Calculations. *J. Chem. Theory Computation* **2017**, *13*, 3829-3845.

(773) Lee, S.; Flood, A. H. Binding Anions in Rigid and Reconfigurable Triazole Receptors. *Topics Heterocyclic Chem.* **2012**, *28*, 85-107.

(774) McDonald, K. P.; Hua, Y.; Lee, S.; Flood, A. H. Shape Persistence Delivers Lock-and-Key Chloride Binding in Triazolophanes. *Chem. Commun.* **2012**, *48*, 5065-5075.

(775) Kim, T.-H.; Kim, I.-J.; Yoo, M.-J.; Swager, T. M. Development of Highly Selective Fluorescent Chemosensors for Fluoride Ion. *J. Korean Chem. Soc.* **2007**, *51*, 258-264.

(776) Marzooghi, S.; Di Toro, D. M. A Critical Review of Polycyclic Aromatic Hydrocarbon Phototoxicity Models. *Environ. Toxicol. Chem.* **2017**, *36*, 1138-1148.

(777) Abbas, I.; Badran, G.; Verdin, A.; Ledoux, F.; Roumie, M.; Courcot, D.; Garcon, G. Polycyclic Aromatic Hydrocarbon Derivatives in Airborne Particulate Matter: Sources, Analysis and Toxicity. *Environ. Chem. Lett.* **2018**, *16*, 439-475.

(778) Davie-Martin, C. L.; Stratton, K. G.; Teeguarden, J. G.; Waters, K. M.; Simonich, S. L. M. Implications of Bioremediation of Polycyclic Aromatic Hydrocarbon-Contaminated Soils for Human Health and Cancer Risk. *Environ. Sci. Technol.* **2017**, *51*, 9458-9468.

(779) Kasala, E. R.; Bodduluru, L. N.; Barua, C. C.; Sriram, C. S.; Gogoi, R. Benzo(a)pyrene Induced Lung Cancer: Role of Dietary Phytochemicals in Chemoprevention. *Pharmacol. Reports* **2015**, *67*, 996-1009.

(780) Wells, P. G.; McCallum, G. P.; Chen, C. S.; Henderson, J. T.; Lee, C. J. J.; Perstin, J.; Preston, T. J.; Wiley, M. J.; Wong, A. W. Oxidative Stress in Developmental Origins of Disease: Teratogenesis, Neurodevelopmental Deficits, and Cancer. *Toxicol. Sci.* **2009**, *108*, 4-18.

(781) Varjani, S. J.; Gnansounou, E.; Pandey, A. Comprehensive Review on Toxicity of Persistent Organic Pollutants from Petroleum Refinery Waste and their Degradation by Microorganisms. *Chemosphere* **2017**, *188*, 280-291.

(782) Sudakin, D. L.; Stone, D. L.; Power, L. Naphthalene Mothballs: Emerging and Recurring Issues and their Relevance to Environmental Health. *Curr. Topic. Toxicol.* **2011**, *7*, 13-19.

(783) Cheruiyot, N. K.; Lee, W.-J.; Mwangi, J. K.; Wang, L.-C.; Lin, N.-H.; Lin, Y.-C.; Cao, J.; Zhang, R.; Chang-Chien, G.-P. An Overview: Polycyclic Aromatic Hydrocarbon Emissions from the Stationary and Mobile Sources and in the Ambient Air. *Aerosol Air Quality Research* **2015**, *15*, 2730-2762.

(784) Evans, M.; Liu, J.; Bacosa, H.; Rosenheim, B. E.; Liu, Z. Petroleum Hydrocarbon Persistence Following the Deepwater Horizon Oil Spill as a Function of Shoreline Energy. *Marine Pollution Bull.* **2017**, *115*, 47-56.

(785) Harwell, M. A.; Gentile, J. H. Assessing Risks to Sea Otters and the Exxon Valdez Oil Spill: New Scenarios, Attributable Risk, and Recovery. *Human Ecological Risk Assessment* **2014**, *20*, 889-916.

(786) DiScenza, D. J.; Gareau, L.; Serio, N.; Roque, J.; Prignano, L.; Verderame, M.; Levine, M. Cyclodextrin-Promoted Detection of Aromatic Toxicants and Toxicant Metabolites in Urine. *Anal. Chem. Lett.* **2016**, *6*, 345-353.

(787) DiScenza, D. J.; Lynch, J.; Verderame, M.; Serio, N.; Prignano, L.; Gareau, L.; Levine, M. Efficient Fluorescence Detection of Aromatic Toxicants and Toxicant Metabolites in Human Breast Milk. *Supramol. Chem.* **2018**, *30*, 267-277.

(788) Sammarco, P. W.; Kolian, S. R.; Warby, R. A. F.; Bouldin, J. L.; Subra, W. A.; Porter, S. A. Concentrations in Human Blood of Petroleum Hydrocarbons Associated with the BP/Deepwater Horizon Oil Spill, Gulf of Mexico. *Archives Toxicol.* **2016**, *90*, 829-837.

(789) Pulkrabova, J.; Stupak, M.; Svarcova, A.; Rossner, P.; Rossnerova, A.; Ambroz, A.; Sram, R.; Hajslova, J. Relationship Between Atmospheric Pollution in the Residential Area and Concentrations of Polycyclic Aromatic Hydrocarbons (PAHs) in Human Breast Milk. *Sci. Total Environ.* **2016**, *562*, 640-647.

(790) Webb, J.; Coomes, O. T.; Mergler, D.; Ross, N. A. Levels of 1-Hydroxypyrene in Urine of People Living in an Oil Producing Region of the Andean Amazon (Ecuador and Peru). *Int. Archives Occupational Environ. Health* **2018**, *91*, 105-115.

(791) Kulkarni, K. S.; Sahu, S. K.; Vaikunta, R. L.; Pandit, G. G.; Lakshmana, D. N. Characterization and Source Identification of Atmospheric Polycyclic Aromatic Hydrocarbons in Visakhapatnam, India. *Int. Res. J. Environ. Sci.* **2014**, *3*, 57-64.

(792) Lintelmann, J.; Wu, X.; Kuhn, E.; Ritter, S.; Schmidt, C.; Zimmermann, R. Detection of Monohydroxylated Polycyclic Aromatic Hydrocarbons in Urine and Particulate Matter Using LC Separations Coupled with Integrated SPE and Fluorescence Detection or Coupled with High-Resolution Time-of-Flight Mass Spectrometry. *Biomed. Chromatography* **2018**, *Ahead of Print*; DOI: 10.1002/bmc.4183.

(793) Ogawa, S.; Wakayama, T.; Watanabe, H.; Hayashi, K.; Ogata, S.; Oaki, Y.; Hasegawa, M.; Imai, H. Enhanced Quantum Yield of Fluorophores in Confined Spaces of Supermicroporous Silicas. *Bull. Chem. Soc. Japan* **2018**, *91*, 87-91.

(794) Qiao, B.; Li, Y.; Meng, X.; Sun, Y.; Hu, P.; Lu, S.; Ren, H.; Liu, Z.; Zhou, Y. Development of an Indirect Competitive ELISA for the Detection of Acenaphthene and Pyrene. *Food Agricultur. Immunology* **2017**, *28*, 789-800.

(795) Mako, T.; Marks, P.; Cook, N.; Levine, M. Fluorescent Detection of Polycyclic Aromatic Hydrocarbons in Ternary Cyclodextrin Complexes. *Supramol. Chem.* **2012**, *24*, 743-747.

(796) Zhou, L.; Hu, Y.; Li, G. Conjugated Microporous Polymers with Built-In Magnetic Nanoparticles for Excellent Enrichment of Trace Hydroxylated Polycyclic Aromatic Hydrocarbons in Human Urine. *Anal. Chem.* **2016**, *88*, 6930-6938.

(797) Bhattacharyya, T.; Singha, A.; Dasgupta, A. K. A Solid-State Chemistry Approach to Sense Polycyclic Aromatic Hydrocarbons from Environment Using Single-Wall Carbon Nanotubes. *IEEE Sensors J.* **2016**, *16*, 6821-6827.

(798) Casida, J. E. Radioligand Recognition of Insecticide Targets. *J. Agricultur. Food Chem.* **2018**, *66*, 3277-3290.

(799) Thind, T. S.; Hollomon, D. W. Thiocarbamate Fungicides: Reliable Tools in Resistance Management and Future Outlook. *Pest Management Sci.* **2018**, *74*, 1547-1551.

(800) Jayakody, N.; Harris, E. C.; Coggon, D. Phenoxy Herbicides, Soft-Tissue Sarcoma and Non-Hodgkin Lymphoma: A Systematic Review of Evidence from Cohort and Case-Control Studies. *British Medical Bulletin* **2015**, *114*, 75-94.

(801) Li, Y. F.; Macdonald, R. W. Sources and Pathways of Selected Organochlorine Pesticides to the Arctic and the Effect of Pathway Divergence on HCH Trends in Biota: A Review. *Sci. Total Environ.* **2005**, *342*, 87-106.

(802) Rogan, W. J.; Chen, A. Health Risks and Benefits of Bis(4-chlorophenyl)-1,1,1-trichloroethane (DDT). *Lancet* **2005**, *366*, 763-773.

(803) Dai, D.; Rose, R. L.; Hodgson, E. Toxicology of Environmentally Persistent Chemicals: Mirex and Chlordecone. *Rev. Toxicol.* **1998**, *2*, 477-499.

(804) DiScenza, D. J.; Lynch, J.; Miller, J.; Verderame, M.; Levine, M. Detection of Organochlorine Pesticides in Contaminated Marine Environments via Cyclodextrin-Promoted Fluorescence Modulation. *ACS Omega* **2017**, *2*, 8591-8599.

(805) Pirsaheb, M.; Hossini, H.; Asadi, F.; Janjany, H. A Systematic Review on Organochlorine and Organophosphorus Pesticides Content in Water Resources. *Toxin Rev.* **2017**, *36*, 210-221.

(806) Schaeffer, A.; Amelung, W.; Hollert, H.; Kaestner, M.; Kandeler, E.; Kruse, J.; Miltner, A.; Ottermanns, R.; Page, H.; Peth, S.; Poll, C.; Rambold, G.; Schloter, M.; Schulzg S.; Streckd, T.; Roß-Nickoll, M. The Impact of Chemical Pollution on the Resilience of Soils Under Multiple Stresses: A Conceptual Framework for Future Research. *Sci. Total Environ.* **2016**, *568*, 1076-1085.

(807) Turusov, V.; Rakitsky, V.; Tomatis, L. Dichlorodiphenyltrichloroethane (DDT): Ubiquity, Persistence, and Risks. *Environ. Health Perspectives* **2002**, *110*, 125-128.

(808) Kaur, N.; Prabhakar, N. Current Scenario in Organophosphates Detection Using Electrochemical Biosensors. *TrAC, Trends Anal. Chem.* **2017**, *92*, 62-85.

(809) Hakme, E.; Lozano, A.; Ferrer, C.; Diaz-Galiano, F. J.; Fernandez-Alba, A. R. Analysis of Pesticide Residues in Olive Oil and Other Vegetable Oils. *TrAC, Trends Anal. Chem*. **2018**, *100*, 167-179.

(810) Ben-Zur, R.; Hake, H.; Hassoon, S.; Bulatov, V.; Schechter, I. Optical Analytical Methods for Detection of Pesticides. *Rev. Anal. Chem.* **2011**, *30*, 123-139.

(811) DiScenza, D. J.; Levine, M. Selective Detection of Non-Aromatic Pesticides via Cyclodextrin-Promoted Fluorescence Modulation. *New J. Chem.* **2016**, *40*, 789-793.

(812) DiScenza, D. J.; Levine, M. Sensitive and Selective Detection of Alcohols via Fluorescence Modulation. *Supramol. Chem.* **2016**, *28*, 881-891.

(813) Talbert, W.; Jones, D.; Morimoto, J.; Levine, M. Turn-On Detection of Pesticides via Reversible Fluorescence Enhancement of Conjugated Polymer Nanoparticles and Thin Films. *New J. Chem.* **2016**, *40*, 7273-7277.

(814) Mogos, V. T.; Dondoi, C. I.; Bajko, D. E. Carcinogenic Substances Naturally Occuring in the Human Diet. *Romanian Journal of Diabetes Nutrition and Metabolic Diseases.* **2018**, *25*, 105-108.

(815) Holck, A.; Axelsson, L.; McLeod, A.; Rode, T. M.; Heir, E. Health and Safety Considerations of Fermented Sausages. *J. Food Qual.* **2017**, 9753894/1-9753894/25.

(816) Pickworth, W. B.; Rosenberry, Z. R.; Yi, D.; Pitts, E. N.; Lord-Adem, W.; Koszowski, B. Cigarillo and Little Cigar Mainstream Smoke Constituents from Replicated Human Smoking. *Chem. Res. Toxicol.* **2018**, *31*, 251-258.

(817) Park, S.-J.; Jeong, M-J.; Park, S.-R.; Choi, J. C.; Choi, H.; Kim, M. Release of *N*-nitrosamines and *N*-nitrosatable Substances from Baby Bottle Teats and Rubber Kitchen Tools in Korea. *Food Sci. Biotechnol.* **2018**, *27*, 1041-1046.

(818) Son, S.; Nam, K.; Kim, H.; Gye, M. C.; Shin, I. Cytotoxicity Measurements of Bisphenol A (BPA) and its Substitutes using Human Keratinocytes. *Environ. Res.* **2018**, *164*, 655-659.

(819) Kotzebue, L. R. V.; de Oliveira, J. R.; da Silva, J. B.; Mazzetto, S. E.; Ishisa, H.; Lomonaco, D. Development of Fully Biobased High-Performance Bis-Benzoxazine under Environmentally Friendly Conditions. *ACS Sustainable Chem. Eng.* **2018**, *6*, 5485-5494.

(820) Rochester, J. R. Bisphenol A and Human Health: A Review of the Literature. *Reproductive Toxicology* **2013**, *42*, 132-155.

(821) Zhou, Y.-Y.; Yang, J.; Liu, M.; Wang, S.-F.; Lu, Q. A Novel Fluorometric Determination of Melamine using Cucurbit[7]uril. *J. Luminescence* **2010**, *130*, 817-820.

(822) Duan, X.; Dai, X.-X.; Wang, T.; Liu, H.-L.; Sun, S.-C. Melamine Negatively Affects Oocyte Architecture, Oocyte Development and Fertility in Mice. *Human Reproduction* **2015**, *30*, 1643-1652.

(823) Lam, H. S.; Ng, P. C.; Chu, W. C. W.; Wong, W.; Chean, D. F. Y.; Ho, S. S.; Wong, K. T.; Ahuja, A. T.; Li, C. K. Renal Screening in Children After Exposure to Low Dose Melamine in Hong Kong: Cross Sectional Study. *BMJ* **2009**, *338*, 92-95.

(824) Wu, S. Electric Cable with Melamine as Flame Retardant and its Manufacture Method. CN Patent 106967248, July 21, 2017.

(825) Rahman, M. M.; Ahmed, J. Cd-Doped Sb2O4 Nanostructures Modified Glassy Carbon Electrode for Efficient Detection of Melamine by Electrochemical Approach. *Biosens. Bioelectron.* **2018**, *102*, 631-636.

(826) Filazi, A.; Sireli, U. T.; Ekici, H.; Can, Y.; Karagoz, A. Determination of Melamine in Milk and Dairy Products by High Performance Liquid Chromatography. *J. Dairy. Sci.* **2011**, *95*, 602-608.

(827) Wahlang, B.; Perkins, J. T.; Petriello, M. C.; Hoffman, J. B.; Stromberg, A. J.; Hennig, B. A Compromised Liver Alters Polychlorinated Biphenyl-Mediated Toxicity. *Toxicology* **2017**, *380*, 11-22.

(828) Andersson, M.; Ottesen, R. T.; Volden, T. Building Materials as a Source of PCB Pollution in Bergen, Norway. *Sci. Total Environ.* **2004**, *325*, 139-144.

(829) Heinzow, B.; Mohr, S.; Ostendorp, G.; Kerst, M.; Körner, W. PCB and Dioxin-Like PCB in Indoor Air of Public Buildings Contaminated with Different PCB Sources – Deriving Toxicity Equivalent Concentrations from Standard PCB Congeners. *Chemosphere* **2007**, *67*, 1746-1753.

(830) Gupta, P.; T, B. L.; Wahlang, B.; Jordan, C. T.; Hilt, J. Z.; Hennig, B.; Dziubla, T. The Environmental Pollutant, Polychlorinated Biphenyls, and Cardiovascular Disease: A Potential Target for Antioxidant Nanotherapeutics. *Drug Deliv. Transl. Res.* **2018**, *8*, 740-759.

(831) Breivik, K.; Vestreng, V.; Rozovskaya, O.; Pacyna, J. M. Atmospheric Emissions of Some POPs in Europe: A Discussion of Existing Inventories and Data Needs. *Environ. Sci. Policy* **2006**, *9*, 663-674.

(832) Vorkamp, K.; An Overlooked Environmental Issue? A Review of the Inadvertent Formation of PCB-11 and other PCB Congeners and their Occurrence in Consumer Products and in the Environment. *Sci. Total Environ.* **2016**, *541*, 1463-1476.

(833) Waugh, C. A.; Arukwe, A.; Jaspers, V. L. B. Deregulation of microRNA-115 and its Transcription Factor NF-kB by Polychlorinated Biphenyls During Viral Infections. *APMIS* **2018**, *126*, 234-240.

(834) Abliz, A.; Chen, C.; Deng, W.; Wang W.; Sun, R. NADPH Oxidase Inhibitor Apocynin Attenuates PCB153-Induced Thyroid Injury in Rats. *Int. J. Endocrinol.* **2016**, *2016*, 8354745.

(835) Shanmugaraju, S.; Mukherjee, P. S. π-Electron Rich Small Molecule Sensors for the Recognition of Nitroaromatics. *Chem. Commun.* **2015**, *51*, 16014-16032.

(836) Venkatramaiah, N.; Pereira, C. F.; Mendes, R. F.; Paz, F. A. A.; Tome, J. P. C. Phosphonate Appended Porphyrins as Versatile Chemosensors for Selective Detection of Trinitrotoluene. *Anal. Chem.* **2015**, *87*, 4515-4522.

(837) Yang, J. S.; Swager, T. M. Porous Shape Persistent Fluorescent Polymer Films: An Approach to TNT Sensory Materials. *J. Am. Chem. Soc.* **1998**, *120*, 5321-5322.

(838) Yang, J. S.; Swager, T. M. Fluorescent Porous Polymer Films as TNT Chemosensors: Electronic and Structural Effects. *J. Am. Chem. Soc.* **1998**, *120*, 11864-1173.

(839) Marks, P.; Cohen, S.; Levine, M. Highly Efficient Quenching of Nanoparticles for the Detection of Electron-Deficient Nitroaromatics. *J. Polym. Sci. A Polym. Chem.* **2013**, *51*, 4150-4155.

(840) Martinez, H. P.; Grant, C. D.; Reynolds, J. G.; Trogler, W. C. Silica Anchored Fluorescent Organosilicon Polymers for Explosives Separation and Detection. *J. Mater. Chem.* **2012**, *22*, 2908-2914.

(841) Bonnot, K.; Bernhardt, P.; Hassler, D.; Baras, C.; Comet, M.; Keller, V.; Spitzer, D. Tunable Generation and Adsorption of Energetic Compounds in the Vapor Phase at Trace Levels: A Tool for Testing and Developing Sensitive and Selective Substrates for Explosive Detection. *Anal. Chem.* **2010**, *82*, 3389-3393.

(842) Sheaff, C. N.; Eastwood, D.; Wai, C. M.; Addleman, R. S. Fluorescence Detection and Identification of Tagging Agents and Impurities Found in Explosives. *Appl. Spectroscopy* **2008**, *62*, 739-746.

(843) Osborn, T.; Kaimal, S.; Burns, W.; Ford, A. R.; Reeve, S. W. Spectral Signatures for Volatile Impurities in TNT and RDX Based Explosives. *Proc. SPIE* **2008**, *6945*, 69451B/1-69451B/11.

(844) Willer, U.; Schade, W. Photonic Sensor Devices for Explosive Detection. *Anal. Bioanal. Chem.* **2009**, *395*, 275-282.

(845) Kumari, S.; Joshi, S.; Cordova-Sintjago, T. C.; Pant, D. D.; Sakhuja, R. Highly Sensitive Fluorescent Imidazolium-Based Sensors for Nanomolar Detection of Explosive Picric Acid in Aqueous Medium. *Sensors Actuators B: Chem.* **2016**, *229*, 599-608.

(846) Andrew, T. L.; Swager, T. M. A Fluorescence Turn-On Mechanism to Detect High Explosives RDX and PETN. *J. Am. Chem. Soc.* **2007**, *129*, 7254-7255.

(847) Kranz, W.; Kitts, K.; Strange, N.; Cummins, J.; Lotspeich, E.; Goodpaster, J. On the Smell of Composition C-4. *Forensic Sci. Int.* **2014**, *236*, 157-163.

(848) Marks, P.; Radaram, B.; Levine, M.; Levitsky, I. A. Highly Efficient Detection of Hydrogen Peroxide in Solution and in the Vapor Phase via Fluorescence Quenching. *Chem. Commun.* **2015**, *51*, 7061-7064.

(849) Jiang, D.; Peng, L.; Wen, M.; Zhou, Q.; Chen, C.; Wang, X.; Chen, W.; Li, H. Dopant-Assisted Positive Photoionization Ion Mobility Spectrometry Coupled with Time-Resolved Thermal Desorption for On-Site Detection of Triacetone Triperoxide and Hexamethylene Trioxide Diamine in Complex Matrices. *Anal. Chem.* **2016**, *88*, 4391-4399.

(850) de Perre, C.; Prado, A.; McCord, B. R. Rapid and Specific Detection of Urea Nitrate and Ammonium Nitrate by Electrospray Ionization Time-of-Flight Mass Spectrometry Using Infusion with Crown Ethers. *Rapid Commun. Mass Spectrometry* **2012**, *26*, 154-162.

(851) Sun, R.; Huo, X.; Lu, H.; Feng, S.; Wang, D.; Liu, H. Recyclable Fluorescent Paper Sensor for Visual Detection of Nitroaromatic Explosives. *Sensors Actuators B: Chem.* **2018**, *265*, 476-487.

(852) Li, X.; Shorter, D.; Kosten, T. R. Buprenorphine in the Treatment of Opioid Addiction: Opportunities, Challenges and Strategies. *Exp. Opinion Pharmacotherapy* **2014**, *15*, 2263-2275.

(853) Sangion, A.; Gramatica, P. PBT Assessment and Prioritization of Contaminants of Emerging Concern: Pharmaceuticals. *Environ. Res.* **2016**, *147*, 297-306.

(854) Asimakopoulos, A. G.; Kannan, K. Neuropsychiatric Pharmaceuticals and Illicit Drugs in Wastewater Treatment Plants: A Review. *Environ. Chem.* **2016**, *13*, 541-576.

(855) Priya, S. S.; Radha, K. V. A Review on the Adsorption Studies of Tetracycline onto Various Types of Adsorbents. *Chem. Engineering Commun.* **2017**, *204*, 821-839.

(856) Zmirou, D.; Deloraine, A.; Balducci, F.; Boudet, C.; Dechenaux, J. Health Effects Costs of Particulate Air Pollution. *J. Occupational Environ. Medicine* **1999**, *41*, 847-856.

(857) Brox, S.; Seiwert, B.; Kuester, E.; Reemtsma, T. Toxicokinetics of Polar Chemicals in Zebrafish Embryo (*Danio rerio*): Influence of Physicochemical Properties and of Biological Processes. *Environ. Sci. Technol.* **2016**, *50*, 10264-10272.

(858) Arini, A.; Mittal, K.; Dornbos, P.; Head, J.; Rutkiewicz, J.; Basu, N. A Cell-Free Testing Platform to Screen Chemicals of Potential Neurotoxic Concern Across Twenty Vertebrate Species. *Environ. Toxicol. Chem.* **2017**, *36*, 3081-3090.

(859) Karmaus, W.; Osuch, J. R.; Eneli, I.; Mudd, L. M.; Zhang, J.; Mikucki, D.; Haan, P.; Davis, S. Maternal Levels of Dichlorodiphenyl-Dichloroethylene (DDE) May Increase Weight and Body Mass Index in Adult Female Offspring. *Occupational Environ. Medicine* **2009**, *66*, 143-149.

(860) Kumar, B.; Baldi, A. The Challenge of Counterfeit Drugs: A Comprehensive Review on Prevalence, Detection and Preventive Measures. *Curr. Drug Safety* **2016**, *11*, 112-120.

(861) Zou, W.-B.; Yin, L.-H.; Jin, S.-H. Advances in Rapid Drug Detection Technology. *J. Pharmaceutical Biomed. Anal.* **2018**, *147*, 81-88.

(862) Bassat, Q.; Tanner, M.; Guerin, P. J.; Stricker, K.; Hamed, K. Combating Poor-Quality Anti-Malarial Medicines: A Call to Action. *Malaria J.* **2016**, *15*, 302/1-302/12.

(863) Sadones, N.; Capiau, S.; De Kesel, P. M. M.; Lambert, W. E.; Stove, C. P. Spot Them in the Spot: Analysis of Abused Substances Using Dried Blood Spots. *Bioanal.* **2014**, *6*, 2211-2227.

(864) Gardon, O.; Faget, L.; Chu Sin Chung, P.; Matifas, A.; Massotte, D.; Kieffer, B. L. Expression of Mu Opioid Receptor in Dorsal Diencephalic Conduction System: New Insights for the Medial Habenula. *Neuroscience* **2014**, *277*, 595-609.

(865) Rodriguez-Munoz, M.; Sanchez-Blazquez, P.; Bailon, C.; Garzon, J. Detecting Zinc Release Induced by Mu-Opioid Receptor Agonists in Brain Slices. *Methods Molec. Biol.* **2015**, *1230*, 233-241.

(866) Koohsarian, M.; Mokhtari, A. Direct Chemiluminescence Determination of Oxymorphone Using Potassium Permanganate and Polyphosphoric Acid. *Anal. Bioanal. Chem. Res.* **2017**, *4*, 127-139.

(867) Bari, V.; Dhorda, U. J.; Sundaresan, M. High Performance Liquid Chromatographic Determination of Acetaminophen in Human Blood Plasma Using Electrochemical Detection. *Indian Drugs* **1998**, *35*, 222-225.

(868) Deokar, G. S.; Pagare, I. S.; Naseem, A. Md.; Kshirsagar, S.; Shindhe, L. Chemical Derivatization UV Spectrophotometric Method for Detection of p-Amino Phenol and Energy of Activation Approach to Set Degradation Protocol for Forced Degradation Studies. *Int. J. Pharma Res. Rev.* **2016**, *5*, 1-12.

(869) Vergeynst, L.; K'oreje, K.; De Wispelaere, P.; Harinck, L.; Van Langenhove, H.; Demeestere, K. Statistical Procedures for the Determination of Linearity, Detection Limits and Measurement Uncertainty: A Deeper Look into SPE-LC-Orbitrap Mass Spectrometry of Pharmaceuticals in Wastewater. *J. Hazardous Mater.* **2017**, *323*, 2-10.

(870) Kumar, P. A.; Thirupathi, D.; Kumar, Y. R.; Jayashree, A. Simultaneous Determination of Related Organic Impurities of Ibuprofen and Paracetamol in Combination Solid Dosage Form by Rp-Hplc With Qbd Approach. *Oriental J. Chem.* **2017**, *33*, 1461-1468.

(871) Yang, Y.; Yin, S.; Li, Y.; Lu, D.; Zhang, J.; Sun, C. Application of Aptamers in Detection and Chromatographic Purification of Antibiotics in Different Matrices. *TrAC, Trends Anal. Chem.* **2017**, *95*, 1-22.

(872) Xu, N.; Yuan, Y.; Yin, J.-H.; Wang, X.; Meng, L. One-Pot Hydrothermal Synthesis of Luminescent Silicon-Based Nanoparticles for Highly Specific Detection of Oxytetracycline via Ratiometric Fluorescent Strategy. *RSC Adv.* **2017**, *7*, 48429-48436.

(873) Zhou, Y.; Gu, G.-H.; Geng, M.-Y.; Lu, Z.-H. Rapid Detection of Anabolic Steroids in Urine by Protein Arrays. *Int. J. Sports Medicine* **2006**, *27*, 526-532.

(874) Liu, X.; Na, W.; Liu, H.; Su, X. Fluorescence Turn-Off-On Probe Based on Polypyrrole/Graphene Quantum Composites for Selective and Sensitive Detection of Paracetamol and Ascorbic Acid. *Biosensors Bioelectronics* **2017**, *98*, 222-226.

(875) Yang, Q.; Zhou, L.; Wu, Y.-X.; Zhang, K.; Cao, Y.; Zhou, Y.; Wu, D.; Hu, F.; Gan, N. A Two Dimensional Metal-Organic Framework Nanosheets-Based Fluorescence Resonance Energy Transfer Aptasensor with Circular Strand-Replacement DNA Polymerization Target-Triggered Amplification Strategy for Homogeneous Detection of Antibiotics. *Anal. Chim. Acta* **2018**, *1020*, 1-8.

(876) Wilson, D. F. Oxidative Phosphorylation: Regulation and Role in Cellular and Tissue Metabolism. *J. Physiol.* **2017**, *595*, 7023-7038.

(877) D'Alessandro, M.; Melandri, B. A. ATP Hydrolysis in ATP Synthases Can Be Differently Coupled to Proton Transport and Modulated by ADP and Phosphate: A Structure Based Model of the Mechanism. *Biochim. Biophys. Acta* **2010**, *1797*, 755-762.

(878) Dzeja, P. P.; Terzic, A. Phosphotransfer Reactions in the Regulation of ATP-Sensitive K+ Channels. *FASEB J.* **1998**, *12*, 523-529.

(879) McLarnon, J. G. Purinergic Mediated Changes in Ca2+ Mobilization and Functional Responses in Microglia: Effects of Low Levels of ATP. *J. Neurosci. Res.* **2005**, *81*, 349-356.

(880) Carling, D.; Thornton, C.; Woods, A.; Sanders, M. J. AMP-Activated Protein Kinase: New Regulation, New Roles? *Biochem. J.* **2012**, *445*, 11-27.

(881) Yu, C.-J.; Wu, S.-M.; Tseng, W.-L. Magnetite Nanoparticle-Induced Fluorescence Quenching of Adenosine Triphosphate-BODIPY Conjugates: Application to Adenosine Triphosphate and Pyrophosphate Sensing. *Anal. Chem.* **2013**, *85*, 8559-8565.

(882) Farias, P. A. M.; Castro, A. A.; Wagener, A. d. L. R.; Miguel, E. M. Adenine Determination in the Presence of Copper in Diluted Alkaline Electrolyte by Adsorptive Stripping Voltammetry at the Mercury Film Electrode. *Electroanal.* **2008**, *20*, 1445-1453.

(883) Zhao, Q.; Zhang, Z.; Tang, Y. A New Conjugated Polymer-Based Combination Probe for ATP Detection Using a Multisite-Binding and FRET Strategy. *Chem. Commun.* **2017**, *53*, 9414-9417.

(884) Li, X.; Yang, J.; Xie, J.; Jiang, B.; Yuan, R.; Xiang, Y. Cascaded Signal Amplification via Target-Triggered Formation of Aptazyme for Sensitive Electrochemical Detection of ATP. *Biosensors Bioelectronics* **2018**, *102*, 296-300.

(885) Hoffman, M. A.; Fang, B.; Haura, E. B.; Rix, U.; Koomen, J. M. Comparison of Quantitative Mass Spectrometry Platforms for Monitoring Kinase ATP Probe Uptake in Lung Cancer. *J. Proteome Res.* **2018**, *17*, 63-75.

(886) Ng, S.; Lim, H. S.; Ma, Q.; Gao, Z. Optical Aptasensors for Adenosine Triphosphate. *Theranostics* **2016**, *6*, 1683-1702.

(887) Zhao, J.; Gao, J.; Xue, W.; Di, Z.; Xing, H.; Lu, Y.; Li, L. Upconversion Luminescence-Activated DNA Nanodevice for ATP Sensing in Living Cells. *J. Am. Chem. Soc.* **2018**, *140*, 578-581.

(888) Paulines, M. J.; Limbach, P. A. Stable Isotope Labeling for Improved Comparative Analysis of RNA Digests by Mass Spectrometry. *J. Am. Soc. Mass Spectrometry* **2017**, *28*, 551-561.

(889) Buchholz, A.; Hurlebaus, J.; Wandrey, C.; Takors, R. Metabolomics: Quantification of Intracellular Metabolite Dynamics. *Biomolecular Engineering* **2002**, *19*, 5-15.

(890) Maity, D.; Li, M.; Ehlers, M.; Schmuck, C. A Metal-Free Fluorescence Turn-On Molecular Probe for Detection of Nucleoside Triphosphates. *Chem. Commun.* **2017**, *53*, 208-211.

(891) Zhang, P.; Yuly, J. L.; Lubner, C. E.; Mulder, D. W.; King, P. W.; Peters, J. W.; Beratan, D. N. Electron Bifurcation: Thermodynamics and Kinetics of Two-Electron Brokering in Biological Redox Chemistry. *Acc. Chem. Res.* **2017**, *50*, 2410-2417.

(892) Xiao, W.; Wang, R.-S.; Handy, D. E.; Loscalzo, J. NAD(H) and NADP(H) Redox Couples and Cellular Energy Metabolism. *Antioxidants Redox Signaling* **2018**, *28*, 251-272.

(893) Iitani, K.; Chien, P.-J.; Suzuki, T.; Toma, K.; Arakawa, T.; Iwasaki, Y.; Mitsubayashi, K. Fiber-Optic Bio-Ssniffer (Biochemical Gas Sensor) Using Reverse Reaction of Alcohol Dehydrogenase for Exhaled Acetaldehyde. *ACS Sensors* **2018**, *3*, 425-431.

(894) Zhang, X.; Zhu, M.; Xu, B.; Cui, Y.; Tian, G.; Shi, Z.; Ding, M. Indirect Electrochemical Detection for Total Bile Acids in Human Serum. *Biosensors Bioelectronics* **2016**, *85*, 563-567.

(895) Ito, H.; Uchida, T.; Makita, K. Ketamine Causes Mitochondrial Dysfunction in Human Induced Pluripotent Stem Cell-Derived Neurons. *PLoS One* **2015**, *10*, e0128445/1-e0128445/20.

(896) Ma, Y.; Nie, H.; Chen, H.; Li, J.; Hong, Y.; Wang, B.; Wang, C.; Zhang, J.; Cao, W.; Zhang, M.; Xu, Y.; Ding, X.; Yin, S. K.; Qu, X.; Ying, W. NAD+/NADH Metabolism and NAD+-Dependent Enzymes in Cell Death and Ischemic Brain Injury: Current Advances and Therapeutic Implications. *Curr. Med. Chem.* **2015**, *22*, 1239-1247.

(897) Teng, H.; Lv, M.; Liu, L.; Zhang, X.; Zhao, Y.; Wu, Z.; Xu, H. Quantitative Detection of NADH Using a Novel Enzyme-Assisted Method Based on Surface-Enhanced Raman Scattering. *Sensors* **2017**, *17*, 788/1-788/8.

(898) Blandon-Naranjo, L.; Della Pelle, F.; Vazquez, M. V.; Gallego, J.; Santamaria, A.; Alzate-Tobon, M.; Compagnone, D. Electrochemical Behaviour of Microwave-Assisted Oxidized MWCNTs Based Disposable Electrodes: Proposal of a NADH Electrochemical Sensor. *Electroanal.* **2018**, *30*, 509-516.

(899) Wang, L.; Zhang, J.; Kim, B.; Peng, J.; Berry, S. N.; Ni, Y.; Su, D.; Lee, J.; Yuan, L.; Chang, Y.-T. Boronic Acid: A Bio-Inspired Strategy to Increase the Sensitivity and Selectivity of Fluorescent NADH Probe. *J. Am. Chem. Soc.* **2016**, *138*, 10394-10397.

(900) Malinovsky, A. V. Reason for Indispensability of Threonine in Humans and Other Mammals in Comparative Aspect. *Biochem.* **2017**, *82*, 1055-1060.

(901) Wang, X.; Lin, M.; Xu, D.; Lai, D.; Zhou, L. Structural Diversity and Biological Activities of Fungal Cyclic Peptides, Excluding Cyclodipeptides. *Molecules* **2017**, *22*, 2069/1-2069/47.

(902) Sperringer, J. E.; Addington, A.; Hutson, S. M. Branched-Chain Amino Acids and Brain Metabolism. *Neurochem. Res.* **2017**, *42*, 1697-1709.

(903) van Galen, K. A.; ter Horst, K. W.; Booij, J.; la Fleur, S. E.; Serlie, M. J. The Role of Central Dopamine and Serotonin in Human Obesity: Lessons Learned from Molecular Neuroimaging Studies. *Metabolism* **2018**, *85*, 325-339.

(904) Riessland, M.; Kolisnyk, B.; Greengard, P. Reactive Dopamine Leads to Triple Trouble in Nigral Neurons. *Biochem*. **2017**, *56*, 6409-6410.

(905) Kostrzewa, J. P.; Kostrzewa, R. A.; Kostrzewa, R. M.; Brus, R.; Nowak, P. Perinatal 6-Hydroxydopamine to Produce a Lifelong Model of Severe Parkinson's Disease. *Curr. Topics Behavioral Neuroscience* **2016**, *29*, 313-332.

(906) Verdurand, M.; Zimmer, L. Hippocampal 5-HT1A Receptor Expression Changes in Prodromal Stages of Alzheimer's Disease: Beneficial or Deleterious? *Neuropharmacol.* **2017**, *123*, 446-454.

(907) Jamwal, S.; Sharma, S. Vascular Endothelium Dysfunction: A Conservative Target in Metabolic Disorders. *Inflammation Res.* **2018**, *67*, 391-405.

(908) Fu, Y.; Wang, X.; Kong, W. Hyperhomocysteinaemia and Vascular Injury: Advances in Mechanisms and Drug Targets. *British J. Pharmacol.* **2018**, *175*, 1173-1189.

(909) De Bandt, J.-P. Leucine and Mammalian Target of Rapamycin-Dependent Activation of Muscle Protein Synthesis in Aging. *J. Nutrition* **2016**, *146*, 2616S-2624S.

(910) Colovic, M. B.; Vasic, V. M.; Djuric, D. M.; Krstic, D. Z. Sulphur-Containing Amino Acids: Protective Role Against Free Radicals and Heavy Metals. *Curr. Med. Chem.* **2018**, *25*, 324-335.

(911) Nguyen, H. T. H.; Shaffer, C. J.; Pepin, R.; Turecek, F. UV Action Spectroscopy of Gas-Phase Peptide Radicals. *J. Phys. Chem. Lett.* **2015**, *6*, 4722-4727.

(912) Danielson, N. D.; Mansour, F. R.; Zhou, L.; Connell, C. V.; Dotlich, E. M.; Gibler, J. N.; Norman, B. E.; Grossman, S.; Wei, W.; Zhang, Y. Liquid Chromatography with Alkylammonium Formate Ionic Liquid Mobile Phases and Fluorescence Detection. *J. Chromatography A* **2018**, *1559*, 128-135.

(913) Guo, C.; Yang, X.; Yang, X.; Zhu, W.; Pei, M.; Zhang, G. Fluorescent Probes for Cu2+, Hg2+ and Amino Acids in Aqueous Solutions Based on Two Mechanisms. *Sensors Actuators B: Chem.* **2014**, *205*, 345-351.

(914) Sol, H.; Lei, C.; Han, X. X.; Zhang, X.; Wang, X.; Bing, Z. Quantitative Determination of Total Amino Acids Based on Surface-Enhanced Raman Scattering and Ninhydrin Derivatization. *Anal. Sci.* **2017**, *33*, 53-57.

(915) Eissa, S.; Zourob, M. Aptamer- Based Label-Free Electrochemical Biosensor Array for the Detection of Total and Glycated Hemoglobin in Human Whole Blood. *Sci. Reports* **2017**, *7*, 1-8.

(916) Yu, H.; Yong, X.; Liang, J.; Deng, J.; Wu, Y. Materials Established for Enantioselective Release of Chiral Compounds. *Ind. Eng. Chem. Res.* **2016**, *55*, 6037-6048.

(917) Habala, L.; Horákova, R.; Čižmáriková, R. Chromatographic Separations Based on Tartaric Acid and its Derivatives. *Monatsh. Chem.* **2018**, *149*, 873-882.

(918) Zhang, C.; Rodriguez, E.; Bi, C.; Zheng, X.; Suresh, D.; Suh, K.; Li, Z.; Elsebaei, F.; Hage, D. S. High Performance Affinity Chromatography and Related Separation Methods for the Analysis of Biological and Pharmaceutical Agents. *Analyst* **2018**, *143*, 374-391.

(919) Yu, X.; Yao, Z.-P. Chiral Recognition and Determination of Enantiomeric Excess by Mass Spectrometry: A Review. *Anal. Chim. Acta* **2017**, *968*, 1-20.

(920) Qiu, X.; Xie, L.; Liu, X.; Luo, L.; Zhang, Z.; Du, J. Estimation of Optical Rotation of Chiral Molecules with Weak Measurements. *Opt. Lett.* **2016**, *41*, 4032-4035.

(921) Nakai, H.; Nonaka, K.; Goto, T.; Seo, J.; Matsumoto, T.; Ogo, S. A Macrocyclic Tetraamine Bearing Four Phenol Groups: A New Class of Heptadentate Ligands to Provide an Oxygen-Sensitive Luminescent Tb(III) Complex with an Extendable Phenol Pendant Arm. *Dalton Trans.* **2015**, *44*, 10923-10927.

(922) Florea, M.; Nau, W. M. Strong Binding of Hydrocarbons to Cucurbituril Probed by Fluorescent Dye Displacement: A Supramolecular Gas-Sensing Ensemble. *Angew. Chem. Int. Ed.* **2011**, *50*, 9338-9342.

(923) Yan, Y.; Zhang, K.; Yu, H.; Zhu, H.; Sun, M.; Hayat, T.; Alsaedi, A.; Wang, S. Sensitive Detection of Sulfide Based on the Self-Assembly of Fluorescent Silver Nanoclusters on the Surface of Silica Nanospheres. *Talanta* **2017**, *174*, 387-393.

(924) Dilonardo, E.; Penza, M.; Alvisi, M.; Cassano, G.; Di Franco, C.; Palmisano, F.; Torsi, L.; Cioffi, N. Sensitive Detection of Hydrocarbon Gases using Electrochemically Pd-modified ZnO Chemiresistors. *Beilstein J. Nanotechnol.* **2017**, *8*, 82-90.

(925) Martínez-Hurtado, J. L.; Davidson, C. A. B.; Blyth, J. Lowe, C. R. Holographic Detection of Hydrocarbon Gases and Other Volatile Organic Compounds. *Langmuir* **2010**, *26*, 15694-15699.

(926) Yvon-Durocher, G.; Allen, A. P.; Bastwiken, D.; Conrad, R.; Gudasz, C.; St-Pierre, A.; Thanh-Duc, N.; del Giorgio, P. A. Methane Fluxes Show Consistent Temperature Dependence Across Microbial to Ecosystem Scales. *Nature* **2014**, *507*, 488-491.

(927) Zhang, J.; Cheng, D.; Wang, B.; Khan, I.; Ni, Y. Ethylene Control Technologies in Extending Postharvest Shelf Life of Climacteric Fruit. *J. Agricultur. Food Chem.* **2017**, *65*, 7308-7319.

(928) Chang, C. Q&A: How Do Plants Respond to Ethylene and What Is Its Importance? *BMC Biol.* **2016**, *14*, 7/1-7/7.

(929) Pugh, C. W.; Ratcliffe, P. J. New Horizons in Hypoxia Signaling Pathways. *Experimental Cell Research* **2017**, *356*, 116-121.

(930) O'Mara, P.; Farrell, A.; Bones, J.; Twomey, K. Staying Alive! Sensors Used for Monitoring Cell Health in Bioreactors. *Talanta* **2018**, *176*, 130-139.

(931) Sjöberg, F.; Singer, M. The Medical Use of Oxygen: A Time for Critical Reappraisal. *J. Intern. Med.* **2013**, *274*, 505-528.

(932) Zahra, S. A.; Butt, Y. N.; Nasar, S.; Akram, S.; Fatima, Q.; Ikram, J. Food Packaging in Perspective of Microbial Activity: A Review. *J. Microbiol. Biotechnol. Food Sci.* **2016,** *6*, 752-757.

(933) O'Callaghan, K. A. M.; Papkovsky, D. B. Kerry, J. P. An Assessment of the Influence of the Industry Distribution Chain on the Oxygen Levels in Commercial Modified Atmosphere Packaged Cheddar Cheese Using Non-Destructive Oxygen Sensor Technology. *Sensors* **2016**, *16*, 916/1-916/11.

(934) National Research Council. *Prudent Practices in the Laboratory: Handling and Management of Chemical Hazards, Updated Version.* The National Academic Press: Washington, DC, 2011.

(935) Erker, W.; Schoen, A.; Basche, T.; Decker, H. Fluorescence Labels as Sensors for Oxygen Binding of Arthropod Hemocyanins. *Biochem. Biophys. Res. Commun.* **2004**, *324*, 893-900.

(936) Dane, E. L.; King, S. B.; Swager, T. M. Conjugated Polymers That Respond to Oxidation with Increased Emission. *J. Am. Chem. Soc.* **2010**, *132*, 7758-7768.

(937) Frausto, F.; Thomas, S. W. Ratiometric Singlet Oxygen Detection in Water Using Acene-Doped Conjugated Polymer Nanoparticles. *ACS Appl. Mater. Interfaces* **2017**, *9*, 15768-15775.

(938) Jianwen, Z.; Da, L.; Wenxing, F. Analysis of Chemical Disasters Caused by Release of Hydrogen Sulfide-Bearing Natural Gas. *Procedia Engineering* **2011**, *26*, 1878-1890.

(939) Dosmukhamedov, N.; Kaplan, V.; Zholdasbay, Y.; Wachtel, E.; Lubomirsky, I. Natural Gas Regeneration of Carbonate Melts Following SO2 Capture from Non-Ferrous Smelter Emissions. *RSC Adv.* **2017**, *7*, 21406-21411.

(940) Palanisamy, S.; Lee, L.-Y.; Wang, Y.-L.; Chen, Y.-J.; Chen. C-Y.; Wang, Y.-M. A Water Soluble and Fast Response Fluorescent Turn-On Copper Complex Probe for H2S Detection in Zebra Fish. *Talanta* **2016**, *147*, 445-452.

(941) Wu, H.; Krishnakumar, S.; Yu, J.; Liang, D.; Qi, H.; Lee, Z.-W.; Deng, L.-W.; Huang, D. Highly Selective and Sensitive Near-Infrared-Fluorescent Probes for the Detection of Cellular Hydrogen Sulfide and the Imaging of H2S in Mice. *Chem. Asian. J.* **2014**, *9*, 3604-3611.

(942) Liu, J.; Yee, K.-K.; Lo, K. K.-W.; Zhang, K. Y.; To, W.-P.; Che, C.-M.; Xu, Z. Selective Ag(I) Binding, H2S Sensing, and White-Light Emission from an Easy-to-Make Porous Conjugated Polymer. *J. Am. Chem. Soc.* **2014**, *136*, 2818-2824.

(943) Fenech, M.; Nersesyan, A.; Knasmueller, S. A Systematic Review of the Association Between Occupational Exposure to Formaldehyde and Effects on Chromosomal DNA Damage Measured Using the Cytokinesis-Block Micronucleus Assay in Lymphocytes. *Mutation Res. Rev. Mutation Res.* **2016**, *770*, 46-57.

(944) Salthammer, T. The Formaldehyde Dilemma. *Int. J. Hygiene Environ. Health* **2015**, *218*, 433-436.

(945) Huang, B.; Lei, C.; Wei, C.; Zeng, G. Chlorinated Volatile Organic Compounds (Cl-VOCs) in Environment - Sources, Potential Human Health Impacts, and Current Remediation Technologies. *Environ. Int.* **2014**, *71*, 118-138.

(946) Balwant, K.; Kumar, S. U.; Sukanta, N. A Review of Some Specific Air Pollutants and its Exposure Related to Human Health. *Int. Res. J. Environ. Sci.* **2015**, *4*, 63-68.

(947) Singh, Z.; Chadha, P. Textile Industry and Occupational Cancer. *J. Occupational Medicine Toxicol.* **2016**, *11*, 39/1-39/6.

(948) Wang, Z.; Wang, C. Is Breath Acetone a Biomarker of Diabetes? A Historical Review on Breath Acetone Measurements. *J. Breath Res.* **2013**, *7*, 037109/1-037109/18.

(949) Huang, J.; Kumar, S.; Hanna, G. B. Investigation of C3-C10 Aldehydes in the Exhaled Breath of Healthy Subjects Using Selected Ion Flow Tube-Mass Spectrometry (SIFT-MS). *J. Breath Res.* **2014**, *8*, 037104/1-037104/7.

(950) Moscarella, S.; Laffi, G.; Coletta, D.; Arena, U.; Cappellini, A. Paola; Gentilini, P. Volatile Hydrocarbons in the Breath of Patients with Chronic Alcoholic Liver Disease: A Possible Marker of Ethanol-Induced Lipoperoxidation. *Frontiers Gastrointestinal Res.* **1984**, *8*, 208-216.

(951) Mochalski, P.; King, J.; Haas, M.; Unterkofler, K.; Amann, A.; Mayer, G. Blood and Breath Profiles of Volatile Organic Compounds in Patients with End-Stage Renal Disease. *BMC Nephrology* **2014**, *15*, 43/1-43/14, 14.

(952) Smolinska, A.; Tedjo, D. I.; Blanchet, L.; Bodelier, A.; Pierik, M. J.; Masclee, Ad A. M.; Dallinga, J.; Savelkoul, P. H. M.; Jonkers, D. M. A. E.; Penders, J.; van Schooten, F.-J. Volatile Metabolites in Breath Strongly Correlate with Gut Microbiome in CD Patients. *Anal. Chim. Acta* **2018**, *1025*, 1-11.

(953) Kischkel, S.; Miekisch, W.; Sawacki, A.; Straker, E. M.; Trefz, P.; Amann, A.; Schubert, J. K. Breath Biomarkers for Lung Cancer Detection and Assessment of Smoking Related Effects - Confounding Variables, Influence of Normalization and Statistical Algorithms. *Clinical Chim. Acta* **2010**, *411*, 1637-1644.

(954) Yoon, J.-W.; Lee, J.-H. Toward Breath Analysis on a Chip for Disease Diagnosis Using Semiconductor-Based Chemiresistors: Recent Progress and Future Perspectives. *Lab on a Chip* **2017**, *17*, 3537-3557.

(955) Amann, A.; de Lacy Costello, B.; Miekisch, W.; Schubert, J.; Buszewski, B.; Pleil, J.; Ratcliffe, N.; Risby, T. The Human Volatilome: Volatile Organic Compounds (VOCs) in Exhaled Breath, Skin Emanations, Urine, Feces and Saliva. *J. Breath Res.* **2014**, *8*, 034001/1-034001/17.

(956) Demichelis, A.; Pascale, C.; Lecuna, M.; Niederhauser, B.; Sassi, G.; Sassi, M. P. Compact Devices for Generation of Reference Trace VOC Mixtures: A New Concept in Assuring Quality at Chemical and Biochemical Laboratories. *Anal. Bioanal. Chem.* **2018**, *410*, 2619-2628.

(957) Brock, B.; Kamysek, S.; Silz, J.; Trefz, P.; Schubert, J. K.; Miekisch, W. Monitoring of Breath VOCs and Electrical Impedance Tomography Under Pulmonary Recruitment in Mechanically Ventilated Patients. *J. Breath Res.* **2017**, *11*, 016005/1-016005/9.

(958) Guntner, A. T.; Pineau, N. J.; Mochalski, P.; Wiesenhofer, H.; Agapiou, A.; Mayhew, C. A.; Pratsinis, S. E. Sniffing Entrapped Humans with Sensor Arrays. *Anal. Chem.* **2018**, *90*, 4940-4945.

(959) Gherghel, S.; Morgan, R. M.; Arrebola-Liebanas, J.; Romero-Gonzalez, R.; Blackman, C. S.; Garrido-Frenich, A.; Parkin, I. P. Development of a HS-SPME/GC-MS Method for the Analysis of Volatile Organic Compounds from Fabrics for Forensic Reconstruction Applications. *Forensic Sci. Int.* **2018**, *290*, 207-218.

(960) Erler, A.; Riebe, D.; Beitz, T.; Loehmannsroeben, H.-G.; Grothusheitkamp, D.; Kunz, T.; Methner, F.-J. Detection of Volatile Organic Compounds in the Headspace Above Mold Fungi by GC-Soft X-Radiation-Based APCI-MS. *J. Mass Spectrometry* **2018**, *Ahead of Print*; DOI: 10.1002/jms.4210.

(961) Romano, A.; Doran, S.; Belluomo, I.; Hanna, G. B. High-Throughput Breath Volatile Organic Compound Analysis Using Thermal Desorption Proton Transfer Reaction Time-of-Flight Mass Spectrometry. *Anal. Chem.* **2018**, *90*, 10204-10210.

(962) Bi, A.; Yang, S.; Liu, M.; Wang, X.; Liao, W.; Zeng, W. Fluorescent Probes and Materials for Detecting Formaldehyde: From Laboratory to Indoor for Environmental and Health Monitoring. *RSC Adv.* **2017**, *7*, 36421-36432.

(963) Hatanaka, S.; Ono, T.; Hisaeda, Y. Turn-On Fluorogenic and Chromogenic Detection of Small Aromatic Hydrocarbon Vapors by a Porous Supramolecular Host. *Chem. Eur. J.* **2016**, *22*, 10346-10350.

(964) Xia, H.; Liu, G.; Zhao, C.; Meng, X.; Li, F.; Wang, F.; Duan, L.; Chen, H. Fluorescence Sensing of Amine Vapours Based on ZnS-Supramolecular Organogel Hybrid Films. *RSC Adv.* **2017**, *7*, 17264-17270.

(965) Wen, J. T.; Roper, J. M.; Tsutsui, H. Polydiacetylene Supramolecules: Synthesis, Characterization, and Emerging Applications. *Industrial Engineering Chem. Res.* **2018**, *57*, 9037-9053.

(966) Delehanty, J. B.; Susumu, K.; Manthe, R. L.; Algar, W. R.; Medintz, I. L. Active Cellular Sensing with Quantum Dots: Transitioning from Research Tool to Reality; A Review. *Anal. Chim. Acta* **2012**, *750*, 63-81.

(967) Ivanova, I. A.; Tsacheva, I. Microbial Sensors Based on Nanostructures. *Recent Patents Nanomedicine* **2015**, *5*, 59-65.

(968) Bertsche, U.; Mayer, C.; Goetz, F.; Gust, A. A. Peptidoglycan Perception - Sensing Bacteria by their Common Envelope Structure. *Int. J. Medical Microbiol.* **2015**, *305*, 217-223.

(969) Xia, J.; Wang, H.; Li, S.; Wu, Q.; Sun, L.; Huang, H.; Zeng, M. Ion Channels or Aquaporins as Novel Molecular Targets in Gastric Cancer. *Molec. Cancer* **2017**, *16*, 54/1-54/10.

(970) Avrahami, D.; Wang, Y. J.; Klochendler, A.; Dor, Y.; Glaser, B.; Kaestner, K. H. β-Cells Are Not Uniform After All-Novel Insights into Molecular Heterogeneity of Insulin-Secreting Cells. *Diabetes, Obesity and Metabolism* **2017**, *19*, 147-152.

(971) Leon, G.; MacDonagh, L.; Finn, S. P.; Cuffe, S.; Barr, M. P. Cancer Stem Cells in Drug Resistant Lung Cancer: Targeting Cell Surface Markers and Signaling Pathways. *Pharmacol. Therapeutics* **2016**, *158*, 71-90.

(972) Holowka, D.; Baird, B. Roles for Lipid Heterogeneity in Immunoreceptor Signaling. *Biochim. Biophys. Acta* **2016**, *1861*, 830-836.

(973) Sonoi, R.; Kim, M.-H.; Yamada, K.; Kino-oka, M. Phenotypic Heterogeneity of Human Retinal Pigment Epithelial Cells in Passaged Cell Populations. *J. Bioscience Bioengineering* **2017**, *124*, 227-233.

(974) Lam, B. Y. H.; Cimino, I.; Polex-Wolf, J.; Nicole Kohnke, S.; Rimmington, D.; Iyemere, V.; Heeley, N.; Cossetti, C.; Schulte, R.; Saraiva, L. R.; Logan, D. W.; Blouet, C.; O'Rahilly, S.; Coll, A. P.; Yeo, G. S. H. Heterogeneity of Hypothalamic Pro-Opiomelanocortin-Expressing Neurons Revealed by Single-Cell RNA Sequencing. *Molecular Metabolism* **2017**, *6*, 383-392.

(975) Desimone, M. F.; Alvarez, G. S.; Foglia, M. L.; Copello, G. J.; Diaz, L. E. Development of Biocompatible Matrices for Whole Cell Biosensors. *Adv. Mater. Res.* **2011**, *2*, 1-19.

(976) Vadgama, P. Sensor Biocompatibility: Final Frontier in Bioanalytical Measurement. *Analyst* **2007**, *132*, 495-499.

(977) Kim, I.-B.; Shin, H.; Garcia, A. J.; Bunz, U. H. F. Use of a Folate-PPE Conjugate to Image Cancer Cells in Vitro. *Bioconjugate Chem.* **2007**, *18*, 815-820.

(978) Le, N. D. B.; Yazdani, M.; Rotello, V. M. Array-Based Sensing Using Nanoparticles: An Alternative Approach for Cancer Diagnostics. *Nanomedicine* **2014**, *9*, 1487-1498.

(979) Rana, S.; Singla, A. K.; Bajaj, A.; Elci, S. G.; Miranda, O. R.; Mout, R.; Yan, B.; Jirik, F. R.; Rotello, V. M. Array-Based Sensing of Metastatic Cells and Tissues Using Nanoparticle-Fluorescent Protein Conjugates. *ACS Nano* **2012**, *6*, 8233-8240.

(980) Modena, M. M.; Chawla, K.; Misun, P. M.; Hierlemann, A. Smart Cell Culture Systems: Integration of Sensors and Actuators into Microphysiological Systems. *ACS Chem. Biol.* **2018**, *13*, 1767-1784.

(981) Altunbek, M.; Kuku, G.; Culha, M. Gold Nanoparticles in Single-Cell Analysis for Surface Enhanced Raman Scattering. *Molecules* **2016**, *21*, 1617/1-1617/18.

(982) Shekhar, S.; Cambi, A.; Figdor, C. G.; Subramaniam, V.; Kanger, J. S. A Method for Spatially Resolved Local Intracellular Mechanochemical Sensing and Organelle Manipulation. *Biophys. J.* **2012**, *103*, 395-404.

(983) Niu, X.; Mo, Z.; Yang, X.; Sun, M.; Zhao, P.; Li, Z.; Ouyang, M.; Liu, Z.; Gao, H.; Guo, R.; Liu, N. Advances in the Use of Functional Composites of β-Cyclodextrin in Electrochemical Sensors. *Microchim. Acta* **2018**, *185(7)*, 1-17.

(984) Rezanka, M. Synthesis of Substituted Cyclodextrins. *Environ. Chem. Lett.* **2018**, *Ahead of Print*; DOI: 10.1007/s10311-018-0779-7.

(985) Cong, H. Ni, X. L.; Xiao, X.; Huang, Y.; Zhu, Q.-J.; Xue, S.-F.; Tao, Z.; Lindoy, L. F.; Wei, G. Synthesis and Separation of Cucurbit[n]urils and their Derivatives. *Org. Biomol. Chem.* **2016**, *14*, 4335-4364.

(986) Rusalov, M. V.; Uzhinov, B. M.; Alfimov, M. V.; Gromov, S. P. Photoinduced Recoordination of Metal Cations in Complexes with Chromogenic Crown Ethers. *Russian Chem. Rev.* **2010**, *79*, 1099-1121.

(987) Li, J.; Yim, D.; Jang, W.-D.; Yoon, J. Recent Progress in the Design and Applications of Fluorescence Probes Containing Crown Ethers. *Chem. Soc. Rev.* **2017**, *46*, 2437-2458.

(988) Cram, D. J. Cavitands: Organic Hosts with Enforced Cavities. *Science* **1983**, *219*, 1177-1183.

(989) Kobayashi, K.; Yamanaka, M. Self-Assembled Capsules Based on Tetrafunctionalized Calix[4]resorcinarene Cavitands. *Chem. Soc. Rev.* **2015**, *44*, 449-466.

(990) Pinalli, R.; Pedrini, A.; Dalcanale, E. Environmental Gas Sensing with Cavitands. *Chem. Eur. J.* **2018**, *24*, 1010-1019.

(991) Szejtli, J. Past, Present, and Future of Cyclodextrin Research. *Pure Appl. Chem.* **2004**, *76*, 1825-1845.

(992) Szejtli, J. Introduction and General Overview of Cyclodextrin Chemistry. *Chem. Rev.* **1998**, *98*, 1743-1753.

(993) Fernandez, J. M. G.; Mellet, C. O.; Defaye, J. Glyco-Nano-Cavities: Cyclodextrins and Beyond. *J. Inclusion Phenom. Macrocyclic Chem.* **2006**, *56*, 149-159.

(994) Harata, K. Structural Aspects of Stereodifferentiation in the Solid State. *Chem. Rev.* **1998**, *98*, 1803-1827.

(995) Guzman-Maldonado, H.; Paredes-Lopez, O. Amylolytic Enzymes and Products Derived from Starch: A Review. *Critical Rev. Food Sci. Nutrition* **1995**, *35*, 373-403.

(996) Li, Z.; Chen, S.; Gu, Z.; Chen, J.; Wu, J. Alpha-Cyclodextrin: Enzymatic Production and Food Applications. *Trends Food Sci. Technol.* **2014**, *35*, 151-160.

(997) Dardeer, H. M. Importance of Cyclodextrins into Inclusion Complexes. *Int. J. Adv. Res.* **2014**, *2*, 414-428.

(998) Saokham, P.; Loftsson, T. γ-Cyclodextrin. *Int. J. Pharmaceutics* **2017**, *516*, 278-292.

(999) Schneider, H.-J. Dispersive Interactions in Solution Complexes. *Acc. Chem. Res.* **2015**, *48*, 1815-1822.

(1000) Chen, Y.; Liu, Y. Construction and Functions of Cyclodextrin-Based 1D Supramolecular Strands and their Secondary Assemblies. *Adv. Mater.* **2015**, *27*, 5403-5409.

(1001) Cai, W.; Sun, T.; Shao, X.; Chipot, C. Can the Anomalous Aqueous Solubility of β-Cyclodextrin be Explained by its Hydration Free Energy Alone? *Phys. Chem. Chem. Phys.* **2008**, *10*, 3236-3243.

(1002) Naidoo, K. J.; Chen, J. Y.-J.; Jansson, J. L. M.; Widmalm, G.; Maliniak, A. Molecular Properties Related to the Anomalous Solubility of β-Cyclodextrin. *J. Phys. Chem. B* **2004**, *108*, 4236-4238.

(1003) Gurbuz, S.; Idris, M.; Tuncel, D. Cucurbituril-Based Supramolecular Engineered Nanostructured Materials. *Org. Biomol. Chem.* **2015**, *13*, 330-347.

(1004) Buschmann, H.-J. From Small Cucurbituril Complexes to Large Ordered Networks. *Israel J. Chem.* **2011**, *51*, 533-536.

(1005) Pinalli, R.; Boccini, F.; Dalcanale, E. Cavitand-Based Coordination Cages: Achievements and Current Challenges. *Israel J. Chem.* **2011**, *51*, 781-797.

(1006) Dodziuk, H. Rigidity versus Flexibility. A Review of Experimental and Theoretical Studies Pertaining to the Cyclodextrin Non-Rigidity. *J. Molec. Structure* **2002**, *614*, 33-45.

(1007) Guo, D.-S.; Uzunova, V. D.; Assaf, K. I.; Lazar, A. I.; Liu, Y.; Nau, W. M. Inclusion of Neutral Guests by Water-Soluble Macrocyclic Hosts - A Comparative Thermodynamic Investigation with Cyclodextrins, Calixarenes and Cucurbiturils. *Supramol. Chem.* **2016**, 28, 384-395.

(1008) Takezawa, K.; Hirai, T.; Yamamoto, T.; Yoshikiyo, K. Thermodynamic and Structural Studies on the Complexation of Guanidino-Appended α-Cyclodextrin Derivatives with p-Nitrophenolate Ion. *J. Molec. Structure* **2016**, *1108*, 80-86.

(1009) Harata, K. Crystallographic Analysis of the Thermal Motion of the Inclusion Complex of Cyclomaltoheptaose (β-Cyclodextrin) with Hexamethylenetetramine. *Carbohydr. Res.* **2003**, *338*, 353-359.

(1010) Zerbetto, M.; Kotsyubynskyy, D.; Kowalewski, J.; Widmalm, G.; Polimeno, A. Stochastic Modeling of Flexible Biomolecules Applied to NMR Relaxation. I. Internal Dynamics of Cyclodextrins: γ-Cyclodextrin as a Case Study. *J. Phys. Chem. B* **2012**, *116*, 13159-13171.

(1011) Zhang, N.; Chen, Y.; Yu, M.; Liu, Y. Benzenesulfonamidoquinolino-β-Cyclodextrin as a Cell-Impermeable Fluorescent Sensor for Zn2+. *Chem. Asian J.* **2009**, *4*, 1697-1702.

(1012) Hayashida, O.; Hamachi, I. Fluorophore Appended Saccharide Cyclophane: Self-Association, Fluorescent Properties, Hetero-Dimers with Cyclodextrins, and Cross-Linking Behavior with Peanut Agglutinin of Dansyl-Modified Saccharide Cyclophane. *J. Org. Chem.* **2004**, *69*, 3509-3516.

(1013) Corradini, R.; Dossena, A.; Marchelli, R.; Panagia, A.; Sartor, G.; Saviano, M.; Lombardi, A.; Pavone, V. A Modified Cyclodextrin with a Fully Encapsulated Dansyl Group: Self-Inclusion in the Solid State and in Solution. *Chem. Eur. J.* **1996**, *2*, 373-381.

(1014) Agbaria, R. A.; Gill, D. Extended 2,5-Diphenyloxazole-γ-Cyclodextrin Aggregates Emitting 2,5-Diphenyloxazole Excimer Fluorescence. *J. Phys. Chem.* **1988**, *92*, 1052-1055.

(1015) Sikorski, C. T.; Petter, R. C. The Effect of Tether Length on the Affinity of Ligands for Bis(cyclodextrins). *Tetrahedron Lett.* **1994**, *35*, 4275-4278.

(1016) Tungala, K.; Adhikary, P.; Azmeera, V.; Kumar, K.; Krishnamoorthi, S. Dendritic Star Polymer of Polyacrylamide Based on a β-Cyclodextrin Trimer: A Flocculant and Drug Vehicle. *New J. Chem.* **2017**, *41*, 611-618.

(1017) Arslan, M.; Yilmaz Sengel, T.; Guler, E.; Gumus, Z. P.; Aldemir, E.; Akbulut, H.; Coskunol, H.; Timur, S.; Yagci, Y. Double Fluorescence Assay via a β-Cyclodextrin Containing Conjugated Polymer as a Biomimetic Material for Cocaine Sensing. *Polym. Chem.* **2017**, *8*, 3333-3340.

(1018) Chen, G.; Jiang, M. Cyclodextrin-Based Inclusion Complexation Bridging Supramolecular Chemistry and Macromolecular Self-Assembly. *Chem. Soc. Rev.* **2011**, *40*, 2254-2266.

(1019) Gould, S.; Scott, R. C. 2-Hydroxypropyl-β-Cyclodextrin (HP-β-CD): A Toxicology Review. *Food Chem. Toxicol.* **2005**, *43*, 1451-1459.

(1020) Tolnai, G. L.; Nilsson, U. J.; Olofsson, B. Efficient O-Functionalization of Carbohydrates with Electrophilic Reagents. *Angew. Chem. Int. Ed.* **2016**, *55*, 11226-11230.

(1021) Guo, Z.; Chen, X.; Zhang, X.; Xin, J.; Li, J.; Xiao, H. Effective Syntheses of Per-2,3-Di- and Per-3-O-Chloroacetyl-β-Cyclodextrins: A New Kind of ATRP Initiators for Star Polymers. *Tetrahedron Lett.* **2010**, *51*, 2351-2353.

(1022) Lopez, O.; Bols, M. Effective Synthesis of Negatively Charged Cyclodextrins. Selective Access to Phosphate Cyclodextrins. *Tetrahedron* **2008**, *64*, 7587-7593.

(1023) Coleman, A. W.; Zhang, P.; Ling, C. C.; Parrot-Lopez, H.; Galons, H. The Use of Chlorodimethylthexylsilane for Protecting the Hydroxyl Groups in Cyclomaltoheptaose (β-Cyclodextrin). *Carbohydr. Res.* **1992**, *224*, 307-309.

(1024) Balbuena, P.; Goncalves-Pereira, R.; Jimenez Blanco, J. L.; Garcia-Moreno, M. I.; Lesur, D.; Ortiz Mellet, C.; Garcia Fernandez, J. M. o-Xylylene Protecting Group in Carbohydrate Chemistry: Application

to the Regioselective Protection of a Single vic-Diol Segment in Cyclodextrins. *J. Org. Chem.* **2013**, *78*, 1390-1403.

(1025) Rezanka, M. Monosubstituted Cyclodextrins as Precursors for Further Use. *Eur. J. Org. Chem.* **2016**, *2016*, 5322-5334.

(1026) Armspach, D.; Matt, D. The Tris(4-tert-butylphenyl)methyl Group: A Bulky Substituent for Effective Regioselective Difunctionalization of Cyclomaltohexaose. *Carbohydr. Res.* **1998**, *310*, 129-133.

(1027) Letort, S.; Mathiron, D.; Grel, T.; Albaret, C.; Daulon, S.; Djedaini-Pilard, F.; Gouhier, G.; Estour, F. The First 2IB,3IA-Hetero-Difunctionalized β-Cyclodextrin Derivatives as Artificial Enzymes. *Chem. Commun.* **2015**, *51*, 2601-2604.

(1028) Oliveri, V.; Bellia, F.; Pietropaolo, A.; Vecchio, G. Unusual Cyclodextrin Derivatives as a New Avenue to Modulate Self- and Metal-Induced Aβ Aggregation. *Chem. Eur. J.* **2015**, *21*, 14047-14059.

(1029) Atsumi, M.; Izumida, M.; Yuan, D.-Q.; Fujita, K. Selective Synthesis and Structure Determination of 6A,6C,6E-Tri(O-sulfonyl)-β-Cyclodextrins. *Tetrahedron Lett.* **2000**, *41*, 8117-8120.

(1030) Jouffroy, M.; Armspach, D.; Matt, D.; Toupet, L. Regioselective Di- and Tetra-Functionalization of γ-Cyclodextrin Using Capping Methodology. *Org. Biomol. Chem.* **2013**, *11*, 3699-3705.

(1031) Gu, J.; Chen, T.; Zhang, P.; Ling, C.-C. Controlled Acid-Mediated Regioselective O-Desilylation for Multi-Functionalization of Cyclodextrins. *Eur. J. Org. Chem.* **2014**, *2014*, 5793-5805.

(1032) Zhao, Y.-L.; Zhang, H.-Y.; Wang, M.; Yu, H.-M.; Yang, H.; Liu, Y. Organic Anion Recognition of Naphthalenesulfonates by Steroid-Modified β-Cyclodextrins: Enhanced Molecular Binding Ability and Molecular Selectivity. *J. Org. Chem.* **2006**, *71*, 6010-6019.

(1033) Luzardo-Alvarez, A.; Antelo-Queijo, A.; Soto, V. H.; Blanco-Mendez, J. Preparation and Characterization of β-Cyclodextrin-Linked Chitosan Microparticles. *J. Appl. Polym. Sci.* **2012**, *123*, 3595-3604.

(1034) Pettiwala, A. M.; Singh, P. K. Supramolecular Dye Aggregate Assembly Enables Ratiometric Detection and Discrimination of Lysine and Arginine in Aqueous Solution. *ACS Omega* **2017**, *2*, 8779-8787.

(1035) Zaruba, K.; Vasek, P.; Kral, V. Study of Molecular Recognition of 5,10,15,20-Tetrakis(pentafluorophenyl)porphyrin-β-Cyclodextrin Conjugate Covalently Immobilized on a Silica Surface. *Supramol. Chem.* **2004**, *16*, 529-536.

(1036) Plazzo, A. P.; Hoefer, C. T.; Jicsinszky, L.; Fenyvesi, E.; Szente, L.; Schiller, J.; Herrmann, A.; Mueller, P. Uptake of a Fluorescent Methyl-β-Cyclodextrin via Clathrin-Dependent Endocytosis. *Chem. Phys. Lipids* **2012**, *165*, 505-511.

(1037) Maciollek, A.; Ritter, H.; Beckert, R. Superstructures of Fluorescent Cyclodextrin via Click-Reaction. *Beilstein J. Org. Chem.* **2013**, *9*, 827-831.

(1038) Sun, J.; Wang, S.; Gao, F. Covalent Surface Functionalization of Semiconducting Polymer Dots with β-Cyclodextrin for Fluorescent Ratiometric Assay of Cholesterol through Host-Guest Inclusion and FRET. *Langmuir* **2016**, *32*, 12725-12731.

(1039) Luo, M.; Hua, Y.; Liang, Y.; Han, J.; Liu, D.; Zhao, W.; Wang, P. Synthesis of Novel β-Cyclodextrin Functionalized S, N Codoped Carbon Dots for Selective Detection of Testosterone. *Bios. Bioelectron.* **2017**, *98*, 195-201.

(1040) Tian, S.; D'Souza, V. T. Selective Protection of the Secondary Side of β-Cyclodextrin. *Tetrahedron Lett.* **1994**, *35*, 9339-9342.

(1041) Khan, A. R.; Barton, L.; D'Souza, V. T. Epoxides of the Secondary Side of Cyclodextrins. *J. Org. Chem.* **1996**, *61*, 8301-8303.

(1042) Ward, S.; Ling, C.-C. Efficient and Versatile Modification of the Secondary Face of Cyclodextrins through Copper-Catalyzed Huisgen 1,3-Dipolar Cycloaddition. *Eur. J. Org. Chem.* **2011**, *2011*, 4853-4861.

(1043) Vurgun, N.; Gomez-Biagi, R. F.; Nitz, M. Access to Versatile β-Cyclodextrin Scaffolds through Guest-Mediated Monoacylation. *Chem. Eur. J.* **2016**, *22*, 1062-1069.

(1044) Bistri, O.; Sinay, P.; Sollogoub, M. Expeditious Selective Synthesis of Primary Rim Tri-Differentiated α-Cyclodextrin. *Tetrahedron Lett.* **2006**, *47*, 4137-4139.

(1045) Chiu, S.-H.; Myles, D. C. Efficient Mono-modification of the Secondary Hydroxyl Groups of β-Cyclodextrin. *J. Org. Chem.* **1999**, *64*, 332-333.

(1046) Menuel, S.; Doumert, B.; Saitzek, S. Ponchel, A.; Delevoye, L.; Monflier, E.; Hapoit, F. Selective Secondary Face Modification of Cyclodextrins by Mechanosynthesis. *J. Org. Chem.* **2015**, *80*, 6259-6266.

(1047) Schmidt, B. V. K. J.; Barner-Kowollik, C. Dynamic Macromolecular Material Design-The Versatility of Cyclodextrin-Based Host-Guest Chemistry. *Angew. Chem. Int. Ed.* **2017**, *56*, 8350-8369.

(1048) Antoniuk, I.; Amiel, C. Cyclodextrin-Mediated Hierarchical Self-Assembly and Its Potential in Drug Delivery Applications. *J. Pharm. Sci.* **2016**, *105*, 2570-2588.

(1049) Sharma, N.; Baldi, A. Exploring Versatile Applications of Cyclodextrins: An Overview. *Drug Delivery* **2016**, *23*, 729-747.

(1050) Baron, R.; Setny, P.; McCammon, J. A. Hydrophobic Association and Volume-Confined Water Molecules. *Methods Principles Med. Chem.* **2012**, *53*, 145-170.

(1051) Liu, L.; Guo, Q.-X. The Driving Forces in the Inclusion Complexation of Cyclodextrins. *J. Incl. Phenom. Macrocycl. Chem.* **2002**, *42*, 1-14.

(1052) Loftsson, T. Drug Solubilization by Complexation. *Int. J. Pharm.* **2017**, *531*, 276-280.

(1053) Adeoye, O.; Cabral-Marques, H. Cyclodextrin Nanosystems in Oral Drug Delivery: A Mini Review. *Int. J. Pharm.* **2017**, *531*, 521-531.

(1054) Peng, L.; Liu, S.; Feng, A.; Yuan, J. Polymeric Nanocarriers Based on Cyclodextrins for Drug Delivery: Host-Guest Interaction as Stimuli Responsive Linker. *Mol. Pharm.* **2017**, *14*, 2475-2486.

(1055) Karoyo, A. H.; Wilson, L. D. Nano-Sized Cyclodextrin-Based Molecularly Imprinted Polymer Adsorbents for Perfluorinated Compounds-A Mini-Review. *Nanomaterials* **2015**, *5*, 981-1003.

(1056) Xiao, L.; Ling, Y.; Alsbaiee, A.; Li, C.; Helbling, D. E.; Dichtel, W. R. β-Cyclodextrin Polymer Network Sequesters Perfluorooctanoic Acid at Environmentally Relevant Concentrations. *J. Am. Chem. Soc.* **2017**, *139*, 7689-7692.

(1057) DiScenza, D. J.; Verderame, M.; Levine, M. Detection of Benzene and Alkylated Benzene Derivatives in Fuel Contaminated Environments. *Clean: Soil, Air, Water* **2016**, *44*, 1621-1627.

(1058) Kumar, A.; Sharma, G.; Naushad, M.; Thakur, S. SPION/β-Cyclodextrin Core-Shell Nanostructures for Oil Spill Remediation and Organic Pollutant Removal from Wastewater. *Chem. Eng. J.* **2015**, *280*, 175-187.

(1059) Serio, N.; Chanthalyma, C.; Prignano, L.; Levine, M. Cyclodextrin-Enhanced Extraction and Energy Transfer of Carcinogens in Complex Oil Environments. *ACS Appl. Mater. Interfaces* **2013**, *5*, 11951-11957.

(1060) Setthayanond, J.; Sodsangchan, C.; Suwanruji, P.; Tooptompong, P.; Avinc, O. Influence of MCT-β-Cyclodextrin Treatment on Strength, Reactive Dyeing and Third-Hand Cigarette Smoke Odor Release Properties of Cotton Fabric. *Cellulose* **2017**, *24*, 5233-5250.

(1061) Alzate-Sanchez, D. M.; Smith, B. J.; Alsbaiee, A.; Hinestroza, J. P.; Dichtel, W. R. Cotton Fabric Functionalized with a β-Cyclodextrin Polymer Captures Organic Pollutants from Contaminated Air and Water. *Chem. Mater.* **2016**, *28*, 8340-8346.

(1062) Celebioglu, A.; ipek, S.; Durgun, E.; Uyar, T. Selective and Efficient Removal of Volatile Organic Compounds by Channel-type Gamma-Cyclodextrin Assembly through Inclusion Complexation. *Ind. Eng. Chem. Res.* **2017**, *56*, 7345-7354.

(1063) Zerkoune, L.; Angelova, A.; Lesieur, S. Nano-Assemblies of Modified Cyclodextrins and their Complexes with Guest Molecules: Incorporation in Nanostructured Membranes and Amphiphile Nanoarchitectonics Design. *Nanomaterials* **2014**, *4*, 741-765.

(1064) Sardella, R.; Ianni, F.; Marinozzi, M.; Macchiarulo, A.; Natalini, B. Laboratory-Scale Preparative Enantioseparations of Pharmaceutically Relevant Compounds on Commercially Available Chiral Stationary Phases for HPLC. *Curr. Med. Chem.* **2017**, *24*, 796-817.

(1065) Zohrehvand, S.; Evans, C. H. 2-Naphthol-Containing β-Cyclodextrin-Epichlorohydrin Copolymers: Synthesis, Characterization and Fluorescence Studies. *Polym. Int.* **2005**, *54*, 744-753.

(1066) Benkovics, G.; Malanga, M.; Fenyvesi, E. The 'Visualized' Macrocycles: Chemistry and Application of Fluorophore Tagged Cyclodextrins. *Int. J. Pharmaceutics* **2017**, *531*, 689-700.

(1067) Ashton, P. R.; Boyd, S. E.; Gattuso, G.; Hartwell, E. Y.; Koeniger, R.; Spencer, N.; Stoddart, J. F. A Novel Approach to the Synthesis of Some Chemically-Modified Cyclodextrins. *J. Org. Chem.* **1995**, *60*, 3898-3903.

(1068) Bistri, O.; Sinay, P.; Sollogoub, M. Diisobutylaluminum Hydride (DIBAL-H) is Promoting a Selective Clockwise Debenzylation of Per-Benzylated 6A,6D-Dideoxy-α-Cyclodextrin. *Tetrahedron Lett.* **2005**, *46*, 7757-7760.

(1069) Xiao, S.; Yang, M.; Sinay, P.; Bleriot, Y.; Sollogoub, M.; Zhang, Y. Diisobutylaluminium Hydride (DIBAL-H) Promoted Secondary Rim Regioselective Demethylations of Permethylated β-Cyclodextrin: A Mechanistic Proposal. *Eur. J. Org. Chem.* **2010**, 1510-1516.

(1070) Ghosh, R.; Hennigan, C.; Ling, C.-C. DIBAL-H-Mediated O-Desilylation with Highly Sterically Hindered Cyclodextrin Substrates. *Tetrahedron* **2013**, *69*, 5227-5233.

(1071) Xiao, S. L.; Zhou, D. M.; Yang, M.; Yu, F.; Zhang, L. H.; Sinay, P.; Zhang, Y. M. Synthesis of Two Mono-Deoxy β-Cyclodextrin Derivatives as Useful Tools for Confirming DIBAL-H Promoted Bis-de-O-Methylation Mechanism. *Chinese Chem. Lett.* **2012**, *23*, 1315-1318.

(1072) Lindbaeck, E.; Zhou, Y.; Pedersen, C. M.; Bols, M. Two Diastereomeric Artificial Enzymes with Different Catalytic Activity. *Eur. J. Org. Chem.* **2012**, *2012*, 5366-5372.

(1073) Tripodo, G.; Wischke, C.; Neffe, A. T.; Lendlein, A. Efficient Synthesis of Pure Monotosylated beta-Cyclodextrin and its Dimers. *Carbohydrate Res.* **2013**, *381*, 59-63.

(1074) Benkovics, G.; Hodek, O.; Havlikova, M.; Bosakova, Z.; Coufal, P.; Malanga, M.; Fenyvesi, E.; Darcsi, A.; Beni, S.; Jindrich, J. Supramolecular Structures Based on Regioisomers of Cinnamyl-α-Cyclodextrins - New Media for Capillary Separation Techniques. *Beilstein J. Org. Chem.* **2016**, *12*, 97-109.

(1075) Deege, A.; Husmann, H.; Huebinger, E.; Kobor, F.; Schomburg, G. Purification and Analysis of Partially Alkylated Cyclodextrins by Liquid and Gas Chromatography. *J. High Resolution Chromatography* **1993**, *16*, 587-589.

(1076) Mutai, T.; Araki, K. Fluorescent Oligopyridines and their Photo-Functionality as Tunable Fluorophores. *Curr. Org. Chem.* **2007**, *11*, 195-211.

(1077) Shin, I. S.; Lee, D. G.; Lee, J. H.; Jeong, H.-J.; Seo, Y. J. Characterization and Histone Deacetylase Inhibitory Activity of Three Novel Fluorescent Benzamide Derivatives. *Bull. Korean Chem. Soc.* **2015**, *36*, 553-558.

(1078) Yoshizawa, M.; Klosterman, J. K. Molecular Architectures of Multi-Anthracene Assemblies. *Chem. Soc. Rev.* **2014**, *43*, 1885-1898.

(1079) Kerr, E.; West, C.; Hartwell, S. K. Quantitative TLC-Image Analysis of Urinary Creatinine Using Iodine Staining and RGB Values. *J. Chromatographic Sci.* **2016**, *54*, 639-646.

(1080) Yang, C.; Spinelli, N.; Perrier, S.; Defrancq, E.; Peyrin, E. Macrocyclic Host-Dye Reporter for Sensitive Sandwich-Type Fluorescent Aptamer Sensor. *Anal. Chem.* **2015**, *87*, 3139-3143.

(1081) Zhang, L.; Hu, W.; Yu, L.; Wang, Y. Click Synthesis of a Novel Triazole Bridged AIE Active Cyclodextrin Probe for Specific Detection of Cd2+. *Chem. Commun.* **2015**, *51*, 4298-4301.

(1082) He, X.-P.; Li, R.-H.; Maisonneuve, S.; Ruan, Y.; Chen, G.-R.; Xie, J. Fluorogenic Supramolecular Complexes Formed Between Pyrenyl-β-Cyclodextrin and Glyco-Rhodamine for the Selective Detection of Lectins. *Chem. Commun.* **2014**, *50*, 14141-14144.

(1083) Martos-Maldonado, M. C.; Quesada-Coriano, I.; Casas-Solvas, J. M.; García-Fuentes, L.; Vargas-Berenguel, A. Secondary Face-to-Face 2-2' β-Cyclodextrin Dimers Linked with Fluorescent Rigid Spacer Arms: A Cyclodextrin-Based Ratiometric Sensor for Bile Salts. *Eur. J. Org. Chem.* **2012**, *2012*, 2560-2571.

(1084) Feng, L.; Tong, C.; He, Y.; Liu, B.; Wang, C.; Sha, J.; Lu, C. A Novel FRET-Based Chemosensor of β-Cyclodextrin Derivative for TNT Detection in Aqueous Solution. *J. Luminescence* **2014**, *146*, 502-507.

(1085) Zhang, F.; Zhao, Y.-Y.; Chen, H.; Wang, X.-H.; Chen, Q.; He, P.-G. Sensitive Fluorescence Detection of Lysozyme Using a Tris(bipyridine)ruthenium(II) Complex Containing Multiple Cyclodextrins. *Chem. Commun.* **2015**, *51*, 6613-6616.

(1086) Pagliari, S.; Corradini, R.; Galaverna, G.; Sforza, S.; Dossena, A.; Montalti, M.; Prodi, L.; Zaccheroni, N.; Marchelli, R. Enantioselective Fluorescence Sensing of Amino Acids by Modified Cyclodextrins: Role of the Cavity and Sensing Mechanism. *Chem. Eur. J.* **2004**, *10*, 2749-2758.

(1087) Fukuhara, G.; Inoue, Y. Peptide Chirality Sensing by a Cyclodextrin-Polythiophene Conjugate. *Chem. Eur. J.* **2012**, *18*, 11459-11464.

(1088) Lepinay, S.; Laffont, G.; Volet, G.; Wintgens, V.; Ferdinand, P.; Millot, M.-C.; Carbonnier, B. Cyclodextrin-Based Supramolecular Multilayer Assemblies for the Design of Biological Optical Sensors Using Tilted Fiber Bragg Gratings. *Key Engineering Mater.* **2012**, *495*, 45-48.

(1089) Clements, A. R.; Pattabiraman, M. γ-Cyclodextrin Mediated Photo-Heterodimerization Between Cinnamic Acids and Coumarins. *J. Photochem. Photobiol. A: Chem.* **2015**, *297*, 1-7.

(1090) Liu, N.; Higashi, K.; Ueda, K.; Moribe, K. Effect of Guest Drug Character Encapsulated in the Cavity and Intermolecular Spaces of γ-Cyclodextrins on the Dissolution Property of Ternary γ-Cyclodextrin Complex. *Int. J. Pharmaceutics* **2017**, *531*, 543-549.

(1091) ten Brummelhuis, N.; Heilmann, M. T. Polymerization of Ternary Inclusion Complexes of Interacting Monomer Pairs with γ-Cyclodextrin. *Macromolecules* **2016**, *49*, 6879-6887.

(1092) Santos, C. I. A. V.; Teijeiro, C.; Ribeiro, A. C. F.; Rodrigues, D. F. S. L.; Romero, C. M.; Esteso, M. A. Drug Delivery Systems: Study of Inclusion Complex Formation for Ternary Caffeine-β-Cyclodextrin-Water Mixtures from Apparent Molar Volume Values at 298.15 K and 310.15 K. *J. Molec. Liquids* **2016**, *223*, 209-216.

(1093) Mendez, S. G.; Otero Espinar, F. J.; Alvarez, A. L.; Longhi, M. R.; Quevedo, M. A.; Zoppi, A. Ternary Complexation of Benzoic Acid with β-Cyclodextrin and Aminoacids - Experimental and Theoretical Studies. *J. Inclusion Phenom. Macrocyclic Chem.* **2016**, *85*, 33-48.

(1094) Serio, N.; Prignano, L.; Peters, S.; Levine, M. Detection of Medium-Sized Polycyclic Aromatic Hydrocarbons via Fluorescence Energy Transfer. *Polycyclic Aromatic Hydrocarbons* **2014**, *34*, 561-572.

(1095) Serio, N.; Chanthalyma, C.; Peters, S.; Levine, D.; Levine, M. 2-Hydroxypropyl beta-Cyclodextrin for the Enhanced Performance of Dual Function Extraction and Detection Systems in Complex Oil Environments. *J. Incl. Phenom. Macrocycl. Chem.* **2015**, *81*, 341-346.

(1096) Serio, N.; Levine, M. Solvent Effects in the Extraction and Detection of Polycyclic Aromatic Hydrocarbons from Complex Oils in Complex Environments. *J. Incl. Phenom. Macrocycl. Chem.* **2016**, *84*, 61-70.

(1097) Serio, N.; Levine, M. Efficient Extraction and Detection of Aromatic Toxicants from Crude Oil and Tar Balls Using Multiple Cyclodextrin Derivatives. *Marine Pollution Bulletin* **2015**, *95*, 242-247.

(1098) Jin, F.; Lian, Y.; Li, J.; Zheng, J.; Hu, Y.; Liu, J.; Huang, J.; Yang, R. Molecule-Binding Dependent Assembly of Split Aptamer and γ-Cyclodextrin: A Sensitive Excimer Signaling Approach for Aptamer Biosensors. *Anal. Chim. Acta* **2013**, *799*, 44-50.

(1099) Khan, R. I.; Pitchumani, K. β-Cyclodextrin Included Coumarin Derivatives as Selective Fluorescent Sensors for Cu2+ Ions in HeLa Cells. *RSC Adv.* **2016**, *6*, 20269-20275.

(1100) Jullian, C.; Fernández-Sandoval, S.; Rojas-Aranguiz, M.; Gómez-Machuca, H.; Salgado-Figueroa, P.; Celis-Barros, C.; Zapata-Torres, G.; Adam, R.; Abarca, B. Detecting Ni(II) in Aqueous Solution by 3-(2-Pyridyl)-[1,2,3]triazolo[1,5-α]pyridine and Dimethyl-β-Cyclodextrin. *Carbohydr. Polym.* **2014**, *107*, 124-131.

(1101) Maniyazagan M.; Mohandoss, S.; Sivakumar, K.; Stalin, T. N-Phenyl-1-Naphthylamine/β-Cyclodextrin Inclusion Complex as a New Fluorescent Probe for Rapid and Visual Detection of Pd2+. *Spectrochim. Acta, Part A* **2014**, *133*, 73-79.

(1102) Liu, M.; Deng, J.; Lai, C.; Chen. Q.; Zhao, Q.; Zhang, Y.; Li, H.; Yao, S. Synthesis, Characterization of Conjugated Oligo-Phenylene-Ethynylenes and their Supramolecular Interaction with β-Cyclodextrin for Salicylaldehyde Detection. *Talanta* **2012**, *100*, 229-238.

(1103) Jalali, F.; Ezzati, N. Spectrofluorimetric Study and Determination of Desipramine in the Presence of β-Cyclodextrin. *J. Anal. Chem*. **2014**, *69*, 367-370.

(1104) Alremrithi, R. H; Meetani, M. A.; Mousa, M. K.; Saleh, N. I.; Graham, J. Determination of *p*-Aminohippuric Acid with β-Cyclodextrin Sensitized Fluorescence Spectrometry. *RSC Adv*. **2016**, *6*, 114296-114303.

(1105) Abdel-Aziz, O.; Kosasy, A. M. E.; Okeil, S. M. E.-S. Novel Comparative Synchronous Spectrofluorimetric Study of Benzo(a)pyrene Using beta-Cyclodextrin and Calix(8)arene as Fluorescence Enhancers. *J. Fluorescence* **2014**, *24*, 549-556.

(1106) Martínez-Tomé, M. J.; Esquembre, R.; Mallavia, R.; Mateo, C. R. Development of a Dual-Analyte Fluorescent Sensor for the Determination of Bioactive Nitrite and Selenite in Water Samples. *J. Pharm. Biomed. Anal.* **2010**, *51*, 484-489.

(1107) Ning, J.; Zhao, J.; Meng, L.; Bi, L. Vortex-Assisted Surfactant-Enhanced Emulsification Microextraction Combined with High Performance Liquid Chromatography-Fluorescence Detector for Determination of Nitrite in Urine. *Asian J. Chem.* **2014**, *26*, 7129-7132.

(1108) Kavitha, R.; Stalin, T. A Highly Selective Chemosensor for Colorimetric Detection of Hg2+ and Fluorescence Detection of pH Changes in Aqueous Solution. *J. Luminescence* **2014**, *149*, 12-18.

(1109) Ferey, L.; Delaunay, N.; Rutledge, D. N.; Cordella, C. B. Y.; This, H.; Huertas, A.; Raoul, Y.; Gareil, P. Optimizing Separation Conditions of 19 Polycyclic Aromatic Hydrocarbons by Cyclodextrin-Modified Capillary Electrophoresis and Applications to Edible Oils. *Talanta* **2014**, *119*, 572-581.

(1110) Ferey, L.; Delaunay, N.; Rutledge, D. N.; Huertas, A.; Raoul, Y.; Gareil, P.; Vial, J. Use of Response Surface Methodology to Optimize the Simultaneous Separation of Eight Polycyclic Aromatic Hydrocarbons by Capillary Zone Electrophoresis with Laser-Induced Fluorescence Detection. *J. Chromatogr.* **2013**, *1302*, 181-190.

(1111) Liang, G.; Choi, K.; Ahmed, A. Y. B. H.; Alothman, Z. A.; Chung, D. S. Highly Sensitive Chiral Analysis of Amino Acids by In-Line Single Drop Microextraction and Capillary Electrophoresis with Laser-Induced Fluorescence Detection. *Anal. Chim. Acta* **2010**, *677*, 37-42.

(1112) Lin, K.-C.; Hsieh, M.-M.; Chang, C.-W.; Lin, E.-P.; Wu T.-H. Stacking and Separation of Aspartic Acid Enantiomers Under Discontinuous System by Capillary Electrophoresis with Light-Emitting Diode-Induced Fluorescence Detection. *Talanta* **2010**, *82*, 1912-1918.

(1113) Wahl, O.; Holzgrabe, U. Evaluation of Enantiomeric Purity of Magnesium-L-Aspartate Dehydrate. *J. Pharm. Biomed. Anal.* **2015**, *102*, 100-109.

(1114) Liu, K.; Wang, L. Enantioseparations of Amino Acids by Capillary Array Electrophoresis with 532 nm Laser-induced Fluorescence Detection. *J. Chromatogr. A.* **2013**, *1295*, 142-146.

(1115) Stephen, T. K. L.; Guillemette, K. L.; Green, T. K. Analysis of Trinitrophenylated Adenosine and Inosine by Capillary Electrophoresis and γ-Cyclodextrin-Enhanced Fluorescence Detection. *Anal. Chem.* **2016**, *88*, 7777-7785.

(1116) Shi, X.; Liang, P.; Song, D.; Yang, W.; Gao, X. Quantification of γ-Aminobutyric Acid in the Heads of Houseflies (*Musca domestica*) and Diamondback Moths (*Plutella xylostella* (L.)), Using Capillary Electrophoresis with Laser-Induced Fluorescence. *J. Separation Sci.* **2012**, *35*, 548-555.

(1117) Uzaşçı, S.; Erim, F. B. Enhancement of Native Fluorescence Intensity of Berberine by (2-Hydroxypropyl)-β-Cyclodextrin in Capillary Electrophoresis Coupled by Laser-Induced Fluorescence Detection: Application to Quality Control of Medicinal Plants. *J. Chromatogr. A* **2014**, *1338*, 184-187.

(1118) Zhang, F.; Sun, Y.; Tian, D.; Shin, W. S.; Kim, J. S.; Li, H. Selective Molecular Recognition on Calixarene-Functionalized 3D Surfaces. *Chem. Commun.* **2016**, *52*, 12685-12693.

(1119) Hanna, T. A.; Liu, L.; Angeles-Boza, A. M.; Kou, X.; Gutsche, C. D.; Ejsmont, K.; Watson, W. H.; Zakharov, L. N.; Incarvito, C. D.; Rheingold, A. L. Synthesis, Structures, and Conformational Characteristics of Calixarene Monoanions and Dianions. *J. Am. Chem. Soc.* **2003**, *125*, 6228-6238.

(1120) Dondoni, A.; Marra, A. Multivalent Glycocalixarenes: Synthesis and Molecular Recognition. *RSC Polym. Chem. Series* **2015**, *15*, 96-148.

(1121) Boehmer, V. Calixarenes, Macrocycles with (Almost) Unlimited Possibilities. *Angew. Chem. Int. Ed.* **1995**, *34*, 713-745.

(1122) Gangemi, C. M. A.; Pappalardo, A.; Sfrazzetto, G. T. Assembling of Supramolecular Capsules with Resorcin[4]arene and Calix[n]arene Building Blocks. *Curr. Org. Chem.* **2015**, *19*, 2281-2308.

(1123) Hussain, M. A.; Ashraf, M. U.; Muhammad, G.; Tahir, M. N.; Bukhari, S. N. A. Calixarene: A Versatile Material for Drug Design and Applications. *Curr. Pharmaceutical Design* **2017**, *23*, 2377-2388.

(1124) Kudo, H.; Mitani, K.; Nishikubo, T.; Mitsuishi, M.; Miyashita, T. The Synthesis and Photo-Induced Deprotection Reaction of Calix[4]resorcinarene Derivatives Containing t-Butyl Ester Moieties. *Bull. Chem. Soc. Japan* **2004**, *77*, 819-826.

(1125) Bayrakcı, M.; Ertul, Ş.; Yilmaz, M. Transportation of Poorly Soluble Drug Molecules from the Organic Phase to the Aqueous Phase by Using Phosphorylated Calixarenes. *J. Chem. Eng. Data* **2011**, *56*, 4473-4479.

(1126) Chen, M.-X.; Li, T.; Peng, S.; Tao, D. Supramolecular Nanocapsules from the Self-Assembly of Amphiphilic Calixarene as a Carrier for Paclitaxel. *New. J. Chem.* **2016**, *40*, 9923-9929.

(1127) Mari, E.; Berthault, P. 129Xe NMR-Based Sensors: Biological Applications and Recent Methods. *Analyst* **2017**, *142*, 3298-3308.

(1128) Song, M.; Sun, Z.; Han, C.; Tian, D.; Li, H.; Kim, J. S. Calixarene-Based Chemosensors by Means of Click Chemistry. *Chem. Asian J.* **2014**, *9*, 2344-2357.

(1129) Giuliani, M.; Morbioli, I.; Sansone, F.; Casnati, A. Moulding Calixarenes for Biomacromolecule Targeting. *Chem. Commun.* **2015**, *51*, 14140-14159.

(1130) Chawla, H. M.; Shukla, R.; Pandey, S. Novel Fluorescein Appended Calix[4]arenes for Preferential Recognition of Cu2+ Ions. *Tetrahedron Lett.* **2013**, *54*, 2063-2066.

(1131) Chawla, H. M.; Gupta, T. Evaluation of a New Calix[4]arene Based Molecular Receptor for Sensitive and Selective Recognition of F- and Cu2+ Ions. *J. Luminescence* **2014**, *154*, 89-94.

(1132) Zadmard, R.; Akbari-Moghaddam, P.; Darvishi, S. Calix[4]arene-Based Crab-Like Molecular Sensors for Highly Selective Detection of Mercury and Copper Ions. *Supramol. Chem.* **2017**, *29*, 17-23.

(1133) Xie, D.-H.; Wang, X.-J.; Sun, C.; Han, J. Calix[4]arene Based 1,3,4-Oxadiazole as a Fluorescent Chemosensor for Copper(II) Ion Detection. *Tetrahedron Lett.* **2016**, *57*, 5834-5836.

(1134) Rahimi, Y.; Goulding, A.; Shrestha, S.; Mirpuri, S.; Deo, S. K. Mechanism of Copper Induced Fluorescence Quenching of Red Fluorescent Protein, DsRed. *Biochem. Biophys. Res. Commun.* **2008**, *370*, 57-61.

(1135) Beaune, G.; Tamang, S.; Bernardin, A.; Bayle-Guillemaud, P.; Fenel, D.; Schoehn, G.; Vinet, F.; Reiss, P.; Texier, I. Luminescence of Polyethylene Glycol Coated CdSeTe/ZnS and InP/ZnS Nanoparticles in the Presence of Copper Cations. *ChemPhysChem* **2011**, *12*, 2247-2254.

(1136) Lehrer, S. S. Fluorescence and Absorption Studies of the Binding of Copper and Iron to Transferrin. *J. Biol. Chem.* **1969**, *244*, 3613-3617.

(1137) Tamil Selvan, G.; Varadaraju, C.; Tamil Selvan, R.; Enoch, I. V. M. V.; Mosae Selvakumar, P. On /Off Fluorescent Chemosensor for Selective Detection of Divalent Iron and Copper Ions: Molecular Logic Operation and Protein Binding. *ACS Omega* **2018**, *3*, 7985-7992.

(1138) Wu, W.-N.; Mao, P.-D.; Wang, Y.; Mao, X.-J.; Xu, Z.-Q.; Xu, Z.-H.; Zhao, X.-L.; Fan, Y.-C.; Hou, X.-F. AEE Active Schiff Base-Bearing Pyrene Unit and Further Cu2+-Induced Self-Assembly Process. *Sens. Actuators B* **2018**, *258*, 393-401.

(1139) Xia, Y.; Yu, T.; Li, F.; Zhu, W.; Ji, Y.; Kong, S.; Li, C.; Huang, B.; Zhang, X.; Tian, Y.; Zhou, H. A Lipid Droplet-Targeted Fluorescence Probe for Visualizing Exogenous Copper (II) Based on LLCT and LMCT. *Talanta* **2018**, *188*, 178-182.

(1140) Ghosh, S.; Ali Khan, M.; Ganguly, A.; Al Masum, A.; Alam, Md. A.; Guchhait, N. Binding Mode Dependent Signaling for the Detection of Cu2+: An Experimental and Theoretical Approach with Practical Applications. *Spectrochim. Acta A* **2018**, *190*, 471-477.

(1141) Maher, N. J.; Diao, H.; O'Sullivan, J.; Fadda, E.; Heaney, F.; McGinley, J. Lower Rim Isoxazole-Calix[4]arene Derivatives as Fluorescence Sensors for Copper(II) Ions. *Tetrahedron* **2015**, *71*, 9223-9233.

(1142) Khan, B.; Shah, M. R.; Ahmed, D.; Rabnawaz, M.; Anis, I.; Afridi, S.; Makhmoor, T.; Tahir, M. N. Synthesis, Characterization and Cu2+ Triggered Selective Fluorescence Quenching of Bis-Calix[4]arene Tetra-Triazole Macrocycle. *J. Hazardous Mater.* **2016**, *309*, 97-106.

(1143) Joseph, R.; Chinta, J. P.; Rao, C. P. Benzothiazole Appended Lower Rim 1,3-Di-Amido-Derivative of Calix[4]arene: Synthesis, Structure, Receptor Properties Towards Cu2+, Iodide Recognition and Computational Modeling. *Inorg. Chim. Acta* **2010**, *363*, 2833-2839.

(1144) Pathak, R. K.; Hinge, V. K.; Mondal, P.; Rao, C. P. Ratiometric Fluorescence Off-On-Off Sensor for Cu2+ in Aqueous Buffer by a Lower Rim Triazole Linked Benzimidazole Conjugate of Calix[4]arene. *Dalton Trans.* **2012**, *41*, 10652-10660.

(1145) Xie, D.-H.; Wang, X.-J.; Sun, C.; Han, J. Calix[4]arene Based 1,3,4-Oxadiazole as a Fluorescent Chemosensor for Copper(II) Ion Detection. *Tetrahedron Lett.* **2016**, *57*, 5834-5836.

(1146) Sahin, O.; Akceylan, E. A Phenanthrene-Based Calix[4]arene as a Fluorescent Sensor for Cu2+ and F-. *Tetrahedron* **2014**, *70*, 6944-6950.

(1147) Sahin, O.; Yilmaz, M. Synthesis and Fluorescence Sensing Properties of a New Naphthalimide Derivative of Calix[4]arene. *Tetrahedron Lett.* **2012**, *53*, 2319-2324.

(1148) Maity, D.; Chakraborty, A.; Gunupuru, R.; Paul, P. Calix[4]arene Based Molecular Sensors with Pyrene as Fluorogenic Unit: Effect of Solvent in Ion Selectivity and Colorimetric Detection of Fluoride. *Inorg. Chim. Acta* **2011**, *372*, 126-135.

(1149) Pathak, R. K.; Dikundwar, A. G.; Row, T. N. G.; Rao, C. P. A Lower Rim Triazole Linked Calix[4]arene Conjugate as a Fluorescence Switch for Zn2+ in Blood Serum Milieu. *Chem. Commun.* **2010**, *46*, 4345-4347.

(1150) Sutariya, P. G.; Modi, N. R.; Pandya, A.; Joshi, B. K.; Joshi, K. V.; Menon, S. K. An ICT Based "*Turn On/Off*" Quinolone Armed Calix[4]arene Fluoroionophore: Its Sensing Efficiency Towards Fluoride From Waste Water and Zn2+ from Blood Serum. *Analyst* **2012**, *137*, 5491-5494.

(1151) Jiang, X.-K.; Ikejiri, Y.; Jin, C.-C.; Wu, C.; Zhao, J.-L.; Ni, X.-L.; Zeng, X.; Redshaw, C.; Yamato, T. Synthesis and Evaluation of a Novel Fluorescent Sensor Based on Hexahomotrioxacalix[3]arene for Zn2+ and Cd2+. *Tetrahedron* **2016**, *72*, 4854-4858.

(1152) Ullman, S.; Schnorr, R.; Handke, M.; Laube, C.; Abel, B.; Matysik, J.; Findeisen, M.; Rüger, R.; Heine, T.; Kersting, B. Zn2+-Ion Sensing by Fluorescent Schiff Base Calix[4]arene Macrocycles. *Chem. Eur. J.* **2017**, *23*, 3824-3827.

(1153) Pathak, R. K.; Dessingou, J.; Rao, C. P. Multiple Sensor Array of Mn2+, Fe2+, Co2+, Ni2+, Cu2+, and Zn2+ Complexes of a Triazole Linked Imino-Phenol Based Calix[4]arene Conjugate for the Selective Recognition of Asp, Glu, Cys, and His. *Anal. Chem.* **2012**, *84*, 8294-8300.

(1154) Mummidivarapu, V. V. S.; Tabbasum, K.; Chinta, J. P.; Rao, C. P. 1,3-Di-Aminoquinoline Conjugate of Calix[4]arene (L) as a Ratiometric and Colorimetric Sensor for Zn2+: Spectroscopy, Microscopy and Computational Studies. *Dalton Trans.* **2012**, *41*, 1671-1674.

(1155) Mummidivarapu, V. V. S.; Bandaru, S.; Yarramala, D. S.; Samanta, K.; Mhatre, D. S.; Rao, C. P. Binding and Ratiometric Dual Ion Recognition of Zn2+ and Cu2+ by 1,3,5-Tris-Amidoquinoline Conjugate of Calix[6]arene by Spectroscopy and its Supramolecular Features by Microscopy. *Anal. Chem.* **2015**, *87*, 4988-4995.

(1156) Darjee, S. M.; Modi, K. M.; Panchal, U.; Patel, C.; Jain, V. K. Highly Selective and Sensitive Fluorescent Sensor: Thiacalix[4]arene-1-Napthalene Carboxylate for Zn2+ Ions. *J. Mol. Struct.* **2017**, *1133*, 1-8.

(1157) Zhang, J. F.; Bhuniya, S.; Lee, Y. H.; Bae, C.; Lee, J. H.; Kim, J. S. Novel 2,2'-Bipyridine-Modified Calix[4]arenes: Ratiometric Fluorescent Chemosensors for Zn2+ Ion. *Tetrahedron Lett.* **2010**, *51*, 3719-3723.

(1158) Li, L.; Du, L.-t.; Sun, J.; Yan, C.-g. Synthesis, Crystal Structure of Bis-Terpyridinyl-Calix[4]arene Derivatives and Fluorescent Sensor for Zn2+. *Chem. Res. Chin. Univ.* **2013**, *29*, 874-878.

(1159) Sulak, M.; Kursunlu, A. N.; Girgin, B.; Karakuş, Ö.; Güler, E. A Highly Selective Fluorescent Sensor for Mercury (II) Ion Based on Bodipy and Calix[4]arene Bearing Triazolenaphthylene Groups; Synthesis and Photophysical Investigations. *J. Photochem. Photobiol. A* **2017**, *349*, 129-137.

(1160) Arena, G.; Attanasio, F.; Zhang, D.; Yang, Y.; Bartsch, R. A.; Sgarlata, C. Selective Sensing of Hg2+ by a Proton-Ionizable Calix[4]arene Fluoroionophore. *Anal. Bioanal. Chem.* **2013**, *405*, 1133-1137.

(1161) Ocak, Ü.; Ocak, M.; Shen, X.; Gorman, A. H.; Surowiec, K.; Bartsch, R. A. Metal Ion Complexation in Acetonitrile by Upper-Rim Benzyl-Substituted, Di-Ionized Calix[4]arenes Bearing Two Dansyl Fluorophores. *Arkivoc* **2010**, *vii*, 81-97.

(1162) Oguz, M.; Bhatti, A. A.; Karakurt, S.; Aktas, M.; Yilmaz, M. New Water Soluble Hg2+ Selective Fluorescent Calix[4]arenes: Synthesis and Application in Living Cells Imaging. *Spectrochim. Acta A* **2017**, *171*, 340-345.

(1163) Erdemir, S.; Malkondu, S.; Kocyigit, O.; Alıcı, O. A Novel Colorimetric and Fluorescent Sensor Based on Calix[4]arene Possessing Triphenylamine Units. *Spectrochem. Acta A* **2013**, *114*, 190-196.

(1164) Kumar, M.; Babu, J. N.; Bhalla, V.; Kumar, R. Ratiometric/'On-Off' Sensing of Pb2+ Ion Using Pyrene-Appended Calix[4]arenes. *Sens. Actuators B* **2010**, *144*, 183-191.

(1165) Sahin, O.; Yilmaz, M. Synthesis and Fluorescence Sensing Properties of Novel Pyrene-Armed Calix[4]arene Derivatives. *Tetrahedron* **2011**, *67*, 3501-3508.

(1166) Depauw, A.; Kumar, N.; Ha-Thi, M.-H.; Leray, I. Calixarene-Based Fluorescent Sensors for Cesium Cations Containing BODIPY Fluorophore. *J. Phys. Chem. A* **2015**, *119*, 6065-6073.

(1167) Kumar, N.; Pham-Xuan, Q.; Depaw, A.; Hemadi, M.; Ha-Duong, N.-T.; Lefevre, J.-P.; Ha-Thi, M.-H.; Leray, I. New Sensitive and Selective Calixarene-Based Fluorescent Sensors for the Detection of Cs+ in an Organoaqueous Medium. *New. J. Chem.* **2017**, *41*, 7162-7170.

(1168) Zhan, J.; Wen, L.; Miao, F.; Tian, D.; Zhu, X.; Li, H. Synthesis of a Pyridyl-Appended Calix[4]arene and its Application to the Modification of Silver Nanoparticles as Fe3+ Colorimetric Sensor. *New J. Chem.* **2012**, *36*, 656-661.

(1169) Zheng, X.; Zhang, W.; Mu, L.; Zeng, X.; Xue, S.; Tao, Z.; Yamatob, T. A Novel Rhodamine-Based Thiacalix[4]arene Fluorescent Sensor for Fe3+ and Cr3+. *J. Incl. Phenom. Macrocycl. Chem.* **2010**, *68*, 139-146.

(1170) Lotfi, B.; Tarlani, A.; Akbari-Moghaddam, P.; Mirza-Aghayan, M.; Peyghan, A. A.; Muzart, J.; Zadmard, R. Multivalent Calix[4]arene-Based Fluorescent Sensor for Detecting Silver Ions in Aqueous Media and Physiological Environment. *Biosens. Bioelectron.* **2017**, *90*, 290-297.

(1171) Memon, S.; Bhatti, A. A. Bhatti, A. A.; Ocak, Ü.; Ocak, M. Calix[4]arene Based Highly Efficient Fluorescent Sensor for Au3+ and I-. *J. Fluorescence* **2015**, *25*, 1507-1515.

(1172) Memon, S.; Bhatti, A. A.; Bhatti, A. A.; Ocak, Ü.; Ocak, M. Calix[4]arene Based Dual Fluorescent Sensor for Al3+ and S2O72-. *J. Fluorescence* **2016**, *26*, 1591-1599.

(1173) Nemati, M.; Hosseinzadeh, R.; Zadmard, R.; Mohadjerani, M. Highly Selective Colorimetric and Fluorescent Chemosensor for Fluoride Based On Fluorenone Armed Calix[4]arene. *Sens. Actuators B* **2017**, *241*, 690-697.

(1174) Gómez-Machuca, H.; Quiroga-Campano, C.; Jullian, C.; De la Fuente, J.; Pessoa-Mahana, H.; Escobar, C. A.; Dobado, J. A.; Saitz, C. Study by Fluorescence of Calix[4]arenes Bearing Heterocycles with Anions: Highly Selective Detection of Iodide. *J. Incl. Phenom. Macrocycl. Chem.* **2014**, *80*, 369-375.

(1175) Kim, J.-S.; Park, S.-Y.; Kim, S.-H.; Thuery, P.; Souane, R.; Matthews, S. E.; Vicens, J. Pyrenyl-Appended Triazole-Based Calix[4]arene as a Fluorescent Sensor for Iodide Ion. *Bull. Korean Chem. Soc.* **2010**, *31*, 624-629.

(1176) Chen, Y.-C.; Liu, X.-X.; Huang, H.; Wu, W.-W.; Zheng, Y.-S. Sensitive Fluorescence Probes for Dihydrogen Phosphate Anion Based on Calix[4]arene Bearing Naphthol-Hydrazone Groups. *Sci. China Chem.* **2010**, *53,* 569-575.

(1177) Erdemir, S.; Tabakci, B.; Tabakci, M. A Highly Selective Fluorescent Sensor Based on Calix[4]arene Appended Benzothiazole Units for Cu2+, S2-, HSO4- Ions in Aqueous Solution. *Sens. Actuators B* **2016**, *228*, 109-116.

(1178) Joseph, R.; Chinta, J. P.; Rao, C. P. Lower Rim 1,3-Diderivative of Calix[4]arene-Appended Salicylidene Imine (H2L): Experimental and Computational Studies of the Selective Recognition of H2L Toward Zn2+ and Sensing Phosphate and Amino Acid by [ZnL]. *J. Org. Chem.* **2010**, *75*, 3387-3395.

(1179) Joseph, R.; Chinta, J. P.; Rao, C. P. Calix[4]arene-Based 1,3-Diconjugate of Salicylyl Imine Having Dibenzyl Amine Moiety (L): Synthesis, Characterization, Receptor Properties Toward Fe2+, Cu2+, and Zn2+, Crystal Structures of its Zn2+ and Cu2+ Complexes, and Selective Phosphate Sensing by the [ZnL]. *Inorg. Chem.* **2011**, *50,* 7050-7058.

(1180) Pathak, R. K.; Hinge, V. K.; Mondal, M.; Rao, C. P. Triazole-Linked-Thiophene Conjugate of Calix[4]arene: Its Selective Recognition of Zn2+ and as a Biomimetic Model in Supporting the Events of Metal Detoxification and Oxidative Stress Involving Metallothionein. *J. Org. Chem.* **2011**, *76*, 10039-10049.

(1181) Pathak, R. K.; Tabbasum K.; Rai, A.; Panda, D.; Rao, C. P. Pyrophosphate Sensing by a Fluorescent Zn2+ Bound Triazole Linked Imino-Thiophenyl Conjugate of Calix[4]arene in HEPES Buffer Medium: Spectroscopy, Microscopy, and Cellular Studies. *Anal. Chem.* **2012**, *84*, 5117-5123.

(1182) Pathak, R. K.; Tabbasum, K.; Rai, A.; Panda, D.; Rao, C. P. A Zn2+ Specific Triazole Based Calix[4]arene Conjugate (L) as a Fluorescence Sensor for Histidine and Cysteine in HEPES Buffer Milieu. *Analyst* **2012**, *137*, 4069-4075.

(1183) Pathak, R. K.; Hinge, V. K.; Rai, A.; Panda, D.; Rao, C. P. Imino-Phenolic-Pyridyl Conjugates of Calix[4]arene (L1 and L2) as Primary Fluorescence Switch-On Sensors for Zn2+ in Solution and in HeLa Cells and the Recognition of Pyrophosphate and ATP by [ZnL2]. *Inorg. Chem.* **2012**, *51*, 4994-5005.

(1184) Mummidivarapu, V. V. S.; Hinge, V. K.; Rao, C. P. Interaction of a Dinuclear Fluorescent Cd(II) Complex of Calix[4]arene Conjugate with Phosphates and Its Applicability in Cell Imaging. *Dalton Trans.* **2015**, *44*, 1130-1141.

(1185) Ozman, M.; Ozbek, Z.; Bayarkci, M.; Ertul, S.; Ersoz, M.; Capan, R. Preparation and Gas Sensing Properties of Langmuir-Blodgett Thin Films of Calix[*n*]arenes: Investigation of Cavity Effect. *Sens. Actuators B* **2014**, *195*, 156-164.

(1186) Mummidivarapu, V. V. S.; Nehra, A.; Hinge, V. K.; Rao, C. P. Triazole Linked Picolylimine Conjugate of Calix[6]arene as a Sequential Sensor for La3+ Followed by F-. *Org. Lett.* **2012**, *14*, 2968-2971.

(1187) Rémy, C.; Guyon, H.; Rebilly, J.-N.; Leray, I.; Reinaud, O. Selective Fluorimetric Detection of Primary Alkylamines by a Calix[6]arene Funnel Complex. *Chem. Eur. J.* **2017**, *23*, 8669-8677.

(1188) Erdemir, S.; Kocyigit, O.; Karakurt, S. A New Perylene Bisimide-Armed Calix[4]-Aza-Crown as "Turn-On" Fluorescent Sensor for Hg2+ Ion and its Application to Living Cells. *Sens. Actuators B* **2015**, *220*, 381-388.

(1189) Chawla, H. M.; Shukla, R.; Goel, P. Sensitive Recognition of Cyanide Through Supramolecularly Complexed New Calix[4]arenes. *New J. Chem.* **2014**, *38*, 5264-5267.

(1190) Zhang, S.; Yang, H.; Ma, Y.; Fang, Y. A Fluorescent Bis-NBD Derivative of Calix[4]arene: Switchable Response to Ag+ and HCHO in Solution Phase. *Sens. Actuators B* **2016**, *227*, 271-276.

(1191) Qazi, M. A.; Ocak, Ü.; Ocak, M.; Memon, S.; Solangi, I. B. Bifunctional Calix[4]arene Sensor for Pb(II) and Cr2O72- Ions. *J. Fluorescence* **2013**, *23*, 575-590.

(1192) Boonkitpatarakul, K.; Yodta, Y.; Niamnont, N.; Sukwattanasinitt, M. Fluorescent Phenylethynylene Calix[4]arenes for Sensing TNT in Aqueous Media and Vapor Phase. *RSC Adv.* **2015**, *5*, 33306-33311.

(1193) Kandpal, M.; Bandela, A. K.; Hinge, V. K.; Rao, V. R.; Rao, C. P. Fluorescence and Piezoresistive Cantilever Sensing of Trinitrotoluene by an Upper-Rim Tetrabenzimidazole Conjugate of Calix[4]arene and Delineation of the Features of the Complex by Molecular Dynamics. *ACS Appl. Mater. Interfaces* **2013**, *5*, 13448-13456.

(1194) Lee, Y. H.; Liu, H.; Lee, J. Y.; Kim, S. H.; Kim, S. K.; Sessler, J. L.; Kim, Y.; Kim, J. S. Dipyrenylcalix[4]arene-A Fluorescence-Based Chemosensor for Trinitroaromatic Explosives. *Chem. Eur. J.* **2010**, *16,* 5895-5901.

(1195) Cao, X.; Luo, L.; Zhang, F.; Miao, F.; Tian, D.; Li, H. Synthesis of a Deep Cavity Calix[4]arene by Fourfold Sonogashira Cross-Coupling Reaction and Selective Fluorescent Recognition Toward *p*-Nitrophenol. *Tetrahedron Lett.* **2014**, *55*, 2029-2032.

(1196) Zhang, F.; Luo, L.; Sun, Y.; Miao, F.; Bi, J.; Tan, S.; Tian, D.; Li, H. Synthesis of a Novel Fluorescent Anthryl Calix[4]arene as Picric Acid Sensor. *Tetrahedron* **2013**, *69*, 9886-9889.

(1197) Zhan, J.; Zhu, X.; Fang, F.; Miao, F.; Tian, D.; Li, H. Sensitive Fluorescence Sensor for Nitroaniline Isomers Based on Calix[4]arene Bearing Naphthyl Groups. *Tetrahedron* **2012**, *68*, 5579-5582.

(1198) Teixeira, C. M.; Costa, A. I.; Prata, J. V. A New Fluorescent Double-Cavity Calix[4]arene: Synthesis and Complexation Studies Toward Nitroanilines. *Tetrahedron Lett.* **2013**, *54*, 6602-6606.

(1199) Jin, T. Near-Infrared Fluorescence Detection of Acetylcholine in Aqueous Solution Using a Complex of Rhodamine 800 and *p*-Sulfonato-calix[8]arene. *Sensors* **2010**, *10*, 2438-2449.

(1200) Guo, D.-S.; Uzunova, V. D.; Su, X.; Liu, Y.; Nau, W. M. Operational Calixarene-Based Fluorescent Sensing Systems for Choline and Acetylcholine and their Application to Enzymatic Reactions. *Chem. Sci.* **2011**, *2*, 1722-1734.

(1201) Xu, Y.-W.; Tan, L.-L.; Liu, J.-M.; Xiao, L.-M.; Li, S.-Y.; Su, C.-Y. Fluorescent Calix[4]arene Chemosensor for Acidic and Basic Amino Acids in Pure Aqueous Media. *RSC Adv.* **2014**, *4*, 28046-28051.

(1202) Han, F.; Xu, Y.; Jiang, D.; Qin, Y.; Chen. H. A BODIPY-Derived Fluorescent Probe for Cellular pH Measurements. *Anal. Biochem.* **2013**, *435*, 106-113.

(1203) Van Dienst, E.; Bakker, W. I. I.; Engbersen, J. F. J.; Verboom, W. Reinhoudt, D. N. Calixarenes, Chemical Chameleons. *Pure Appl. Chem.* **1993**, *65*, 387-392.

(1204) Niederl, J. B.; Vogel, H. J. Aldehyde-Resorcinol Condensation. *J. Am. Chem. Soc.* **1940**, *62*, 2512-2514.

(1205) Natarajan, N.; Brenner, E.; Sémeril, D.; Matt, D.; Harrowfield, J. The Use of Resorcinarene Cavitands in Metal-Based Catalysis. *Eur. J. Org. Chem.* **2017**, 6100-6113.

(1206) Biradha, K.; Ramanan, A.; Vittal, J. J. Coordination Polymers Versus Metal-Organic Frameworks. *Cryst. Growth Des.* **2009**, *9*, 2969-2970.

(1207) Zhang, H.; Yang, J.; Liu, Y.-Y.; Song, S.; Ma, J.-F. A Family of Metal-Organic Frameworks with a New Chair-Conformation Resorcin[4]arene-Based Ligand: Selective Luminescent Sensing of Amine and Aldehyde Vapors, and Solvent-Mediated Structural Transformations. *Cryst. Growth Des.* **2016**, *16*, 3244-3255.

(1208) Li, N.; Harrison, R. G.; Lamb, J. D. Application of Resorcinarene Derivatives in Chemical Separations. *J. Inclusion Phenom. Macrocyclic Chem.* **2014**, *78*, 39-60.

(1209) Gropp, C.; Quigley, B. L.; Diederich, F. Molecular Recognition with Resorcin[4]arene Cavitands: Switching, Halogen-Bonded Capsules, and Enantioselective Complexation. *J. Am. Chem. Soc.* **2018**, *140*, 2705-2717.

(1210) Zhang, S.-T.; Yang, J.; Wu, H.; Liu, Y.-Y.; Ma, J.-F. Systematic Investigation of High-Sensitivity Luminescent Sensing for Polyoxometalates and Iron(III) by MOFs Assembled with a New Resorcin[4]arene-Functionalized Tetracarboxylate. *Chem. Eur. J.* **2015**, *21*, 15806-15819.

(1211) Zhao, S.-S.; Yang, J.; Liu, Y.-Y.; Ma, J.-F. Fluorescent Aromatic Tag-Functionalized MOFs for Highly Selective Sensing of Metal Ions and Small Organic Molecules. *Inorg. Chem.* **2016**, *55*, 2261-2273.

(1212) Lu, B.-B.; Jiang, W.; Yang, J.; Liu, Y.-Y.; Ma, J.-F. Resorcin[4]arene-Based Microporous Metal-Organic Framework as an Efficient Catalyst for CO2 Cycloaddition with Epoxides and Highly Selective Luminescent Sensing of Cr2O72-. *ACS Appl. Mater. Interfaces* **2017**, *9*, 39441-39449.

(1213) Jin, S.-S.; Han, X.; Yang, J.; Zhang, H.-M.; Liu, X.-L.; Ma, J.-F. Luminescent Coordination Polymers Based on a New Resorcin[4]arene Functionalized Tetracarboxylate: Highly Selective Luminescent Detection of Metal Cations, Anions, and Small Organic Molecules. *J. Lumin.* **2017**, *188*, 346-355.

(1214) Han, X.; Lu, B.-B.; Yang, J.; Wu, H.; Liu, Y.-Y.; Ma, J.-F. Four Coordinate Complexes Based on Two Novel Carboxylate-Functionalized Resorcin[4]arenes: Structures, Fluorescence and Sensing of Nitrobenzene and Dichromate Anions. *Inorg. Chimica Acta* **2018**, *482*, 579-587.

(1215) Lv, L.-L.; Yang, J.; Zhang, H.-M.; Liu, Y.-Y.; Ma, J.-F. Metal-Ion Exchange, Small-Molecule Sensing, Selective Dye Adsorption, and Reversible Iodine Uptake of Three Coordinate Polymers Constructed by a New Resorcin[4]arene-Based Tetracarboxylate. *Inorg. Chem.* **2015**, *54*, 1744-1755.

(1216) Kubo, Y.; Tsuruzoe, K.; Okuyama, S.; Nishiyabu, R.; Fujihara, T.; Resorcin[4]arene Cavitand with 1,3,2-Benzodiazaborolyl Walls as a Fluorescence Receptor for Ammonium Cations. *Chem. Commun.* **2010**, *46*, 3604-3606.

(1217) Otsuka, K.; Kondo, T.; Nishiyabu, R.; Kubo, Y. Solvent-Manipulated Guest Binding and Signaling of a Fluorescent Resorcin[4]arene Cavitand with 1,3,2-Benzodiazaboryl D-π-A Conjugation Flaps. *J. Org. Chem.* **2013**, *78*, 5782-5787.

(1218) Mettra, B.; Bretonnière, Y.; Mulatier, J.-C.; Bibal, B.; Tinant, B.; Aronica, C.; Dutasta, J.-P.; Design of Differently P-Substituted *4i*PO Fluorescent Tetraphosphonate Cavitands. *Supramol. Chem.* **2013**, *25*, 672-681.

(1219) Gale, P. A.; Sessler, J. L.; Král, V. Calixpyrroles. *Chem. Commun.* **1998**, 1-8**.**

(1220) Gale, P. A.; Anzenbacher, P., Jr.; Sessler, J. L. Calixpyrroles II. *Coord. Chem. Rev.* **2001**, *222*, 57-102.

(1221) Lee, C. H. Versatilities of Calix[4]pyrrole Based Anion Receptors. *Bull. Korean Chem. Soc.* **2011**, *32*, 768-778.

(1222) Baeyer, A. Condensation Product of Pyrroline with Acetone. *Ber. Dtsch. Chem. Ges.* **1886**, *19*, 2184-2185.

(1223) Gale, P. A.; Sessler, J. L.; Král, V.; Lynch, V. Calix[4]pyrroles: Old Yet New Anion-Binding Agents. *J. Am. Chem. Soc.* **1996**, *118*, 5140-5141.

(1224) Taner, B.; Kursunlu, A. N.; Güler, E.; The Example of Calix[4]pyrrole Derivative Containing Bodipy Unit: Fluorometric and Colorimetric Sensor for F- Ion. *Spectrochim. Acta A* **2014**, *118*, 903-907.

(1225) Sareen, D.; Lee, J. H.; Hwang, H.; Yoo, S.; Lee, C.-H. Ion-Mediated Single-Molecule Orbital Switching and Sensing Based on Fluorophore-Tethered Calix[4]pyrrole. *Chem. Commun.* **2016**, *52*, 5852-5855.

(1226) Sokkalingam, P.; Kim, D. S.; Hwang, H.; Sessler, J. L.; Lee, C.-H. A Dicationic Calix[4]pyrrole Derivative and its Use for the Selective Recognition and Displacement-Based Sensing of Pyrophosphate. *Chem. Sci.* **2012**, *3*, 1819-1824.

(1227) Gotor, R.; Costero, A. M.; Gaviña, P.; Gil, S.; Parra, M. Binding and Fluorescent Sensing of Di-Carboxylates by a Bis(calix[4]pyrrole)-Substituted BODIPY Dye. *Eur. J. Org. Chem.* **2013**, 1515-1520.

(1228) Liu, Y.; Minami, T.; Nishiyabu, R.; Wang, Z.; Anzenbacher, P. Sensing of Carboxylate Drugs in Urine by a Supramolecular Sensor Array. *J. Am. Chem. Soc.* **2013**, *135*, 7705-7712.

(1229) Yoo, J.; Kim, Y.; Kim, S.-J.; Lee, C.-H. Anion-Modulated, Highly Sensitive Supramolecular Fluorescent Chemosensor for C70. *Chem. Commun.* **2010**, *46*, 5449-5451.

(1230) Park, K.; Yoo, J.; Ka, J.-W.; Lee, C.-H. Calix[2]pyreno[2]pyrrole as a Fluorescent Chemical Probe for Polynitroaromatics. *Bull. Korean Chem. Soc.* **2012**, *33*, 675-677.

(1231) Jung, K.-B.; Kim, S. K.; Lynch, V. M.; Cho, D.-G.; Sessler, J. L. A Calix[2]phenol[2]pyrrole and a Fused Pyrrolidine-Containing Derivative. *Chem. Commun.* **2012**, *48*, 2495-2497.

(1232) Pushina, M.; Koutnik, P.; Nishiyabu, R.; Minami, T.; Savechenkov, P.; Anzenbacher, P., Jr. Anion Sensing by Fluorescent Expanded Calixpyrroles. *Chem. Eur. J.* **2018**, *24*, 4879-4884.

(1233) Park, G.; Park, K.; Lee, C.-H. Pyrrole-Strapped Calix[4]pyrrole Bearing Pyrene Moiety: Synthesis and Anion Binding Property. *Bull. Korean Chem. Soc.* **2013**, *34*, 283-286.

(1234) Samanta, R.; Mahanta, S. P.; Ghanta, S.; Panda, P. K. Naphthalene Strapped Fluorescent Calix[4]pyrrole Isomers: Halide Ion Selectivity Based on Strap Topography. *RSC Adv.* **2012**, *2*, 7974-7977.

(1235) Lv, Y.; Xu, J.; Guo, Y.; Shao, S. A Novel Colorimetric and Fluorometric Anion Sensor Based on BODIPY-Calix[4]pyrrole Conjugate. *J. Inclusion Phenom. Macrocyclic Chem.* **2012**, *72*, 95-101.

(1236) Lv, Y.; Xu, J.; Guo, Y.; Shao, S. A Sandwich Anion Receptor by a BODIPY Dye Bearing Two Calix[4]pyrrole Units. *Chemical Papers* **2011**, *65*, 553-558.

(1237) Saha, I.; Lee, J. H.; Hwang, H.; Kim, T. S.; Lee, C.-H. Remarkably Selective Non-Linear Allosteric Regulation of Anion Binding by a Tetracationic Calix[4]pyrrole Homodimer. *Chem. Commun.* **2015**, *51*, 5679-5682.

(1238) Samanta, R.; Kumar, B. S.; Panda, P. K. Calix[4]pyrroles with Shortest Possible Strap: Exclusively Selective Toward Fluoride Ion. *Org. Lett.* **2015**, *17*, 4140-4143.

(1239) Yoo, J.; Park, I.-w.; Kim, T.-Y.; Lee, C.-H. Calix[4]pyrrole Bearing Pyrene-Pickets at Diametrical *Meso*-Positions with Amide Linkages. *Bull. Korean Chem. Soc.* **2010**, *31*, 630-634.

(1240) Kataev, E. A.; Backmann, N.; Shumilova, T. A.; Rüffer, T.; Lang, H. Calix[4]pyrroles Bearing Quinolinium Moiety for Halide Sensing in Aqueous Solution. *Supramol. Chem.* **2016**, *28*, 53-61.

(1241) Anzenbacher, P., Jr.; Liu, Y.; Palacios, M. A.; Minami, T.; Wang, Z.; Nishiyabu, R. Leveraging Material Properties in Fluorescence Anion Sensor Arrays: A General Approach. *Chem. Eur. J.* **2013**, *19*, 8497-8506.

(1242) Bhatt, K. D.; Makwana, B. A.; Vyas, D. J.; Mishra, D. R.; Jain, V. K. Selective Recognition by Novel Calix System: ICT Based Chemosensor for Metal Ion. *J. Lumin.* **2014**, *146*, 450-457.

(1243) Bhatt, K. D.; Shah, H. D.; Panchal, M. A Switch-Off Fluorescence Probe Towards Pb(II) and Cu(II) Ions Based on a Calix[4]pyrrole Bearing Amino-Quinoline Group. *Luminescence* **2017**, *32*, 1398-1404.

(1244) Yoo, J.; Jeoung, E.; Lee, C.-H.; Fluorophore-Appended Calix[4]pyrrole: Conformationally Flexible Fluorometric Chemosensors. *Supramol. Chem.* **2009**, *21*, 164-172.

(1245) Gotor, R.; Costero, A. M.; Gil, S.; Gaviña, P.; Rurack, K. On the Ion-Pair Recognition and Indication Features of a Fluorescent Heteroditopic Host Based on a BODIPY Core. *Eur. J. Org. Chem.* **2014**, 4005-4013.

(1246) Sun, Q.; Lün, Y.; Liu, L.; Liu, K.; Miao, R.; Fang, Y. Experimental Studies on a New Fluorescent Ensemble of Calix[4]pyrrole and Its Sensing Performance in the Film State. *ACS Appl. Mater. Interfaces* **2016**, *8*, 29128-29135.

(1247) Bähring, S.; Martín-Gomis, L.; Olsen, G.; Nielsen, K. A.; Kim, D. S.; Duedal, T.; Sastra-Santos, Á.; Jeppesen, J. O.; Sessler, J. L. Design and Sensing Properties of a Self-Assembled Supramolecular Oligomer. *Chem. Eur. J.* **2016**, *22*, 1958-1967.

(1248) Ogoshi, T.; Kanai, S.; Fujinami, S.; Yamagishi, T.-a.; Nakamoto, Y. *para*-Bridged Symmetrical Pillar[5]arenes: Their Lewis Acid Catalyzed Synthesis and Host-Guest Property. *J. Am. Chem. Soc.* **2008**, *130*, 5022-5023.

(1249) Ogoshi, T.; Yamagishi, T.-a.; Nakamoto, Y. Pillar-Shaped Macrocyclic Hosts Pillar[n]arenes: New Key Players for Supramolecular Chemistry. *Chem. Rev.* **2016**, *116*, 7937-8002.

(1250) Ogoshi, T.; Demachi, K.; Kitajima, K.; Yamagishi, T.-a. Monofunctionalized Pillar[5]arenes: Synthesis and Supramolecular Structure. *Chem. Commun.* **2011**, *47*, 7164-7166.

(1251) Guan, Y.; Liu, P.; Deng, C.; Ni, M.; Xiong, S.; Lin, C.; Hu, X.-Y.; Ma, J.; Wang, L. Dynamic Self-Inclusion Behavior of Pillar[5]arene-Based Pseudo[1]rotaxanes. *Org. Biomol. Chem.* **2014**, *12*, 1079-1089.

(1252) Strutt, N. L.; Forgan, R. S.; Spruell, J. M.; Botros, Y. Y.; Stoddart, J. F. Monofunctionalized Pillar[5]arene as a Host for Alkanediamines. *J. Am. Chem. Soc.* **2011**, *133*, 5668-5671.

(1253) Ogoshi, T.; Iizuka, R.; Kotera, D.; Yamagishi, T.-a. Synthesis of a Pillar[5]arene-Based [2]Rotaxane with Two Equivalent Stations via Copper(I)-Catalyzed Alkyne-Azide Cycloaddition. *Org. Lett.* **2015**, *17*, 350-353.

(1254) Ke, C.; Strutt, N. L.; Li, H.; Hou, X.; Hartlieb, K. J.; McGonigal, P. R.; Ma, Z.; Iehl, J.; Stern, C. L.; Cheng, C.; Zhu, Z.; Vermeulen, N. A.; Meade, T. J.; Botros, Y. Y; Stoddart, J. F. Pillar[5]arene as a Co-Factor in Templating Rotaxane Formation. *J. Am. Chem. Soc.* **2013**, *135*, 17019-17030.

(1255) Ogoshi, T.; Nishida, Y.; Yamagishi, T.-a.; Nakamoto, Y. High Yield Synthesis of Polyrotaxane Constructed from Pillar[5]arene and Viologen Polymer and Stabilization of its Radical Cation. *Macromolecules* **2010**, *43*, 7068-7072.

(1256) Ogoshi, T.; Hasegawa, Y.; Aoki, T.; Ishimori, Y.; Inagi, S.; Yamagishi, T.-a. Reduction of Emeraldine Base Form of Polyaniline by Pillar[5]arene Based on Formation of Poly(pseudorotaxane) Structure. *Macromolecules* **2011**, *44*, 7639-7644.

(1257) Kitajima, K.; Ogoshi, T.; Yamagishi, T.-a. Diastereoselective Synthesis of a [2]Catenane From a Pillar[5]arene and a Pyridinium Derivative. *Chem. Commun.* **2014**, *50*, 2925-2927.

(1258) Yan, X.; Wei, P.; Li, Z.; Zheng, B.; Dong, S.; Huang, F.; Zhou, Q. A Dynamic [1]Catenane with pH-Responsiveness Formed via Threading-Followed-By-Complexation. *Chem. Commun.* **2013**, *49*, 2512-2514.

(1259) Nishimura, T.; Sanada, Y.; Matsuo, T.; Okobira, T.; Mylonas, E.; Yagi, N.; Sakurai, K. A. Biomolecular Micelle Constructed from Amphiphilic Pillar[5]arene Molecules. *Chem. Commun.* **2013**, *49*, 3052-3054.

(1260) Yao, Y.; Wei, P.; Yue, S.; Li, J.; Xue, M. Amphiphilic Pillar[5]arenes: Influence of Chemical Structure on Self-Assembly Morphology and Application in Gas Response and λ-DNA Condensation. *RSC Adv.* **2014**, *4*, 6042-6047.

(1261) Nierengarten, I.; Guerra, S.; Holler, M.; Nierengarten, J.-F.; Deschenaux, R. Building Liquid Crystals from the 5-Fold Symmetrical Pillar[5]arene Core. *Chem. Commun.* **2012**, *48*, 8072-8074.

(1262) Pan, S.; Ni, M.; Mu, B.; Li, Q.; Hu, X.-Y.; Lin, C.; Chen. D.; Wang, L. Well-Defined Pillararene-Based Azobenzene Liquid Crystalline Photoresponsive Materials and Their Thin Films with Photomodulated Surfaces. *Adv. Funct. Mater.* **2015**, *25*, 3571-3580.

(1263) Tan, L.-L.; Li, H.; Qiu, Y.-C.; Chen, D.-X.; Wang, X.; Pan, R.-Y.; Wang, Y.; Zhang, S. X.-A.; Wang, B.; Yang, Y.-W. Stimuli-Responsive Metal-Organic Frameworks Gated by Pillar[5]arene Supramolecular Switches. *Chem. Sci.* **2015**, *6*, 1640-1644.

(1264) Yao, Q.; Lü, B.; Ji, C.; Cai, Y.; Yin, M. Supramolecular Host-Guest System as Ratiometric Fe3+ Ion Sensor Based on Water-Soluble Pillar[5]arene. *ACS Appl. Mater. Interfaces* **2017**, *9*, 36320-26326.

(1265) Wei, T.-B.; Cheng, X.-B.; Li, H.; Zheng, F.; Lin, Q.; Yao, H.; Zhang, Y.-M. Novel Functionalized Pillar[5]arene: Synthesis, Assembly and Application in Sequential Fluorescent Sensing for Fe3+ and F- in Aqueous Media. *RSC Adv*. **2016**, *6*, 20987-20993.

(1266) Zhang, Y.; Su, J.; Li, Q.; Li, W.; Liang, G.; Li, H.; Ma, H.; Lin, Q.; Yao, H.; Wei, T. Novel Fluorescent Chemosensor for Detection of F- Anions Based on a Single Functionalized Pillar[5]arene Iron(III) Complex. *Chin. J. Chem*. **2016**, *34*, 1263-1267.

(1267) Fang, Y.; Li, C.; Wu, L.; Bai, B.; Li, X.; Jia, Y.; Feng, W.; Yuan, L. A Non-Symmetric Pillar[5]arene Based on Triazole-Linked 8-Oxyquinolines as a Sequential Sensor for Thorium(IV) Followed by Fluoride Ion. *Dalton Trans.* **2015**, *44*, 14584-14588.

(1268) Lin, Q.; Liu, L.; Zheng, F.; Mao, P.-P.; Liu, J.; Zhang, Y.-M.; Yao, H.; Wei, T.-B. A Novel Water Soluble Self-Assembled Supramolecular Sensor Based on Pillar[5]arene for Fluorescent Detection of CN- in Water. *Tetrahedron* **2017**, *73*, 5307-5310.

(1269) Cheng, X.; Li, H.; Zheng, F.; Lin, Q.; Zhang, Y.; Yao, H.; Wei, T. A Pillar[5]arene-Based Cyanide Sensor Bearing on a Novel Cyanide-Induced Self-Assemble Mechanism. *Dyes and Pigments* **2016**, *127*, 59-66.

(1270) Wang, K.; Wang, C.-Y.; Zhang, Y.; Zhang, S. X.-A.; Yang, B.; Yang, Y.-W. Ditopic Pillar[5]arene-Based Fluorescence Enhancement Material Mediated by [c2]Daisy Chain Formation. *Chem. Commun*. **2014**, *50*, 9458-9461.

(1271) Wei, T.-B.; Chen, J.-F.; Cheng, X.-B.; Li, H.; Han. B.-B.; Zhang, Y.-M.; Yao, H.; Lin, Q. A Novel Functionalized Pillar[5]arene-Based Selective Amino Acid Sensor for L-Tryptophan. *Org. Chem. Front.* **2017**, *4*, 210-213.

(1272) Lin, Q.; Liu, L.; Zheng, F.; Mao, P.-P.; Liu, J.; Zhang, Y.-M.; Yao, H.; Wei, T.-B. A Water-Soluble Pillar[5]arene-Based Chemosensor for Highly Selective and Sensitive Fluorescence Detection of L-Methionine. *RSC Adv.* **2017**, *7*, 34411-34414.

(1273) Bojtár, M.; Kozma, J.; Szakács, Z.; Hessz, D.; Kubinyi, M.; Bitter, I. Pillararene-Based Fluorescent Indicator Displacement Assay for the Selective Recognition of ATP. *Sensors Actuators B* **2017**, *248*, 305-310.

(1274) Hua, B.; Shao, L.; Yu, G.; Huang, F. Fluorescence Indicator Displacement Detection Based on Pillar[5]arene-Assisted Dye Deprotonation. *Chem. Commun.* **2016**, *52*, 10016-10019.

(1275) Isaacs, L. Stimuli Responsive Systems Constructed Using Cucurbit[n]uril-Type Molecular Containers. *Acc. Chem. Res.* **2014**, *47*, 2052-2062.

(1276) Isaacs, L. Cucurbit[n]urils: From Mechanism to Structure and Function. *Chem. Commun.* **2009**, 619-629.

(1277) Dsouza, R. N.; Pischel, U.; Nau, W. M. Fluorescent Dyes and Their Supramolecular Host/Guest Complexes with Macrocycles in Aqueous Solution. *Chem. Rev.* **2011**, *111*, 7941-7980.

(1278) Das, D.; Scherman, O. A. Cucurbituril: At the Interface of Small Molecule Host-Guest Chemistry and Dynamic Aggregates. *Israel J. Chem.* **2011**, *51*, 537-550.

(1279) Isaacs, L. The Mechanism of Cucurbituril Formation. *Israel J. Chem.* **2011**, *51*, 578-591.

(1280) Sekutor, M.; Molcanov, K.; Cao, L.; Isaacs, L.; Glaser, R.; Mlinaric-Majerski, K. Design, Synthesis, and X-ray Structural Analyses of Diamantane Diammonium Salts: Guests for Cucurbit[n]uril (CB[n]) Hosts. *Eur. J. Org. Chem.* **2014**, *2014*, 2533-2542.

(1281) Babjakova, E.; Branna, P.; Kuczynska, M.; Rouchal, M.; Pruckova, Z.; Dastychova, L.; Vicha, J.; Vicha, R. An Adamantane-Based Disubstituted Binding Motif with Picomolar Dissociation Constants for Cucurbit[n]urils in Water and Related Quaternary Assemblies. *RSC Adv.* **2016**, *6*, 105146-105153.

(1282) Sigwalt, D.; Sekutor, M.; Cao, L.; Zavalij, P. Y.; Hostas, J.; Ajani, H.; Hobza, P.; Mlinaric-Majerski, K.; Glaser, R.; Isaacs, L. Unraveling the Structure-Affinity Relationship between Cucurbit[n]urils (n = 7, 8) and Cationic Diamondoids. *J. Am. Chem. Soc.* **2017**, *139*, 3249-3258.

(1283) Ward, T. R. Artificial Metalloenzymes Based on the Biotin-Avidin Technology: Enantioselective Catalysis and Beyond. *Acc. Chem. Res.* **2011**, *44*, 47-57.

(1284) Sakahara, H.; Saga, T. Avidin-Biotin System for Delivery of Diagnostic Agents. *Adv. Drug Delivery Rev.* **1999**, *37*, 89-101.

(1285) Kaifer, A. E. Portal Effects on the Stability of Cucurbituril Complexes. *Israel J. Chem.* **2018**, *58*, 244-249.

(1286) Meschke, C.; Buschmann, H.-J.; Schollmeyer, E. Complexes of Cucurbituril with Alkyl Mono- and Diammonium Ions in Aqueous Formic Acid Studied by Calorimetric Titrations. *Thermochim. Acta* **1997**, *297*, 43-48.

(1287) Ling, X.; Saretz, S.; Xiao, L.; Francescon, J.; Masson, E. Water vs. Cucurbituril Rim: A Fierce Competition for Guest Solvation. *Chem. Sci.* **2016**, *7*, 3569-3573.

(1288) Khurana, R.; Barooah, N.; Bhasikuttan, A. C.; Mohanty, J. Modulation in the Acidity Constant of Acridine Dye with Cucurbiturils: Stimuli-Responsive pKa Tuning and Dye Relocation into Live Cells. *Org. Biomol. Chem.* **2017**, *15*, 8448-8457.

(1289) Khorwal, V.; Nudurupati, U.; Mondal, S. I.; Datta, A. Interplay of Hydrophobic and Electrostatic Interactions in Modulation of Protonation-Deprotonation Equilibria of Two Positional Isomers in Their Complexes with Cucurbiturils. *J. Phys. Chem. C* **2017**, *121*, 5379-5388.

(1290) Galego, L. R.; Rodrigues, M. A. A.; Mendes, D. C.; Jockusch, S.; Da Silva, J. P. Quantitative Analysis of Biogenic Polyamines in Distilled Drinks by Direct Electrospray Ionization Tandem Mass Spectrometry Using a Nanocontainer. *Rapid Commun. Mass Spectrometry* **2016**, *30*, 1963-1968.

(1291) Minami, T.; Esipenko, N. A.; Akdeniz, A.; Zhang, B.; Isaacs, L.; Anzenbacher, P. Jr. Multianalyte Sensing of Addictive Over-the-Counter (OTC) Drugs. *J. Am. Chem. Soc.* **2013**, *135*, 15238-15243.

(1292) del Pozo, M.; Fernández, Á.; Quintana, C. On-Line Competitive Host-Guest Interactions in a Turn-On Fluorometric Method to Amantadine Determination in Human Serum and Pharmaceutical Formulations. *Talanta* **2018**, *179*, 124-130.

(1293) Yang, H.; Liu, T.; Yang, L.; Liu, K.; Wang, Z.; Zhang, X. Cucurbit[7]uril as a "Protective Agent": Controlling Photochemistry and Detecting 1-Adamantanamine. *Chem. Commun.* **2013**, *49*, 3905-3907.

(1294) Liu, S.; Ruspic, C.; Mukhopadhyay, P.; Chakrabarti, S.; Zavalij, P. Y.; Isaacs, L. The Cucurbit[*n*]uril Family: Prime Components for Self-Sorting Systems. *J. Am. Chem. Soc.* **2005**, *127*, 15959-15967.

(1295) Li, C.; Feng, J.; Ju, H. Supramolecular Interaction of Labetalol with Cucurbit[7]uril for its Sensitive Fluorescence Detection. *Analyst* **2015**, *140*, 230-235.

(1296) Li, Y.; Li, C.-F.; Du, L.-M.; Feng, J.-X.; Liu, H.-L.; Fu, Y.-L. A Competitive Strategy Based on Cucurbit[7]uril Supramolecular Interaction for Simple and Sensitive Detection of Dibucaine. *Talanta* **2015**, *132*, 653-657.

(1297) Aryal, G. H.; Battle, C. H.; Grusenmeyer, T. A.; Zhu, M.; Jayawickramarajah, J. A Naphthalimide Derived Fluorescent Sensor for Solid-Phase Screening of Cucurbit[7]uril-Guest Interactions. *Chem. Commun.* **2016**, *52*, 2307-2310.

(1298) Lazar, A. I.; Biedermann, F.; Mustafina, K. R.; Assaf, K. I.; Hennig, A.; Nau, W. M. Nanomolar Binding of Steroids to Cucurbit[n]urils: Selectivity and Applications. *J. Am. Chem. Soc.* **2016**, *138*, 13022-13029.

(1299) Huang, Y.; Wang, J.; Xue, S.-F.; Tao, Z.; Zhu, Q.-J.; Tang, Q. Determination of Thiabendazole in Aqueous Solutions Using a Cucurbituril-Enhanced Fluorescence Method. *J. Incl. Phenom. Macrocycl. Chem.* **2012**, *72*, 397-404.

(1300) del Pozo, M.; Hernández, L.; Quintana, C. A Selective Spectrofluorimetric Method for Carbendazim Determination in Oranges Involving Inclusion-Complex Formation with Cucurbit[7]uril. *Talanta* **2010**, *81*, 1542-1546.

(1301) Minami, T.; Esipenko, N. A.; Zhang, B.; Kozelkova, M. E.; Isaacs, L.; Nishiyabu, R.; Kubo, Y.; Anzenbacher, P. Jr. Supramolecular Sensor for Cancer-Associated Nitrosamines. *J. Am. Chem. Soc*. **2012**, *134*, 20021-20024.

(1302) Wang, S.; Wan, B.; Zhang, L.; Yang, Y.; Guo, L.-H. In Vitro Inhibition of Lysine Decarboxylase Activity by Organophosphate Esters. *Biochemical Pharmacology* **2014**, *92*, 506-516.

(1303) Biedermann, F.; Hathazi, D.; Nau, W. M. Associative Chemosensing by Fluorescent Macrocycle-Dye Complexes – A Versatile Enzyme Assay Platform Beyond Indicator Displacement. *Chem. Commun*. **2015**, *51*, 4977-4980.

(1304) Ye, R.; Cui, Q.; Yao, C.; Liu, R.; Li, L. Tunable Fluorescence Behaviors of a Supramolecular System Based on a Fluorene Derivative and Cucurbit[8]uril and its Applications for ATP Sensing. *Phys. Chem. Chem. Phys*. **2017**, *19*, 31306-31315.

(1305) Cheng, X.-J.; Liang, L.-L.; Chen, K.; Ji, N.-N.; Xiao, X.; Zhang, J.-X.; Zhang, Y.-Q.; Xue, S.-F.; Zhu, Q.-J.; Ni, X.-L.; Tao, Z. Twisted Cucurbit[14]uril. *Angew. Chem. Int. Ed.* **2013**, *125*, 7393-7396.

(1306) Zhang, J.; Tang, Q.; Gao, Z.-Z.; Qui, S.-C.; Huang, Y.; Tao, Z. Supramolecular Assembly Mediated by Metal Ions in Aqueous Solution and its Applications in their Analysis. *Chem. Eur. J.* **2017**, *23*, 10092-10099.

(1307) Sinha, M. K.; Reany, O.; Parvari, G.; Karmaker, A.; Keinan, E. Switchable Cucurbituril-Bipyridine Beacons. *Chem. Eur. J.* **2010**, *16*, 9056-9067.

(1308) Pedersen, C. J. New Macrocyclic Polyethers. *J. Am. Chem. Soc.* **1967**, *89*, 391-394.

(1309) Pedersen, C. J. Cyclic Polyethers and Their Complexes with Metal Salts. *J. Am. Chem. Soc.* **1967**, *89*, 7107-7036.

(1310) Pedersen, C. J. The Discovery of Crown Ethers. *Science* **1988**, *241*, 536-540.

(1311) Fabbrizzi, L. *Cryptands and Cryptates*; World Scientific: Singapore, 2018.

(1312) Sam, D. J.; Simmons, H. E. Crown Polyether Chemistry. Potassium Permanganate Oxidations in Benzene. *J. Am. Chem. Soc.* **1972**, *94*, 4024-4025.

(1313) Ghale, G.; Nau, W. M. Dynamically Analyte-Responsive Macrocyclic Host-Fluorophore Systems. *Acc. Chem. Res.* **2014**, *47*, 2150-2159.

(1314) Swidan, A.; Macdonald, C. L. B. Polyether Complexes of Groups 13 and 14. *Chem. Soc. Rev.* **2016**, *45*, 3883-3915.

(1315) Zhang, M.; Yan, X.; Huang, F.; Niu, Z.; Gibson, H. W. Stimuli-Responsive Host-Guest Systems Based on the Recognition of Cryptands by Organic Guests. *Acc. Chem. Res.* **2014**, *47*, 1995-2005.

(1316) Denat, F.; Brandès, S.; Guilard, R. Strategies for the Regioselective N-Functionalization of Tetraazacycloalkanes. From Cyclam and Cylen Towards More Sophisticated Molecules. *Synlett* **2000**, *5*, 561-574.

(1317) Joshi, T.; Graham, B.; Spiccia, L. Macrocyclic Metal Complexes for Metalloenzyme Mimicry and Sensor Development. *Acc. Chem. Soc.* **2015**, *48*, 2366-2379.

(1318) Cakić, N.; Gündüz, S.; Rengerasu, R.; Angelovski, G. Synthetic Strategies for Preparation of Cyclen-Based MRI Contrast Agents. *Tetrahedron Lett.* **2015**, *56*, 759-765.

(1319) Delgado, R.; Félix, V.; Lima, L. M. P.; Price, D. W. Metal Complexes of Cyclen and Cyclam Derivatives Useful for Medical Applications: A Discussion Based on Thermodynamic Stability Constants and Structural Data. *Dalton Trans.* **2007**, 2734-2745.

(1320) Cooper, S. R. Crown Thioether Chemistry. *Acc. Chem. Res.* **1988**, *21*, 141-146.

(1321) Tian, M.; Ihmels, H.; Benner, K. Selective Detection of Hg2+ in the Microenvironment of Double-Stranded DNA with an Intercalator Crown-Ether Conjugate. *Chem. Commun.* **2016**, *46*, 5719-5721.

(1322) Li, Y.-P.; Yang, H.-R.; Zhao, Q.; Song, W.-C.; Han, J.; Bu, X.-H. Ratiometric and Selective Fluorescent Sensor for Zn2+ as an "Off-On-Off" Switch and Logic Gate. *Inorg. Chem.* **2012**, *51*, 9642-9648.

(1323) Safin, D. A.; Babashkina, M. G.; Garcia, Y. Crown Ether-Containing Schiff Base as a Highly Efficient "Turn-On" Fluorescent Sensor for Determination and Separation of Zn2+ in Water. *Dalton. Trans.* **2013**, *42*, 1969-1972.

(1324) Kikot, L.; Lyapunov, A.; Bogaschenko, T.; Smola, S.; Kulygina, C.; Kirichenko, T. Facile Synthesis of Bis(Crown Ether) Benzils: Prospective Building Blocks for Metal Ion Sensors. *Synth. Commun.* **2014**, *45*, 478-484.

(1325) Ma, Y.; Marszalek, T.; Yuan, Z.; Strangenberg, R.; Pisula, W.; Chen. L.; Müllen, K. A Crown Ether Decorated Dibenzocoronene Tetracarboxdiimide Chromophore: Synthesis, Sensing, and Self-Organization. *Chem. Asian J.* **2015**, *10*, 139-143.

(1326) Shiraishi, T.; Kagechika, H.; Hirano, T. 6-Arylcoumarins: Versatile Scaffolds for Fluorescent Sensors. *New J. Chem.* **2015**, *39*, 8389-8396.

(1327) Basa, P. N.; Bhowmick, A.; Schulz, M. M.; Sykes, A. G. Site-Selective Imination of an Anthracenone Sensor: Selective Fluorescence Detection of Barium(II). *J. Org. Chem.* **2011**, *76*, 7866-7871.

(1328) Ncube, P.; Krause, R. W. M.; Ndinteh, D. T.; Mamba, B. B. Fluorescent Sensing and Determination of Mercury (II) Ions in Water. *Water SA* **2014**, *40*, 175-182.

(1329) Şahin, D.; Yılmaz, H.; Hayvalı, Z. Synthesis, Spectroscopic and Spectrophotometric Study of BODIPY Appended Crown Ether Sensor for Ion Detection. *Res. Chem. Intermed.* **2016**, *42*, 6337-6350.

(1330) Du, J.; Huang, Z.; Yu, X.-Q.; Pu, L. Highly Selective Fluorescent Recognition of Histidine by a Crown Ether-Terpyridine-Zn(II) Sensor. *Chem. Commun.* **2013**, *49*, 5399-5401.

(1331) Ast, S.; Schwarze, T.; Müller, H.; Sukhanov, A.; Michaelis, S.; Wegener, J.; Wolfbeis, O. S.; Körzdörfer, T.; Dürkop, A., Holdt, H.-J. A Highly K+-Selective Phenylaza[18]Crown-6-Lariat-Ether-Based Fluoroionophore and its Applications in the Sensing of K+ Ions with an Optical Sensor Film and in Cells. *Chem. Eur. J.* **2013**, *19*, 14911-14917.

(1332) Yetisen, A. K.; Jiang, N.; Tamayol, A.; Ruiz-Esparza, G. U.; Zhang, Y. S.; Medina-Pando, S.; Gupta, A.; Wolddshon, J. S.; Butt, H.; Khademhosseini, A.; Yun, S.-H. Paper-Based Microfluidic System for Tear Electrolyte Analysis. *Lab Chip* **2017**, *17*, 1137-1148.

(1333) Tanha, M.; Chakraborty, S. K.; Gabris, B.; Waggoner, A. S.; Salama, G.; Yaron, D. Computational and Experimental Characterization of a Fluorescent Dye for Detection of Potassium Ion Concentration. *J. Phys. Chem. A* **2014**, *118*, 9837-9843.

(1334) Hughes, W.; Rananaware, A.; La, D. D.; Jones, L. A.; Bhargava, S.; Bhosale, S. V. Aza-Crown Ether-Core Substituted Naphthalene Diimide Fluorescence “Turn-On” Probe for Selective Detection of Ca2+. *Sens. Actuators B* **2017**, *244*, 854-860.

(1335) Nakatsuji, Y.; Nakamura, M.; Oka, T.; Muraoka, M. Selective Fluorometric Sensing of Calcium Cation by C-Pivot Lariat Monoaza-Crown Ether with Two Pyrene Moieties. *Chem. Lett.* **2011**, *40*, 1226-1228.

(1336) Balasubramanian, V.; Srinivasan, R.; Miskimins, R.; Sykes, A. G. A Simple Aza-Crown Ether Containing an Anthraquinone Fluorophore for the Selective Detection of Mg(II) in Living Cells. *Tetrahedron* **2016**, *72*, 205-209.

(1337) Poronik, Y. M.; Clermont, G.; Blanchard-Desce, M.; Gryko, D. T. Nonlinear Optical Chemosensor for Sodium Ion Based on Rhodol Chromophore. *J. Org. Chem.* **2013**, *78*, 11721-11732.

(1338) Volchkov, V. V.; Gostev, F. E.; Shelaev, I. V.; Nadtochenko, V. A.; Dmitrieva, S. N.; Gromov, S. P.; Alfimov, M. V.; Melnikov, M. Y. Complexation of Donor-Acceptor Substituted Aza-Crowns with Alkali and Alkaline Earth Metal Cation. Charge Transfer and Recoordination in Excited State. *J. Fluorescence* **2016**, *26*, 585-592.

(1339) Goswami, S.; Maity, S.; Maity, A. C.; Das, A. K.; Khanra, K.; Mandal, T. K.; Bhattacharyya, N. A Macrocyclic Piperazine Linked Extremely Zn2+ Selective Fluorescent Chemosensor with Bio-Imaging and for H2PO4- Sensing. *Tetrahedron Lett.* **2014**, *55*, 5993-5997.

(1340) Bhanja, A. K.; Patra, C.; Mondal, S.; Mishra, S.; Saha, K. D.; Sinha, C. Macrocycle Aza-Crown Chromogenic Reagent to Al3+ and Fluorescence Sensor for Zn2+ and Al3+ Along with Live Cell Application and Logic Operation. *Sens. Actuators B* **2017**, *252*, 257-267.

(1341) Azadbakht, R.; Keypour, H.; Rudbari, H. A.; Zaheri, A. H. M.; Menati, S. Synthesis and Characterization of Two New Fluorescent Macrocycles: A Novel Fluorescent Chemosensor for Zinc Ion. *J. Luminescence* **2012**, *132*, 1860-1866.

(1342) Ghanbari, B.; Zarepour-jevinani, M.; Kubicki, M. Selective and Sensitive Fluorescent Chemosensor Based on N2O2-Donor Naphthodiaza-Crown Macrocyclic Ligands for Detection of Cu(II), and Zn(II). *J. Photochem. Photobiol. A: Chem.* **2018**, *356*, 689-699.

(1343) Ambrosi, G.; Formica, M.; Fusi, V.; Giorgi, L.; Macedi, E.; Micheloni, M.; Paoli, P.; Pontellini, R.; Rossi, P. Efficient Fluorescence Sensors Based on 2,5-Diphenyl[1,3,4]oxadiazole: A Case of Specific Response to Zn(II) at Physiological pH. *Inorg. Chem.* **2010**, *49*, 9940-9948.

(1344) Hsieh, Y.-C.; Chir, J.-L.; Yang, S.-T.; Chen, S.-J.; Hu, C.-H.; Wu, A.-T. A Sugar-Aza-Crown Ether-Based Fluorescent Sensor for Cu2+ and Hg2+ Ions. *Carbohydr. Res.* **2011**, *346*, 978-981.

(1345) Hou, C.; Urbanec, A. M.; Cao, H. A Rapid Hg2+ Sensor Based on Aza-15-Crown-5 Ether Functionalized 1,8-Napthalimide. *Tetrahedron Lett.* **2011**, *52*, 4903-4905.

(1346) Li, Y.; Yoon, U.-C.; Hyun, M.-H. Phosphorescent Azacrown Ether-Appended Iridium(III) Complex for the Selective Detection of Hg2+ in Aqueous Acetonitrile. *Bull. Korean Chem. Soc.* **2011**, *32*, 122-126.

(1347) Abel, A. S.; Mitrofanov, A. Y.; Rousselin, Y.; Denat, F.; Bessmertnykh-Lemeune, A.; Averin, A. D.; Beletskaya, I. P. Ditopic Macrocyclic Receptors with a 4,7-Diamino-1,10-Phenanthroline Fragment for Multimodal Detection of Toxic Metal Ions. *ChemPlusChem* **2016**, *81*, 35-39.

(1348) Yang, L.; Liao, D.-J.; Wu, A.-T.; Yan, H. Synthesis and Fluorescent Properties of Aza-Crown Ether Tethered BODIPY Fluorophores. *Tetrahedron Lett.* **2017**, *58*, 889-891.

(1349) Qiu, L.; Zhu, C.; Chen, H.; Hu, M.; He, W.; Guo, Z. A Turn-On Fluorescent Fe3+ Sensor Derived from an Anthracene-Bearing Bisdiene Macrocycle and its Intracellular Imaging Application. *Chem. Commun.* **2014**, *50*, 4631-4634.

(1350) Li, H.; Li, L.; Yin, B. Highly Selective Fluorescent Chemosensor for Fe3+ Detection Based on Diaza-18-Crown-6 Ether Appended with Dual Coumarins. *Inorg. Chem. Commun.* **2014**, *42*, 1-4.

(1351) Azadbakht, R.; Khanabadi, J. A Highly Sensitive and Selective Off-On Fluorescent Chemosensor for Al3+ Based on Naphthalene Derivative. *Inorg. Chem. Commun.* **2013**, *30*, 21-25.

(1352) Azadbakht, R.; Khanabadi, J. A Novel Fluorescent Nano-Chemosensor for Al(III) Ions Using a New Macrocyclic Receptor. *Spectrochem. Acta A* **2014**, *124*, 249-255.

(1353) Liu, D.; Pang, T.; Ma, K.; Jiang, W.; Bao, X. A New Highly Sensitive and Selective Fluorescence Chemosensor for Cr3+ Based on Rhodamine B and a 4,13-Diaza-18-Crown 6-Ether Conjugate. *RSC Adv.* **2014**, *4*, 2563-2567.

(1354) Yang, S.-T.; Liao, D.-J.; Chen, S.-J.; Hu, C.-H.; Wu, A.-T. A Fluorescence Enhancement-Based Sensor for Hydrogen Sulfate Ion. *Analyst* **2012**, *137*, 1553-1555.

(1355) Li, M.; Liang, Q.; Zheng, M.; Fang, C.; Peng, S.; Zhao, M. An Efficient Ruthenium Tris(bipyridine)-Based Luminescent Chemosensor for Recognition of Cu(II) and Sulfide Anion in Water. *Dalton Trans.* **2013**, *42*, 13509-13515.

(1356) Wang, M.; Zhang, D.; Li, M.; Fan, M.; Ye, Y.; Zhao, Y.-F. A Rhodamine-Cyclen Conjugate as Chromogenic and Fluorescent Chemosensor for Copper Ion in Aqueous Media. *J. Fluorescence* **2013**, *23*, 417-423.

(1357) Majzoub, A. E.; Cadiou, C.; Déchamps-Olivier, I.; Tinant, B.; Chuburu, F. Cyclam-Methylbenzimidazole: A Selective OFF-ON Fluorescent Sensor for Zinc. *Inorg. Chem.* **2011**, *50*, 4029-2038.

(1358) Wang, X.; Zhang, Z.; Ma, X.; Wen, J.; Geng, Z.; Wang, Z. Real-Time Fluorescence Assays of Alkaline Phosphatase and ATP Sulfurylase Activities Based on a Novel PPi Fluorescent Probe. *Talanta* **2015**, *137*, 156-160.

(1359) Bazzicalupi, C.; Bencini, A.; Matera, I.; Puccioni, S.; Valtancoli, B. Selective Binding and Fluorescence Sensing of ZnII with Acridine-Based Macrocycles. *Inorg. Chim. Acta* **2012**, *381*, 162-169.

(1360) Puccioni, S.; Bazzicalupi, C.; Bencini, A.; Giorgi, C.; Valtancoli, B.; De Filippo, G.; Lippolis, V.; Salvi, P. R.; Pietraperzia, G.; Chelli, R.; Gellini, C. Tuning the Emission Properties of Fluorescent Ligands by Changing pH: The Unusual Case of an Acridine-Containing Polyamine Macrocycle. *J. Phys. Chem. A* **2013**, *117*, 3798-3808.

(1361) Wang, X.; Ma, X.; Yang, Z.; Zhang, Z.; Wen, J.; Geng, Z.; Wang, Z. An NBD-Armed Tetraaza Macrocyclic Lysosomal-Targeted Fluorescent Probe for Imaging Copper(II) Ions. *Chem. Commun.* **2013**, *49*, 11263-11265.

(1362) Zhou, R.; Li, B.; Wu, N.; Gao, G.; You, J.; Lan, J. Cyclen-Functionalized Perylenebisimides as Sensitive and Selective Fluorescent Sensors for Pb2+ in Aqueous Solution. *Chem. Commun.* **2011**, *47*, 6668-6670.

(1363) Shim, S.-Y.; Tae, J.-S. Rhodamine Cyclen-Based Fluorescent Chemosensor for the Detection of Cd2+. *Bull. Korean Chem. Soc.* **2011**, *32*, 2928-2932.

(1364) Bakthavatsalam, S.; Sarkar, A.; Rakshit, A.; Jain, S.; Kumar, A.; Datta, A. Tuning Macrocycles to Design 'Turn-On' Fluorescence Probes for Manganese (II) Sensing in Live Cells. *Chem. Commun.* **2015**, *51*, 2605-2608.

(1365) Do-Thanh, C.-L.; Rowland, M. M.; Best, M. D. Fluorescent Bis-Cyclen Tweezer Receptors for Inositol (1,4,5)-Trisphosphate. *Tetrahedron* **2011**, *67*, 3803-3808.

(1366) Granzhan, A.; Ihmels, H.; Viola, G. 9-Donor-Substituted Acridizinium Salts: Versatile Environment-Sensitive Fluorophores for the Detection of Biomacromolecules. *J. Am. Chem. Soc.* **2007**, *129*, 1254-1267.

(1367) Dai, H.; Liu, F.; Gao, Q.; Fu T.; Kou, X. A Highly Selective Fluorescent Sensor for Mercury Ion (II) Based on Azathia-Crown Ether Possessing a Dansyl Moiety. *Luminescence* **2011**, *26*, 523-530.

(1368) Mameli, M.; Lippolis, V.; Caltagirone, C.; Capelo, J. L.; Faza, O. N.; Lodeiro, C. Hg2+ Detection by New Anthracene Pendant-Arm Derivatives of Mixed N/S and N/S/O-Donor Macrocycles: Fluorescence, Matrix-Assisted Laser Desorption/Ionization Time-of-Flight Mass Spectrometry and Density Functional Theory Studies. *Inorg. Chem.* **2010**, *49*, 8276-8286.

(1369) Jiang, Y.; Huang, Z.; Dai, H.; Wang, L.; Ying, L.; Kou, X. A Highly Selective and Sensitive Fluorescent Sensor for Copper(II) Ion Characterized by One Dichlorofluorescein Moiety and Two Azathia-Crown Ether. *Asian J. Chem.* **2013**, *25*, 8292-8296.

(1370) Boricha, V. P.; Patra, S.; Parihar, S.; Chouhan, Y. S.; Paul, P. Luminescent Metalloreceptors with Pendant Macrocyclic Ionophores with NS2O3 Donor Sites: Synthesis, Characterization and Ion-Binding Property. *Polyhedron* **2012**, *43*, 104-113.

(1371) Wang, H.; Xue, L.; Jiang, H. Ratiometric Fluorescent Sensor for Silver Ion and its Resultant Complex for Iodide Anion in Aqueous Solution. *Org. Lett.* **2011**, *13*, 3844-3847.

(1372) Kaur, P.; Kaur, N.; Kaur, M.; Dhuna, V.; Singh, J.; Singh, K. 'Turn-On' Coordination Based Detection of Pd2+ and Bioimaging Applications. *RSC Adv.* **2014**, *4*, 16104-16108.

(1373) Mesquita, L. M.; André, V.; Esteves, C. V.; Palmeira, T.; Berberan-Santos, M. N.; Mateus, P.; Delgado, R. Dinuclear Zinc(II) Macrocyclic Complex as Receptor for Selective Fluorescence Sensing of Pyrophosphate. *Inorg. Chem.* **2016**, *55*, 2212-2219.

(1374) Bhuyan, M.; Katayev, E.; Stadlbauer, S.; Nonaka, H.; Ojida, A.; Hamachi, I.; König, B. Rigid Luminescent Bis-Zinc(II)-Bis-Cyclen Complexes for the Detection of Phosphate Anions and Non-Covalent Protein Labeling in Aqueous Solution. *Eur. J. Org. Chem.* **2011**, *2011*, 2807-2817.

(1375) Saeed, M. A.; Powell, D. R.; Hossain, M. A. Fluorescent Detection of Phosphate Anion by a Highly Selective Chemosensor in Water. *Tetrahedron Lett.* **2010**, *51*, 4904-4907.

(1376) Rhaman, M. M.; Fronczek, F. R.; Powell, D. R.; Hossain, M. A. Colourimetric and Fluorescent Detection of Oxalate in Water by a New Macrocycle-Based Dinuclear Nickel Complex: A Remarkable Red Shift of the Fluorescence Band. *Dalton Trans.* **2014**, *43*, 4618-4621.

(1377) Hu, M.; Feng, G. Highly Selective and Sensitive Fluorescent Sensing of Oxalate in Water. *Chem. Commum*. **2012**, *48*, 6951-6953.

(1378) Li, Z.; Geng, Z.-R.; Zhang, C.; Wang, X.-B.; Wang, Z.-L. BODIPY-Based Azamacrocyclic Ensemble for Selective Fluorescence Detection and Quantification of Homocysteine in Biological Applications. *Biosens. Bioelectron.* **2015**, *72*, 1-9.

(1379) Ito, H.; Shinoda, S. Chirality Sensing and Size Recognition of *N*-Boc-Amino Acids by Cage-Type Dimeric Lanthanide Complexes: Chirality Detection of *N*-Boc-Aspartate Anions via Luminescence Color Change. *Chem. Commun.* **2015**, *51*, 3808-3811.

(1380) Azab, H. A.; Anwar, Z. M.; Kamel, R. M.; Rashwan, M. S. Sensing of Nucleosides, Nucleotides and DNA Using Luminescent Eu Complex by Normal and Time Resolved Fluorescence Techniques. *J. Luminescence* **2016**, *169*, 173-181.

(1381) Comby, S.; Tuck, S. A.; Truman, L. K.; Kotova, O.; Gunnlaugsson, T. New Trick for an Old Ligand! The Sensing of Zn(II) Using a Lanthanide Based Ternary Yb(III)-Cyclen-8-hydroxyquinoline System as a Dual Emissive Probe for Displacement Assay. *Inorg. Chem.* **2012**, *51*, 10158-10168.

(1382) Rivas, C.; Stasiuk, G. J.; Sae-Heng, M.; Long, N. J. Towards Understanding the Design of Dual-Modal MR/Fluorescent Probes to Sense Zinc Ions. *Dalton Trans.* **2015**, *44*, 4976-4985.

(1383) McMahon, B. K.; Gunnlaugsson, T. Lanthanide Luminescence Sensing of Copper and Mercury Ions Using an Iminodiacetate-Based Tb(III)-Cyclen Chemosensor. *Tetrahedron Lett.* **2010**, *51*, 5406-5410.

(1384) Kotova, O.; Comby, S.; Gunnlaugsson, T. Sensing of Biologically Relevant d-Metal Ions Using a Eu(III)-Cyclen Based Luminescent Displacement Assay in Aqueous pH 7.3 Buffered Solution. *Chem. Commun.* **2011**, *47*, 6810-6812.

(1385) Leonenko, I. I.; Aleksandrova, D. I.; Yegorova, A. V.; Antonovitch, V. P.; Basok, S. S. Luminescence Determination of Sodium and Potassium Using Molecular Sensors on the Basis of Terbium(III) Complexes of 4-Carbocybenzocrown Ethers. *J. Anal. Chem.* **2011**, *66*, 158-165.

(1386) Caffrey, D. F.; Gunnlaugsson, T. Displacement Assay Detection by a Dimeric Lanthanide Luminescent Ternary Tb(III)-Cyclen Complex: High Selectivity for Phosphate and Nitrate Anions. *Dalton Trans.* **2014**, *43*, 17964-17970.

(1387) Hardie, M. J. Recent Advances in the Chemistry of Cyclotriveratrylene. *Chem. Soc. Rev.* **2010**, *39*, 516-527.

(1388) Henkelis, J. J.; Hardie, M. J. Controlling the Assembly of Cyclotriveratrylene-Derived Coordination Cages. *Chem. Commun.* **2015**, *51*, 11929-11943.

(1389) Erieau-Peyrard, L.; Coiffier, C.; Bordat, P.; Bégué, D.; Chierici, S.; Pinet, D.; Gosse, I.; Baraille, I.; Brown, R. Selective, Direct Detection of Acetylcholine in PBS Solution, with Self-Assembled Fluorescent Nano-Particles: Experiment and Modelling. *Phys. Chem. Chem. Phys.* **2015**, *17*, 4168-4174.

(1390) Dumartin, M.-L.; Givelet, C.; Meyrand, P.; Bibal, B.; Gosse, I. A Fluorescent Cyclotriveratrylene: Synthesis, Emission Properties, and Acetylcholine Recognition in Water. *Org. Biomol. Chem.* **2009**, *7*, 2725-2728.

(1391) Peyrard, L.; Chierici, S.; Pinet, S.; Bata, P.; Jonusauskas, G.; Pinaud, N.; Meyrand, P.; Gosse, I. C3-Triiodocyclotriveratrylene as a Key Intermediate to Fluorescent Probes: Application to Selective Choline Recognition. *Org. Biomol. Chem.* **2011**, *9*, 8489-8494.

(1392) Moriuchi-Kawakami, T.; Sato, J.; Shibutani, Y. *C3*-Functionalized Cyclotriveratrylene Derivative Bearing Quinolinyl Group as a Fluorescent Probe for Cu2+. *Anal. Sci.* **2009**, *25*, 449-452.

(1393) Ma, L.; Zhang, Q.; Wu, H.; Yang, J.; Liu, Y.-Y.; Ma, J.-F. Multifunctional Luminescence Sensors Assembled with Lanthanide and a Cyclotriveratrylene-Based Ligand. *Eur. J. Inorg. Chem.* **2017**, 4221-4230.

(1394) Yang, F.; Chen, Q.; Cheng, Q.-Y.; Yan, C.-G.; Han, B.-H. Sugar-Functionalized Water-Soluble Cyclotriveratrylene Derivatives: Preparation and Interaction with Fullerene. *J. Org. Chem.* **2012**, *77*, 971-976.

(1395) Deschamps, J.; Langlois, A.; Martin, G.; Bucher, L.; Desbois, N.; Gros, C. P.; Harvey, P. D. Cyclotriveratrylene-Containing Porphyrins. *Inorg. Chem.* **2016**, *55*, 9230-9239.

(1396) Hamblin, M. R. Fullerenes as Photosensitizers in Photodynamic Therapy: Pros and Cons. *Photochem. Photobiol. Sci.* **2018**, *17*, 1003-1017.

(1397) Cook, T. R.; Stang, P. J. Recent Developments in the Preparation and Chemistry of Metallacages and Metallacycles via Coordination. *Chem. Rev.* **2015**, *115*, 7001-7045.

(1398) Saha, M. L.; Yan, X.; Stang, P. J. Photophysical Properties of Organoplatinum(II) Compounds and Derived Self-Assembled Metallacycles and Metallacages: Fluorescence and its Applications. *Acc. Chem. Res.* **2016**, *49*, 2527-2539.

(1399) Pollock, J. B.; Schneider, G. L.; Cook, T. R.; Davies, A. S.; Stang, P. J. Tunable Visible Light Emission of Self-Assembled Rhomboidal Metallacycles. *J. Am. Chem. Soc.* **2013**, *135*, 13676-13679.

(1400) Shanmugaraju, S.; Bar, A. K.; Chi, K.-W.; Mukherjee, P. S. Coordination-Driven Self-Assembly of Metallamacrocycles via a New Pt(II)2 Organometallic Building Block with 90o Geometry and Optical Sensing of Anions. *Organometallics* **2010**, *29*, 2971-2980.

(1401) Mishra, A.; Vajpayee, V.; Kim, H.; Lee, M. H.; Jung, H.; Wang, M.; Stang, P. J.; Chi, K.-W. Self-Assembled Metalla-Bowls for Selective Sensing of Multi-Carboxylate Anions. *Dalton Trans*. **2012**, *41*, 1195-1201.

(1402) Wu, X.; Zhang, D.; Deng, S.; Wang, J.; Yang, C.; Wang, D.-H.; Bi, Y. Functional Metal-Organic Quadrangular Macrocycle as Luminescent Sensor for ATP in Aqueous Media. *Inorg. Chem. Comm*. **2017**, *84*, 195-199.

(1403) Vajpayee, V.; Kim, H. Mishra, A.; Mukherjee, P. S.; Stang, P. J.; Lee, M. H.; Kim, H. K.; Chi, K.-W. Self-Assembled Molecular Squares Containing Metal-Based Donor: Synthesis and Application in the Sensing of Nitro-Aromatics. *Dalton. Trans.* **2011**, *40*, 3112-3115.

(1404) Guzmán-Percástegui, E.; Vonlanthen, M.; Quiroz-García, B.; Flores-Alamo, M.; Rivera, E.; Castillo, I. Supramolecular Fluorescence Enhancement via Coordination-Driven Self-Assembly in Bis-Picolylcalixarene Blue-Emitting M2L2Xn Macrocycles. *Dalton Trans.* **2015**, *44*, 15966-15975.

(1405) Luther, A.; Bisang, C.; Obrecht, D. Advances in Macrocyclic Peptide-Based Antibiotics. *Bioorg. Med. Chem.* **2018**, *26*, 2850-2858.

(1406) Jiang, Y.; Long, H.; Zhu, Y.; Zeng, Y. Macrocyclic Peptides as Regulators of Protein-Protein Interactions. *Chinese Chem. Lett*. **2018**, *29*, 1067-1073.

(1407) Kreutzer, A. G.; Nowick, J. S. Elucidating the Structures of Amyloid Oligomers with Macrocyclic β-Hairpin Peptides: Insights into Alzheimer's Disease and Other Amyloid Diseases. *Acc. Chem. Res.* **2018**, *51*, 706-718.

(1408) Nielsen, D. S.; Lohman, R.-J.; Hoang, H. N.; Hill, T. A.; Jones, A.; Lucke, A. J.; Fairlie, D. P. Flexibility versus Rigidity for Orally Bioavailable Cyclic Hexapeptides. *ChemBioChem* **2015**, *16*, 2289-2293.

(1409) Kwon, I.; Lim, S. I. Non-Natural Amino Acids for Protein Engineering and New Protein Chemistries. *Macromol. Chem. Phys.* **2013**, *214*, 1295-1301.

(1410) Wu, J.; Tang, J.; Chen, H.; He, Y.; Wang, H.; Yao, H. Recent Developments in Peptide Macrocyclization. *Tetrahedron Lett.* **2018**, *59*, 325-333.

(1411) Abdel Monaim, S. A. H.; Acosta, G. A.; Royo, M.; El-Faham, A.; de la Torre, B. G.; Albericio, F. Solid-Phase Synthesis of Homodetic Cyclic Peptides from Fmoc-MeDbz-Resin. *Tetrahedron Lett.* **2018**, *59*, 1779-1782.

(1412) Appavoo, S. D.; Kaji, T.; Frost, J. R.; Scully, C. C. G.; Yudin, A. K. Development of Endocyclic Control Elements for Peptide Macrocycles. *J. Am. Chem. Soc.* **2018**, *140*, 8763-8770.

(1413) Webster, A. M.; Cobb, S. L. Recent Advances in the Synthesis of Peptoid Macrocycles. *Chem. Eur. J.* **2018**, *24*, 7560-7573.

(1414) Jongkees, S. A. K.; Hipolito, C. J.; Rogers, J. M.; Suga, H. Model Foldamers: Applications and Structures of Stable Macrocyclic Peptides Identified Using in Vitro Selection. *New J. Chem.* **2015**, *39*, 3197-3207.

(1415) Shi, Y.; Teng, P.; Sang, P.; She, F.; Wei, L.; Cai, J. γ-AApeptides: Design, Structure, and Applications. *Acc. Chem. Res.* **2016**, *49*, 428-441.

(1416) Fairlie, D. P.; Abbenante, G.; March, D. R. Macrocyclic Peptidomimetics - Forcing Peptides into Bioactive Conformations. *Curr. Med. Chem.* **1995**, *2*, 654-686.

(1417) Iwasaki, K.; Goto, Y.; Katoh, T.; Yamashita, T.; Kaneko, S.; Suga, H. A Fluorescent Imaging Probe Based on a Macrocyclic Scaffold That Binds to Cellular EpCAM. *J. Molec. Evolution* **2015**, *81*, 210-217.

(1418) Curtin, B. H.; Manoni, F.; Park, J.; Sisto, L. J.; Lam, Y.-h.; Gravel, M.; Roulston, A.; Harran, P. G. Assembly of Complex Macrocycles by Incrementally Amalgamating Unprotected Peptides with a Designed Four-Armed Insert. *J. Org. Chem.* **2018**, *83*, 3090-3108.

(1419) Zhou, Z.; Han, Z.; Lu, Z.-R. A Targeted Nanoglobular Contrast Agent from Host-Guest Self-Assembly for MR Cancer Molecular Imaging. *Biomater.* **2016**, *85*, 168-179.

(1420) Krueger, D. M.; Glas, A.; Bier, D.; Pospiech, N.; Wallraven, K.; Dietrich, L.; Ottmann, C.; Koch, O.; Hennig, S.; Grossmann, T. N. Structure-Based Design of Non-Natural Macrocyclic Peptides That Inhibit Protein-Protein Interactions. *J. Med. Chem.* **2017**, *60*, 8982-8988.

(1421) Chen, X.; Liu, L.; Chen, Y.; Yang, Y.; Yang, C.-Y.; Guo, T.; Lei, M.; Sun, H.; Wang, S. Cyclic Peptidic Mimetics of Apollo Peptides Targeting Telomeric Repeat Binding Factor 2 (TRF2) and Apollo Interaction. *ACS Med. Chem. Lett.* **2018**, *9*, 507-511.

(1422) Saludes, J. P.; Morton, L. A.; Ghosh, N.; Beninson, L. A.; Chapman, E. R.; Fleshner, M.; Yin, H. Detection of Highly Curved Membrane Surfaces Using a Cyclic Peptide Derived from Synaptotagmin-I. *ACS Chem. Biol.* **2012**, *7*, 1629-1635.

(1423) Penas, C.; Pazos, E.; Mascarenas, J. L.; Vazquez, M. E. A Folding-Based Approach for the Luminescent Detection of a Short RNA Hairpin. *J. Am. Chem. Soc.* **2013**, *135*, 3812-3814.

(1424) Li, Y.; Han, Z.; Roelle, S.; DeSanto, A.; Sabatelle, R.; Schur, R.; Lu, Z.-R. Synthesis and Assessment of Peptide Gd-DOTA Conjugates Targeting Extradomain B Fibronectin for Magnetic Resonance Molecular Imaging of Prostate Cancer. *Molec. Pharmaceutics* **2017**, *14*, 3906-3915.

(1425) Ito, T.; Inoue, M.; Akamatsu, K.; Kusaka, E.; Tanabe, K.; Nishimoto, S.-i. αvβ3-Integrin-Targeting Lanthanide Complex: Synthesis and Evaluation as a Tumor-Homing Luminescent Probe. *Bioorg. Med. Chem. Lett.* **2011**, *21*, 3515-3518.

(1426) Mohandessi, S.; Rajendran, M.; Magda, D.; Miller, L. W. Cell-Penetrating Peptides as Delivery Vehicles for a Protein-Targeted Terbium Complex. *Chem. Eur. J.* **2012**, *18*, 10825-10829.

(1427) Wang, X.; Wang, C.; Qu, K.; Song, Y.; Ren, J.; Miyoshi, D.; Sugimoto, N.; Qu, X. Ultrasensitive and Selective Detection of a Prognostic Indicator in Early-Stage Cancer Using Graphene Oxide and Carbon Nanotubes. *Adv. Functional Mater.* **2010**, *20*, 3967-3971.

(1428) Wolgemuth, D. J. Function of Cyclins in Regulating the Mitotic and Meiotic Cell Cycles in Male Germ Cells. *Cell Cycle* **2008**, *7*, 3509-3513.

(1429) Yasmeen, A.; Berdel, W. E.; Serve, H.; Mueller-Tidow, C. E- and A-Type Cyclins as Markers for Cancer Diagnosis and Prognosis. *Expert Rev. Mol. Diagn.* **2003**, *3*, 617-633.

(1430) Bachrach, S. M.; Andrews, A. E. All-Carbon Neutral Analogue of ExBox4+: A DFT Study of Polycyclic Aromatic Hydrocarbon Binding. *J. Phys. Chem. A* **2014**, *118*, 6014-6111.

(1431) Nakatani, Y.; Furusho, Y.; Yashima, E. Synthesis of Helically Twisted [1+1] Macrocycles Assisted by Amidinium-Carboxylate Salt Bridges and Control of their Chiroptical Properties. *Org. Biomol. Chem.* **2013**, *11*, 1614-1623.

(1432) Fu, Y.; Xing, Z.; Zhu, C.; Yang, H.; He, W.; Zhu, C.; Cheng, Y. A Novel Calixsalen Macrocycle: Metal Sensing Behavior for Zn(II) and Intracellular Imaging Application. *Tetrahedron Lett.* **2012**, *53*, 804-807.

(1433) Ishida, M.; Naruta, Y.; Tani, F. A Porphyrin-Related Macrocycle with an Embedded 1,10-Phenanthroline Moiety: Fluorescent Magnesium(II) Ion Sensor. *Angew. Chem. Int. Ed.* **2010**, *49*, 91-94.

(1434) Goswami, S.; Das, N. K.; Aich, K.; Sen, D. A Naphthyridine Based Macrocycle "Switching On" Fluorescent Receptor for Cadmium. *J. Luminescence* **2011**, *131*, 2185-2188.

(1435) Dai, B.-N.; Cao, Q.-Y.; Wang, L.; Wang Z.-C.; Yang, Z. A New Naphthalene-Containing Triazolophane for Fluorescence Sensing of Mercury(II) Ion. *Inorg. Chim. Acta* **2014**, *423*, 163-167.

(1436) Baxter, P. N. W.; Gisselbrecht, J.-P.; Karmazin-Brelot, L.; Varnek, A.; Allouche, L. Synthesis of a Strained Acetylenic Macrocycle Incorporating a *para*-Oligo[2]cruciform Bridge Bent Over Nanoscopic Dimensions: Structural, Electronic, Spectroscopic, and Ion-Sensing Properties. *Chem. Eur. J.* **2013**, *19*, 12336-12349**.**

(1437) Baxter, P. N. W.; Ouahabi, A. A.; Gisselbrecht, J.-P.; Brelot, L.; Varnek, A. Electronic, Spectroscopic, and Ion-Sensing Properties of a Dehydro[*m*]pyrido[14]- and [15]Annulene Isomer Library. *J. Org. Chem.* **2012**, *77*, 126-142.

(1438) Ganapathi, E.; Lee, W.-Z.; Ravikanth, M. Stable Nonaromatic [20]Dithiaporphyrun (2.1.1.1) Macrocycles: Synthesis, Structure, Spectral, Electrochemical, and Metal Ion Sensing Studies. *J. Org. Chem.* **2014**, *79*, 9603-9612.

(1439) Núñex, C.; Aldrey, A.; García, V.; Bastida, R.; Macías, A.; Lodeiro, C. Novel Emissive Phenylurea-Based Macrocyclic Chemosensor: Synthesis, Fluorescent and Complexation Studies. *Inorg. Chim. Acta* **2012**, *381*, 85-94.

(1440) Zhang, D.; Jiang, X.; Yang, H.; Martinez, A.; Feng, M.; Dong, Z.; Gao, G. Acridine-Based Macrocyclic Fluorescent Sensors: Self-Assembly Behavior Characterized by Crystal Structures and a Tunable Bathochromic-Shift in Emission Induced by H2PO4- via Adjusting Ring Size and Rigidity. *Org. Biomol. Chem.* **2013**, *11*, 3375-3381.

(1441) Zhang, D.; Jiang, X.; Yang, H.; Su, Z.; Gao, E.; Martinez, A.; Gao, G. Novel Benzimidazolium-Urea-Based Macrocyclic Fluorescence Sensors: Synthesis, Ratiometric Sensing of H2PO4- and Improvement of the Anion Binding Performance via a Synergistic Binding Strategy. *Chem. Commun.* **2013**, *49*, 6149-6151.

(1442) Ghosh, K.; Saha, I. *Ortho*-Phenylenediamine-Based Open and Macrocyclic Receptors in Selective Sensing of H2PO4-, ATP and ADP Under Different Conditions. *Org. Biomol. Chem.* **2012**, *10*, 9383-9392.

(1443) Vonnegut, C. L.; Shonkwiler, A. M.; Zakharov, L. N.; Haley, M. M.; Johnson, D. W. Harnessing Solid-State Packing for Selective Detection of Chloride in a Macrocyclic Anionophore. *Chem. Commun.* **2016**, *52*, 9506-9509.

(1444) Zhou, H.; Zhao, Y.; Gao, G.; Li, S.; Lan, J.; You, J. Highly Selective Fluorescent Recognition of Sulfate in Water by Two Rigid Tetrakisimidazolium Macrocycles with Peripheral Chains. *J. Am. Chem. Soc.* **2013**, *135*, 14908-14911.

(1445) Do-Thanh, C.-L.; Khanal, N.; Lu, Z.; Cramer, S. A.; Jenkins, D. M.; Best, M. D. Chloride Binding by a Polyimidazolium Macrocycle Detected via Fluorescence, NMR, and X-ray Crystallography. *Tetrahedron* **2012**, *68*, 1669-1673.

(1446) Feng, H.-T.; Wang, J.-H.; Zheng, Y.-S. CH3-π Interaction of Explosives with Cavity of a TPE Macrocycle: The Key Cause for Highly Selective Detection of TNT. *ACS Appl. Mater. Interfaces* **2014**, *6*, 20067-20074.

(1447) Li, G.; Zhao, L.; Yang, P.; Yang, Z.; Tian, Z.; Chen, Y.; Shen, H.; Hu, C. Engineering 1,3-Alternate Calixcarbazole for Recognition and Sensing of Bisphenol F in Water. *Anal. Chem.* **2016**, *88*, 10751-10756.

(1448) Ryan, S. T. J.; Del Barrio, J.; Ghosh, I.; Biedermann, F.; Lazar, A. I.; Lan, Y.; Coulston, R. J.; Nau, W. M.; Scherman, O. A. Efficient Host-Guest Energy Transfer in Polycationic Cyclophane-Perylene Diimide Complexes in Water. *J. Am. Chem. Soc.* **2014**, *136*, 9053-9060.

(1449) Ema, T.; Okuda, K.; Watanabe, S.; Yamasaki, T.; Minami, T.; Esipenko, N. A.; Anzenbacher, P. Jr. Selective Anion Sensing by Chiral Macrocyclic Receptors with Multiple Hydrogen-Bonding Sites. *Org. Lett.* **2014**, *16*, 1302-1305.

(1450) Akdeniz, A.; Minami, T.; Watanabe, S.; Yokoyama, M.; Ema, T.; Anzenbacher, P. Jr. Determination of Enantiomeric Excess of Carboxylates by Fluorescent Macrocyclic Sensors. *Chem. Sci.* **2016**, *7*, 2016-2022.

(1451) Xu, X.; Jiao, S.; Yao, W.; Xie, E.; Tang, B.; Wang, C. Synthesis and Highly Enantioselective Fluorescent Recognition of α-Aminocarboxylic Acid Anions Using Chiral Oxacalix[2]arene[2]bisbinaphthes. *Chirality* **2012**, *24*, 646-651.

(1452) Burguete, M. I.; Galindo, F.; Luis, S. V.; Vigara, L. Ratiometric Fluorescence Sensing of Phenylalanine Derivatives by Synthetic Macrocyclic Receptors. *J. Photochem. Photobiol, A: Chem.* **2010**, *209*, 61-67.

(1453) Suzuki, A.; Kondo, K.; Sei, Y.; Akita, M.; Yoshizawa, M. A Fluorescent Molecular Capsule with a Flexible Polyaromatic Shell for Detection of Monoterpene Compounds in Water. *Chem. Commun.* **2016**, *52*, 3151-3154.

(1454) Liu, W.; Gómez-Durán, C. F. A.; Smith, B. D. Fluorescent Neuraminidase Assay Based on Supramolecular Dye Capture After Enzymatic Cleavage. *J. Am. Chem. Soc*. **2017**, *139*, 6390-6395.

(1455) Lewis, J. E. M.; Beer, P. D.; Loeb, S. J.; Goldup, S. M. Metal Ions in the Synthesis of Interlocked Molecules and Materials. *Chem. Soc. Rev.* **2017**, *46*, 2577-2591.

(1456) Evans, N. H.; Beer, P. D. Progress in the Synthesis and Exploitation of Catenanes Since the Millennium. *Chem. Soc. Rev.* **2014**, *43*, 4658-4683.

(1457) Gil-Ramírez, G.; Leigh, D. A.; Stephens, A. J. Catenanes: Fifty Years of Molecular Links. *Angew. Chem. Int. Ed.* **2015**, *54*, 6110-6150.

(1458) Wasserman, E. The Preparation of Interlocking Rings: A Catenane. *J. Am. Chem. Soc.* **1960**, *82*, 4433-4434.

(1459) Frisch, H. L.; Wasserman, E. Chemical Topology. *J. Am. Chem. Soc.* **1961**, *83*, 3789-3795.

(1460) Schill, G.; Lüttringhaus, A. Catenane Synthesis. *Angew. Chem.* **1964**, *76*, 567-568.

(1461) Dietrich-Buchecker, C. O.; Sauvage. J.-P.; Kern, J.-M. Templated Synthesis of Interlocked Macrocyclic Ligands: The Catenands. *J. Am. Chem. Soc.* **1984**, *106*, 3043-3045.

(1462) Philp, D.; Stoddart, J. F. Self-Assembly in Natural and Unnatural Systems. *Angew. Chem. Int. Ed.* **1996**, *35*, 1154-1196.

(1463) Hamilton, D. G.; Sanders, J. K. M.; Davies, J. E.; Clegg, W.; Teat, S. J. Neutral [2]Catenanes From Oxidative Coupling of π-Stacked Components. *Chem. Commun.* **1997**, 897-898.

(1464) Amabilino, D. B.; Stoddart, J. F. Interlocked and Intertwined Structures and Superstructures. *Chem. Rev.* **1995**, *95*, 2725-2828.

(1465) Jäger, R.; Vögtle, F. A New Synthetic Strategy Towards Molecules with Mechanical Bonds: Nonionic Template Synthesis of Amide-Linked Catenanes and Rotaxanes. *Angew. Chem. Int. Ed.* **1997**, *36*, 930-944.

(1466) Gaviña, P.; Tatay, S. Synthetic Strategies for the Construction of Threaded and Interlocked Molecules. *Curr. Org. Synth.* **2010**, *7*, 24-43.

(1467) Sauvage, J.-P. From Chemical Topology to Molecular Machines (Nobel Lecture) *Angew. Chem. Int. Ed.* **2017**, *56*, 11080-11093.

(1468) Durot, S.; Heitz, V.; Sour, A.; Sauvage, J.-P. Transition-Metal-Complexed Catenanes and Rotaxanes: From Dynamic Systems to Functional Molecular Machines. *Top. Curr. Chem.* **2014**, *354*, 35-70.

(1469) Wang, Y.; Frasconi, M.; Stoddart, J. F. Introducing Stable Radicals into Molecular Machines. *ACS Cent. Sci.* **2017**, *3*, 927-935.

(1470) Langton, M. J.; Beer, P. D. Rotaxane and Catenane Host Structures for Sensing Charged Guest Species. *Acc. Chem. Res.* **2014**, *47*, 1935-1949.

(1471) Hudson, B.; Vinograd, J. Catenated Circular DNA Molecules in HeLa Cell Mitochondria. *Nature* **1967**, *216*, 647-652.

(1472) Clayton, D. A.; Vinograd, J. Circular Dimer and Catenate Forms of Mitrochondrial DNA in Human Leukaemic Leucocytes. *Nature* **1967**, *216*, 652-657.

(1473) Caballero, A.; Zapata, F.; White, N. G.; Costa, P. J.; Félix, V.; Beer, P. D. A Halogen-Bonding Catenane for Anion Recognition and Sensing. *Angew. Chem. Int. Ed.* **2012**, *124*, 1 1912-1916.

(1474) Brown, A.; Langton, M. J.; Kilah, N. L.; Thompson, A. L.; Beer, P. D. Chloride-Anion-Templated Synthesis of a Strapped-Porphyrin-Containing Catenane Host System. *Chem. Eur. J.* **2015**, *21*, 17664-17675.

(1475) Mercurio, J. M.; Caballero, A.; Cookson, J.; Beer, P. D. A Halogen- and Hydrogen-Bonding [2]Catenane for Anion Recognition and Sensing. *RSC Adv.* **2015**, *5*, 9298-9306.

(1476) Barendt, T. A.; Ferreira, L.; Marques, I.; Félix, V.; Beer, P. D. Anion- and Solvent-Induced Rotary Dynamics and Sensing in a Perylene Diimide [3]Catenane. *J. Am. Chem. Soc.* **2017**, *139*, 9026-9037.

(1477) Harrison, I. T.; Harrison, S. The Synthesis of a Stable Complex of a Macrocycle and a Threaded Chain. *J. Am. Chem. Soc.* **1967**, *89*, 5723-5724.

(1478) Xue, M.; Yang, Y.; Chi, X.; Yan, X.; Huang, F. Development of Pseudorotaxanes and Rotaxanes: From Synthesis to Stimula-Responsive Motors to Applications. *Chem. Rev.* **2015**, *115*, 7398-7501.

(1479) Li, S.; Liu, M; Zheng, B.; Zhu, K.; Wang, F.; Li, N.; Zhao, X.-L.; Huang, F. Taco Complex Template Synthesis of a Cryptand/Paraquat [2]Rotaxane and a [2]Catenane by Olefin Metathesis. *Org. Lett.* **2009**, *11*, 3350-3353.

(1480) Johnston, A. G.; Leigh, D. A.; Murphy, A.; Smart, J. P.; Deegan, M. D. The Synthesis and Solubilization of Amide Macrocycles via Rotaxane Formation. *J. Am. Chem. Soc.* **1996,** *118*, 10662-10663.

(1481) Sambrook, M. R.; Beer, P. D.; Lankshear, M. D. Ludlow, R. F.; Wisner, J. A. Anion-Templated Assembly of [2]Rotaxanes. *Org. Biomol. Chem.* **2006**, *4*, 1529-1538.

(1482) Nepogodiev, S. A.; Stoddart, J. F. Cyclodextrin-Based Catenanes and Rotaxanes. *Chem. Rev.* **1998**, *98*, 1959-1976.

(1483) Chambron, J-C.; Heitz, V.; Sauvage, J.-P. Transition Metal Template Formation of [2]-and [3]-Rotaxanes with Porphyrins as Stoppers. *J. Am. Chem. Soc.* **1993**, *115*, 12378-12384.

(1484) Hänni, K. D.; Leigh, D. A. The Application of CuAAC 'Click' Chemistry to Catenane and Rotaxane Synthesis. *Chem. Soc. Rev.* **2010**, *39*, 1240-1251.

(1485) Zhao, Y.; Li, Y.; Lai, S.-W.; Yang, J.; Liu, C.; Liu, H.; Che, C.-M.; Li, Y. Construction of a Functional [2]Rotaxane with Multilevel Fluorescence Responses. *Org. Biomol. Chem.* **2011**, *9*, 7500-7503.

(1486) Jiang, Y.; Guo, J-B.; Chen, C.-F. A Bifunctionalized [3]Rotaxane and its Incorporation into a Mechanically Interlocked Polymer. *Chem. Commun.* **2010**. *46*, 5536-5538.

(1487) Langton, M. J.; Beer, P. D. Sulfate-Selective Binding and Sensing of a Fluorescent [3]Rotaxane Host System. *Chem. Eur. J.* **2012**, *18*, 14406-14412.

(1488) Fu, X.; Zhang, Q.; Rao, S.-J.; Qu, D.-H.; Tian, H. One-Pot Synthesis of a [c2]Daisy-Chain-Containing Hetero[4]rotaxane via a Self-Sorting Strategy. *Chem. Sci.* **2016**, *7*, 1696-1701.

(1489) Waelès, P.; Riss-Yaw, B.; Coutrot, F. Synthesis of a pH-Sensitive Hetero[4]rotaxane Molecular Machine that Combines [c2]Daisy and [2]Rotaxane Arrangements. *Chem. Eur. J.* **2016**, *22*, 6837-6845.

(1490) Iijima, K.; Aoki, D.; Otsuka, H.; Takata, T. Synthesis of Rotaxane Cross-Linked Polymers with Supramolecular Cross-Linkers Based on γ-CD and PTHF Macromonomers: The Effect of the Macromonomer Structure on the Polymer Properties. *Polymer* **2017**, *128*, 392-396.

(1491) Sun, N.; Xiao, X.; Li, W.; Jiang, J. Multistimuli Sensitive Behavior of Novel Bodipy-Involved Pillar[5]arene-Based Fluorescent [2]Rotaxane and its Supramolecular Gel. *Adv. Sci.* **2015**, *2*, 1500082.

(1492) Goujon, A.; Lang, T.; Mariani, G.; Moulin, E.; Fuks, G.; Raya, J.; Buhler, E.; Giuseppone, N. Bistable [c2] Daisy Chain as Reversible Muscle-Like Actuators in Mechanically Active Gels. *J. Am. Chem. Soc.* **2017**, *139*, 14825-14828.

(1493) Bruns, C. J.; Frasconi, M.; Iehl, J.; Hartlieb, K. J.; Schneebeli, S. T.; Cheng, C.; Stupp, S. I.; Stoddart, J. F. Redox Switchable Daisy Chain Rotaxanes Driven by Radical-Radical Interactions. *J. Am. Chem. Soc.* **2014**, *136*, 4714-4723.

(1494) Liu, J.; Du, X. pH- and Competitor-Driving Nanovalves of Cucurbit[7]uril Pseudorotaxanes Based on Mesoporous Silica Supports for Controlled Release. *J. Mater. Chem.* **2010**, *20*, 3642-3649.

(1495) Zhu, K.; Vukotic, V. N.; O'Keefe, C. A.; Schurko, R. W. Loeb, S. J. Metal-Organic Frameworks with Mechanically Interlocked Pillars: Controlling Ring Dynamics in the Solid-State via a Reversible Phase Change. *J. Am. Chem. Soc.* **2014**, *136*, 7403-7409.

(1496) Vukotic, V. N.; O'Keefe, C. A.; Zhu, K.; Harris, K. J.; To, C.; Schurko, R. W.; Loeb, S. J. Mechanically Interlocked Linkers Inside Metal-Organic Frameworks: Effects of Ring Size on Rotational Dynamics. *J. Am. Chem. Soc.* **2015**, *137*, 9643-9651.

(1497) Hu, C.; Lan, Y.; Tian, F.; West, K. R.; Scherman, O. A. Facile Method for Preparing Surface-Mounted Cucurbit[8]uril-Based Rotaxanes. *Langmuir* **2014**, *30*, 10926-10932.

(1498) Lehr, J.; Lang, T.; Blackburn, O. A.; Barendt, T. A.; Faulkner, S.; Davis, J. J.; Beer, P. D. Anion Sensing by Solution- and Surface-Assembled Osmium(II) Bipyridyl Rotaxanes. *Chem. Eur. J.* **2013**, *19*, 15898-15906.

(1499) Brown, A.; Lang, T.; Mullen, K. M.; Beer, P. D. Active Metal Template Synthesis of a Neutral Indolocarbazole-Containing [2]Rotaxane Host System for Selective Oxoanion Recognition. *Org. Biomol. Chem.* **2017**, *15*, 4587-4594.

(1500) Mullaney, B. R.; Thompson, A. L.; Beer, P. D. An All-Halogen Bonded Rotaxane for Selective Sensing of Halides in Aqueous Media. *Angew. Chem. Int. Ed.* **2014**, *53*, 11458-11462.

(1501) Langton, M. J.; Blackburn, O. A.; Lang, T.; Faulkner, S.; Beer, P. D. Nitrite-Templated Synthesis of Lanthanide-Containing [2]Rotaxanes for Anion Sensing. *Angew. Chem. Int. Ed.* **2014**, *53*, 11463-11466.

(1502) Langton, M. J.; Marques, I.; Robinson, S. W.; Félix, V.; Beer, P. D. Iodide Recognition and Sensing in Water by a Halogen-Bonding Ruthenium(II)-Based Rotaxane. *Chem. Eur. J.* **2016**, *22*, 185-192.

(1503) Gassensmith, J. J.; Matthys, S.; Lee, J.-J.; Wojcik, A.; Kamat, P. V.; Smith, B. D. Squaraine Rotaxane as a Reversible Optical Chloride Sensor. *Chem. Eur. J.* **2010**, *16*, 2916-2921.

(1504) Collins, C. G.; Peck, E. M.; Kramer, P. J.; Smith, B. D. Squaraine Rotaxane Shuttle as a Ratiometric Deep-Red Optical Chloride Sensor. *Chem. Sci.* **2013**, *4*, 2557-2563.

(1505) Raju, M. V. R.; Lin, H.-C. A Novel Diketopyrrolopyrrole (DPP)-Based [2]Rotaxane for Highly Selective Optical Sensing of Fluoride. *Org. Lett.* **2013**, *15*, 1274-1277.

(1506) Arumugaperumal, R.; Srinivasadesikan, V.; Raju, M. V. R.; Lin, M.-C.; Shukla, T.; Singh, R.; Lin, H.-C. Acid/Base and H2PO4- Controllable High-Contrast Optical Molecular Switches with a Novel BODIPY Functionalized [2]Rotaxane. *ACS. Appl. Mater. Interfaces* **2015**, *7*, 26491-26503.

(1507) Shi, J.; Cao, X.; Wang, X.; Nie, X.; Zhou, B.; Bao, X.; Zhu, J. A Novel Switchable [2]Rotaxane Driven by Light Energy with Rhodamine B Stopper. *Tetrahedron* **2015**, *71*, 4116-4123.

(1508) Wu, R.; Chen, R.; Qin, C.; Gao, Y.; Qiao, Z.; Zhang, G.; Xiao, L.; Jia, S. An Electric Field Induced Reversible Single-Molecule Fluorescence Switch. *Chem. Commun.* **2015**, *51*, 7368-7371.

(1509) Toal, S. J.; Trogler, W. C. Polymer Sensors for Nitroaromatic Explosives Detection. *J. Mater. Chem.* **2006**, *16*, 2871-2883.

(1510) Kim, H. N.; Ren, W. X.; Kim, J. S.; Yoon, J. Fluorescent and Colorimetric Sensors for Detection of Lead, Cadmium, and Mercury Ions. *Chem. Soc. Rev.* **2012**, *41*, 3210-3244.

(1511) Chen, D.; Zhan, J.; Zhang, M.; Zhang, J.; Tao, J.; Tang, D.; Shen, A.; Qiu, H.; Yin, S. A Fluorescent Supramolecular Polymer with Aggregation Induced Emission (AIE) Properties Formed by Crown Ether-Based Host-Guest Interactions. *Polym. Chem.* **2015**, *6*, 25-29.

(1512) Zhou, L.; Zhao, K.; Hu, Y.-J.; Feng, X.-C.; Shi, P.-D.; Zheng, H.-G. A Bifunctional Photoluminescent Metal-Organic Framework for Detection of Fe3+ Ion and Nitroaromatics. *Inorganic Chem. Commun.* **2018**, *89*, 68-72.

(1513) Nian, S.; Pu, L. Amphiphilic Polymer-Based Fluorescent Probe for Enantioselective Recognition of Amino Acids in Immiscible Water and Organic Phases. *Chem. Eur. J.* **2017**, *23*, 18066-18073.

(1514) Rochat, S.; Swager, T. M. Conjugated Amplifying Polymers for Optical Sensing Applications. *ACS Appl. Mater. Interfaces* **2013**, *5*, 4488-4502.

(1515) Swager, T. M. The Molecular Wire Approach to Sensory Signal Amplification. *Acc. Chem. Res.* **1998**, *31*, 201-207.

(1516) Andrew, T. L.; Swager, T. M. Structure-Property Relationships for Exciton Transfer in Conjugated Polymers. *J. Polym. Sci. B Polym. Phys.* **2011**, *49*, 476-498.

(1517) Saini, S.; Bagchi, B. Photophysics of Conjugated Polymers: Interplay Between Foerster Energy Migration and Defect Concentration in Shaping a Photochemical Funnel in PPV. *Phys. Chem. Chem. Phys.* **2010**, *12*, 7427-7433.

(1518) Correia, H. M. G.; Barbosa, H. M. C.; Marques, L.; Ramos, M. M. D. Unravelling the Effect of Strand Orientation on Exciton Migration in Conjugated Polymers. *Computational Mater. Sci.* **2013**, *75*, 18-23.

(1519) Fan, L.-J.; Jones, W. E., Jr. Studies of Photoinduced Electron Transfer and Energy Migration in a Conjugated Polymer System for Fluorescence "Turn-On" Chemosensor Applications. *J. Phys. Chem. B* **2006**, *110*, 7777-7782.

(1520) Emelianova, E. V.; van der Auweraer, M.; Bassler, H. Hopping Approach Towards Exciton Dissociation in Conjugated Polymers. *J. Chem. Phys.* **2008**, *128*, 24709/1-224709/8.

(1521) de Oliveira Neto, P. H.; da Silva Filho, D. A.; da Cunha, W. F.; Acioli, P. H.; e Silva, G. M. Limit of Exciton Diffusion in Highly Ordered π-Conjugated Systems. *J. Phys. Chem. C* **2015**, *119*, 19654-19659.

(1522) Fakis, M.; Polyzos, I.; Tsigaridas, G.; Giannetas, V.; Persephonis, P.; Spiliopoulos, I.; Mikroyannidis, J. Dual Amplified Spontaneous Emission and Laser Action from a Model Oligo(phenylene Vinylene): Comparison with the Corresponding Polymer. *Optical Mater.* **2004**, *27*, 503-507.

(1523) Mathy, A.; Ueberhofen, K.; Schenk, R.; Gregorius, H.; Garay, R.; Muellen, K.; Bubeck, C. Third-Harmonic-Generation Spectroscopy of Poly(p-phenylenevinylene): A Comparison with Oligomers and Scaling Laws for Conjugated Polymers. *Phys. Rev. B: Condensed Matt.* **1996**, *53*, 4367-4376.

(1524) Larsen, R. E. Simple Extrapolation Method To Predict the Electronic Structure of Conjugated Polymers from Calculations on Oligomers. *J. Phys. Chem. C* **2016**, *120*, 9650-9660.

(1525) Zhang, L.; Yu, M.; Zhao, H.; Wang, Y.; Gao, J. Theoretical Investigations on the Electronic and Optical Characteristics of Fused-Ring Homopolymers: Comparison of Oligomer Method and PBC-DFT Method. *Chem. Phys. Lett.* **2013**, *570*, 153-158.

(1526) Bunz, U. H. F.; Seehafer, K.; Geyer, F. L.; Bender, M.; Braun, I.; Smarsly, E.; Freudenberg, J. Porous Polymers Based on Aryleneethynylene Building Blocks. *Macromol. Rapid Commun.* **2014**, *35*, 1466-1496.

(1527) Soloducho, J.; Cabaj, J.; Idzik, K.; Nowakowska-Oleksy, A.; Swist, A.; Lapkowski, M. Synthesis, Structure and Properties of Crowded Symmetric Arylenes. *Curr. Org. Chem.* **2010**, *14*, 1234-1244.

(1528) Schiedel, M.-S.; Briehn, C. A.; Bauerle, P. C-C Cross-Coupling Reactions for the Combinatorial Synthesis of Novel Organic Materials. *J. Organometallic Chem.* **2002**, *653*, 200-208.

(1529) Geng, Y. H.; Huang, L.; Wu, S. P.; Wang, F. S. Kumada Chain-Growth Polycondensation as a

Universal Method for Synthesis of Well-Defined Conjugated Polymers. *Sci. China: Chem.* **2010**, *53*, 1620-1633.

(1530) Yokozawa, T.; Nanashima, Y.; Ohta, Y. Precision Synthesis of n-Type π-Conjugated Polymers in Catalyst-Transfer Condensation Polymerization. *ACS Macro Lett.* **2012**, *1*, 862-866.

(1531) Haque, T.; Nomura, K. Acyclic Diene Metathesis (ADMET) Polymerization for Precise Synthesis of Defect-Free Conjugated Polymers with Well-Defined Chain Ends. *Catalysts* **2015**, *5*, 500-517.

(1532) Suraru, S.-L.; Lee, J. A.; Luscombe, C. K. C-H Arylation in the Synthesis of π-Conjugated Polymers. *ACS Macro Lett.* **2016**, *5*, 724-729.

(1533 Pouliot, J.-R.; Grenier, F.; Blaskovits, J. T.; Beaupre, S.; Leclerc, M. Direct (Hetero)arylation Polym0erization: Simplicity for Conjugated Polymer Synthesis. *Chem. Rev.* **2016**, *116*, 14225-14274.

(1534) Bura, T.; Beaupre, S.; Legare, M.-A.; Quinn, J.; Rochette, E.; Blaskovits, J. T.; Fontaine, F.-G.; Pron, A.; Li, Y.; Leclerc, M. Direct Heteroarylation Polymerization: Guidelines for Defect-Free Conjugated Polymers. *Chem. Sci.* **2017**, *8*, 3913-3925.

(1535) Arroyave, F. A.; Reynolds, J. R. 3,4-Propylenedioxypyrrole-Based Conjugated Oligomers via Pd-Mediated Decarboxylative Cross Coupling. *Org. Lett.* **2010**, *12*, 1328-1331.

(1536) Manna, C. M.; Kaur, A.; Yablon, L. M.; Haeffner, F.; Li, B.; Byers, J. A. Stereoselective Catalysis Achieved through in Situ Desymmetrization of an Achiral Iron Catalyst Precursor. *J. Am. Chem. Soc.* **2015**, *137*, 14232-14235.

(1537) Yang, S.-C.; Graupner, W.; Guha, S.; Puschnig, P.; Martin, C.; Chandrasekhar, H. R.; Chandrasekhar, M.; Leising, G.; Ambrosch-Draxl, C. Influence of the Molecular Geometry on the Photoexcitations of Highly Emissive Organic Semiconductors. *Proc. SPIE* **1999**, *3797*, 26-37.

(1538) Wilhelm, P.; Vogelsang, J.; Poluektov, G.; Schoenfelder, N.; Keller, T. J.; Jester, S.-S.; Hoeger, S.; Lupton, J. M. Molecular Polygons Probe the Role of Intramolecular Strain in the Photophysics of π-Conjugated Chromophores. *Angew. Chem. Int. Ed.* **2017**, *129*, 1254-1258.

(1539) Tilley, A. J.; Danczak, S. M.; Browne, C.; Young, T.; Tan, T.; Ghiggino, K. P.; Smith, T. A.; White, J. Synthesis and Fluorescence Characterization of MEHPPV Oligomers. *J. Org. Chem.* **2011**, *76*, 3372-3380.

(1540) Wong, K. S.; Wang, H.; Lanzani, G. Ultrafast Excited-State Planarization of the Hexamethylsexithiophene Oligomer Studied by Femtosecond Time-Resolved Photoluminescence. *Chem. Phys. Lett.* **1998**, *288*, 59-64.

(1541) Ishow, E.; Bouffard, J.; Kim, Y.; Swager, T. M. Anthryl-Based Poly(phenylene Ethynylene)s: Tuning Optical Properties with Diels-Alder Reactions. *Macromolecules* **2006**, *39*, 7854-7858.

(1542) Swager, T. M.; Gil, C. J.; Wrighton, M. S. Fluorescence Studies of Poly(p-phenyleneethynylene)s: The Effect of Anthracene Substitution. *J. Phys. Chem.* **1995**, *99*, 4886-4893.

(1543) Amonoo, J. A.; Li, A.; Purdum, G. E.; Sykes, M. E.; Huang, B.; Palermo, E. F.; McNeil, A. J.; Shtein, M.; Loo, Y.-L.; Green, P. F. An All-Conjugated Gradient Copolymer Approach for Morphological Control of Polymer Solar Cells. *J. Mater. Chem. A* **2015**, *3*, 20174-20184.

(1544) Wang, J.-L.; Luo, J.; Liu, L.-H.; Zhou, Q.-F.; Ma, Y.; Pei, J. Nanosized Gradient π-Conjugated Thienylethynylene Dendrimers for Light Harvesting: Synthesis and Properties. *Org. Lett.* **2006**, *8*, 2281-2284.

(1545) Zhao, D.; Swager, T. M. Sensory Responses in Solution vs Solid State: A Fluorescence Quenching Study of Poly(iptycenebutadiynylene)s. *Macromolecules* **2005**, *38*, 9377-9384.

(1546) Kim, J.; McQuade, D. T.; Rose, A.; Zhu, Z.; Swager, T. M. Directing Energy Transfer within

Conjugated Polymer Thin Films. *J. Am. Chem. Soc.* **2001**, *123*, 11488-11489.

(1547) Jiang, Y.; McNeill, J. Light-Harvesting and Amplified Energy Transfer in Conjugated Polymer Nanoparticles. *Chem. Rev.* **2017**, *117*, 838-859.

(1548) McQuade, D. T.; Hegedus, A. H.; Swager, T. M. Signal Amplification of a "Turn-On" Sensor: Harvesting the Light Captured by a Conjugated Polymer. *J. Am. Chem. Soc.* **2000**, *122*, 12389-12390.

(1549) Liao, J. H.; Swager, T. M. Quantification of Amplified Quenching for Conjugated Polymer Microsphere Systems. *Langmuir* **2007**, *23*, 112-115.

(1550) Pangeni, D.; Nesterov, E. E. "Higher Energy Gap" Control in Fluorescent Conjugated Polymers: Turn-On Amplified Detection of Organophosphorous Agents. *Macromolecules* **2013**, *46*, 7266-7273.

(1551) Liu, X.; Ouyang, L.; Cai, X.; Huang, Y.; Feng, X.; Fan, Q.; Huang, W. An Ultrasensitive Label-Free Biosensor for Assaying of Sequence-Specific DNA-Binding Protein Based on Amplifying Fluorescent Conjugated Polymer. *Biosensors Bioelectronics* **2013**, *41*, 218-224.

(1552) Wang, M.; Guo, L.; Cao, D. Metal-Organic Framework as Luminescence Turn-On Sensor for Selective Detection of Metal Ions: Absorbance Caused Enhancement Mechanism. *Sensors Actuators B: Chem.* **2018**, *256*, 839-845.

(1553) Noguchi, T.; Roy, B.; Yoshihara, D.; Tsuchiya, Y.; Yamamoto, T.; Shinkai, S. Tailoring of the Desired Selectivity and the Turn-On Detection Range in a Self-Assembly-Based Fluorescence Sensory System. *Chem. Sci.* **2015**, *6*, 3863-3867.

(1554) Gaylord, B. S.; Wang, S.; Heeger, A. J.; Bazan, G. C. Water-Soluble Conjugated Oligomers: Effect of Chain Length and Aggregation on Photoluminescence-Quenching Efficiencies. *J. Am. Chem. Soc.* **2001**, *123*, 6417-6418.

(1555) Fan, C.; Wang, S.; Hong, J. W.; Bazan, G. C.; Plaxco, K. W.; Heeger, A. J. Beyond Superquenching: Hyper-Efficient Energy Transfer from Conjugated Polymers to Gold Nanoparticles. *Proc. Natl. Acad. Sci. U.S.A.* **2003**, *100*, 6297-6301.

(1556) Feng, F.; Yang, J.; Xie, D.; McCarley, T. D.; Schanze, K. S. Remarkable Photophysics and Amplified Quenching of Conjugated Polyelectrolyte Oligomers. *J. Phys. Chem. Lett.* **2013**, *4*, 1410-1414.

(1557) Swager, T. M. Iptycenes in the Design of High Performance Polymers. *Acc. Chem. Res.* **2008**, *41*, 1181-1189.

(1558) Miao, Y.-J.; Kim, J.; Swager, T. M. Design of Specific Fluorescence Sensory Polymers for the Detection of TNT. *Polym. Preprints* **1999**, *40*, 825-826.

(1559) Rose, A.; Lugmair, C. G.; Miao, Y.-J.; Kim, J.; Levitsky, I. A.; Williams, V. E.; Swager, T. M. Optimization of TNT Sensory Polymers. *Proceedings SPIE* **2000**, *4038*, 512-518.

(1560) Huang, W.; Smarsly, E.; Han, J.; Bender, M.; Seehafer, K.; Wacker, I.; Schroeder, R. R.; Bunz, U. H. F. Truxene-Based Hyperbranched Conjugated Polymers: Fluorescent Micelles Detect Explosives in Water. *ACS Appl. Mater. Interfaces* **2017**, *9*, 3068-3074.

(1561) Dong, W.; Fei, T.; Scherf, U. Conjugated Polymers Containing Tetraphenylethylene in the Backbones and Side-Chains for Highly Sensitive TNT Detection. *RSC Adv.* **2018**, *8*, 5760-5767.

(1562) Ma, X.; Tao, F.; Zhang, Y.; Li, T.; Raymo, F. M.; Cui, Y. Detection of Nitroaromatic Explosives by a 3D Hyperbranched σ-π Conjugated Polymer Based on a POSS Scaffold. *J. Mater. Chem. A* **2017**, *5*, 14343-14354.

(1563) Ma, X.-S.; Cui, Y.-Z.; Ding, Y.-Q.; Tao, F.-R.; Zheng, B.; Yu, R.-H.; Huang, W. 2D Hyperbranched Conjugated Polymer for Detecting TNT with Excellent Exciton Migration. *Sensors Actuators B: Chem.* **2017**, *238*, 48-57.

(1564) Wu, X.; Hang, H.; Li, H.; Chen, Y.; Tong, H.; Wang, L. Water-Dispersible Hyperbranched Conjugated Polymer Nanoparticles with Sulfonate Terminal Groups for Amplified Fluorescence Sensing of Trace TNT in Aqueous Solution. *Mater. Chem. Frontiers* **2017**, *1*, 1875-1880.

(1565) Malik, A. H.; Hussain, S.; Kalita, A.; Iyer, P. K. Conjugated Polymer Nanoparticles for the Amplified Detection of Nitro-Explosive Picric Acid on Multiple Platforms. *ACS Appl. Mater. Interfaces* **2015**, *7*, 26968-26976.

(1566) Levine, M.; Song, I.; Andrew, T. L.; Kooi, S. E.; Swager, T. M. Photoluminescent Energy Transfer from Poly(phenyleneethynylene)s to Near-Infrared Emitting Fluorophores. *J. Polym. Sci. A Polym. Chem.* **2010**, *48*, 3382-3391.

(1567) Tian, Z.; Yu, J.; Wu, C.; Szymanski, C.; McNeill, J. Amplified Energy Transfer in Conjugated Polymer Nanoparticle Tags and Sensors. *Nanoscale* **2010**, *2*, 1999-2011.

(1568) Wang, C.; Tang, Y.; Guo, Y. Adenosine Deaminase Biosensor Combining Cationic Conjugated Polymer-Based FRET with Deoxyguanosine-Based Photoinduced Electron Transfer. *ACS Appl. Mater. Interfaces* **2014**, *6*, 21686-21691.

(1569) Chiang, C.-H.; Pangeni, D.; Nesterov, E. E. Higher Energy Gap Control of Fluorescence in Conjugated Polymers: Turn-On Amplifying Chemosensor for Hydrogen Sulfide. *Macromolecules* **2017**, *50*, 6961-6966.

(1570) Wu, C.; Peng, H.; Jiang, Y.; McNeill, J. Energy Transfer Mediated Fluorescence from Blended Conjugated Polymer Nanoparticles. *J. Phys. Chem. B* **2006**, *110*, 14148-14154.

(1571) Murphy, C. B.; Zhang, Y.; Troxler, T.; Ferry, V.; Martin, J. J.; Jones, W. E., Jr. Probing Forster and Dexter Energy-Transfer Mechanisms in Fluorescent Conjugated Polymer Chemosensors. *J. Phys. Chem. B* **2004**, *108*, 1537-1543.

(1572) Sajid, H.; Mahmood, T.; Ayub, K. An Accurate Comparative Theoretical Study of the Interaction of Furan, Pyrrole, and Thiophene with Various Gaseous Analytes. *J. Molec. Modeling* **2017**, *23*, 295.

(1573) Wang, J.; Gu, J.; Leszczynski, J. Effect of Stacking Interactions on the Spectra of the Monomer of PFBT: A Theoretical Study. *J. Phys. Chem. A* **2009**, *113*, 10224-10230.

(1574) Dong, W.; Fei, T.; Palma-Cando, A.; Scherf, U. Aggregation Induced Emission and Amplified Explosive Detection of Tetraphenylethylene-Substituted Polycarbazoles. *Polym. Chem.* **2014**, *5*, 4048-4053.

(1575) Clavaguera, S.; Dautel, O. J.; Hairault, L.; Methivier, C.; Montmeat, P.; Pasquinet, E.; Pradier, C.-M.; Serein-Spirau, F.; Wakim, S.; Veignal, F.; Moreau, J. J. E.; Lere-Porte, J.-P. Alternated π-Conjugated Polymers Based on a 1,2-Diiminocyclohexane Chiral Unit for Nitroaromatics Sensing. *J. Polym. Sci. A Polym. Chem.* **2009**, *47*, 4141-4149.

(1576) Li, H.; Wang, L.; Zhai, J.; Zhang, Y.; Tian, J.; Sun, X. Coordination Polymer Nanobelts as an Effective Sensing Platform for Fluorescence-Enhanced Nucleic Acid Detection. *Macromol. Rapid Commun.* **2011**, *32*, 899-904.

(1577) Gopalakrishnan, D.; Dichtel, W. R. Real-Time, Ultrasensitive Detection of RDX Vapors Using Conjugated Network Polymer Thin Films. *Chem. Mater.* **2015**, *27*, 3813-3816.

(1578) Chen, L.; Wang, H.; Liu, J.; Xing, R.; Yu, X.; Han, Y. Tuning the π-π Stacking Distance and J-Aggregation of DPP-Based Conjugated Polymer via Introducing Insulating Polymer. *J. Polym. Sci. B: Polym. Phys.* **2016**, *54*, 838-847.

(1579) Letizia, J. A.; Salata, M. R.; Tribout, C. M.; Facchetti, A.; Ratner, M. A.; Marks, T. J. n-Channel Polymers by Design: Optimizing the Interplay of Solubilizing Substituents, Crystal Packing, and Field-Effect Transistor Characteristics in Polymeric Bithiophene-Imide Semiconductors. *J. Am. Chem. Soc.* **2008**,

130, 9679-9694.

(1580) Sun, X.; Zhang, Z.; Hou, R.; Huang, M.; Zhao, B.; Tan, S. The Effect of the Length of Alkyl Side-Chains on the Molecular Aggregation and Photovoltaic Performance of the Isoindigo-Based Polymers. *Dyes Pigments* **2017**, *139*, 403-411.

(1581) Lee, D.; Swager, T. M. Defining Space Around Conjugated Polymers: New Vistas in Self-Amplifying Sensory Materials. *Synlett* **2004**, 149-154.

(1582) Pinto, M. R.; Schanze, K. S. Conjugated Polyelectrolytes: Synthesis and Applications. *Synthesis* **2002**, 1293-1309.

(1583) Jiang, H.; Taranekar, P.; Reynolds, J. R.; Schanze, K. S. Conjugated Polyelectrolytes: Synthesis, Photophysics, and Applications. *Angew. Chem. Int. Ed.* **2009**, *48*, 4300-4316.

(1584) Das, S.; Routh, P.; Ghosh, R.; Chatterjee, D. P.; Nandi, A. K. Water-Soluble Ionic Polythiophenes for Biological and Analytical Applications. *Polym. Int.* **2017**, *66*, 623-639.

(1585) Yao, Z.; Bai, H.; Li, C.; Shi, G. Analyte-Induced Aggregation of Conjugated Polyelectrolytes: Role of the Charged Moieties and its Sensing Application. *Chem. Commun.* **2010**, *46*, 5094-5096.

(1586) Duan, X.; Liu, L.; Feng, F.; Wang, S. Cationic Conjugated Polymers for Optical Detection of DNA Methylation, Lesions, and Single Nucleotide Polymorphisms. *Acc. Chem. Res.* **2010**, *43*, 260-270.

(1587) Liu, B.; Bazan, G. C. Methods for Strand-Specific DNA Detection with Cationic Conjugated Polymers Suitable for Incorporation into DNA Chips and Microarrays. *Proc. Natl. Acad. Sci. U.S.A.* **2005**, *102*, 589-593.

(1588) Watanabe, K.; Sun, Z.; Akagi, K. Interchain Helically π-Stacked Assembly of Cationic Chiral Poly(para-phenylene) Derivatives Enforced by Anionic π-Conjugated Molecules through Both Electrostatic and π-π Interactions. *Chem. Mater.* **2015**, *27*, 2895-2902.

(1589) Zhan, R.; Liu, B. Functionalized Conjugated Polyelectrolytes for Biological Sensing and Imaging. *Chem. Rec.* **2016**, *16*, 1715-1740.

(1590) Cui, Q.; Bazan, G. C. Narrow Band Gap Conjugated Polyelectrolytes. *Acc. Chem. Res.* **2018**, *51*, 202-211.

(1591) Chanphai, P.; Agudelo, D.; Tajmir-Riahi, H. A. PEG and mPEG-Anthracene Conjugate with Trypsin and Trypsin Inhibitor: Hydrophobic and Hydrophilic Contacts. *J. Biomol. Structure Dynamics* **2017**, *35*, 2257-2268.

(1592) Pu, K.-Y.; Liu, B. Fluorescence Turn-on Responses of Anionic and Cationic Conjugated Polymers toward Proteins: Effect of Electrostatic and Hydrophobic Interactions. *J. Phys. Chem. B* **2010**, *114*, 3077-3084.

(1593) Ruelle, P.; Kesselring, U. W. The Hydrophobic Effect. 2. Relative Importance of the Hydrophobic Effect on the Solubility of Hydrophobes and Pharmaceuticals in H-Bonded Solvents. *J. Pharmaceutical Sci.* **1998**, *87*, 998-1014.

(1594) Yu, M.; He, F.; Tang, Y.; Wang, S.; Li, Y.; Zhu, D. Non-Ionic Water-Soluble Crown-Ether-Substituted Polyfluorene as Fluorescent Probe for Lead Ion Assays. *Macromol. Rapid Commun.* **2007**, *28*, 1333-1338.

(1595) Khan, A.; Mueller, S.; Hecht, S. Practical Synthesis of an Amphiphilic, Non-Ionic Poly(para-phenyleneethynylene) Derivative with a Remarkable Quantum Yield in Water. *Chem. Commun.* **2005**, 584-586.

(1596) Huang, Y.-Q.; Fan, Q.-L.; Zhang, G.-W.; Chen, Y.; Lu, X.-M.; Huang, W. A Fluorene-Containing Water-Soluble Poly(p-phenyleneethynylene) Derivative: Highly Fluorescent and Sensitive Conjugated

Polymer with Minor Aggregation in Aqueous Solution. *Polym.* **2006**, *47*, 5233-5238.

(1597) Kuroda, K.; Swager, T. M. Synthesis of a Nonionic Water Soluble Semiconductive Polymer. *Chem. Commun.* **2003**, 26-27.

(1598) Higgins, S. J. Conjugated Polymers Incorporating Pendant Functional Groups - Synthesis and Characterization. *Chem. Soc. Rev.* **1997**, *26*, 247-258.

(1599) Esser, B.; Swager, T. M. Detection of Ethylene Gas by Fluorescence Turn-On of a Conjugated Polymer. *Angew. Chem. Int. Ed.* **2010**, *49*, 8872-8875.

(1600) Esser, B.; Schnorr, J. M.; Swager, T. M. Selective Detection of Ethylene Gas Using Carbon Nanotube-Based Devices: Utility in Determination of Fruit Ripeness. *Angew. Chem. Int. Ed.* **2012**, *51*, 5752-5756.

(1601) Giovannitti, A.; Nielsen, C. B.; Rivnay, J.; Kirkus, M.; Harkin, D. J.; White, A. J. P.; Sirringhaus, H.; Malliaras, G. G.; McCulloch, I. Sodium and Potassium Ion Selective Conjugated Polymers for Optical Ion Detection in Solution and Solid State. *Adv. Functional Mater.* **2016**, *26*, 514-523.

(1602) Casanovas, J.; Rodriguez-Ropero, F.; Zanuy, D.; Aleman, C. Microscopic Details of the Sensing Ability of 15-Crown-5-Ether Functionalized Poly(bithiophene). *Polym.* **2010**, *51*, 4267-4272.

(1603) Yamaguchi, I.; Mitsuno, H. Synthesis of n-Type π-Conjugated Polymers with Pendant Crown Ether and Their Stability of n-Doping State against Air. *Macromolecules* **2010**, *43*, 9348-9354.

(1604) Wosnick, J. H.; Mello, C. M.; Swager, T. M. Synthesis and Application of Poly(phenylene Ethynylene)s for Bioconjugation: A Conjugated Polymer-Based Fluorogenic Probe for Proteases. *J. Am. Chem. Soc.* **2005**, *127*, 3400-3405.

(1605) Hu, Z.; Willard, A. P.; Ono, R. J.; Bielawski, C. W.; Rossky, P. J.; Vanden Bout, D. A. An Insight into Non-Emissive Excited States in Conjugated Polymers. *Nature Commun.* **2015**, *6*, 8246.

(1606) Takagi, K.; Momiyama, M.; Ohta, J.; Yuki, Y.; Matsuoka, S.-i.; Suzuki, M. Polymeric Oligothiophene Fluorophores Spatially Isolated by Spirobifluorene and Their Emission Properties. *Macromolecules* **2007**, *40*, 8807-8811.

(1607) Zeng, G.; Li, J.; Liang, H.; Yuan, Y.; Li, X.; Yin, C.; Yang, Z.; Fan, Q.; Lu, X.; Huang, W. A Water-soluble Conjugated Polymer for Thiol Detection Based on "Turn-off" Effect. *Chinese J. Chem.* **2015**, *33*, 881-887.

(1608) Liu, J.; Zhong, Y.; Lam, J. W. Y.; Lu, P.; Hong, Y.; Yu, Y.; Yue, Y.; Faisal, M.; Sung, H. H. Y.; Williams, I. D.; Wong, K. S.; Tang, B. Z. Hyperbranched Conjugated Polysiloles: Synthesis, Structure, Aggregation-Enhanced Emission, Multicolor Fluorescent Photopatterning, and Superamplified Detection of Explosives. *Macromolecules* **2010**, *43*, 4921-4936.

(1609) Shi, W.; Sun, X.; Chen, X.; Zhao, S.; Xie, Z. Diphenylphosphoryl-Triazole-Tethered, AIEE-Type Conjugated Polymer as Optical Probe for Silver Ion in Relatively High-Water-Fraction Medium. *Macromol. Chem. Phys.* **2015**, *216*, 2263-2269.

(1610) Wei, G.; Jiang, Y.; Wang, F. A Novel AIEE Polymer Sensor for Detection of Hg2+ and Ag+ in Aqueous Solution. *J. Photochem. Photobiol. A: Chem.* **2018**, *358*, 38-43.

(1611) Saha, S. K.; Ghosh, K. R.; Gao, J. P.; Wang, Z. Y. Highly Sensitive Dual-Mode Fluorescence Detection of Lead Ion in Water Using Aggregation-Induced Emissive Polymers. *Macromol. Rapid Commun.* **2014**, *35*, 1592-1597.

(1612) Ghosh, K. R.; Saha, S. K.; Wang, Z. Y. Ultra-Sensitive Detection of Explosives in Solution and Film as Well as the Development of Thicker Film Effectiveness by Tetraphenylethene Moiety in AIE Active Fluorescent Conjugated Polymer. *Polym. Chem.* **2014**, *5*, 5638-5643.

(1613) Yamaguchi, I.; Miyawaki, K. Synthesis of Polyfluorene and Oligofluorene with N1-Hexylcytosine Side Chains and their Sensing Ability for Nucleosides. *Reactive Functional Polym.* **2017**, *120*, 14-19.

(1614) Ma, X.-S.; Wang, D.-H.; Cui, Y.-Z.; Tao, F.-R.; Wang, Y.-T.; Li, T.-D. A Novel Hydrophilic Conjugated Polymer Containing Hydroxyl Groups: Syntheses and Sensing Performance for NACs in Aqueous Solution. *Sensors Actuators B: Chem.* **2017**, *251*, 851-857.

(1615) Nketia-Yawson, B.; Jung, A.-R.; Noh, Y.; Ryu, G.-S.; Tabi, G. D.; Lee, K.-K.; Kim, B.; Noh, Y.-Y. Highly Sensitive Flexible NH3 Sensors Based on Printed Organic Transistors with Fluorinated Conjugated Polymers. *ACS Appl. Mater. Interfaces* **2017**, *9*, 7322-7330.

(1616) Sanyakamdhorn, S.; Agudelo, D.; Bekale, L.; Tajmir-Riahi, H. A. Targeted Conjugation of Breast Anticancer Drug Tamoxifen and its Metabolites with Synthetic Polymers. *Colloids Surfaces B: Biointerfaces* **2016**, *145*, 55-63.

(1617) Kranz, W. D.; Strange, N. A.; Goodpaster, J. V. "Fooling Fido"-Chemical and Behavioral Studies of Pseudo-Explosive Canine Training Aids. *Anal. Bioanal. Chem.* **2014**, *406*, 7817-7825.

(1618) Aleman, J.; Parra, A.; Jiang, H.; Jorgensen, K. A. Squaramides: Bridging from Molecular Recognition to Bifunctional Organocatalysis. *Chem. Eur. J.* **2011**, *17*, 6890-6899.

(1619) Hu, R.; Kang, Y.; Tang, B. Z. Recent Advances in AIE Polymers. *Polym. J.* **2016**, *48*, 359-370.

(1620) Lv, F.; Qiu, T.; Liu, L.; Ying, J.; Wang, S. Recent Advances in Conjugated Polymer Materials for Disease Diagnosis. *Small* **2016**, *12*, 696-705.

(1621) Sakai, R. Conjugated Polymers Applicable to Colorimetric and Fluorescent Anion Detection. *Polym. J.* **2016**, *48*, 59-65.

(1622) BBC News. Underwear Bomber Abdulmutallab Sentenced to Life. http://www.bbc.com/news/world-us-canada-17065130 (accessed April 21, 2018).

(1623) Elliot, M. The Shoe Bomber's World. *Time* [Online] Feb 16, 2002. http://content.time.com/time/world/article/0,8599,203478,00.html (accessed April 21, 2018)

(1624) Peng, L.; Hua, L.; Wang, W.; Zhou, Q.; Li, H. On-Site Rapid Detection of Trace Non-Volatile Inorganic Explosives by Stand-Alone Ion Mobility Spectrometry via Acid-Enhanced Evaporization. *Sci. Reports* **2014**, *4*, 6631.

(1625) Akmalov, A. E.; Chistyakov, A. A.; Kotkovskii, G. E. Laser Desorption of Explosives Traces with Low Vapors Pressure. *Phys. Procedia* **2015**, *71*, 207-211.

(1626) Wang, J.; Muto, M.; Yatabe, R.; Onodera, T.; Tanaka, M.; Okochi, M.; Toko, K. Rational Design of Peptide-Functionalized Surface Plasmon Resonance Sensor for Specific Detection of TNT Explosive. *Sensors* **2017**, *17*, 2249/1-2249/8.

(1627) Pettersson, A.; Wallin, S.; Oestmark, H.; Ehlerding, A.; Johansson, I.; Nordberg, M.; Ellis, H.; Al-Khalili, A.; Harmon, R. S.; Holloway, J. H., Jr.; Broach, J. T. Explosives Standoff Detection Using Raman Spectroscopy: From Bulk Towards Trace Detection. *Proc. SPIE* **2010**, *7664*, 76641K/1-76641K/12.

(1628) Hakonen, A.; Andersson, P. O.; Stenbaek Schmidt, M.; Rindzevicius, T.; Kall, M. Explosive and Chemical Threat Detection by Surface-Enhanced Raman Scattering: A Review. *Anal. Chim. Acta* **2015**, *893*, 1-13.

(1629) Novotney, J. L.; Dichtel, W. R. Conjugated Porous Polymers for TNT Vapor Detection. *ACS Macro Lett.* **2013**, *2*, 423-426.

(1630) Chen, J.; Cao, Y. Silole-Containing Polymers: Chemistry and Optoelectronic Properties. *Macromol. Rapid Commun.* **2007**, *28*, 1714-1742.

(1631) Tennyson, A. G.; Do, L.; Smith, R. C.; Lippard, S. J. Selective Fluorescence Detection of Nitroxyl over Nitric Oxide in Buffered Aqueous Solution Using a Conjugated Metallopolymer. *Polyhedron* **2007**, *26*, 4625-4630.

(1632) Li, X.; Wang, M.; Tan, H.; Yang, Q.; Wang, A.; Bai, L.; Zhao, H.; Wu, Y. Preparation of the Water-Soluble Pyrene-Containing Fluorescent Polymer by One-Pot Method. *Polym.* **2015**, *7*, 2625-2637.

(1633) Schmatz, B.; Yuan, Z.; Lang, A. W.; Hernandez, J. L.; Reichmanis, E.; Reynolds, J. R. Aqueous Processing for Printed Organic Electronics: Conjugated Polymers with Multistage Cleavable Side Chains. *ACS Central Sci.* **2017**, *3*, 961-967.

(1634) Joly, G. D.; Geiger, L.; Kooi, S. E.; Swager, T. M. Highly Effective Water-Soluble Fluorescence Quenchers of Conjugated Polymer Thin Films in Aqueous Environments. *Macromolecules* **2006**, *39*, 7175-7177.

(1635) De-La-Cuesta, J.; Gonzalez, E.; Pomposo, J. A. Advances in Fluorescent Single-Chain Nanoparticles. *Molecules* **2017**, *22*, 1819/1-1819/14.

(1636) Szymanski, C.; Wu, C.; Hooper, J.; Salazar, M. A.; Perdomo, A.; Dukes, A.; McNeill, J. Single Molecule Nanoparticles of the Conjugated Polymer MEH-PPV, Preparation and Characterization by Near-Field Scanning Optical Microscopy. *J. Phys. Chem. B* **2005**, *109*, 8543-8546.

(1637) Wu, C.; Szymanski, C.; McNeill, J. Preparation and Encapsulation of Highly Fluorescent Conjugated Polymer Nanoparticles. *Langmuir* **2006**, *22*, 2956-2960.

(1638) MacNeill, C. M.; Graham, E. G.; Levi-Polyachenko, N. H. Soft Template Synthesis of Donor-Acceptor Conjugated Polymer Nanoparticles: Structural Effects, Stability, and Photothermal Studies. *J. Polym. Sci. A: Polym. Chem.* **2014**, *52*, 1622-1632.

(1639) Childress, E. S.; Roberts, C. A.; Sherwood, D. Y.; LeGuyader, C. L. M.; Harbron, E. J. Ratiometric Fluorescence Detection of Mercury Ions in Water by Conjugated Polymer Nanoparticles. *Anal. Chem.* **2012**, *84*, 1235-1239.

(1640) Wang, J.; Lv, F.; Liu, L.; Ma, Y.; Wang, S. Strategies to Design Conjugated Polymer Based Materials for Biological Sensing and Imaging. *Coordination Chem. Rev.* **2018**, *354*, 135-154.

(1641) Izquierdo, M. A.; Wadhavane, P. D.; Vigara, L.; Burguete, M. I.; Galindo, F.; Luis, S. V. The Interaction of Amino Acids with Macrocyclic pH Probes of Pseudopeptidic Nature. *Photochem. Photobiol. Sci.* **2017**, *16*, 1320-1326.

(1642) Del Bonis-O'Donnell, J. T.; Thakrar, A.; Hirschberg, J. W.; Vong, D.; Queenan, B. N.; Fygenson, D. K.; Pennathur, S. DNA-Stabilized Silver Nanoclusters as Specific, Ratiometric Fluorescent Dopamine Sensors. *ACS Chem. Neurosci.* **2018**, *9*, 849-857.

(1643) Gavvala, K.; Sengupta, A.; Hazra, P. Modulation of Photophysics and pKa Shift of the Anti-Cancer Drug Camptothecin in the Nanocavities of Supramolecular Hosts. *ChemPhysChem* **2013**, *14*, 532-542.

(1644) Kim, Y.; Whitten, J. E.; Swager, T. M. High Ionization Potential Conjugated Polymers. *J. Am. Chem. Soc.* **2005**, *127*, 12122-12130.

(1645) Lim, J.; Swager, T. M. Fluorous Biphase Synthesis of a Poly(p-phenyleneethynylene) and its Fluorescent Aqueous Fluorous-Phase Emulsion. *Angew. Chem. Int. Ed.* **2010**, *49*, 7486-7488.

(1646) Izuhara, D.; Swager, T. M. Poly(Pyridinium Phenylene)s: Water-Soluble N-Type Polymers. *J. Am. Chem. Soc.* **2009**, *131*, 17724-17725.

(1647) Kim, Y.; Swager, T. M. Sensory Polymers for Electron-Rich Analytes of Biological Interest. *Macromolecules* **2006**, *39*, 5177-5179.

(1648) Satrijo, A.; Swager, T. M. Anthryl-Doped Conjugated Polyelectrolytes as Aggregation-Based

Sensors for Nonquenching Multicationic Analytes. *J. Am. Chem. Soc.* **2007**, *129*, 16020-16028.

(1649) Santos, C. I. M.; Oliveira, E.; Menezes, J. C. J. M. D. S.; Barata, J. F. B.; Faustino, M. A. F.; Ferreira, V. F.; Cavaleiro, J. A. S.; Neves, M. G. P. M. S.; Lodeiro, C. New Coumarin-Corrole and -Porphyrin Conjugate Multifunctional Probes for Anionic or Cationic Interactions: Synthesis, Spectroscopy, and Solid Supported Studies. *Tetrahedron* **2014**, *70*, 3361-3370.

(1650) Jin, Y.; Yang, R.; Suh, H.; Woo, H. Y. Cationic and Anionic Conjugated Polyelectrolytes: Aggregation-Mediated Fluorescence Energy Transfer to Dye-Labeled DNA. *Macromol. Rapid Commun.* **2008**, *29*, 1398-1402.

(1651) Wang, S.; Zeman, C. J.; Jiang, J.; Pan, Z.; Schanze, K. S. Intercalation of Alkynylplatinum(II) Terpyridine Complexes into a Helical Poly(phenylene ethynylene) Sulfonate: Application to Protein Sensing. *ACS Appl. Mater. Interfaces* **2017**, *9*, 33461-33469.

(1652) Fu, N.; Wang, Y.; Liu, D.; Zhang, C.; Su, S.; Bao, B.; Zhao, B.; Wang, L. A Conjugated Polyelectrolyte with Pendant High Dense Short-Alkyl-Chain-Bridged Cationic Ions: Analyte-Induced Light-Up and Label-Free Fluorescent Sensing of Tumor Markers. *Polym.* **2017**, *9*, 227/1-227/14.

(1653) Zhang, Z.; Lu, X.; Fan, Q.; Hu, W. Conjugated Polyelectrolyte Brushes with Extremely High Charge Density for Improved Energy Transfer and Fluorescence Quenching Applications. *Polym. Chem.* **2011**, *2*, 2369-2377.

(1654) Lu, X.; Jiang, R.; Yang, M.; Fan, Q.; Hu, W.; Zhang, L.; Yang, Z.; Deng, W.; Shen, Q.; Huang, Y.; Liu, X.; Huang, W. Monodispersed Grafted Conjugated Polyelectrolyte-Stabilized Magnetic Nanoparticles as Multifunctional Platform for Cellular Imaging and Drug Delivery. *J. Mater. Chem. B* **2014**, *2*, 376-386.

(1655) Nilsson, K. P. R.; Inganaes, O. Optical Emission of a Conjugated Polyelectrolyte: Calcium-Induced Conformational Changes in Calmodulin and Calmodulin-Calcineurin Interactions. *Macromolecules* **2004**, *37*, 9109-9113.

(1656) Hu, W.; Lu, X.; Jiang, R.; Fan, Q.; Zhao, H.; Deng, W.; Zhang, L.; Huang, L.; Huang, W. Water-Soluble Conjugated Polyelectrolyte Brush Encapsulated Rare-Earth Ion Doped Nanoparticles with Dual-Upconversion Properties for Multicolor Cell Imaging. *Chem. Commun.* **2013**, *49*, 9012-9014.

(1657) Alvaro, M.; Corma, A.; Ferrer, B.; Galletero, M. S.; Garcia, H.; Peris, E. Increasing the Stability of Electroluminescent Phenylenevinylene Polymers by Encapsulation in Nanoporous Inorganic Materials. *Chem. Mater.* **2004**, *16*, 2142-2147.

(1658) Hussain, S.; Malik, A. H.; Iyer, P. K. Highly Precise Detection, Discrimination, and Removal of Anionic Surfactants Over the Full pH Range via Cationic Conjugated Polymer: An Efficient Strategy to Facilitate Illicit-Drug Analysis. *ACS Appl. Mater. Interfaces* **2015**, *7*, 3189-3198.

(1659) Giri, D.; Patra, S. K. Benzodithieno-Imidazole Based π-Conjugated Fluorescent Polymer Probe for Selective Sensing of Cu2+. *RSC Adv.* **2015**, *5*, 79011-79021.

(1660) Tanwar, A. S.; Iyer, P. K. Fluorescence "Turn-On" Indicator Displacement Assay-Based Sensing of Nitroexplosive 2,4,6-Trinitrophenol in Aqueous Media via a Polyelectrolyte and Dye Complex. *ACS Omega* **2017**, *2*, 4424-4430.

(1661) Bunz, U. H. F.; Rotello, V. M. Gold Nanoparticle-Fluorophore Complexes: Sensitive and Discerning "Noses" for Biosystems Sensing. *Angew. Chem. Int. Ed.* **2010**, *49*, 3268-3279.

(1662) Bajaj, A.; Miranda, O. R.; Phillips, R.; Kim, I.-B.; Jerry, D. J.; Bunz, U. H. F.; Rotello, V. M. Array-Based Sensing of Normal, Cancerous, and Metastatic Cells Using Conjugated Fluorescent Polymers. *J. Am. Chem. Soc.* **2010**, *132*, 1018-1022.

(1663) Bajaj, A.; Miranda, O. R.; Kim, I.-B.; Phillips, R. L.; Jerry, D. J.; Bunz, U. H. F.; Rotello, V. M. Detection and Differentiation of Normal, Cancerous, and Metastatic Cells Using Nanoparticle-Polymer

Sensor Arrays. *Proc. Natl. Acad. Sci. U.S.A.* **2009**, *106*, 10912-10916.

(1664) Rana, S.; Elci, S. G.; Mout, R.; Singla, A. K.; Yazdani, M.; Bender, M.; Bajaj, A.; Saha, K.; Bunz, U. H. F.; Jirik, F. R.; Rotello, V. M. Ratiometric Array of Conjugated Polymers-Fluorescent Protein Provides a Robust Mammalian Cell Sensor. *J. Am. Chem. Soc.* **2016**, *138*, 4522-4529.

(1665) Grandclement, C.; Tannieres, M.; Morera, S.; Dessaux, Y.; Faure, D. Quorum Quenching: Role in Nature and Applied Developments. *FEMS Microbiol. Rev.* **2016**, *40*, 86-116.

(1666) Reis e Sousa, C. Sensing Infection and Tissue Damage. *EMBO Molecular Medicine* **2017**, *9*, 285-288.

(1667) Xue, C.; Velayudham, S.; Johnson, S.; Saha, R.; Smith, A.; Brewer, W.; Murthy, P.; Bagley, S. T.; Liu, H. Highly Water-Soluble, Fluorescent, Conjugated Fluorene-Based Glycopolymers with Poly(ethylene glycol)-Tethered Spacers for Sensitive Detection of Escherichia coli. *Chem. Eur. J.* **2009**, *15*, 2289-2295.

(1668) Sankarankutty, K. M. Biosensors and their Applications for Ensuring Food Safety. *Global J. Pathol. Microbiol.* **2014**, *2*, 15-21.

(1669) Ceto, X.; Voelcker, N. H.; Prieto-Simon, B. Bioelectronic Tongues: New Trends and Applications in Water and Food Analysis. *Biosensors Bioelectronics* **2016**, *79*, 608-626.

(1670) Luthria, D. L. Significance of Sample Preparation in Developing Analytical Methodologies for Accurate Estimation of Bioactive Compounds in Functional Foods. *J. Sci. Food Agriculture* **2006**, *86*, 2266-2272.

(1671) Stewart, D.; Shepherd, L. V. T.; Hall, R. D.; Fraser, P. D. Crops and Tasty, Nutritious Food - How Can Metabolomics Help? *Annual Plant Rev.* **2011**, *43*, 181-217.

(1672) Blanke, M. M. Reducing Ethylene Levels Along the Food Supply Chain: A Key to Reducing Food Waste? *J. Sci. Food Agriculture* **2014**, *94*, 2357-2361.

(1673) Chowdhury, R. B.; Moore, G. A.; Weatherley, A. J.; Arora, M. Key Sustainability Challenges for the Global Phosphorus Resource, their Implications for Global Food Security, and Options for Mitigation. *J. Cleaner Production* **2017**, *140*, 945-963.

(1674) Silva, N. F. D.; Magalhaes, J. M. C. S.; Freire, C.; Delerue-Matos, C. Electrochemical Biosensors for Salmonella: State of the Art and Challenges in Food Safety Assessment. *Biosensors Bioelectronics* **2018**, *99*, 667-682.

(1675) van Asselt, E. D.; van der Fels-Klerx, H. J.; Marvin, H. J. P.; van Bokhorst-van de Veen, H.; Groot, M. N. Overview of Food Safety Hazards in the European Dairy Supply Chain. *Comprehensive Rev. Food Sci. Food Safety* **2017**, *16*, 59-75.

(1676) Calas-Blanchard, C.; Catanante, G.; Noguer, T. Electrochemical Sensor and Biosensor Strategies for ROS/RNS Detection in Biological Systems. *Electroanal*. **2014**, *26*, 1277-1286.

(1677) Wu, C.; Bull, B.; Christensen, K.; McNeill, J. Ratiometric Single-Nanoparticle Oxygen Sensors for Biological Imaging. *Angew. Chem. Int. Ed.* **2009**, *48*, 2741-2745.

(1678) Qin, A.; Lam, J. W. Y.; Tang, B. Z. Luminogenic Polymers with Aggregation-Induced Emission Characteristics. *Progress Polym. Sci.* **2012**, *37*, 182-209.

(1679) Padmanaban, G.; Ramakrishnan, S. Segmented Conjugated Polymers. *Pramana* **2003**, *61*, 425-434.

(1680) Schmidt, B. V. K. J.; Barner-Kowollik, C. Living Radical Polymerization of Ethylene: A Challenge Overcome? *ChemCatChem* **2014**, *6*, 3060-3062.

(1681) Noble, B. B.; Coote, M. L. First Principles Modelling of Free-Radical Polymerisation Kinetics. *Int. Rev. Phys. Chem.* **2013**, *32*, 467-513.

(1682) Ibrahim, A.; Stefano, L. D.; Tarzi, O.; Tar, H.; Ley, C.; Allonas, X. High-Performance Photoinitiating Systems for Free Radical Photopolymerization. Application to Holographic Recording. *Photochem. Photobiol.* **2013**, *89*, 1283-1290.

(1683) Yokozawa, T.; Ohta, Y. Transformation of Step-Growth Polymerization into Living Chain-Growth Polymerization. *Chem. Rev.* **2016**, *116*, 1950-1968.

(1684) Chen, Y.; Abdellatif, M. M.; Nomura, K. Olefin Metathesis Polymerization: Some Recent Developments in the Precise Polymerizations for Synthesis of Advanced Materials (by ROMP, ADMET). *Tetrahedron* **2018**, *74*, 619-643.

(1685) Bazban-Shotorbani, S.; Hasani-Sadrabadi, M. M.; Karkhaneh, A.; Serpooshan, V.; Jacob, K. I.; Moshaverinia, A.; Mahmoudi, M. Revisiting Structure-Property Relationship of pH-Responsive Polymers for Drug Delivery Applications. *J. Controlled Release* **2017**, *253*, 46-63.

(1686) Kim, Y.-J.; Matsunaga, Y. T. Thermo-Responsive Polymers and Their Application as Smart Biomaterials. *J. Mater. Chem. B* **2017**, *5*, 4307-4321.

(1687) Zhang, Q. M.; Serpe, M. J. Responsive Polymers as Sensors, Muscles, and Self-Healing Materials. *Topics Curr. Chem.* **2015**, *369*, 377-424.

(1688) Alvarez, A.; Costa-Fernandez, J. M.; Pereiro, R.; Sanz-Medel, A.; Salinas-Castillo, A. Fluorescent Conjugated Polymers for Chemical and Biochemical Sensing. *TrAC, Trends Anal. Chem.* **2011**, *30*, 1513-1525.

(1689) Gonzalez-Juarez, E.; Guizado-Rodriguez, M.; Barba, V.; Melgoza-Ramirez, M.; Rodriguez, M.; Ramos-Ortiz, G.; Maldonado, J. L. Polythiophenes Based on Pyrene as Pendant Group: Synthesis, Structural Characterization and Luminescent Properties. *J. Molec. Structure* **2016**, *1103*, 25-34.

(1690) Maiti, B.; Haldar, U.; Rajasekhar, T.; De, P. Functional-Polymer Library through Post-Polymerization Modification of Copolymers Having Oleate and Pentafluorophenyl Pendants. *Chem. Eur. J.* **2017**, *23*, 15156-15165.

(1691) Lutz, P. J. Control of Macromolecular Architectures by Various Polymerization Methods: Advantages and Drawbacks. *Macromolecular Symposia* **2000**, *161*, 53-61.

(1692) Ngororabanga, J. M. V.; Du Plessis, J.; Mama, N. Fluorescent Polymer Incorporating Triazolyl Coumarin Units for Cu2+ Detection via Planarization of ICT-Based Fluorophore. *Sensors* **2017**, *17*, 1980/1-1980/13.

(1693) Ishiwari, F.; Hasebe, H.; Matsumura, S.; Hajjaj, F.; Horii-Hayashi, N.; Nishi, M.; Someya, T.; Fukushima, T. Bioinspired Design of a Polymer Gel Sensor for the Realization of Extracellular Ca2+ Imaging. *Sci. Reports* **2016**, *6*, 24275.

(1694) La, D. D.; Bhosale, S. V.; Jones, L. A.; Bhosale, S. V. Tetraphenylethylene-Based AIE-Active Probes for Sensing Applications. *ACS Appl. Mater. Interfaces* **2018**, *10*, 12189-12216.

(1695) Zhou, H.; Li, J.; Chua, M. H.; Yan, H.; Tang, B. Z.; Xu, J. Poly(acrylate) with a Tetraphenylethene Pendant with Aggregation-Induced Emission (AIE) Characteristics: Highly Stable AIE-Active Polymer Nanoparticles for Effective Detection of Nitro Compounds. *Polym. Chem.* **2014**, *5*, 5628-5637.

(1696) Li, G.; Du, F.; Wang, H.; Bai, R. Synthesis and Self-Assembly of Carbazole-Based Amphiphilic Triblock Copolymers with Aggregation-Induced Emission Enhancement. *Reactive Functional Polym.* **2014**, *75*, 75-80.

(1697) Li, X.; Li, C.; Wang, S.; Dong, H.; Ma, X.; Cao, D. Synthesis and Properties of Photochromic Spirooxazine with Aggregation-Induced Emission Fluorophores Polymeric Nanoparticles. *Dyes and Pigments* **2017**, *142*, 481-490.

(1698) Chien, R.-H.; Lai, C.-T.; Hong, J.-L. Enhanced Aggregation Emission of Vinyl Polymer Containing Tetraphenylthiophene Pendant Group. *J. Phys. Chem. C* **2011**, *115*, 5958-5965.

(1699) Pablos, J. L.; Vallejos, S.; Ibeas, S.; Munoz, A.; Serna, F.; Garcia, F. C.; Garcia, J. M. Acrylic Polymers with Pendant Phenylboronic Acid Moieties as "Turn-Off" and "Turn-On" Fluorescence Solid Sensors for Detection of Dopamine, Glucose, and Fructose in Water. *ACS Macro Lett.* **2015**, *4*, 979-983.

(1700) Zhai, W.; Sun, X.; James, T. D.; Fossey, J. S. Boronic Acid-Based Carbohydrate Sensing. *Chem. – Asian J.* **2015**, *10*, 1836-1848.

(1701) Wu, X.; Chen, X.-X.; Jiang, Y.-B. Recent Advances in Boronic Acid-Based Optical Chemosensors. *Analyst* **2017**, *142*, 1403-1414.

(1702) Tashkhourian, J.; Dehbozorgi, A. Determination of Dopamine in the Presence of Ascorbic and Uric Acids by Fluorometric Method Using Graphene Quantum Dots. *Spectroscopy Lett.* **2016**, *49*, 319-325.

(1703) Mao, Q.; Liu, K.; Li, W.; Yan, J.; Zhang, A. OEGylated Cyclodextrin-Based Thermoresponsive Polymers and their Switchable Inclusion Complexation with Fluorescent Dyes. *Polym. Chem.* **2015**, *6*, 1300-1308.

(1704) McBrierty, V. J.; Martin, S. J.; Karasz, F. E. Understanding Hydrated Polymers: The Perspective of NMR. *J. Molec. Liquids* **1999**, *80*, 179-205.

(1705) Wang, Y.; Sun, C.; Li, H.; Gong, Q.; Chen, J. Self-Reference Plasmonic Sensors Based on Double Fano Resonances. *Nanoscale* **2017**, *9*, 11085-11092.

(1706) Fekete, Z; Csernai, M.; Kocsis, K.; Horvath, A. C.; Pongracz, A.; Bartho, P. Simultaneous In Vivo Recording of Local Brain Temperature and Electrophysiological Signals with a Novel Neural Probe. *J. Neural Engineering* **2017**, *14*, 034001.

(1707) Cheung, S. S.; Reynolds, L. F.; Macdonald, M. A. B.; Tweedie, C. L; Urquhart, R. L.; Westwood, D. A. Effects of Local and Core Body Temperature on Grip Force Modulation During Movement-Induced Load Force Fluctuations. *Eur. J. Appl. Physiol.* **2008**, *103*, 59-69.

(1708) Wang, H.; Cui, H.; Liu, X.; Li, L.; Cao, Y.; Liu, T.; Fang, Y. Alternative Copolymerization of a Conjugated Segment and a Flexible Segment and Fabrication of a Fluorescent Sensing Film for HCl in the Vapor Phase. *Chem Asian J.* **2013**, *8*, 101-107.

(1709) Almassio, M. F.; Romagnoli, M. J.; Del Rosso, P. G.; Schvval, A. B.; Garay, R. O. Distyrylbenzene-Based Segmented Conjugated Polymers: Synthesis, Thin Film Morphology and Chemosensing of Hydrophobic and Hydrophilic Nitroaromatics in Aqueous Media. *Polym.* **2017**, *113*, 167-179.

(1710) Kumpf, J.; Freudenberg, J.; Schwaebel, S. T.; Bunz, U. H. F. Amine Sensing with Distyrylbenzenes and Their Hexamethylene-Linked Polymers: Spraying Them On. *Macromolecules* **2014**, *47*, 2569-2573.

(1711) Tolosa, J.; Zucchero, A. J.; Bunz, U. H. F. Water-Soluble Cruciforms: Response to Protons and Selected Metal Ions. *J. Am. Chem. Soc.* **2008**, *130*, 6498-6506.

(1712) Del Rosso, P. G.; Almassio, M. F.; Garay, R. O. Chemosensing of Nitroaromatics with a New Segmented Conjugated Quaterphenylene Polymer. *Tetrahedron Lett.* **2011**, *52*, 4911-4915.

(1713) Del Rosso, P. G.; Romagnoli, M. J.; Almassio, M. F.; Barbero, C. A.; Garay, R. O. Diphenylanthrylene and Diphenylfluorene-Based Segmented Conjugated Polymer Films as Fluorescent Chemosensors for Nitroaromatics in Aqueous Solution. *Sensors Actuators B: Chem.* **2014**, *203*, 612-620.

(1714) Del Rosso, P. G.; Almassio, M. F.; Palomar, G. R.; Garay, R. O. Nitroaromatic Compounds Sensing. Synthesis, Photophysical Characterization and Fluorescence Quenching of a New Amorphous Segmented Conjugated Polymer with Diphenylfluorene Chromophores. *Sensors Actuators B: Chem.* **2011**, *160*, 524-532.

(1715) Gilliard, R. J.; Iacono, S. T.; Budy, S. M.; Moody, J. D.; Smith, D. W.; Smith, R. C. Chromophore-Derivatized Semifluorinated Polymers for Colorimetric and Turn-On Fluorescent Anion Detection. *Sensors Actuators B: Chem.* **2009**, *B143*, 1-5.

(1716) Steed, J. W.; Atwood, J. L. *Supramolecular Chemistry,* 2nd ed.; Wiley: Chippenham, 2009.

(1717) Vikaas, B.; Brahamdutt; Manjusha, C. Nanotechnology: Applications in Pharmaceutical Drug Delivery Systems. *J. Chem. Pharmaceutical Res.* **2016**, *8*, 259-265.

(1718) Verma, P. K.; Shegavi, M. L.; Bose, S. K.; Geetharani, K. A Nano-Catalytic Approach for C-B Bond Formation Reactions. *Org. Biomol. Chem.* **2018**, *16*, 857-873.

(1719) Wang, X.; Yao, C.; Wang, F.; Li, Z. Cellulose-Based Nanomaterials for Energy Applications. *Small* **2017**, *13*; DOI: 10.1002/smll.201702240.

(1720) Waleker, L.; Dutta, T.; Kumar, P.; Ok, Y. S.; Pawar, S.; Deep, A.; Kim, K.-H. Functionalized Fluorescent Nanomaterials for Sensing Pollutants in the Environment: A Critical Review. *Trends in Anal. Chem*. **2017**, *97*, 458-467.

(1721) Kang, K.; Jang, H. Advance in Synthesis of High Surface-to-Volume Gold Nanoparticles. *Bull. Korean Chem. Soc.* **2016**, *37*, 1391-1392.

(1722) Azria, D.; Blanquer, S.; Verdier, J.-M.; Belamie, E. Nanoparticles as Contrast Agents for Brain Nuclear Magnetic Resonance Imaging in Alzheimer's Disease Diagnosis. *J. Mater. Chem. B* **2017**, *5*, 7216-7237.

(1723) Lim, S. A.; Ahmed, M. U. Electrochemical Immunosensors and Their Recent Nanomaterial-Based Signal Amplification Strategies: A Review. *RSC Adv.* **2016**, *6*, 24995-25014.

(1724) Malekzad, H.; Sahandi Zangabad, P.; Mohammadi, H.; Sadroddini, M.; Jafari, Z.; Mahlooji, N.; Abbaspour, S.; Gholami, S.; Ghanbarpoor, M.; Pashazadeh, R.; Beyzavi, A.; Karimi, M.; Hamblin, M. R. Noble Metal Nanostructures in Optical Biosensors: Basics, and Their Introduction to Anti-Doping Detection. *TrAC, Trends Anal. Chem.* **2018**, *100*, 116-135.

(1725) Vasilescu, A.; Hayat, A.; Gaspar, S.; Marty, J.-L. Advantages of Carbon Nanomaterials in Electrochemical Aptasensors for Food Analysis. *Electroanal.* **2018**, *30*, 2-19.

(1726) Ong, Q.; Luo, Z.; Stellacci, F. Characterization of Ligand Shell for Mixed-Ligand Coated Gold Nanoparticles. *Acc. Chem. Res.* **2017**, *50*, 1911-1919.

(1727) Li, Y.; Xu, Y.; Fleischer, C. C.; Huang, J.; Lin, R.; Yang, L.; Mao, H. Impact of Anti-Biofouling Surface Coatings on the Properties of Nanomaterials and their Biomedical Applications. *J. Mater. Chem. B* **2018**, *6*, 9-24.

(1728) Zhao, Q.; Lin, Y.; Han, N.; Li, X.; Geng, H.; Wang, X.; Cui, Y.; Wang, S. Mesoporous Carbon Nanomaterials in Drug Delivery and Biomedical Application. *Drug Delivery* **2017**, *24*, 94-107.

(1729) Wang, Y.; Sun, S.; Zhang, Z.; Shi, D. Nanomaterials for Cancer Precision Medicine. *Adv. Mater.* **2018**, *Ahead of Print*; DOI: 10.1002/adma.201705660.

(1730) Nsibande, S. A.; Forbes, P. B. C. Fluorescence Detection of Pesticides using Quantum Dot Materials – A Review. *Anal. Chim. Acta* **2016**, *945*, 9-22.

(1731) Rasheed, P. A.; Lee, J.-S. Recent Advances in Optical Detection of Dopamine using Nanomaterials. *Microchim. Acta* **2017**, *184*, 1239-1266.

(1732) El-Ansary, A.; Faddah, L. M. Nanoparticles as Biochemical Sensors. *Nanotechnol. Sci. Appl.* **2010**, *3*, 65-76.

(1733) Ma, Q.; Su, X. Recent Advances and Applications in QDs-Based Sensors. *Analyst* **2011**, *136*, 4883-4893.

(1734) Duan, J.; Zhan, J. Recent Developments on Nanomaterials-Based Optical Sensors for Hg2+ Detection. *Sci China Mater*, **2015**, *58*, 223-240.

(1735) Lin, Y.-W.; Huang, C.-C.; Chang, H.-T. Gold Nanoparticle Probes for the Detection of Mercury, Lead and Copper Ions. *Analyst* **2011**, *136*, 863-871.

(1736) Yue, G.; Su, S.; Li, N.; Shuai, M.; Lai, X.; Astruc, D.; Zhao, P. Gold Nanoparticles as Sensors in the Colorimetric and Fluorescence Detection of Chemical Warfare Agents. *Coord. Chem. Rev.* **2016**, *311*, 75-84.

(1737) Saha, K.; Agasti, S. S.; Kim, C.; Li, X.; Rotello, V. M. Gold Nanoparticles in Chemical and Biological Sensing. *Chem. Rev*. **2012**, *112*, 2739-2779.

(1738) Zhang, J. J.; Cheng, F. F.; Li, J. J.; Zhu, J.-J.; Lu, Y. Fluorescent Nanoprobes for Sensing and Imaging of Metal Ions: Recent Advances and Future Perspectives. *Nano Today* **2016**, *11*, 309-329.

(1739) Heinz, H.; Pramanik, C.; Heinz, O.; Ding, Y.; Mishra, R. K.; Marchon, D.; Flatt, R. J.; Estrela-Lopis, I.; Llop, J.; Moya, S.; Ziolo, R. F. Nanoparticle Decoration with Surfactants: Molecular Interactions, Assembly, and Applications. *Surface Sci. Reports* **2017**, *72*, 1-58.

(1740) De Leo, F.; Magistrato, A.; Bonifazi, D. Interfacing Proteins with Graphitic Nanomaterials: From Spontaneous Attraction to Tailored Assemblies. *Chem. Soc. Rev.* **2015**, *44*, 6916-6953.

(1741) Hegazy, M. A.; El-Hameed, A. M. Characterization of CdSe-Nanocrystals used in Semiconductors for Aerospace Applications: Production and Optical Properties. *NRIAG Journal of Astronomy and Geophysics*, **2014***, 3,* 82-87.

(1742) Smith, A.; Nie, S. Semiconductor Nanocrystals: Structure, Properties, and Band Gap Engineering. *Acc. Chem. Res*. **2010**, *43*, 190-200.

(1743) Sun, J.; Goldys, E. M. Linear Absorption and Molar Extinction Coefficients in Direct Semiconductor Quantum Dots. *J. Phys. Chem. C* **2008**, *112*, 9261-9266.

(1744) Yu, W. W.; Qu, L.; Guo, W.; Peng, X. Experimental Determination of the Extinction Coefficient of CdTe, CdSe, and CdS Nanocrystals. *Chem. Mater*. **2003**, *15*, 2854-2860.

(1745) Ng, S. M.; Koneswaran, M.; Narayanaswamy, R. A Review on Fluorescent Inorganic Nanoparticles for Optical Sensing Applications. *RSC Adv.* **2016**, *6*, 21624-21661.

(1746) Erathodiyil, N.; Ying, J. Y. Functionalization of Inorganic Nanoparticles for Bioimaging Applications. *Acc. Chem. Res.* **2011**, *44*, 925-935.

(1747) Park, J. H.; Gu, L.; von Maltzahn, G.; Ruoslahti, E.; Bhatia, S. N.; Sailor, M. J. Biodegradable Luminescent Porous Silicon Nanoparticles for in Vivo Applications. *Nat. Mater.* **2009**, *8*, 331-336.

(1748) Sung, T.-W.; Lo, Y.-L. Highly Sensitive and Selective Sensor Based on Silica-Coated CdSe/ZnS Nanoparticles for Cu2+ Ion Detection. *Sens. Actuators B* **2012**, *165*, 119-125.

(1749) Zhao, J.; Deng, J.; Yi, Y.; Li, H.; Zhang, Y.; Yao, S. Label-Free Silicon Quantum Dots as Fluorescent Probe for Selective and Sensitive Detection of Copper Ions. *Talanta* **2014**, *125*, 372-377.

(1750) Xu, S.; Xu, S.; Zhu, Y.; Xu, W.; Zhou, P.; Zhou, C.; Dong, B.; Song, H. A Novel Upconversion, Fluorescence Resonance Energy Transfer Biosensor (FRET) for Sensitive Detection of Lead Ions in Human Serum. *Nanoscale* **2014**, *6*, 12573-12579.

(1751) Liu, Y.-L.; Kang, N.; Ke, X.-B.; Wang, D.; Ren, L.; Wang, H.-J. A Fluorescent Nanoprobe Based on Metal-Enhanced Fluorescence Combined with Förster Resonance Energy Transfer for the Trace Detection of Nitrite Ions. *RSC Adv*. **2016**, *6*, 27395-27403.

(1752) Du, X.; Zhang, X.; Jiang, C.; Zhang, W.; Yang, L. The Trace Detection of Nitrite Ions Using Neutral Red Functionalized SH-β-Cyclodextrin @Au Nanoparticles. *Sensors* **2018**, *18*.

(1753) Yi, Y.; Zhu, G.; Liu, C.; Huang, Y.; Zhang, Y.; Li, H.; Zhao, J.; Yao, S.; A Label-Free Silicon Quantum Dots-Based Photoluminescence Sensor for Ultrasensitive Detection of Pesticides. *Anal. Chem.* **2013**, *85*, 11464-11470.

(1754) Li, Y.; Xu, J.; Wang, L.; Huang, Y.; Guo, J.; Cao, X.; Shen, F.; Luo, Y.; Sun, C. Aptamer-Based Fluorescent Detection of Bisphenol A using Nonconjugated Gold Nanoparticles and CdTe Quantum Dots. *Sens. Actuators B* **2016**, *222*, 815-822.

(1755) Xu, G.; Zeng, S.; Zhang, B.; Swihart, M. T.; Yong, K.-T.; Prasad, P. N. New Generation Cadmium-Free Quantum Dots for Biophotonics and Nanomedicine. *Chem. Rev*. **2016**, *116*, 12234-12327.

(1756) Banerjee, S.; Kar, S.; Santra, S. A Simple Strategy for Quantum Dot Assisted Selective Detection of Cadmium Ions. *Chem. Commun.* **2008**, *26*, 3037-3039.

(1757) Tu, R.; Liu, B.; Wang, Z.; Gao, D.; Wang, F.; Fang, Q.; Zhang, Z. Amine-Capped ZnS-Mn2+ Nanocrystals for Fluorescence Detection of Trace TNT Explosive. *Anal. Chem.* **2008**, *80*, 3458-3465.

(1758) Wu, P.; He, Y.; Wang, H.-F.; Yan, X.-P. Conjugation of Glucose Oxidase onto Mn-doped ZnS Quantum Dots for Phosphorescent Sensing of Glucose in Biological Fluids. *Anal. Chem.* **2010**, *82*, 1427-1433.

(1759) Zhang, C.; Zhang, K.; Zhao, T.; Liu, B.; Wang, Z.; Zhang, Z. Selective Phosphorescence Sensing of Pesticide Based on the Inhibition of Silver (I) Quenched ZnS:Mn2+ Quantum Dots. *Sens. Actuators B* **2017**, *252*, 1083-1088.

(1760) Wang, S.; Wang, L. Lanthanide-Doped Nanomaterials for Luminescence Detection and Imaging. *Trends Anal. Chem.* **2014**, *62*, 123-134.

(1761) dos Santos, C. M. G.; Harte, A. J.; Quinn, S. J.; Gunnlaugsson, T. Recent Developments in the Field of Supramolecular Lanthanide Luminescent Sensors and Self-Assemblies. *Coord. Chem. Rev*. **2008**, *252*, 2512-2527.

(1762) Wang, F.; Banerjee, D.; Liu, Y.; Chen, X.; Liu, X. Upconversion Nanoparticles in Biological Labeling, Imaging, and Therapy. *Analyst* **2010**, *135*, 1839-1854.

(1763) Park, Y. I.; Lee, K. T.; Suh, Y. D.; Hyeon, T. Upconverting Nanoparticles: A Versatile Platform for Wide-Field Two-Photon Microscopy and Multi-Modal In Vivo Imaging. *Chem. Soc. Rev.* **2015**, *44*, 1302-1317.

(1764) Lee, S. Y.; Lin, M.; Lee, A.; Park, Y. I. Lanthanide-Doped Nanoparticles for Diagnostic Sensing. *Nanomaterials* **2017**, *7*, 411/1-411/14.

(1765) Kazemi, S.; Sarabi, A. A.; Abdouss, M. Synthesis and Characterization of Magnetic Molecularly Imprinted Polymer Nanoparticles for Controlled Release of Letrozole. *Korean J. Chem. Eng.* **2016**, *33*, 3289-3297.

(1766) Zheng, W.; Zhou, S.; Chen, Z.; Hu, P.; Liu, Y.; Tu, D.; Zhu, H.; Li, R.; Huang, M.; Chen, X. Sub-10 nm Lanthanide-Doped CaF2 Nanoprobes for Time-Resolved Luminescent Biodetection. *Angew. Chem. Int. Ed.* **2013**, *52*, 6671-6676.

(1767) Huang, P.; Wu, F.; Mao, L. Target-Triggered Switching On and Off the Luminescence of Lanthanide Coordination Polymer Nanoparticles for Selective and Sensitive Sensing of Copper Ions in Rat Brain. *Anal. Chem*. **2015**, *87*, 6834-6841.

(1768) Sarkar, S.; Chatti, M.; Mahalingam, V. Highly Luminescent Colloidal Eu3+-Doped KZnF3 Nanoparticles for the Selective and Sensitive Detection of CuII Ions. *Chem. Eur. J.* **2014**, *20*, 3311-3316.

(1769) Han, J.; Zhang, C.; Liu, F.; Liu, B.; Han, M.; Zou, W.; Yang, L.; Zhang, Z. Upconversion Nanoparticles for Ratiometric Fluorescence Detection of Nitrite. *Analyst* **2014**, *139*, 3032-3038.

(1770) Xie, L.; Qin, Y.; Chen, H.-Y. Polymeric Optodes Based on Upconverting Nanorods for Fluorescent Measurements of pH and Metal Ions in Blood Samples. *Anal. Chem.* **2012**, *84*, 1969-1974.

(1771) Chu, B; Song, B.; Ji, X.; Su, Y.; Wang, H.; He, Y. Fluorescent Silicon Nanorods-Based Ratiometric Sensors for Long-Term and Real-Time Measurements of Intracellular pH in Live Cells. *Anal. Chem*. **2017**, *89*, 12152-12159.

(1772) Zhang, C.-L.; Yuan, Y.-X.; Zhang, S.-M.; Wang, Y.-H.; Liu, Z.-H. Biosensing Platform Based on Fluorescence Resonance Energy Transfer from Upconverting Nanocrystals to Graphene Oxide. *Angew. Chem. Int. Ed.* **2011**, *50*, 6851-6854.

(1773) Tu, N.; Wang, L. Surface Plasmon Resonance Enhanced Upconverion Luminescence in Aqueous Media for TNT Selective Detection. *Chem. Commun.* **2013**, *49*, 6319-6321.

(1774) Ma, Y.; Wang, L. Upconversion Luminescence Nanosensor for TNT Selective and Label-Free Quantification in the Mixture of Nitroaromatic Explosives. *Talanta* **2014**, *120*, 100-105.

(1775) Wang, Y.; Wu, Z.; Liu, Z. Upconversion Fluorescence Resonance Energy Transfer Biosensor with Aromatic Polymer Nanospheres as the Lable-Free Energy Acceptor. *Anal. Chem*. **2013**, *85*, 258-264.

(1776) Wang, J.; Wei, T.; Li, X.; Zhang, B.; Wang, J.; Huang, C.; Yuan, Q. Near-Infrared-Light-Mediated Imaging of Latent Fingerprints Based on Molecular Recognition. *Angew. Chem. Int. Ed.* **2014**, *53*, 1616-1620.

(1777) Huang, D.; Niu, C.; Ruan, M.; Wang, X.; Zeng, G.; Deng, C. Highly Sensitive Strategy for Hg2+ Detection in Water Environmental Samples Using Long Lifetime Fluorescence Quantum Dots and Gold Nanoparticles. *Environ. Sci. Technol.* **2013**, *47*, 4392-4398.

(1778) Li, Q.; Wang, J.; He, Y.; Selective Chemiluminescent Sensor for Detection of Mercury(II) Ions Using Non-Aggregated Luminol-Caped Nanoparticles. *Sens. Actuators B* **2016**, *231*, 64-69.

(1779) Wu, Y.-S.; Huang, F.-F.; Lin, Y.-W. Fluorescent Detection of Lead in Environmental Water and Urine Samples Using Enzyme Mimics of Catechin-Synthesized Au Nanoparticles. *ACS Appl. Mater. Interfaces* **2013**, *5*, 1503-1509.

(1780) Li, D.; Ma, Y.; Duan, H.; Deng, W.; Li, D. Griess Reaction-Based Paper Strip for Colorimetric/Fluorescent/SERS Triple Sensing of Nitrite. *Biosens. Bioelectron.* **2018,** *99*, 389-398.

(1781) Wu, Q.; Long, Q.; Li, H.; Zhang, Y.; Yao, S.; An Upconversion Fluorescence Resonance Energy Transfer Nanosensor for One Step Detection of Melamine in Raw Milk. *Talanta* **2015**, *136*, 47-53.

(1782) Dai, H.; Shi, Y.; Wang, Y.; Sun, Y.; Hu, J.; Ni, P.; Li, Z. A Carbon Dot Based Biosensor for Melamine Detection by Fluorescence Resonance Energy Transfer. *Sens. Actuators B* **2014**, *202,* 201-208.

(1783) Guo, J.; Zhang, Y.; Luo, Y.; Shen, F.; Sun, C. Efficient Fluorescence Resonance Energy Transfer Between Oppositely Charged CdTe Quantum Dots and Gold Nanoparticles for Turn-On Fluorescence Detection of Glyphosate. *Talanta* **2014**, *125*, 385-392.

(1784) Palanisamy, S.; Zhang, X.; He, T. Simple Colorimetric Detection of Dopamine using Modified Silver Nanoparticles. *Sci China Chem*. **2016**, *59*, 387-393.

(1785) Biswal, J.; Misra, N.; Borde, L.; Sabharwal, S. Synthesis of Silver Nanoparticles in Methacrylic Acid Solution by Gamma Radiolysis and Their Application for Estimation of Dopamine at Low Concentrations. *Radiat. Phys. Chem.* **2013**, *83*, 67-73.

(1786) He, Y.; Xu, B.; Li, W.; Yu, H. Silver Nanoparticle-Based Chemiluminescent Sensor Array for Pesticide Discrimination. *J. Agric. Food. Chem*. **2015**, *63*, 2930-2934.

(1787) Das, N. K.; Ghosh, S.; Priya, A.; Datta, S.; Mukherjee, S. Luminescent Copper Nanoclusters as a Specific Cell-Imaging Probe and a Selective Metal Ion Sensor. *J. Phys. Chem. C* **2015**, *119*, 24657-24664.

(1788) Zheng, J.; Nicovich, P. R.; Dickson, R.M. Highly Fluorescent Noble-Metal Quantum Dots. *Annu. Rev. Phys. Chem*. **2007**, *58*, 409-431.

(1789) Ma, Y.; Wang, S.; Wang, L. Nanomaterials for Luminescence Detection of Nitroaromatic Explosives. *Trends Anal. Chem.* **2015**, *65*, 13-21.

(1790) Deng, H.-H.; Zhang, L.-N.; He, S.-B.; Liu, A.-L.; Li, G.-W; Lin, X.-H.; Xia, X.-H.; Chen, W. Methionine-Directed Fabrication of Gold Nanoclusters with Yellow Fluorescent Emission for Cu2+ Sensing. *Biosens. Bioelectron*. **2015**, *65*, 397-403.

(1791) Chen, Q.; Li, Y.; Xu, S.; Tie, W.; Wang, N.; He, Z.; Liu, P.; Zhou, H. Highly Fluorescent Au Nanoclusters: Electrostatically Induced Phase Transfer Synthesis for Cu2+ Sensing. *Luminescence* **2017**, *32*, 271-276.

(1792) Yuan, X.; Yeow, T. J.; Zhang, Q.; Lee, J. Y.; Xie, J. Highly Luminescent Ag+ Nanoclusters for Hg2+ Ion Detection. *Nanoscale* **2012,** *4*, 1968-1971.

(1793) Villar-Vidal, N.; Blanco, M. C.; Lopez-Quintela, M. A.; Rivas, J.; Serra, C. Electrochemical Synthesis of Very Stable Photoluminescent Copper Clusters. *J. Phys. Chem. C* **2010**, *114*, 15924-15930.

(1794) Wei, W.; Lu, Y.; Chen, W.; Chen, S. One-Pot Synthesis, Photoluminescence, and Electrocatalytic Properties of Subnanometer-Sized Copper Clusters. *J. Am. Chem. Soc.* **2011**, *133*, 2060-2063.

(1795) Wang, C.; Huang, Y. Green Route to Prepare Biocompatible and Near Infrared Thiolate-Protected Copper Nanoclusters for Cellular Imaging. *Nano* **2013**, *8*, 1350054/1-1350054/10.

(1796) Ghosh, R.; Sahoo, A. K.; Ghosh, S. S.; Paul, A.; Chattopadhyay, A. Blue-Emitting Copper Nanoclusters Synthesized in the Presence of Lysozyme as Candidates for Cell Labeling. *ACS Appl. Mater. Interfaces* **2014**, *6*, 3822-3828.

(1797) Fernandez-Ujados, M.; Trapiella-Algonso, L.; Costa-Fernandez, J. M.; Pereiro, R.; Sanz-Medel, A. One-Step Aqueous Synthesis of Fluorescent Copper Nanoclusters by Direct Metal Reduction. *Nanotechnology* **2013**, *24*, 495601/1-495601/6.

(1798) Liao, X.; Li, R.; Li, Z.; Sun, X.; Wang, Z.; Liu, J. Fast Synthesis of Copper Nanoclusters Through the Use of Hydrogen Peroxide Additive and their Application for the Fluorescence Detection of Hg2+ in Water Samples. *New J. Chem.* **2015**, *39*, 5240-5248.

(1799) Luo, T.; Zhang, S.; Wang, Y.; Wang, M.; Liao, M.; Kou, X. Glutathione-Stabilized Cu Nanocluster-Based Fluorescent Probe for Sensitive and Selective Detection of Hg2+ in Water. *Luminescence* **2017**, *32*, 1092-1099.

(1800) Zhai, Q.; Xing, H.; Zhang, X.; Li, J.; Wang, E. Enhanced Electrochemiluminescence Behavior of Gold-Silver Bimetallic Nanoclusters and its Sensing Application for Mercury(II). *Anal. Chem*. **2017**, *89*, 7788-7794.

(1801) Niu, C.; Liu, Q.; Shang, Z.; Zhao, L.; Ouyang, J. Dual-Emission Fluorescent Sensor Based on AIE Organic Nanoparticles and Au Nanoclusters for the Detection of Mercury and Melamine. *Nanoscale* **2015**, *7*, 8457-8465.

(1802) Qu, F.; Xu, X.; You, J. A New Dual-Emission Fluorescence Sensor Based on Carbon Nanodots and Gold Nanoclusters for the Detection of Melamine. *New J. Chem.* **2017**, *41*, 9438-9443.

(1803) Bian, R.-X.; Wu, X.-T.; Chai, F.; Li, L.; Zhang, L.-Y.; Wang, T.-T.; Wang, C.-G.; Su, Z.-M. Facile Preparation of Fluorescent Au Nanoclusters-Based Test Papers for Recyclable Detection of Hg2+ and Pb2+. *Sensors Actuators B* **2017**, *241*, 592-600.

(1804) Lin, Z.; Luo, F.; Dong, T.; Zheng, L.; Wang, Y.; Chi, Y.; Chen, G. Recyclable Fluorescent Gold Nanocluster Membrane for Visual Sensing of Copper (II) Ion in Aqueous Solution. *Analyst* **2012**, *137*, 2394-2399.

(1805) Lu, J.; Fu, Y.; Wang, D. L.; Lu, C. A Facile Synthesis of Thermo-Responsive Copolymer Stabilized Fluorescent Silver Nanoclusters and their Application in pH Sensing. *Sensors Actuators B* **2018**, *254*, 996-1004.

(1806) Miao, Z.; Hou, W.; Liu, M.; Zhang, Y.; Yao, S. BSA Capped Bi-Functional Fluorescent Cu Nanoclusters as pH Sensor and Selective Detection of Dopamine. *New J. Chem.* **2017**, *42*, 1446-1456.

(1807) Zhang, Y.; Li, M.; Niu, Q.; Gao, P.; Zhang, G.; Dong, C.; Shuang, S. Gold Nanoclusters as Fluorescent Sensors for Selective and Sensitive Hydrogen Sulfide Detection. *Talanta* **2017***, 171*, 143-151.

(1808) Deng, C.; Zhong, Y.; He, Y.; Ge, Y.; Song, G. Selective Determination of Trace Bisphenol A Using Molecularly Imprinted Silica Nanoparticles Containing Quenchable Fluorescent Silver Nanoclusters. *Microchim. Acta* **2016**, *183,* 431-439.

(1809) Anjali Devi, J. S.; Aswathy, B.; Asha, S.; George, S. Lactose Tailored Boronic Acid Conjugated Fluorescent Gold Nanoclusters for Turn-On Sensing of Dopamine. *J. Anal. Chem.* **2017**, *72*, 445-459.

(1810) Wang, S.; Li, N.; Pan, W.; Tang, B. Advances in Functional Fluorescent and Luminescent Probes for Imaging Intracellular Small-Molecule Reactive Species. *Trends Anal. Chem*. **2012**, *39*, 3-37.

(1811) Yang, S.; Sun, X.; Chen, Y. Fluorescence Enhancement Probe Based on L-Cystine Modified Copper Nanoclusters for the Detection of 2,4,6-Trinitrotoluene. *Mater. Lett*. **2017**, *194*, 5-8.

(1812) Aparna, R.; Devi, J.; Sachidanandan, P.; George, S. Polyethylene Imine Capped Copper Nanoclusters-Fluorescent Colorimetric Onsite Sensor for the Trace Level Detection of TNT. *Sensors Actuators B* **2018**, *254*, 811-819.

(1813) Auger, A.; Samuel, J.; Poncelet, O.; Raccurt, O. A Comparative Study of Non-Covalent Encapsulation Methods for Organic Dyes into Silica Nanoparticles. *Nanoscale Res Lett*. **2011**, *6*, 328.

(1814) Wang, M.; Meng, G.; Huang, Q.; Qian, Y. Electrospun 1,4-DHAQ-Doped Cellulose Nanofiber Films for Reusable Fluorescence Detection of Trace Cu2+ and Further for Cr3+. *Environ. Sci. Technol.* **2012**, *46*, 367-373.

(1815) Tyagi, A. K.; Ramkumar, J.; Jayakumar, O. D. Inorganic-Organic Ag-Rhodamine 6G Hybrid Nanorods: "Turn" On Fluorescent Sensors for Highly Selective Detection of Pb2+ Ions in Aqueous Solution. *Analyst* **2012**, *137*, 760-764.

(1816) Xu, J.; Yu, H.; Hu, Y.; Chen, M.; Shao, S. A Gold Nanoparticle-Based Fluorescence Sensor for High Sensitive and Selective Detection of Thiols in Living Cells. *Biosens. Bioelectron*. **2016**, *75*, 1-7.

(1817) Cao, X.; Shen, F.; Zhang, M.; Guo, J.; Luo, Y.; Xu, J.; Li, Y.; Sun, C. Highly Sensitive Detection of Melamine Based on Fluorescence Resonance Energy Transfer between Rhodamine B and Gold Nanoparticles. *Dyes and Pigments* **2014**, *111*, 99-107.

(1818) Gao, D.; Wang, Z.; Liu, B.; Ni, L. Wu, M.; Zhang, Z. Resonance Energy Transfer-Amplifying Fluorescence Quenching at the Surface of Silica Nanoparticles Toward Ultrasensitive Detection of TNT. *Anal. Chem*. **2008**, *80*, 8545-8553.

(1819) Salinas, Y.; Solano, M. V.; Sorensen, R. E.; Larsen, K. R.; Lycoops, J.; Jeppesen, J. O.; Martinez-Manez, R.; Sancenon, F.; Marcos, M. D.; Amoros, P.; Guillem, C. Chromo-Fluorogenic Detection of Nitroaromatic Explosives by Using Silica Mesoporous Supports Gated with Tetrathiafulvalene Derivatives. *Chem. Eur. J.* **2014**, *20*, 855-866.

(1820) Ma, Y.; Li, H.; Peng, S.; Wang, L. Highly Selective and Sensitive Fluorescent Paper Sensor for Nitroaromatic Explosive Detection. *Anal. Chem.* **2012**, *84*, 8415-8421.

(1821) Liu, Q.; Zhou, Q.; Jiang, G. Nanomaterials for Analysis and Monitoring of Emerging Chemical Pollutants. *Trends Anal. Chem*. **2014**, *58*, 10-22.

(1822) Zhao, A.; Zhao, C.; Li, M.; Ren, J.; Qu, X. Ionic Liquids as Precursors for Highly Luminescent, Surface-Different Nitrogen-Doped Carbon Dots Used for Label-Free Detection of Cu2+/Fe3+ and Cell Imaging. *Anal. Chim. Acta* **2014**, *809*, 128-133.

(1823) Cao, B.; Yuan, C.; Liu, B.; Jiang, C.; Guan, G.; Han, M.-Y. Ratiometric Fluorescence Detection of Mercuric Ions Based on the Nanohybrid of Fluorescence Carbon Dots and Quantum Dots. *Anal. Chim. Acta* **2013***, 786*, 146-152.

(1824) Qu, F.; Huang, W.; You, J. A Fluorescent Sensor for Detecting Dopamine and Tyrosinase Activity by Dual-Emission Carbon Dots and Gold Nanoparticles. *Colloids Surfaces B* **2018**, *162*, 212-219.

(1825) Kim, J.; Kim, F.; Huang, J. Seeing Graphene-Based Sheets. *Materials Today* **2010**, *13*, 28-38.

(1826) Kasry, A.; Ardakani, A. A.; Tulevski, G. S.; Menges, B.; Copel, M.; Vyklicky, L. Highly Efficient Fluorescence Quenching with Graphene. *J. Phys. Chem. C.* **2012**, *116*, 2858-2862.

(1827) Li, Y.; Gao, Y.; Li, Y.; Liu, S.; Zhang, H.; Su, X. A Novel Fluorescence Probing Strategy Based on Mono-[6-(2-aminoethylamino)-6-deoxy]-β-Cyclodextrin Functionalized Graphene Oxide for the Detection of Amantadine. *Sensors Actuators B* **2014**, *202*, 323-329.

(1828) Bao, X. Shi, J.; Zhu, J.; Wang, X. A Novel Sensitive and Selective Nanocomposite Sensor for Doxorubicin Based on Graphene Oxide and Fluorescent [2] Rotaxane. *Sensors Actuators B* **2016**, *237*, 380-386.

(1829) Zor, E.; Esad Saglam, M.; Alpaydin, S.; Bingol, H. A Reduced Graphene Oxide/α-Cyclodextrin Hybrid for the Detection of Methionine: Electrochemical, Fluorometric and Computational Studies. *Anal. Methods* **2014**, *6*, 6522-6530.

(1830) Mondal, A.; Jana, N. R. Fluorescent Detection of Cholesterol using β-Cyclodextrin Functionalized Graphene. *Chem. Commun.* **2012***, 48*, 7316-7318.

(1831) Hu, H.; Xin, J. H.; Hu, H.; Wang, X.; Lu, X. Organic Liquids-Responsive β-Cyclodextrin-Functionalized Graphene-Based Fluorescence Probe: Label-Free Selective Detection of Tetrahydrofuran. *Molecules* **2014**, *19*, 7459-7479.

(1832) Becuwe, M.; Danjou, P.-E.; Cazier, F.; Woisel, P.; Delattre, F. Immobilization of Fluorescent Chemosensor on Pyrogenic Silica: A Promising Device for Gaseous Detection. *J. Colloid Interface Sci.* **2015,** *450*, 62-67.

(1833) Cristaldi, D. A.; Fragala, I.; Pappalardo, A.; Toscano, R. M.; Ballistreri, F. P.; Tomaselli, G. A.; Gulino, A. Sensing of Linear Alkylammonium Ions by a 5-Pyrenoylamide-Calix[5]arene Solution and Monolayer Using Luminescence Measurements. *J. Mater. Chem*. **2012***, 22*, 675-683.

(1834) Zhao, G.; Yang, L.; Wu, S.; Zhao, H.; Tang, E.; Li, C.-P. The Synthesis of Amphiphilic Pillar[5]arene Functionalized Reduced Graphene Oxide and its Application as a Novel Fluorescence Sensing Platform for the Determination of Acetaminophen. *Biosens. Bioelectron*. **2017**, *91*, 863-869.

(1835) Yang, L.; Zhao, H.; Li, Y.; Ran, X.; Deng, G.; Xie, X.; Li, C.-P. Fluorescent Detection of Tadalafil based on Competitive Host-Guest Interaction using p-Sulfonated Calix[6[arene Functionalized Graphene. *ACS Appl. Mater. Interfaces* **2015**, *7*, 26557-26565.

(1836) Sun, Y.; Mao, X.; Luo, L.; Tian, D.; Li, H. Calix[4]arene Triazole-Linked Pyrene: Click Synthesis, Assembly on Graphene Oxide, and Highly Sensitive Carbaryl Sensing in Serum. *Org. Biomol. Chem.* **2015**, *13*, 9294-9299.

(1837) Naseri, A.; Samadi, M.; Pourjavadi, A.; Moshfegh, A. Z.; Ramakrishna, S. Graphitic Carbon Nitride (g-C3N4)-Based Photocatalysts for Solar Hydrogen Generation: Recent Advances and Future Development Directions. *J. Mater. Chem. A* **2017**, *5*, 23406-23433.

(1838) Mousavi, M.; Habibi-Yangjeh, A.; Pouran, S. R. Review on Magnetically Separable Graphitic Carbon Nitride-Based Nanocomposites and Promising Visible-Light-Driven Photocatalysts. *J. Mater. Sci. - Mater. Electron.* **2018**, *29*, 1719-1747.

(1839) Chen, L.; Zeng, X.; Si, P.; Chen, Y.; Chi, Y.; Kim, D.-H.; Chen, G. Gold Nanoparticle-Graphite-Like C3N4 Nanosheet Nanohybrids used for Electroluminescent Immunosensor. *Anal. Chem.* **2014**, *86*, 4188-4195.

(1840) Wang, B.; Wang, H.; Zhong, X.; Chai, Y.; Chen, S.; Yuan, R. A Highly Sensitive Electrochemiluminescence Biosensor for the Detection of Organophosphate Pesticides Based on Cyclodextrin Functionalized Graphitic Carbon Nitride and Enzyme Inhibition. *Chem. Commun.* **2016**, *52*, 5049-5052.

(1841) Sauer, M. Single-Molecule-Sensitive Fluorescent Sensors Based on Photoinduced Intramolecular Charge Transfer. *Angew. Chem. Int. Ed.* **2003**, *42*, 1790-1793.

(1842) McNutt, M. K.; Chu, S.; Lubchenco, J.; Hunter, T.; Dreyfus, G.; Murawski, S. A.; Kennedy, D. M. Applications of Science and Engineering to Quantify and Control the Deepwater Horizon Oil Spill. *Proc. Natl. Acad. Sci. U.S.A.* **2012**, *109*, 20222-20228.

(1843) Vianna, N. J. The Love Canal: Issues and Problems. *Chemosphere* **1983**, *12*, 705-712.

(1844) Whelton, A. J.; McMillan, L.; Connell, M.; Kelley, K. M.; Gill, J. P.; White, K. D.; Gupta, R.; Dey, R.; Novy, C. Residential Tap Water Contamination Following the Freedom Industries Chemical Spill: Perceptions, Water Quality, and Health Impacts. *Environ. Sci. Technol.* **2015**, *49*, 813-823.

(1845) Han, A. A.; Fabyanic, E. B.; Miller, J. V.; Prediger, M. S.; Prince, N.; Mouch, J. A.; Boyd, J. In Vitro Cytotoxicity Assessment of a West Virginia Chemical Spill Mixture Involving 4-Methylcyclohexanemethanol and Propylene Glycol Phenyl Ether. *Environ. Monitoring Assessment* **2017**, *189*, 1-13.

(1846) Chen, D.; Kannan, K.; Tan, H.; Zheng, Z.; Feng, Y.-L.; Wu, Y.; Widelka, M. Bisphenol Analogues Other Than BPA: Environmental Occurrence, Human Exposure, and Toxicity-A Review. *Environ. Sci. Technol.* **2016**, *50*, 5438-5453.

(1847) Andra, S. S.; Austin, C.; Yang, J.; Patel, D.; Arora, M. Recent Advances in Simultaneous Analysis of Bisphenol A and its Conjugates in Human Matrices: Exposure Biomarker Perspectives. *Sci. Total Environ.* **2016**, *572*, 770-781.

(1848) Reineck, P.; Gibson, B. C. Near-Infrared Fluorescent Nanomaterials for Bioimaging and Sensing. *Adv. Optical Mater.* **2017**, *5(2)*; DOI: 10.1002/adom.201600446.

(1849) Chaudhary, S.; Umar, A.; Bhasin, K. K.; Singh, S. Applications of Carbon Dots in Nanomedicine. *J. Biomed. Nanotechnol.* **2017**, *13*, 591-637.

(1850) Zhou, J.-W.; Zou, X.-M.; Song, S.-H.; Chen, G.-H. Quantum Dots Applied to Methodology on Detection of Pesticide and Veterinary Drug Residues. *J. Agricultural Food Chem.* **2018**, *66*, 1307-1319.

(1851) Pinalli, R.; Dalcanale, E. Supramolecular Sensing with Phosphonate Cavitands. *Acc. Chem. Res.* **2013**, *46*, 399-411.

(1852) Kubik, S. Anion Recognition in Aqueous Media by Cyclopeptides and Other Synthetic Receptors. *Acc. Chem. Res.* **2017**, *50*, 2870-2878.

(1853) Liu, B.; Liu, J. Comprehensive Screen of Metal Oxide Nanoparticles for DNA Adsorption, Fluorescence Quenching, and Anion Discrimination. *ACS Appl. Mater. Interfaces* **2015**, *7*, 24833-24838.

(1854) Kwon, H.; Jiang, W.; Kool, E. T. Pattern-Based Detection of Anion Pollutants in Water with DNA Polyfluorophores. *Chem. Sci.* **2015**, *6*, 2575-2583.

(1855) Szumna, A.; Jurczak, J. A New Macrocyclic Polylactam-Type Neutral Receptor for Anions - Structural Aspects of Anion Recognition. *Eur. J. Org. Chem.* **2001**, 4031-4039.

(1856) Zou, J.-Y.; Li, L.; You, S.; Liu, Y.; Cui, H.-M.; Cui, J.-z.; Zhang, S. Two Luminescent Lanthanide(III) Metal-Organic Frameworks as Chemosensors for High-Efficiency Recognition of Cr(VI) Anions in Aqueous Solution. *Dalton Trans.* **2018**, *Ahead of Print*; DOI: 10.1039/c8dt03050b.

(1857) Simon, E.; Lamoree, M. H.; Hamers, T.; de, Boer, J. Challenges in Effect-Directed Analysis with a Focus on Biological Samples. *TrAC, Trends Anal. Chem.* **2015**, *67*, 179-191.

(1858) Winterbourn, C. C. The Challenges of Using Fluorescent Probes to Detect and Quantify Specific Reactive Oxygen Species in Living Cells. *Biochim. Biophys. Acta* **2014**, *1840*, 730-738.

(1859) Weidhaas, J.; Lin, L.-S.; Buzby, K. A Case Study for Orphaned Chemicals: 4-Methylcyclohexanemethanol (MCHM) and Propylene Glycol Phenyl Ether (PPH) in Riverine Sediment and Water Treatment Processes. *Sci. Total Environ.* **2017**, *574*, 1396-1404.